Technical Report Documentation Page

1. Report No. SSRP 2001/17	2. Government Accession No.	3. Recipient's Catalog No.
4. Title and Subtitle TILT: The Treasure Island Liquefaction Test		5. Report Date January 2002 6. Performing Organization Code
7. Author(s) Scott A. Ashford and Kyle M. Rollins		8. Performing Organization Report No. UCSD / SSRP-2001/17
9. Performing Organization Name and Address Department of Structural Engineering School of Engineering University of California, San Diego La Jolla, California 92093-0085		10. Work Unit No. (TRAIS) 11. Contract or Grant No. 59A0051 and 59A0128
12. Sponsoring Agency Name and Address California Department of Transportation Engineering Service Center 1801 30th St., West Building MS-9 Sacramento, California 95807		13. Type of Report and Period Covered Final Report 10/15/98 – 06/30/01 14. Sponsoring Agency Code

15. Supplementary Notes

Prepared in cooperation with the State of California Department of Transportation (lead agency) along with Departments of Transportation from the following States: Alaska, Missouri, New York, Oregon, Utah, and Washington.

16. Abstract

This report presents the results of the Treasure Island Liquefaction Test (TILT), a joint project carried out by University of California, San Diego, and Brigham Young University. To improve our understanding of the lateral load behavior of deep foundations in liquefied soil, a series of full-scale lateral load tests were been performed at the National Geotechnical Experimentation Site (NGES) at Treasure Island in San Francisco, California. The ultimate goal of the (TILT) project was to develop lateral load-displacement relationships for a variety of individual piles and pile groups in liquefied sand under full-scale conditions. The tests were carried out using a high-speed hydraulic loading system after the sand surrounding the piles was liquefied using blasting techniques. This report presents back-calculated *p-y* curves for a single pipe piles, pile groups, and Cast-in-Steel Shell piles before and during liquefaction, as well as through dissipation of excess pore water pressures. In addition, recommendations with regard to design of deep foundations in liquefied soil are presented.

17. Key Words piles, liquefaction, p-y curves, lateral loading		18. Distribution Statement Unlimited	
19. Security Classification (of this report) Unclassified	20. Security Classification (of this page) Unclassified	21. No. of Pages 511	22. Price

Form DOT F 1700.7 (8-72) Reproduction of completed page authorized

DISCLAIMER

The opinions, recommendations and conclusions contained within this report are solely those of the authors, and do not necessarily reflect the views of the California Department of Transportation or other project sponsors.

ACKNOWLEDGMENTS

The authors wish to express their sincere gratitude to the sponsors of the Treasure Island Liquefaction Test (TILT) project, especially the lead agency for the project, Caltrans, and the several other agencies that participated in this pooled fund study. These include the Alaska Department of Transportation and Public Facilities, the Missouri Department of Transportation, the Oregon Department of Transportation, the New York Department of Transportation, the Utah Department of Transportation, and the Washington State Department of Transportation.

Hayward Baker and Geotechnics America/Mustang Construction provided additional project funding as well as donated services for installation of ground improvement measures. Condon–Johnson & Associates and Foundation Constructors donated foundation installation services. Additional services were also donated by Subsurface Consultants and Kleinfelder & Associates. Their support is gratefully acknowledged.

We would like to thank Thomas Weaver and Dusty Lane, the graduate research assistants responsible for the full-scale testing. Travis Gerber, a graduate research assistant, has also contributed significantly to this work. Their contribution to the testing program and this report is greatly appreciated.

Finally, the project could never have taken place without the full cooperation of the United States Navy and the City of San Francisco. Their cooperation is greatly appreciated.

EXECUTIVE SUMMARY

This report presents the results of the Treasure Island Liquefaction Test (TILT), a joint project carried out by University of California, San Diego, and Brigham Young University. To improve our understanding of the lateral load behavior of deep foundations in liquefied soil, a series of full-scale lateral load tests were been performed at the National Geotechnical Experimentation Site (NGES) at Treasure Island in San Francisco, California. The ultimate goal of the TILT project was to develop lateral load-displacement relationships for a variety of individual piles and pile groups in liquefied sand under full-scale conditions. The tests were carried out using a high-speed hydraulic loading system after the sand surrounding the piles was liquefied using blasting techniques. This report presents back-calculated *p-y* curves for single piles, pile groups, and Cast-in-Steel Shell piles before and during liquefaction, as well as through dissipation of excess pore water pressures. Furthermore, the results of studies on the use of stone columns and synthetic earthquake drains as liquefaction mitigation are also presented.

The primary conclusions and recommendations that will have a significant impact on design practice are:

1. The shape of the back-calculated *p-y* curves for liquefied sand are significantly different than those currently recommended for design, using either the p-multiplier approach or the residual strength approach. Specifically, the *p-y* curves for liquefied sand obtained from this study show a concave up shape, rather than a concave down shape typical of clay and non-liquefied sand.

2. Alternative methods for developing *p-y* curves in liquefied sand (i.e. p-multipliers or residual strength curves) may result in computed displacements and bending moments that adequately capture the measured response over only a limited range of depth and load, and may result in significant error elsewhere. If these alternative *p-y* curves are used, the effect of their shape on the computed foundation and superstructure response should be considered for the anticipated loading conditions.

3. Based the limitations of the current p-y analysis procedures mentioned above, it is recommended that analysis procedures be developed that capture the dilational response of the liquefied soil that result in this concave up shape for the p-y curves.

4. Group effects appear to be relatively inconsequential for pile groups in liquefied sand. For both the 4-pile group and the 9-pile group, the load-displacement curves for the individual piles within a group were essentially the same. In addition, the load-displacement curve for the single pile was very similar to that for the piles in the 9-pile group.

5. For design purposes, p-multipliers for group effects can be taken as 1.0 for liquefied sand. However, as the average r_u decreases and the frictional resistance increases, group effects will also become important and will need to be accounted for with appropriate p-multipliers.

6. Installation of stone columns significantly limited the excess pore pressure increase resulting from controlled blasting and significantly increased the rate of excess pore pressure dissipation after blasting, thus effectively mitigating the liquefaction hazard. In addition, the stone columns increased the stiffness of the foundation system 2.5 to 3.5 times that of the system in the liquefied soil. Even in the pre-blast, non-liquefied testing, the stone columns increased the stiffness of the foundation system by approximately 25 to 45 percent.

7. Pushover analyses should only be used if kinematic loads are not expected to contribute significantly to the foundation and superstructure response. Furthermore, when performing a pushover analysis, pile response should be assessed under lateral loads applied before and after the onset of liquefaction.

8. If a dynamic/time history analysis which implements *p-y* curves to model the soil is required, the effect of dilational soil response on the shape of *p-y* curves may have a significant effect on the structural response. Current procedures only account for pore pressure changes due to free-field soil strains and neglect the effect of pore pressure changes resulting from interaction with the foundation.

The results obtained from the full-scale pile testing at Treasure Island compare favorably with centrifuge test results under similar conditions. However, the TILT results are only for sands of relative density of approximately 50 percent. Current research is underway to combine the TILT results with centrifuge test results and other field studies to develop comprehensive design recommendations for deep foundations in liquefied sand.

In summary, the TILT project has resulted in several direct benefits to the project sponsors for application in bridge design. The testing and subsequent analyses have greatly increased our understanding of soil-foundation-structure interaction in liquefied soil, resulting in specific recommendations that can be immediately implemented into design practice, as well as general conclusions and recommendations that will be useful in assessing our current design methodology. Combined with the results of ongoing research, these also can be developed into specific design recommendations. In addition, the general agreement between the TILT full-scale testing and the smaller scale centrifuge test results increases our confidence in the numerous centrifuge studies already completed elsewhere. Finally, the TILT project provides some of the first full-scale quantitative data on two different ground improvement techniques, providing insight into our design procedures and increasing our confidence level in the ability of these methods to mitigate liquefaction hazards.

TABLE OF CONTENTS

Disclaimer ii

Acknowledgements iii

Executive Summary iv

Table of Contents vi

1 INTRODUCTION 1-1

1.1 Background and Research Significance 1-1

1.2 Project Objectives 1-2

1.3 Overview of Testing 1-3

2 PILOT LIQUEFACTION STUDY 2-1

2.1 Pilot Study Site Characterization 2-1

2.2 Pilot Study Test Results 2-2

2.2.1 Excess Pore Pressure Ratio's 2-3

2.2.2 Settlement 2-4

2.2.3 Peak Particle Velocity 2-4

2.3 Summary 2-5

3 SINGLE PILE TESTS 3-1

3.1 Single Pile Site Characterization 3-1

3.2 Single Pile Test Results 3-2

3.2.1 Load-Displacement Results for Test 1 3-3

3.2.2 Excess Pore Pressure Response for Test 1 3-4

3.2.3 Load-Displacement Results for Test 2 3-4

3.2.4 Excess Pore Pressure Response for Test 2 3-5

3.2.5 Settlement 3-5
3.3 Summary of Testing 3-6
4 4-PILE GROUP AND 0.6-m CISS PILE TESTS 4-1
4.1 4-Pile Group and 0.6-m CISS Pile Site Characterization 4-1
4.2 4-Pile Group and 0.6-m CISS Pile Test Results 4-3
4.2.1 Load-Displacement Results for Test 1 4-3
4.2.2 Excess Pore Pressure Response for Test 1 4-4
4.3 Site Characterization after Installation of Stone Columns 4-4
4.4 Stone Column Test Results 4-5
4.4.1 Load-Displacement Results with Stone Columns 4-5
4.4.2 Excess Pore Pressure Response with Stone Columns 4-6
4.5 Blast Induced Settlement 4-6
4.6 Summary 4-7
5 9-PILE GROUP AND 0.9-m CISS PILE TESTS 5-1
5.1 9-Pile Group and 0.9-m CISS Pile Site Characterization 5-1
5.2 9-Pile Group and 0.9-m CISS Pile Test Results 5-3
5.2.1 Load-Displacement Results for Test 1 5-3
5.2.2 Excess Pore Pressure Response for Test 1 5-4
5.2.3 Load-Displacement Results for Test 2 5-5
5.2.4 Excess Pore Pressure Response for Test 2 5-6
5.3 Blast Induced Settlement 5-7
5.4 Summary 5-7
6 THE VERTICAL DRAIN PIPE TESTING 6-1

6.1 Objectives of the Vertical Drain Pipe Testing 6-1

6.2 Site Characterization 6-2

6.3 Drain Properties and Installation Procedures 6-3

6.4 Drain Tests at Pilot Liquefaction Site 6-4

6.5 Drain Tests at Vertical Pipe Drain Site 6-5

6.5.1 Drain Installation and Test Layout 6-5

6.5.1.2 Vibration during Installation 6-7

6.5.1.4 CPT Test After Treatment 6-8

6.5.2 Test Blast 6-9

6.6 Analysis of Drain Test Results 6-16

6.6.1 Description of Computer Model and Input Parameters 6-16

6.6.1.1 Required Soil Properties and Geometry 6-17

6.6.2 Analysis of Pilot Liquefaction Test Results 6-19

6.6.2.1 Model Calibration 6-20

6.6.3 Analysis of Vertical Pipe Drain Site 6-22

6.7 Results and Conclusions Based on Drain Testing and Analysis 6-25

6.7.1 Conclusions Regarding Settlement Mitigation Due to Drainage 6-25

6.7.2 Conclusions Regarding Pore Pressure Response 6-26

6.7.3 Conclusions based on Computer Model Analysis of Measured Response 6-27

7 ANALYSIS OF CISS PILES 7-1

7.1 Methodology for Back-Calculating p-y Curves 7-2

7.1.1 Soil Displacement 7-3

7.1.2 Moment Curvature Analyses 7-3

7.1.3 Soil Reaction 7-4

7.1.4 Modification to Curvature Data 7-5

7.2 0.6-m CISS Pile p-y Curves 7-5

7.2.1 Pre-Blast p-y Curves 7-6

7.2.2 Excess Pore Pressure Ratio's Adjacent to 0.6-m CISS Pile 7-7

7.2.3 Post-Blast p-y Curves 7-7

7.3 0.9-m CISS Pile p-y Curves 7-8

7.3.1 Pre-Blast p-y Curves 7-8

7.3.2 Excess Pore Pressure Ratio's for 0.9-m CISS Pile 7-9

7.3.3 Post-Blast p-y Curves 7-10

7.4 Comparison of 0.6-m and 0.9-m CISS Pile p-y Curves 7-11

7.5 Excess Pore Pressure Response 7-12

7.6 Centrifuge p-y Curves 7-15

7.7 Modified p-y Curves 7-17

7.8 Simplified Analyses 7-20

7.8.1 0.6-m CISS Pile Analyses 7-20

7.8.2 0.9-m CISS Pile Analyses 7-23

7.9 Considerations for Design of Deep Foundations in Liquefied Sand 7-25

7.10 Summary 7-29

8 ANALYSIS OF STEEL PIPES AND PILE GROUPS 8-1

8.1 Analysis of Single Pile Response for Pre-Blast Load Tests 8-1

8.1.1 Summary of Site Conditions and Soil Property Selection 8-1

8.1.2 Test Pile Properties and Instrumentation 8-4

8.1.3 Measured Response 8-5

8.1.4 Computed Response 8-6

8.2 Analysis of 4-Pile Group Response for Pre-Blast Test Before Improvement 8-10

8.2.1 Summary of Site Conditions and Soil Property Selection 8-10

8.2.2 Measured Response 8-11

8.2.3 Computed Response 8-11

8.3 Analysis of 4- Pile Group Response for Pre-Blast Test After Improvement 8-13

8.3.1 Summary of Site Conditions and Soil Property Selection 8-13

8.3.2 Measured Response 8-13

8.3.3 Computed Response 8-14

8.4 Analysis of 9-Pile Group Response for Pre-Blast Test 8-15

8.4.1 Summary of Site Conditions and Soil Property Selection 8-15

8.4.2 Measured Response 8-16

8.4.3 Computed Response 8-17

8.5 Results and Conclusions Relative to Pile Behavior in Non-Liquefied Sand 8-19

8.6 Excess Pore Pressure Measurements at Test Sites After Blast 8-22

8.7 Response of 9-Pile Group Response for Tests after Blasting 8-23

8.7.1 Measured Load versus Deflection 8-23

8.8 Development of p-y Curves 8-24

8.8.1 Analysis Procedure 8-24

8.8.2 Deflection Calculations 8-26

8.8.3 Soil Reaction Calculations 8-27

8.9 P-y Curves for 9 Pile Group 8-29

8.9.1 First Set of Load Cycles 8-29

8.9.2 Last Set of Load Cycles 8-32

8.9.3 Effect of Excess Pore Pressure Ratio and Depth on P-Y Curves 8-33

8.9.4 Validation Using Lateral Response Analysis 8-34

8.9.5 Comparison With Other Methods for p-y Determination 8-35

8.10 P-y Curves for Single Pile 8-37

8.10.1 Validation Using Lateral Response Analysis 8-38

9 CONCLUSIONS AND RECOMMENDATIONS 9-1

10 REFERENCES 10-1

APPENDIX A A-1

A.1 ABSTRACT A-1

A.2 INTRODUCTION A-2

A.3 PROJECT DESCRIPTION A-3

A.4 METHODS AND TESTING PROCEDURE A-5

A.4.1 Test Set-up A-5

A.4.2 Controlled Blasting A-6

A.4.3 Stone Column Installation A-7

A.4.4 Loading Sequence A-8

A.5 RESULTS A-9

A.6 CONCLUSIONS A-12

A.7 REFERENCES A-13

1 INTRODUCTION

The Treasure Island Liquefaction Test (TILT) is a research project that consisted of full-scale lateral load pile tests in non-liquefied and liquefied ground at Treasure Island in the San Francisco Bay. This project is a joint venture between the University of California, San Diego and Brigham Young University, in close interaction with research personnel from the California Department of Transportation (Caltrans) and several other Departments of Transportation. Participants in this pooled fund study include the states of Alaska, California, Missouri, New York, Oregon, Utah, and Washington. Several other organizations collaborated on the project. The University of Michigan carried out visual-cone testing with funding from the National Science Foundation. The United Stated Geological Survey conducted ground-penetrating radar testing at the site. Utah State University conducted shear wave velocity tests at the site also with funding from the National Science Foundation.

1.1 Background and Research Significance

The lateral load capacity of deep foundations is critically important in the design of bridge structures in seismically active regions; however, there is currently little information to guide engineers in the design of piles embedded in liquefiable soils. Typical design procedures for piles in liquefiable soils are conservative and assume that the liquefied soil will provide little or no resistance to lateral movement. However, recent laboratory studies suggest that while the resistance may be reduced from the non-liquefied state, it is not zero and may be substantial (e.g. Wilson et al., 2000; Dobry et al., 1996).

Ongoing centrifuge studies using small-scale models (e.g. Wilson et al., 2000; Dobry et al., 1996) are providing valuable insight on soil-pile interaction in liquefied soil. However, full-scale tests are necessary to verify/calibrate these models and provide ground truth information. To improve our understanding of the lateral load behavior of deep foundations in liquefied soil, we conducted a series of lateral load tests on a full-scale single pile, pile groups, and Cast-in-Steel-Shell (CISS) piles. The testing was conducted near the National Geotechnical Experimentation Site on Treasure Island in San Francisco Bay where liquefaction has been observed in past earthquakes. Both static and cyclic tests were conducted in non-liquefied soil, and then cyclic tests were conducted after a surface layer over 4 m thick was liquefied using controlled blasting techniques.

1.2 Project Objectives

The overall objective of this research is to develop recommendations for soil parameters to use in the design and analysis of deep foundations subjected to lateral loading in liquefied soil based on the results of the proposed full-scale testing, in conjunction with available results of related centrifuge tests. Specifically, our objectives are to:

1. Characterize the proposed site through an extensive field exploration program.

2. Determine optimum charge size, delay and layout, as well as instrumentation layout by conducting a pilot blast program at the site.

3. Determine the lateral load capacity and distribution of load in a full-scale pile, pile group, and CISS pile in non-liquefied sand under static and cyclic loading conditions.

4. Determine the lateral load capacity and distribution of load in a full-scale pile, pile group, and CISS pile in liquefied sand under cyclic loading conditions.

5. Back-calculate p-y curves to model the resistance provided by liquefied sand.

6. Develop appropriate p-multipliers to account for reduction in capacity due to group effects.

1.3 Overview of Testing

Eleven full-scale field tests were conducted at Treasure Island. The testing consisted of two pilot liquefaction tests, two single pile tests, two 4-pile group/0.6-m CISS pile tests, two nine-pile group/0.9-m CISS pile tests, an earthquake drain (E~Quake Drain) test, a pre-stressed concrete pile test, and a concrete filled fiber reinforced polymer (FRP) pile test. The pile load tests consisted of lateral loads being applied to the piles in the free-head condition (no rotational restraint). Down-hole explosives were used to induce liquefaction in all except for the pre-stressed and FRP pile tests. Prior to the second 4-pile group/0.6-m CISS pile test, stone columns were installed to improve soil conditions. A list of field tests conducted and the date of testing is presented in Table 1.1. The tests were conducted in five different excavations within the test site. A site plan of the TILT project is shown in Figure 1.1.

Data was collected from each test using various instrumentation. Pore pressure transducers were used to measure in-situ water pressures. All piles except for the pre-stressed and FRP piles were instrumented with strain gages. Linear potentiometers were used to measure pile head displacement and rotation. Load cells on the hydraulic actuator and individual piles within the pile groups measured the applied lateral force. A slope inclinometer was used with the 0.6-m and 0.9-m CISS piles at the end of testing to obtain the final displaced shape. Peak particle velocity was measured using portable seismographs and settlement measurements were made using driven stakes and a surveyor's rod and level. A summary of data collected from in-situ soil tests as well as lateral load tests is presented in Table 1.2.

The UCSD Mobile Structural Testing (MoST) laboratory, which houses a high speed data acquisition system capable of acquiring over 200 channels of data, and a high speed data acquisition system from BYU were used to obtain data from the load cells, linear potentiometers, strain gages, and pore pressure transducers. The UCSD system collected the strain gage data while the BYU system collected the pore pressure and displacement data. Both systems acquired the lateral force applied by the actuator in order to synchronize the data.

This report contains a comprehensive collection of data obtained from the in-situ testing and full-scale field tests as reported in the Structural Systems Research Report titled "Full-Scale Behavior of Laterally Loaded Deep Foundations in Liquefied Sand: Test Results" as well as p-y curves back-calculated from the full-scale testing. The test results were included in this report to provide a single complete document that can be referenced for both measured test results as well as the back-calculated p-y curves. The

report has been organized to present data from each test site in separate chapters. Data from the pilot liquefaction study will be presented first followed by results from the single pile tests, 4-pile group/0.6-m CISS pile tests, nine- pile group/0.9-m CISS pile and EQ Drain tests. The back-calculated p-y curve are presented for the single pile, 0.6-m and 0.9-m CISS pile, and the 4-Pile and 9-pile group. Conclusions and recommendations based upon the back-calculated p-y curves are presented to assist in pile design at sites where liquefaction is a concern.

Table 1.1 List of Field Tests

Test	Date Performed
Pilot Liquefaction Study Blast 1	10/23/98
Pilot Liquefaction Study Blast 2	10/26/98
Single Pile Blast 1	1/20/99
Single Pile Blast 2	1/28/99
Four Pile Group/0.6-m CISS Pile Blast 1	2/4/99
Four Pile Group/0.6-m CISS Pile Blast 2 (with Stone Columns)	2/27/99
Nine Pile Group/0.9-m CISS Pile Blast 1	2/18/99
Nine Pile Group/0.9-m CISS Pile Blast 2	2/19/99
E~Quake Drain Test	2/25/99
Pre-Stressed Concrete Pile	3/8/99
Concrete Filled FRP Pile	3/8/99

Table 1.2 Summary of Data Collected

	Insitu Tests							Pile Tests							Concrete Tests		
	Nuclear Density	Radar	Soil Boring	CPT	Vs	Pressuremeter	Dilitometer	Load	Displacement	Strain	Inclinometer	Particler Velocity	Pore Pressure	Settlement	Concrete UC	Gamma Logging	Rebar Tension
Pilot Liquefaction Study																	
Field Exploration			x	x	x												
Blast No.1				x								x	x	x			
Blast No.2				x								x	x	x			
Blast No.3				x								x	x	x			
Single Pile Tests																	
Field Exploration			x	x	x	x	x										
Blast No.1								x	x	x		x	x	x			
Blast No.2								x	x	x		x	x	x			
Composite & Pre-stressed Pile Tests								x	x								
0.6-m CISS / 4 Pile Group																	
Field Exploration	x	x	x	x	x										x	x	x
Blast No.1								x	x	x	x	x	x	x			
After Stone Column Installation		x		x	x												
Blast No.2					x			x	x	x	x	x	x	x			
0.9-m CISS / 9 Pile Group																	
Field Exploration		x	x	x	x										x	x	x
Blast No.1					x			x	x	x	x	x	x	x			
Blast No.2					x			x	x	x	x	x	x	x			
Drain Test																	
Field Exploration	x			x													
Blast No.1												x	x	x			

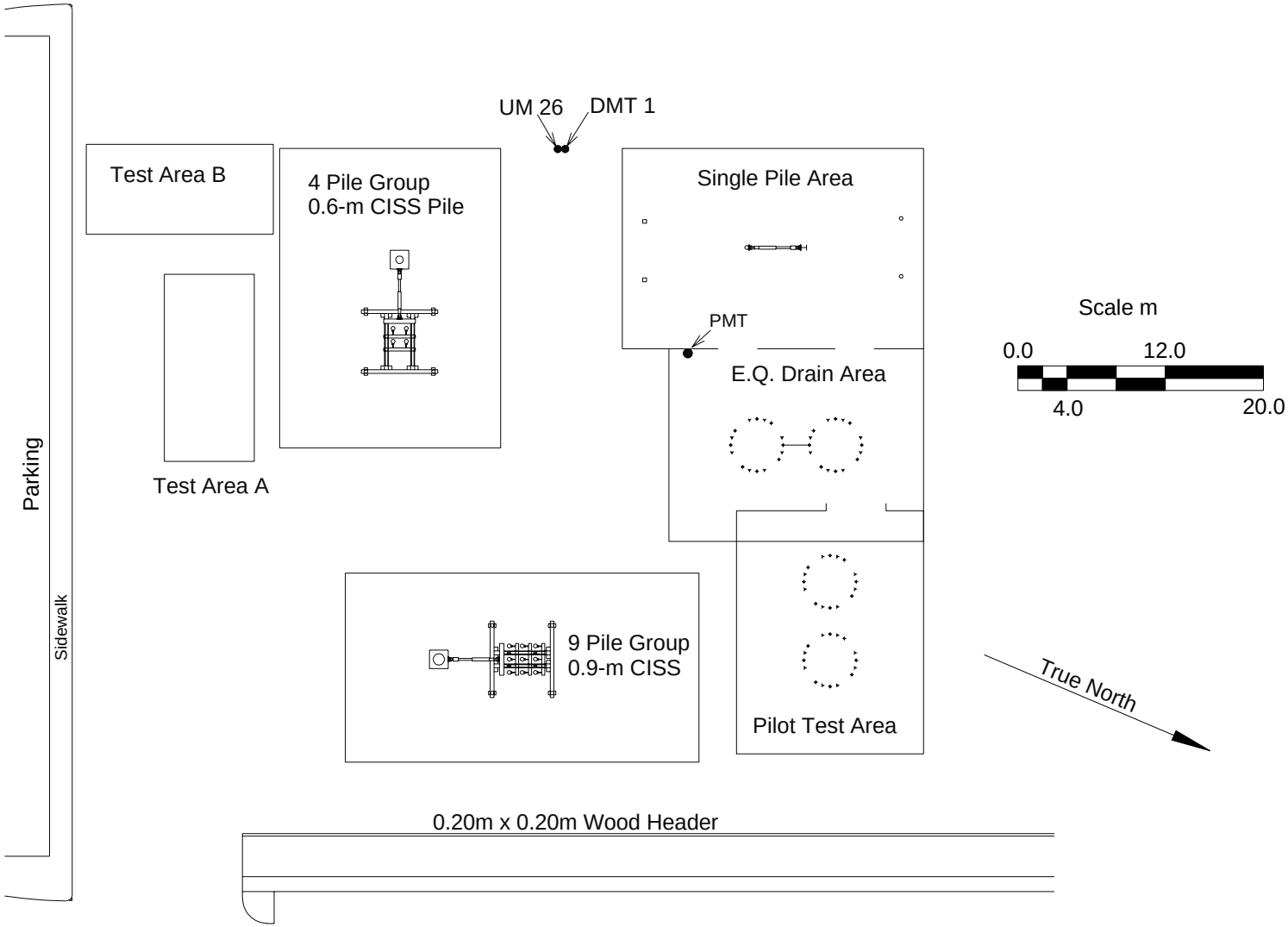

Figure 1.1 Treasure Island Liquefaction Test Site Plan

Figure 1.2 Aerial Photograph of Treasure Island Liquefaction Test Site

2 PILOT LIQUEFACTION STUDY

An area adjacent to the pile test sites was used to conduct a pilot liquefaction study prior to foundation testing. The pilot liquefaction study consisted of two small trial blasts and two pilot blasts. Two trial test blasts were performed in an effort to assess pore-pressure transducer capabilities, while the pilot blasts verified the required charge weight, delay and pattern to induce liquefaction. Although blast densification has been used successfully over the last 50 years in a variety of soil and site conditions, site-specific studies are generally recommended (Narin van Court and Mitchell, 1995). This site-specific pilot study was carried out in order to verify that the controlled blasting was a viable technique to use for this project, prior to any foundations being installed. This chapter presents data from the subsurface investigation and in-situ testing at the pilot study site, followed by plots of excess pore pressure ratios, peak particle velocity as a function of scaled distance and settlement contours resulting from blasting.

The test set-ups for Trial Blasts A and B are shown in Figures 2.1 and 2.2, respectively. We found that the vibrating wire transducers used in Trial Blast A were not capable of withstanding the peak pressure caused by the initial blast. Trial Blast B utilized piezoresistive transducers, which performed well, and were used for the remainder of testing at Treasure Island.

2.1 Pilot Study Site Characterization

Prior to and after blasting, a series of in-situ tests were performed to characterize the soil at the pilot site. Figure 2.3 shows the location and type of in-situ tests performed for this effort. The soil boring log BH-1 is shown in Figure 2.4. This log shows the water table at

approximately 1.5 m below the original ground surface. The low standard penetration test (SPT) blow counts in the sand indicate liquefaction susceptibility of the deposit. For the SPT procedures used in all the soil borings, the measured hammer energy effeciency was approximately 45 to 50 percent. Figures 2.5 through 2.10 show results from six CPT's performed within the excavated test area before blasting. Thirteen additional CPT's were performed after the first pilot blast and are shown in Figures 2.11 through 2.23. Shear and compression wave velocity testing was also carried out at the pilot study site prior to any blasting. A seismic cone test at the location of CPT-3 measured shear wave velocity and a suspension logger was used in the borehole to measure shear and compression wave velocities. The velocity profile is shown in Figure 2.24. Correlation between the measured shear wave velocities using the seismic cone and suspension logger is good. Shear wave velocities in the profile generally vary between 100 m/s and 200 m/s.

2.2 Pilot Study Test Results

The initial pilot liquefaction blast occurred on October 23, 1998, with the second pilot blast occurring three days later on October 26, 1998. A map showing the location and depth of the pore-pressure transducers (PPT's) and location of the down-hole explosives for both pilot blasts is presented in Figure 2.25. The PPT's were placed at depths ranging from 1 to 6 m, and the explosives were placed at a depth of approximately 3 m below the excavated ground surface. Pore pressure transducers remained at the location shown in Figure 2.25 for the second blast while the down-hole explosives were rotated clockwise 0.3 m at the same radial distance and depth used for the first blast. The water table for the pilot study was approximately 0.5 m below the excavated ground surface.

2.2.1 Excess Pore Pressure Ratio's

Excess pore pressure ratios from the first blast are presented in Figures 2.26 through 2.35. The excess pore pressure ratio plots are grouped according to location, starting at the west end of the excavation and moving east. All transducers below a depth of 1 m show excess pore pressure ratios reaching or exceeding a value of 80% initially. Many transducers show excess pore pressure ratios reaching 100%. Approximately five minutes after blasting, the excess pore pressure ratios dropped below 80%. The excess pore pressure ratios generally ranged between 10% and 20% one hour after the blast. In addition to the pore pressure transducers indicating excess pore pressure ratios of 100%, the presence of sand boils after blasting provided evidence that liquefaction had occurred. Sand boils first appeared approximately 5 minutes after the blast, and continued for over 20 minutes.

The second pilot blast was performed on October 26, 1998. The objective of the second blast was to verify that liquefaction could be induced more than once at the same site with the same charge weight and pattern. Again, excess pore pressure ratios below 1 m typically exceeded 80% with many transducers showing values of 100% for the first five minutes after blasting. After one hour, excess pore pressure ratios had dropped to between 10% and 20%. Excess pore pressure ratios for the second blast are shown in Figures 2.36 through 2.45. Again, sand boils provided further evidence that liquefaction had occurred as shown in Figure 2.46.

2.2.2 Settlement

Figure 2.47 shows how we performed an elevation survey to measure settlement due to blasting. Contours of blast induced settlement are presented in Figures 2.48 and 2.49 for the first and second blast respectively. The total settlement resulting from both blasts is presented in Figure 2.50. The contours of settlement are in millimeters, while the coordinates from the edge of the excavation are in meters.

2.2.3 Peak Particle Velocity

Portable seismographs were placed at various distances from the blasts to monitor peak particle velocity to verify that vibration levels were low enough to not disturb residents or cause damage to adjacent structures. The measured peak particle velocity is plotted against scaled distance in Figure 2.51. A general equation for estimating peak radial velocity for saturated soils has been given by Charlie and Abt (1985). The peak radial velocity in mm/sec is given as

$$V_p = 12000\left(\frac{R}{W^{1/3}}\right)^{-1.5} \tag{2.1}$$

where V_p is the peak radial velocity, R is the distance from the charge in meters, and W is the charge mass in kilograms. Results from this equation predict velocities significantly greater than those measured at Treasure Island in the loose sand deposit. A best fit of the recorded data can be approximated using following equation.

$$V_p = 2400\left(\frac{R}{W^{1/3}}\right)^{-1.5} \tag{2.2}$$

Three components of velocity were measured at each seismograph: vertical, longitudinal and transverse. The vertical velocity was the largest for each test.

2.3 Summary

The pilot liquefaction study was quite successful. The trial blasts showed that piezoresistive pore pressure transducers were necessary to resist the initial shock wave produced by the blasting, yet still able to record pore pressures following the blast with sufficient accuracy and precision. The charge size, delay and pattern were found sufficient to liquefy the sand inside the ring of charges. Using the same charge size, delay and pattern, the site was liquefied a second time, thus verifying the repeatability of the test. We were also able to develop a site-specific relationship correlating peak particle velocity and scaled distance. This site-specific relationship may be useful in predicting peak particle velocities at other sites where blast densification is used to mitigate liquefaction hazards. Based on the success of this pilot study, a series of full-scale foundation tests were carried out as presented in the following chapters.

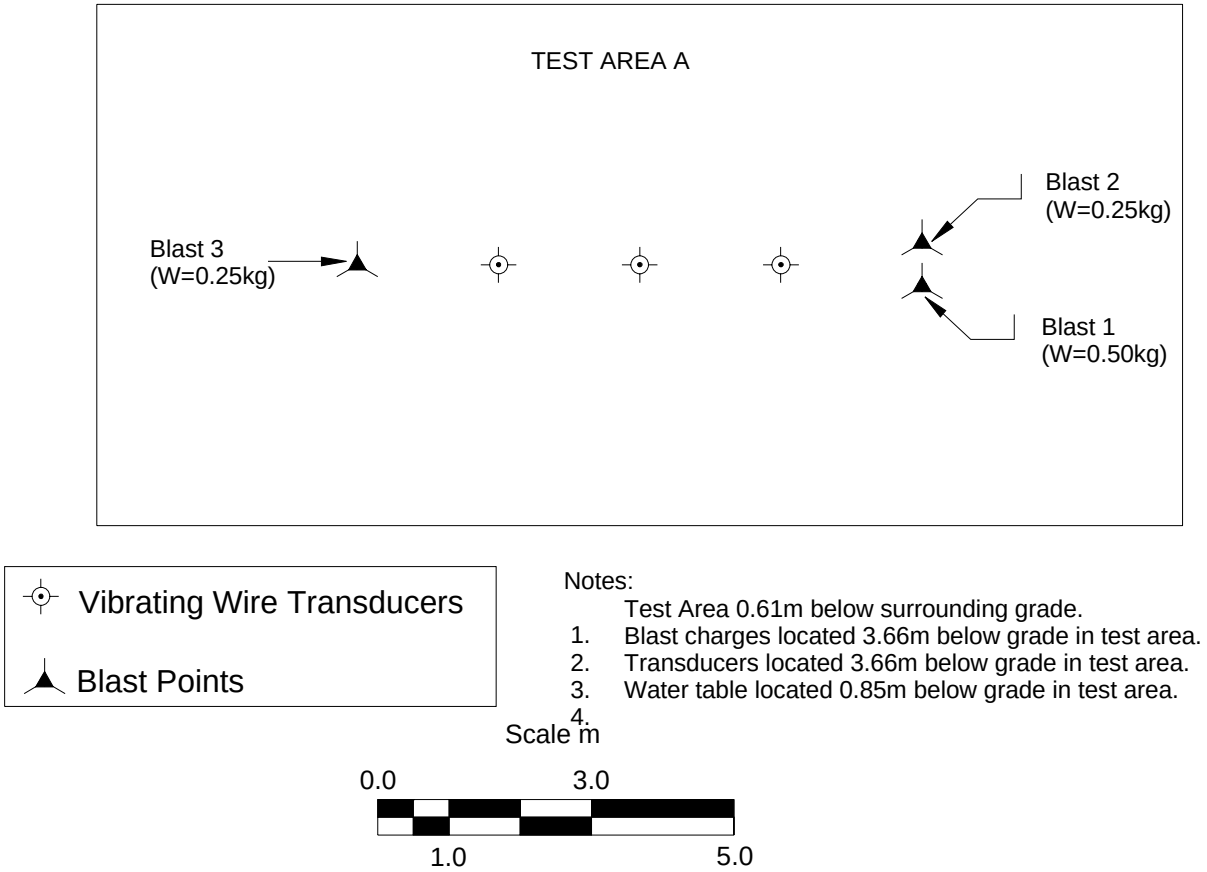

Figure 2.1 Location of Pore Pressure Transducers and Explosives for Trial Blast A

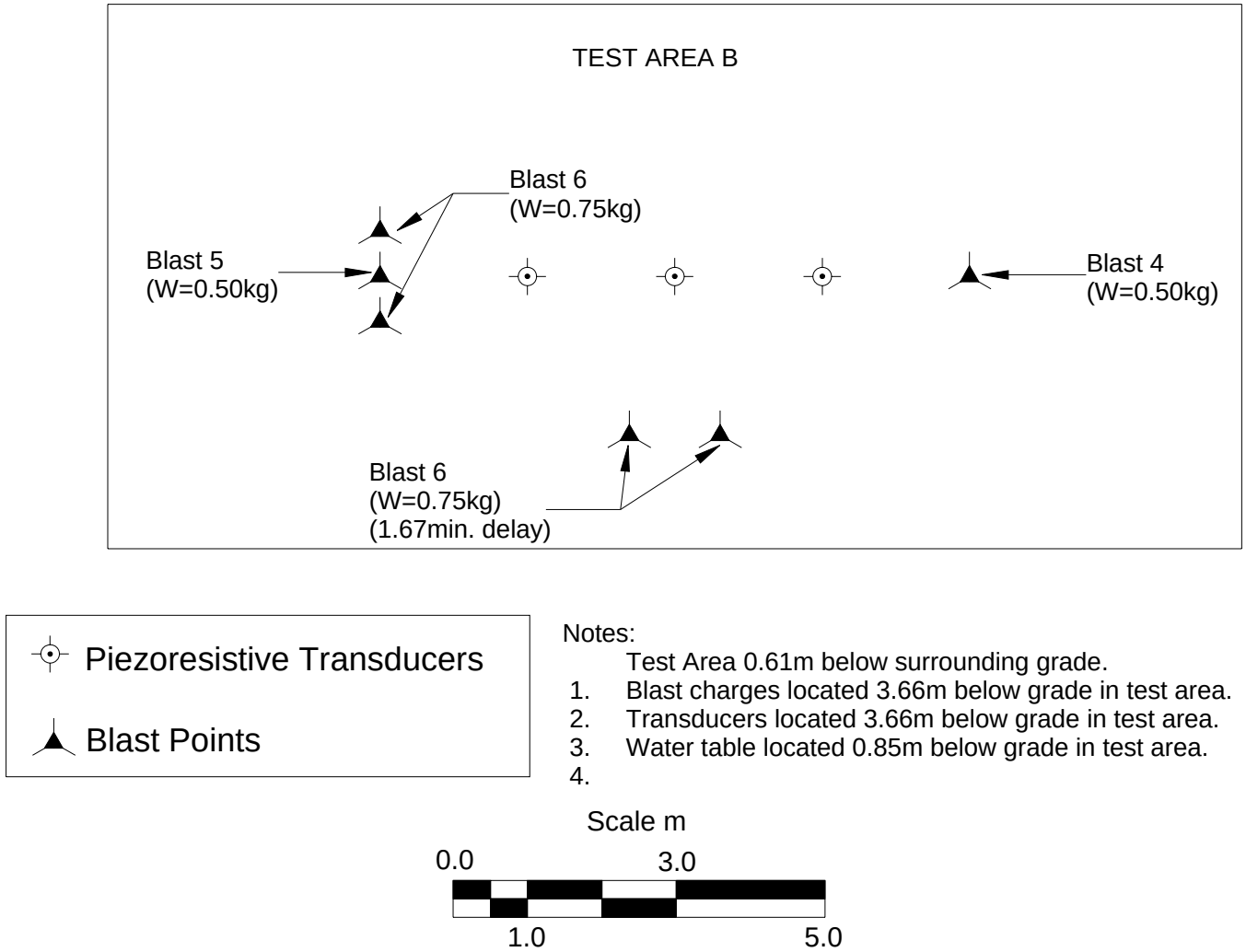

Figure 2.2 Location of Pore Pressure Transducers and Explosives for Trial Blast B

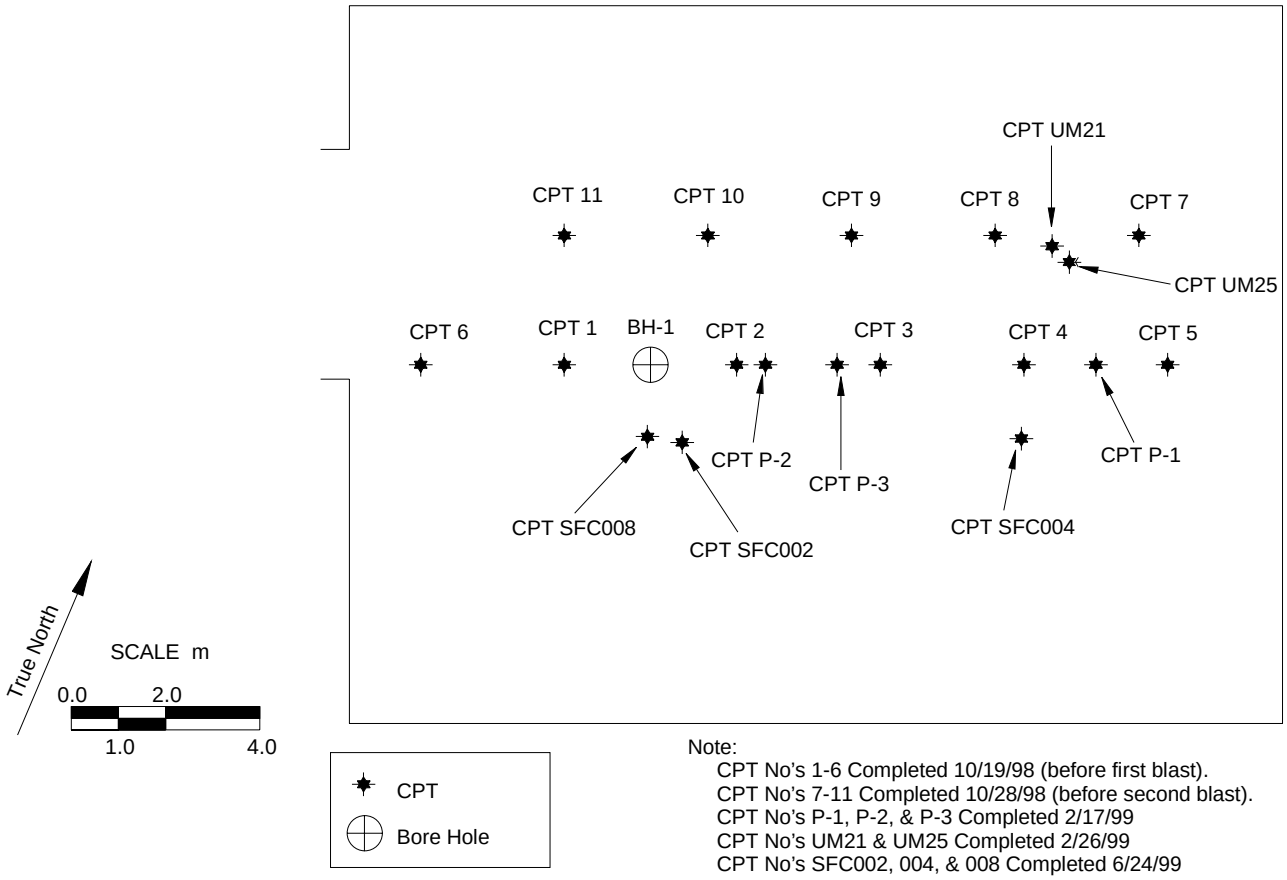

Figure 2.3 Location Map of In-Situ Tests for Pilot Liquefaction Study Area

Brigham Young University
&
University of California - San Diego
Telephone: (801) 378-6334
Fax: (801) 378-4449

Boring No: BH-1 | Sheet 1 of 2
Logged By: tw | Elevation (m): 3.4
Date Started: 9/17/1998 | Drill Contractor: Pitcher
Date Finished: 9/17/1998 | Drilling Method: Rotary Wash

TREASURE ISLAND
SAN FRANCISCO BAY
CALIFORNIA

Location: Pilot Liquefaction Study

Material Description	Water Level	Depth (m)	Graphic Log	Location	Number	Type	Recovery (cm/cm)	Blows/15 cm	$(N_1)_{60}$ Blows/30 cm	Soil Classification USCS	Soil Classification AASHTO	S_u (kPa)	Torvane (kPa)	Pocket Pentometer (kPa)	Dry Density (kN/m3)	Moisture Content %	Atterberg Limits: Liquid Limits LL	Atterberg Limits: Plastic Limits PL	Atterberg Limits: Plasticity Index PI	Passing #200 Sieve (%)	OTHER DATA AND REMARKS
Sand, SP, brown, very moist, medium dense, fine grained		1			S-1	SPT	46/46	5-8-10		SP											Top Has Shells, No Shells at Bottom
		2			S-2	SPT	46/46	6-9-10		SP										3	
		3			S-3	SPT	46/46	4-5-6		SP											
		4			S-4	SPT	46/46	5-4-2		SP										5	
		5			S-5	SPT	46/46	4-5-5		SP											
					S-6	SPT	46/46	4-3-3		SP										7	Encountered Bay Mud @ 19 Feet
Clay, grey, saturated, loose		6			S-7	SPT	46/46	0-1-1		CL											
Sand Lense																					
Clay, grey, saturated, loose																					
Sand, grey, loose, fine grained		7																			
		8			S-8	SPT	30/46	1-2-1		SP										13	Clay In Bit
Clay, grey, soft																					
		9			S-9	SPT	46/46	0-1-3		CL											Clay - First 16", Sand - Last 2"
Sand, black & grey, saturated, loose		10																			

LEGEND AND NOTES
- SPT = Standard Penetration Test, Split Spoon Sample
- US = Undisturbed Shelby Tube, Pushed
- Ring = Dames & Moore Sampler
- Bulk = Bulk Sample From Cuttings

GROUNDWATER DEPTHS:
- = Initial
- = End of Drilling

COMMENTS:

LOG_OF_BORING_METRIC_SANFRAN.GPJ LANE.GDT 9/14/00

Figure 2.4a Soil Boring Log for Pilot Liquefaction Study Area

Brigham Young University
&
University of California - San Diego
Telephone: (801) 378-6334
Fax: (801) 378-4449

Boring No: BH-1 | Sheet 2 of 2
Logged By: tw | Elevation (m): 3.4
Date Started: 9/17/1998 | Drill Contractor: Pitcher
Date Finished: 9/17/1998 | Drilling Method: Rotary Wash

TREASURE ISLAND
SAN FRANCISCO BAY
CALIFORNIA

Location: Pilot Liquefaction Study

Material Description	Water Level	Depth (m)	Graphic Log	Location	Number	Type	Recovery (cm/cm)	Blows/15 cm	$(N_1)_{60}$ Blows/30 cm	Soil Classification USCS	Soil Classification AASHTO	S_u (kPa)	Torvane (kPa)	Pocket Pentometer (kPa)	Dry Density (kN/m3)	Moisture Content %	Atterberg Limits: Liquid Limits LL	Atterberg Limits: Plastic Limits PL	Atterberg Limits: Plasticity Index PI	Passing #200 Sieve (%)	OTHER DATA AND REMARKS
		11			S-10	SPT	46/46	1-1-1		SP										17	
		12			S-11	SPT	46/46	1-1-2		SC										23	Hit More Firm Layer @ 37.5'
Clay, grey, moist/saturated, soft, w/sand grains in clay		13																			
		14			S-12	SPT	46/46	1-0-1		CL											More Clay In Sand
		15			S-13	SPT	46/46	1-2-1		CL											Less Sand
		16																			
		17			S-14	SPT	46/46	0-1-1		CL											
		18																			
		19			S-15	SPT	46/46	2-0-1		CL											
Bottom of Bore Hole		20																			

LEGEND AND NOTES
- SPT = Standard Penetration Test, Split Spoon Sample
- US = Undisturbed Shelby Tube, Pushed
- Ring = Dames & Moore Sampler
- Bulk = Bulk Sample From Cuttings

GROUNDWATER DEPTHS:
- = Initial
- = End of Drilling

COMMENTS:

LOG_OF_BORING_METRIC SANFRAN.GPJ LANE.GDT 9/14/00

Figure 2.4b Soil Boring Log for Pilot Liquefaction Study Area

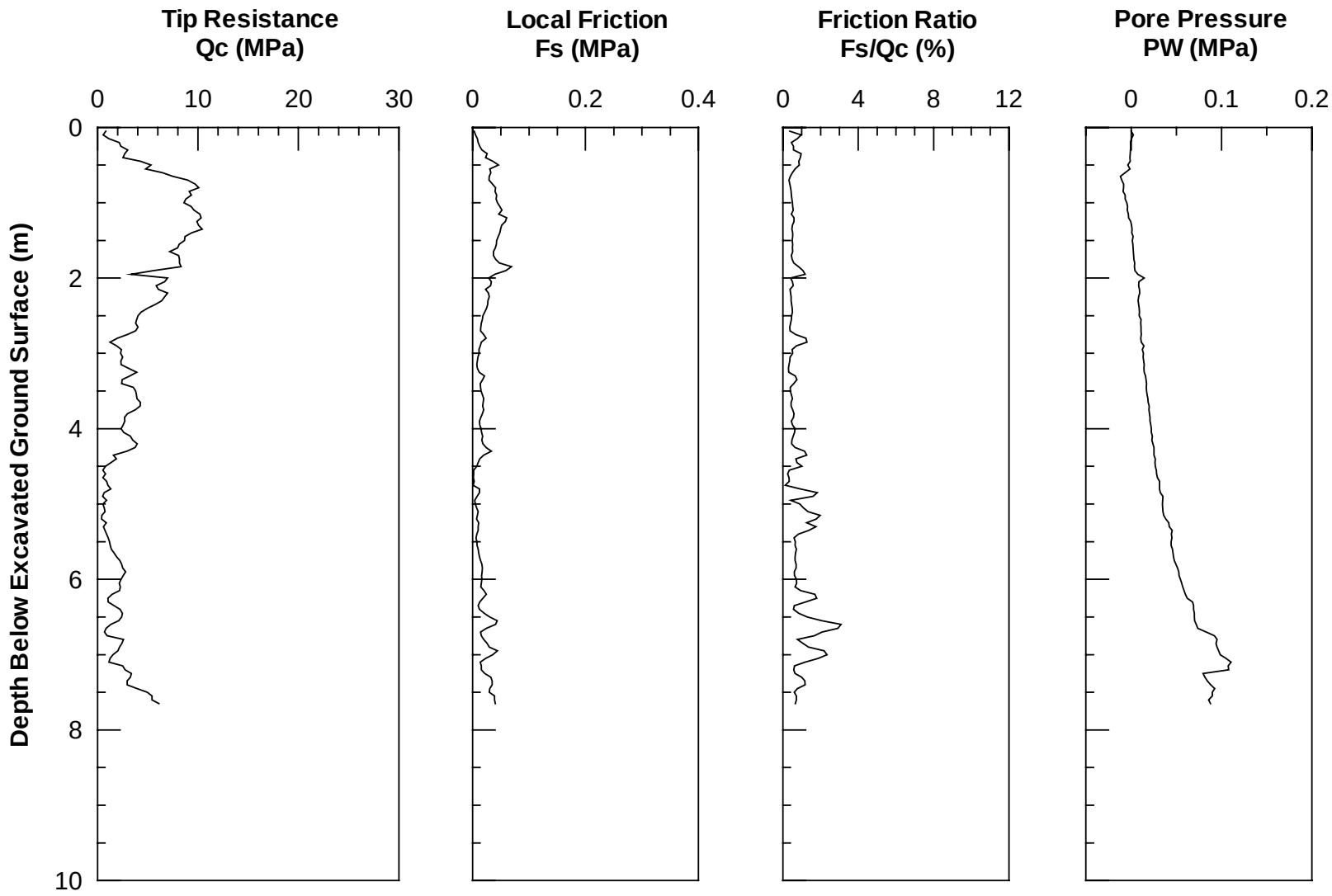

Figure 2.5 CPT-1 Logs for the Pilot Liquefaction Study Area (10-19-98)

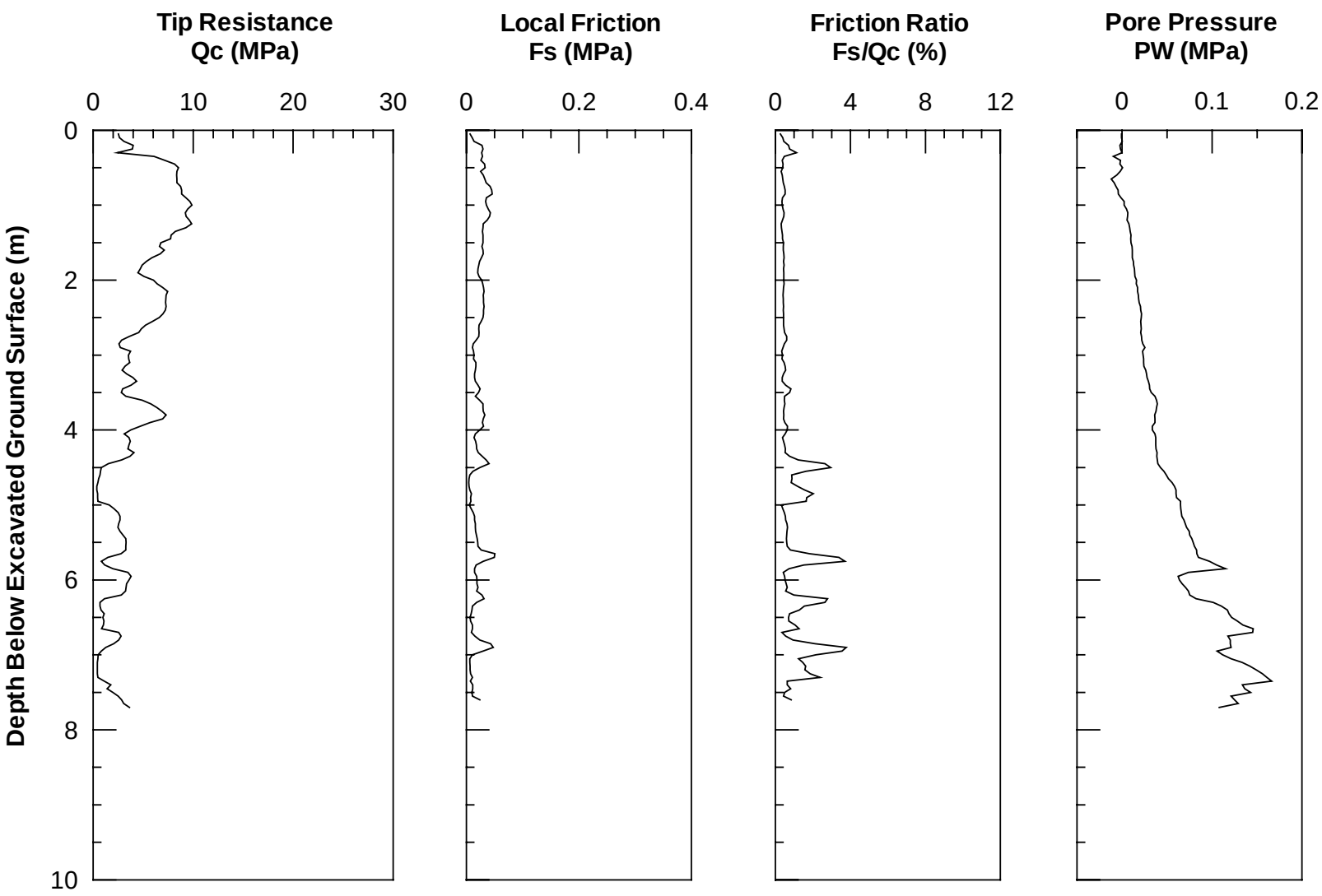

Figure 2.6 CPT-2 Logs for Pilot Liquefaction Study Area (10-19-98)

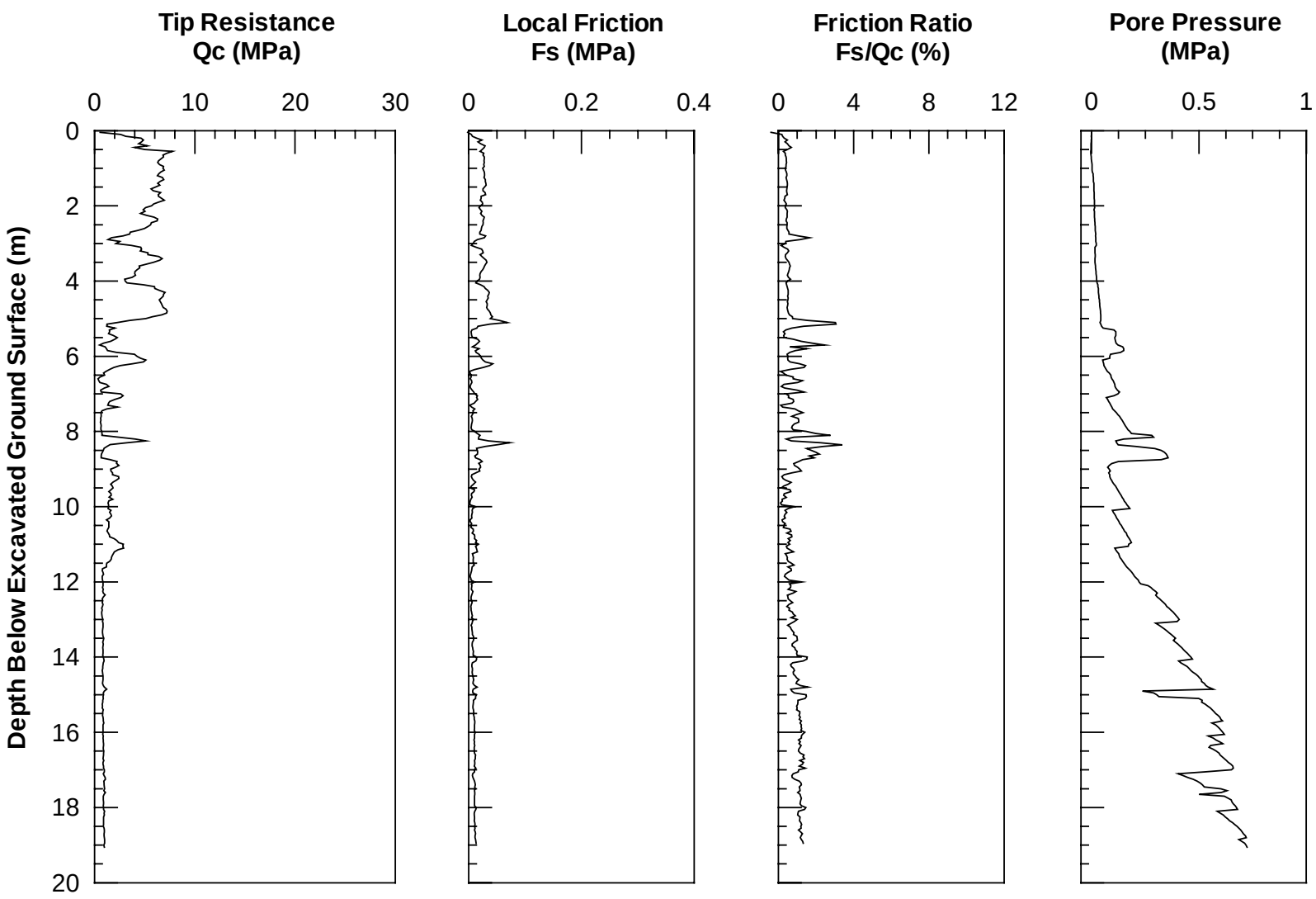

Figure 2.7 CPT-3 Logs for Pilot Liquefaction Study Area (10-19-98)

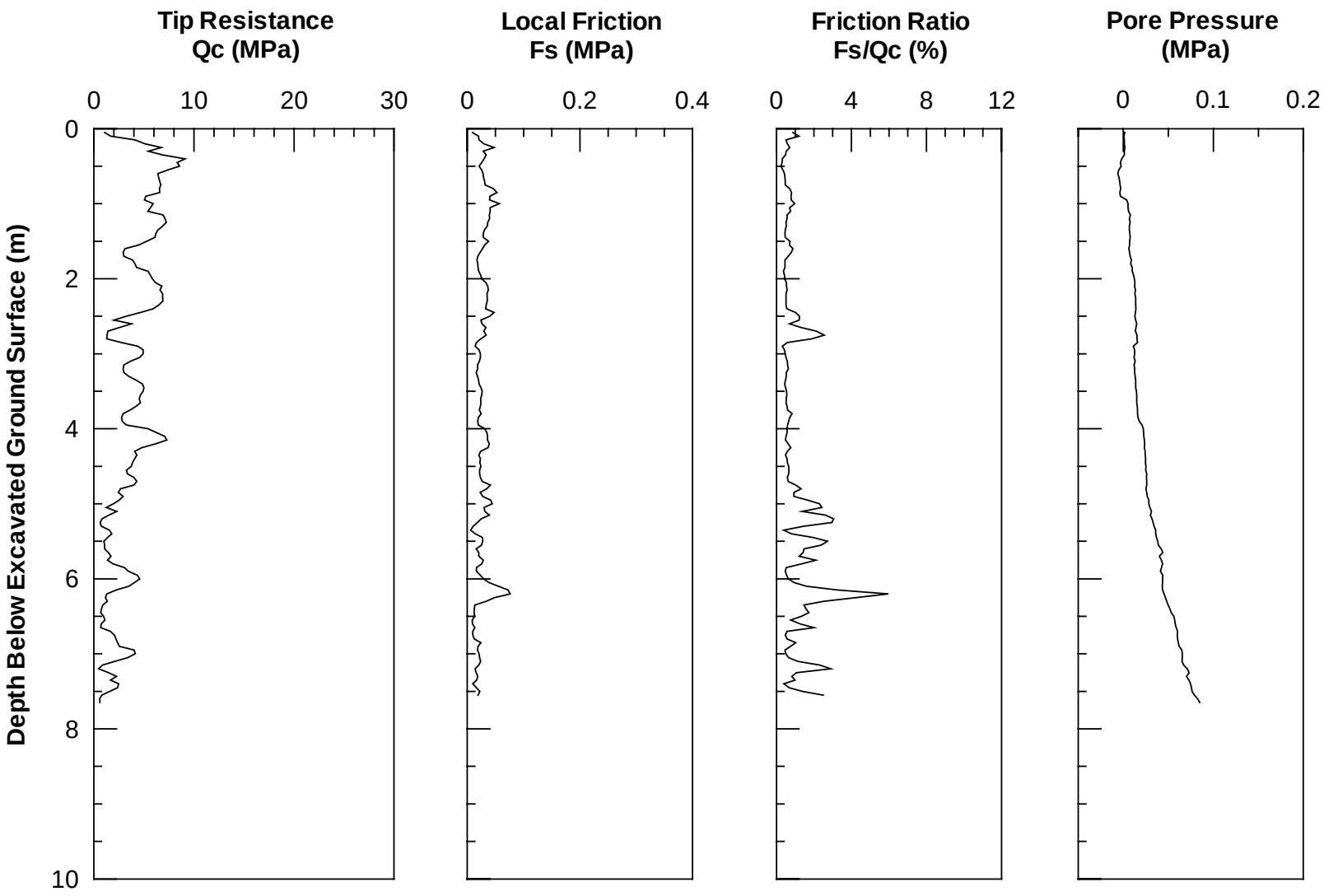

Figure 2.8 CPT-4 Logs for Pilot Liquefaction Study Area (10-19-98)

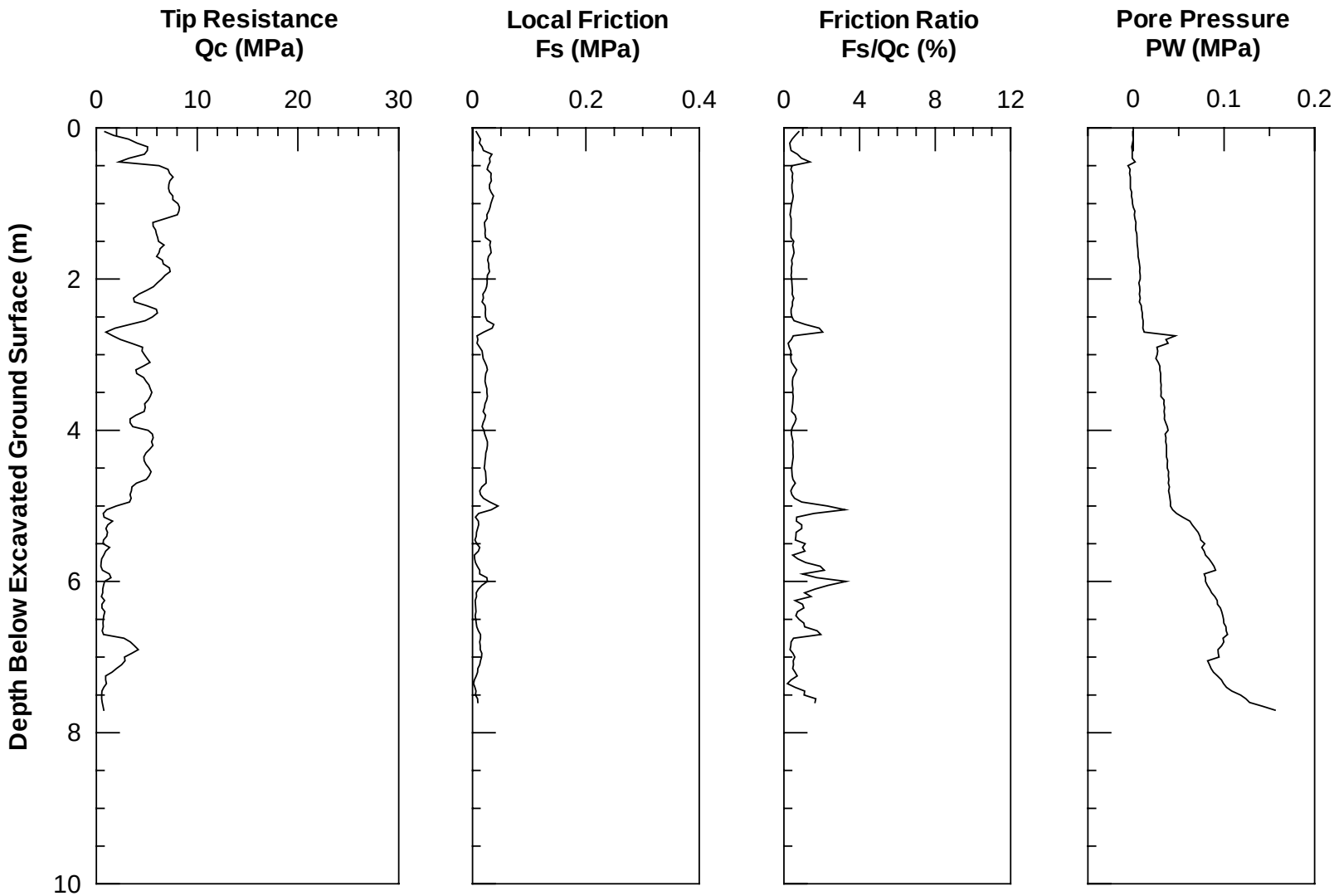

Figure 2.9 CPT-5 Logs for Pilot Liquefaction Study Area (10-19-98)

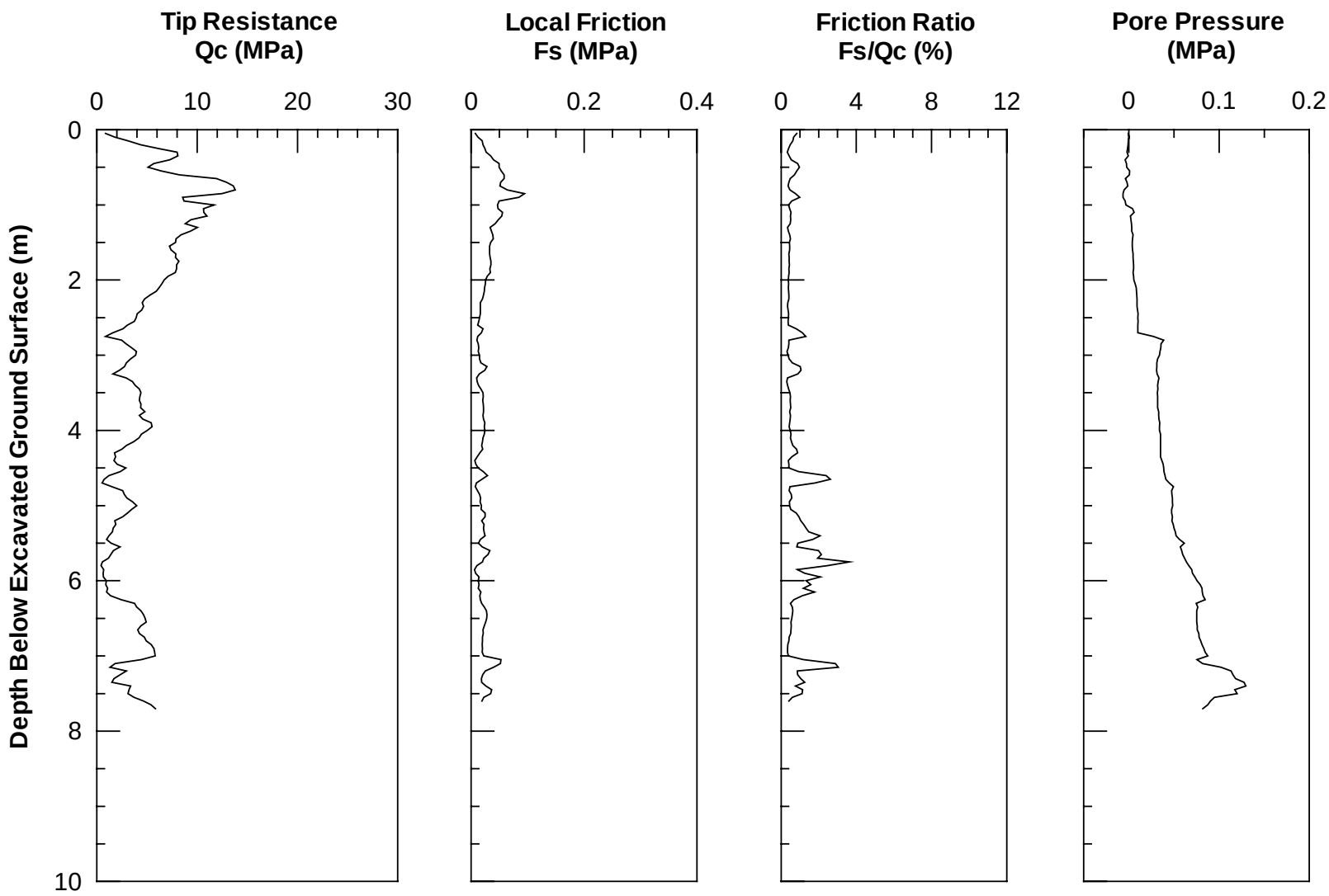

Figure 2.10 CPT-6 Logs for Pilot Liquefaction Study Area (10-19-98)

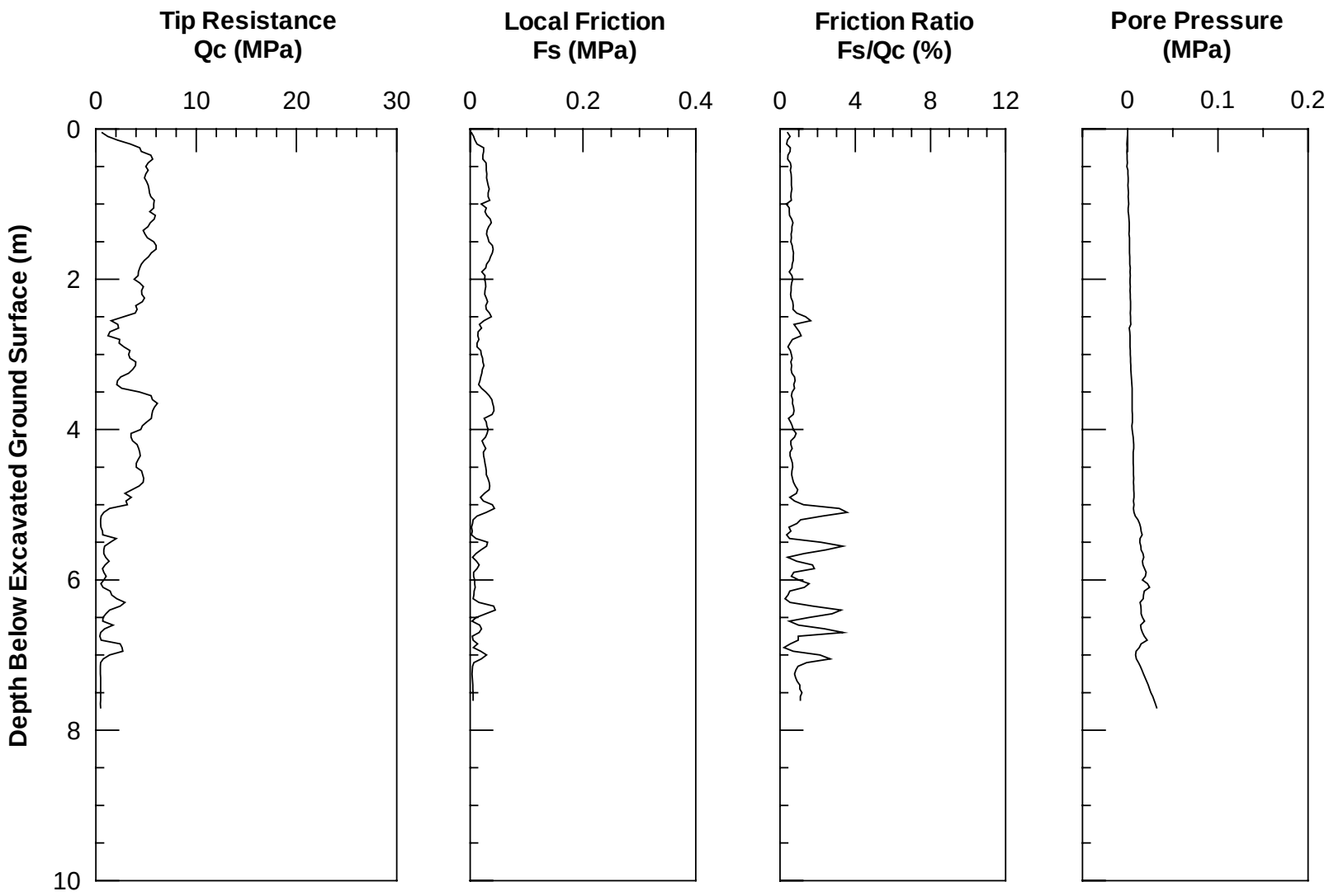

Figure 2.11 CPT-7 Logs for Pilot Liquefaction Study Area (10-28-98)

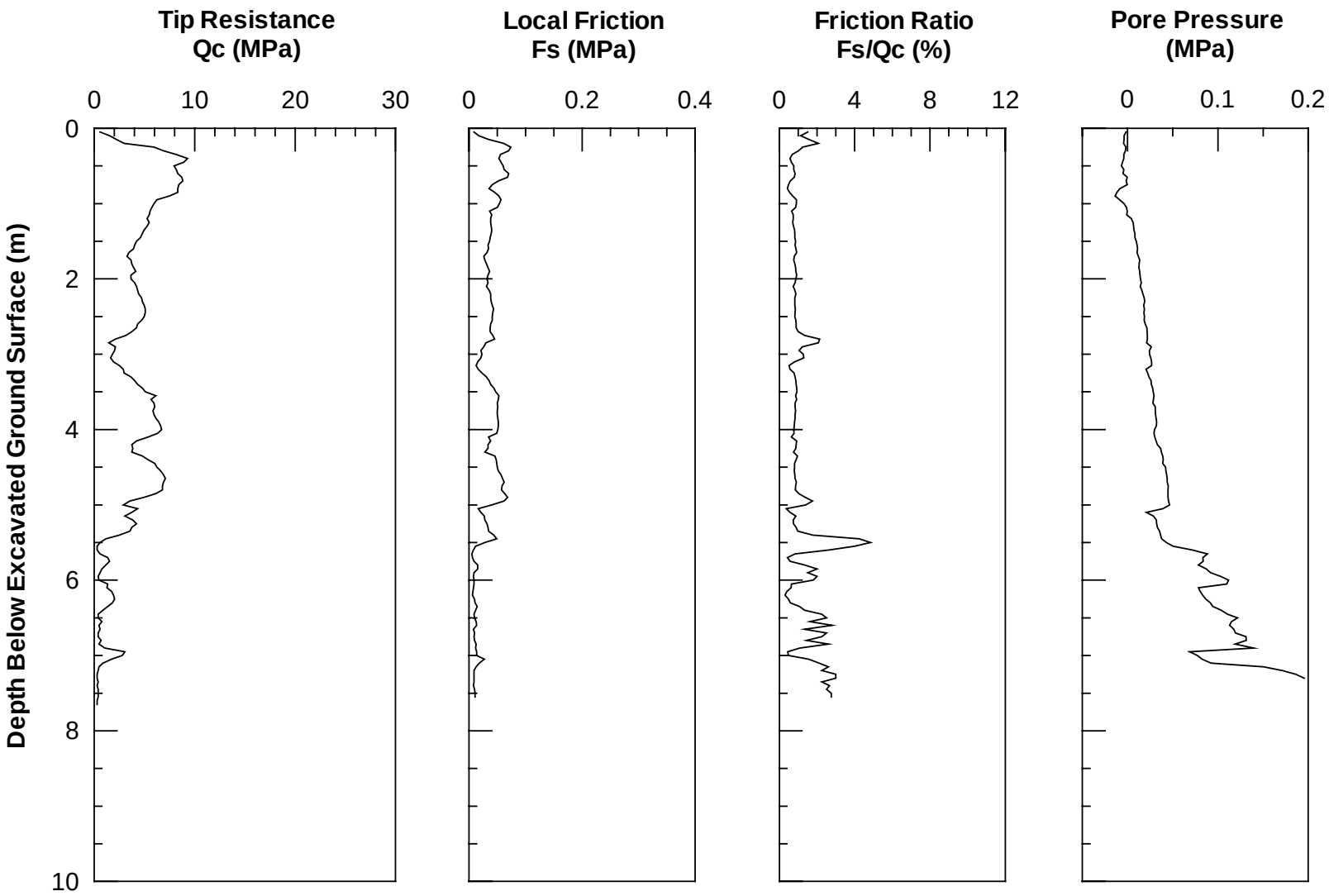

Figure 2.12 CPT-8 Logs for Pilot Liquefaction Study Area (10-28-98)

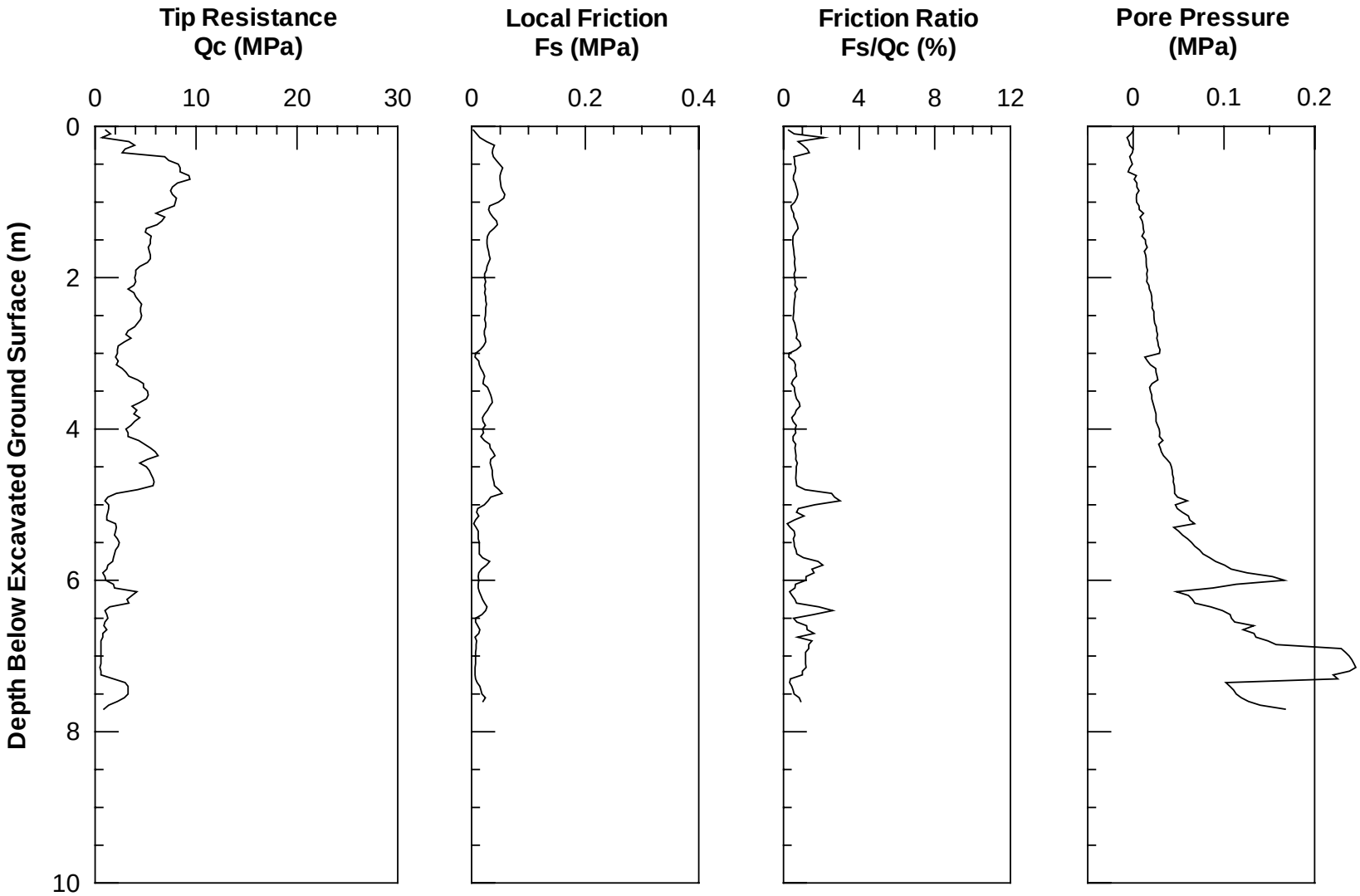

Figure 2.13 CPT-9 Logs for Pilot Liquefaction Study Area (10-28-98)

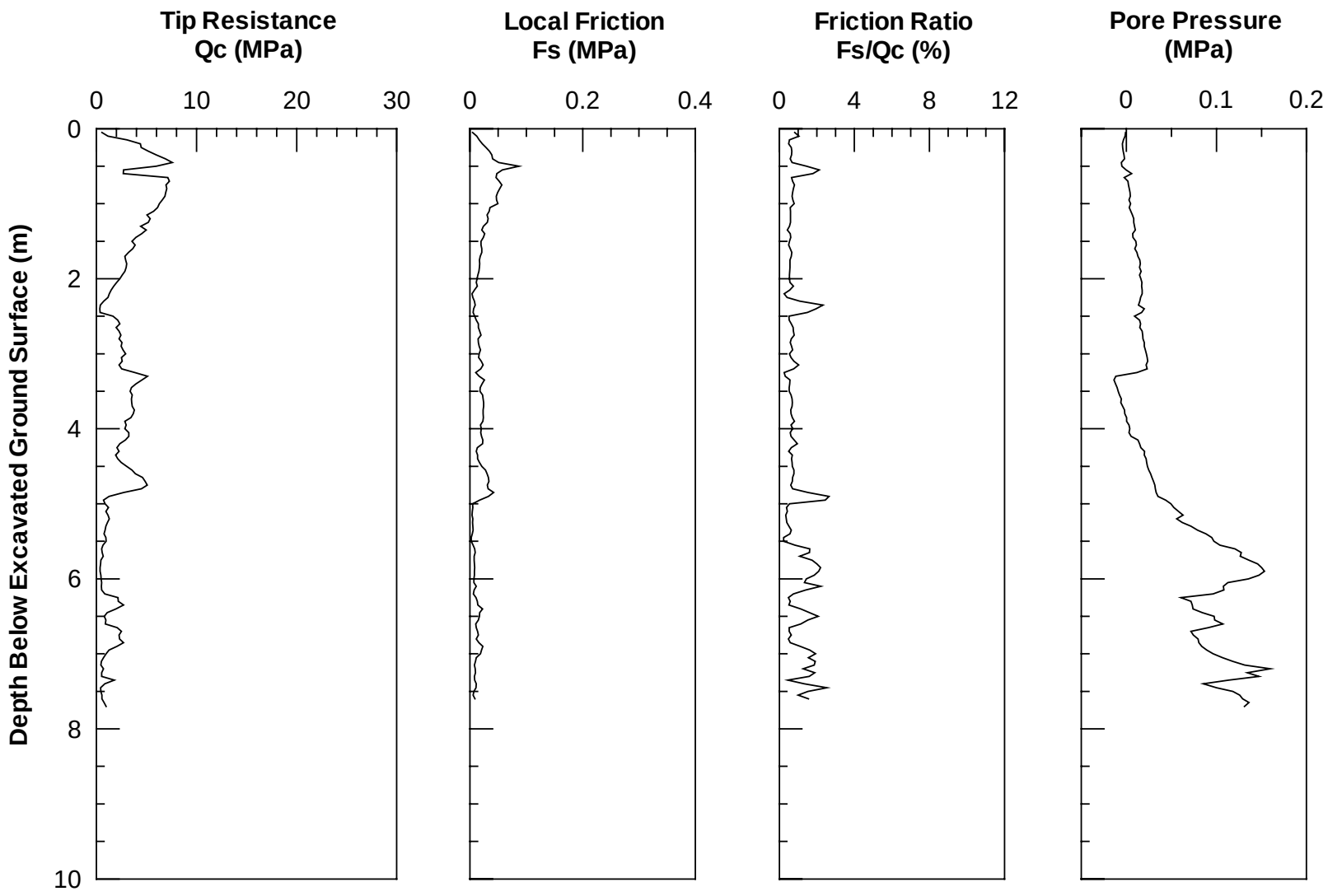

Figure 2.14 CPT-10 Logs for Pilot Liquefaction Study Area (10-28-98)

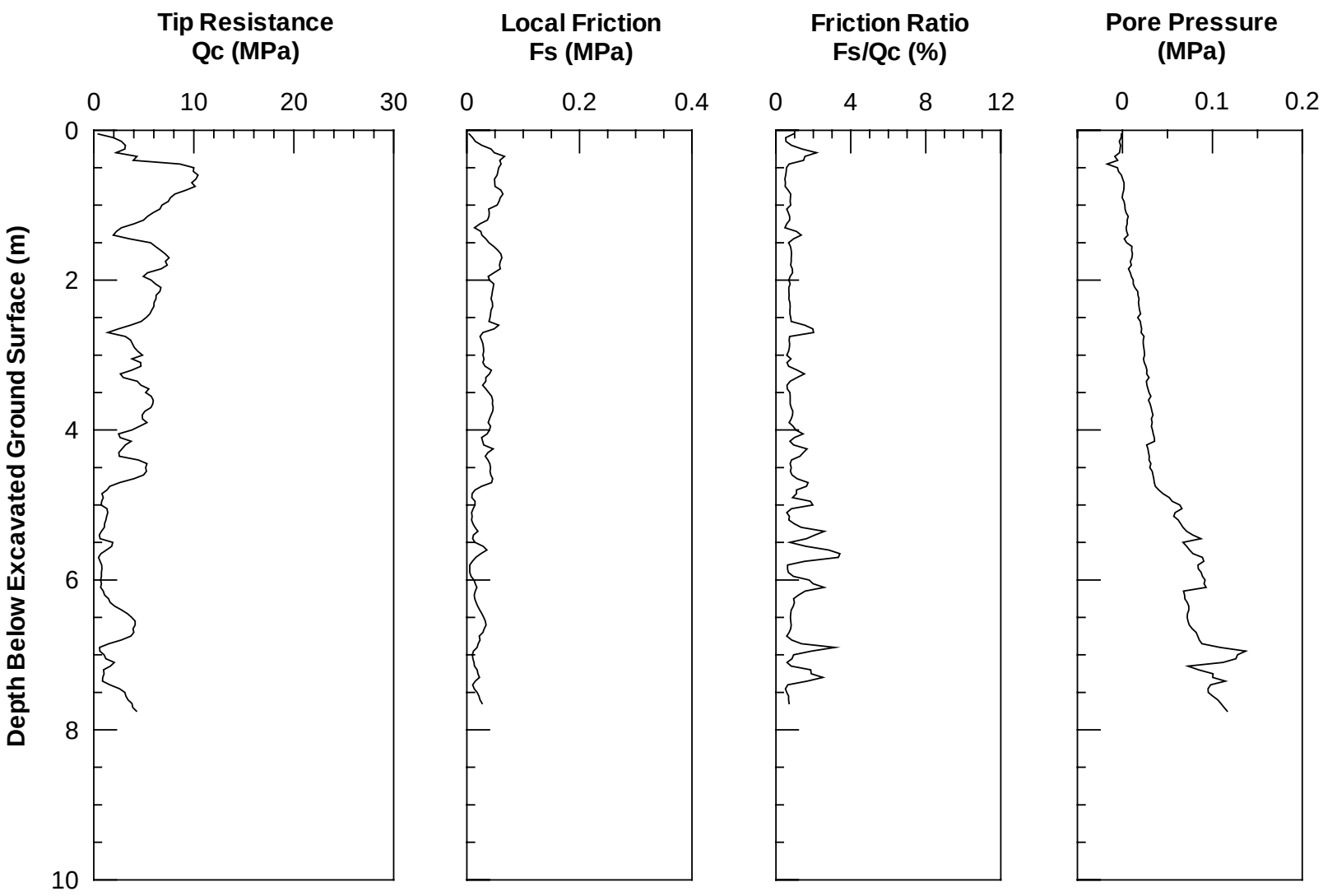

Figure 2.15 CPT-11 Logs for Pilot Liquefaction Study Area (10-28-98)

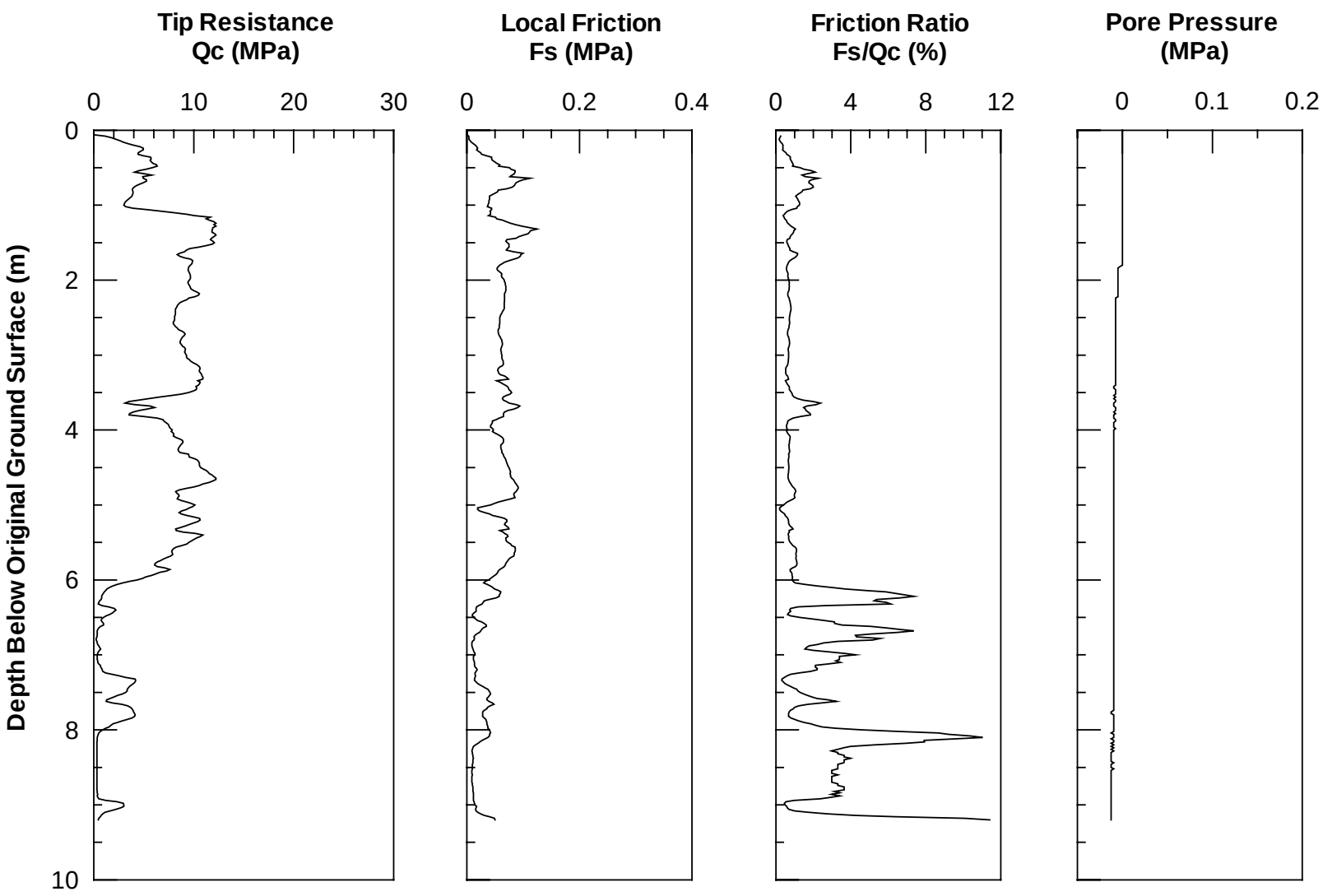

Figure 2.16 CPT P-1 Logs for Pilot Liquefaction Study Area (2-17-99)

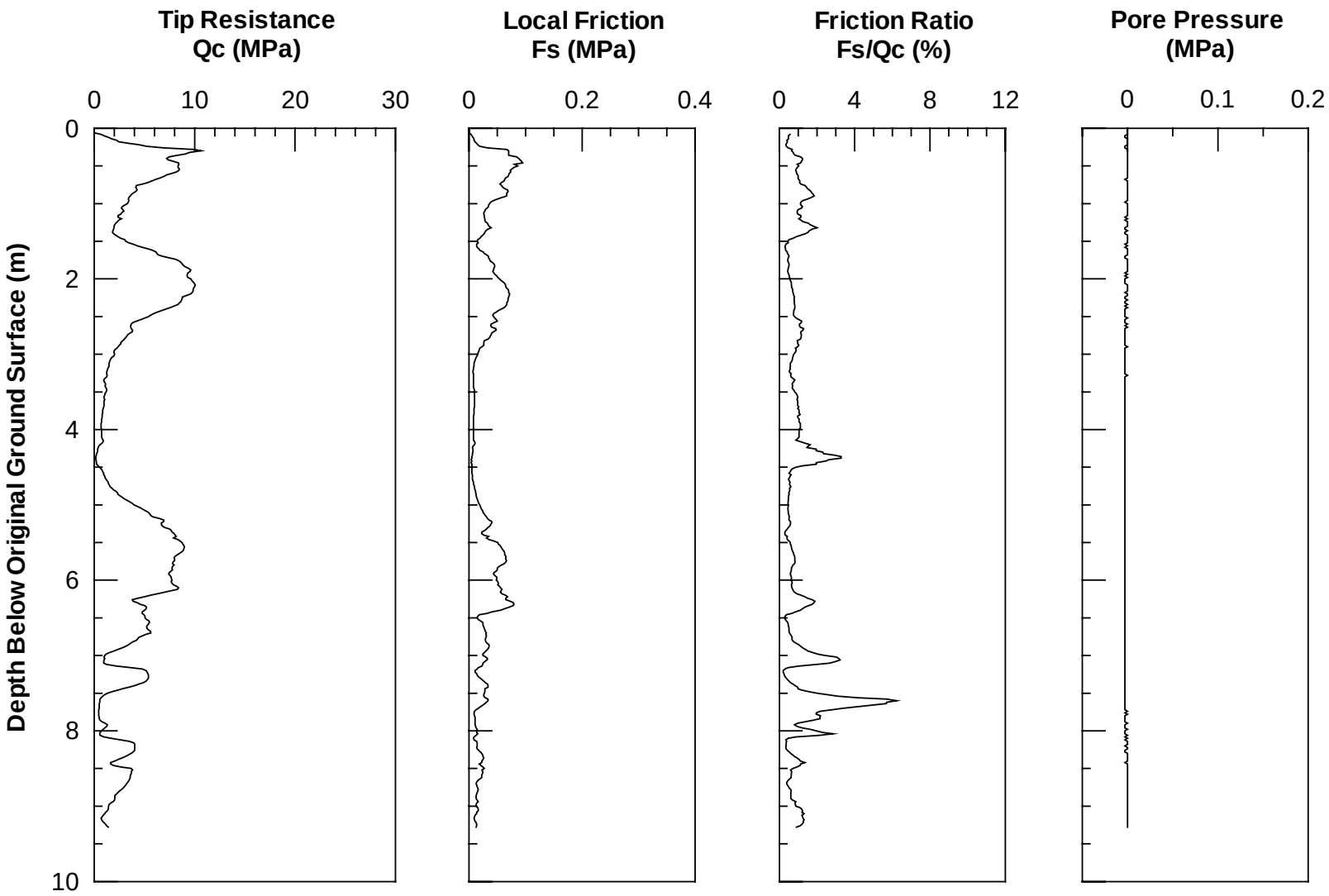

Figure 2.17 CPT P-2 Logs for Pilot Liquefaction Study Area (2-17-99)

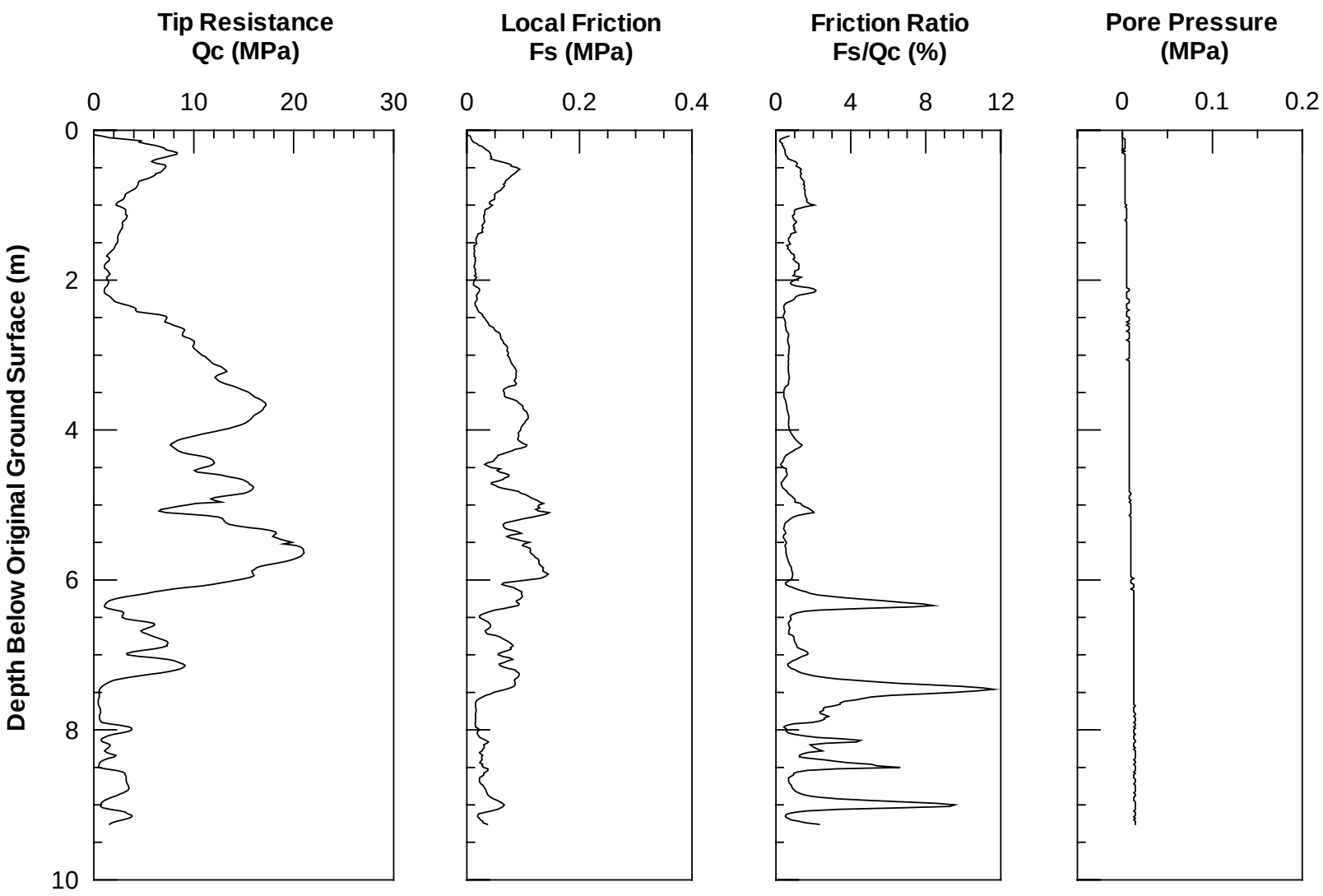

Figure 2.18 CPT P-3 Logs for Pilot Liquefaction Study Area (2-17-99)

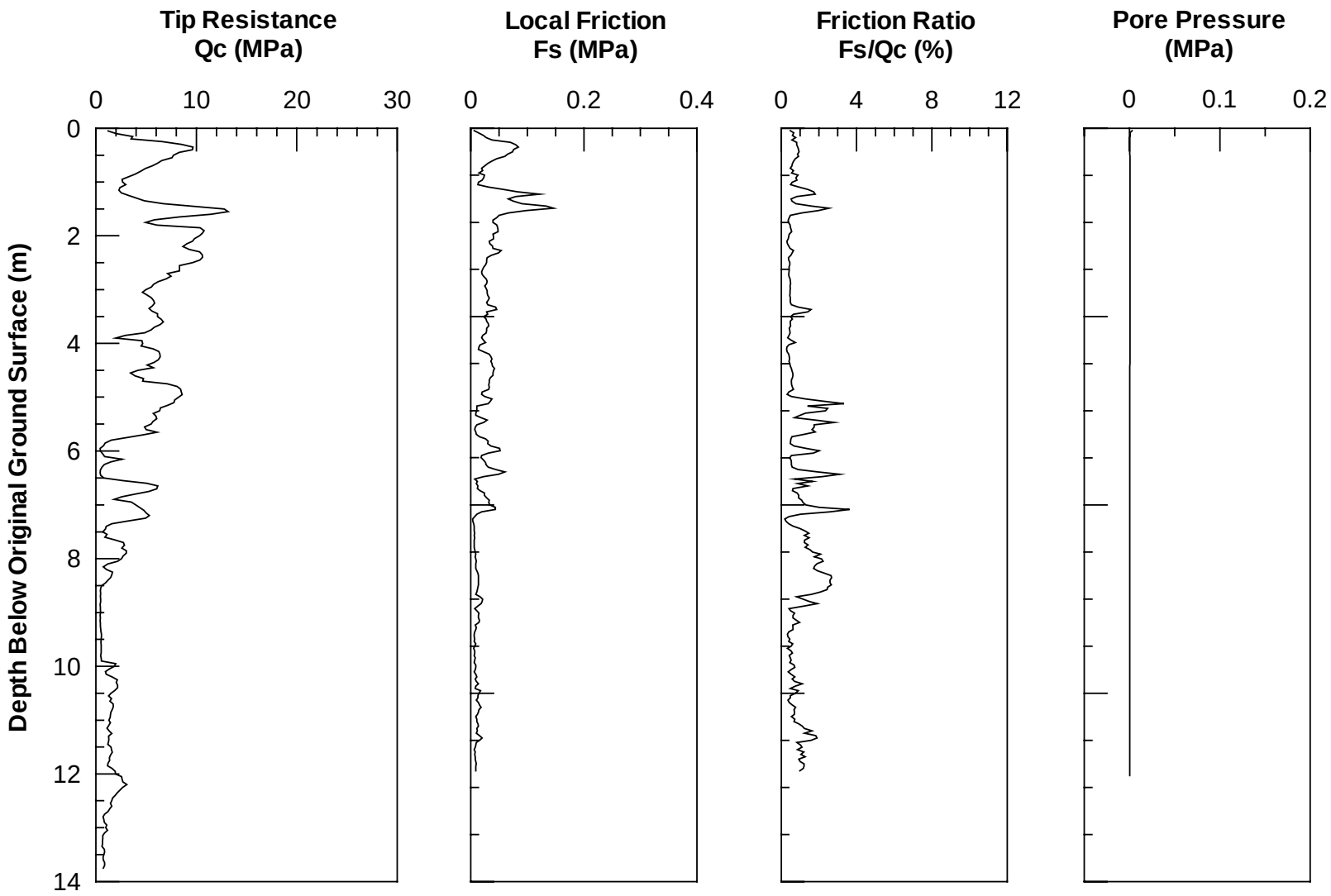

Figure 2.19 CPT UM21 Logs for Pilot Liquefaction Study Area (2-26-99)

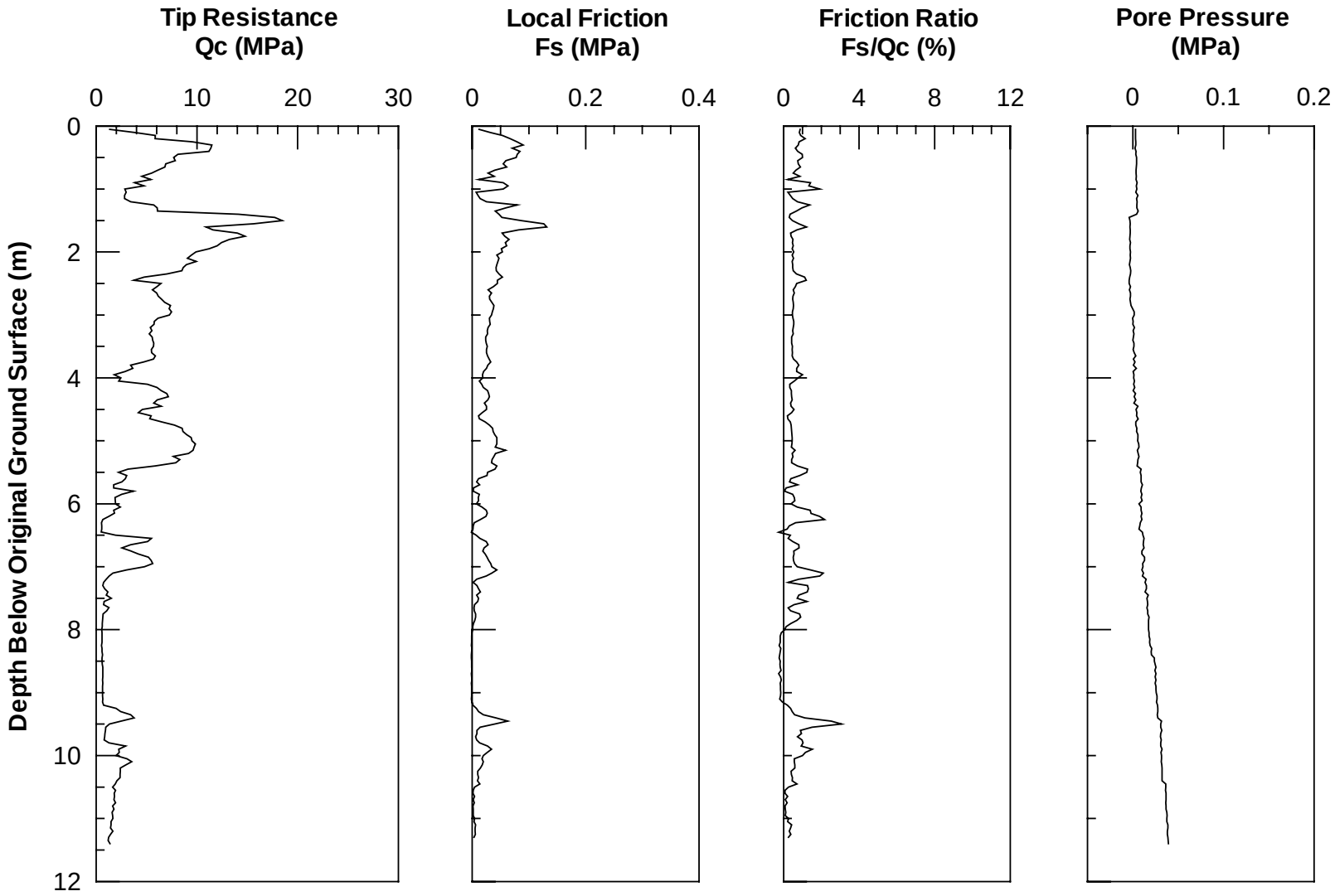

Figure 2.20 CPT UM25 Logs for Pilot Liquefaction Study Area (2-26-99)

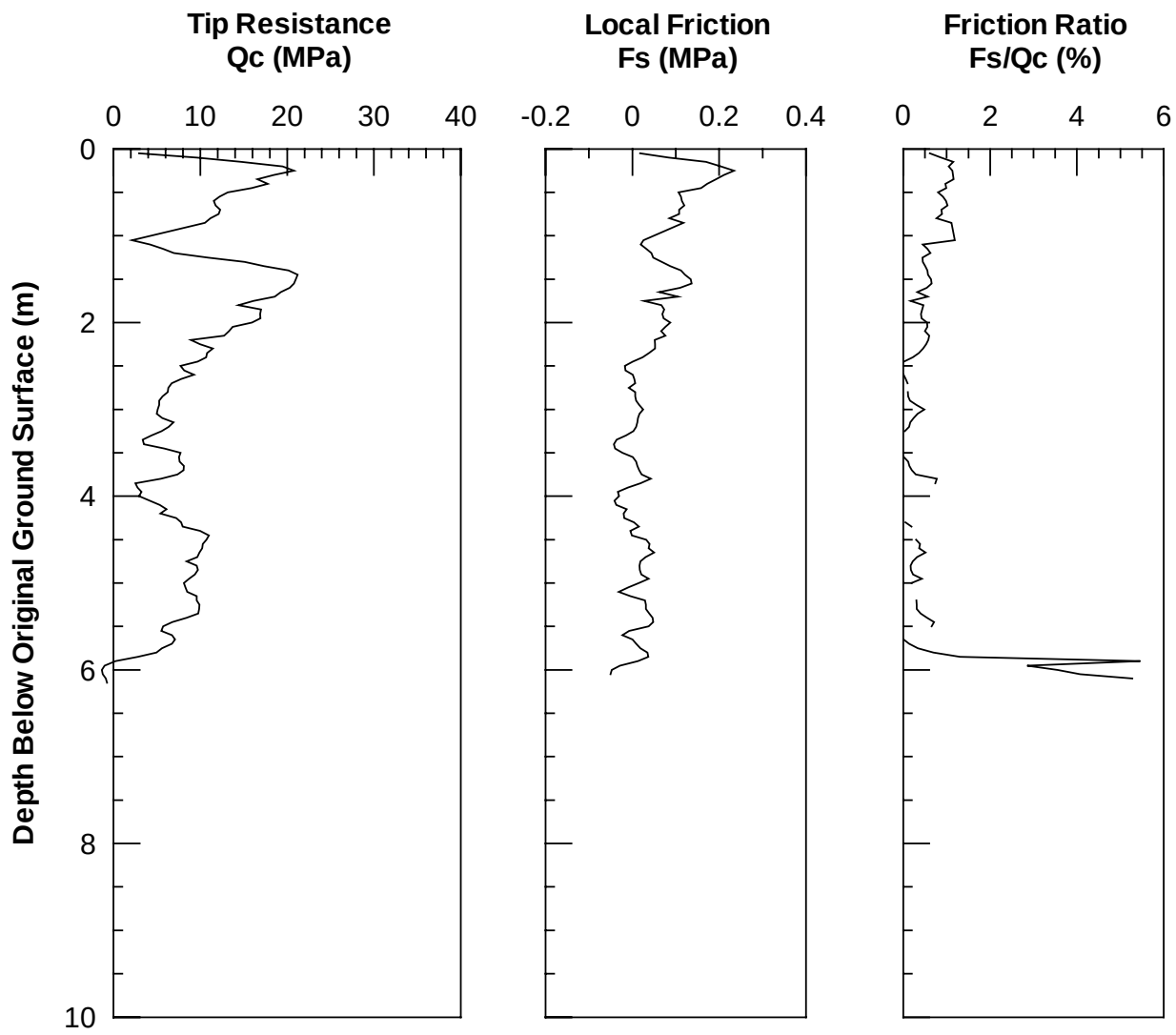

Figure 2.21 CPT SFC002 Logs for Pilot Liquefaction Study Area (6-24-99)

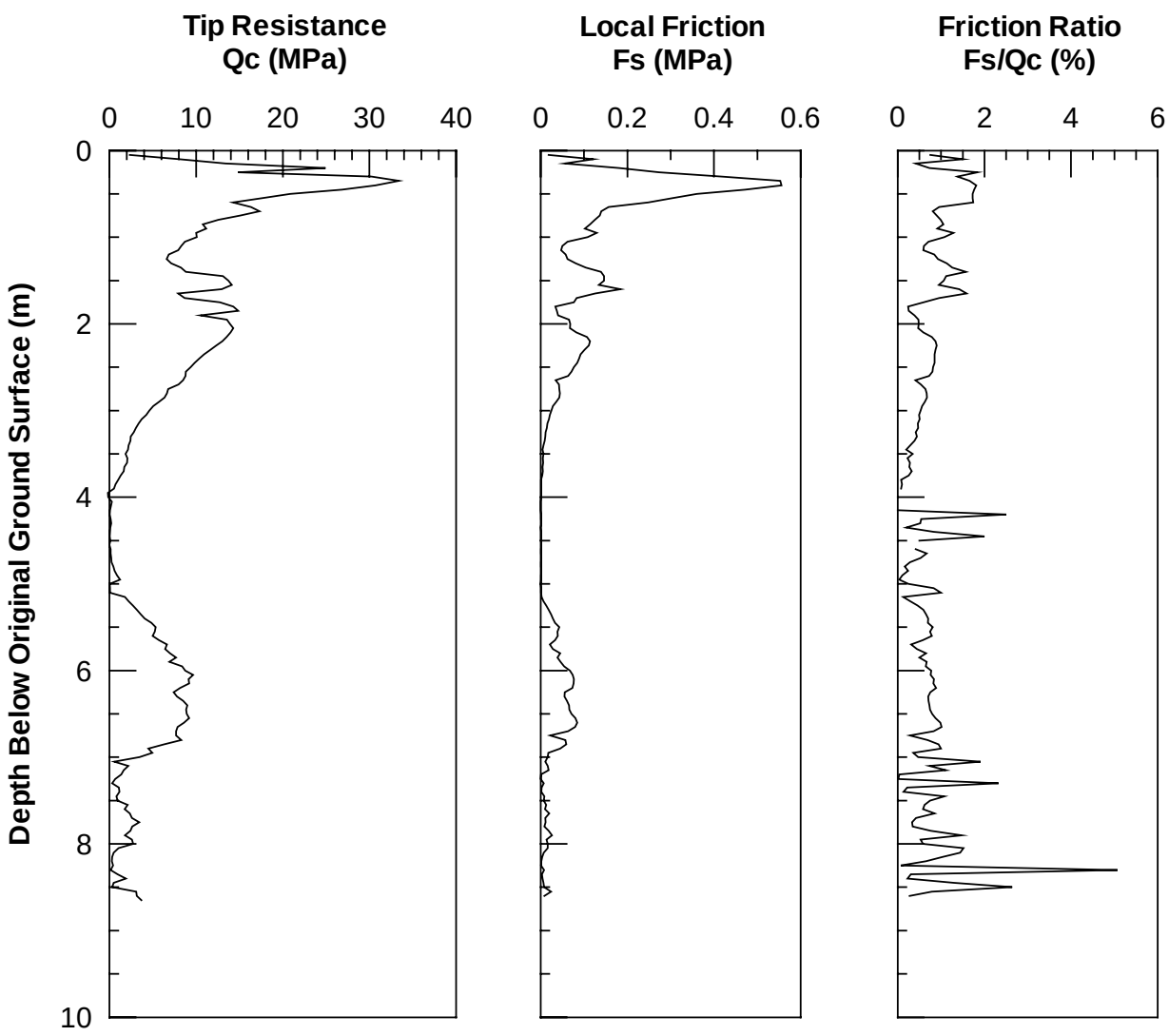

Figure 2.22 CPT SFC004 Logs for Pilot Liquefaction Study Area (6-24-99)

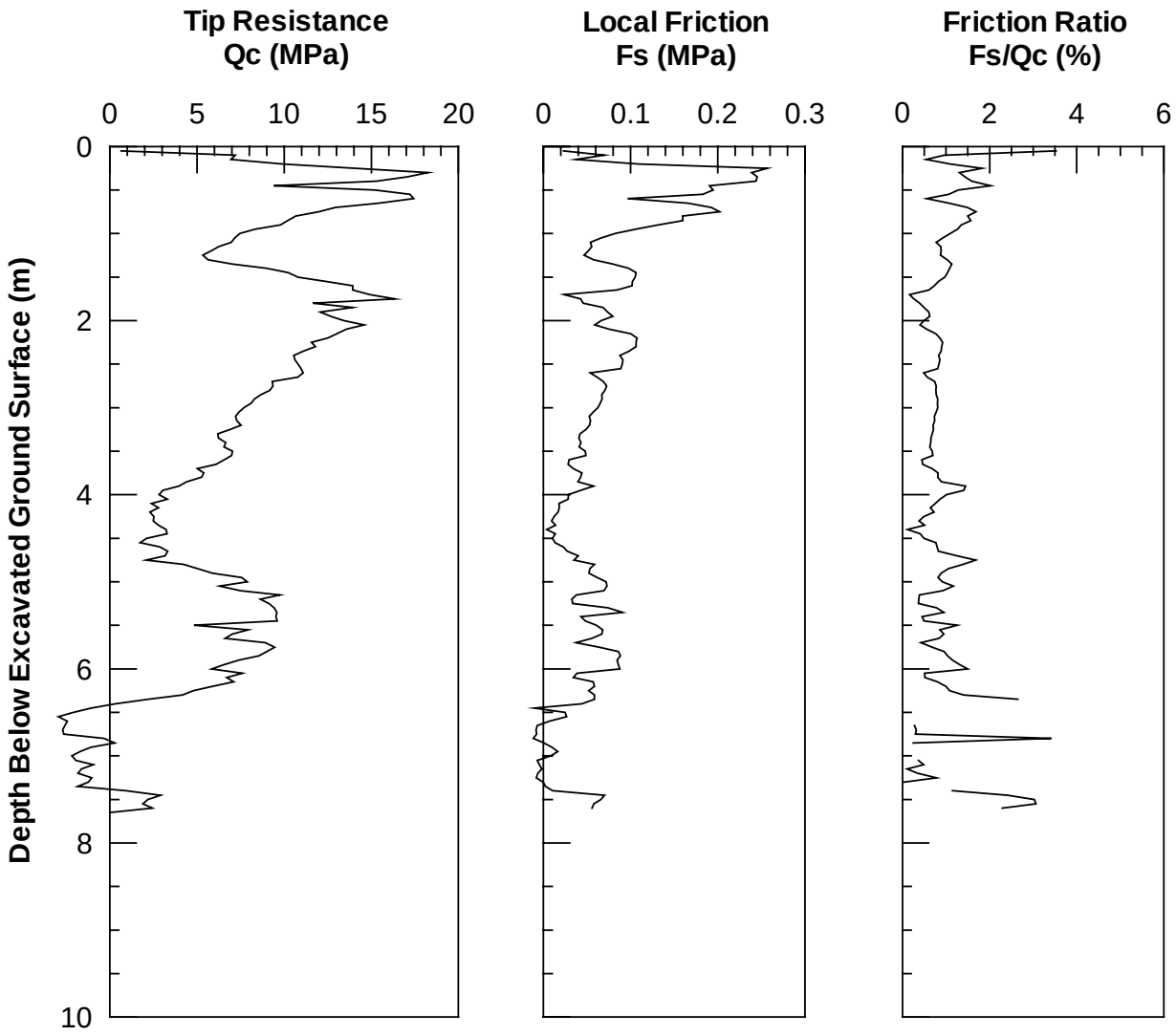

Figure 2.23 CPT SFC008 Logs for Single Pile Test Area 5 Months After 2nd Blast (6-24-99)

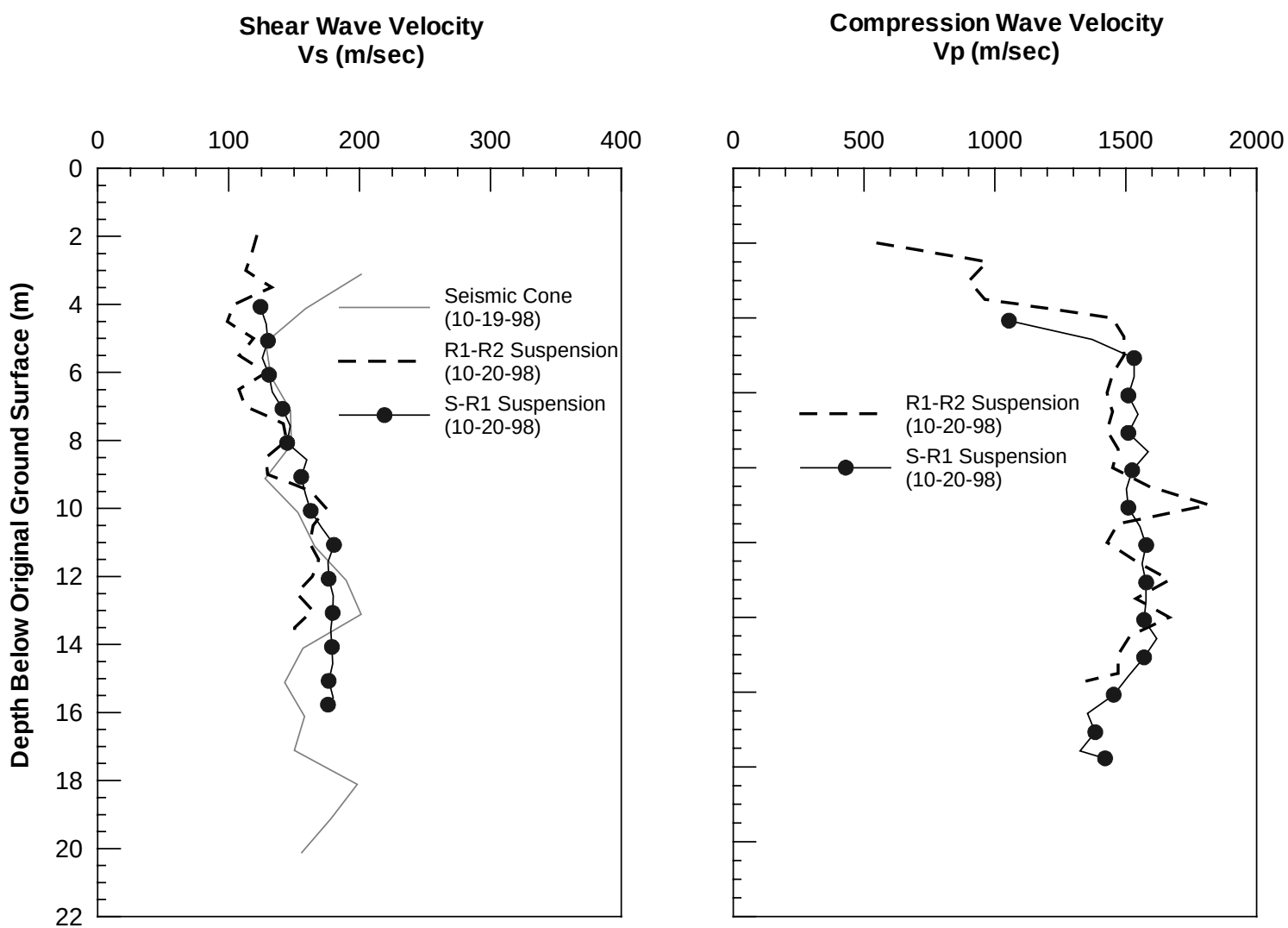

Figure 2.24 Pre-Blast Velocity Profile at Pilot Liquefaction Site a) Shear Wave b) Compression Wave

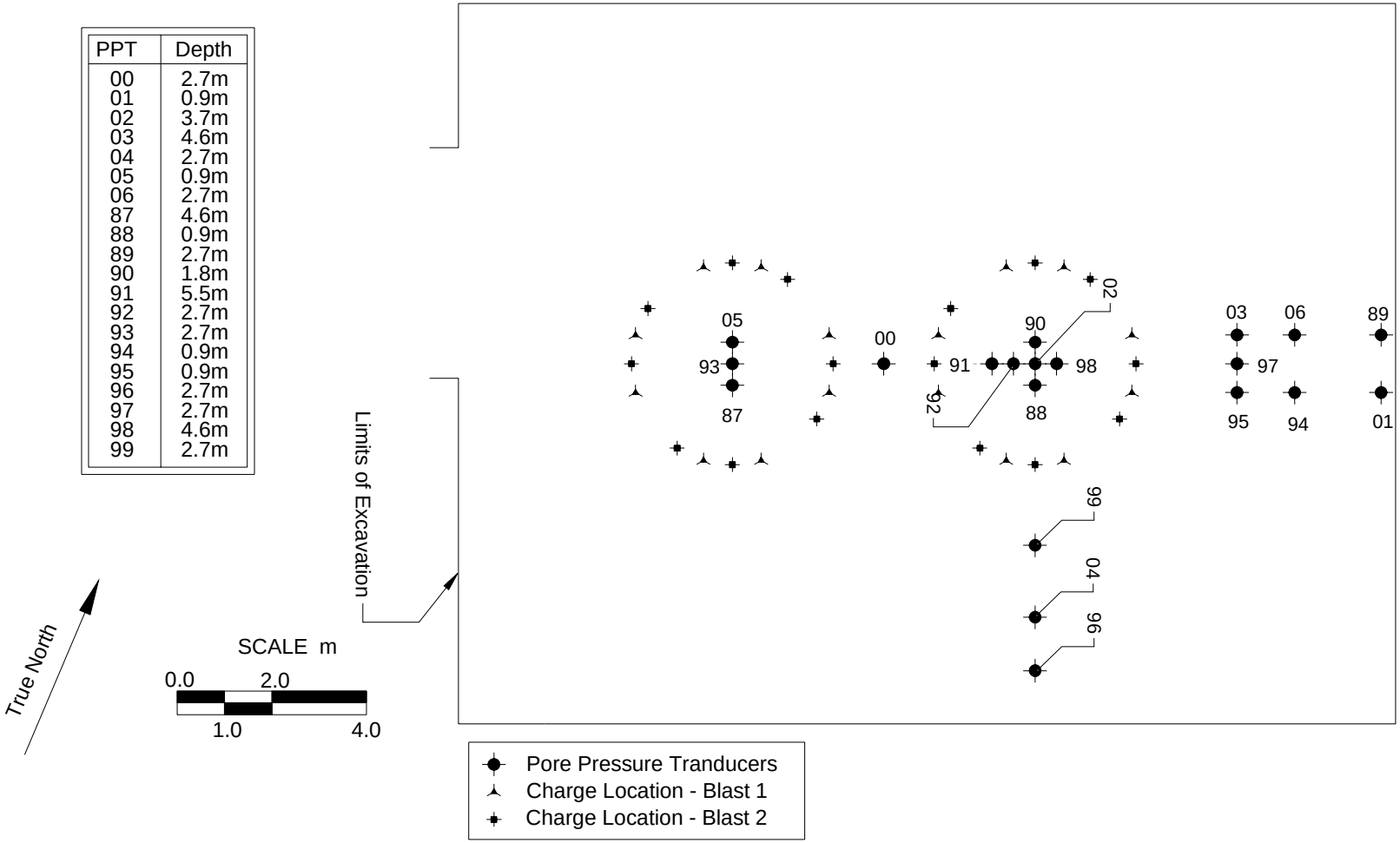

Figure 2.25 Location of Pore Pressure Transducers and Explosives for Pilot Liquefaction Test

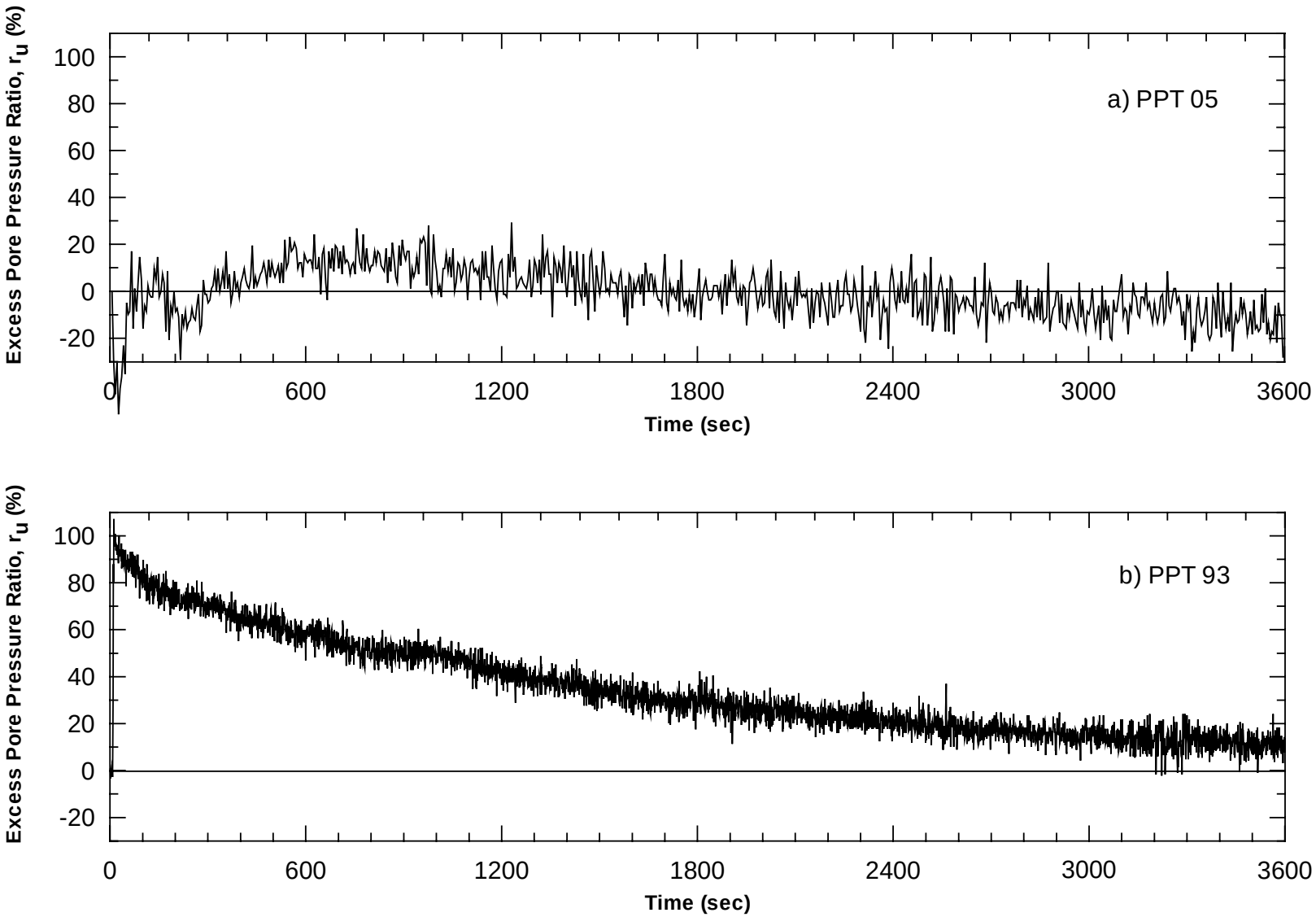

Figure 2.26 Excess Pore Pressure Ratio for Pilot Liquefacti on Test 1st Blast a) PPT 05 and b) PPT 93

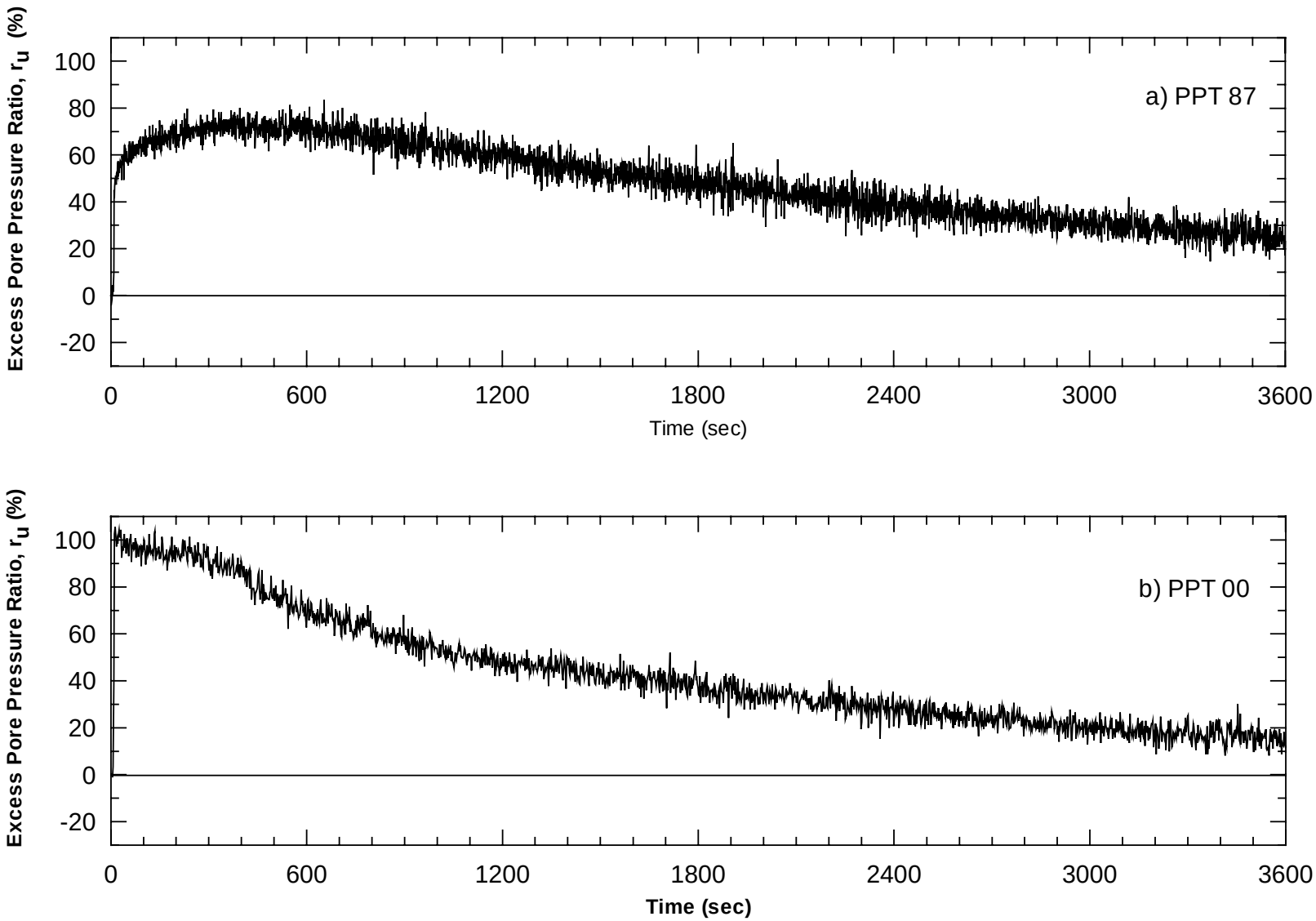

Figure 2.27 Excess Pore Pressure Ratio for Pilot Liquefaction Test 1st Blast a) PPT 87 and b) PPT 00

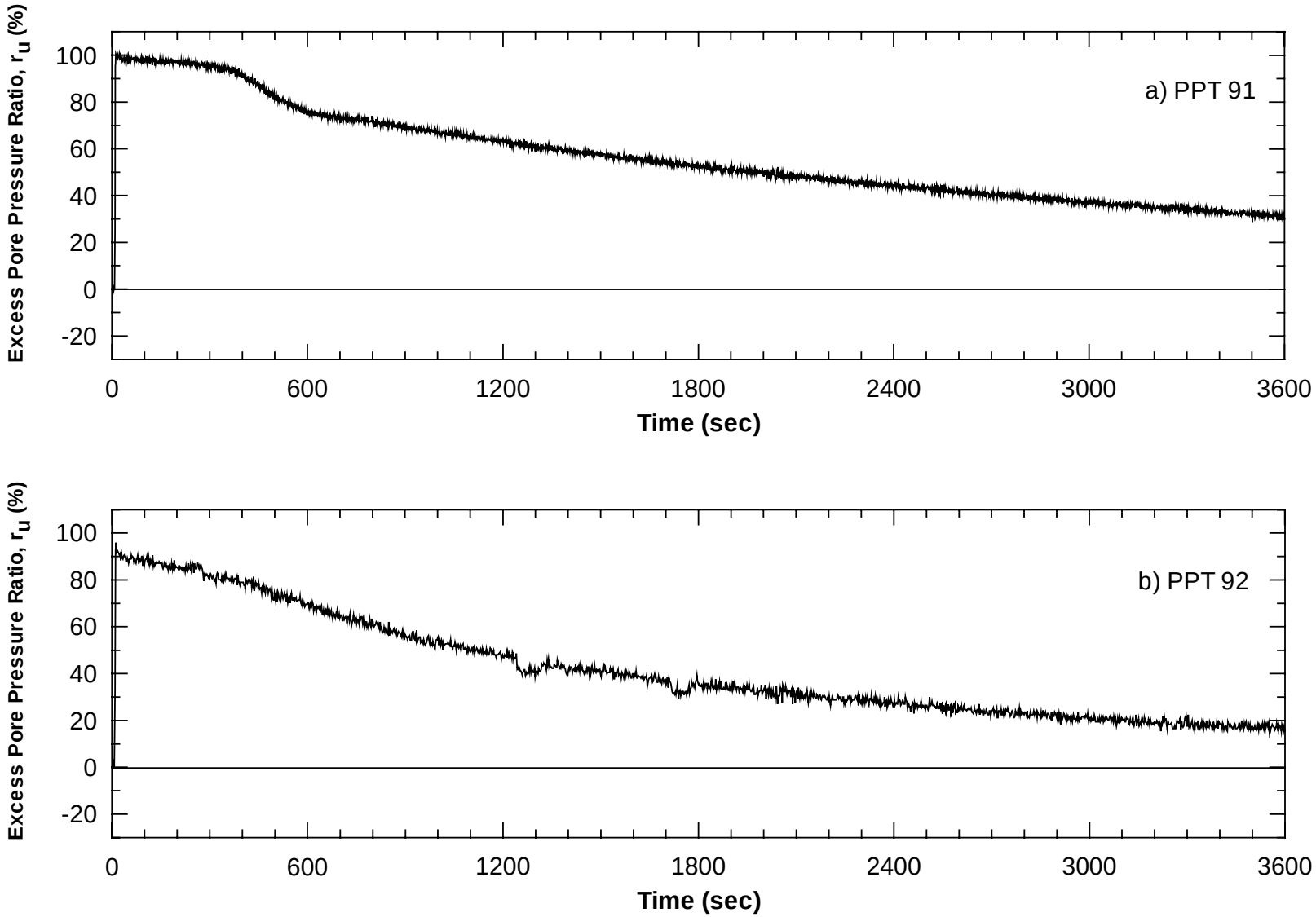

Figure 2.28 Excess Pore Pressure Ratio for Pilot Liquefaction Test 1st Blast a) PPT 91 and b) PPT 9 2

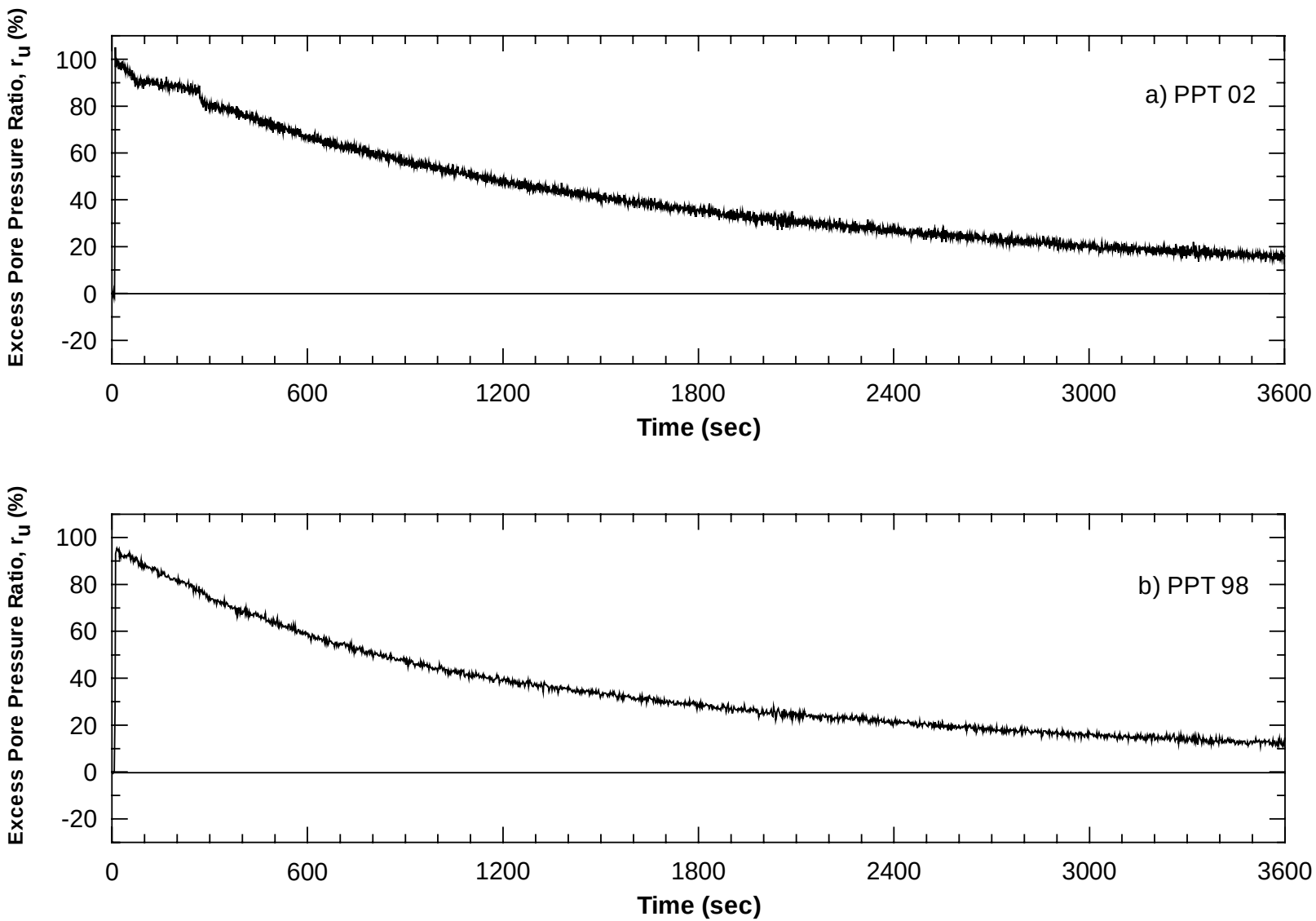

Figure 2.29 Excess Pore Pressure Ratio for Pilot Liquefaction Test 1st Blast a) PPT 02 and b) PPT 98

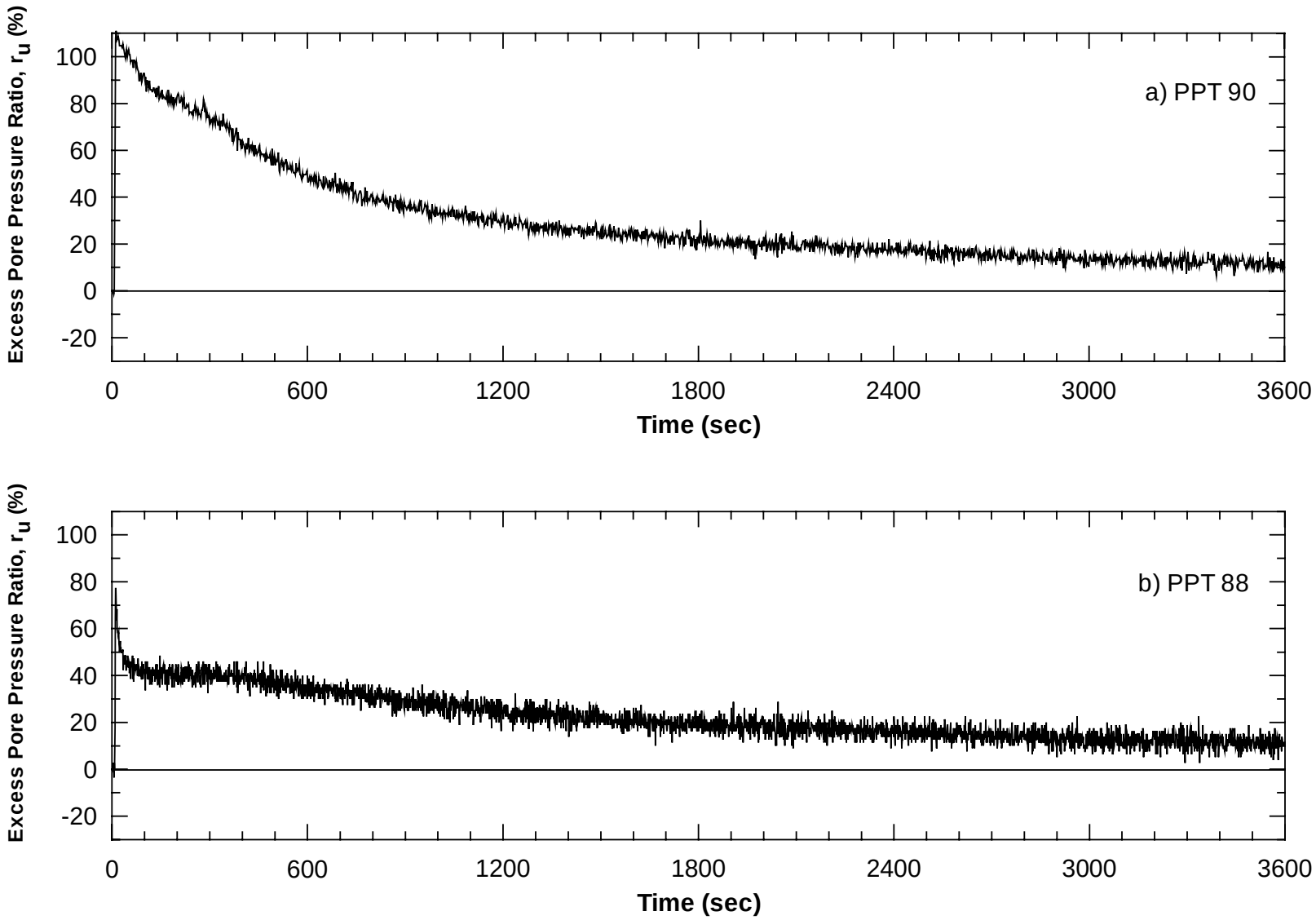

Figure 2.30 Excess Pore Pressure Ratio for Pilot Liquefaction Test 1st Blast a) PPT 90 and b) PPT 88

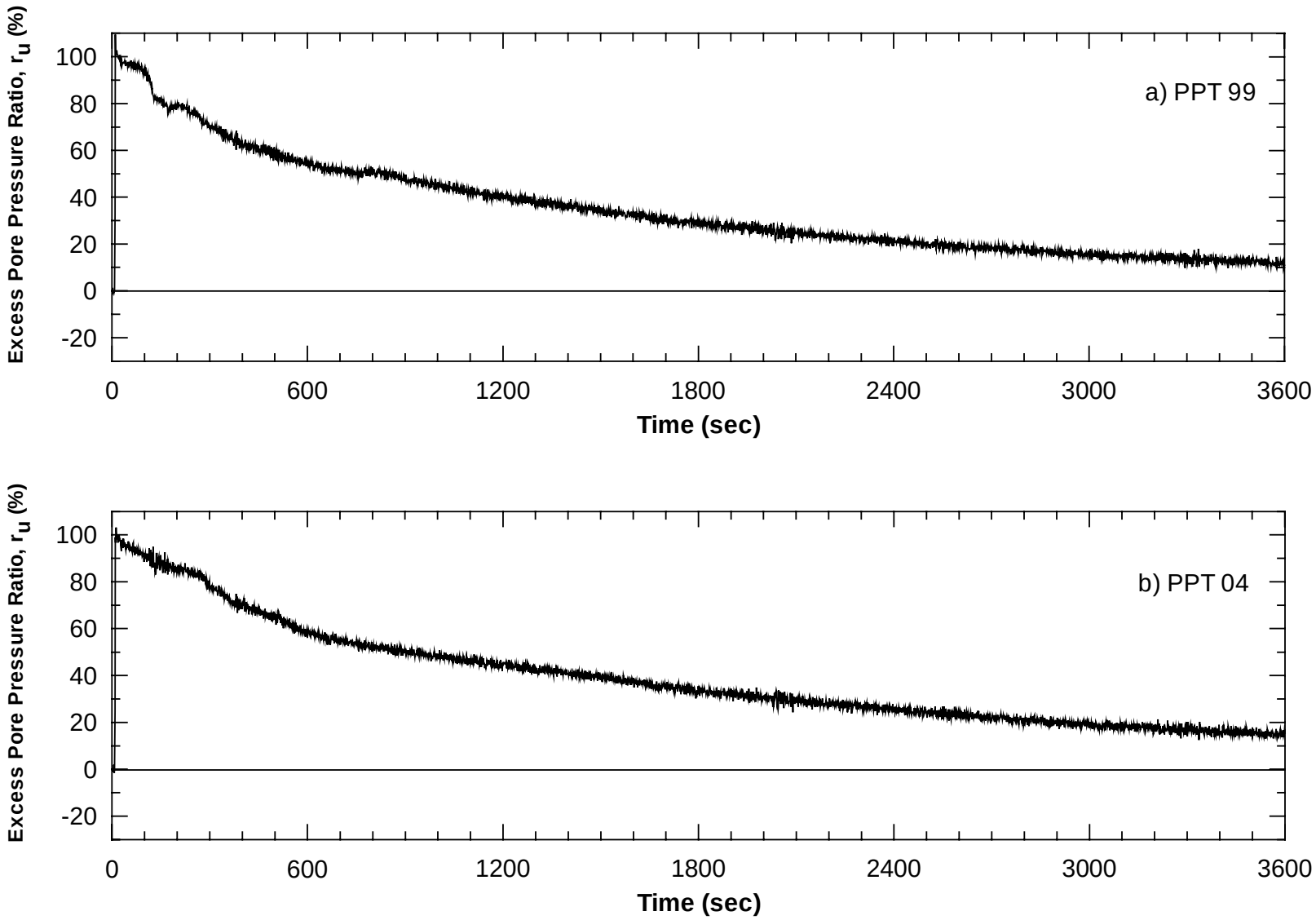

Figure 2.31 Excess Pore Pressure Ratio for Pilot Liquefaction Test 1st Blast a) PPT 99 and b) PPT 04

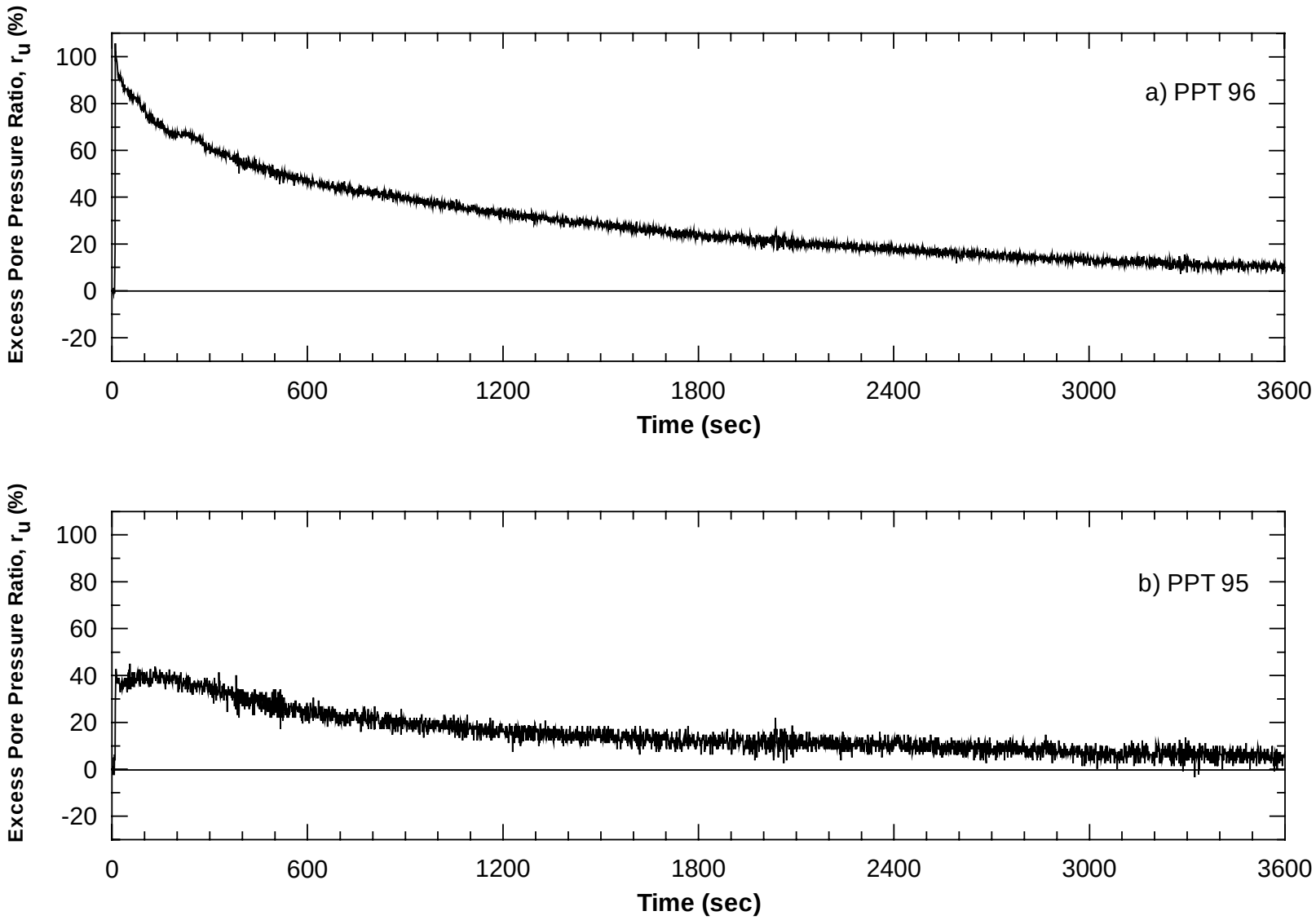

Figure 2.32 Excess Pore Pressure Ratio for Pilot Liquefaction Test 1st Blast a) PPT 96 and b) PPT 95

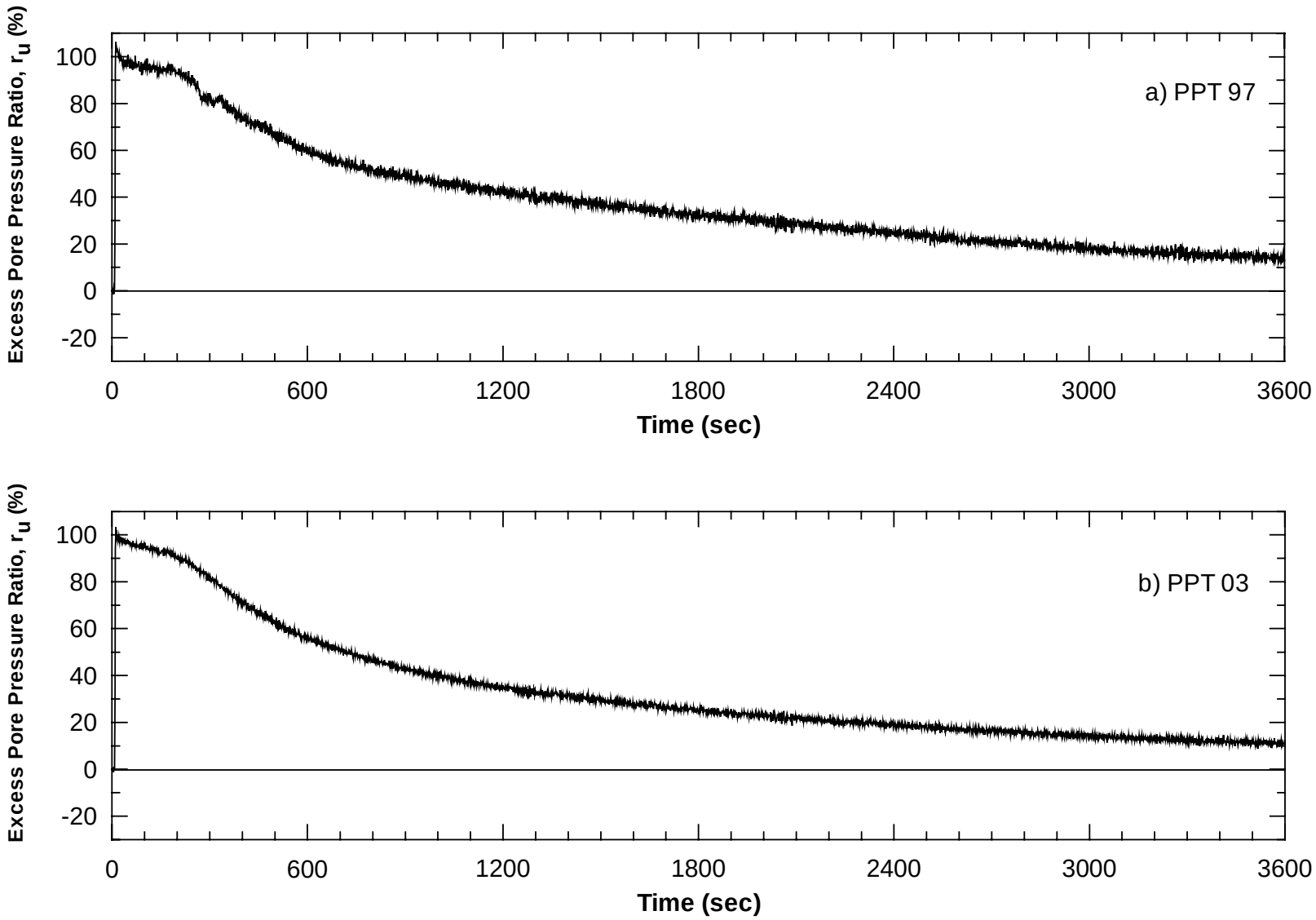

Figure 2.33 Excess Pore Pressure Ratio for Pilot Liquefaction Test 1st Blast a) PPT 97 and b) PPT 03

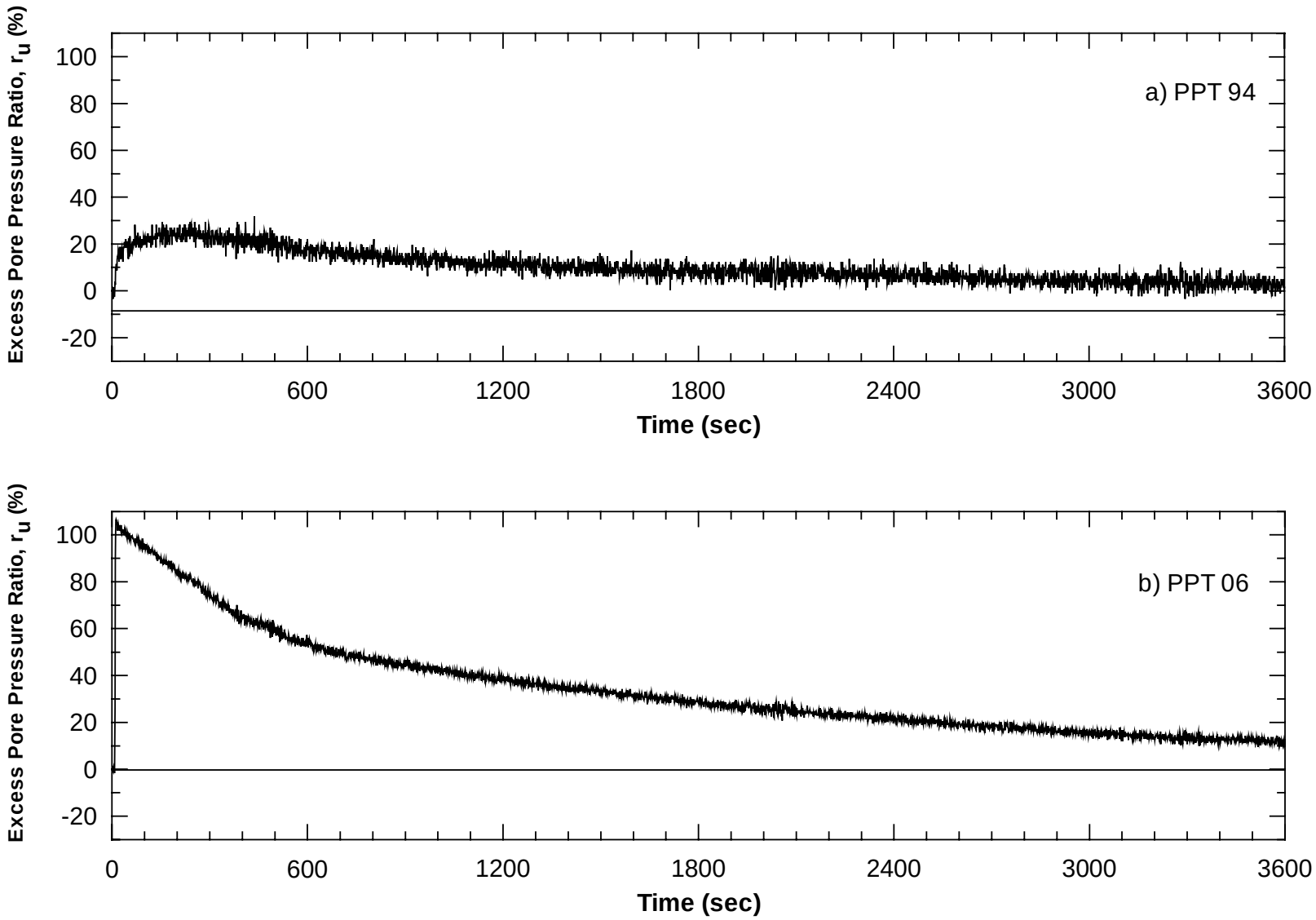

Figure 2.34 Excess Pore Pressure Ratio for Pilot Liquefaction Test 1st Blast a) PPT 94 and b) PPT 06

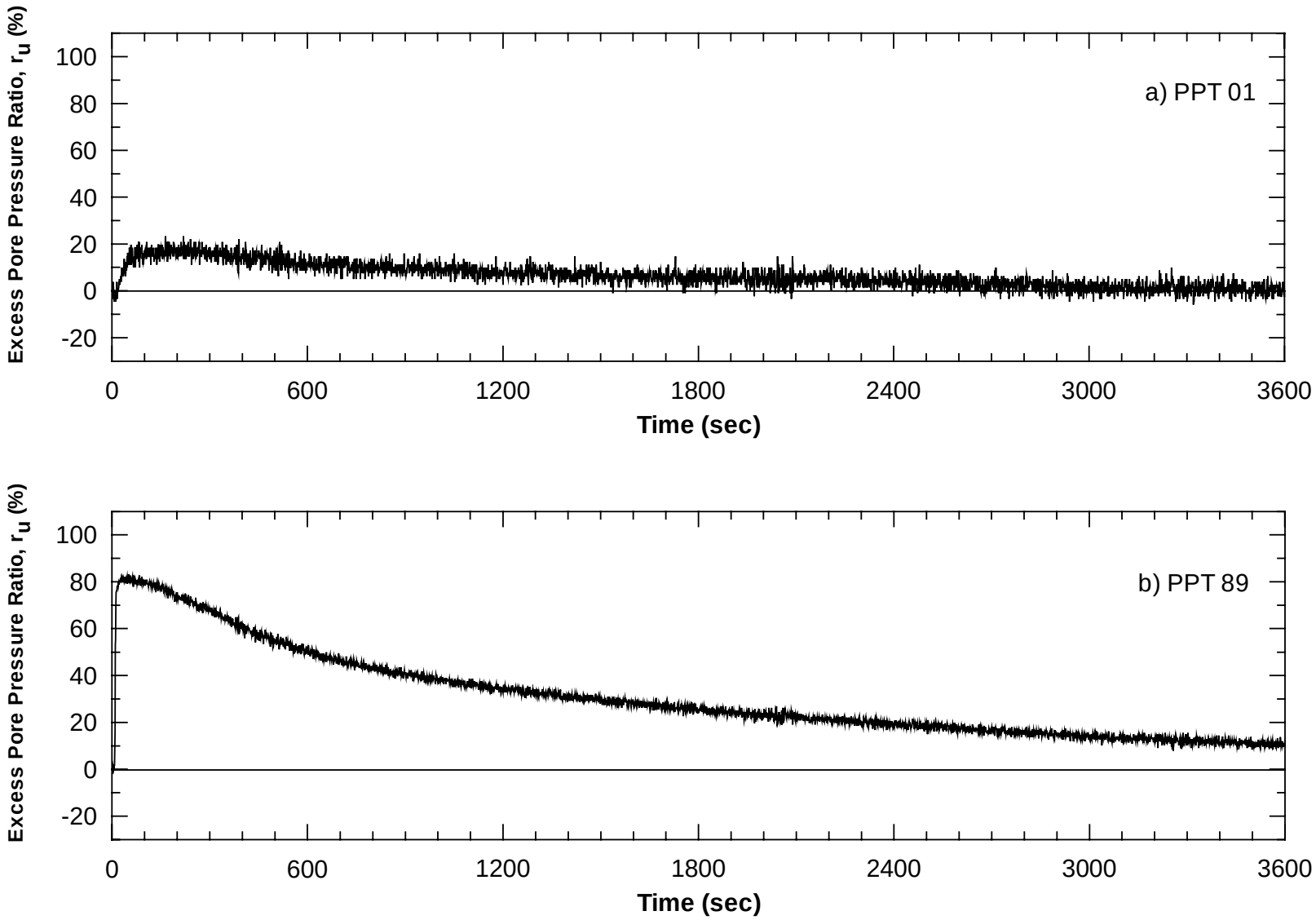

Figure 2.35 Excess Pore Pressure Ratio for Pilot Liquefaction Test 1st Blast a) PPT 01 and b) PPT 89

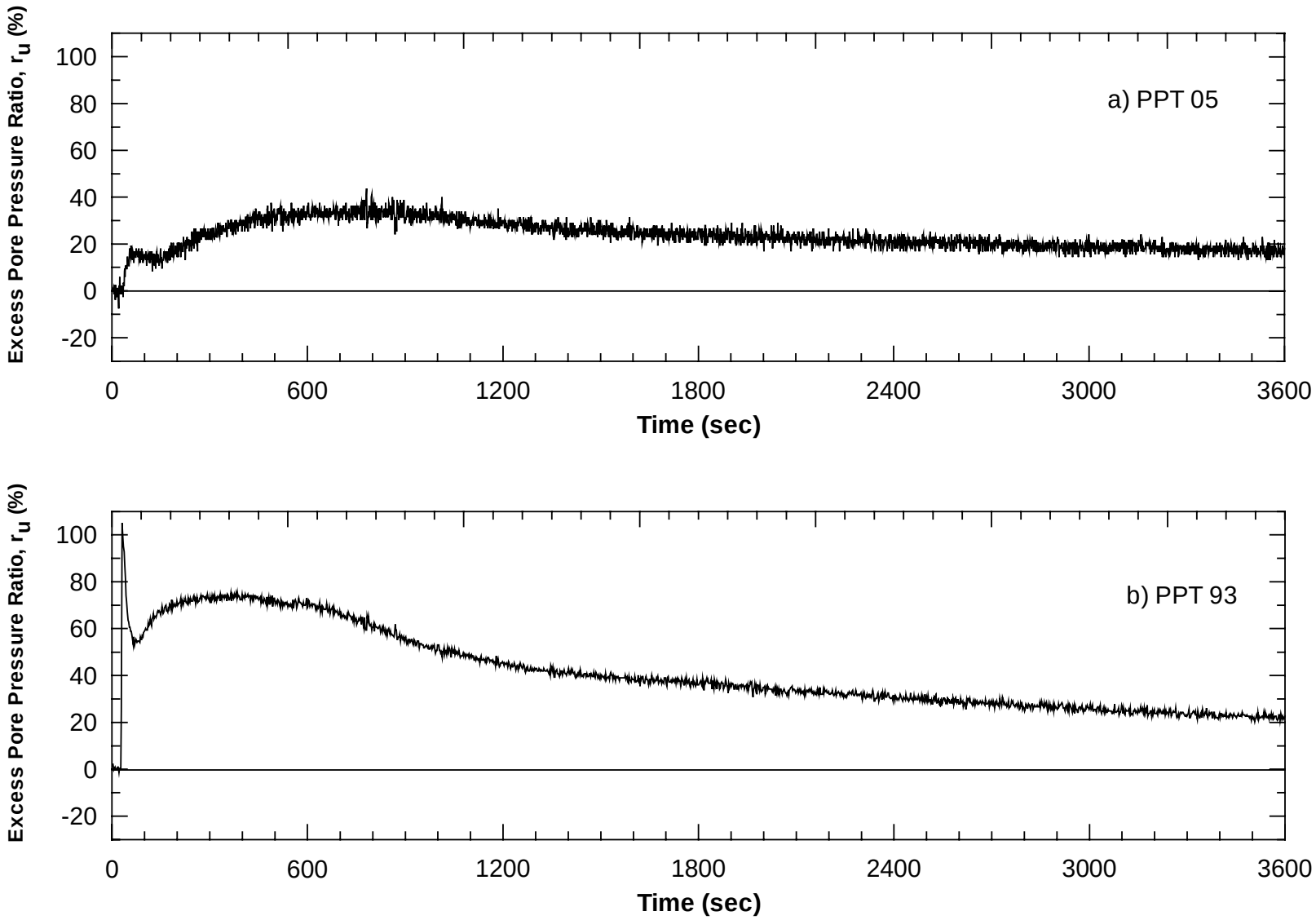

Figure 2.36 Excess Pore Pressure Ratio for Pilot Liquefaction Test 2nd Blast a) PPT 05 and b) PPT 93

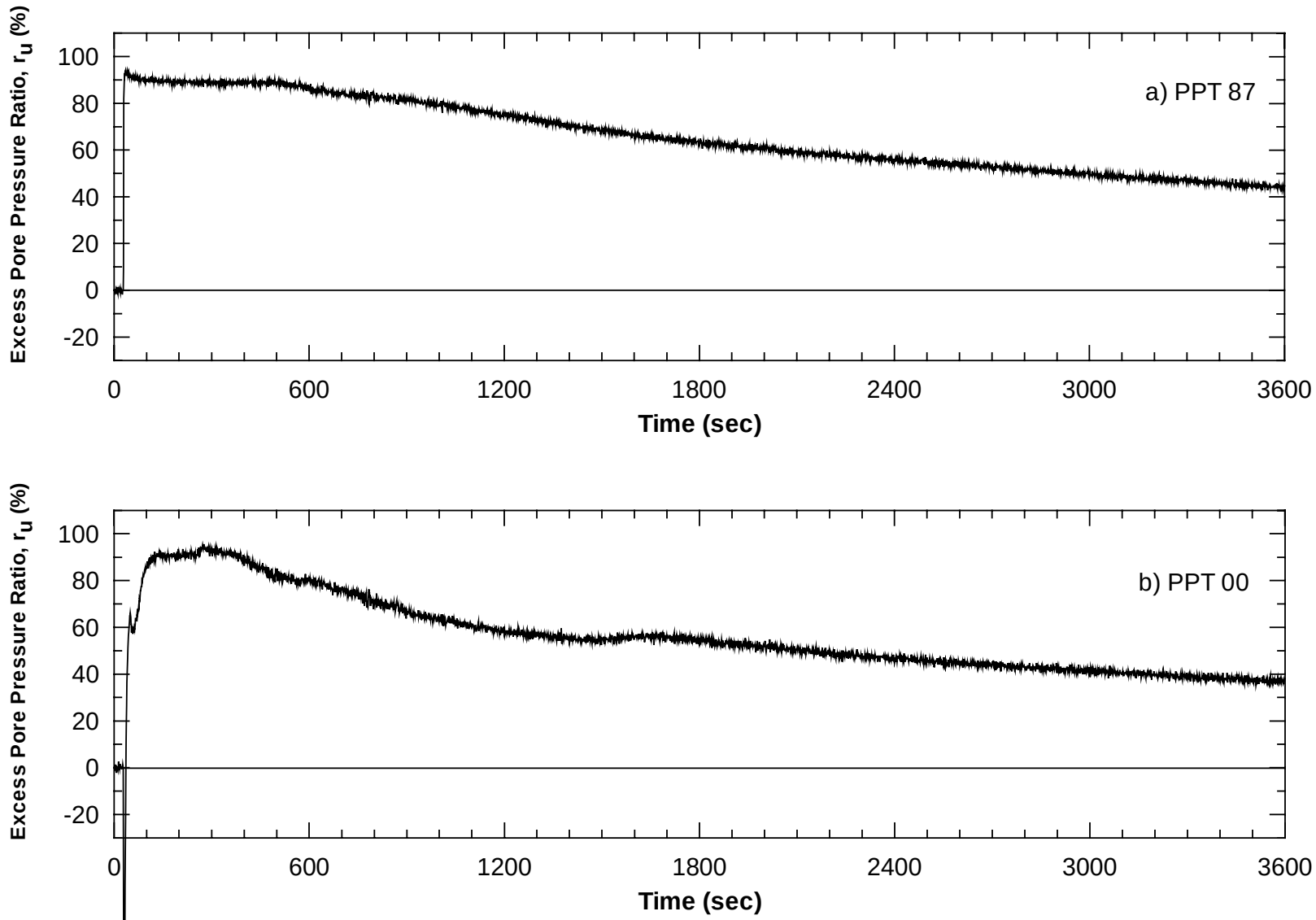

Figure 2.37 Excess Pore Pressure Ratio for Pilot Liquefaction Test 2nd Blast a) PPT 87 and b) PPT 00

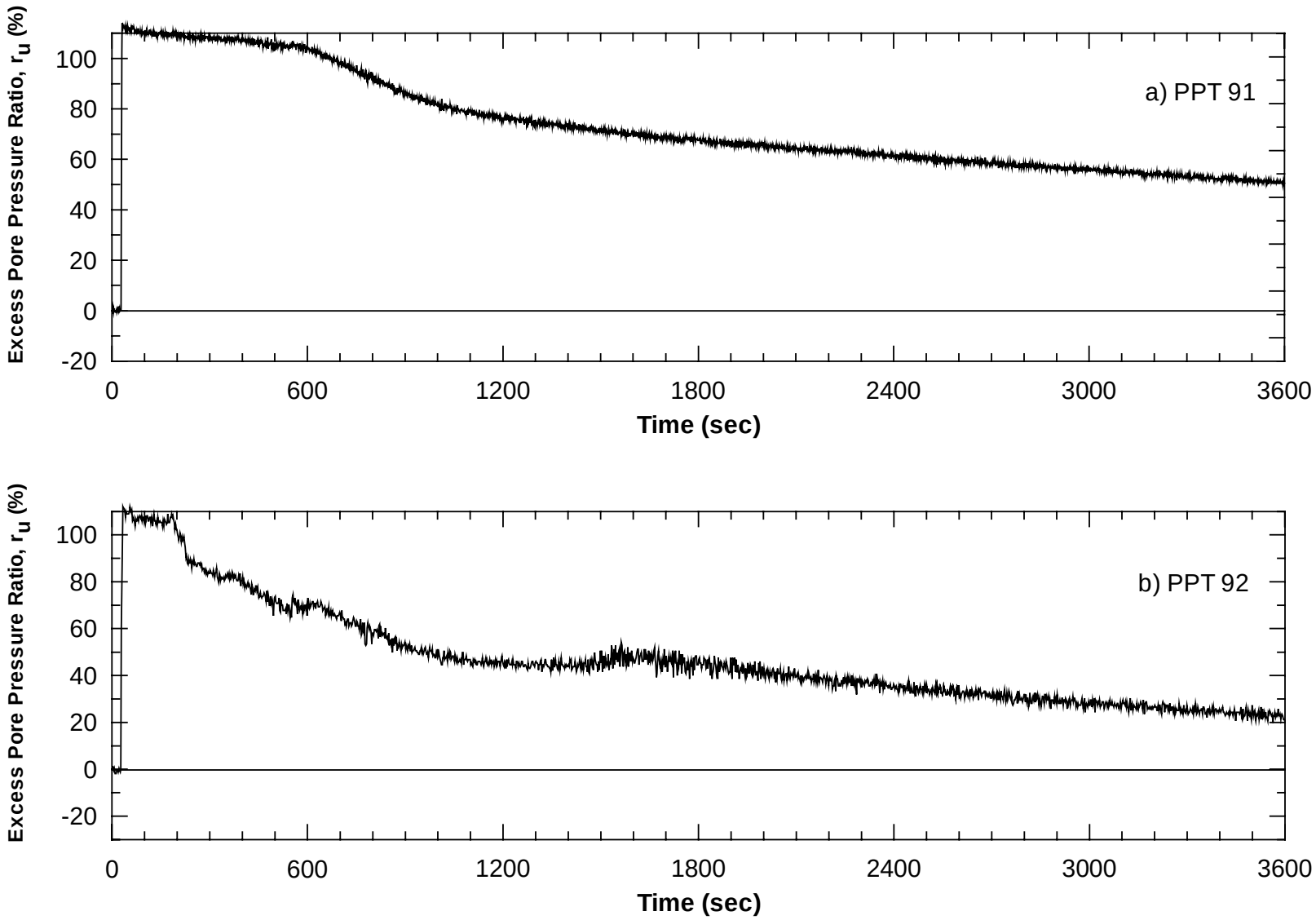

Figure 2.38 Excess Pore Pressure Ratio for Pilot Liquefaction Test 2nd Blast a) PPT 91 and b) PPT 92

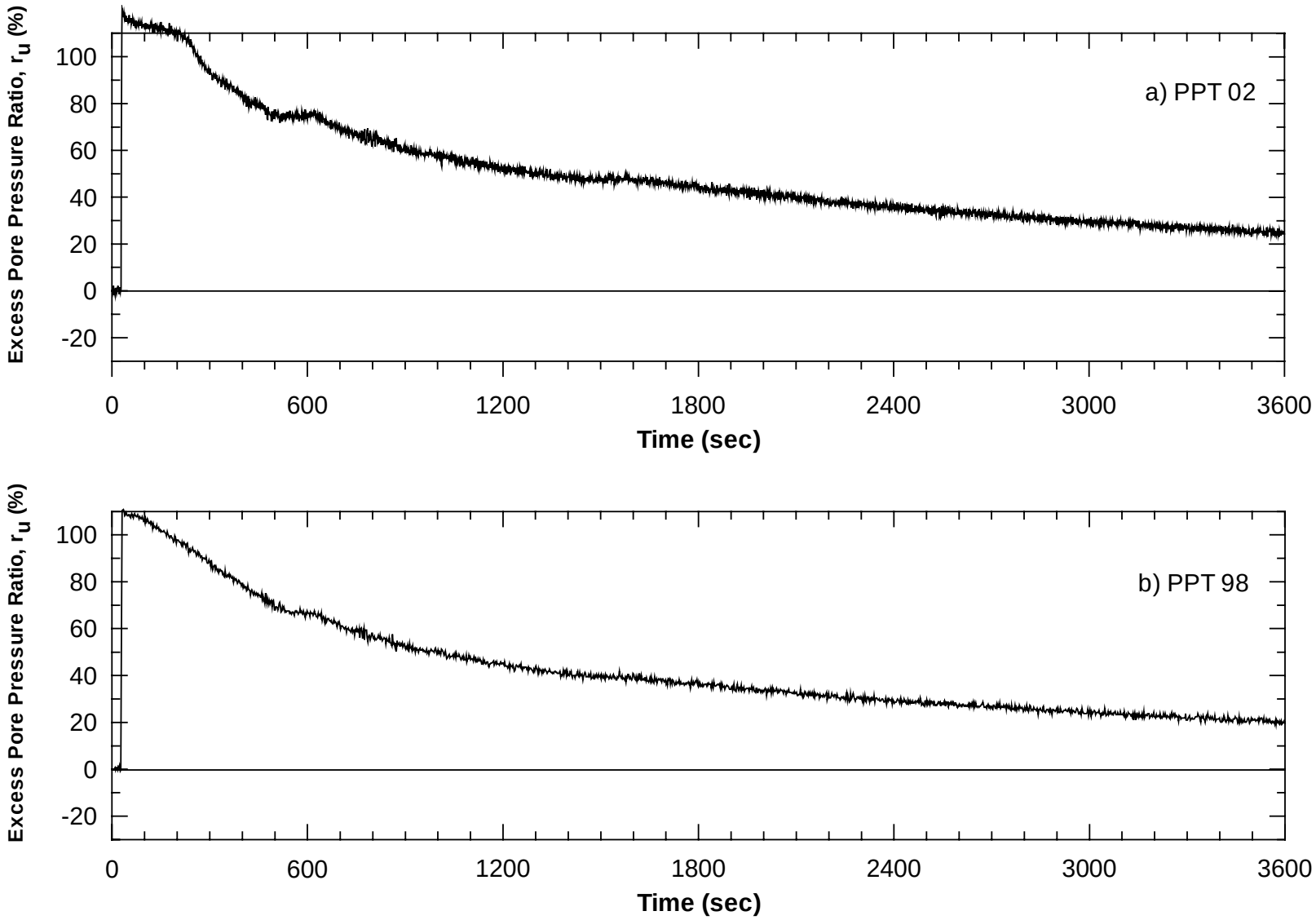

Figure 2.39 Excess Pore Pressure Ratio for Pilot Liquefaction Test 2nd Blast a) PPT 02 and b) PPT 98

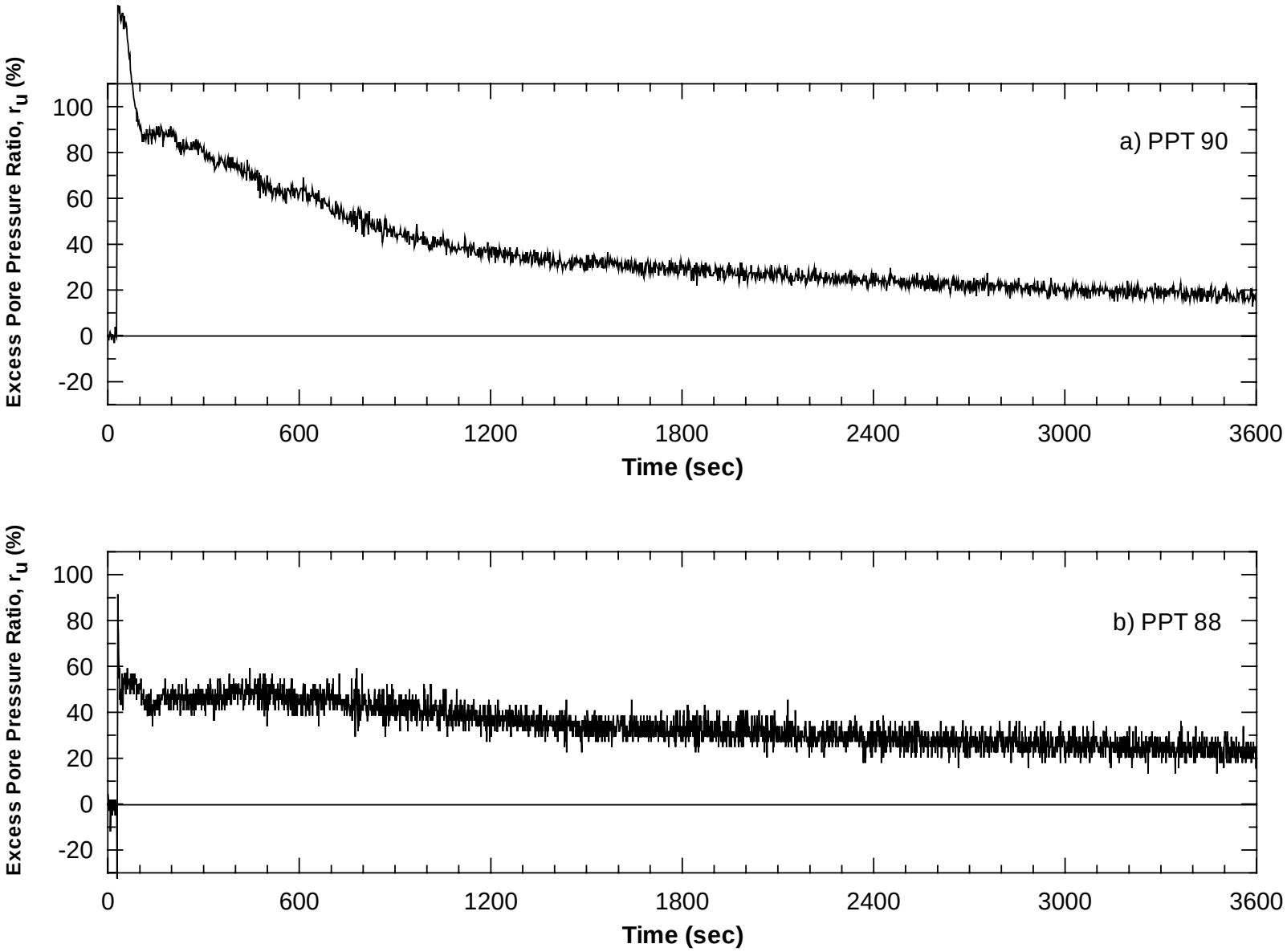

Figure 2.40 Excess Pore Pressure Ratio for Pilot Liquefaction Test 2nd Blast a) PPT 90 and b) PPT 88

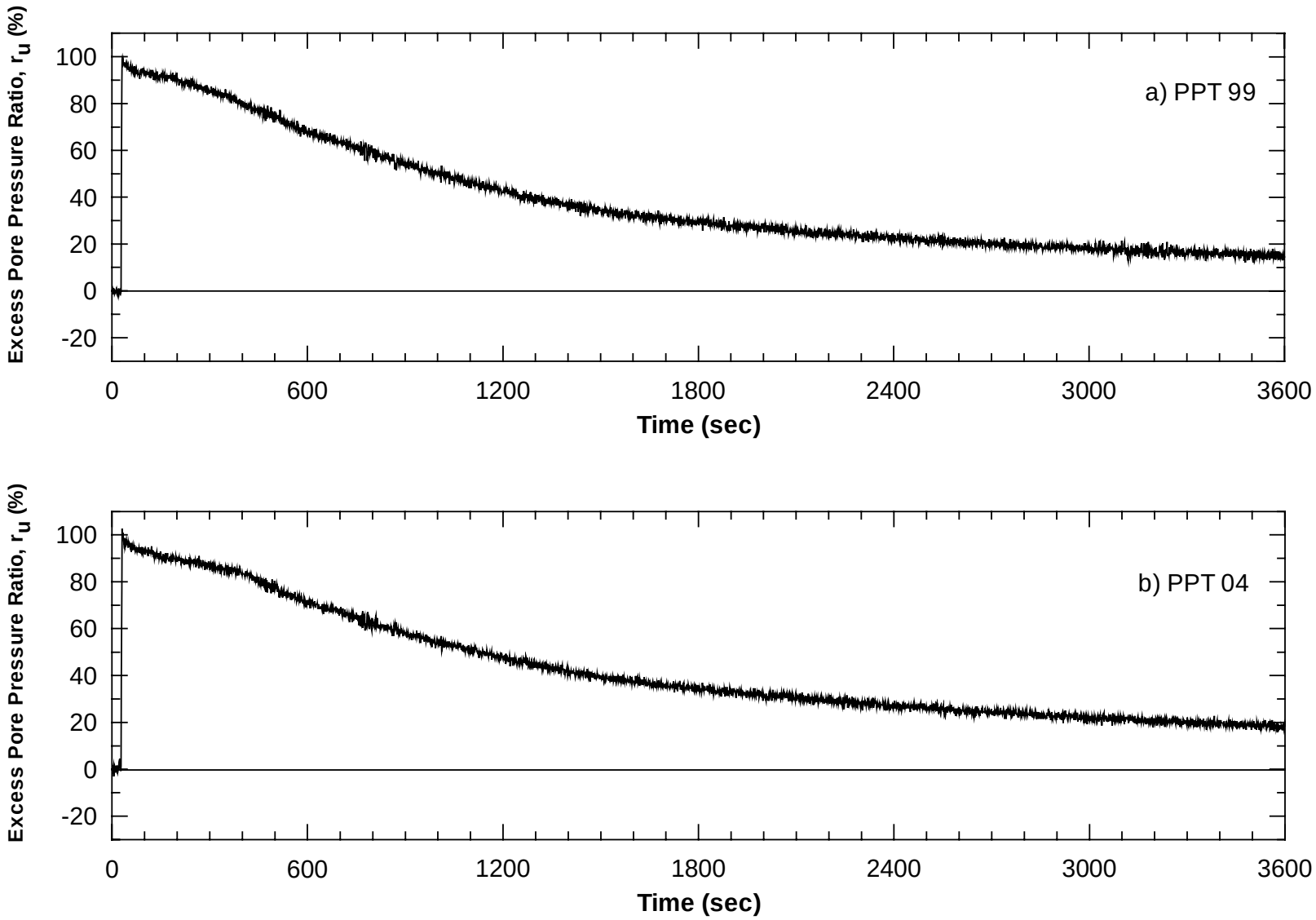

Figure 2.41 Excess Pore PressureRatio for Pilot Liquefaction Test 2nd Blast a) PPT 99 and b) PPT 04

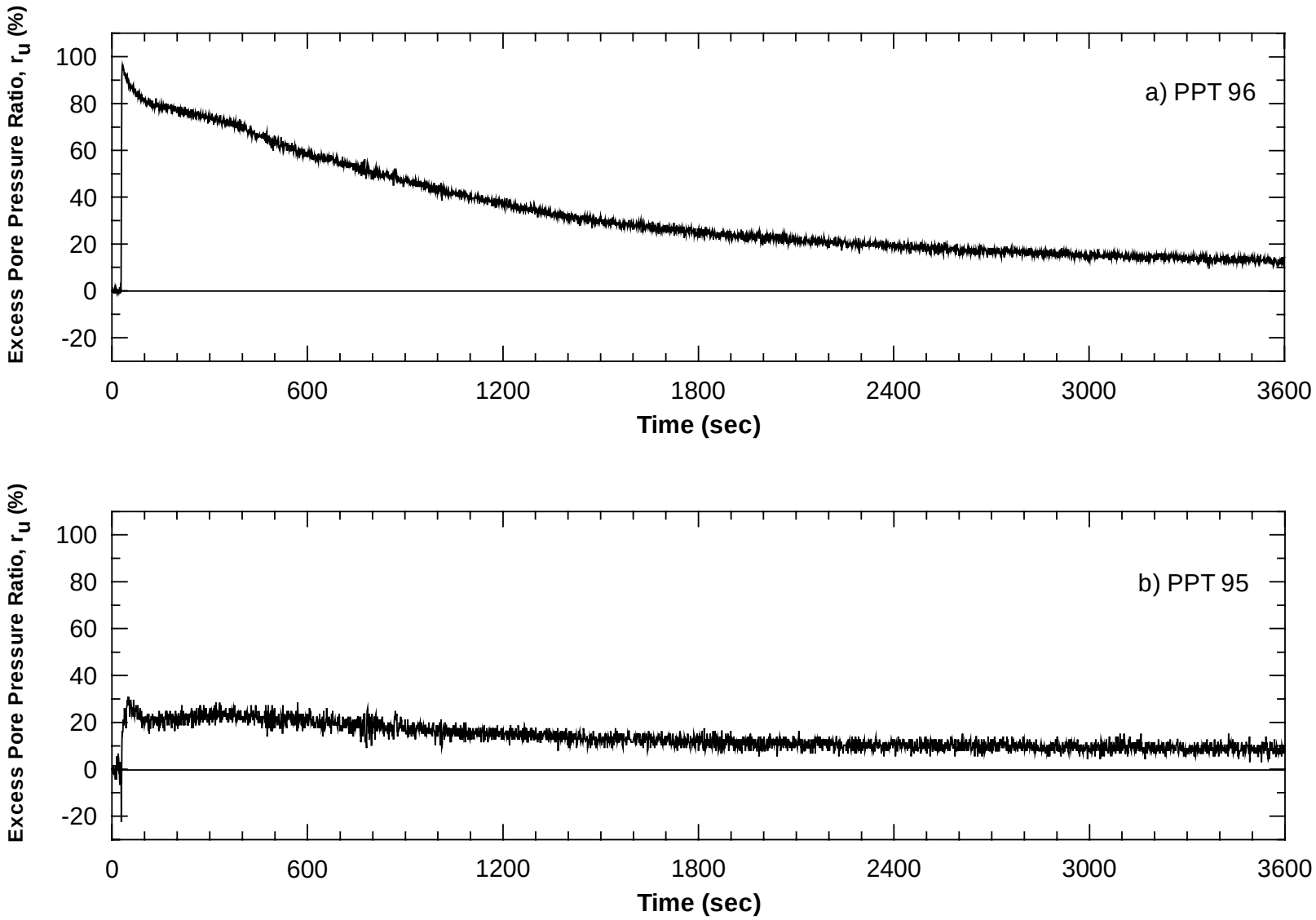

Figure 2.42 Excess Pore Pressure Ratio for Pilot Liquefaction Test 2nd Blast a) PPT 96 and b) PPT 95

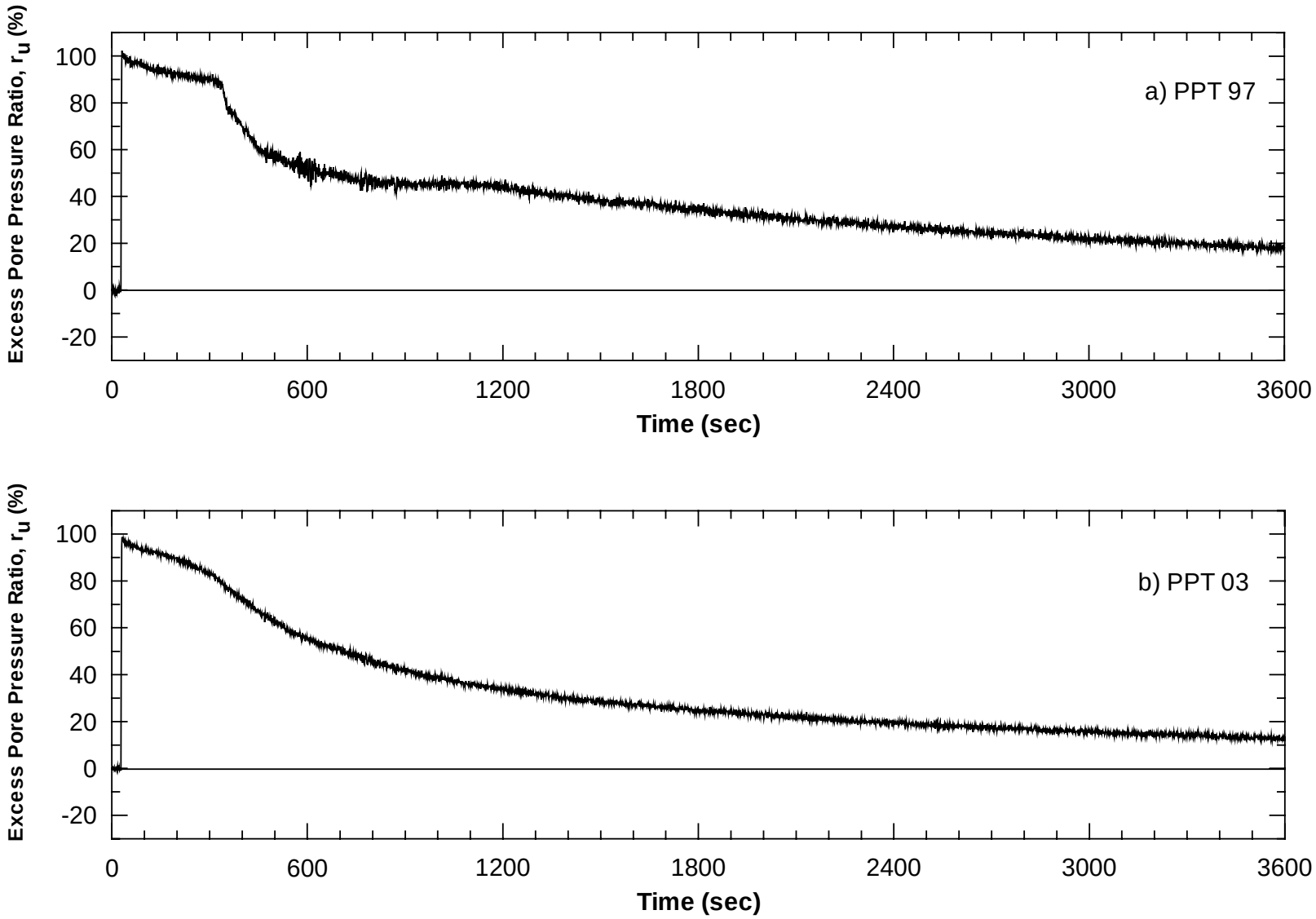

Figure 2.43 Excess Pore Pressure Ratio for Pilot Liquefaction Test 2nd Blast a) PPT 97 and b) PPT 03

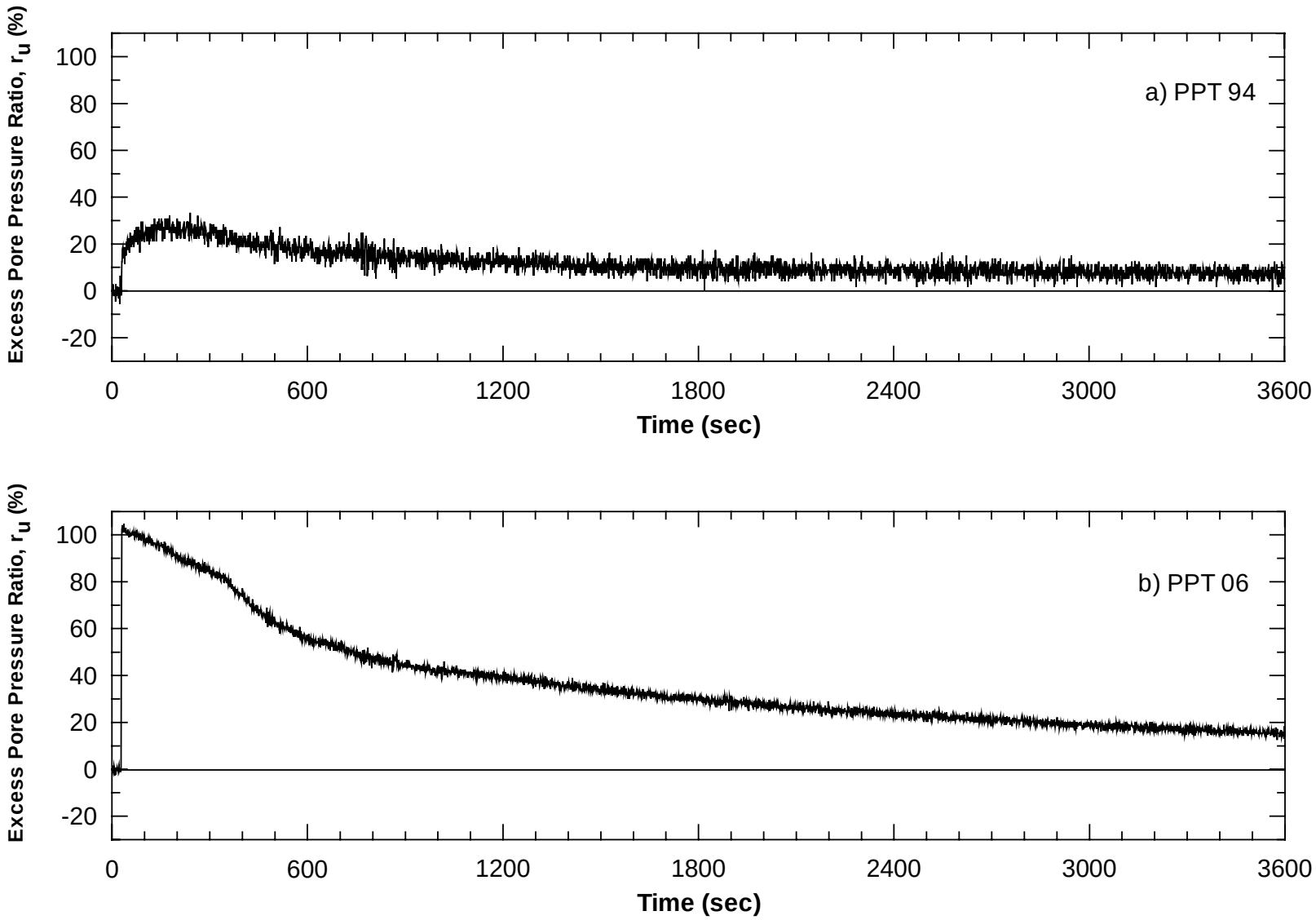

Figure 2.44 Excess Pore Pressure Ratio for Pilot Liquefaction Test 2nd Blast a) PPT 94 and b) PPT 06

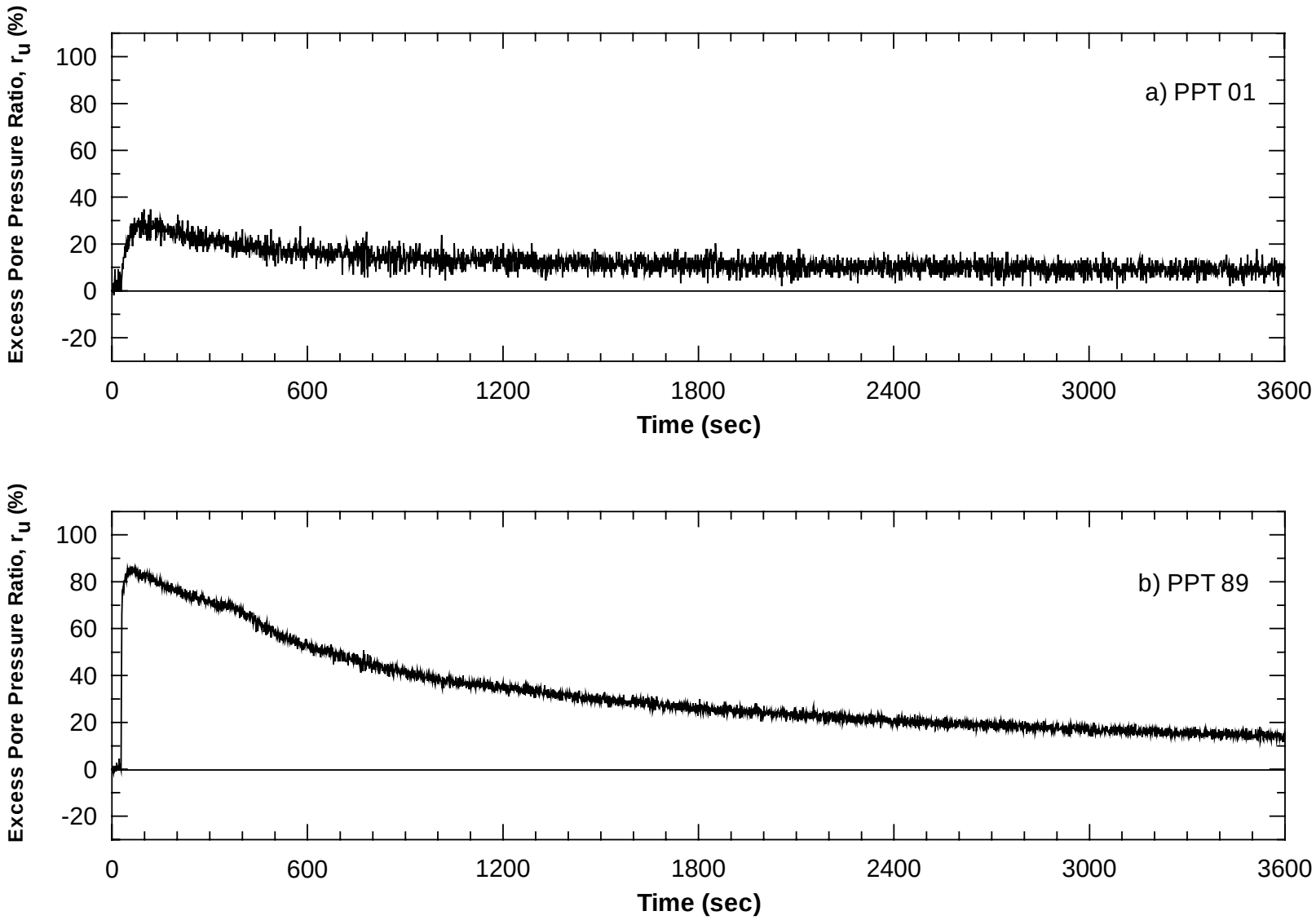

Figure 2.45 Excess Pore Pressure Ratio for Pilot Liquefaction Test 2nd Blast a) PPT 01 and b) PPT 89

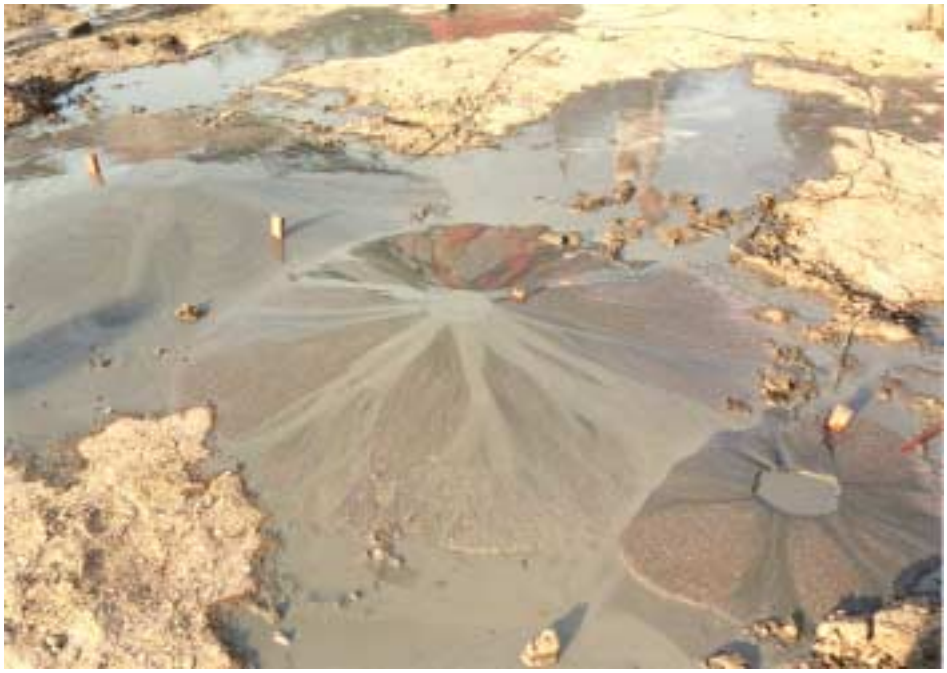

Figure 2.46 Formation of Sand Boils During Pilot Liquefaction Study

Figure 2.47 Settlement Survey after Pilot Liquefaction Test

Note: Contours in millimeters
Coordinates in feet

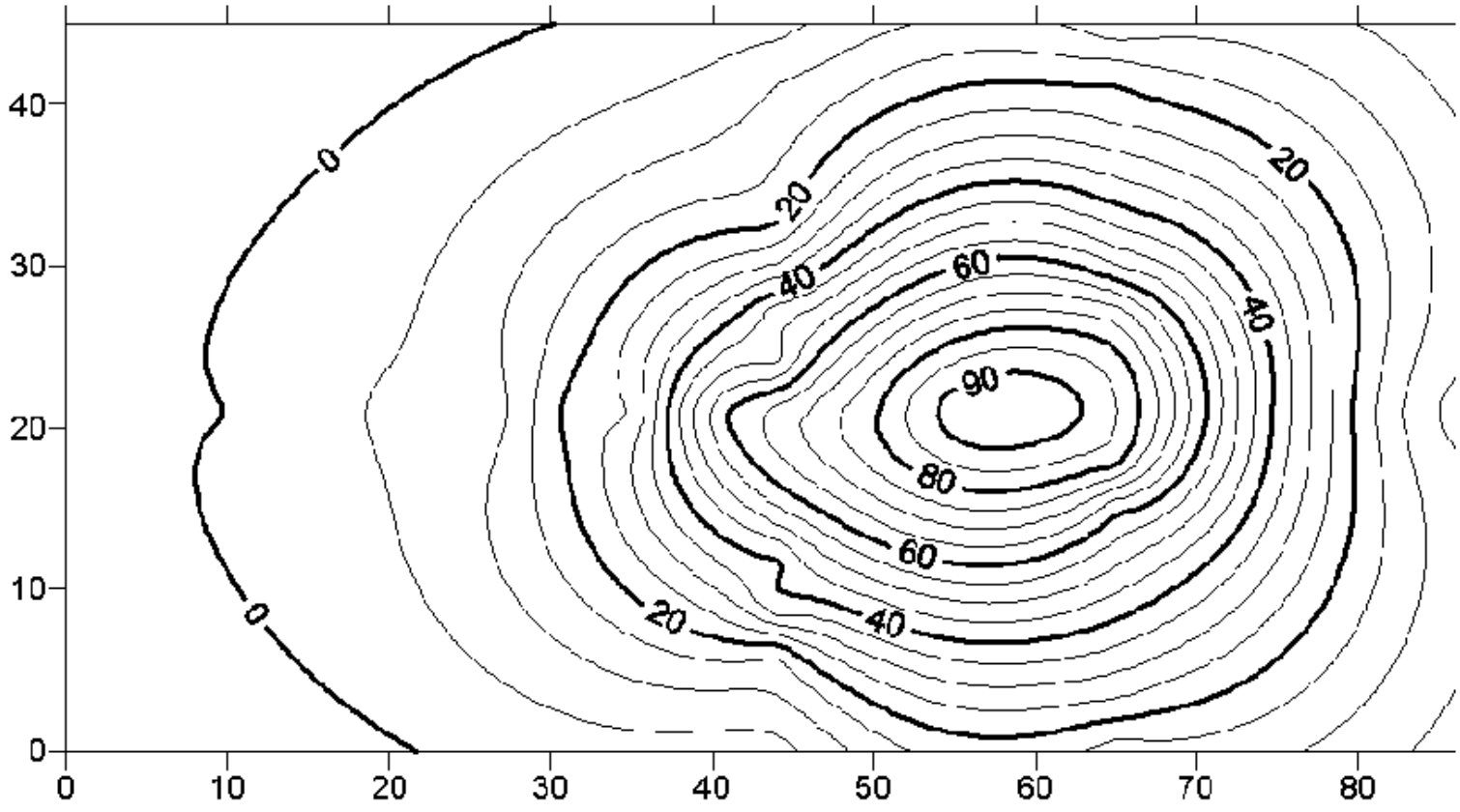

Figure 2.48 Settlement t Contours for 1st Blast of Pilot Liquefaction Study

Note: Contours in millimeters
Coordinates in feet

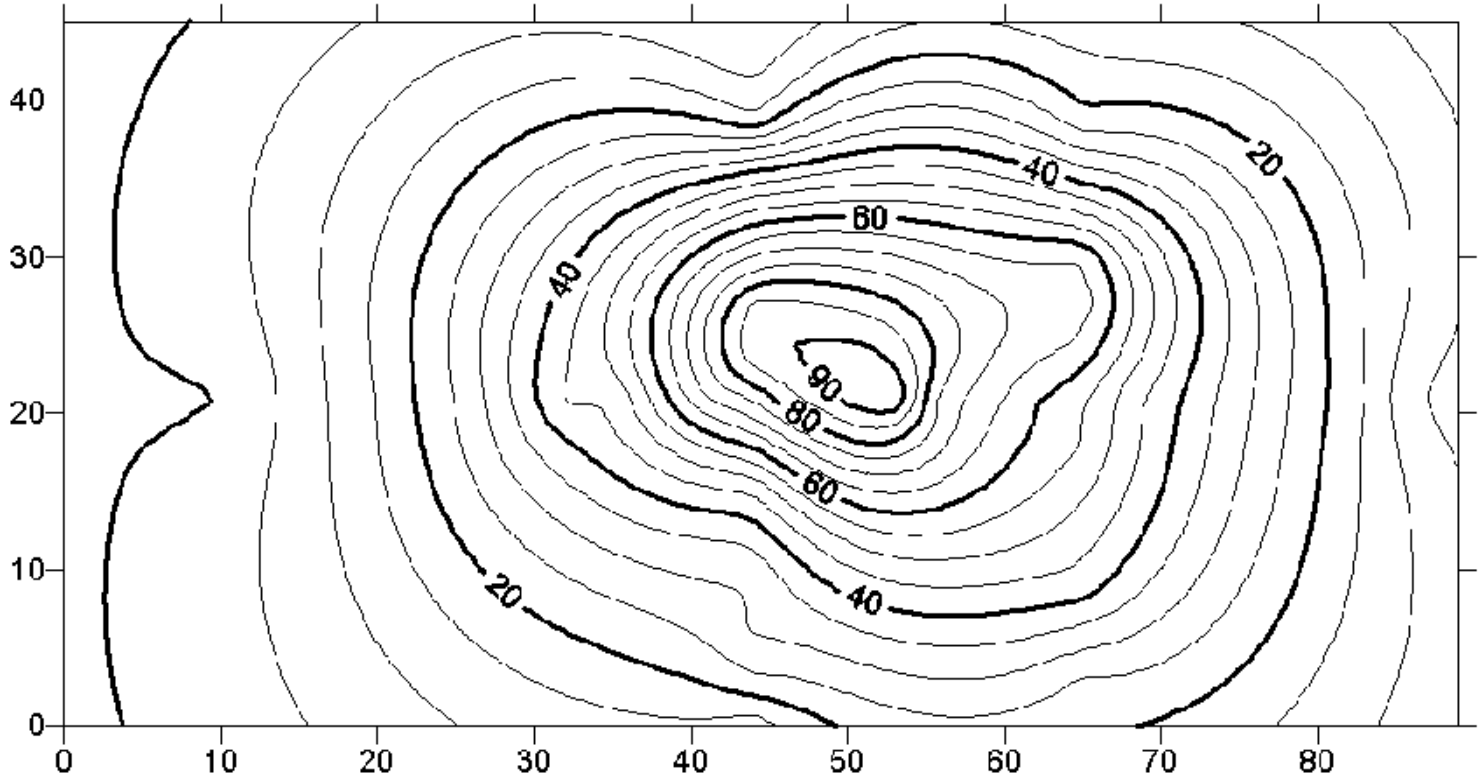

Figure 2.49 Settlement Contours for 2nd Blast of Pilot Liquefaction Study

Note: Contours in millimeters
Coordinates in feet

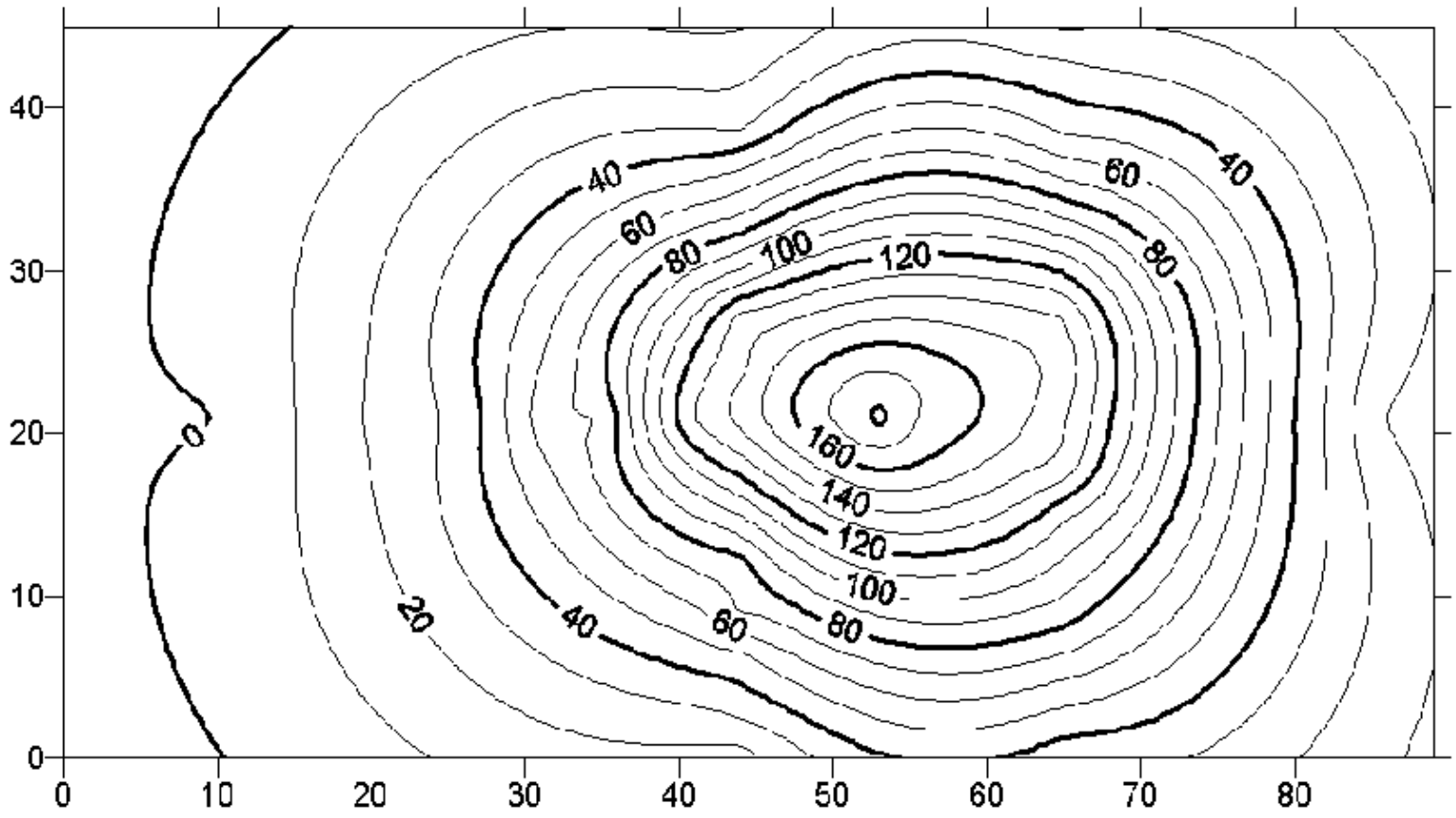

Figure 2.50 Combined Settlement Contours for 1st and 2nd Blast of Pilot Liquefaction Study

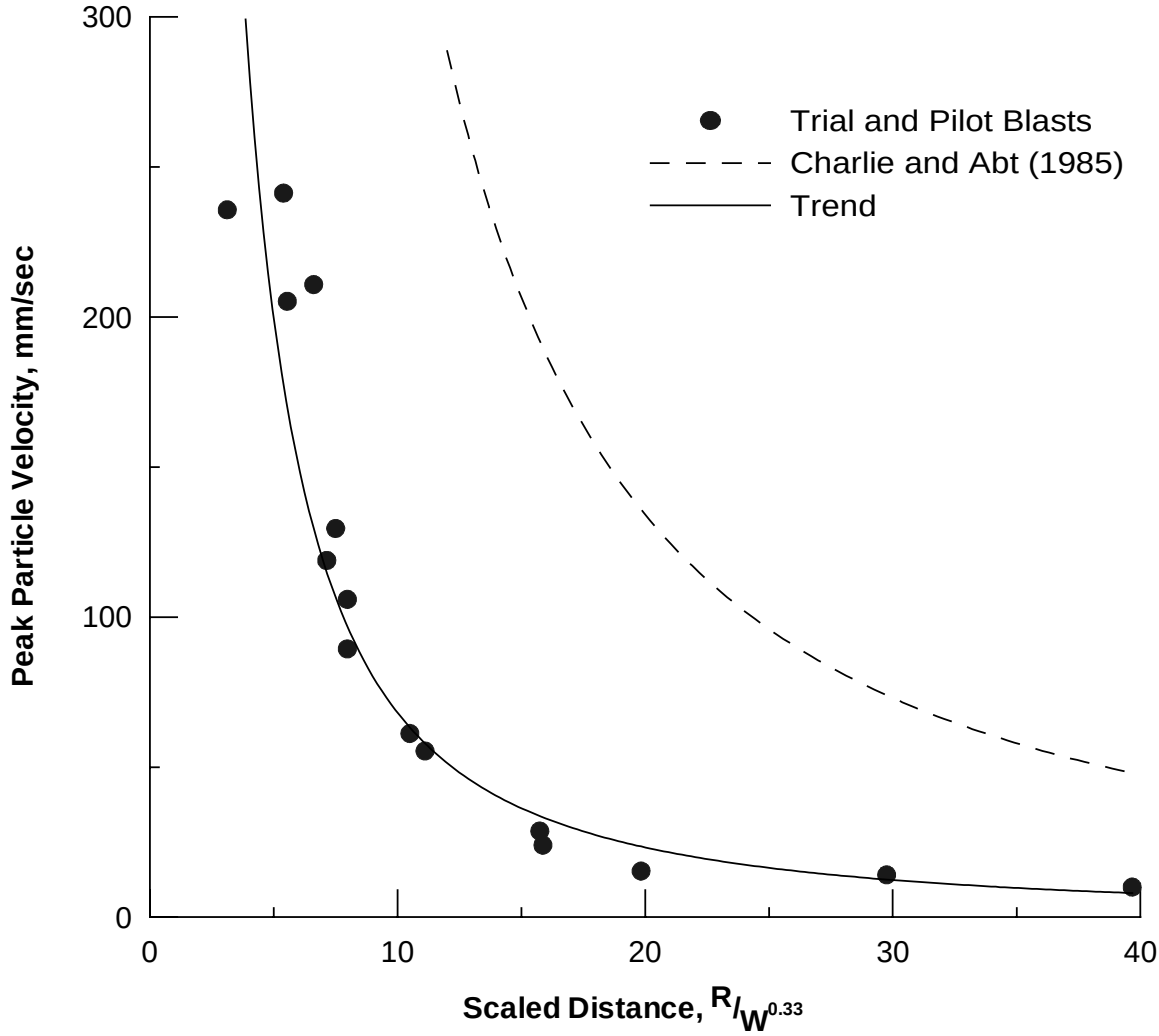

Figure 2.51 Peak Particle Velocity vs. Scaled Distance

3 SINGLE PILE TESTS

The single pile tests investigated the lateral response of a steel pipe pile (0.32-m O.D.) and an H-Pile (HP 12x53). All piles were driven through the sand layer and well into the underlying clay layer to ensure that they performed as “long piles”. Though they would have been driven deeper to a bearing layer on a real bridge, vertical capacity was not a concern for the lateral load testing. In all cases, driving was very easy. The single pile tests were the first ever full-scale lateral load field tests of piles in liquefied soil. Results of the single pile test will be valuable in verifying the validity of model tests performed in the laboratory. The single pile tests also provided baseline information needed to assess the performance of the pile groups and large diameter CISS piles tested at Treasure Island. In this chapter, data from the subsurface investigation and in-situ testing for the single pile tests are presented along with load and displacement test results, excess pore pressure ratios, and settlement contours resulting from blasting.

3.1 Single Pile Site Characterization

A comprehensive field exploration was carried out before any foundation testing was performed. Figure 3.1 shows the location of in-situ tests at the single pile test site. The soil boring log for BH-4 is presented in Figure 3.2. The boring logs from the single pile site show the subsurface conditions as consisting of relatively loose, poorly graded sand from the ground surface to a depth of 9.1 meters. A soft clay layer was observed at a depth of 9.1 meters and extended to the bottom of the boring at 18.3 meters. The water table at the time of the boring was 1.7 meters below the original ground surface. Low

SPT blow counts indicated that the sand below the water table was liquefiable. Six CPT's performed before foundation testing are shown in Figures 3.3 through 3.8. Cone penetration logs generally confirmed SPT results, showing low tip resistance of between 5 and 10 MPa in the sand deposit indicating a relatively low density. An additional six cone penetration tests were conducted after the single pile tests were completed. CPT logs S-1, S-2, and S-3 in Figures 3.10 through 3.12 (20 days after testing) do not show any increase in tip resistance compared to cone logs prior to blasting. CPT logs SFC007 and SFC008 in Figures 3.13 and 3.14 (5 months after testing) show an increase in tip resistance when compared to cone logs prior to blasting and 20 days after blasting.

Shear wave velocity tests shown in Figure 3.15 were conducted before and after the first single pile test. Results of the down-hole test show a reduction in the shear wave velocity of approximately 12 m/sec (approximately 10%) in the upper 3.5 meters within hours of the first blast. After the blast, the shear wave velocity below 3.5 meters increased by 18 m/sec according to down-hole measurements.

3.2 Single Pile Test Results

The first of two single pile tests was conducted on January 20, 1999. The single piles were loaded using a 2200 kN capacity hydraulic actuator. Two linear potentiometers were attached to each pile to measure lateral displacement and rotation at the load point. The lateral load was applied 0.76 m above the excavated ground surface. The piles were also instrumented with strain gages along the depth of the pile. A plan view of the test set-up is shown in Figure 3.16.

3.2.1 Load-Displacement Results for Test 1

Three static tests were performed prior to blasting with a maximum displacement of 38 mm. Two of the static tests consisted of pulling the piles together and one test where the piles were pushed in opposite directions. After the explosives were detonated, the piles were cycled through a series of displacements. Due to the H-pile experiencing failure early in testing, displacement of the pipe pile was used to control cycling. The first series of cycles consisted of pushing the pipe pile to displacements of 76 mm and 152 mm once each. Then the pipe pile was cycled through ten 228 mm displacements. No control was placed on the displacement level of the H-pile during these cycles. As testing progressed, the H-pile became less stiff. As the H-pile reached a displacement of approximately 375 mm, the maximum stroke of the actuator was approached, preventing the pipe pile from being displaced to the target displacement of 228 mm. The pipe pile displaced between 150 and 178 mm upon reaching the maximum actuator stroke. Load-displacement results for the pipe pile are shown in Figures 3.17 and 3.18. Results for the H-pile are shown in Figures 3.19 and 3.20. A review of the pipe pile test results shows that as testing continued past the initial few post blast loading cycles, the soil pile system provided more resistance to lateral loads. This increase in lateral stiffness is attributed to the reduction of the excess pore pressure with time resulting in an increase in soil shear strength. Although the soil strength increased as pore pressures decreased, there was no significant increase in the H-pile lateral stiffness. The low stiffness provided by the H-pile is likely due to the formation of a plastic hinge approximately 1.9 m below the excavated ground surface.

3.2.2 Excess Pore Pressure Response for Test 1

Pore pressures within the soil were measured during the entire loading and for approximately one hour after loading ceased. The location of each pore pressure transducer and blast point is shown in Figure 3.21. The excess pore pressure ratio for each transducer along with a plot of loading with time is presented in Figures 3.22 through 3.33. The excess pore pressure ratio plots are grouped according to location, beginning with the transducers at the south end of the excavation. Excess pore pressure ratios near the piles were significantly affected as the pile was displaced through the soil. As the pile was pushed and pulled, the excess pore pressure ratios would decrease and increase as can be seen in the figures. Excess pore pressures ratios at a distance of 4.2 m and 6.4 m from the pile were minimally affected as the piles were displaced. Similar to the pilot study, sand boils began forming within approximately 5 minutes of the blast as shown in Figure 3.34, and continued for sometime.

3.2.3 Load-Displacement Results for Test 2

Eight days after the first single pile test, a second lateral load test was performed. A 1.5-m square and 0.6-m deep concrete block was placed at grade around the failed H-pile to provide a stiff reaction for the pipe pile. Linear potentiometers were only connected to the pipe pile to measure displacement and rotation. A static load test was again performed prior to detonation of the explosives. Applied load versus lateral displacement plots for the entire test are presented in Figures 3.35 through 3.37. The pipe pile was displaced 38 mm toward the H-pile during the static test. Approximately 10 seconds after detonation of the explosives, the pipe pile was cycled through eleven series of displacements. The

first series consisted of a 76 mm, 152 mm and eleven 228 mm cycles. The cycles consisted of pushing the pile to the target displacement and then returning the pile to a zero displacement at the load point. During the first post blast series, the soil-pile system reduced in stiffness during each 228 mm cycle. Post blast Series 2 through 11 consisted of a 76 mm, 152 mm and four 228 mm cycles. The soil-pile system showed an incremental increase in stiffness from post blast Series 2 through 11. The increase in stiffness can be attributed to the reduction in excess pore pressures with time.

3.2.4 Excess Pore Pressure Response for Test 2

Pore pressure response for the second single pile test are similar to the first test, as can be seen from excess pore pressure ratios and load versus time plots in Figures 3.38 through 3.44. Excess pore pressure ratios at a distance of 4.2 m and 6.4 m from the pile were minimally affected as the pile was displaced. Excess pore pressures were affected the greatest at shallow depths near the pile. Only pore pressure transducers near the pipe pile were used during the second test. The formation of sand boils again provided evidence of liquefaction within the ring of charges.

3.2.5 Settlement

Immediately prior to and after each blast, an elevation survey was performed to measure settlement in the excavation. Figure 3.45 presents settlement contours as measured after the first blast. The contours of settlement are in millimeters, while the coordinates from the edge of the excavation are in meters. It can been seen from the

figure that 200 mm of settlement was observed in the center of the test area, between the two piles.

3.3 Summary of Testing

The single pile test provided valuable results. CPT results showed an increase in soil density approximately 5 months after blasting. Load test results were consistent with previous laboratory testing showing a decrease in pile stiffness when the soil liquefies. As pore pressures decreased, the lateral stiffness of the soil-pile system increased. During the first ten minutes after detonation of the explosives, excess pore pressure ratios remained above 80%. This allowed for the piles to be displaced through a number of cycles while pore pressures were high. In addition to the value of the single pile test data alone, the single pile tests will be used as a reference for the larger diameter pile and pile group tests.

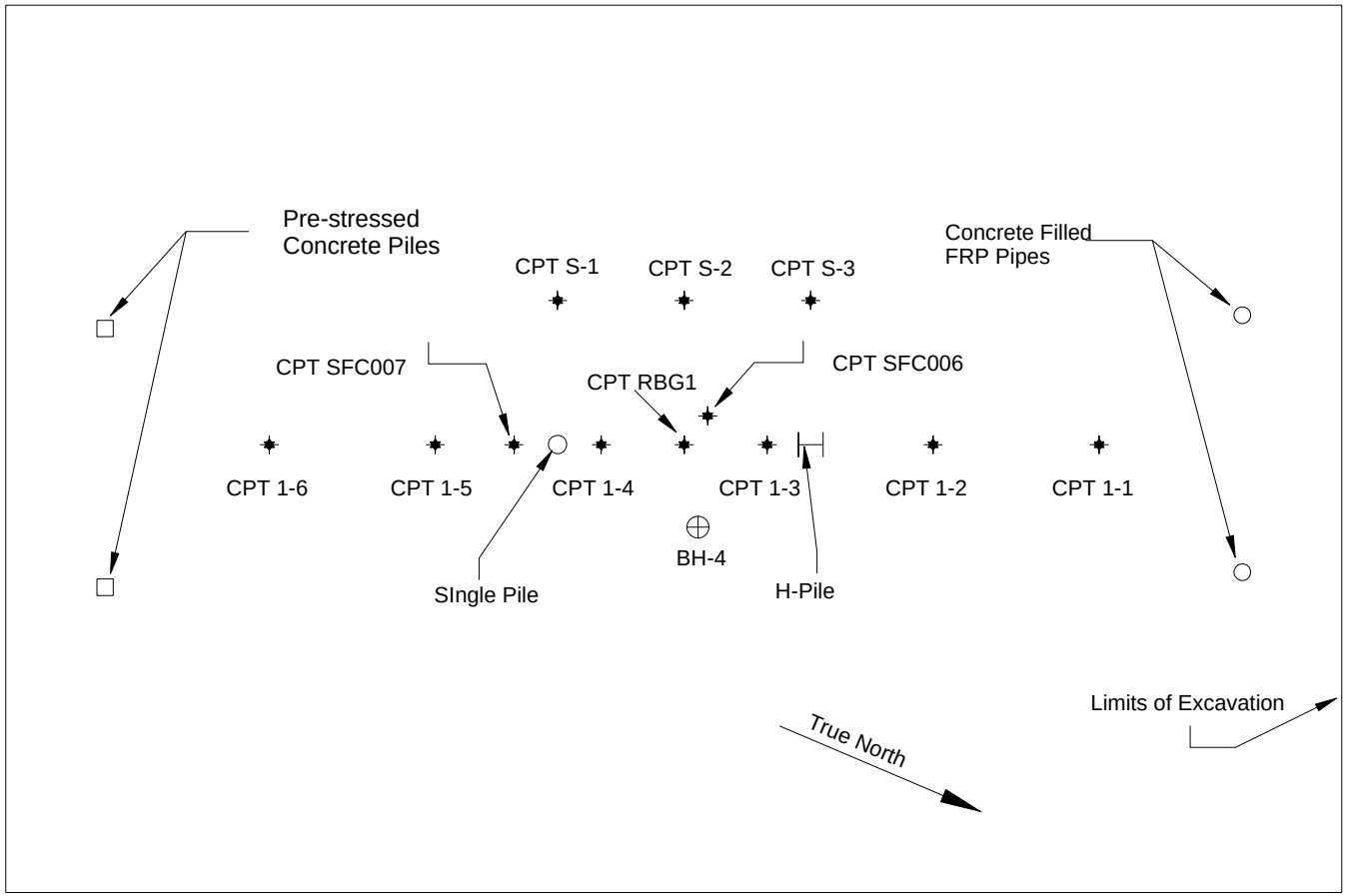

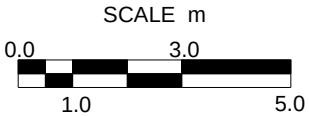

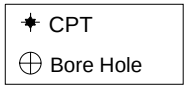

Note:
CPT No's 1-1 through 1-6 Completed 11/06/98 (before first blast)
CPT No RBG1 Completed 2/05/99
CPT No's S-1, S-2, & S-3 Completed 2/17/99
CPT No's SFC006 & SFC007 Completed 6/24/99

Figure 3.1 Location Map of In-Situ Tests for Single Pile Area

Brigham Young University
&
University of California - San Diego
Telephone: (801) 378-6334
Fax: (801) 378-4449

Boring No: BH-4 | Sheet 1 of 2
Logged By: jdl | Elevation (m): 3.4
Date Started: 10/16/1998 | Drill Contractor: Pitcher
Date Finished: 10/16/1998 | Drilling Method: Rotary Wash

TREASURE ISLAND
SAN FRANCISCO BAY
CALIFORNIA

Location: Single Pile

Material Description	Depth (m)	Location	Number	Type	Recovery (cm/cm)	Blows/15 cm	$(N_1)_{60}$ Blows/30 cm	Soil Classification USCS	Soil Classification AASHTO	S_u (kPa)	Torvane (kPa)	Pocket Pentometer (kPa)	Dry Density (kN/m3)	Moisture Content %	Liquid Limits LL	Plastic Limits PL	Plasticity Index PI	Passing #200 Sieve (%)	OTHER DATA AND REMARKS
Brown, moist, Fined-Grained Sand w/Shells	1		S-1	SPT	46/46	8-11-11		SP											
	2		S-2	SPT	30/46	4-4-7		SP											
Black, Saturated, Fine-Grained Silty Sand	3		S-3	SPT	23/46	4-5-5		SP-SM											
	4		S-4	SPT	30/46	3-3-5		SP-SM											
	5		S-5	SPT	33/46	5-7-7		SP-SM											
	6		S-6	SPT	46/46	4-5-2		SP-SM											
	7		S-7	SPT	43/46	2-2-1		SP-SM											
Dark, Clay, Saturated Fine-Medium Sand w/Some Silt	8		S-8	SPT	46/46	2-2-2		SP-SM											
	9		S-9	SPT	46/46	2-0-0		SM											
Saturated, Gray Clay	10		S-10	SPT	46/46			CL											

LEGEND AND NOTES
- SPT = Standard Penetration Test, Split Spoon Sample
- US = Undisturbed Shelby Tube, Pushed
- Ring = Dames & Moore Sampler
- Bulk = Bulk Sample From Cuttings

GROUNDWATER DEPTHS:
- = Initial
- = End of Drilling

COMMENTS:

LOG_OF_BORING_METRIC SANFRAN.GPJ LANE.GDT 9/14/00

Figure 3.2a Soil Boring Log for Single Pile Area

Brigham Young University
&
University of California - San Diego
Telephone: (801) 378-6334
Fax: (801) 378-4449

Boring No: BH-4 | Sheet 2 of 2
Logged By: jdl | Elevation (m): 3.4
Date Started: 10/16/1998 | Drill Contractor: Pitcher
Date Finished: 10/16/1998 | Drilling Method: Rotary Wash

TREASURE ISLAND
SAN FRANCISCO BAY
CALIFORNIA

Location: Single Pile

Material Description	Water Level	Depth (m)	Graphic Log	Sample Data: Location	Number	Type	Recovery (cm/cm)	Blows/15 cm	$(N_1)_{60}$ Blows/30 cm	Soil Classification: USCS	AASHTO	S_u (kPa)	Torvane (kPa)	Pocket Pentometer (kPa)	Dry Density (kN/m3)	Moisture Content %	Atterberg Limits: Liquid Limits LL	Plastic Limits PL	Plasticity Index PI	Passing #200 Sieve (%)	OTHER DATA AND REMARKS
		11			S-11	SH	0/76														
		12			S-12	SH	76/76			CL											
		13			S-13	SH	76/76			CL											
		14																			
		15			S-14	SH	76/76			CL											
		16			S-15	SH	76/76			CL											
		17																			
		18			S-16	SH	76/76			CL											
		19																			
		20																			

LEGEND AND NOTES
- SPT = Standard Penetration Test, Split Spoon Sample
- US = Undisturbed Shelby Tube, Pushed
- Ring = Dames & Moore Sampler
- Bulk = Bulk Sample From Cuttings

GROUNDWATER DEPTHS:
- = Initial
- = End of Drilling

COMMENTS:

LOG_OF_BORING_METRIC SANFRAN.GPJ LANE.GDT 9/14/00

Figure 3.2b Soil Boring Log for Single Pile Area

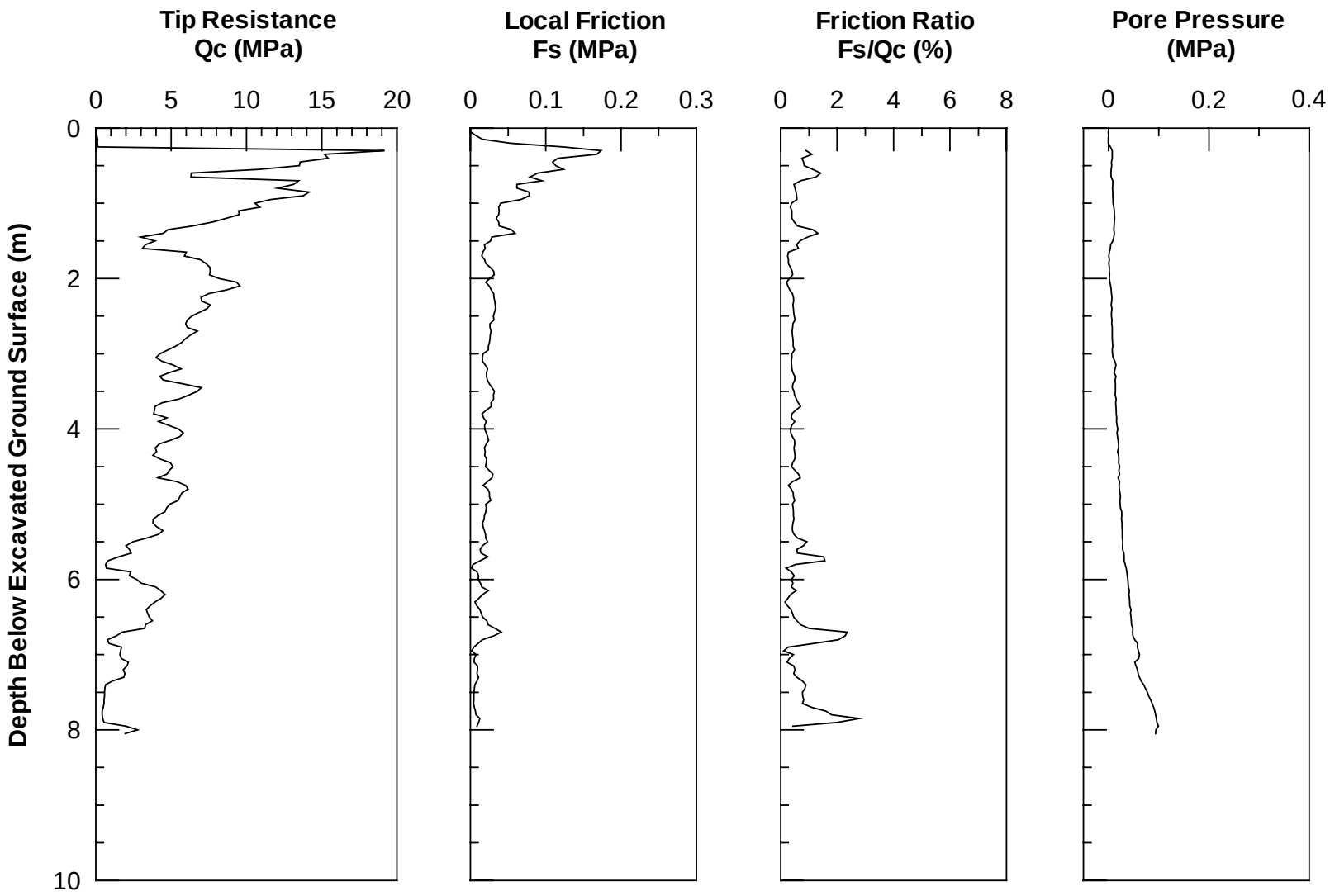

Figure 3.3 CPT1-1 Logs for Single Pile Test Area (10-30-98)

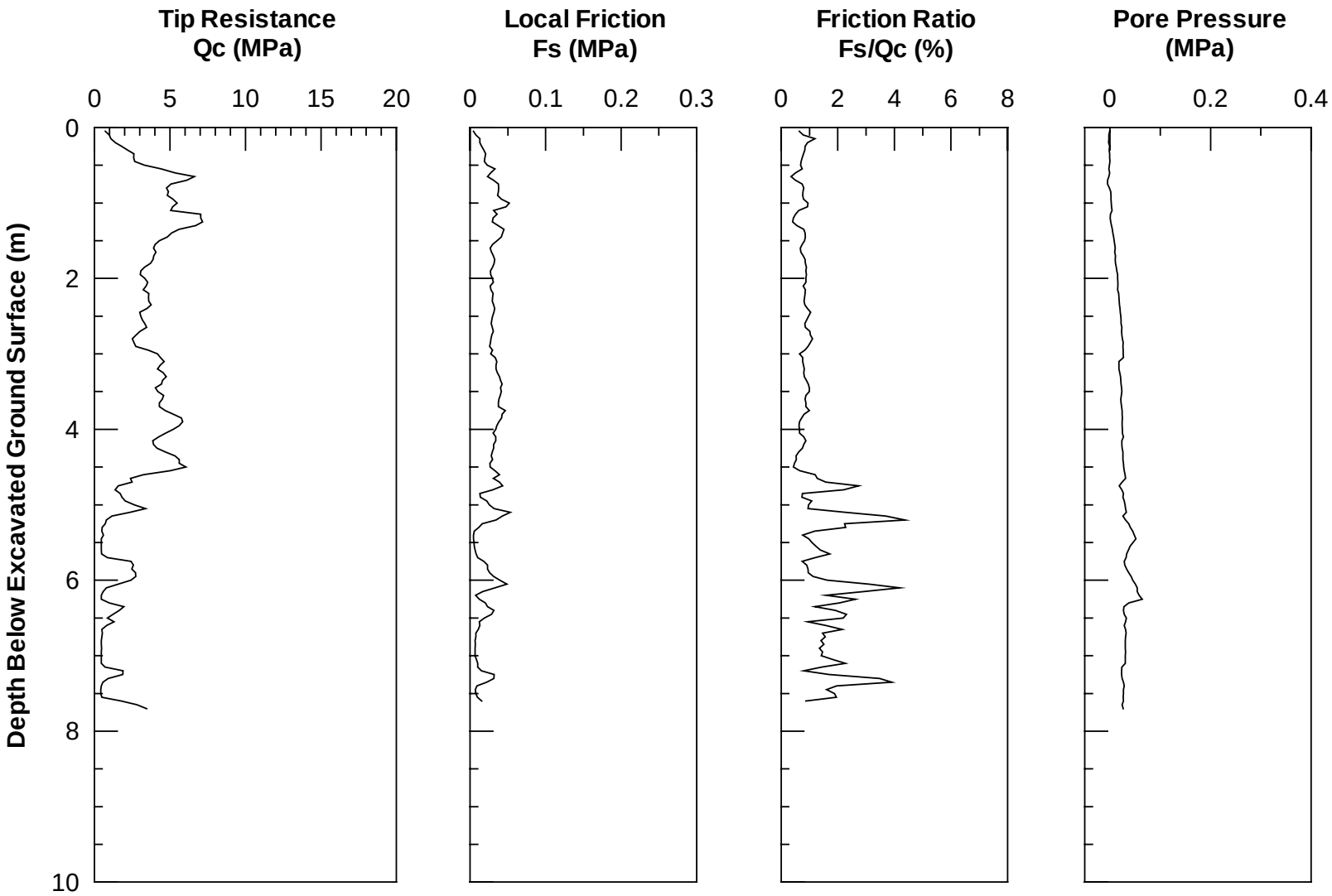

Figure 3.4 CPT1-2 Logs for Single Pile Test Area (11-06-98)

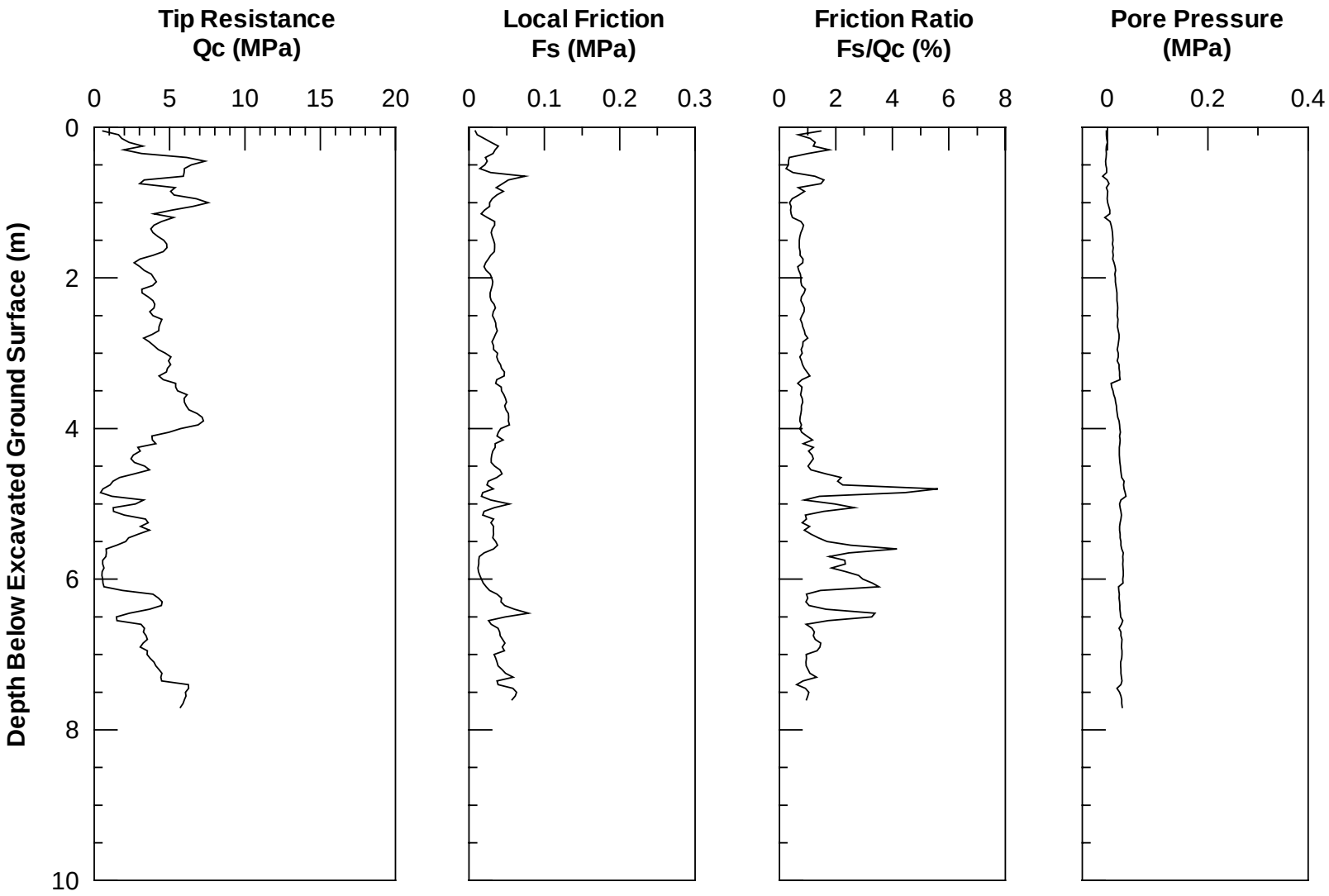

Figure 3.5 CPT1-3 Logs for Single Pile Test Area (11-06-98)

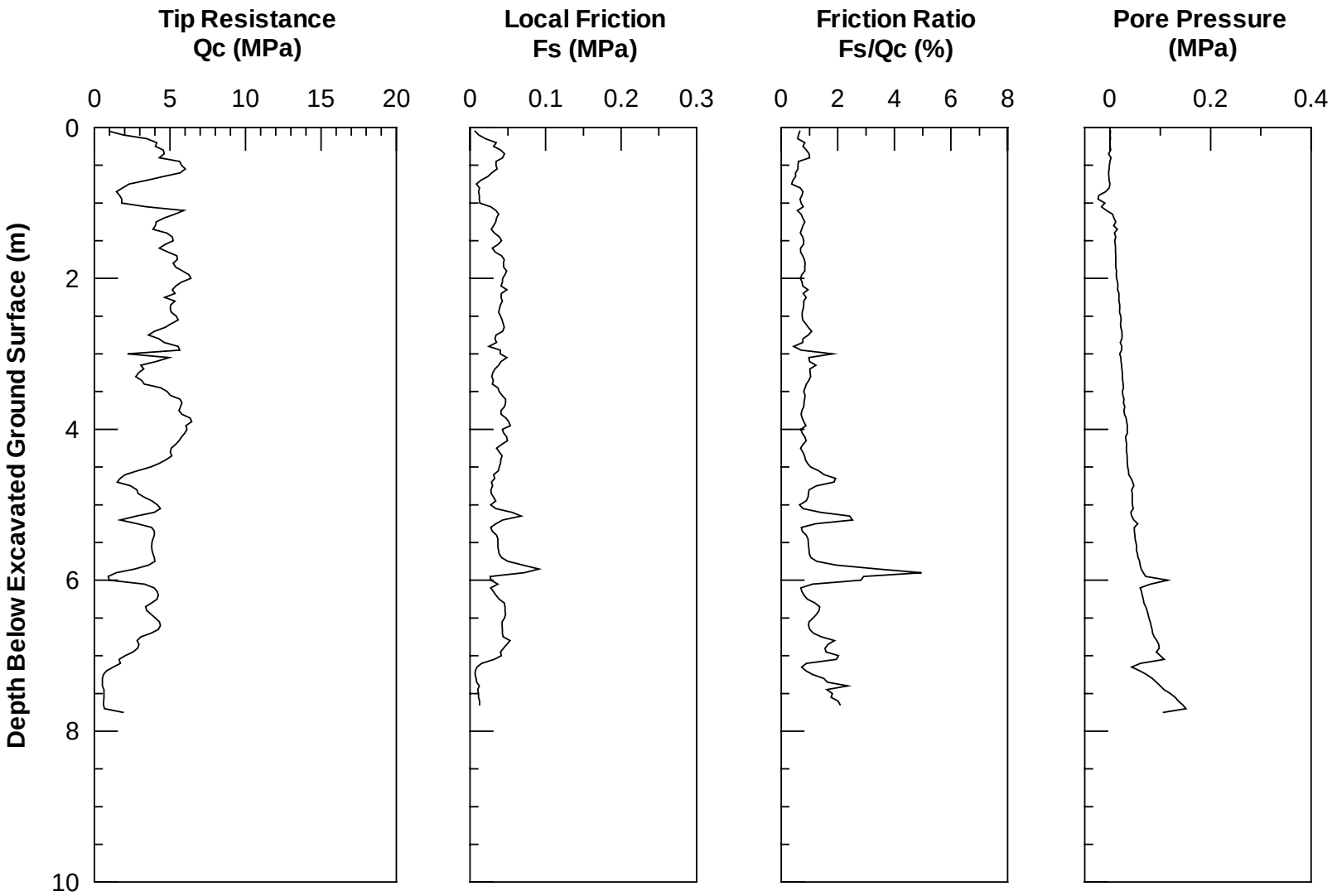

Figure 3.6 CPT1-4 Logs for Single Pile Test Area (11-06-98)

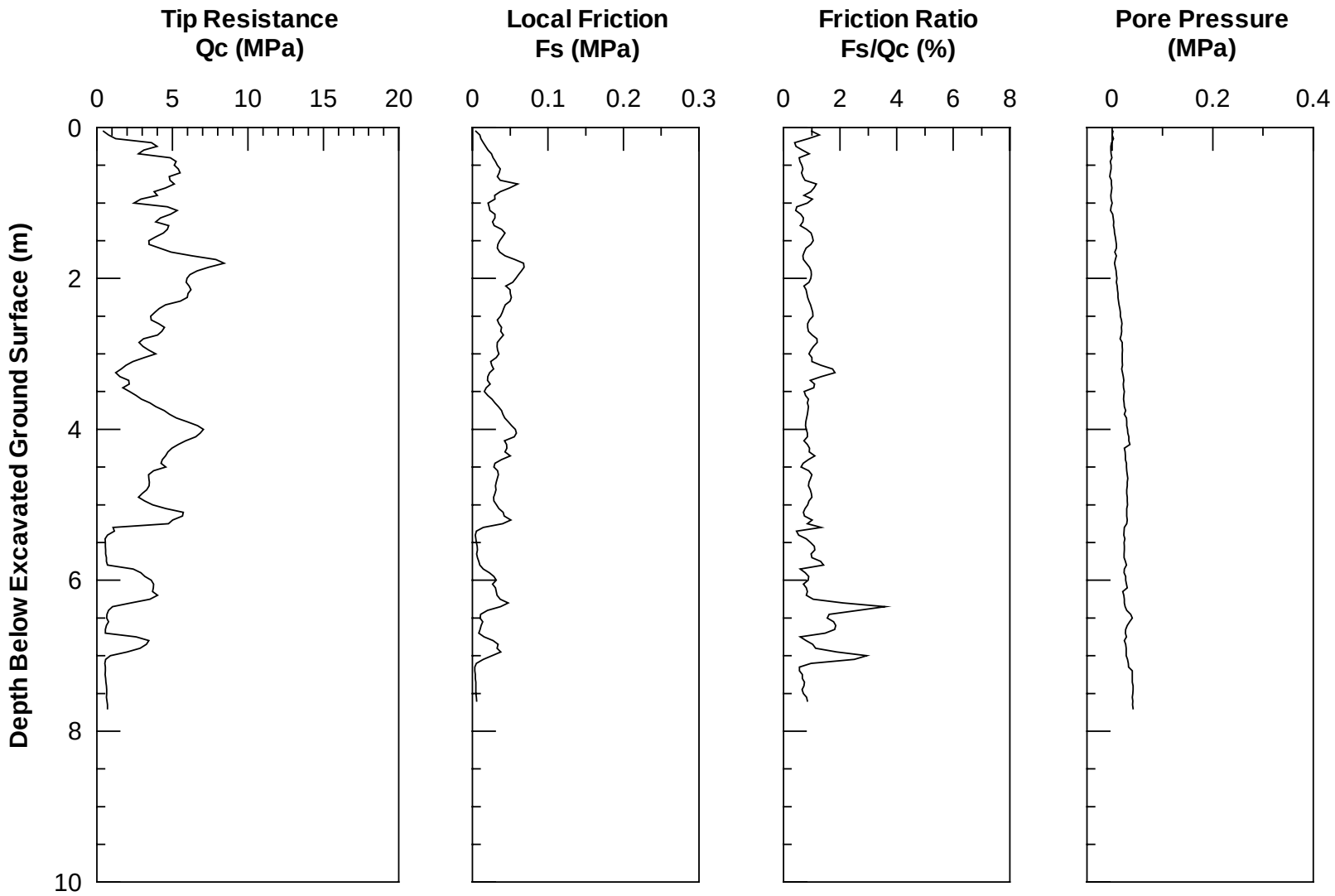

Figure 3.7 CPT1-5 Logs for Single Pile Test Area (11-06-98)

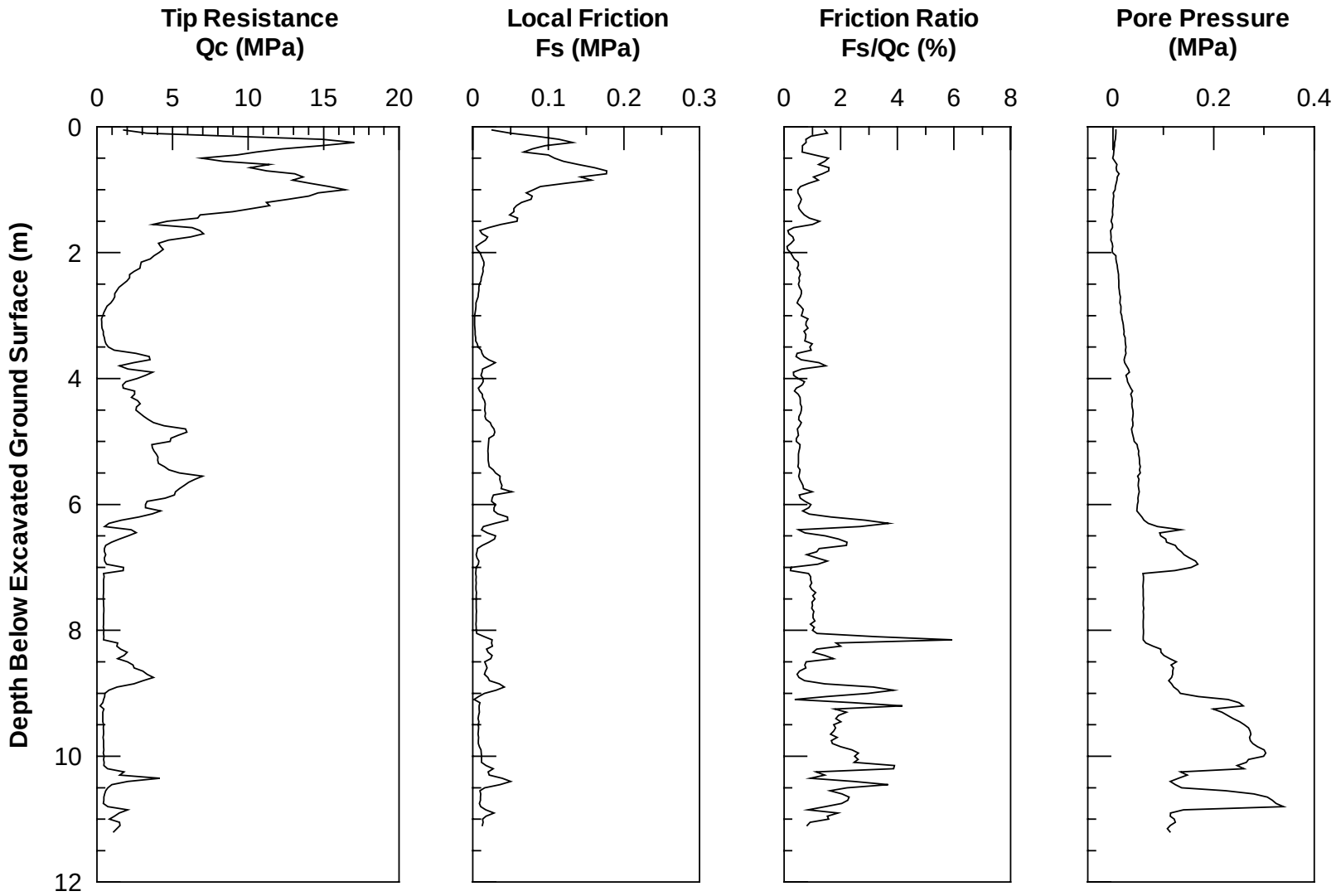

Figure 3.8 CPT1-6 Logs for Single Pile Test Area (10 -30-98)

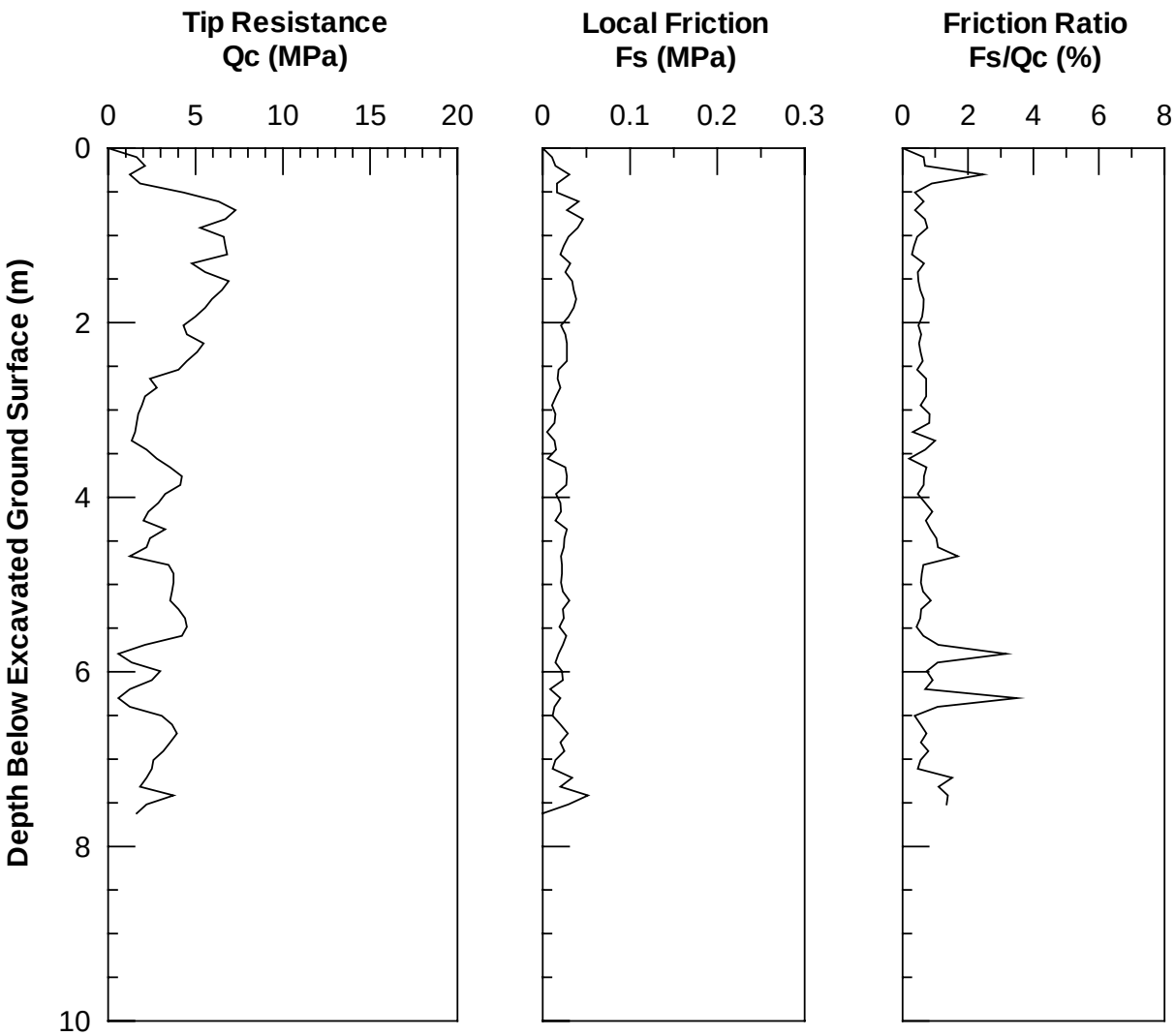

Figure 3.9 CPT RBG1 Logs for Single Pile Test Area (2-05-99)

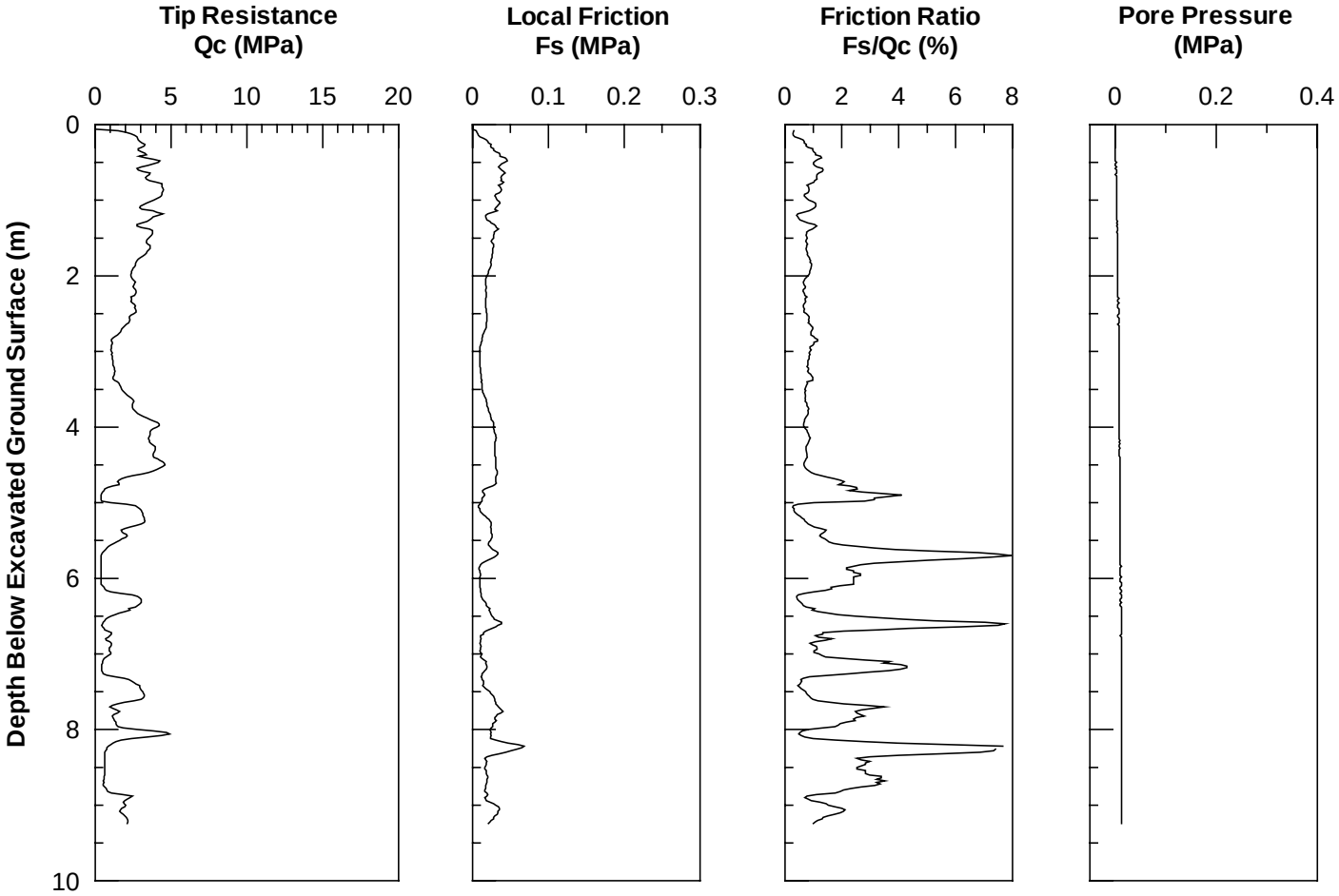

Figure 3.10 CPT S-1 Logs for Single Pile Test Area (2-17-99)

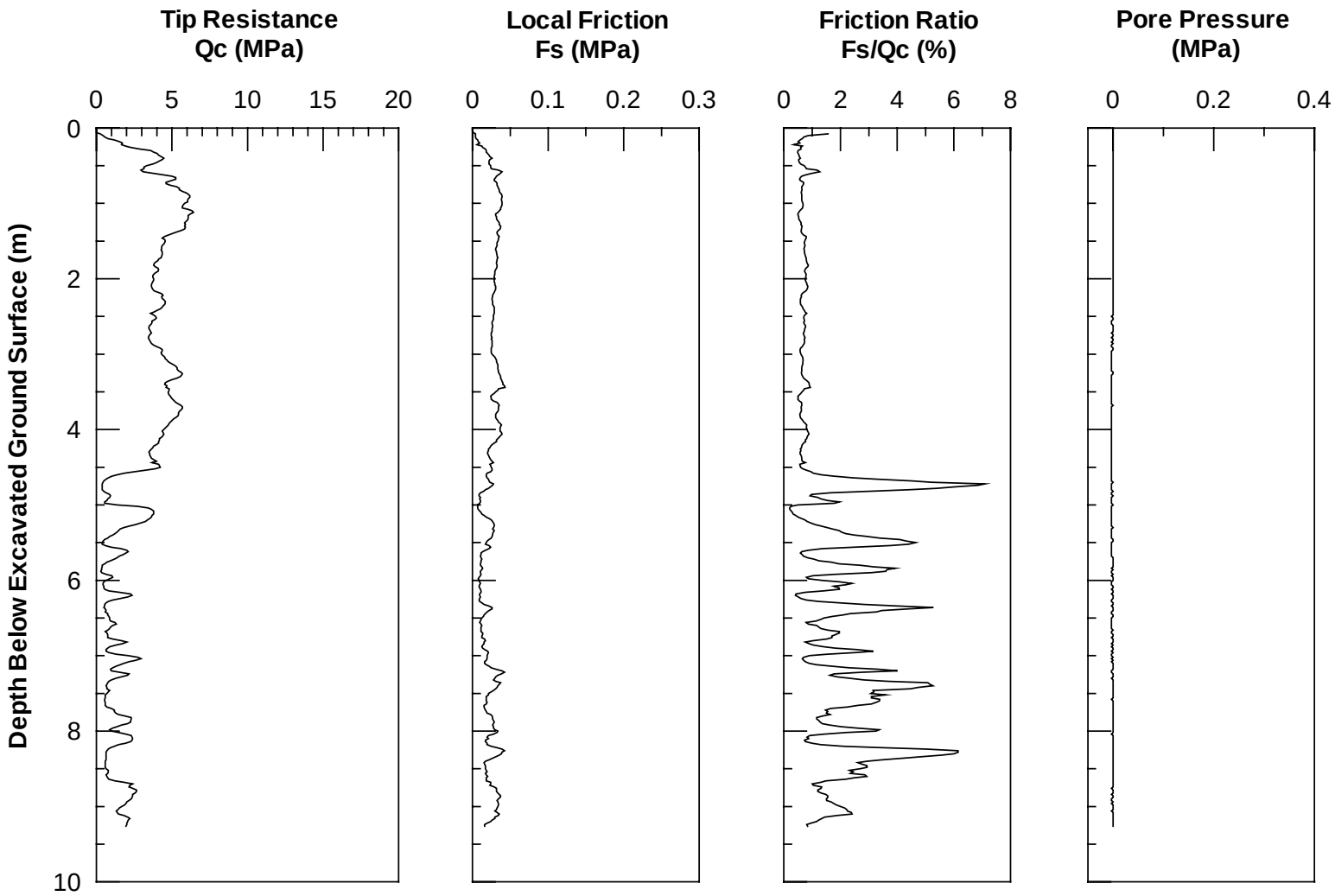

Figure 3.11 CPT S-2 Logs for Single Pile Test Area (2-17-99)

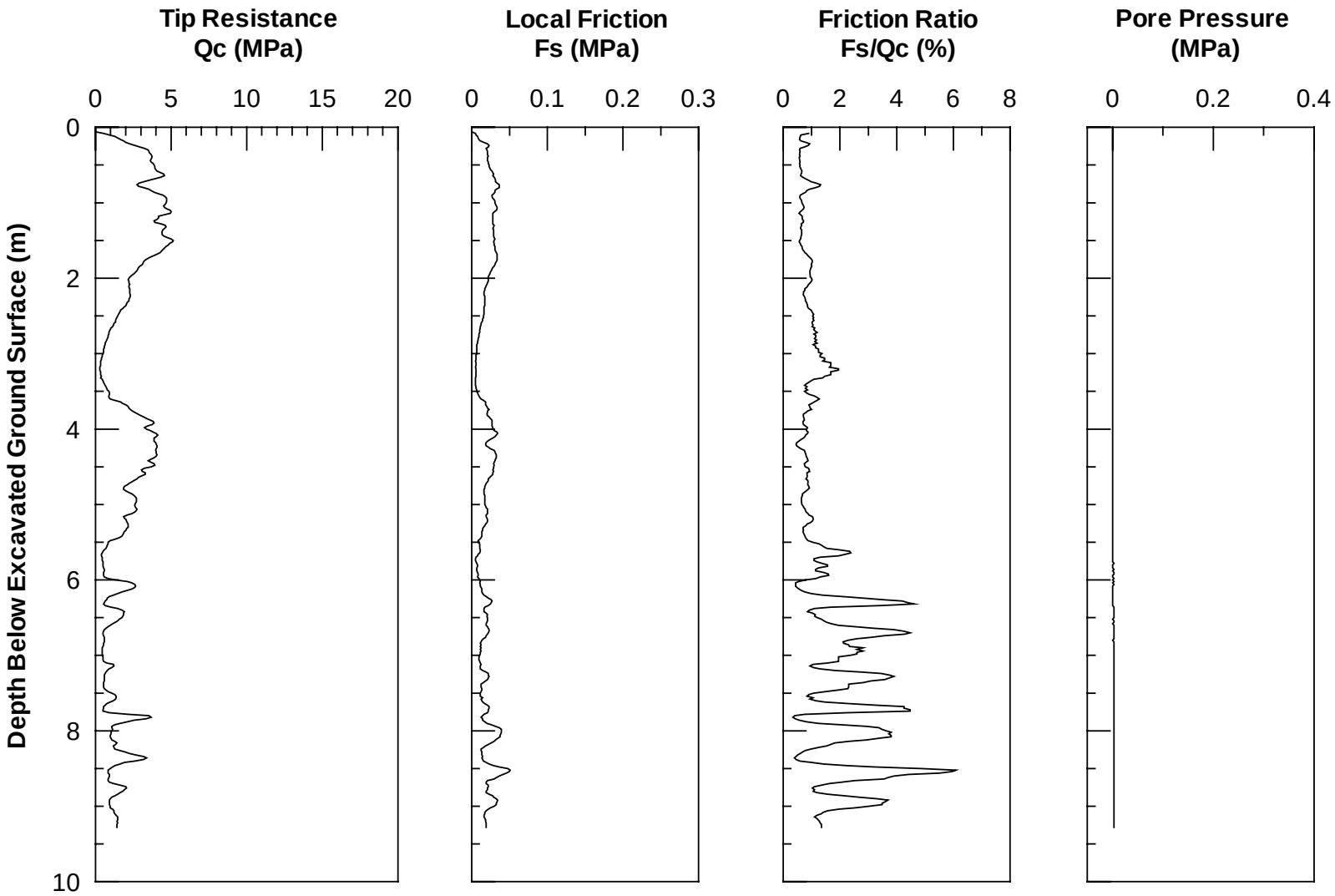

Figure 3.12 CPT S-3 Logs for Single Pile Test Area (2-17-99)

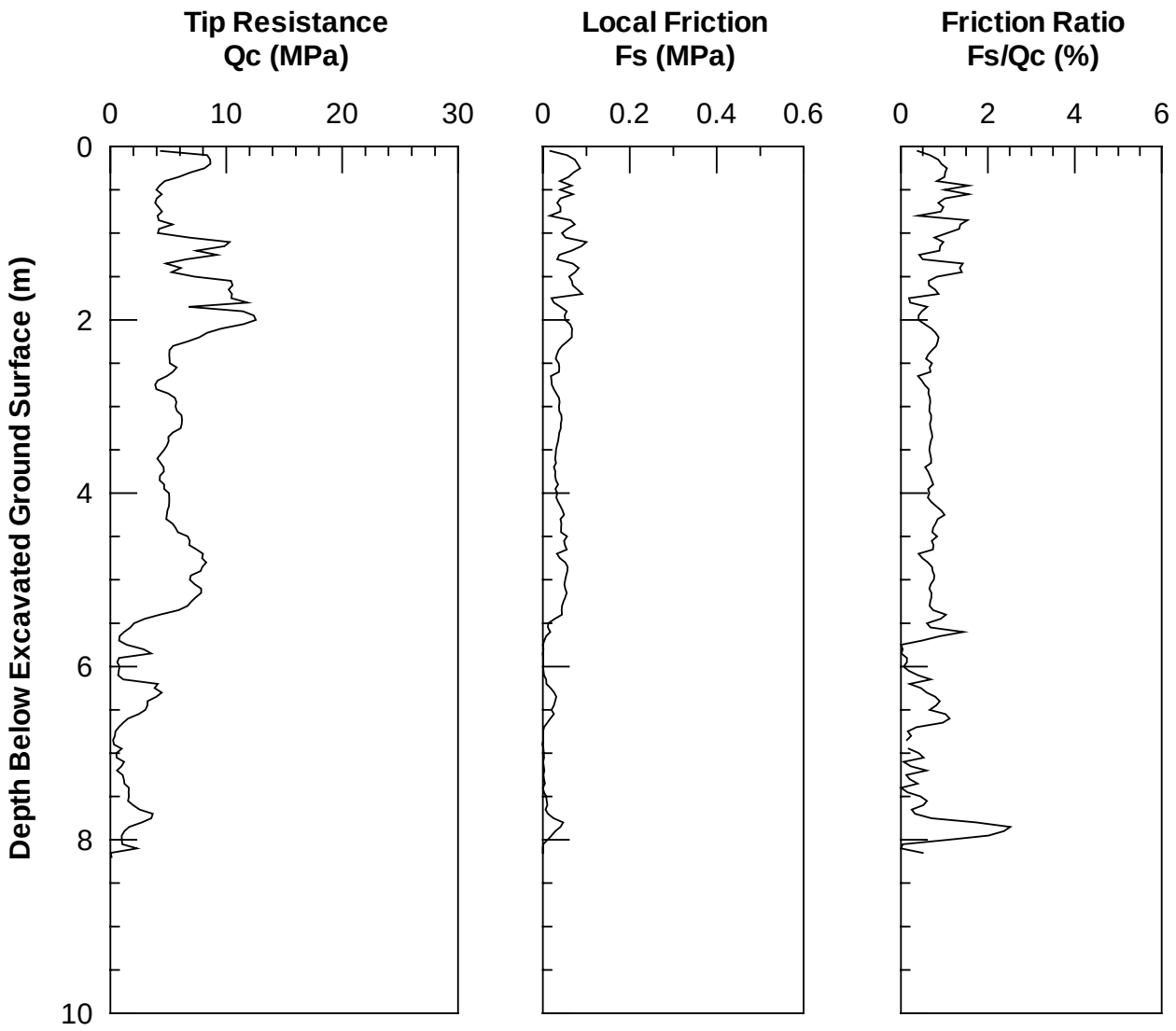

Figure 3.13 CPT SFC006 Logs for Single Pile Test Area (6-24-99)

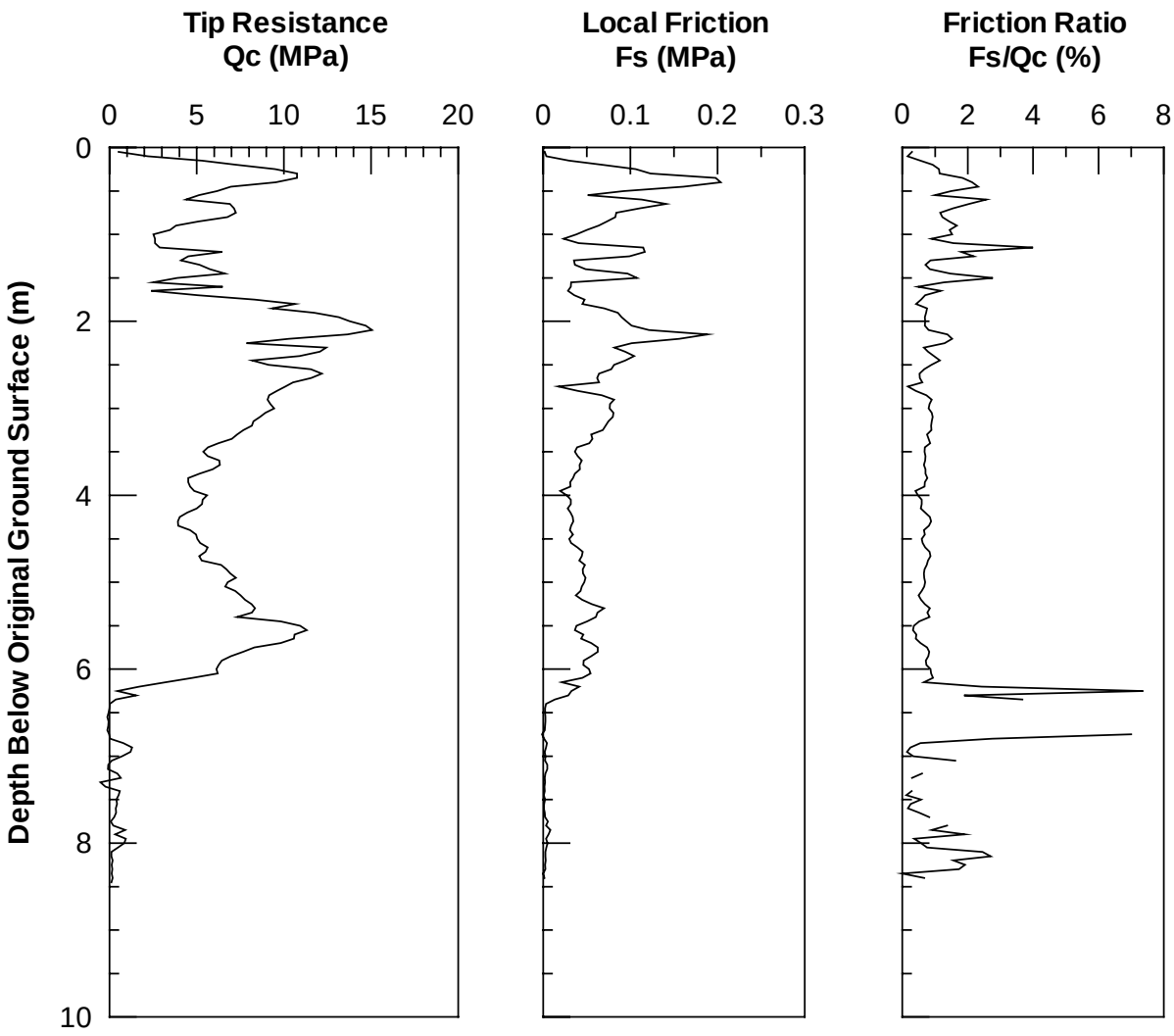

Figure 3.14 CPT SFC007 Logs for Single Pile Test Area (6-24-99)

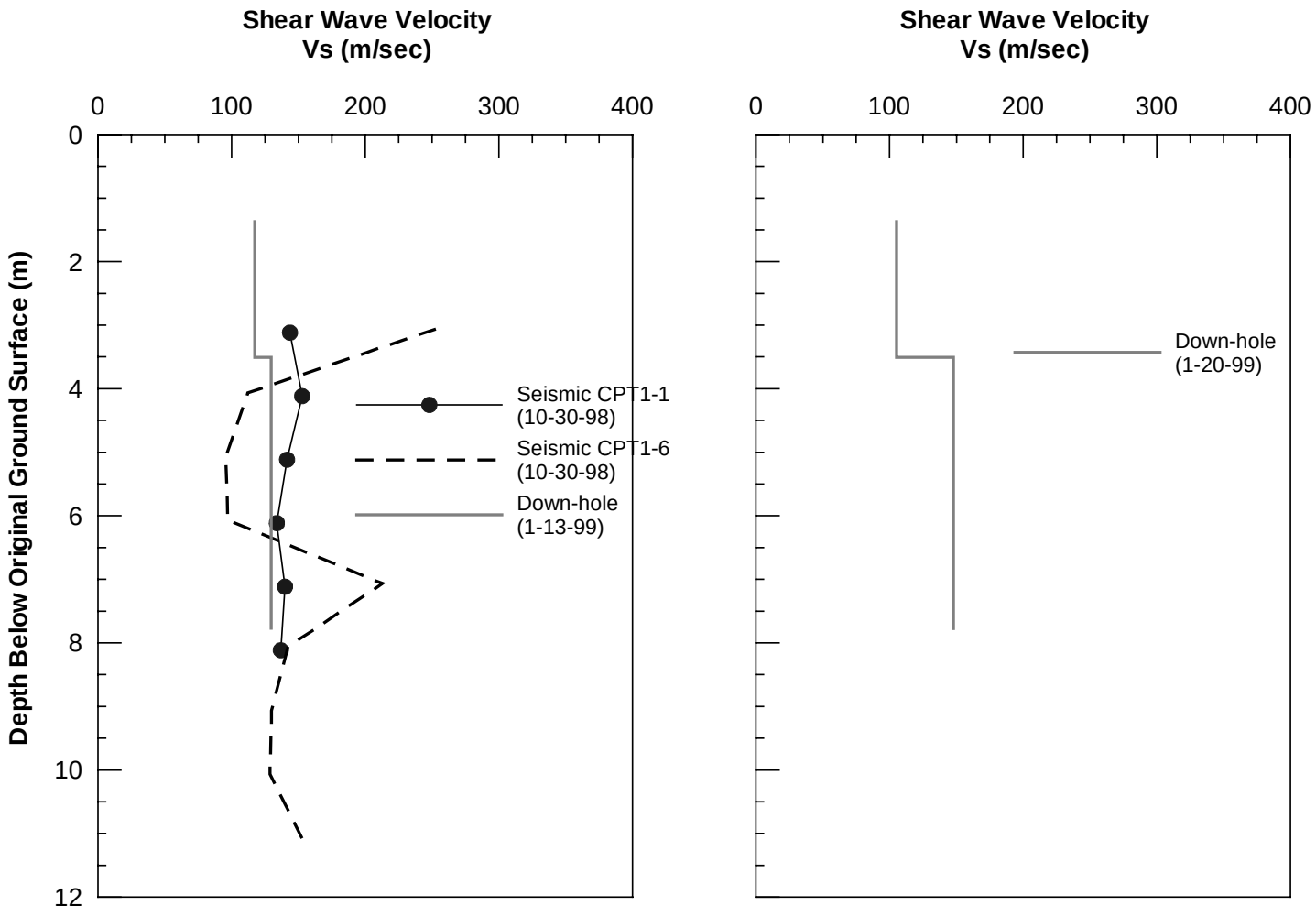

Figure 3.15 Shear Wave Velocity at Single Pile Test Area a) Pre-Blast Velocity b) Post 1st Blast Velocity

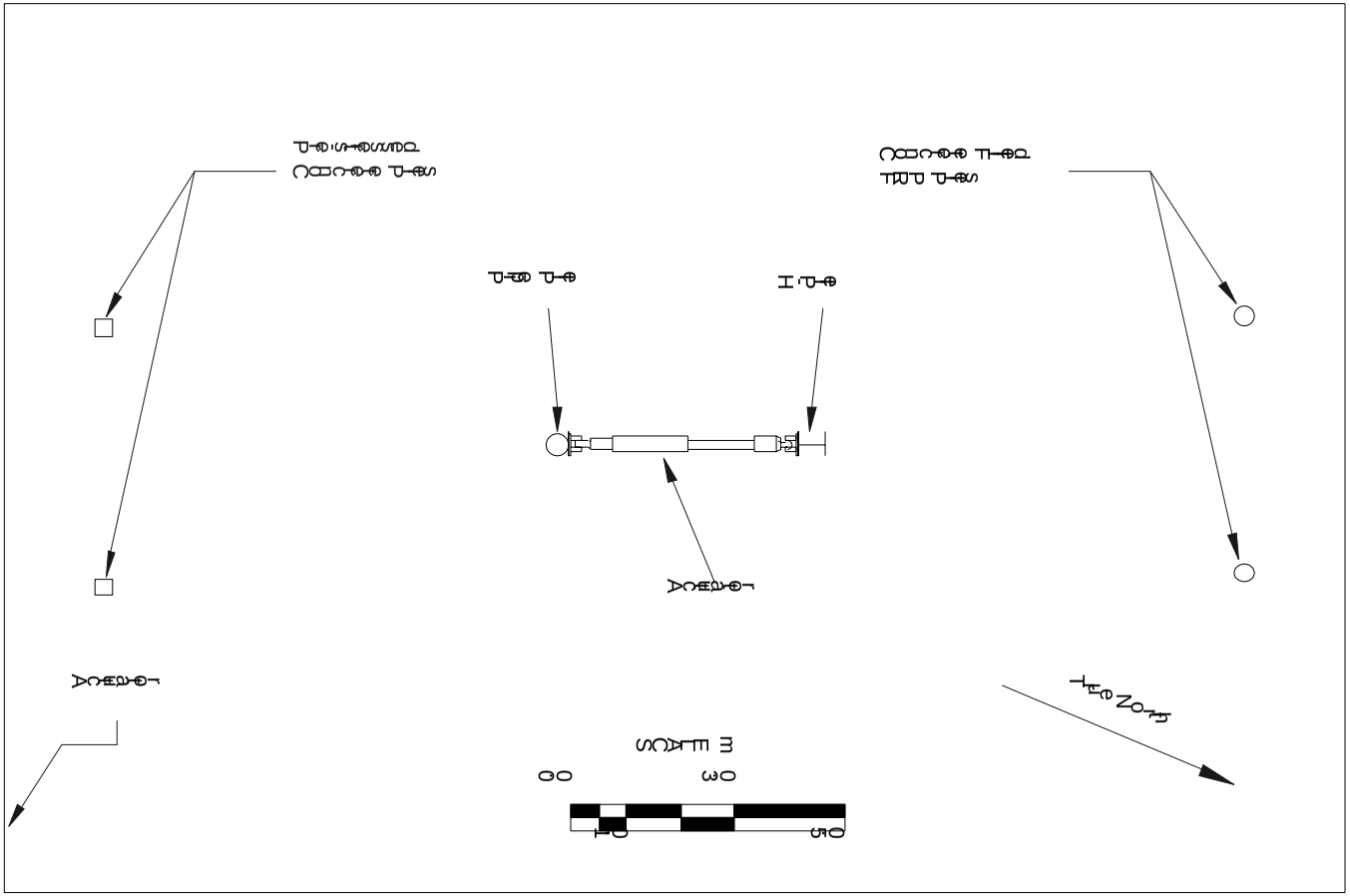

Figure 3.16 Plan View of Single Pilt Test Set-Up

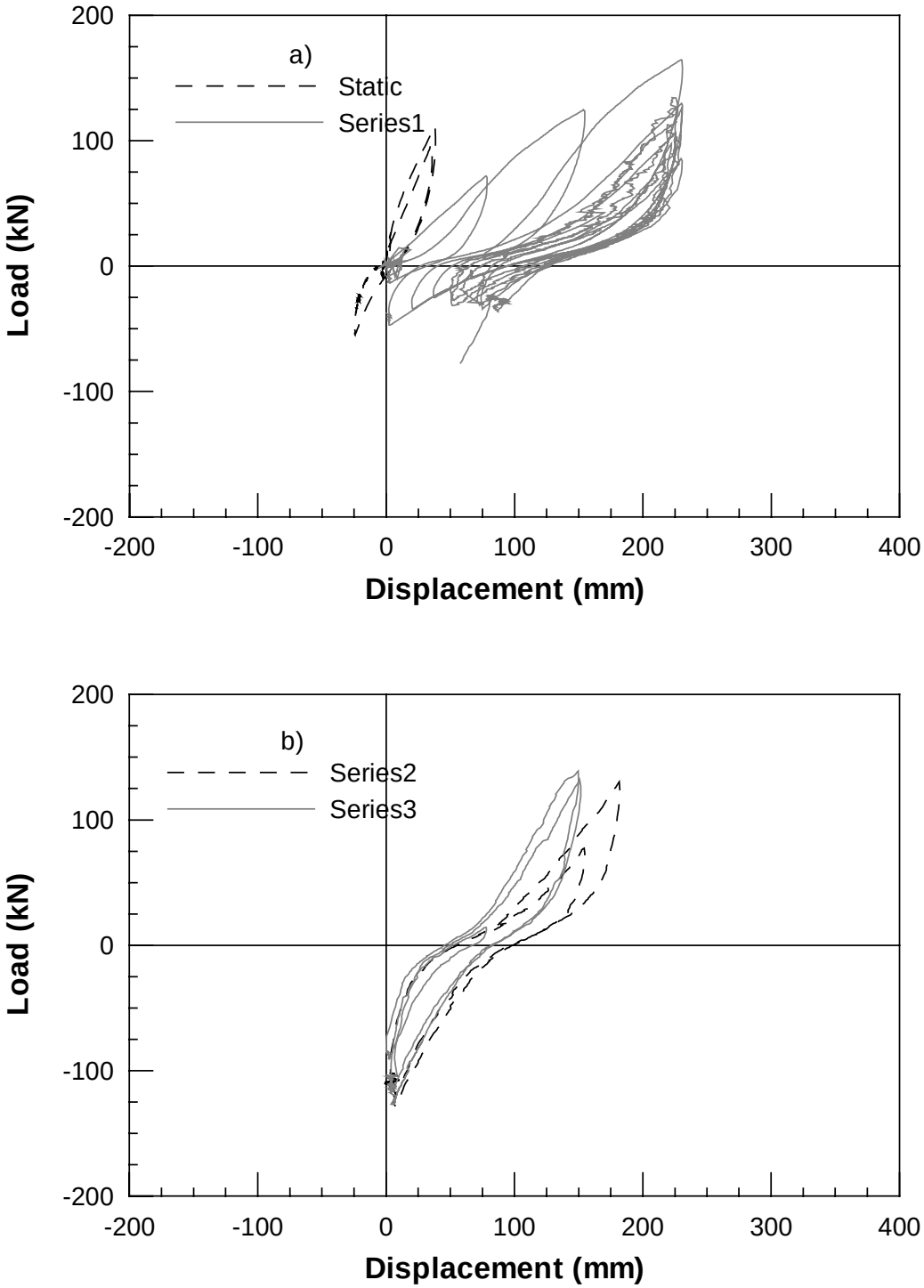

Figure 3.17 Load vs Displacement for Single Pipe Pile 1st Blast a) Static and Post Blast Series 1 b) Post Blast Series 2 and 3

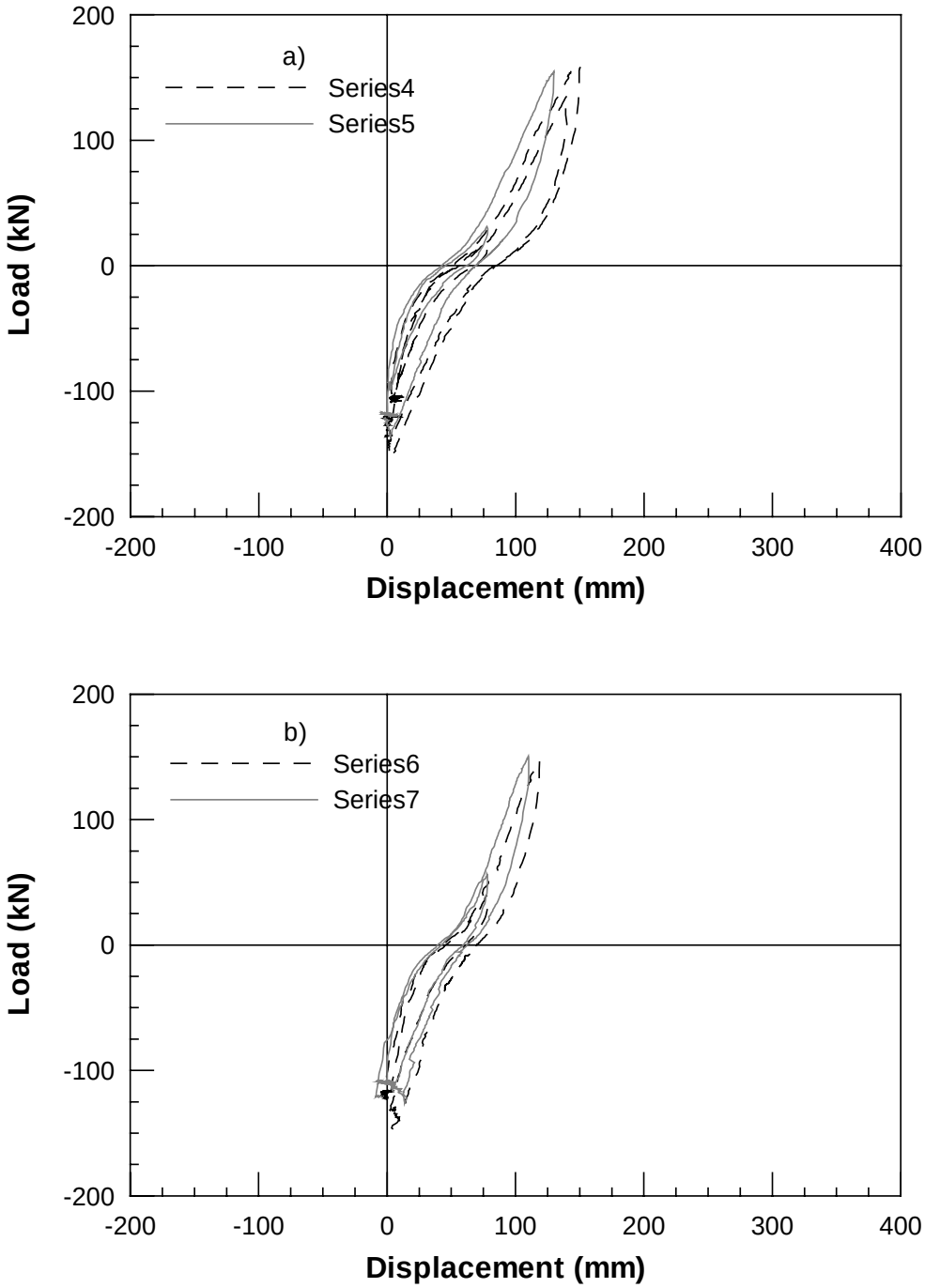

Figure 3.18 Load vs Displacement for Single Pipe Pile 1st Blast a) Post Blast Series 4 and 5 b) Post Blast Series 6 and 7

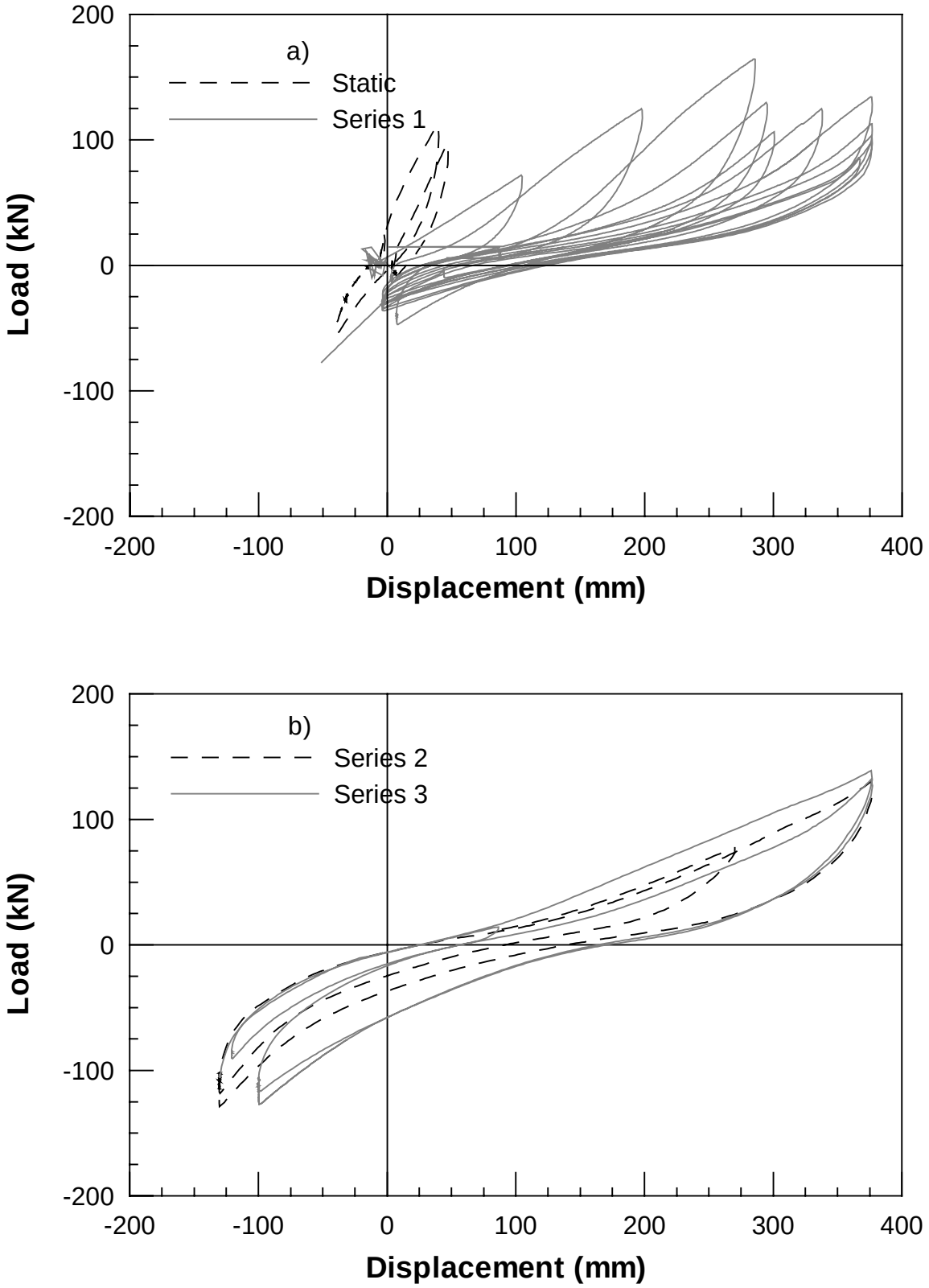

Figure 3.19 Load vs Displacement for H-Pile 1st Blast a) Static and Post Blast Series 1 b) Post Blast Series 2 and 3

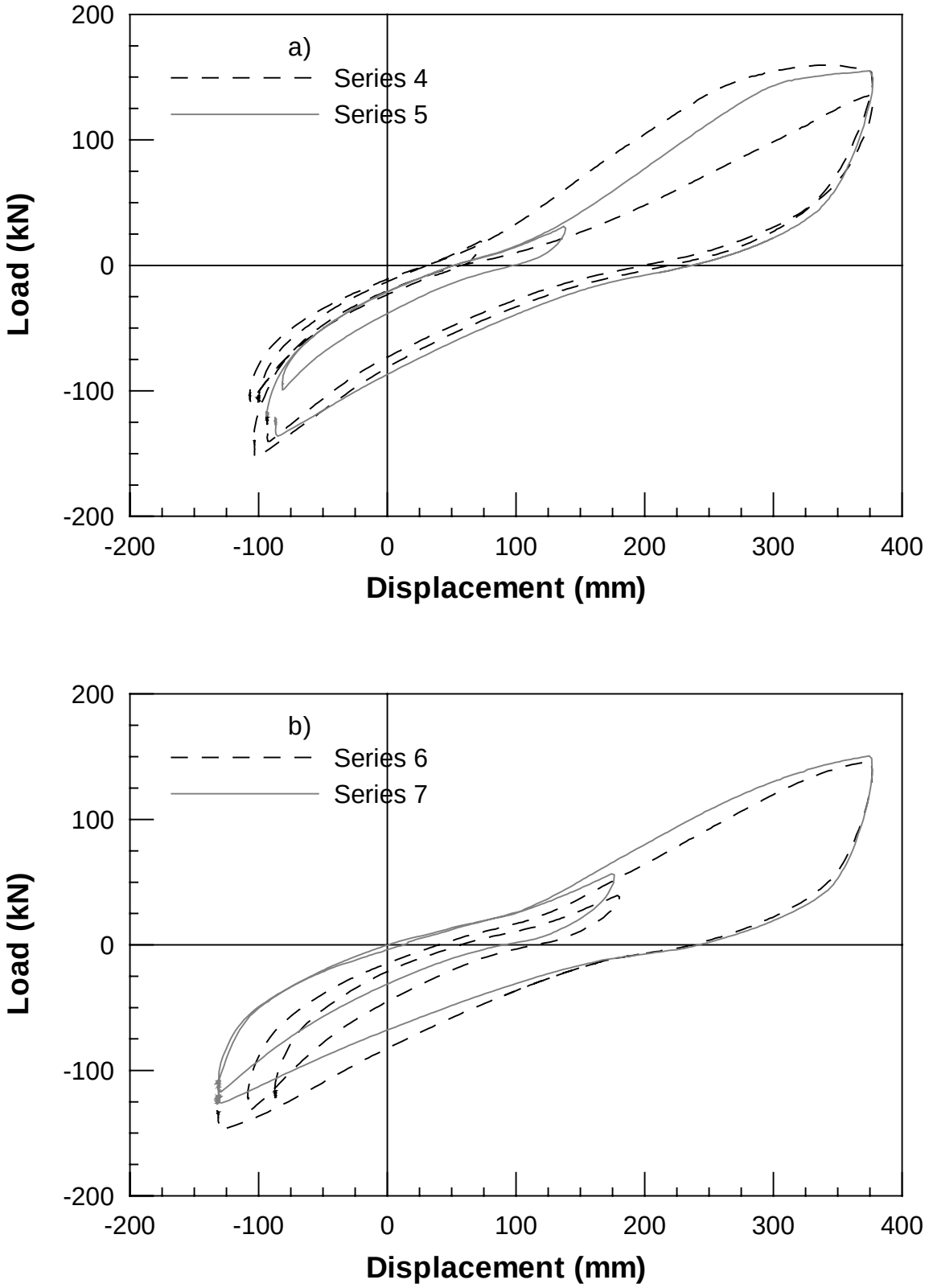

Figure 3.20 Load vs Displacement for H-Pile 1st Blast a) Post Blast Series 4 and 5 b) Post Blast Series 6 and 7

PPT	Depth
01	3.25m
02	3.25m
03	5.08m
04	5.08m
06	1.42m
10	2.34m
16	1.42m
24	1.42m
38	3.25m
39	2.34m
44	4.17m
47	4.17m
54	2.34m
55	3.25m
57	3.25m
87	3.25m
89	1.42m
90	6.00m
92	3.25m
93	2.34m
94	4.17m
95	3.25m
96	2.34m
97	4.17m
98	6.00m
99	3.25m

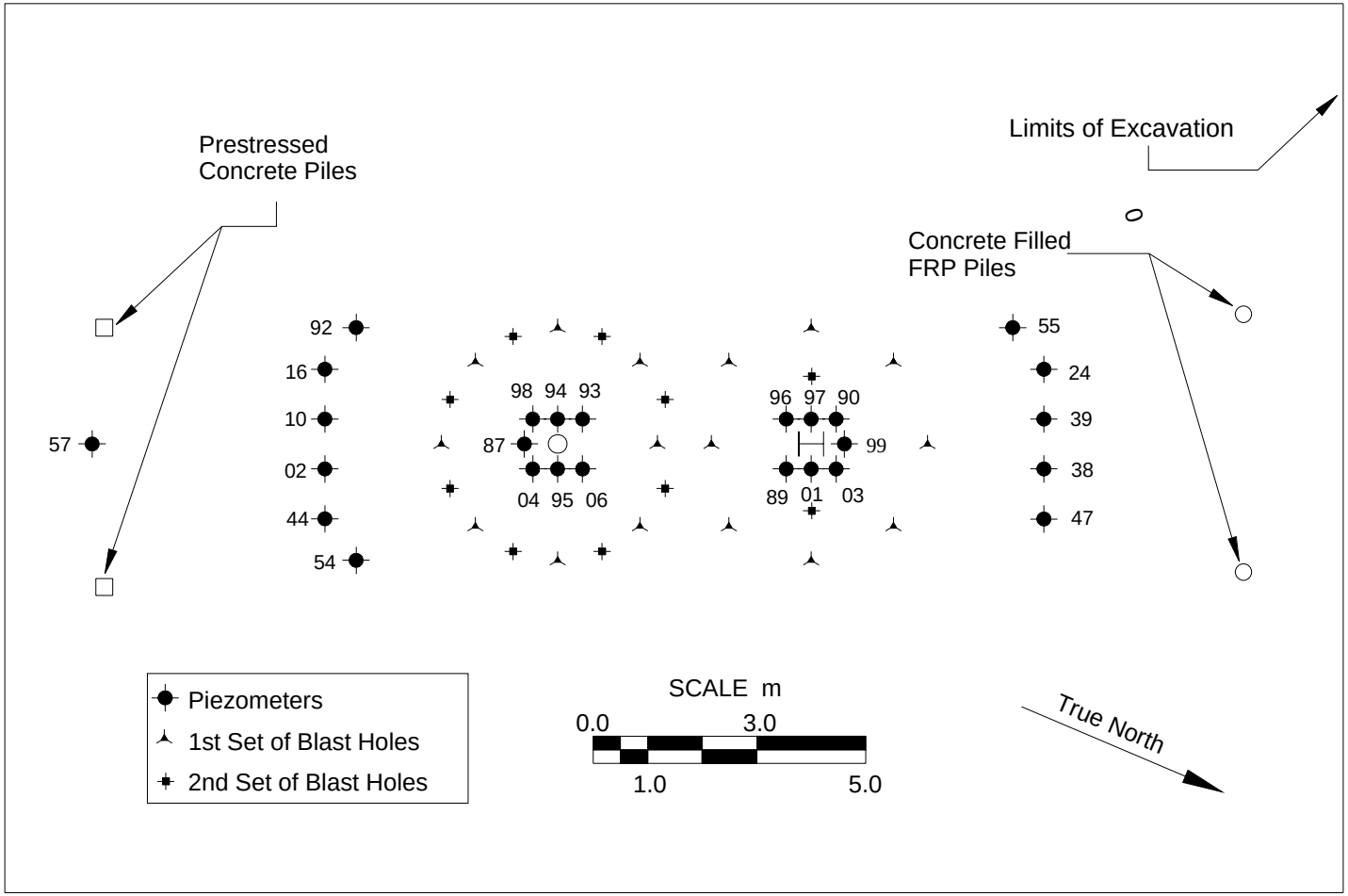

Figure 3.21 Location of Pore Pressure Transducers and Explosives for Single Pile Test

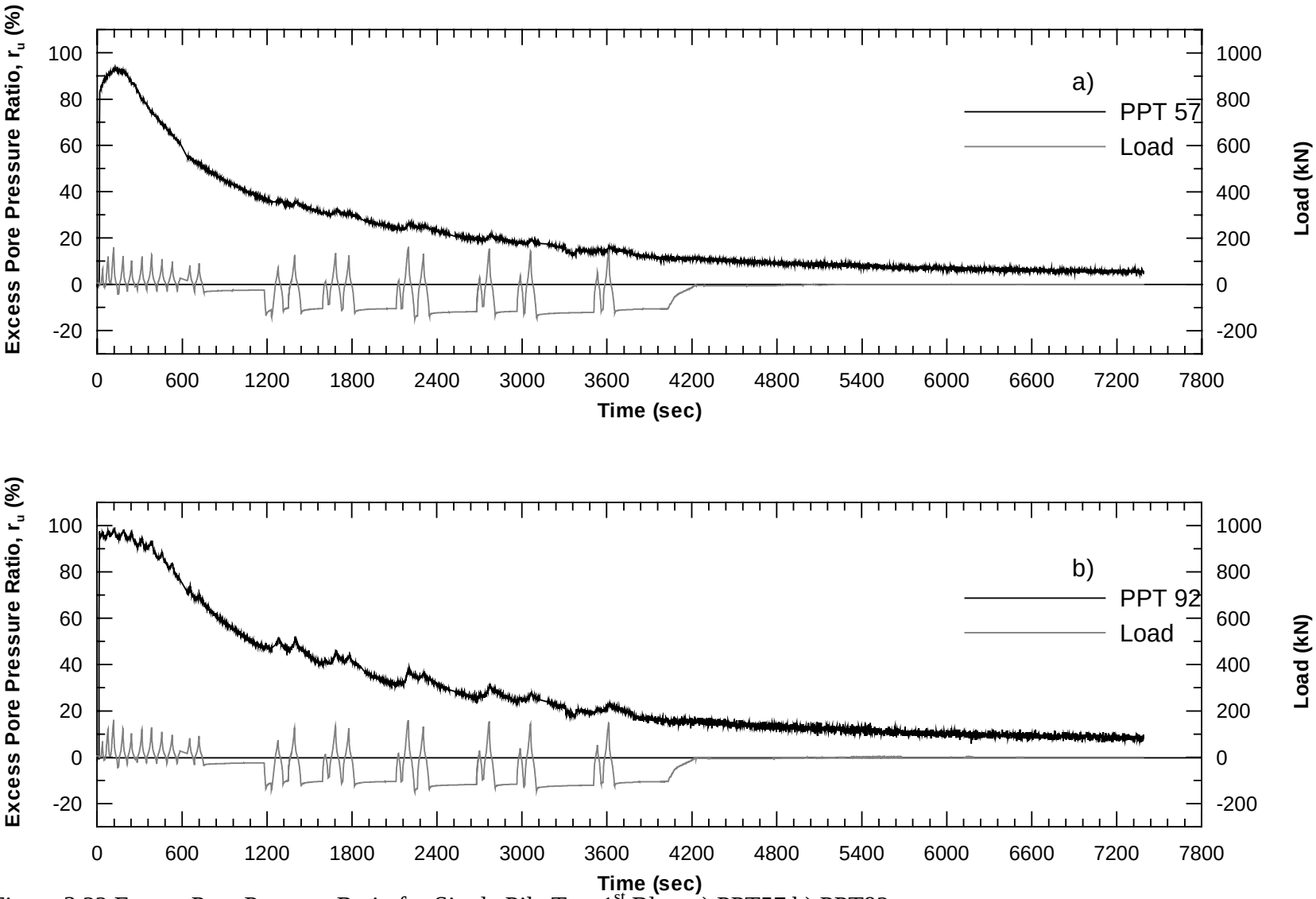

Figure 3.22 Excess Pore Pressure Ratio for Single Pile Test 1st Blast a) PPT57 b) PPT92

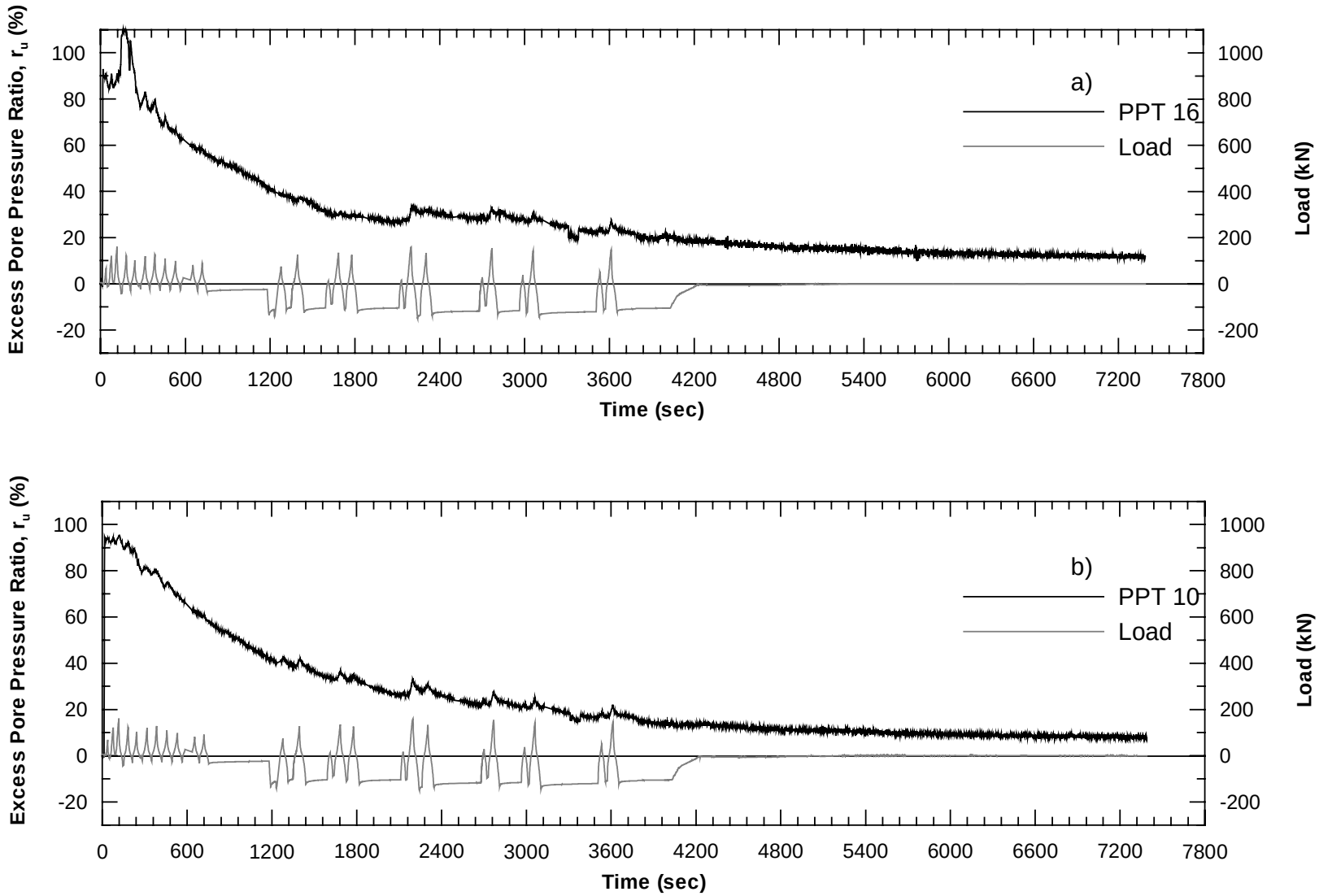

Figure 3.23 Excess Pore Pressure Ratio for Single Pile Test 1st Blast a) PPT16 b) PPT10

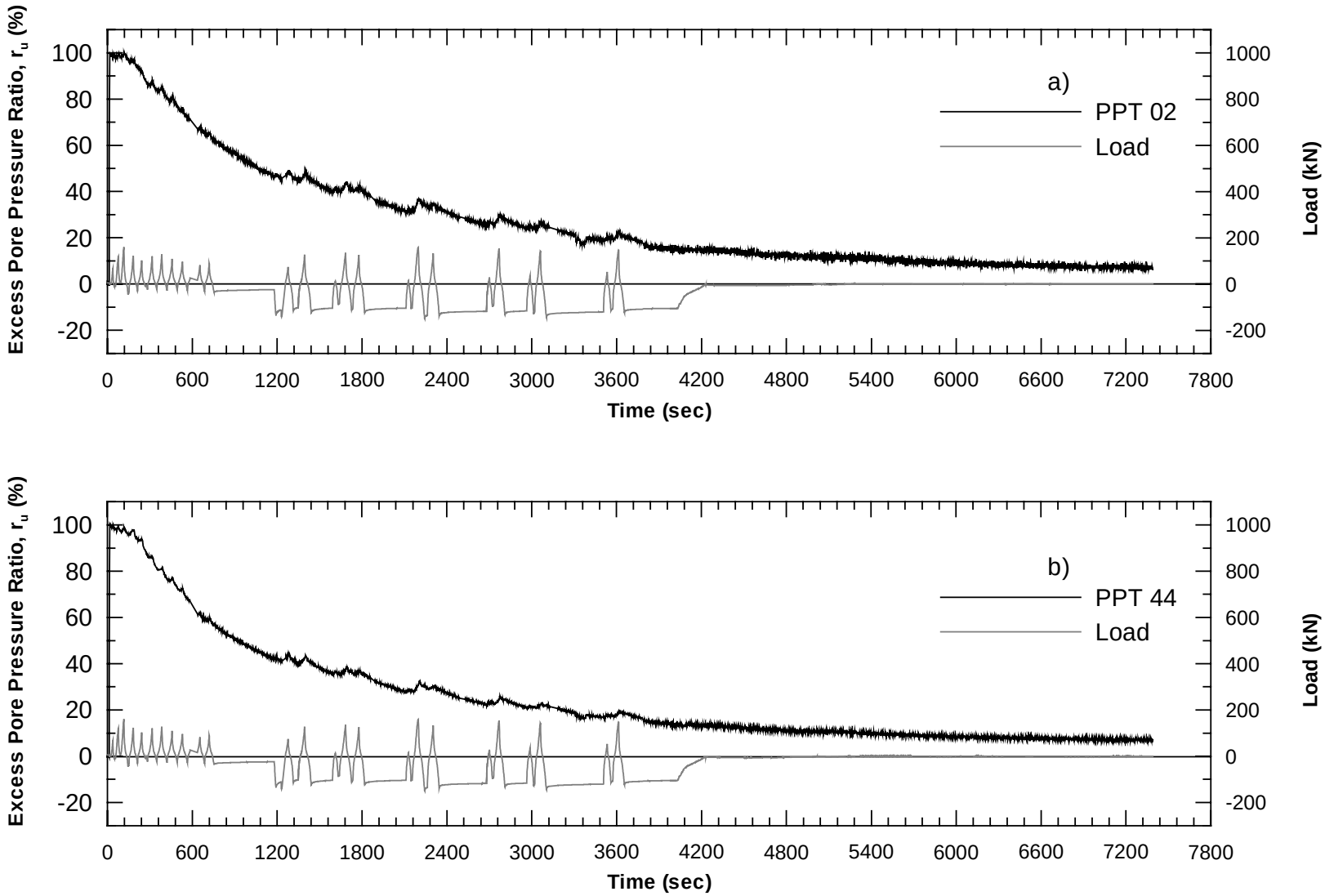

Figure 3.24 Excess Pore Pressure Ratio for Single Pile Test 1st Blast a) PPT02 b) PPT44

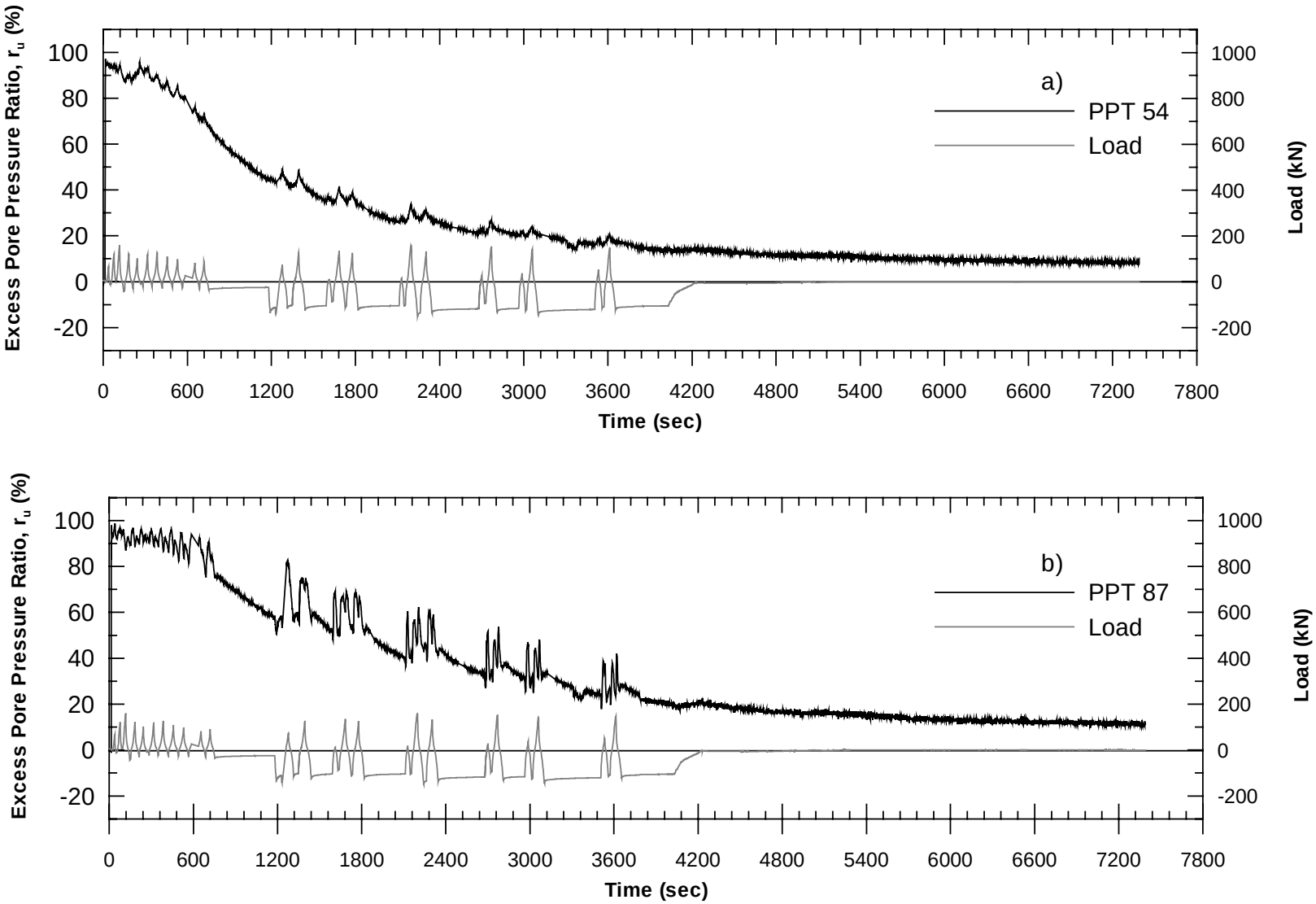

Figure 3.25 Excess Pore Pressure Ratio for Single Pile Test 1st Blast a) PPT54 b) PPT87

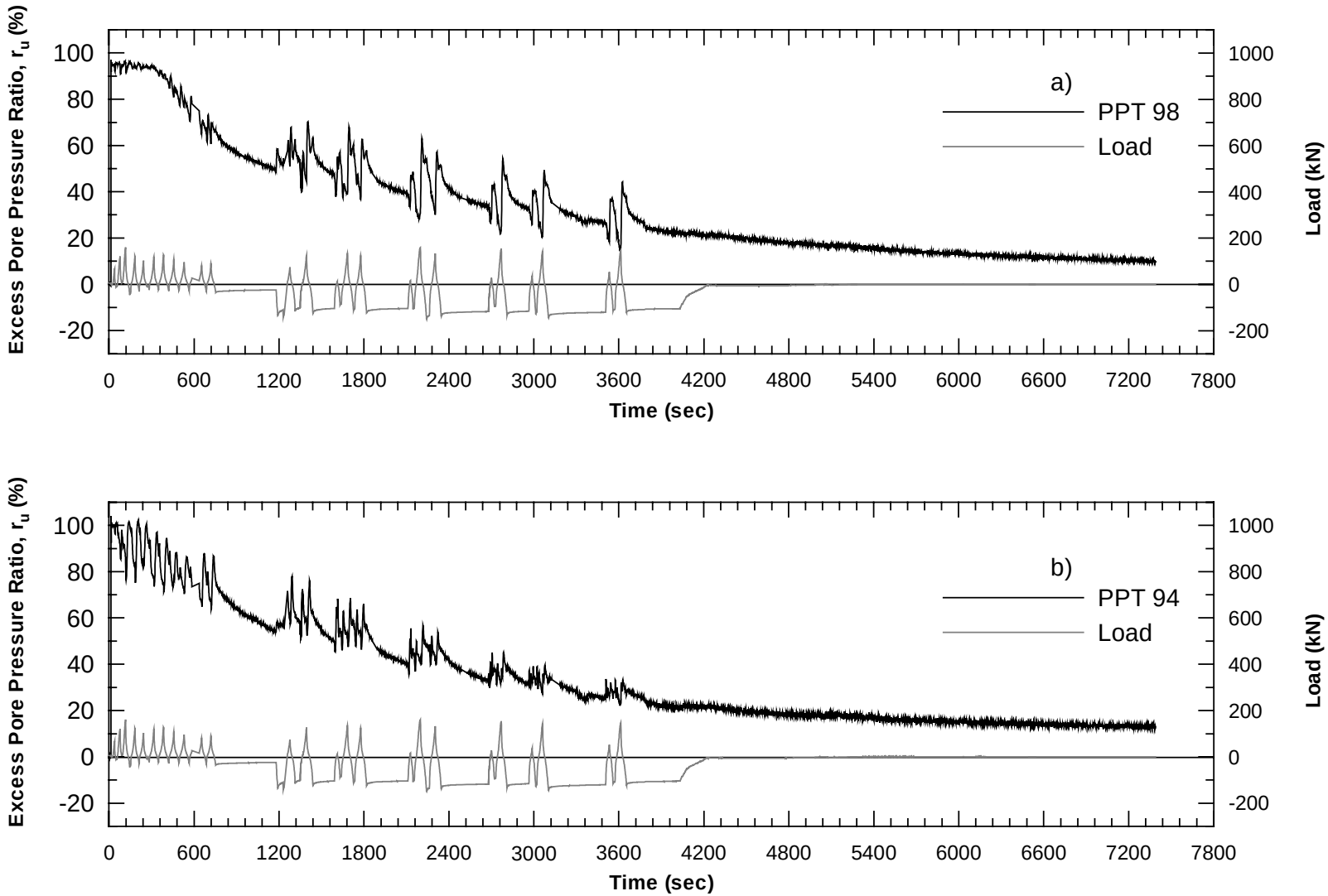

Figure 3.26 Excess Pore Pressure Ratio for Single Pile Test 1st Blast a) PPT98 b) PPT94

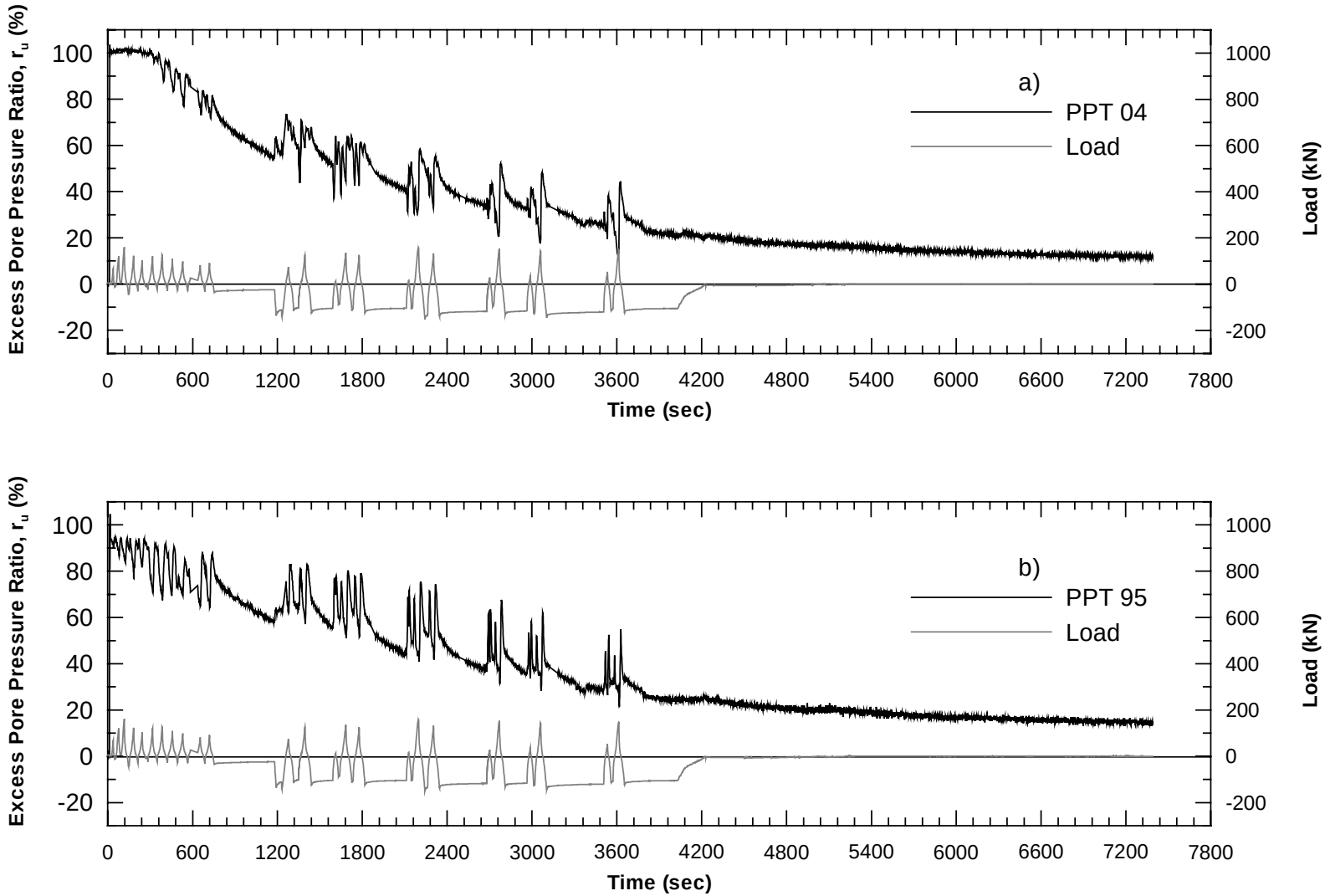

Figure 3.27 Excess Pore Pressure Ratio for Single Pile Test 1st Blast a)PPT04 b)PPT95

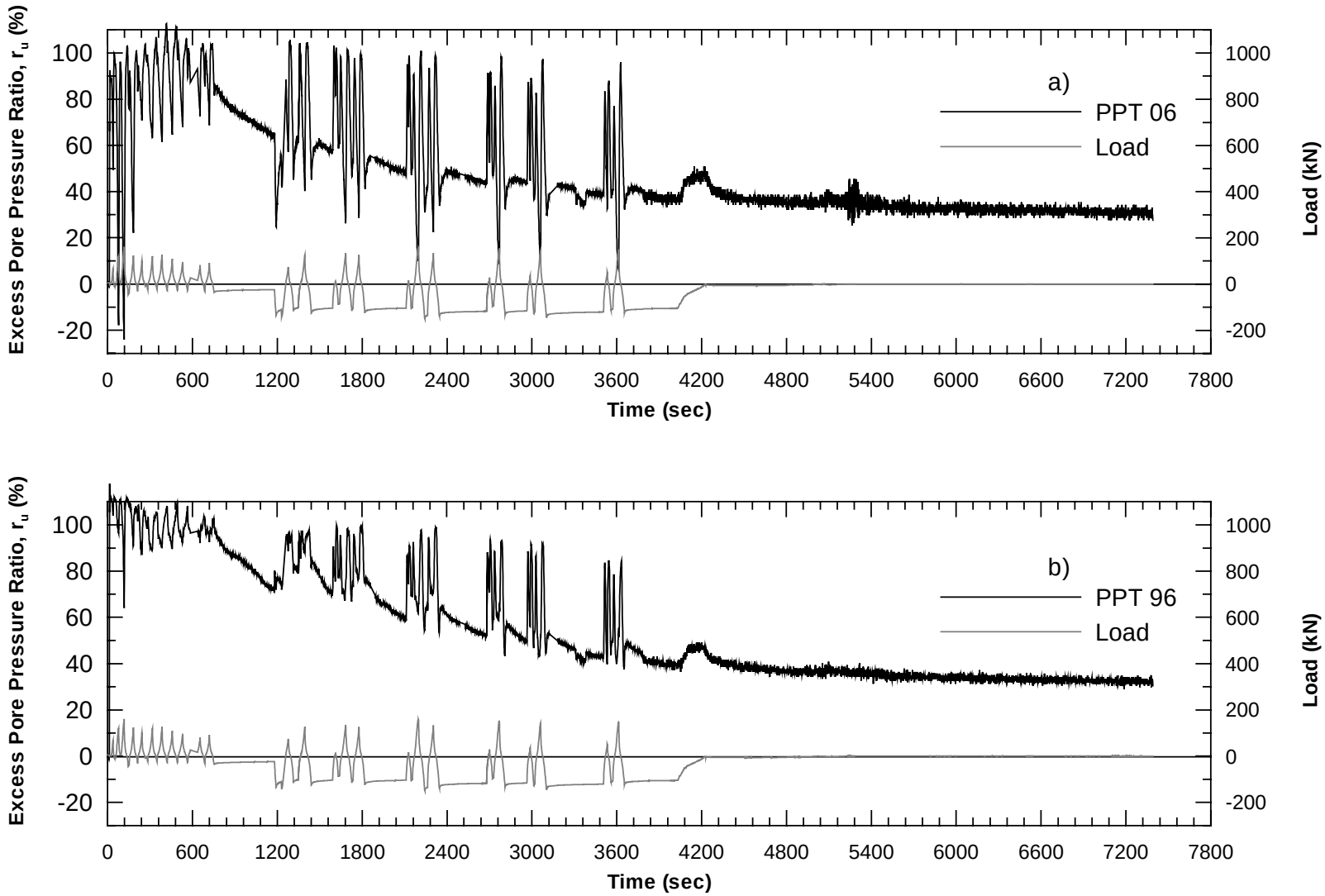

Figure 3.28 Excess Pore Pressure Ratio for Single Pipe Test 1st Blast a) PPT06 b) PPT96

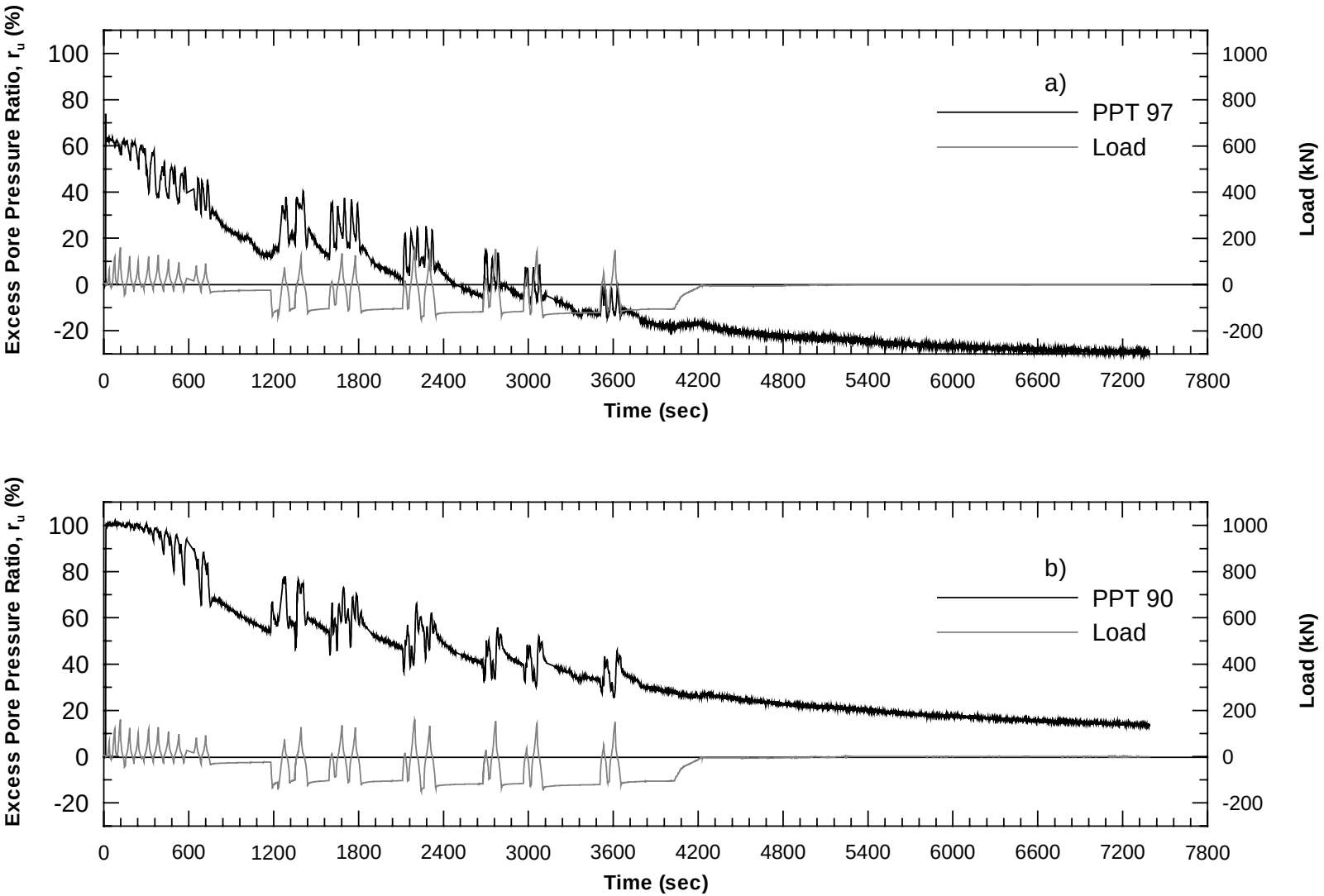

Figure 3.29 Excess Pore Pressure Ratio for Single Pile Test 1st Blast a) PPT97 b)PPT90

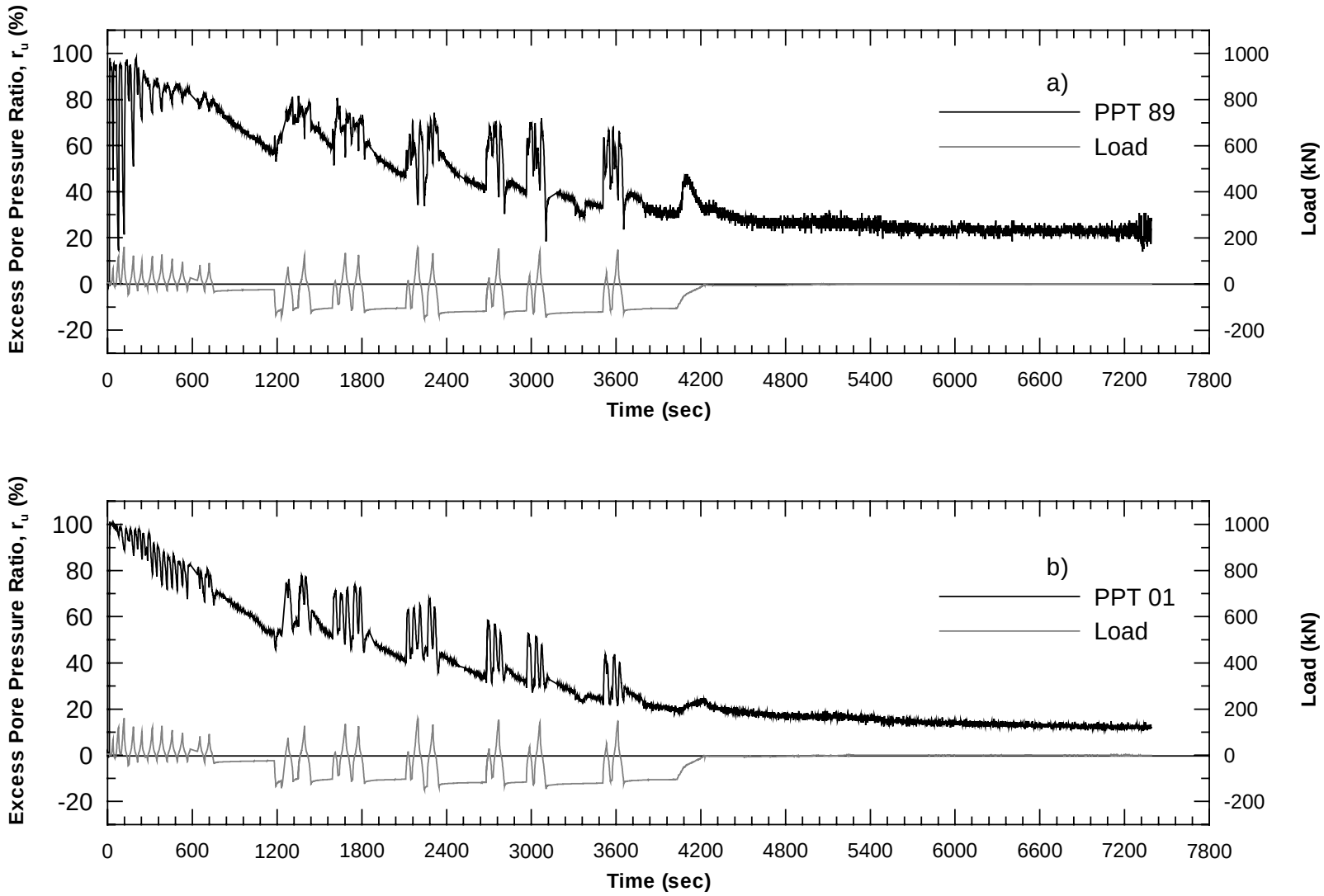

Figure 3.30 Excess Pore Pressure Ratio for Single Pile Test 1st Blast a)PPT89 b)PPT01

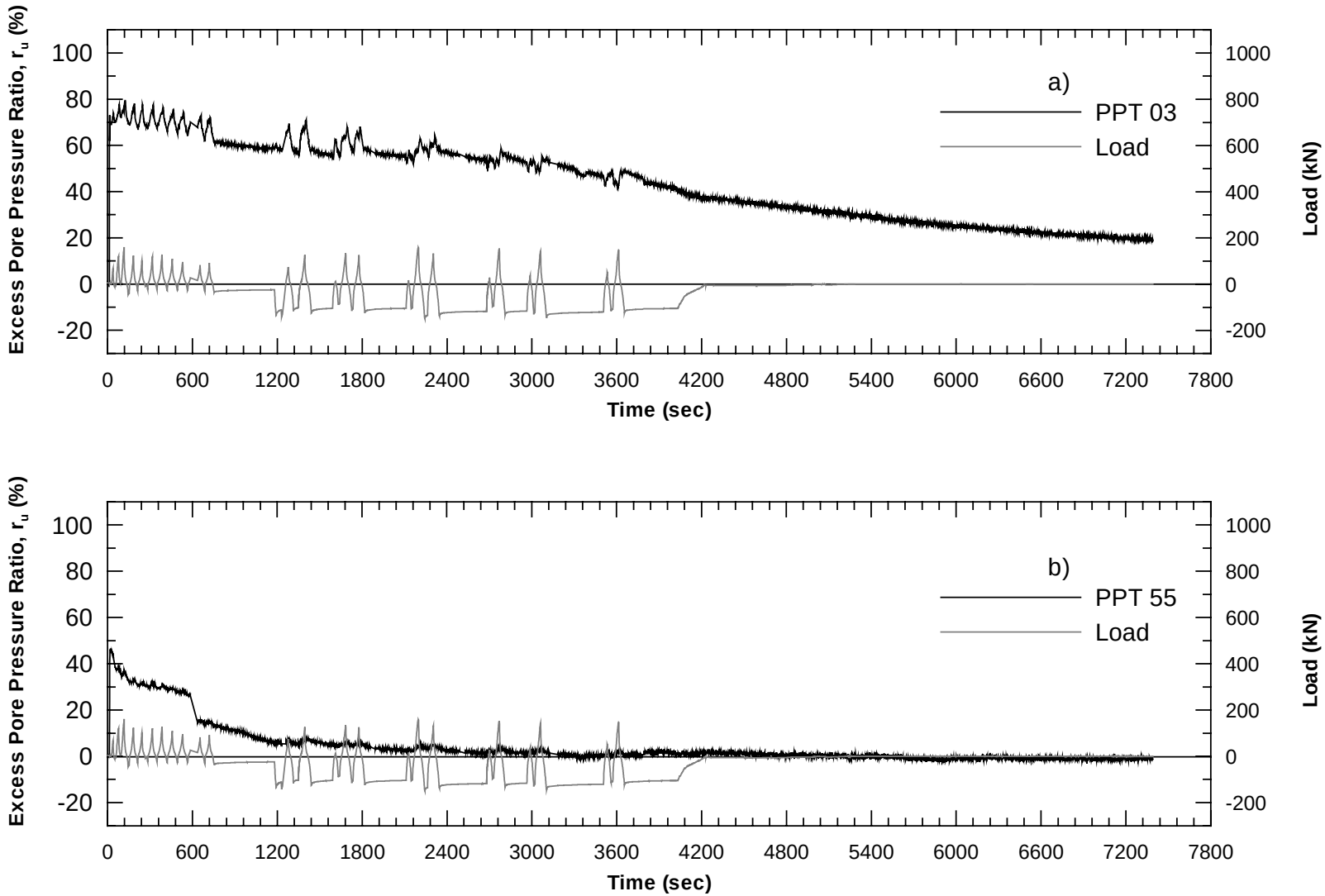

Figure 3.31 Excess Pores Pressure Ratio for Single Pile Test 1st Blast a)PPT03 b)PPT55

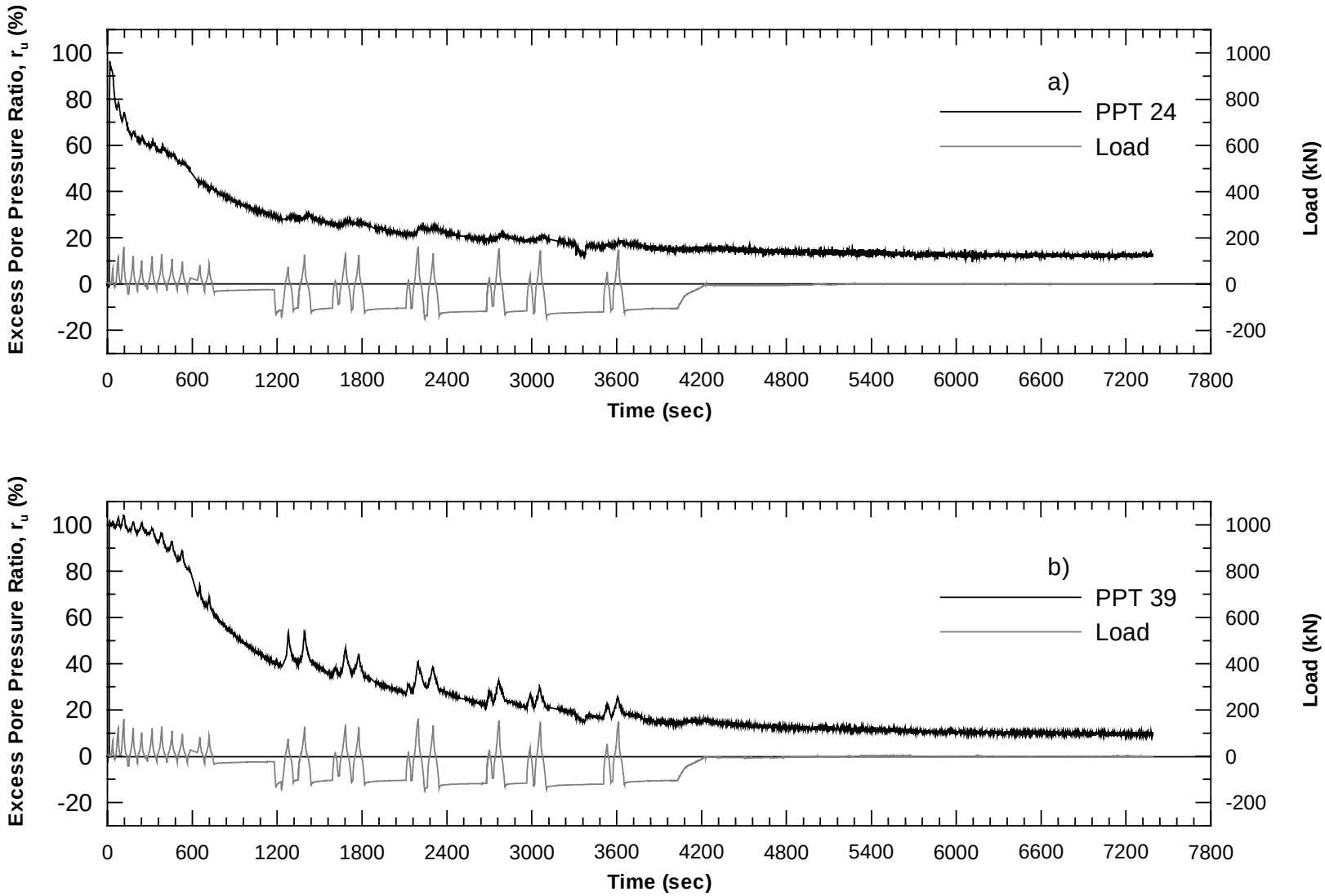

Figure 3.32 Excess Pore Pressure Ratio for Single Pile Test 1st Blast a)PPT24 b)PPT39

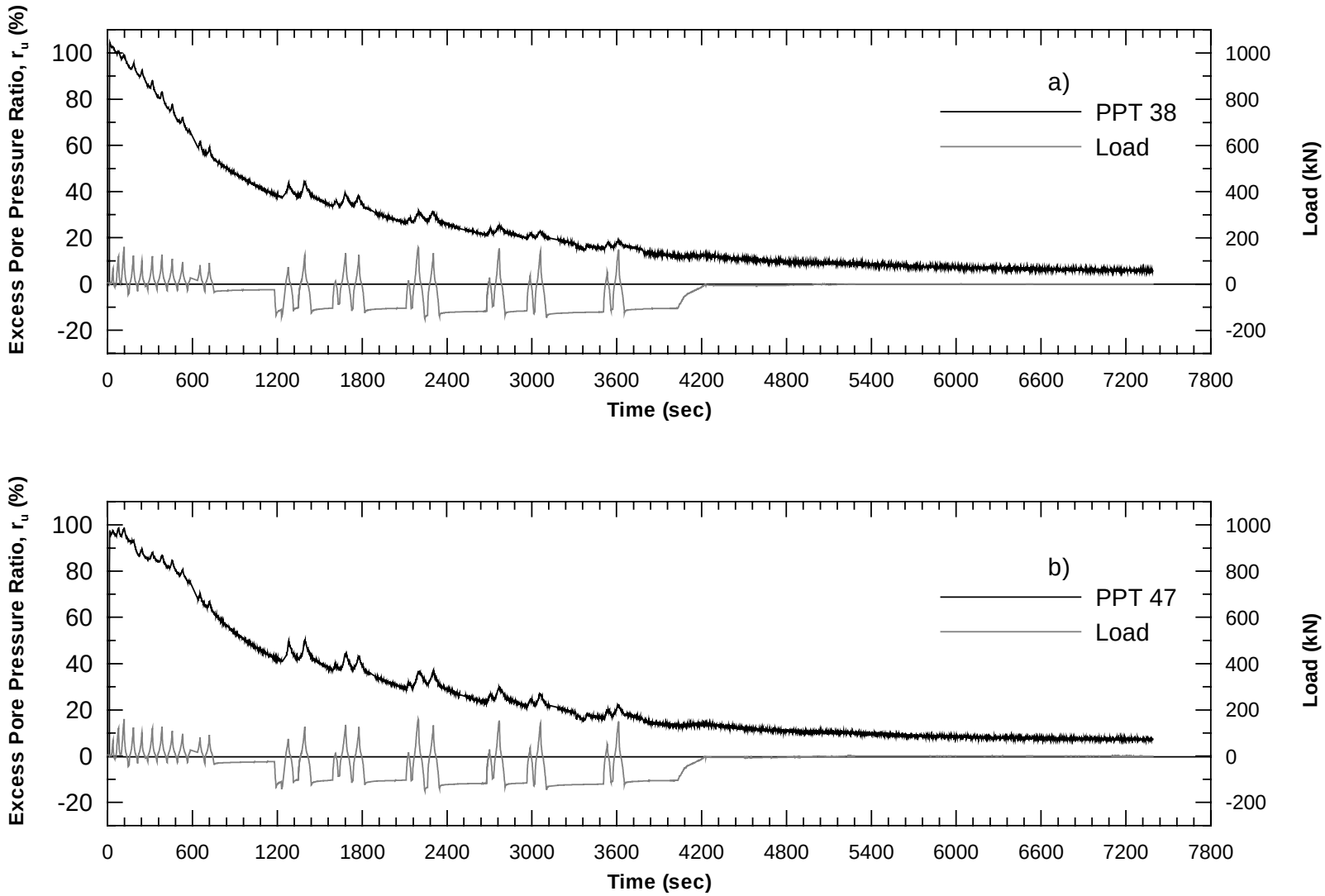

Figure 3.33 Excess Pore Pressure Ratio for Single Pile Test 1 st Blast a)PPT38 b)PPT47

Figure 3.34 Sand Boils Near H-Pile During Single Pile Test

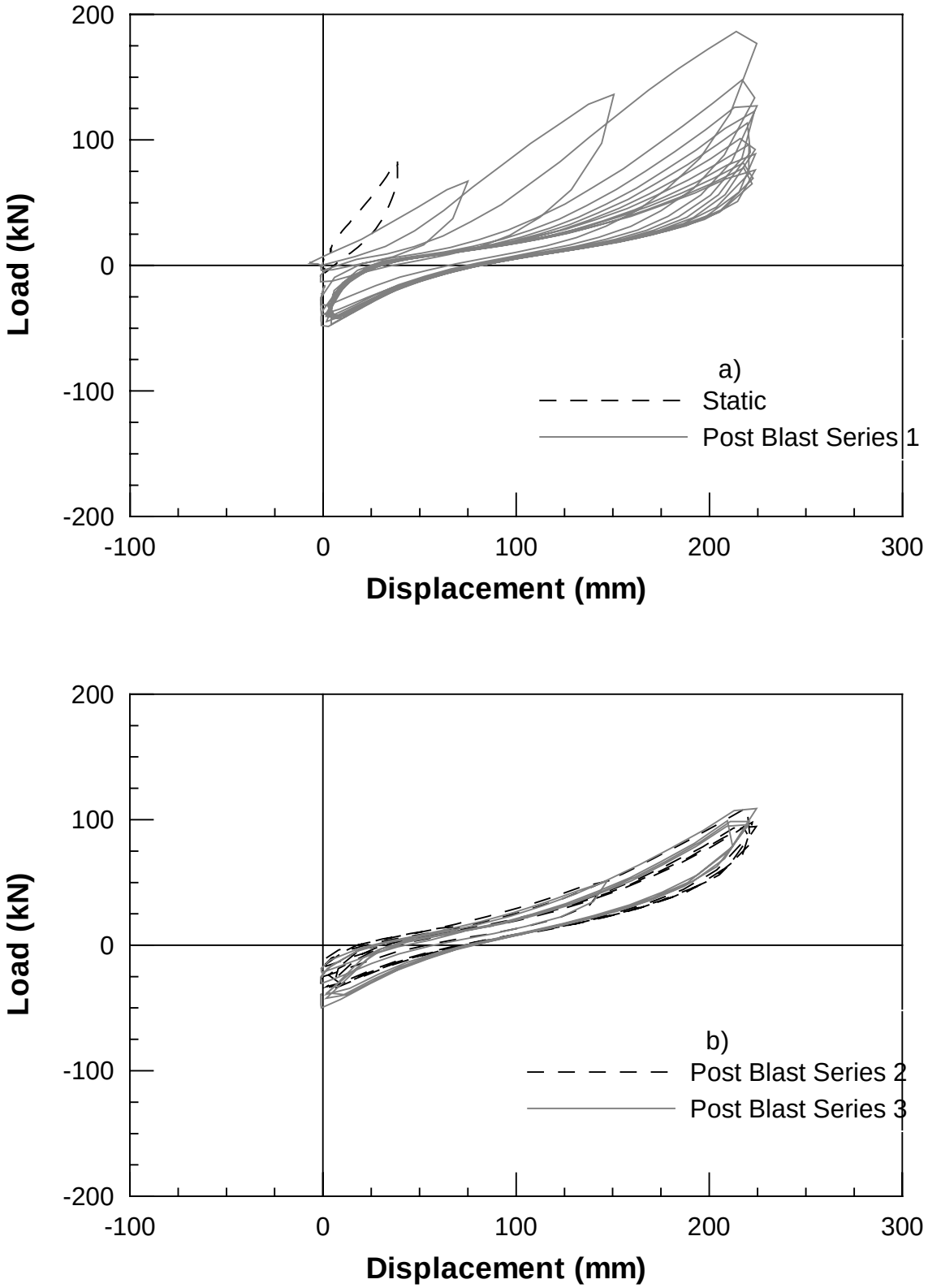

Figure 3.35 Load vs Displacement for Single Pipe Pile 2nd Blast a) Static and Post Blast Series 1 b) Post Blast Series 2 and 3

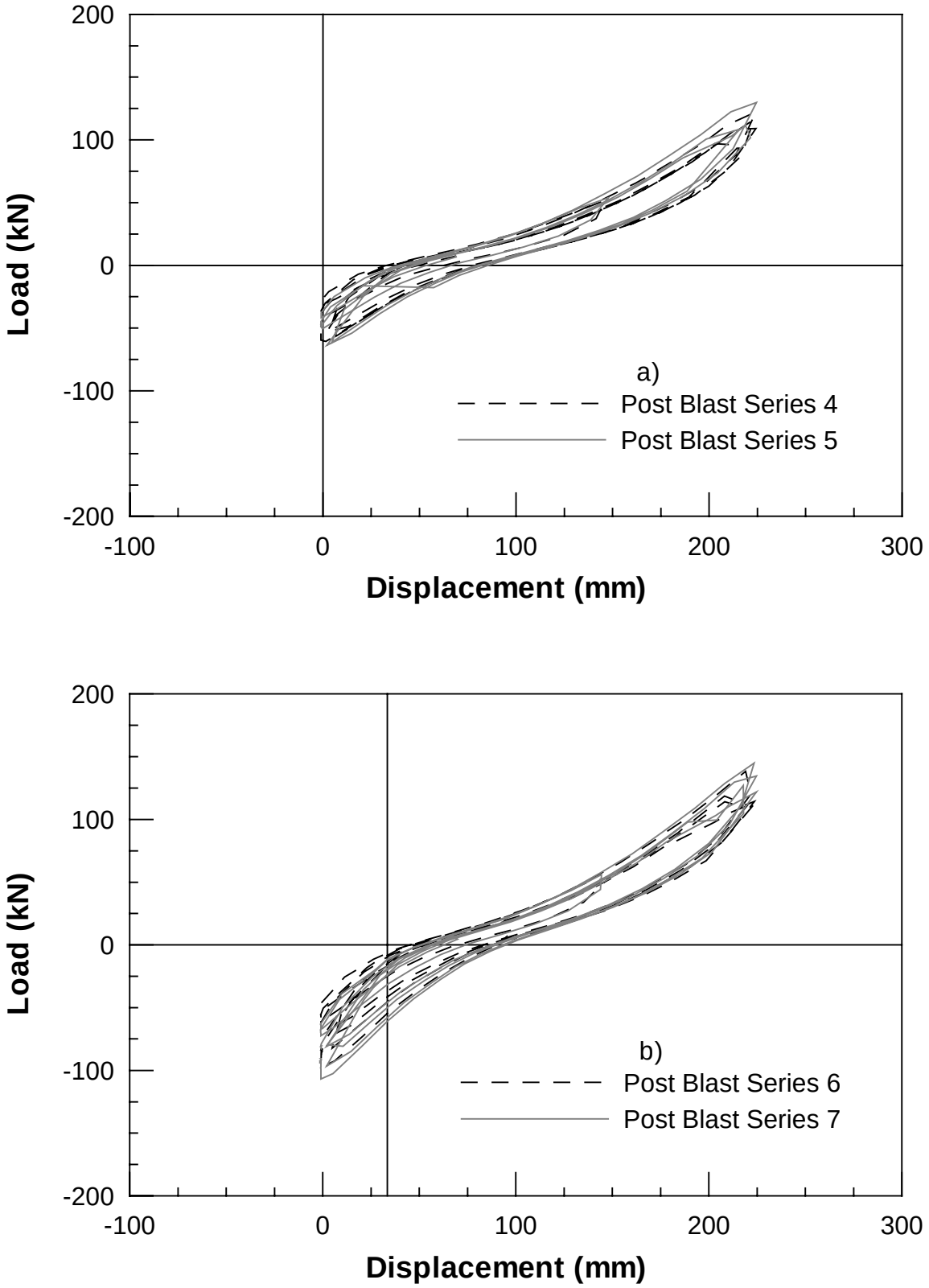

Figure 3.36 Load vs Displacement for Single Pipe Pile 2nd Blast a) Post Blast Series 4 and 5 b) Post Blast Series 6 and 7

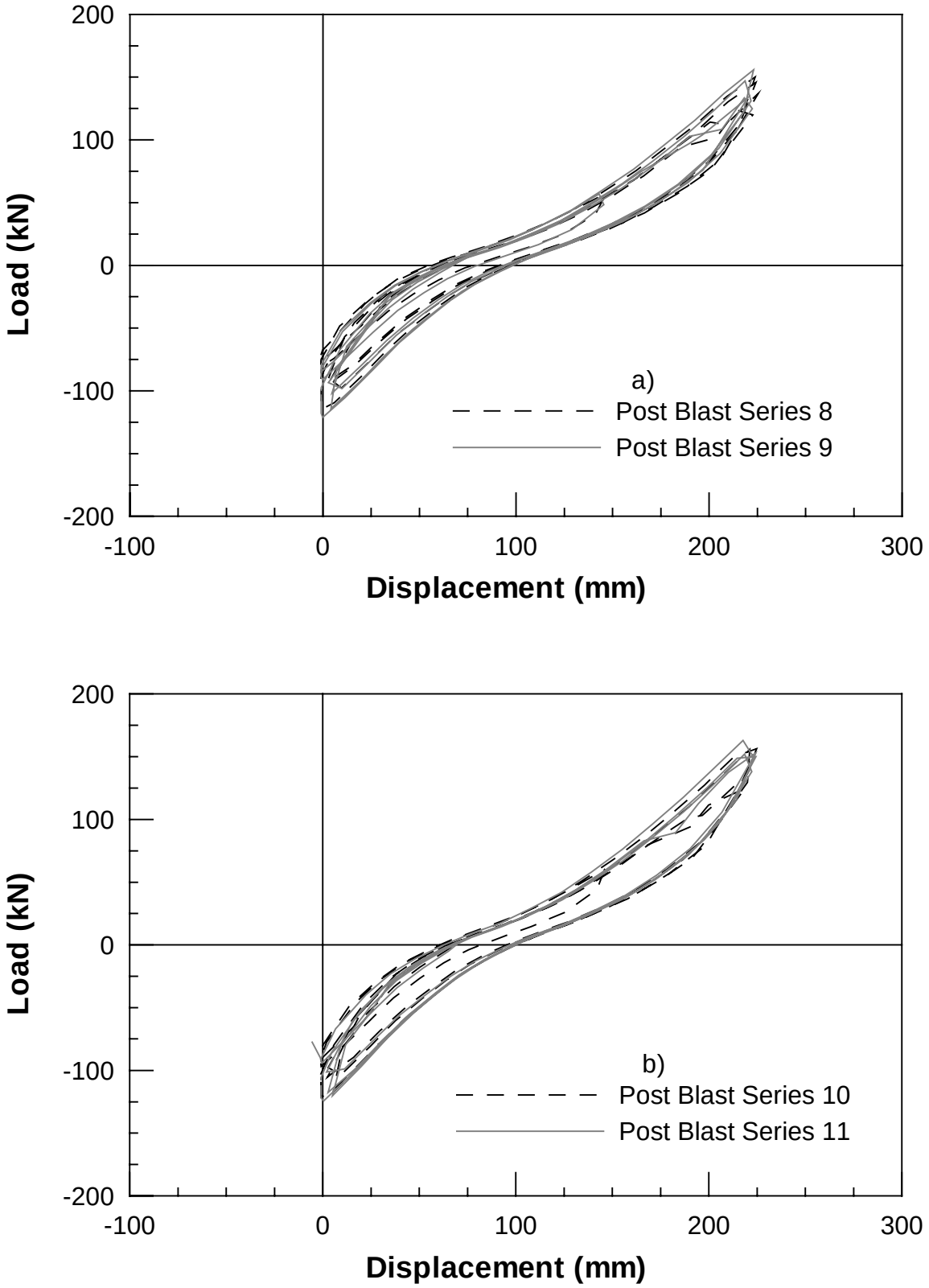

Figure 3.37 Load vs Displacement for Single Pipe Pile 2nd Blast a) Post Blast Series 8 and 9 b) Post Blast Series 10 and 11

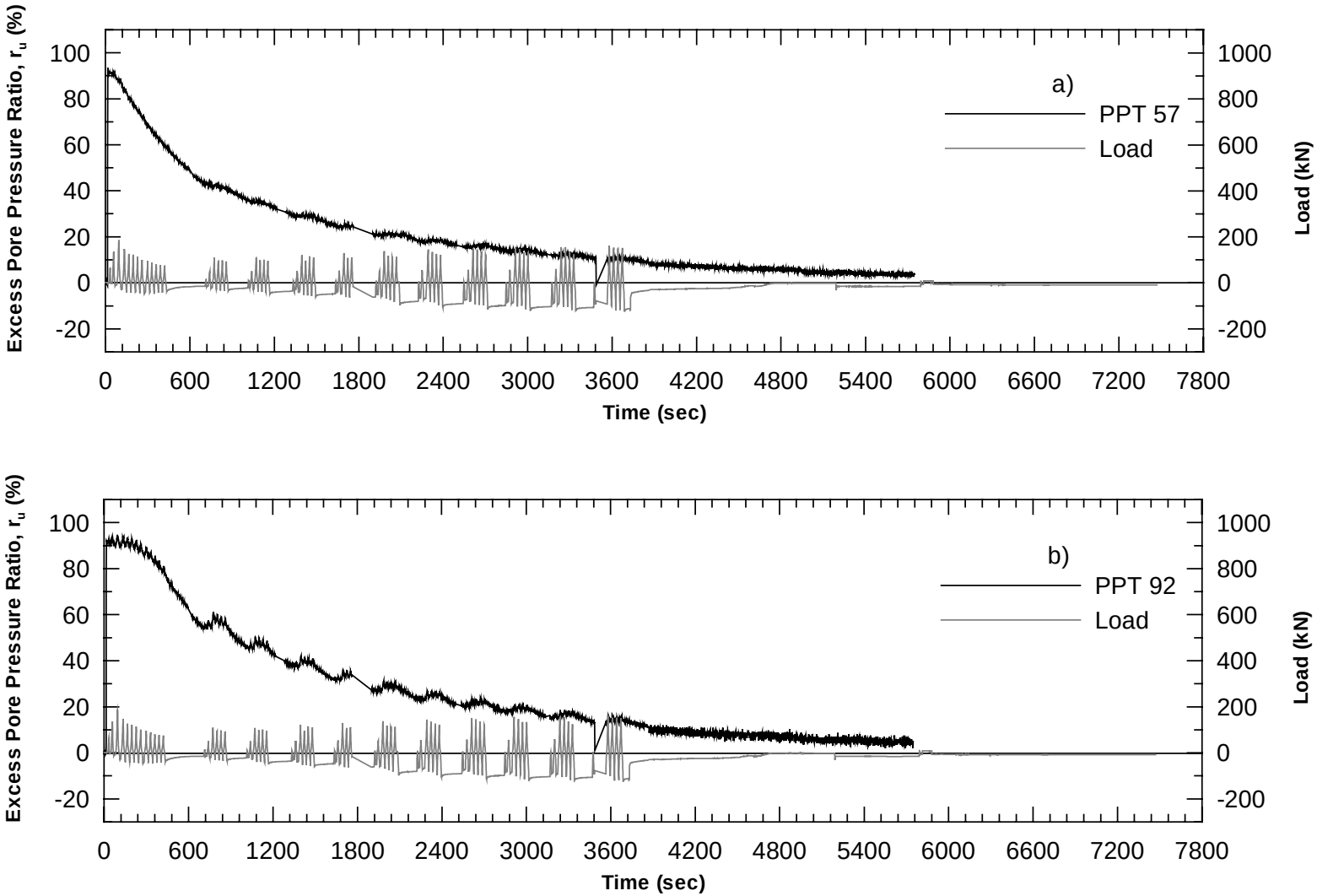

Figure 3.38 Excess Pore Pressure Ratio for Single Pile Test 2 nd Blast a)PPT57 b)PPT92

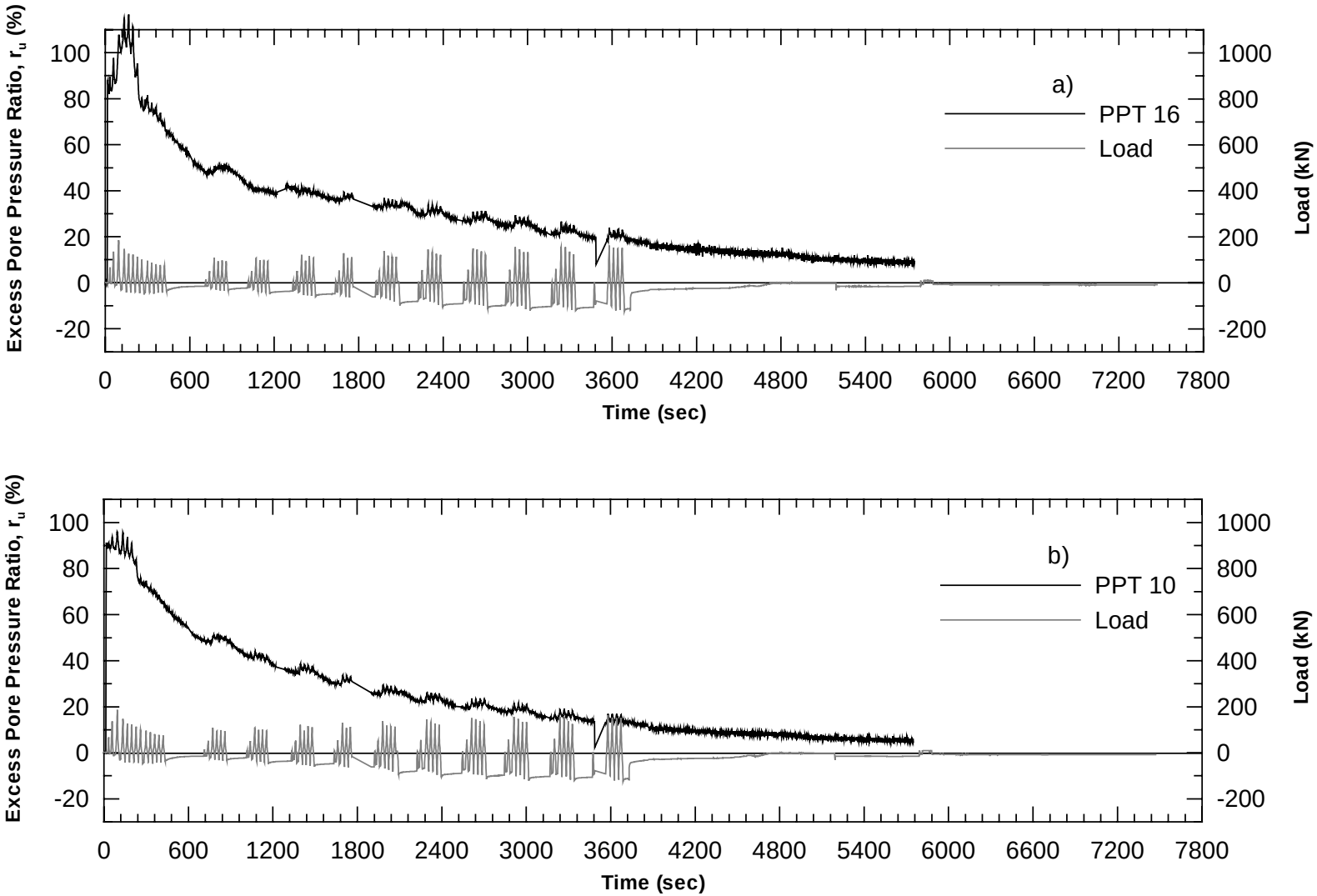

Figure 3.39 Excess Pore Pressure Ratio for Single Pile Test 2 nd Blast a)PPT16 b)PPT10

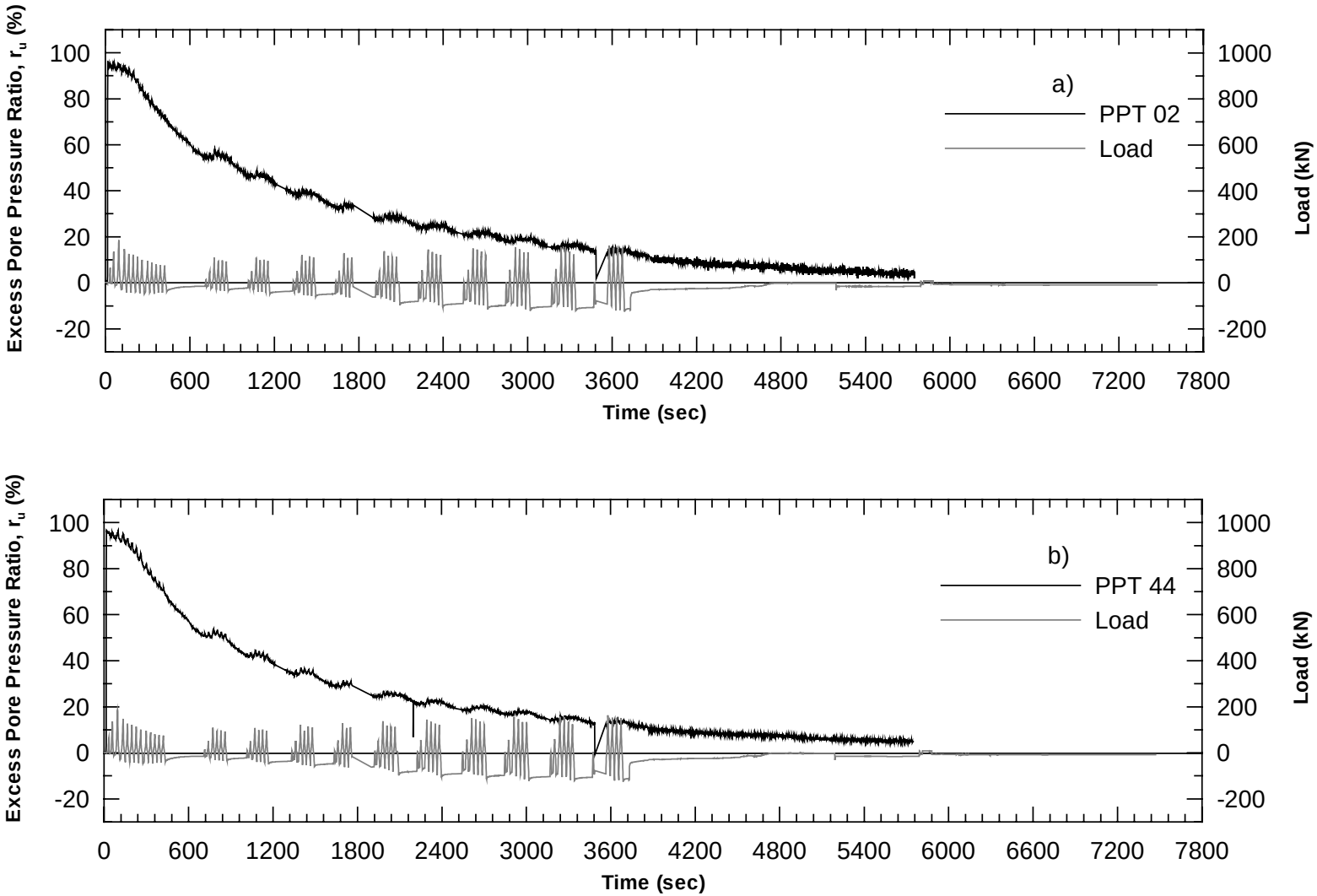

Figure 3.40 Excess Pore Pressure Ratio for Single Pile Test 2 nd Blast a)PPT02 b)PPT44

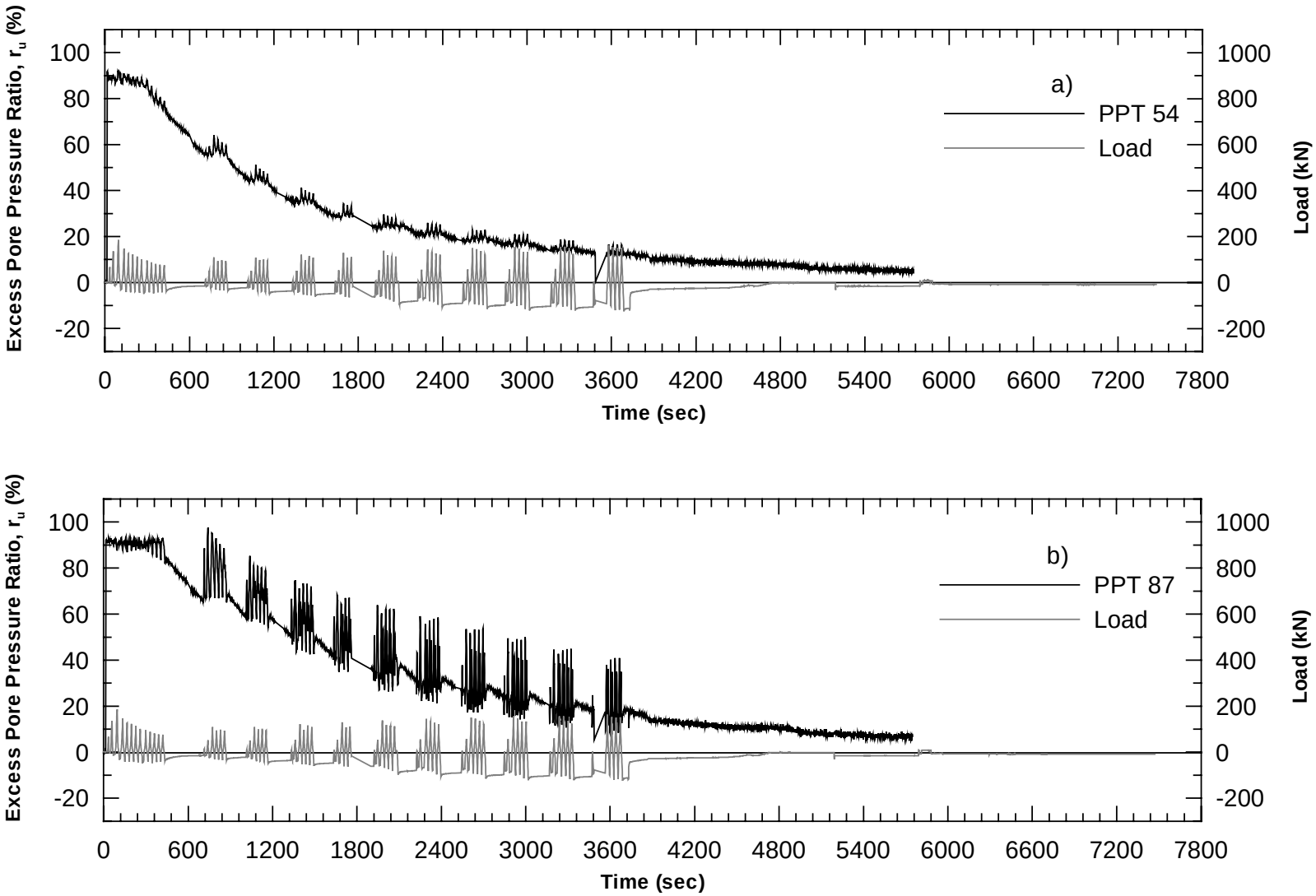

Figure 3.41 Excess Pore Pressure Ratio for Single Pile Test 2 nd Blast a)PPT54 b)PPT87

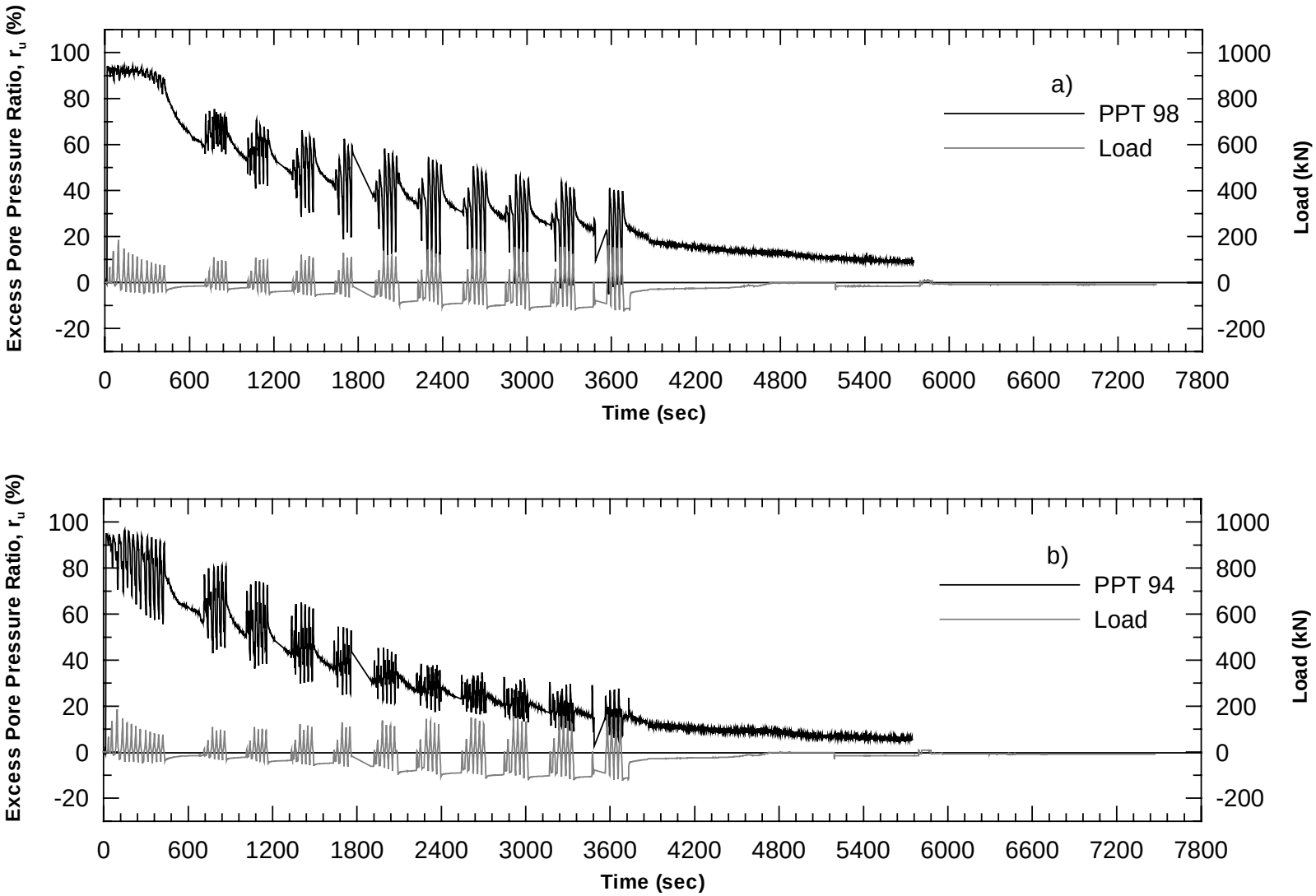

Figure 3.42 Excess Pore Pressure Ratio for Single Pile Test 2 nd Blast a)PPT98 b)PPT94

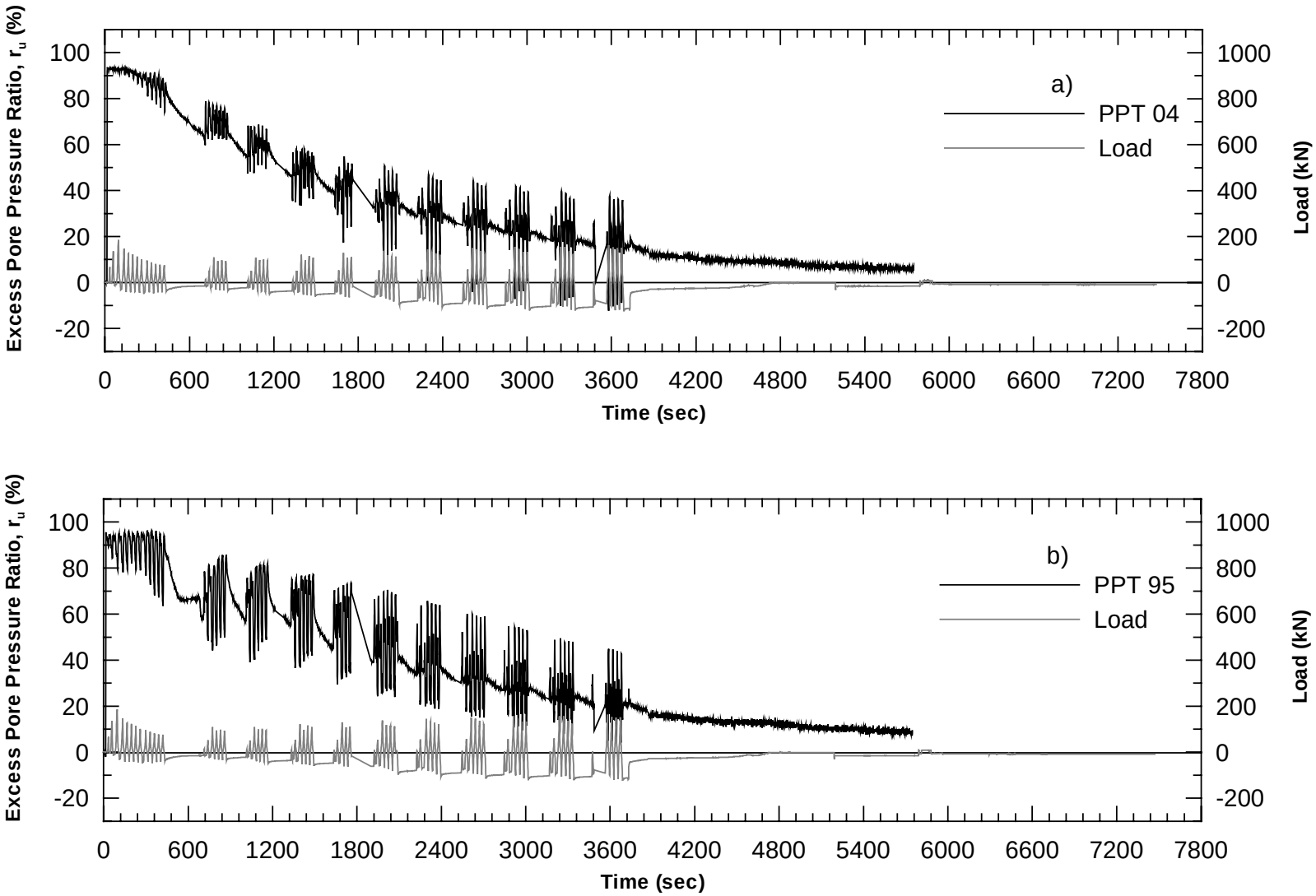

Figure 3.43 Excess Pore Pressure Ratio for Single Pile Test 2 nd Blast a)PPT04 b)PPT95

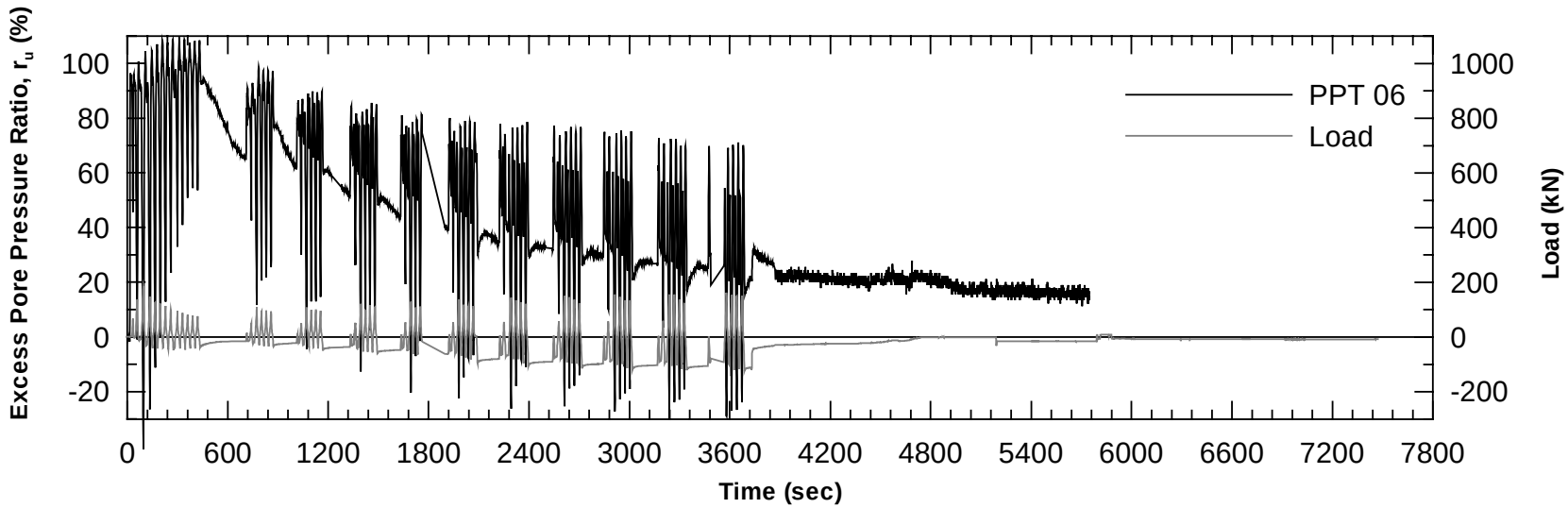

Figure 3.44 Excess Pore Pressure Ratio for Single Pile Test 2 nd Blast PPT06

Note: Contours in millimeters
Coordinates in feet

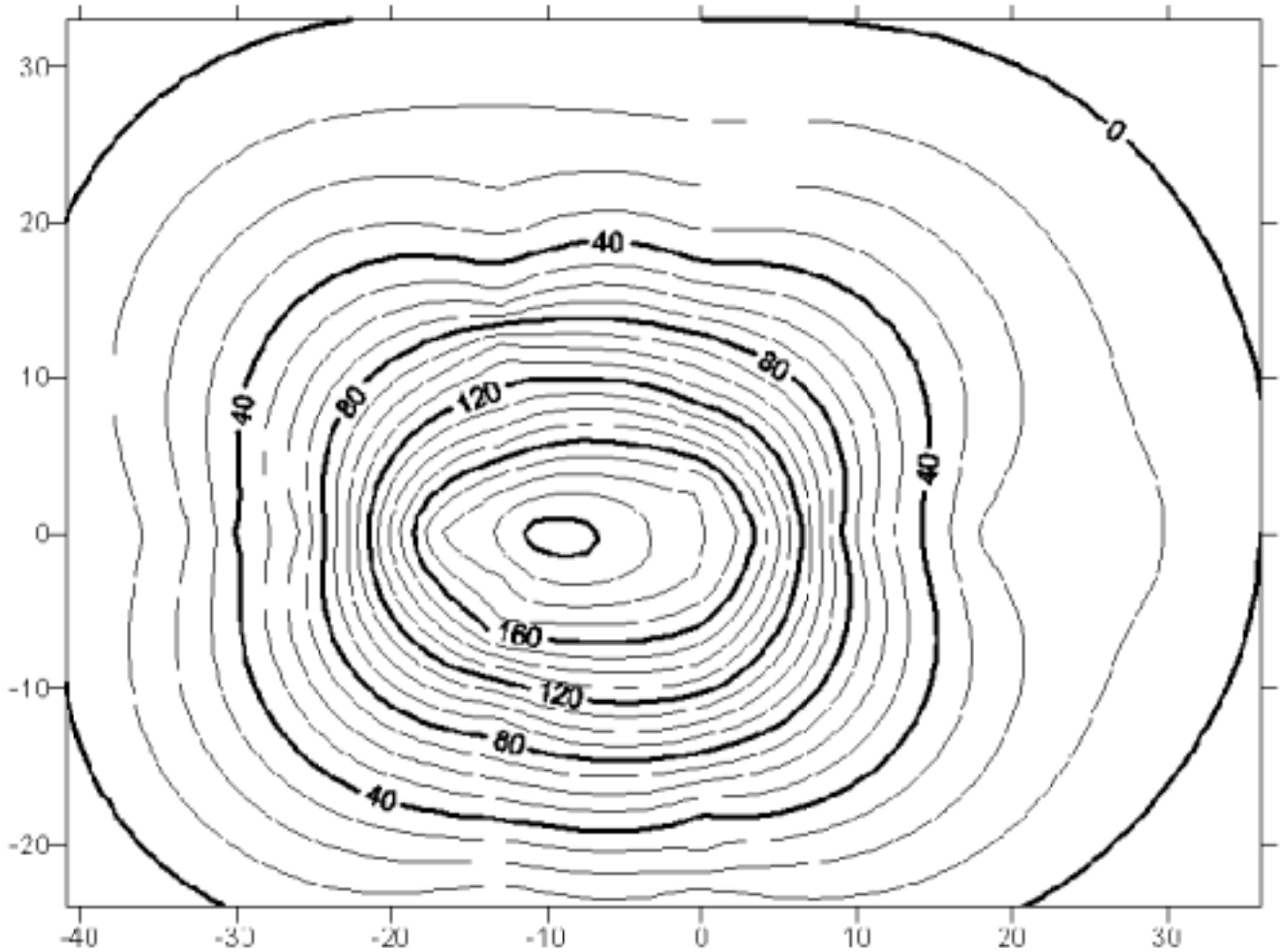

Figure 3.45 Contours of Settlement for Single Pile Test 1 st Blast

4 4-PILE GROUP AND 0.6-m CISS PILE TESTS

The 4-pile group and 0.6-m CISS pile tests were performed to investigate effects of group behavior of closely spaced piles and large diameter piles in liquefied soils. The 4-pile group consisted of 0.32 m outside diameter pipe piles spaced at 3.5 pile diameters driven to a depth of 12 m. The 0.6-m CISS pile consisted of a 0.6-m outside diameter steel shell with a 13 mm wall thickness driven to a depth of 13.8 m. In all cases, driving was very easy. Soil inside the 0.6-m steel shell was augered out, and a rebar cage consisting of nine 28.7 mm (#9) bars spaced at 143 mm on center and a 9.5 mm (#3) spiral with a 114 mm spacing was then placed inside the steel shell. The steel shell was then filled with concrete. A 2.2 MN hydraulic actuator placed between the pile group and CISS pile applied lateral loads during testing. The test set-up is shown in Figure 4.1. Pile instrumentation consisted of strain gages along the depth of the pile and displacement transducers at the pile head. Pore pressure transducers were placed along the sides of the piles and at various distances in front of the piles. Data from the subsurface investigation and in-situ testing are presented along with load and displacement test results, excess pore pressure ratios, and settlement contours resulting from blasting.

4.1 4-Pile Group and 0.6-m CISS Pile Site Characterization

A detailed subsurface investigation was performed at the 4-pile group and 0.6-m CISS pile site. The location of each in-situ test performed prior to foundation testing is presented in Figure 4.2. Soil boring log BH-2 (Figure 4.3) shows a loose poorly graded sand extending from the original ground surface to a depth of 5.6 m. This is underlain by

a soft gray clay layer with occasional sand seams extending to a depth of 10.2 m. A loose silty sand layer was found between 10.2 m and 13.7 m. A soft gray clay extended from 13.7 m to the bottom of the boring at 19 m. SPT blow counts in the saturated sand varied between 5 and 13. The low SPT blow counts are an indication that the sand is susceptible to liquefaction.

Cone penetration tests were performed at various stages in the test program. Seven CPT's were performed prior to lateral load testing. Six of the seven cone logs shown in Figures 4.4 through 4.9 were performed prior to foundation installation. The seventh CPT log (Figure 4.10) presents data between piles within the 4-pile group after foundation installation. There was not a significant change in the measured tip resistance after installation of the pile group. The CPT results generally show a tip resistance varying between 4 and 10 MPa in the saturated sand layer.

Shear and compression wave velocity testing was also performed at the site. Down-hole, suspension logger and seismic CPT's were used to obtain shear wave velocities. The suspension logger and seismic CPT tests were performed prior to foundation installation. The down-hole test utilized a steel pipe pile within the 4-pile group to house the geophone and obtain shear wave velocities. The suspension logger was used to obtain compression wave velocities. Results of the shear and compression wave velocity tests are shown in Figure 4.11. Additional shear wave velocity tests were performed after the first lateral load test and again after stone columns were installed. A comparison of down-hole shear wave velocity profiles at various stages of the testing program is shown in Figure 4.12.

4.2 4-Pile Group and 0.6-m CISS Pile Test Results

The first lateral load test at the 4-pile group/0.6-m CISS pile site was conducted on February 4, 1999. A plan view of this test set-up is shown in Figure 4.13. Similar to the single pile test, a static test was performed prior to blasting. The actuator loading was controlled using displacement limits. When either the CISS pile or the 4-pile group reached the target displacement, loading began to decrease until the zero displacement target was achieved.

4.2.1 Load-Displacement Results for Test 1

The static test consisted of pulling the piles together up to a displacement of 38 mm. The piles were then cyclically loaded through a series of displacements after blasting where the piles were pushed apart. The first of ten post-blast series consisted of the piles being displaced through one 76 mm cycle, one 152 mm cycle, and eleven 228 mm cycles. Post-blast Series 2 through 6 consisted of one 76 mm cycle, one 152 mm cycle and four 228 mm cycles. Post-blast Series 7 through 10 consisted of one 75 mm cycle and four 150 mm cycles. The magnitude of the displacement was reduced for the later series to prevent individual load cells within the 4-pile group from being loaded beyond the calibrated region. Load versus displacement for the 4-pile group is presented in Figures 4.14 through 4.16. Load versus displacement for the 0.6-m CISS pile is presented in Figures 4.17 through 4.19. Both the 4-pile group and 0.6-m CISS pile showed an initial decrease in stiffness with each cycle of loading and then an increase in stiffness as pore water pressures decreased.

4.2.2 Excess Pore Pressure Response for Test 1

Transducers used to measure pore water pressure were placed throughout the test site. The depth and location of each PPT is shown in Figure 4.20. Measured pore water pressures were used to calculate the excess pore pressure ratio at each transducer location. Excess pore pressure ratios and the variation of load with time are shown in Figures 4.21 through 4.31. PPT data to the east (near the 4-pile group) is presented first, and transducer data to the west (around the CISS pile) is presented last. Excess pore pressure ratios varied according to depth and location. Excess pore pressure ratios at a distance of 4.2 m from the CISS pile or pile group generally tend to be lower than ratios near the pile. Initial excess pore pressure ratios ranged from as low as 40 percent to just over 100 percent. The change in excess pore pressure ratio close to the CISS pile and pile group was affected dramatically by loading and unloading of the pile as seen in the figures.

4.3 Site Characterization after Installation of Stone Columns

Within days of the first blast, the excavation was backfilled, and twenty-four 0.9-m diameter stone columns were installed in a 4 by 6 grid centered around the piles. The stone columns extended through the sand layer and were spaced at approximately 2.4 meters on center. Installation of the stone columns is shown in Figure 4.32. A series of CPT's were performed after the first blast prior to stone column installation and after the stone columns were installed. The location of the stone columns and in-situ tests after the first blast is shown in Figure 4.33. CPT results prior to stone column installation are presented in Figures 4.34 through 4.37. CPT results after stone column installation are

presented in Figures 4.38 through 4.47. Measured tip resistance from cone penetration tests prior to stone column installation rarely exceed 10 MPa. Tip resistance values after stone column installation reach as high as 35 MPa. The difference between tip resistance before and after stone column installation provided evidence that the loose sand deposit had been significantly densified as a result of the stone columns.

4.4 Stone Column Test Results

The lateral load tests provided further evidence of improved ground behavior as a result of installing stone columns. In addition to the standard 16 charges used to liquefy the site, an additional 14 charges were placed around the perimeter of the improved area in an attempt to liquefy the area surrounding the stone columns.

4.4.1 Load-Displacement Results with Stone Columns

Load versus displacement for the 4-pile group and 0.6-m CISS pile is presented in Figures 4.48 through 4.50 and Figures 4.51 through 4.53, respectively. The static tests were run using displacement control. The target displacements for the static test were 3 mm and 38 mm. The piles were unloaded between the two target displacements. The post blast testing was controlled using load limits as the piles were pushed apart to prevent individual load cells within the 4-pile group from being loaded beyond the calibrated region. As the piles were unloaded, a zero displacement target was set to control the actuator. The first post blast series consisted of one cycle with a maximum load of 450 kN and twelve cycles at a maximum load of 600 kN. The remaining post blast cycles consisted of one 200 kN loading cycle and four 600 kN loading cycles. Stiffness of the

pile group and the CISS pile reduced during the first post blast series. Displacements continued to increase slightly during each loading cycle. The effect of pore water pressure buildup on the load-displacement response was minimal.

4.4.2 Excess Pore Pressure Response with Stone Columns

The pore water pressure transducers were again placed around the pile group and CISS pile. In addition to the transducers around the piles, an array of transducers in the north-south direction was placed just to the east of the CISS pile. The depth and location of each transducer is shown in Figure 4.54. The excess pore pressure ratios are shown in Figures 4.55 through 4.63 with data to the west (near the CISS pile) presented first, and transducer data to the east (around the 4-pile group) presented last. Immediately after blasting, the excess pore pressure ratios ranged between 30% and 85% adjacent to the CISS pile and between 50% and 95% adjacent to the pile group. Within one minute after blasting, the pore pressure ratios had dropped dramatically, and approximately 10 minutes after blasting, the excess pore pressure ratios were generally 10% ore less. The stone columns sufficiently densified the loose sand to prevent liquefaction from occurring during this test.

4.5 Blast Induced Settlement

Upon completion of each test, a settlement survey was conducted. Settlement contours are presented in Figure 4.64 due to the first blast and Figure 4.65 due to the first and second blast combined. The contours of settlement are in millimeters, while the coordinates from the edge of the excavation are in meters. The amount of settlement

following the first blast was very similar to the single pile test, though essentially no settlement was measured due to the second blast.

4.6 Summary

In summary, two series of lateral load tests were performed on the 4-pile group and a 0.6-m CISS pile. Both static and post-liquefaction tests were performed. Foundation stiffness was observed to decrease after detonation of the explosives due to an increase in the pore water pressure. As the pore water pressure dissipated, foundation stiffness increased. The effect of pore-pressure on foundation stiffness is discussed in more detail in Chapters 7 and 8. It was observed that the 0.6-m CISS pile was stiffer than the 4-pile group during the static test, but was less stiff during the liquefaction testing. The installation of the stone columns dramatically increased the soil density, preventing liquefaction from occurring during the second blast. As a result, the foundation stiffness increased substantially as compared to the liquefied case for the first blast. This is some of the first full-scale quantitative evidence of the effectiveness of stone columns in increasing the lateral capacity of pile foundations in liquefiable soil.

Figure 4.1 4-Pile Group/0.6-m CISS Pile Test Set-Up

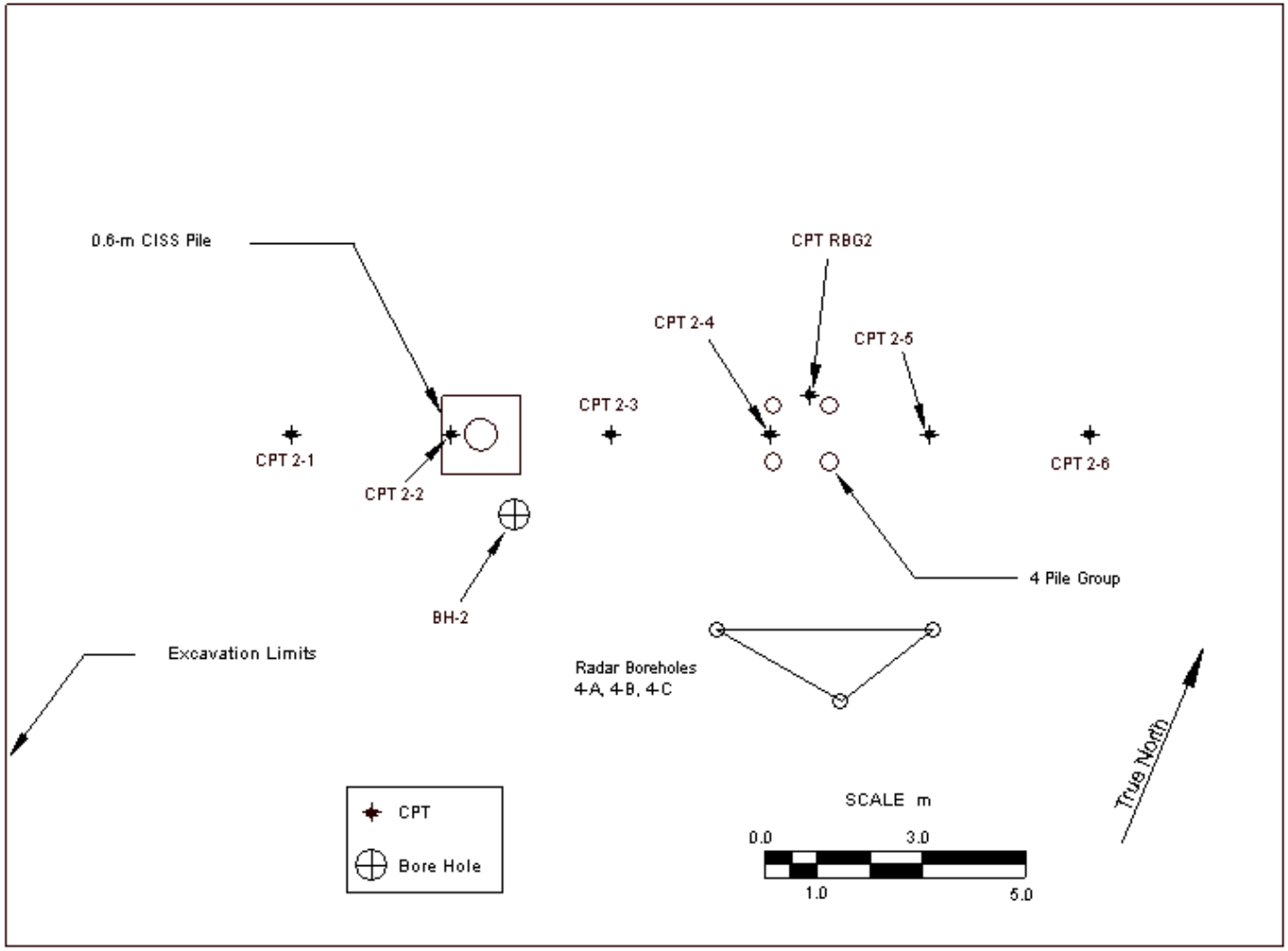

Note:
CPT No's 1-6 Completed 10/19/98
CPT No's RBG-1 Completed 1/30/99

Figure 4.2 Location Map of Insitu Tests Prior to Blasting

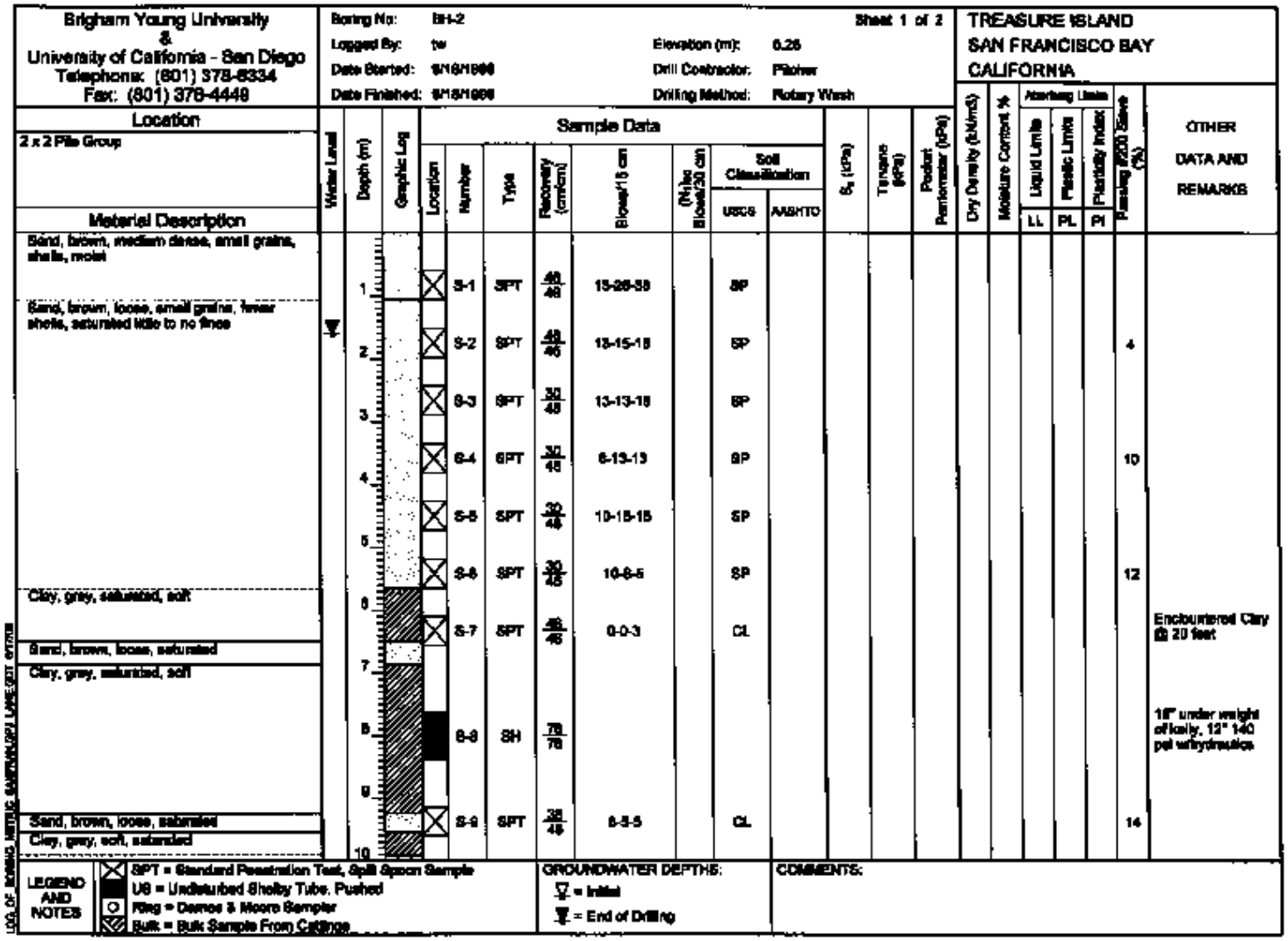

Figure 4.3a Soil Boring Log for 4-Pile Group/0.6m CISS Pile Area

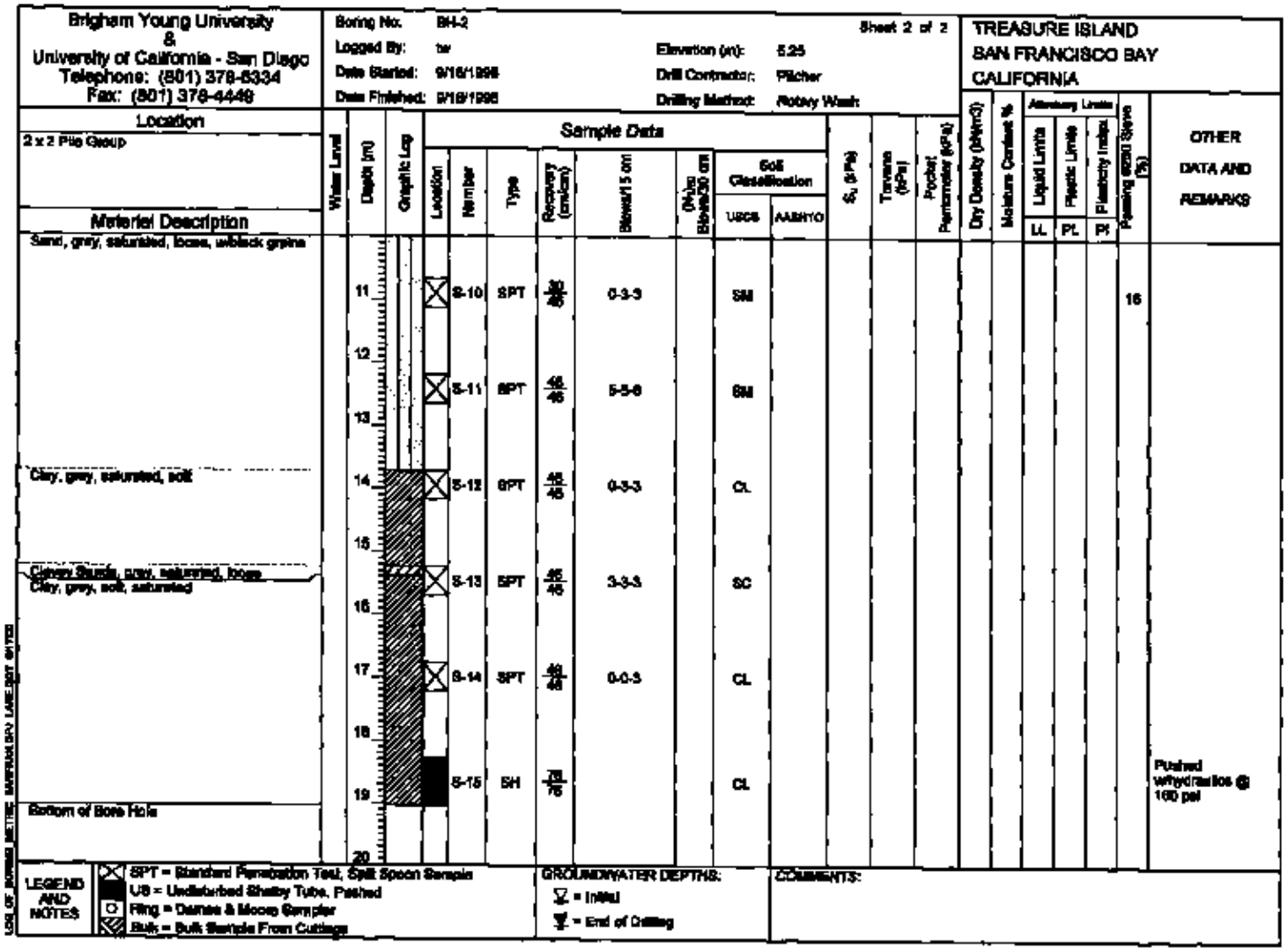

Figure 4.3b Soil Boring Log for 4-Pile Group/0.6m CISS Pile Area

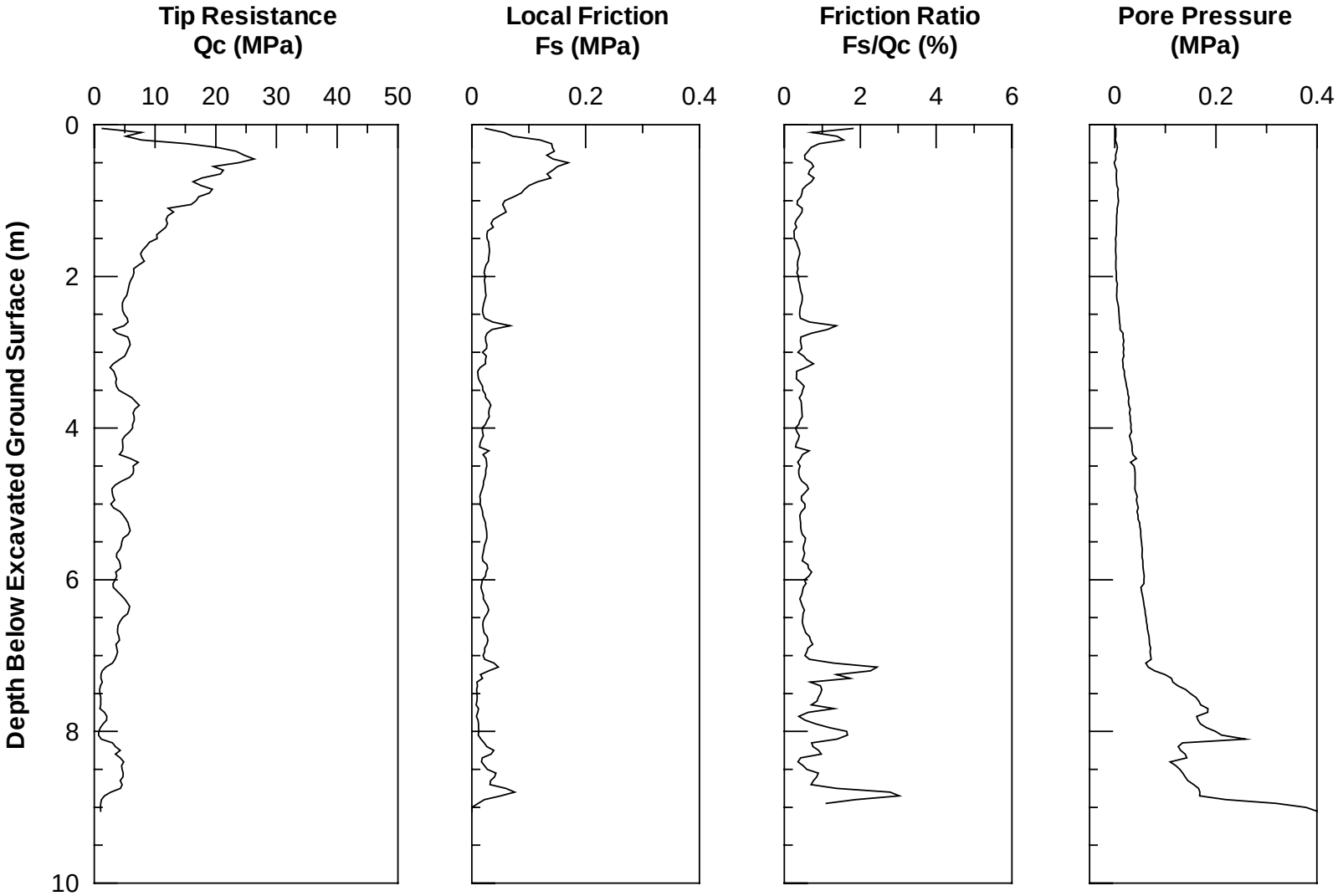

Figure 4.4 CPT2-1 Logs for 4 Pile Group/0.6m CISS Pile Test Area (10-30-98)

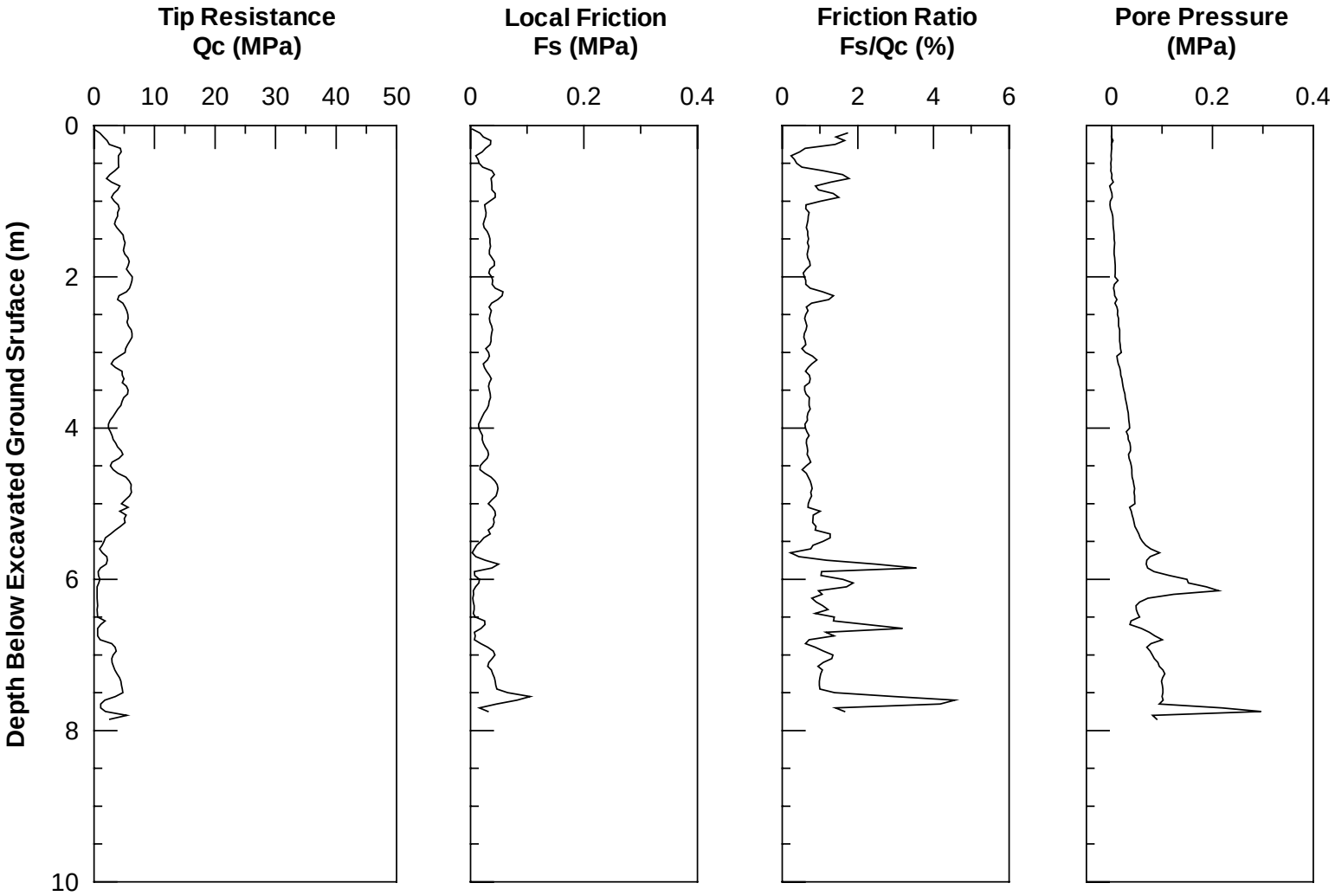

Figure 4.5 CPT2-2 Logs for 4-Pile Group/0.6m CISS Pile Test Area (11-06-98)

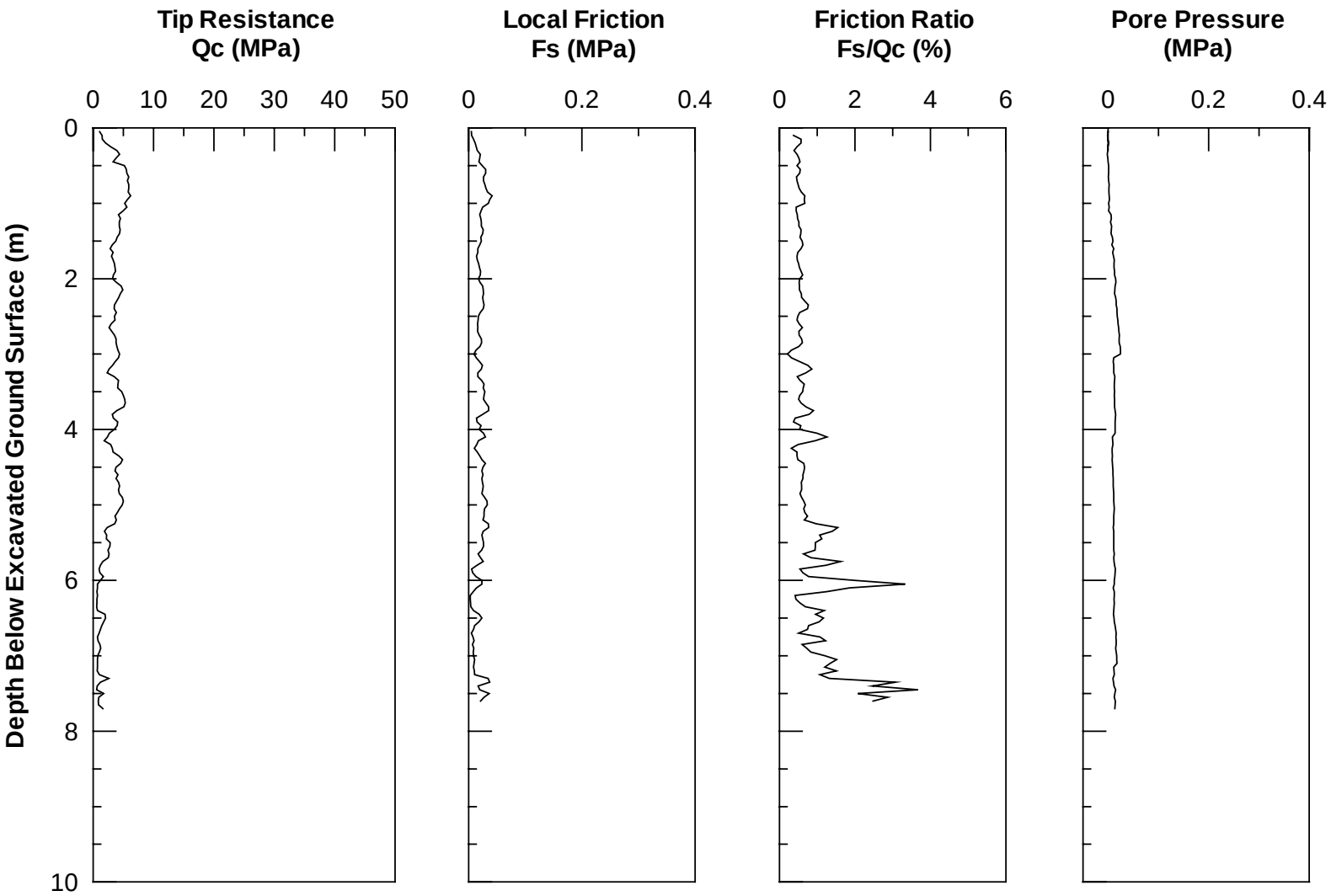

Figure 4.6 CPT2-3A Logs for 4-Pile Group/0.6m CISS Pile Test Area (11-06-98)

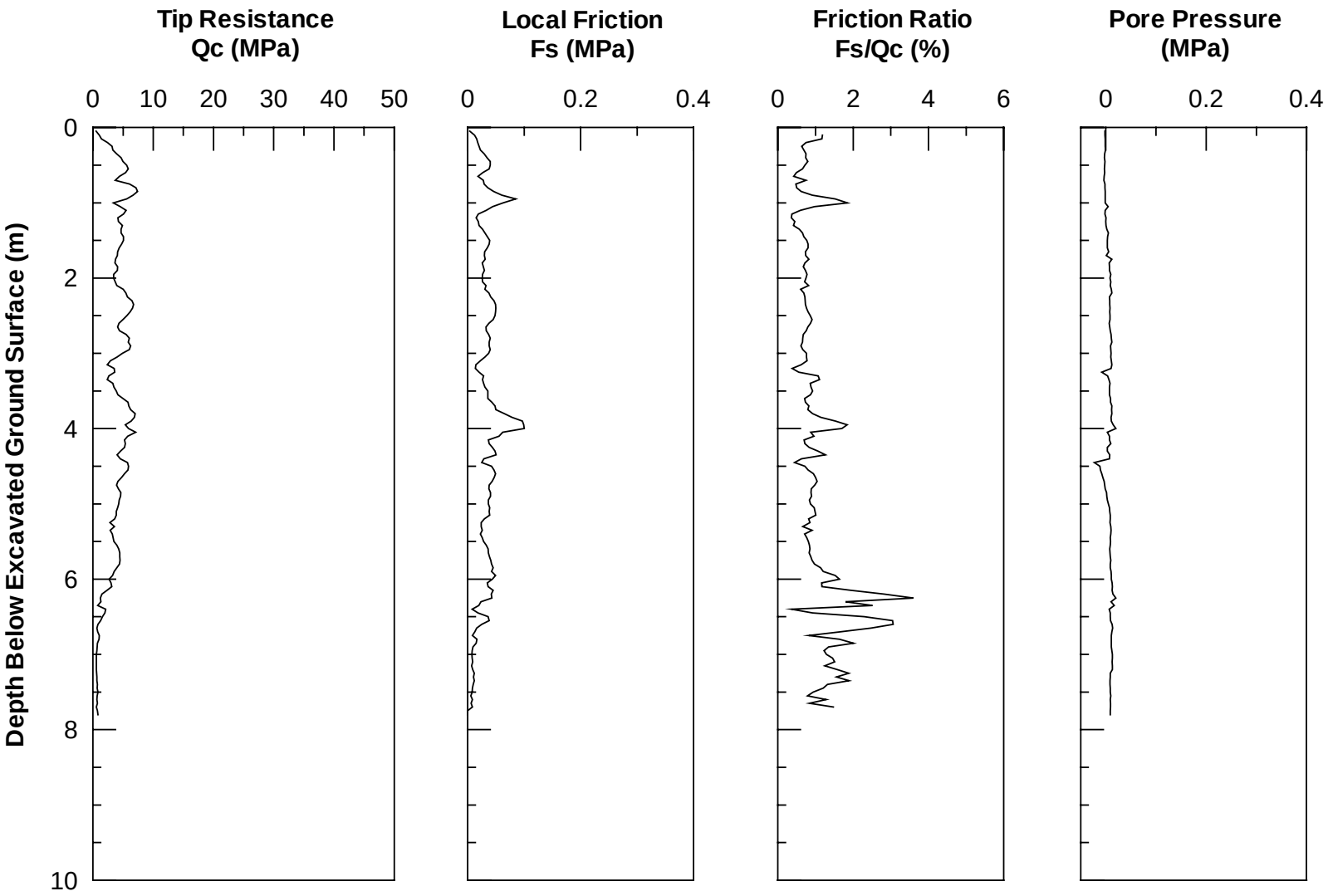

Figure 4.7 CPT2-4 Logs for 4-Pile Group/0.6m CISS Pile Test Area (10-30-98)

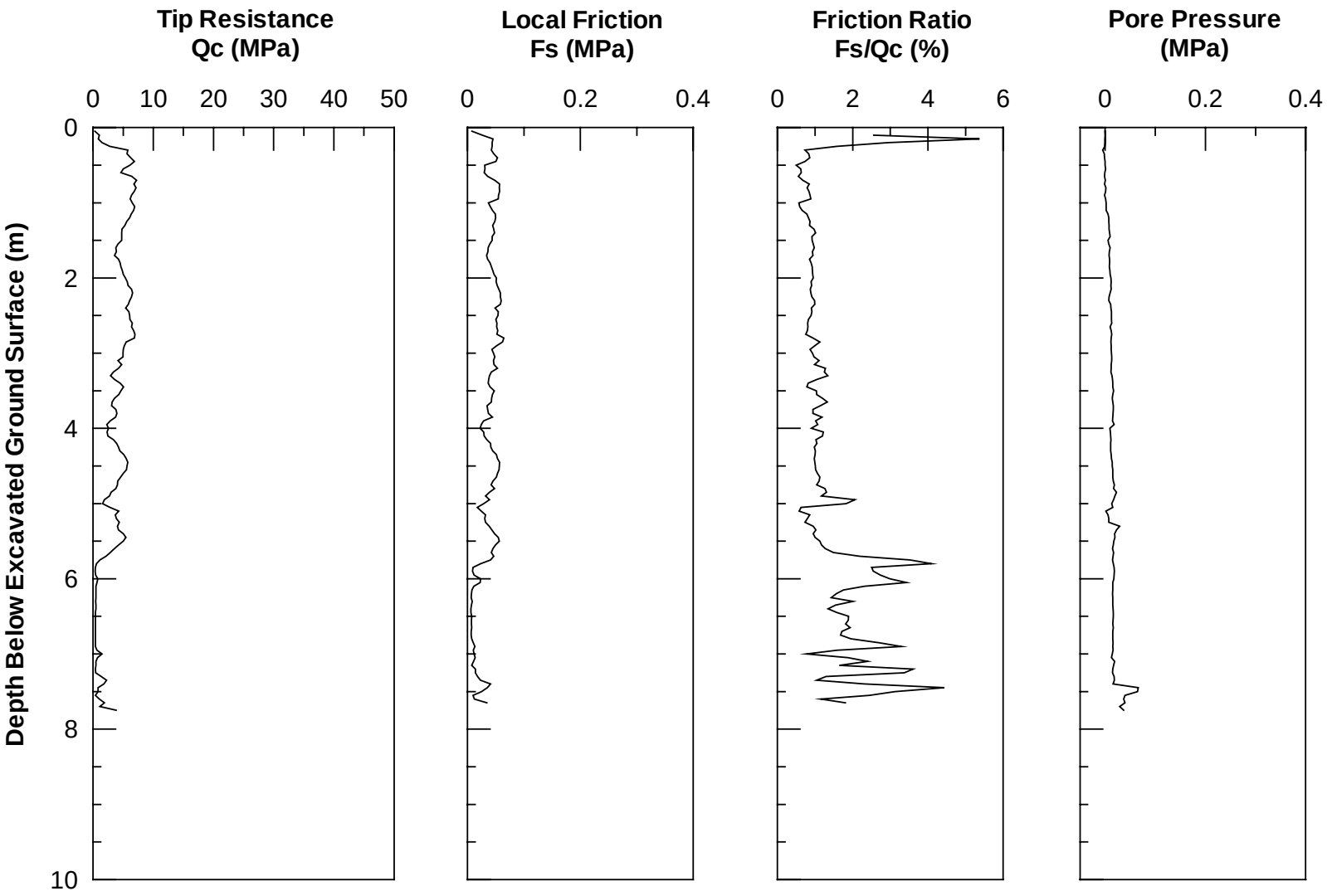

Figure 4.8 CPT2-5 Logs for 4-Pile Group/0.6m CISS Pile Test Area (10-30-98)

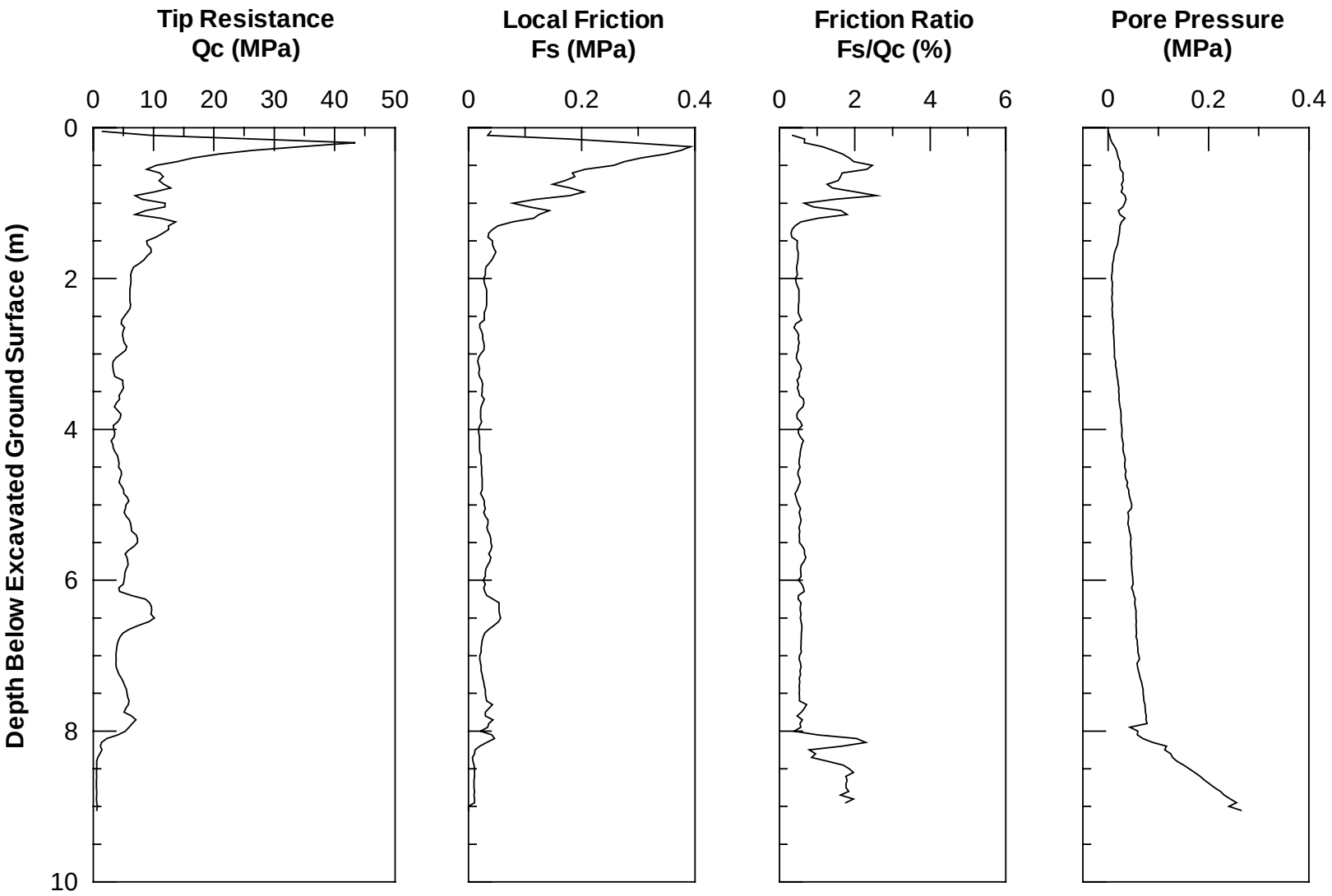

Figure 4.9 CPT2-6 Logs for 4-Pile Group/0.6m CISS Pile Test Area (10-30-98)

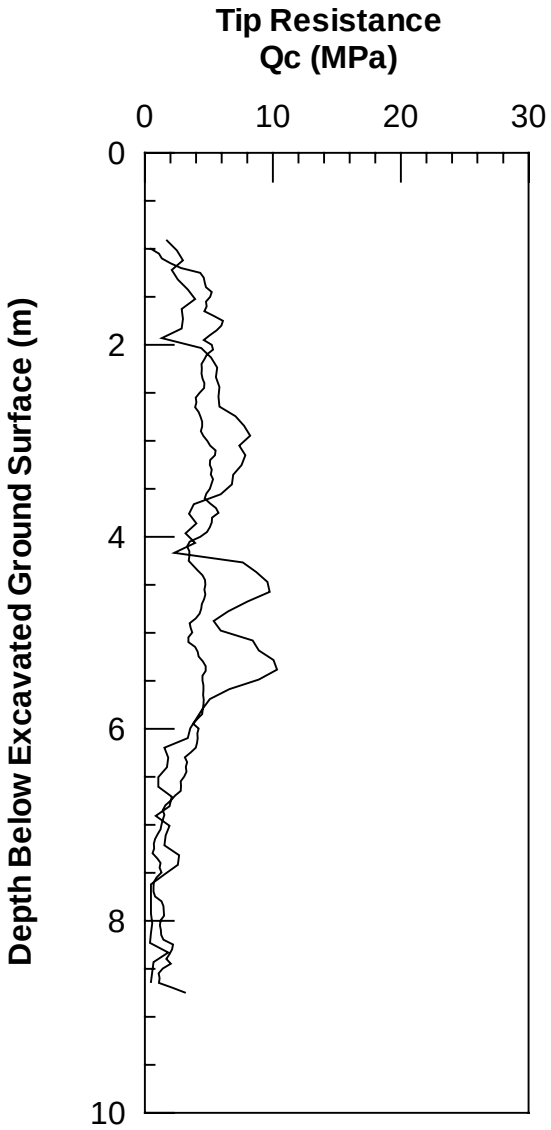

Figure 4.10 CPT RBG2 Logs for 4-Pile Group/0.6m CISS Pile Test Area After Foundation Installation (1-30-99)

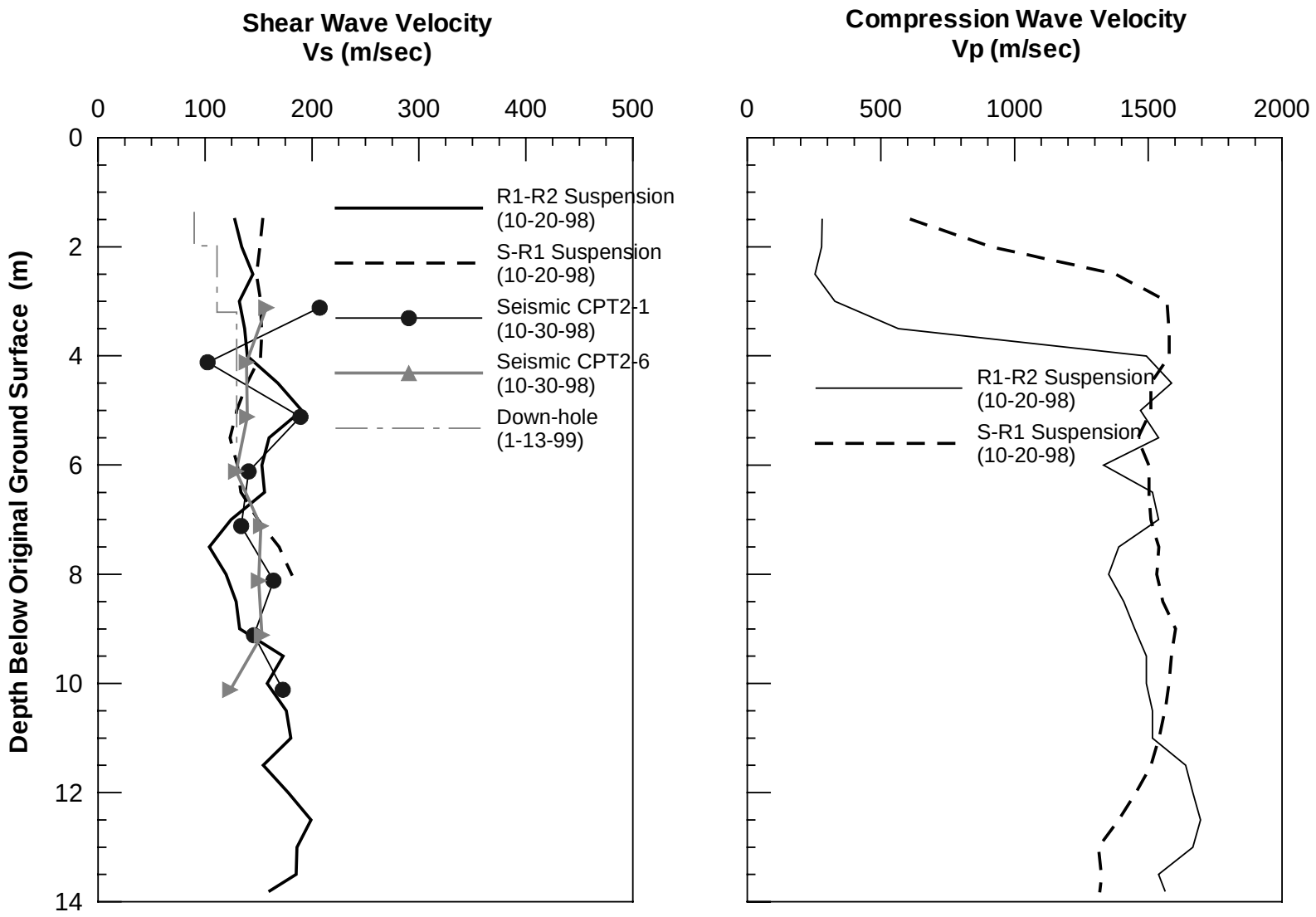

Figure 4.11 Pre-blast Velocity Profile for 4-Pile Group/0.6m CISS Pile a) Shear Wave b) Compression Wave

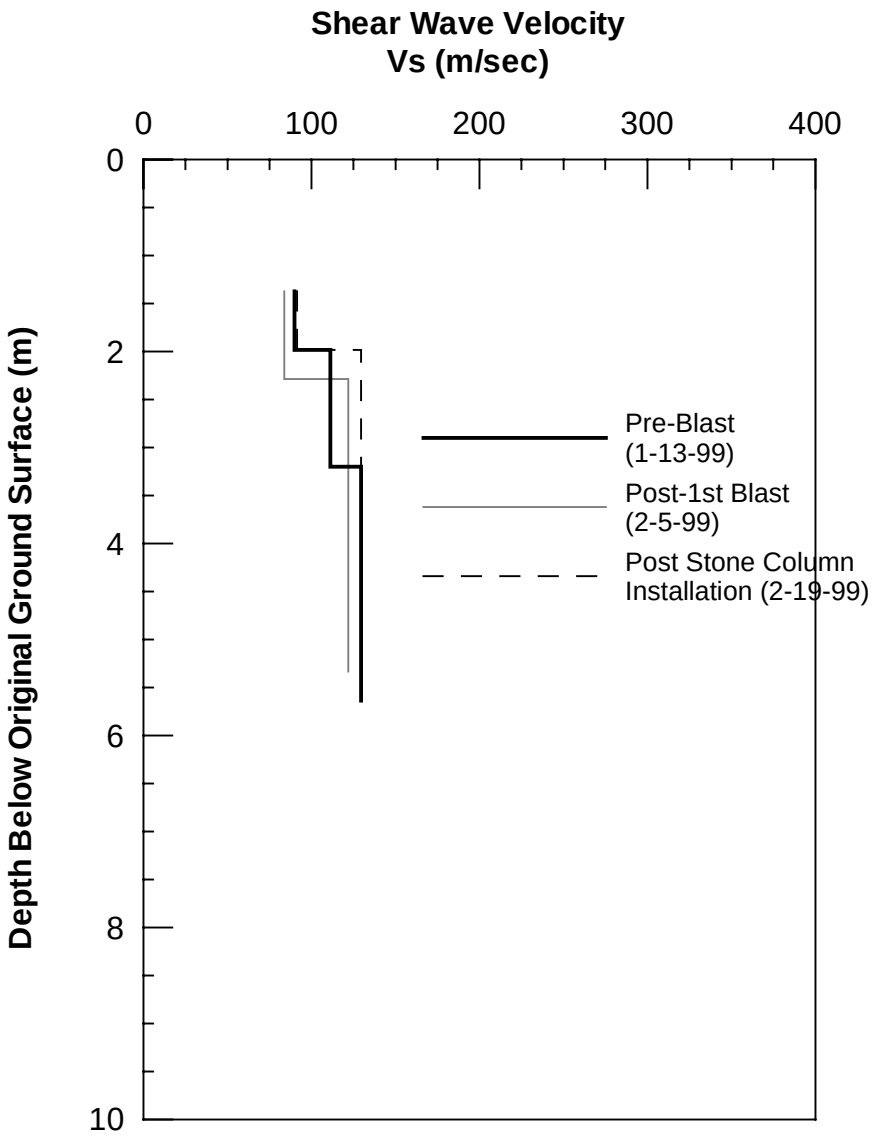

Figure 4.12 Comparison of Down-hole Shear Wave Velocity Profile before 1st Blast, after 1st Blast and after Stone Column Installation for the 4-Pile Group/0.6m CISS Pile Test Area

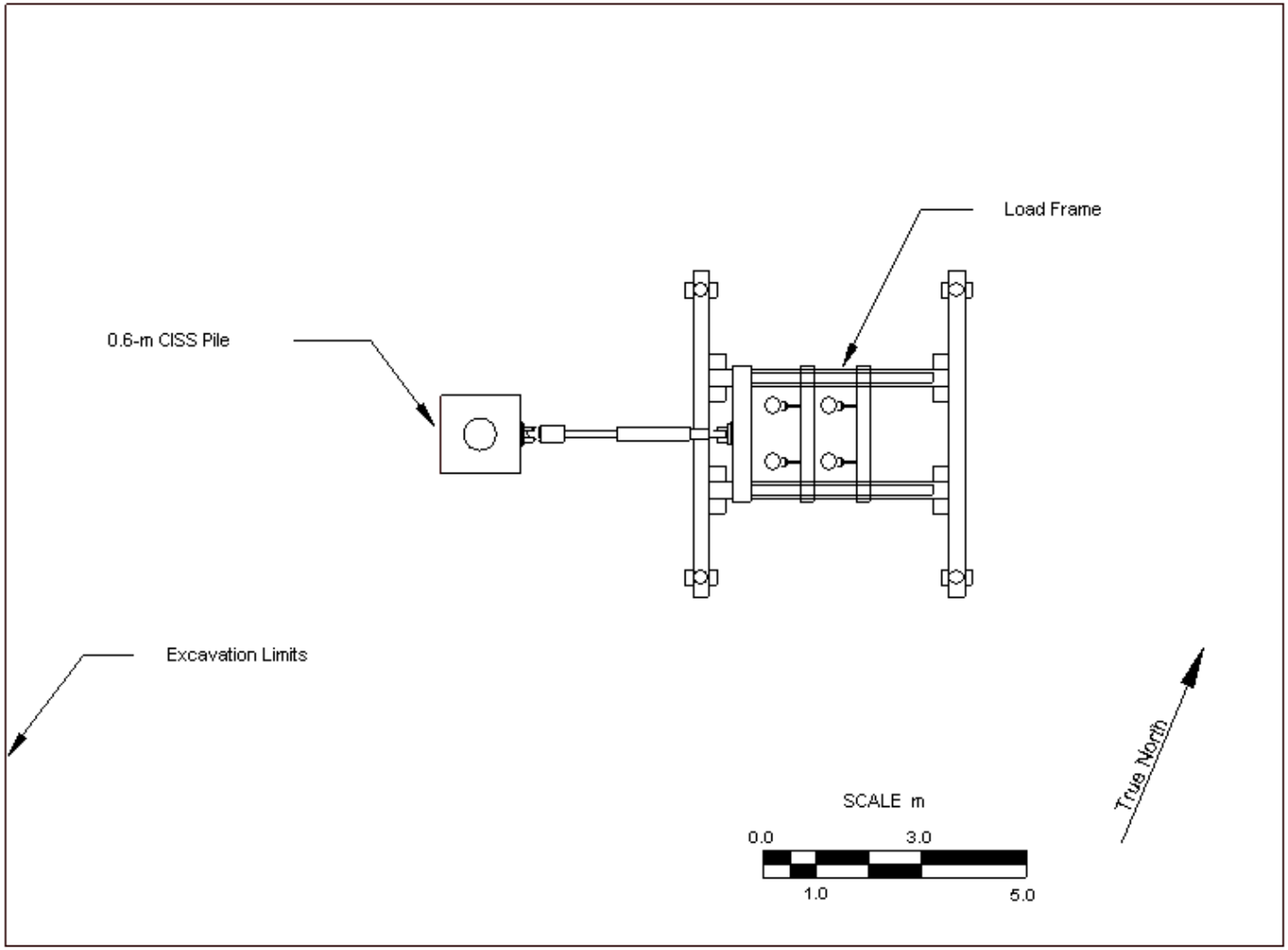

Figure 4.13 Plan View of 4-Pile Group/0.6m CISS Pile Test Set-Up

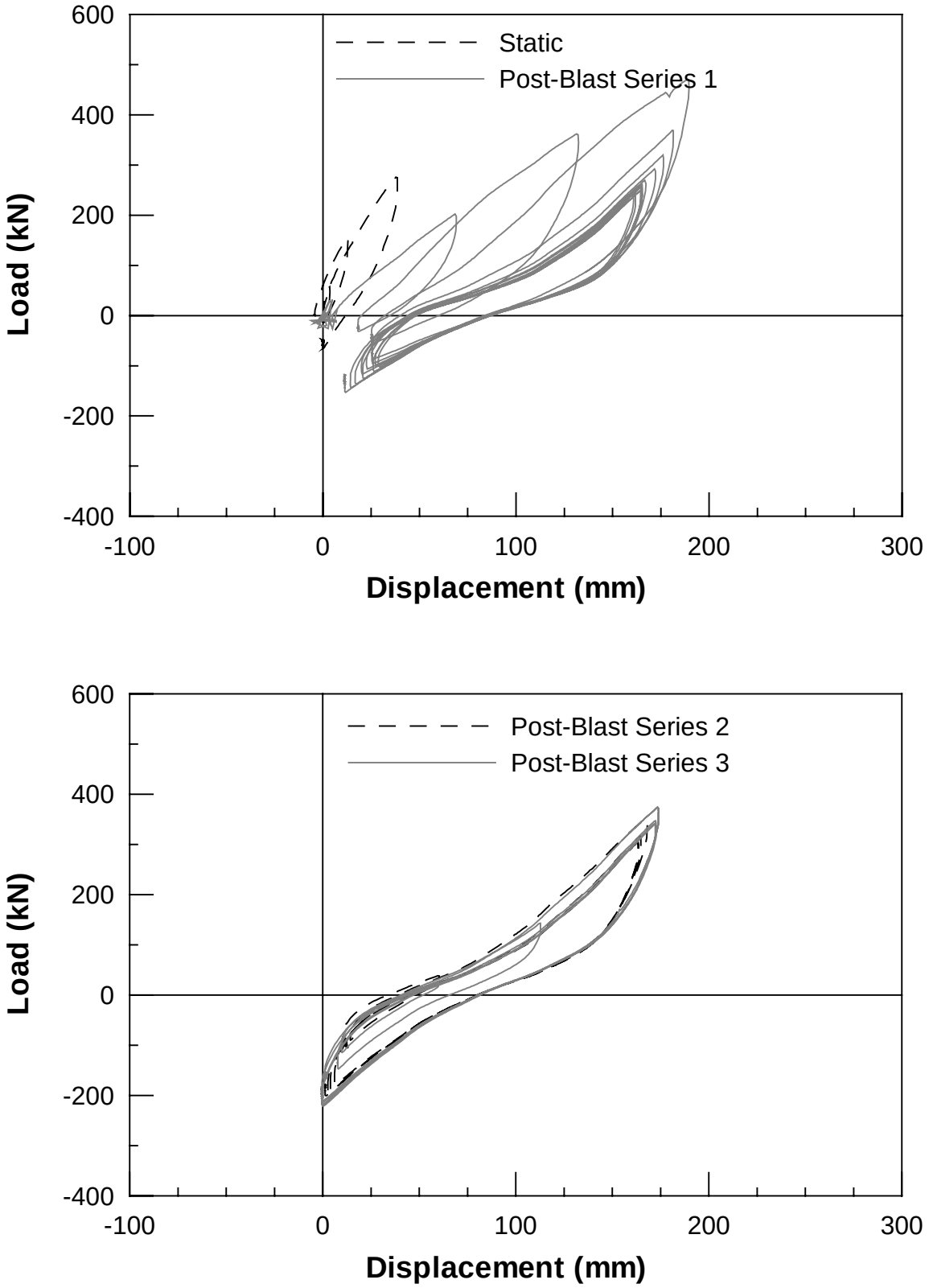

Figure 4.14 4-Pile Group Load vs. Displacement 1st Blast a) Static and Post Blast Series 1 b) Post Blast Series 2 and 3

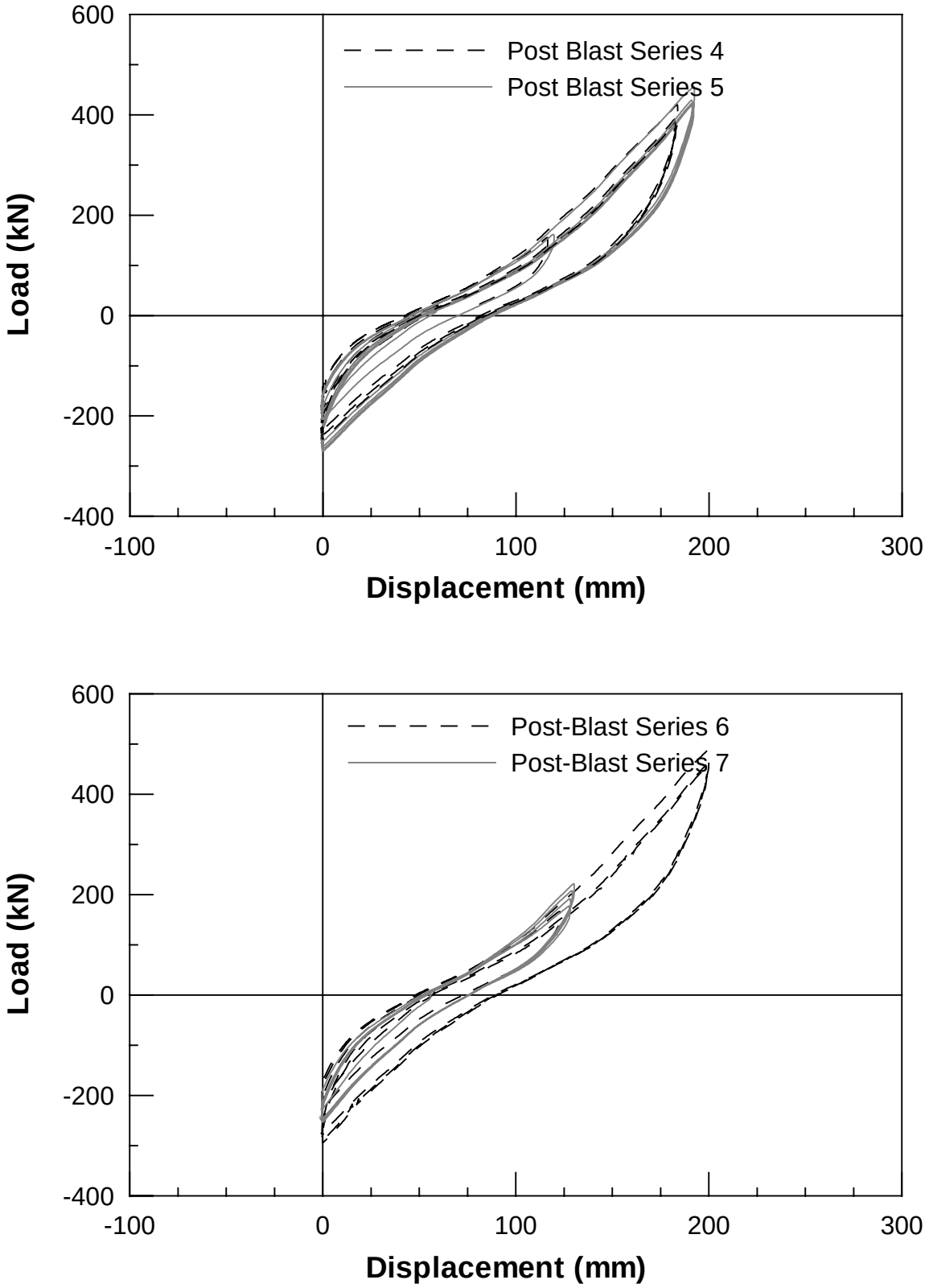

Figure 4.15 4-Pile Group Load vs. Displacement 1st Blast a) Post Blast Series 4 and 5 b) Post Blast Series 6 and 7

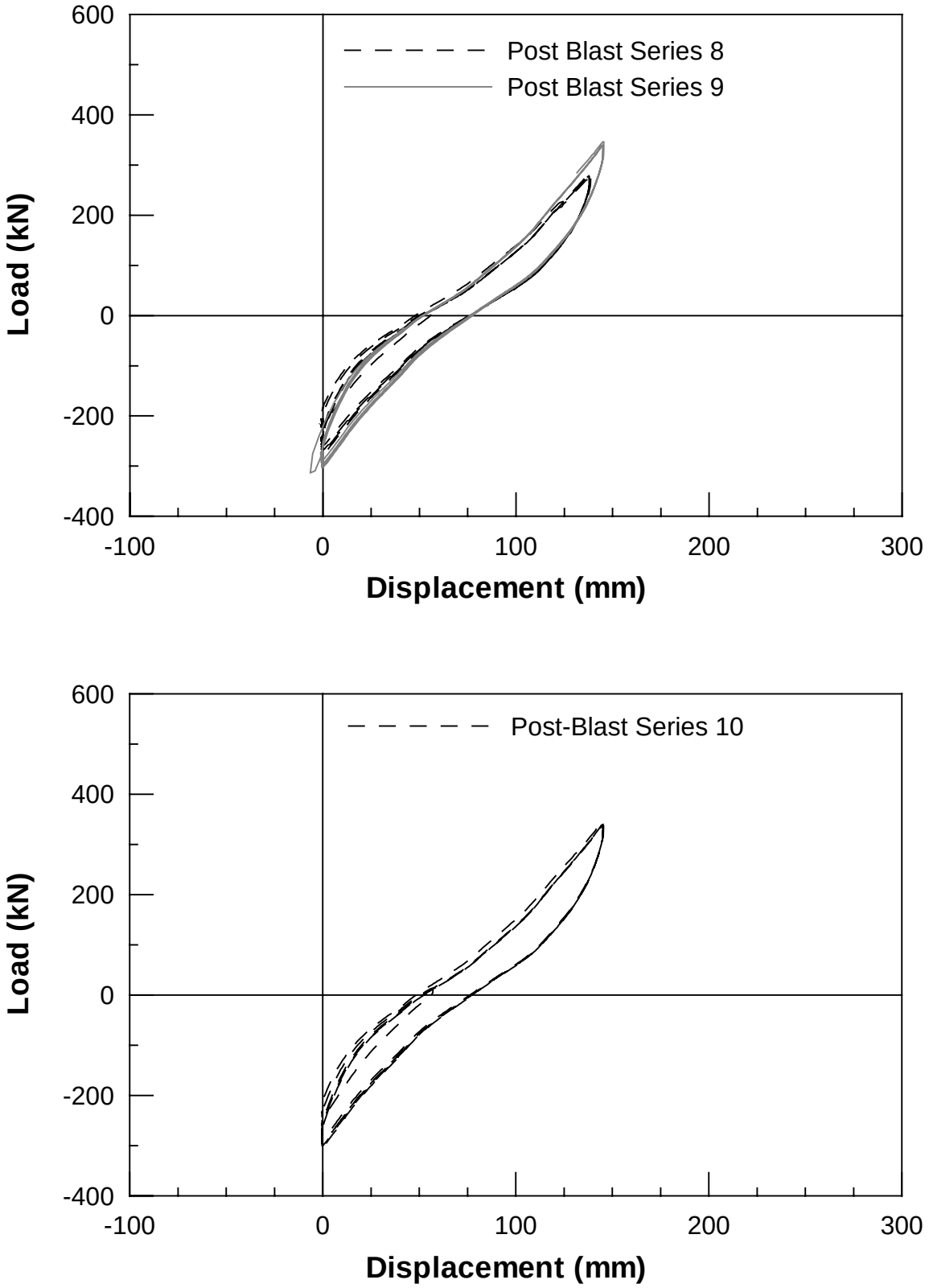

Figure 4.16 Pile Group Load vs. Displacement 1st Blast a) Post Blast Series 8 and 9 b) Post Blast Series 10

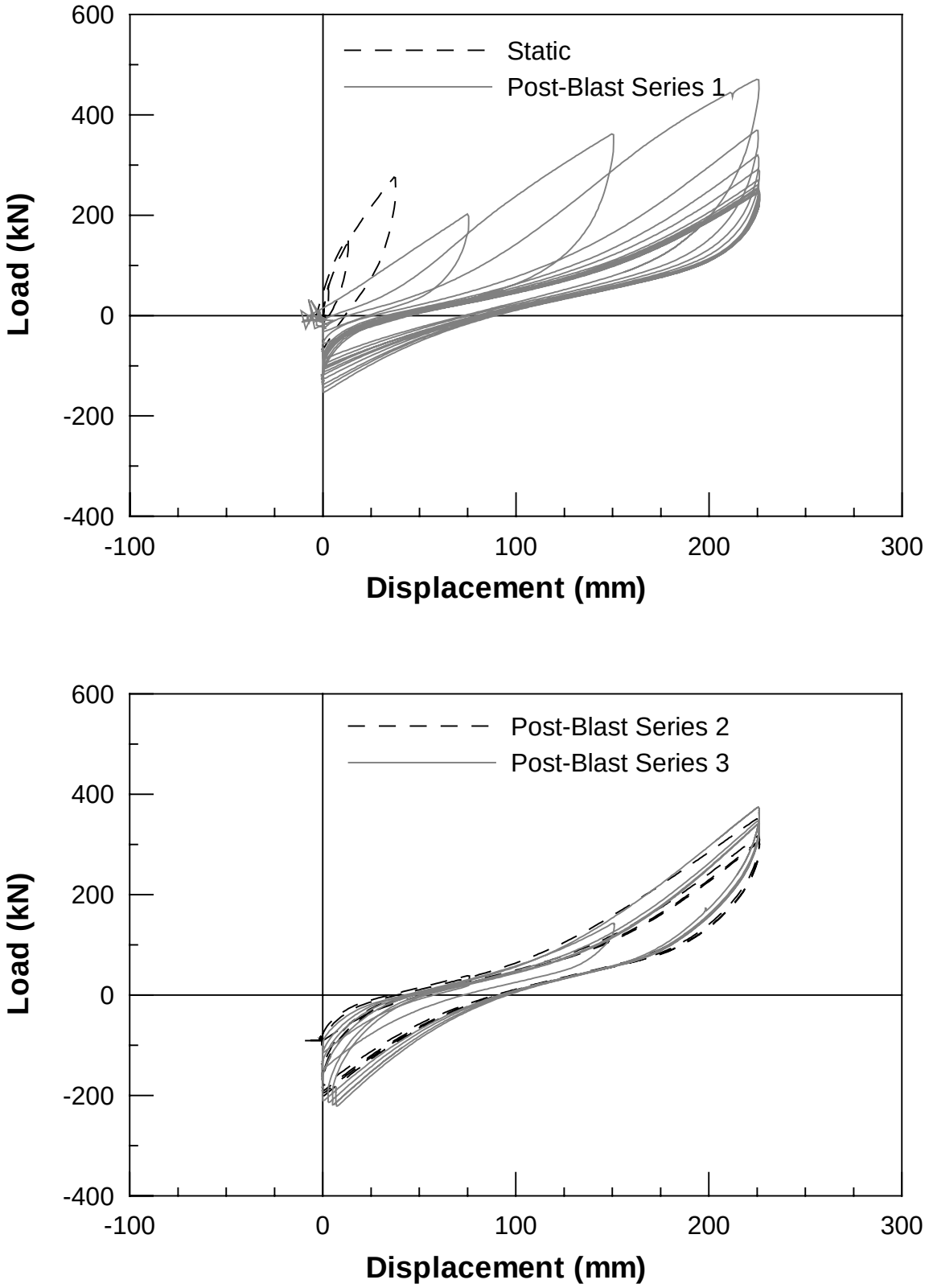

Figure 4.17 0.6m CISS Load vs. Displacement 1st Blast a) Static and Post Blast Series 1 b) Post Blast Series 2 and 3

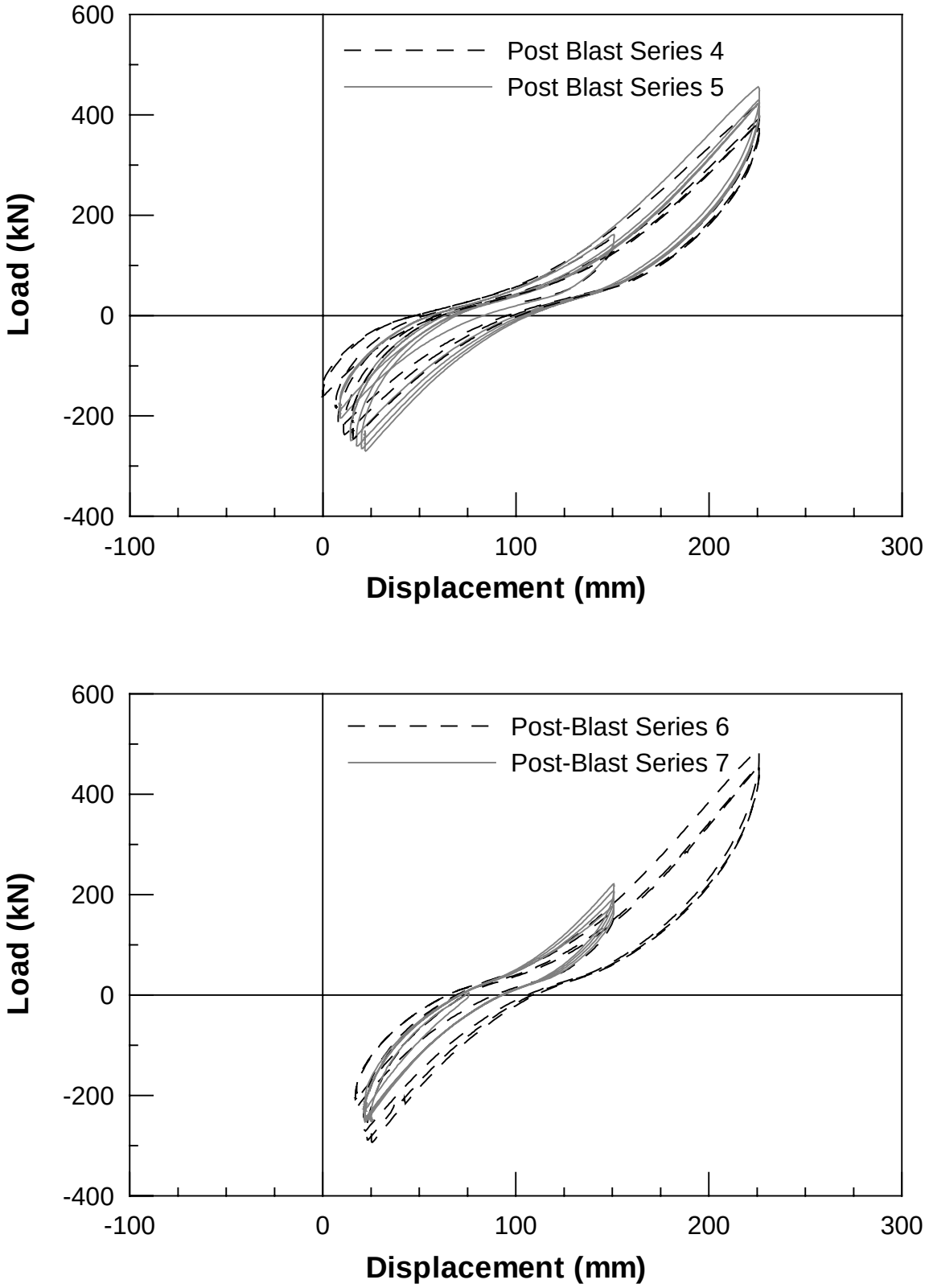

Figure 4.18 0.6m CISS Load vs. Displacement 1st Blast a) Post Blast Series 4 and 5 b) Post Blast Series 6 and 7

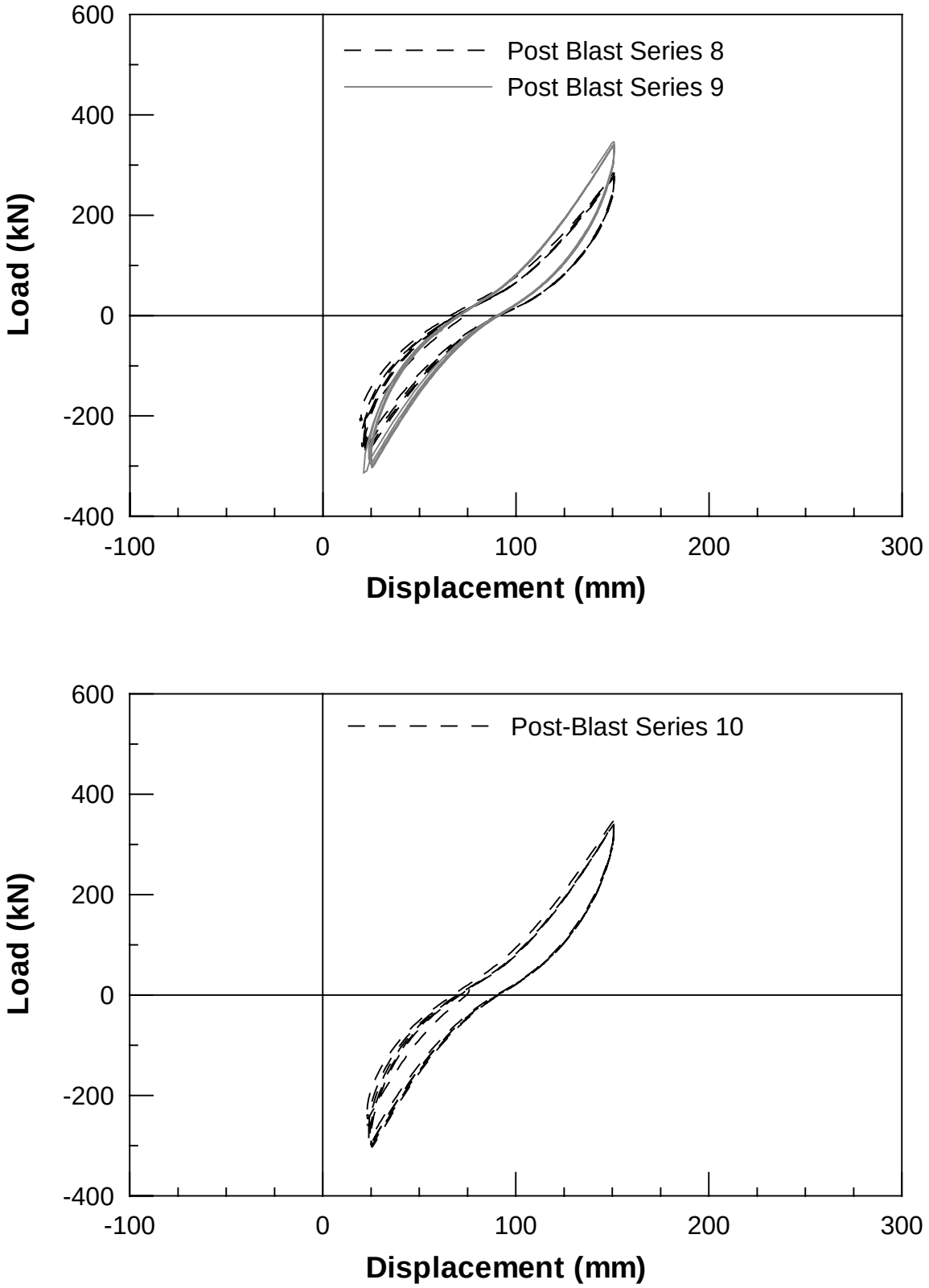

Figure 4.19 0.6m CISS Load vs. Displacement 1st Blast a) Post Blast Series 8 and 9 b) Post Blast Series 10

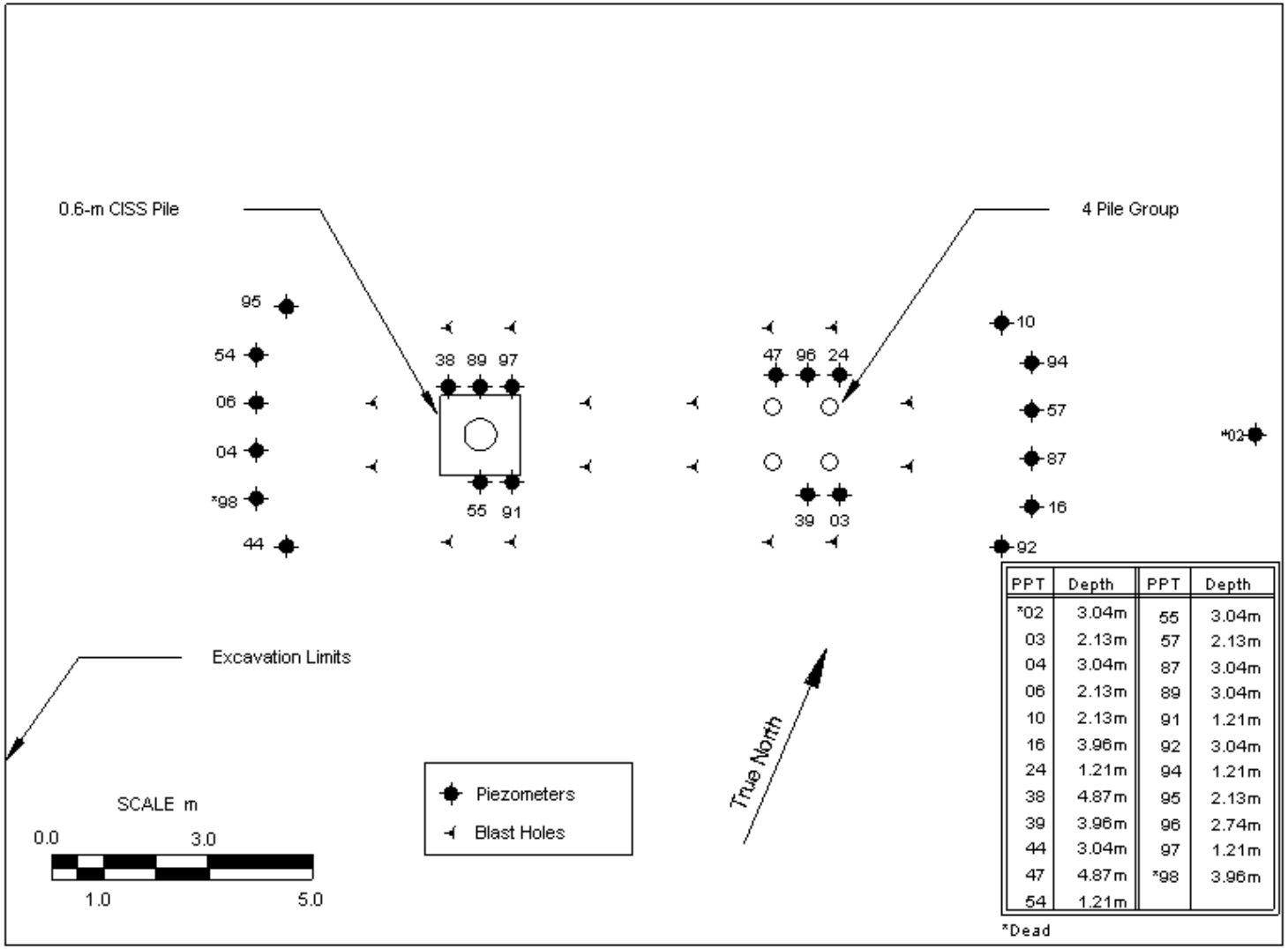

PPT	Depth	PPT	Depth
*02	3.04m	55	3.04m
03	2.13m	57	2.13m
04	3.04m	87	3.04m
06	2.13m	89	3.04m
10	2.13m	91	1.21m
16	3.96m	92	3.04m
24	1.21m	94	1.21m
38	4.87m	95	2.13m
39	3.96m	96	2.74m
44	3.04m	97	1.21m
47	4.87m	*98	3.96m
54	1.21m		

*Dead

Figure 4.20 Location Map of Pore Pressure Transducers for 4-Pile Group/0.6m CISS Pile Site

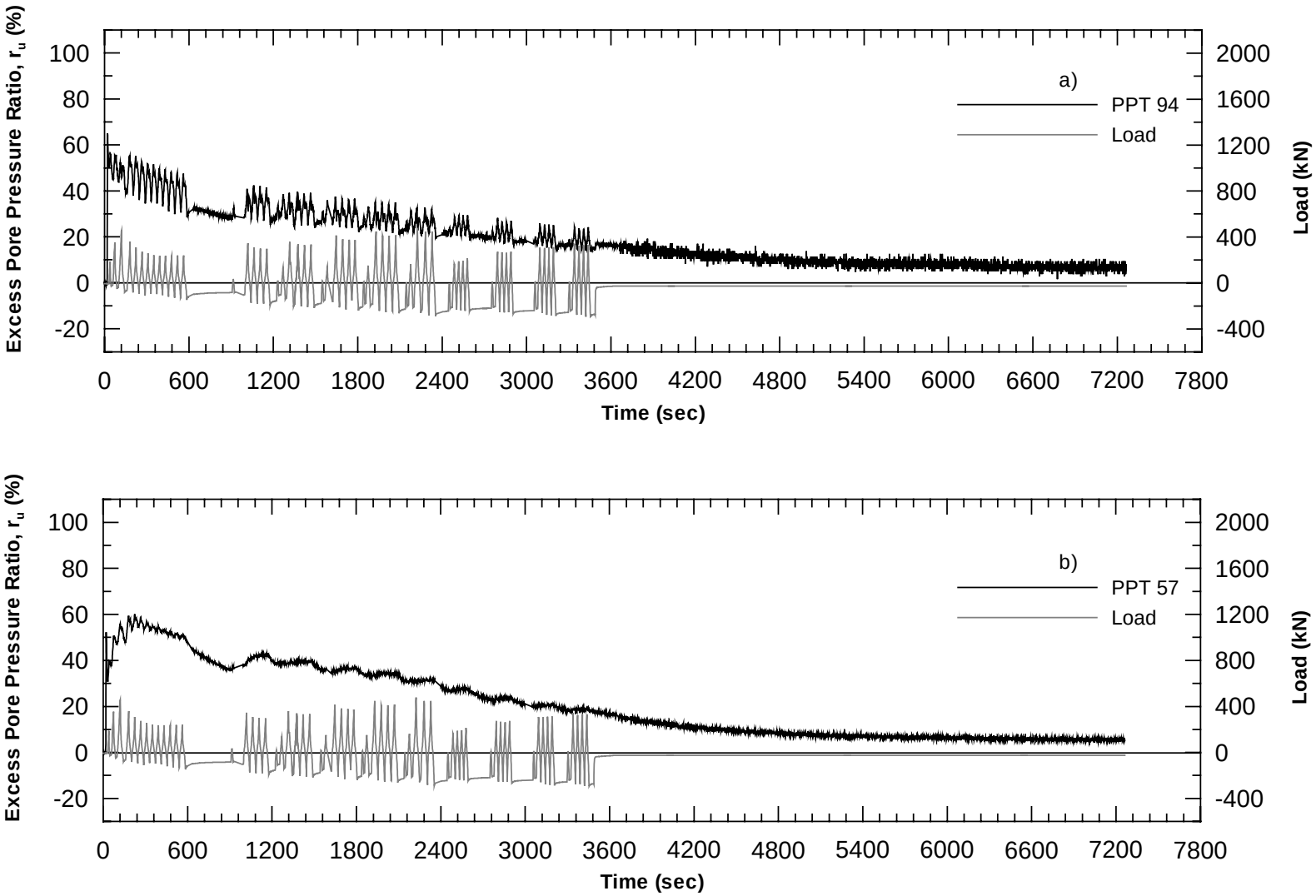

Figure 4.21 Excess Pore Pressure Ratio for 4-Pile Group/0.6m CISS Pile 1 st Blast a)PPT94 b)PPT57

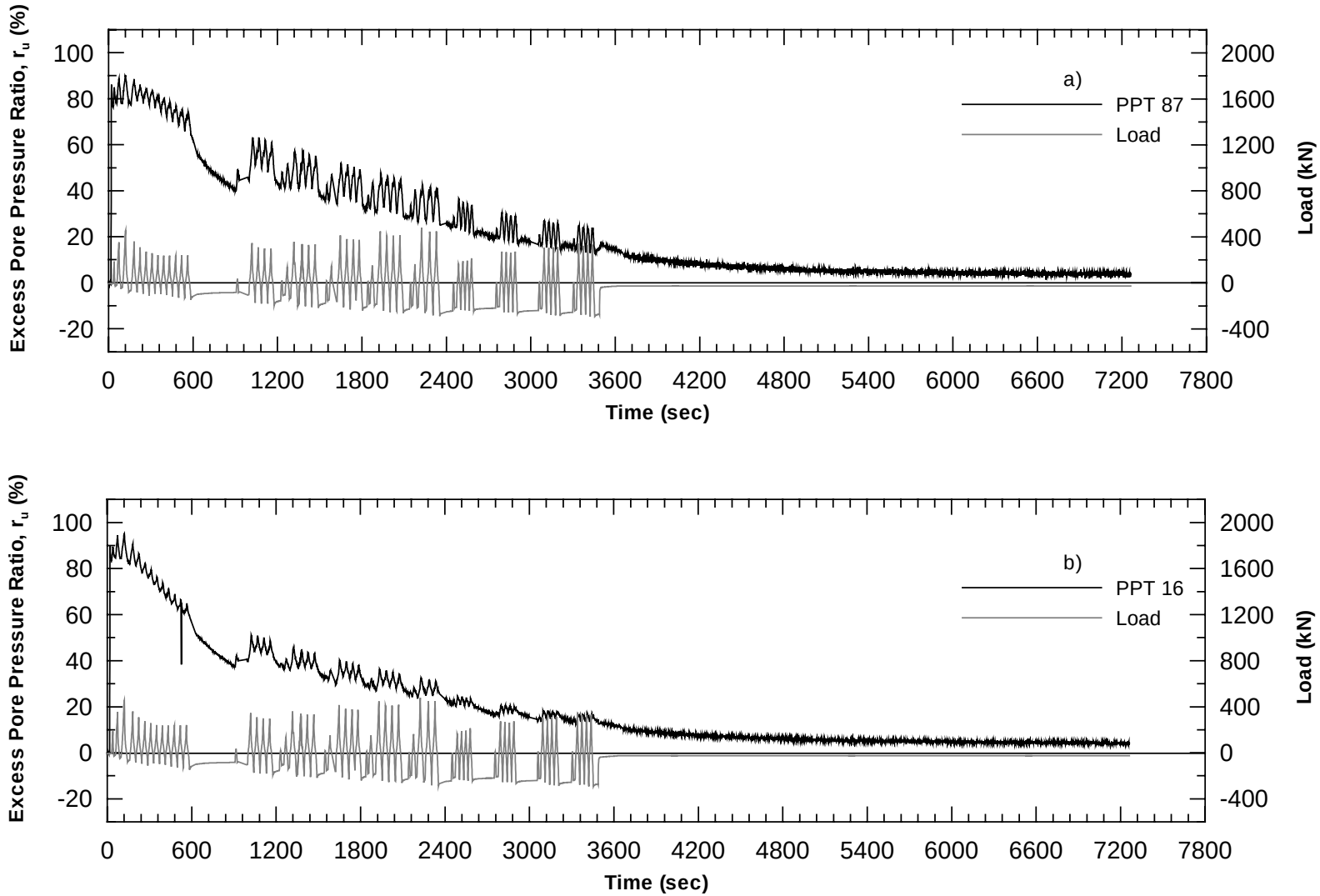

Figure 4.22 Excess Pore Pressure Ratio for 4-Pile Group/0.6m CISS Pile 1 st Blast a)PPT87 b)PPT16

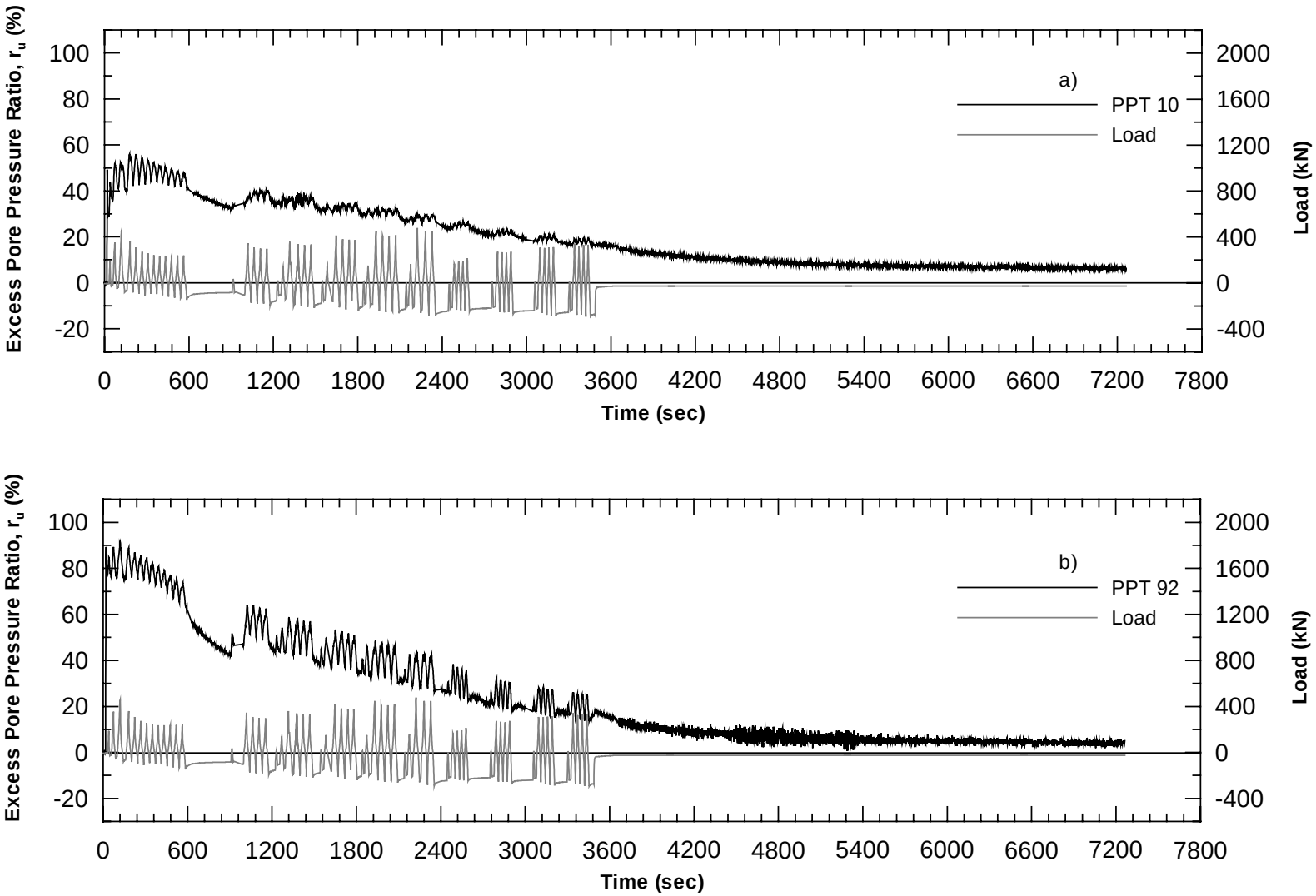

Figure 4.23 Excess Pore Pressure Ratio for 4-Pile Group/0.6m CISS Pile 1 st Blast a)PPT10 b)PPT92

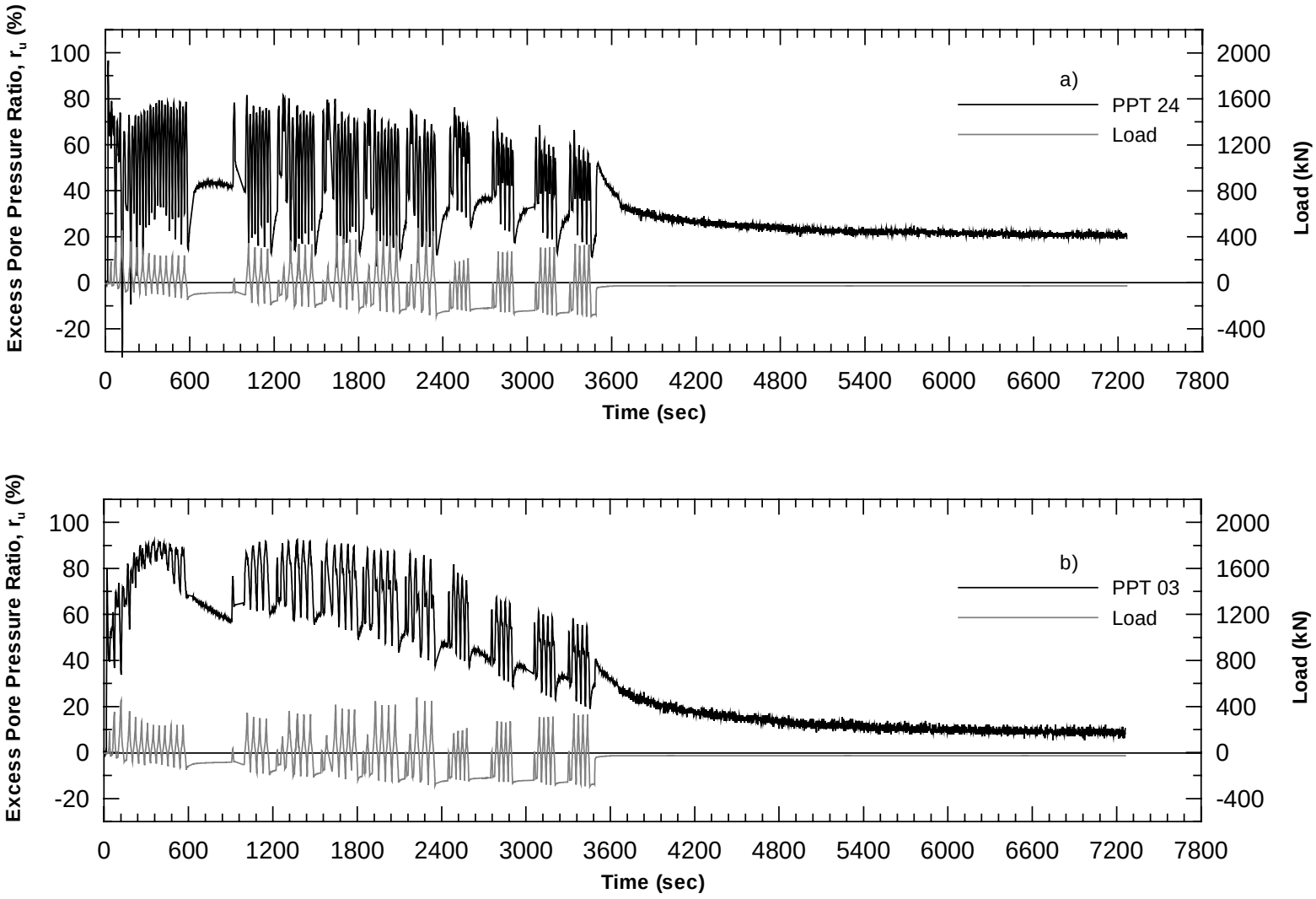

Figure 4.24 Excess Pore Pressure Ratio for 4-Pile Group/0.6m CISS Pile 1 st Blast a)PPT24 b)PPT3

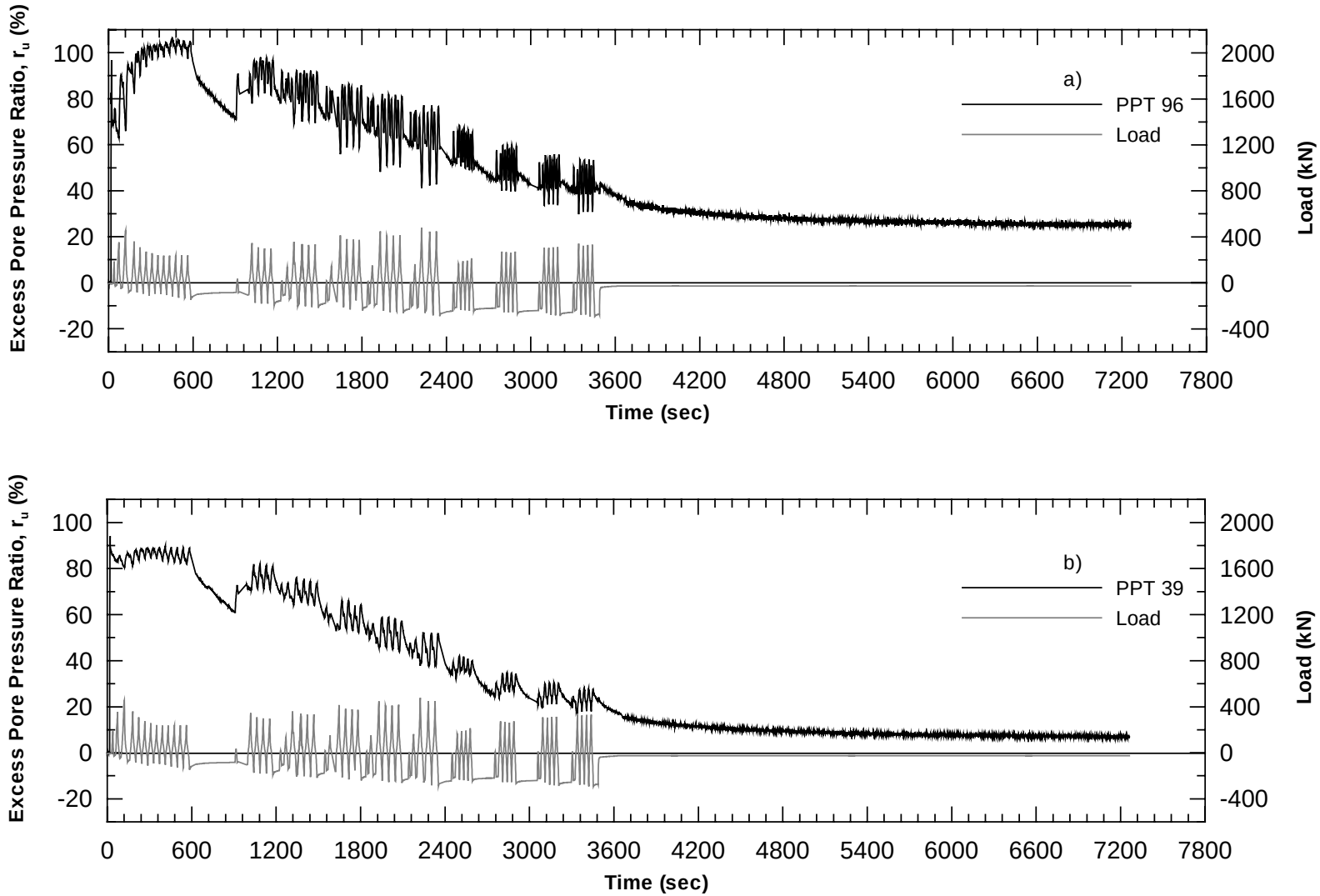

Figure 4.25 Excess Pore Pressure Ratio for 4-Pile Group/0.6m CISS Pile 1 st Blast a)PPT96 b)PPT39

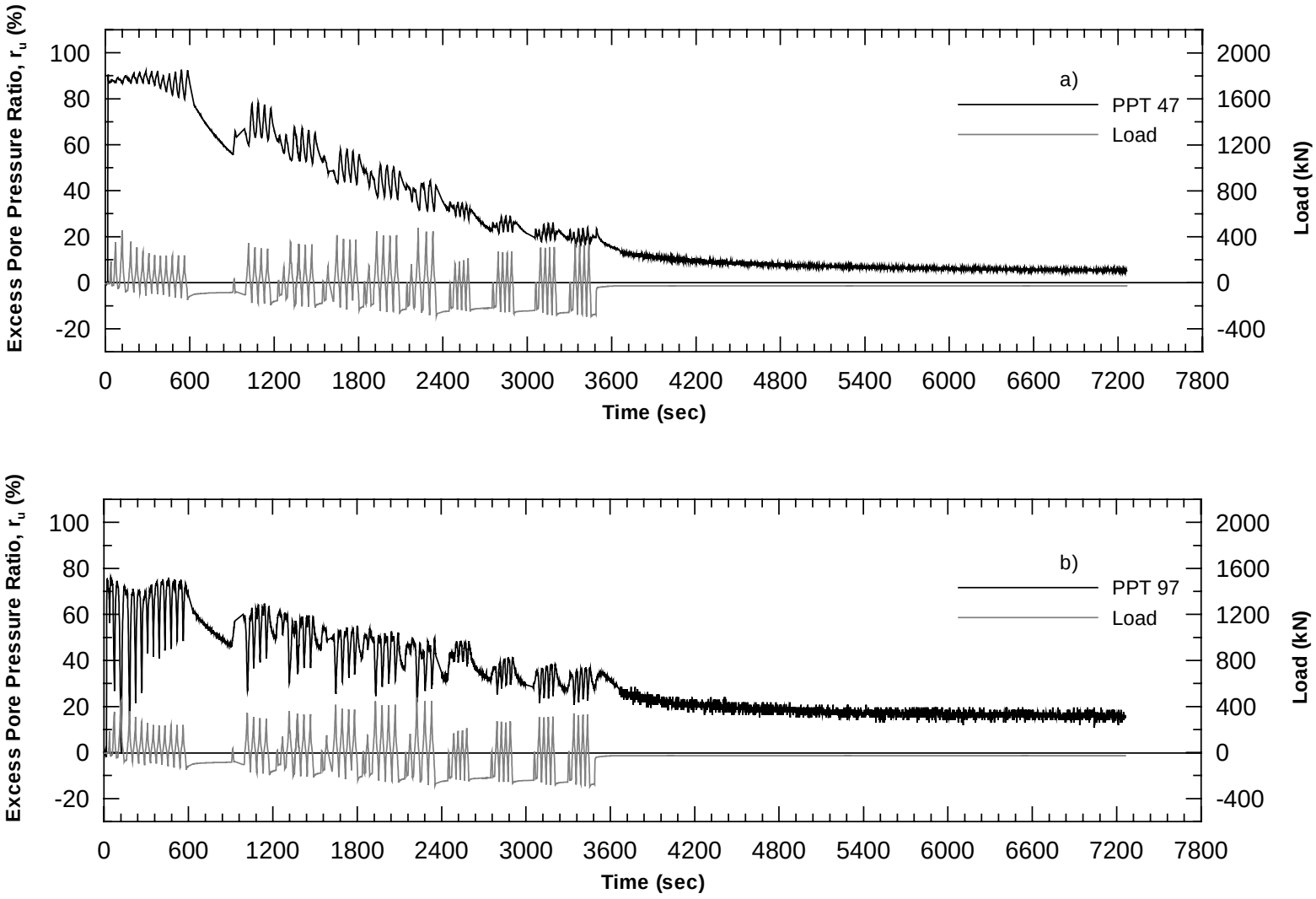

Figure 4.26 Excess Pore Pressure Ratio for 4-Pile Group/0.6m CISS Pile 1 st Blast a)PPT47 b)PPT97

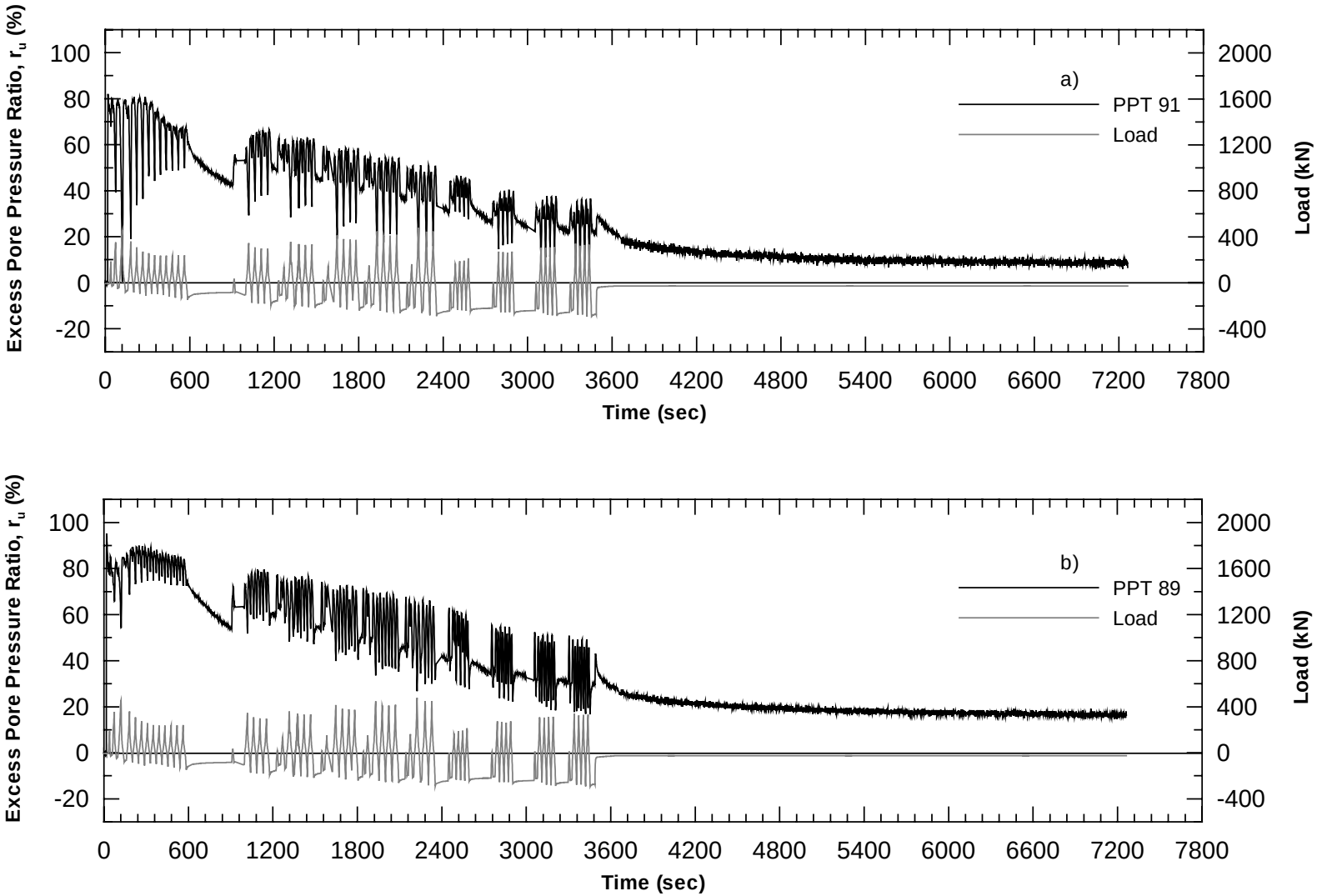

Figure 4.27 Excess Pore Pressure Ratio for 4-Pile Group/0.6m CISS Pile 1 st Blast a)PPT91 b)PPT89

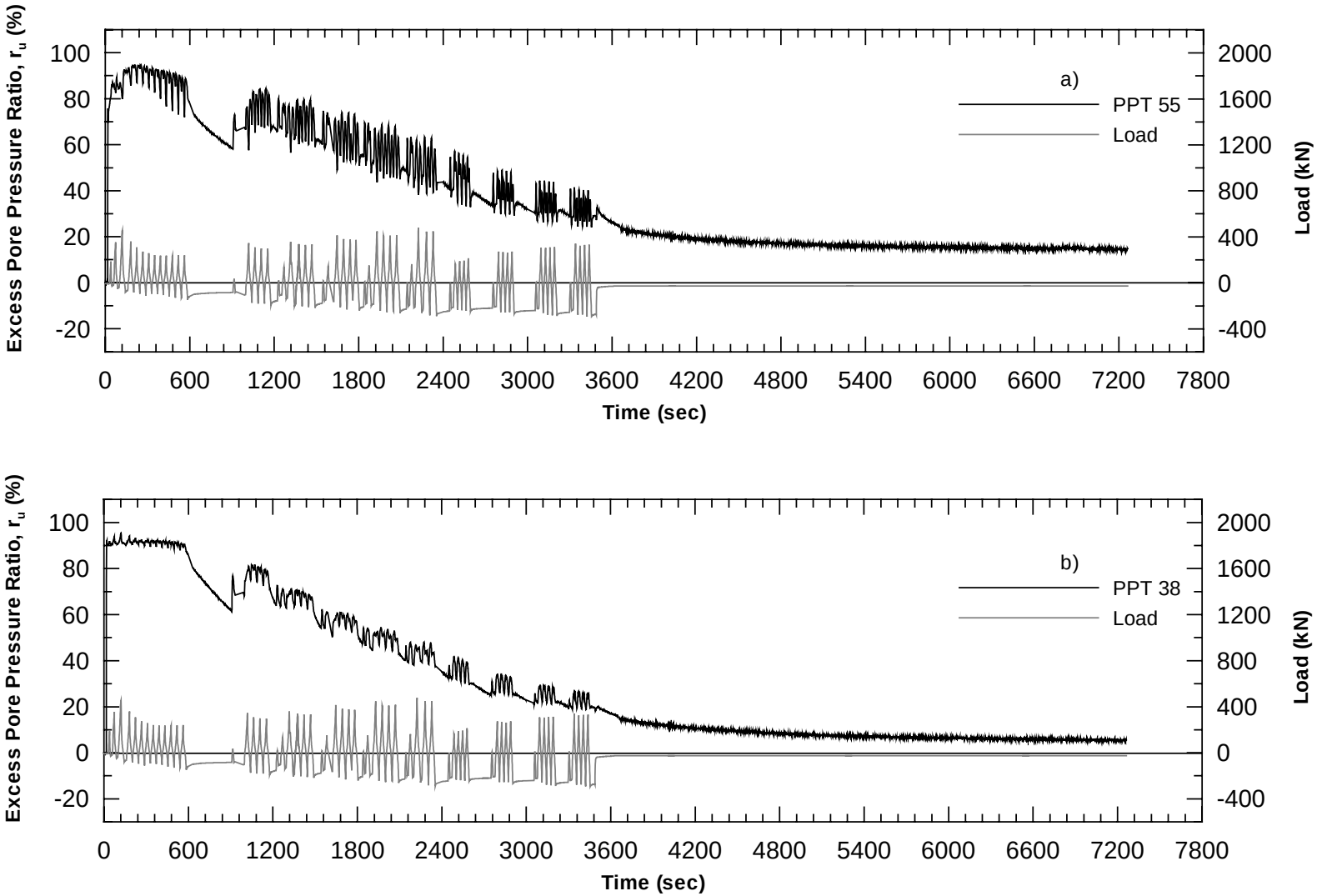

Figure 4.28 Excess Pore Pressure Ratio for 4-Pile Group/0.6m CISS Pile 1 st Blast a)PPT55 b)PPT38

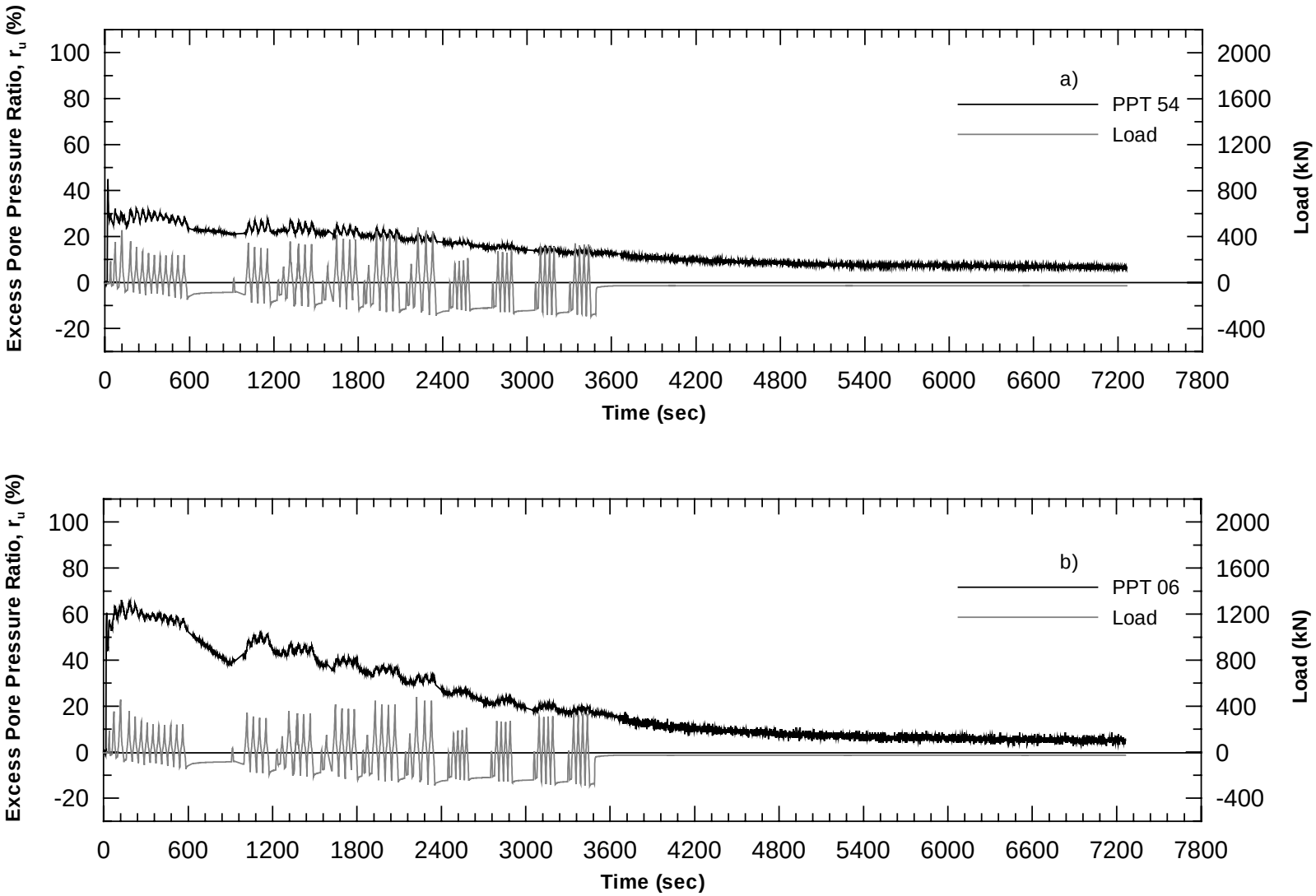

Figure 4.29 Excess Pore Pressure Ratio for 4-Pile Group/0.6m CISS Pile 1 st Blast a)PPT54 b)PPT06

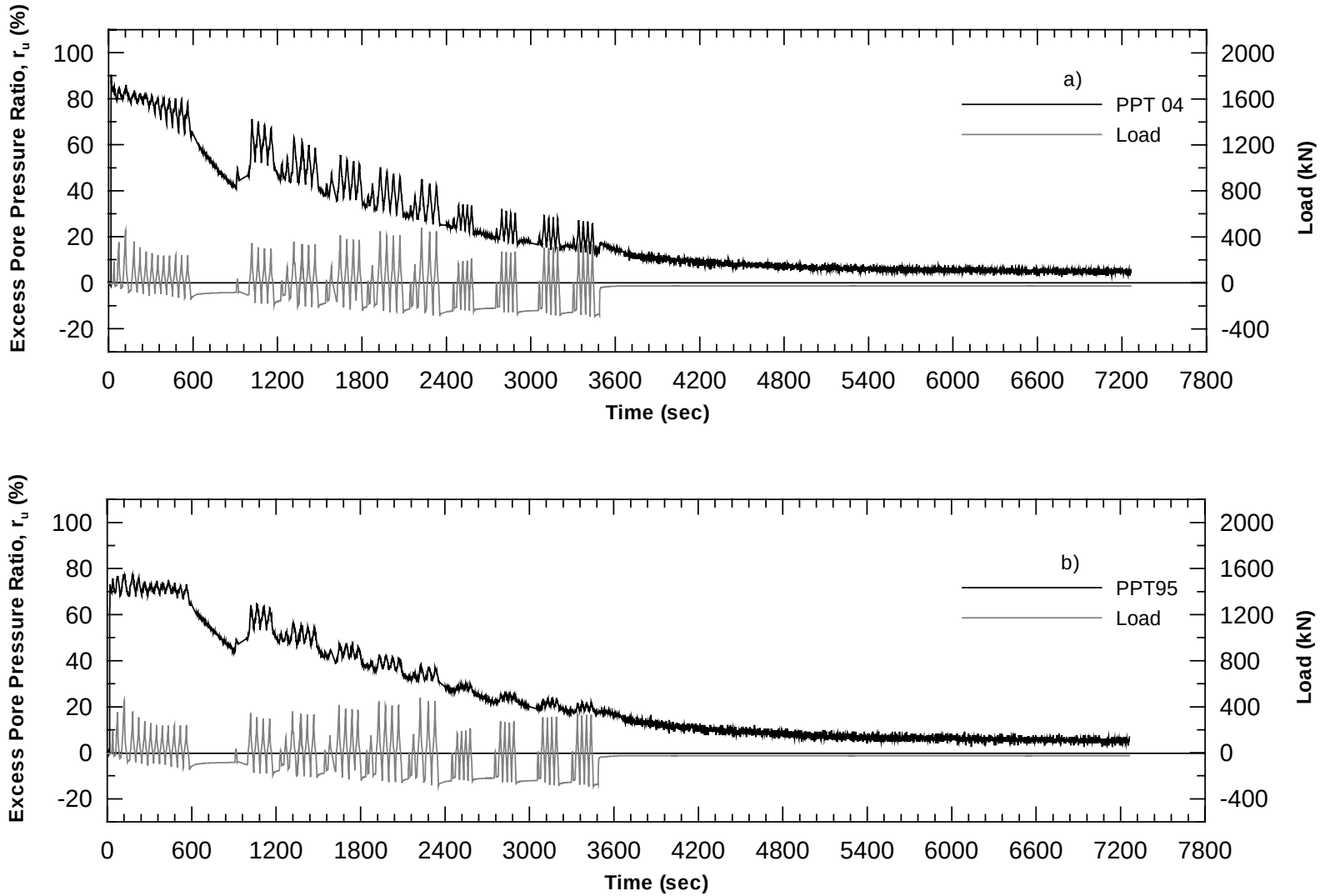

Figure 4.30 Excess Pore Pressure Ratio for 4-Pile Group/0.6m CISS Pile 1 st Blast a)PPT04 b)PPT95

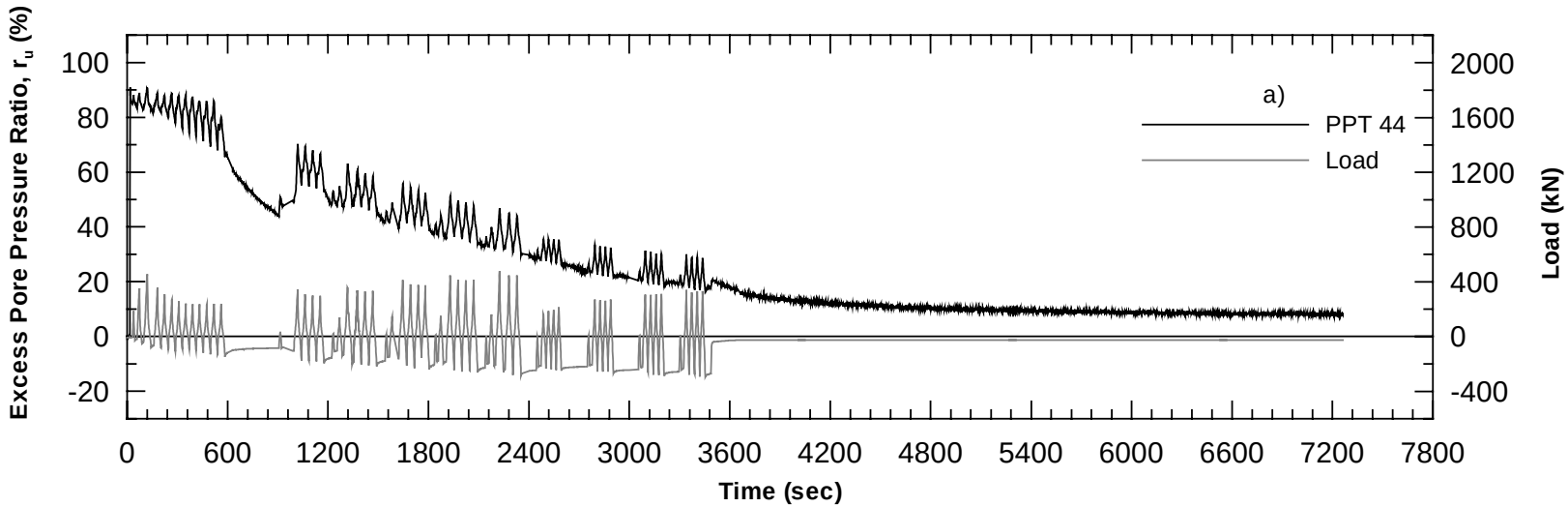

Figure 4.31 Excess Pore Pressure Ratio for 4-Pile Group/0.6m CISS Pile 1 st Blast PPT44

Figure 4.32 Installation of Stone Columns

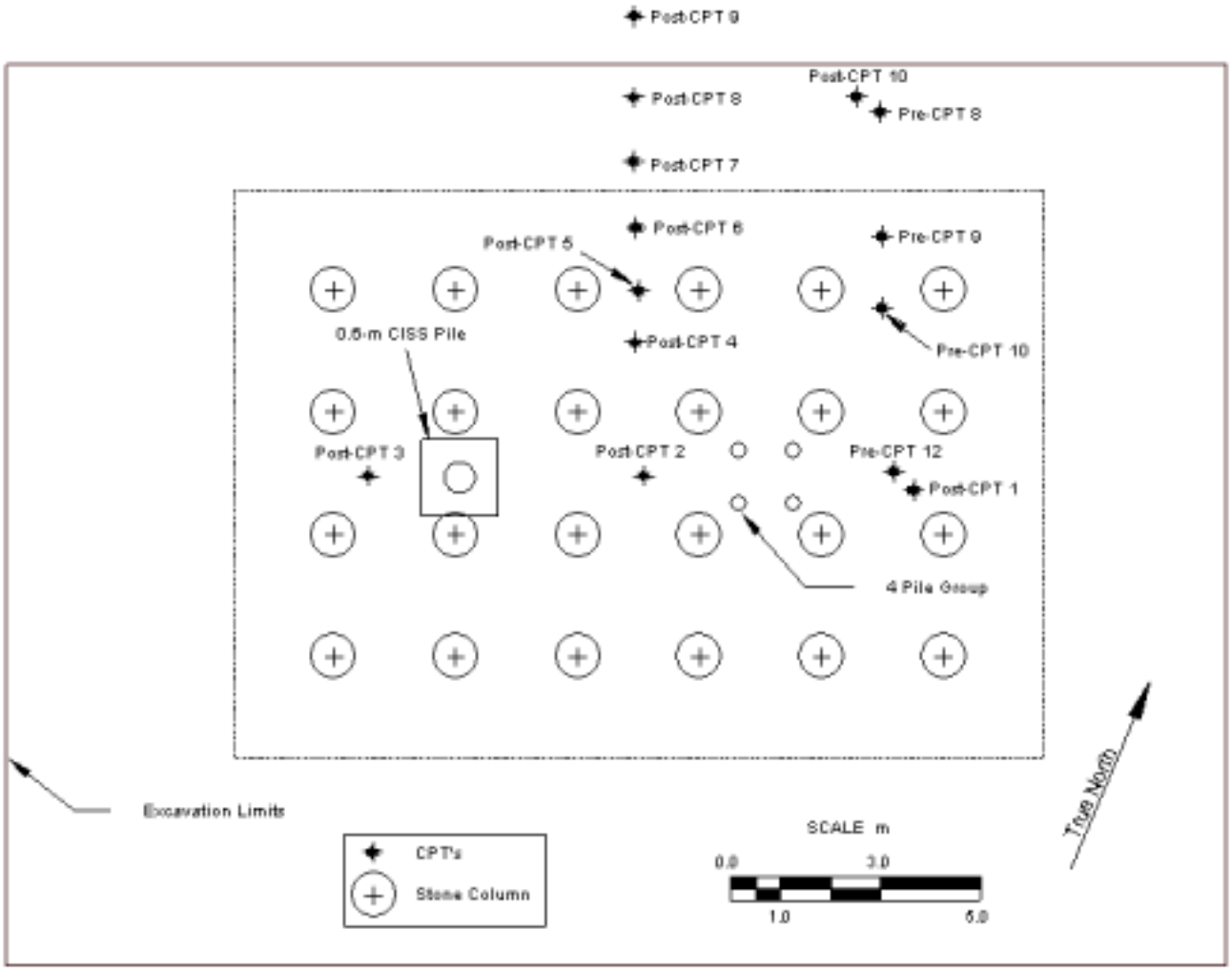

Figure 4.33 Location Map of Secondary In-Situ Tests and Stone Columns for 2 nd Blast

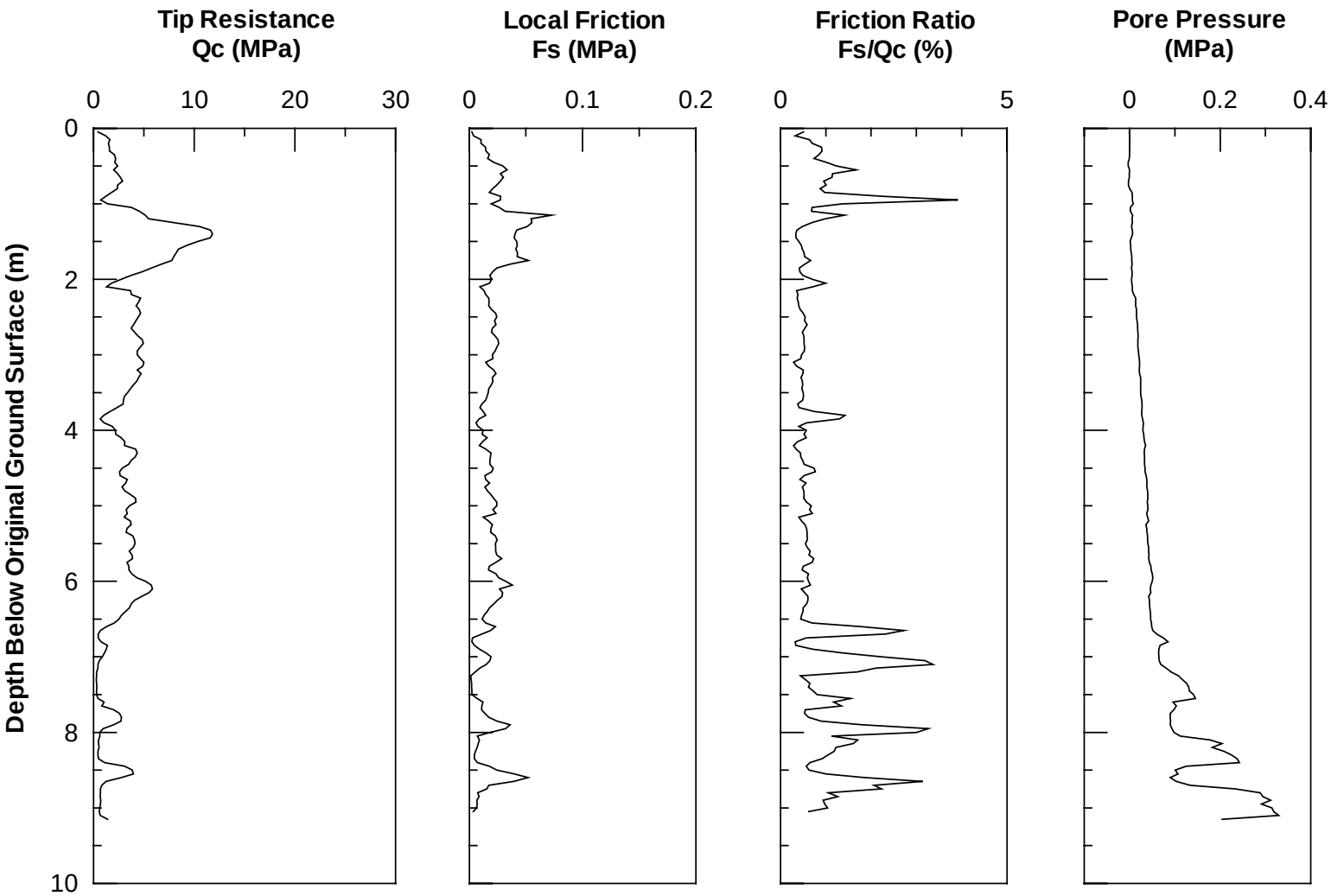

Figure 4.34 Pre-treatment CPT08 Logs for 4-Pile Group/0.6m CISS Pile Test Area (2-08-99)

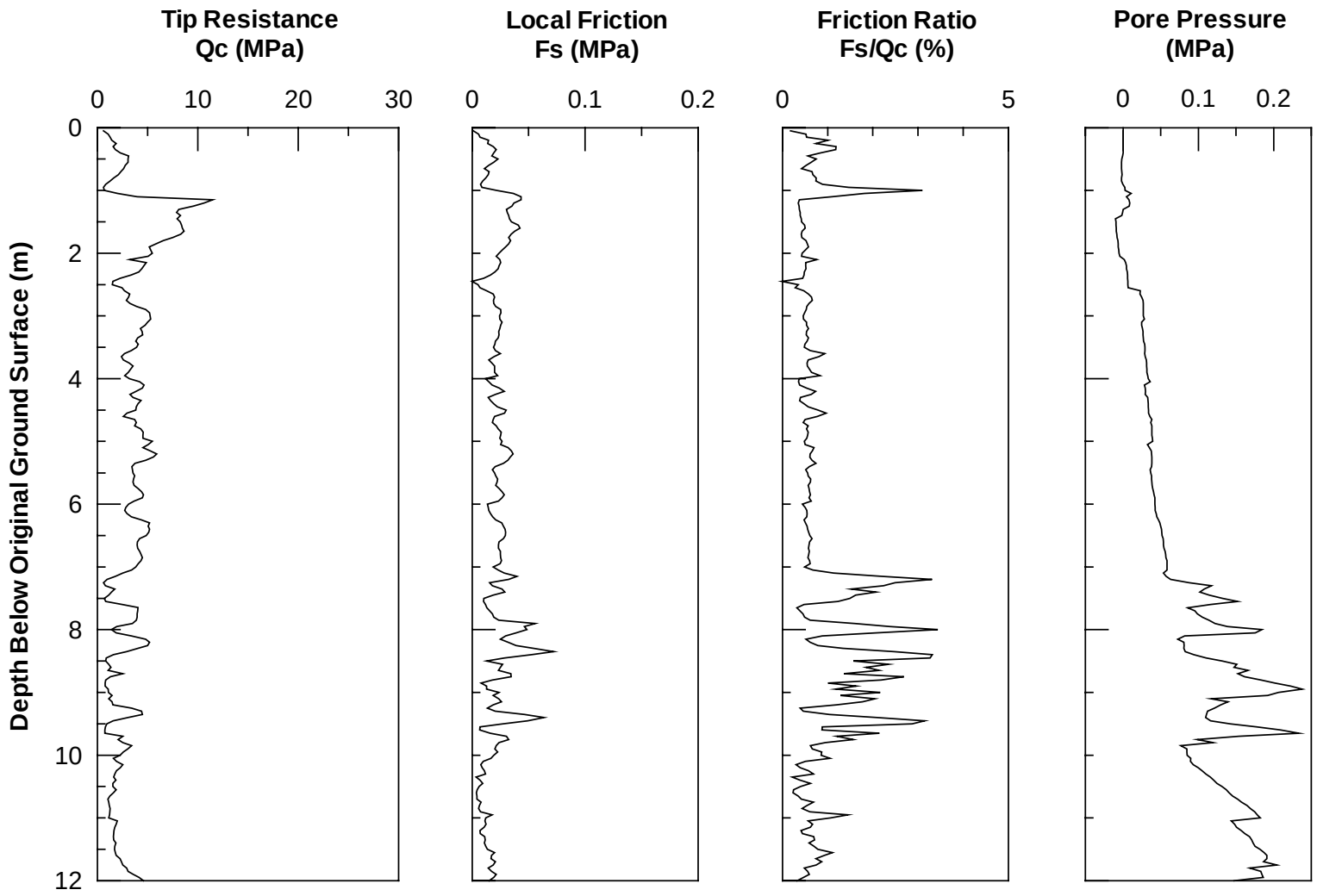

Figure 4.35 Pre-treatment CPT09 Logs for 4-Pile Group/0.6m CISS Pile Test Area (2-08-99)

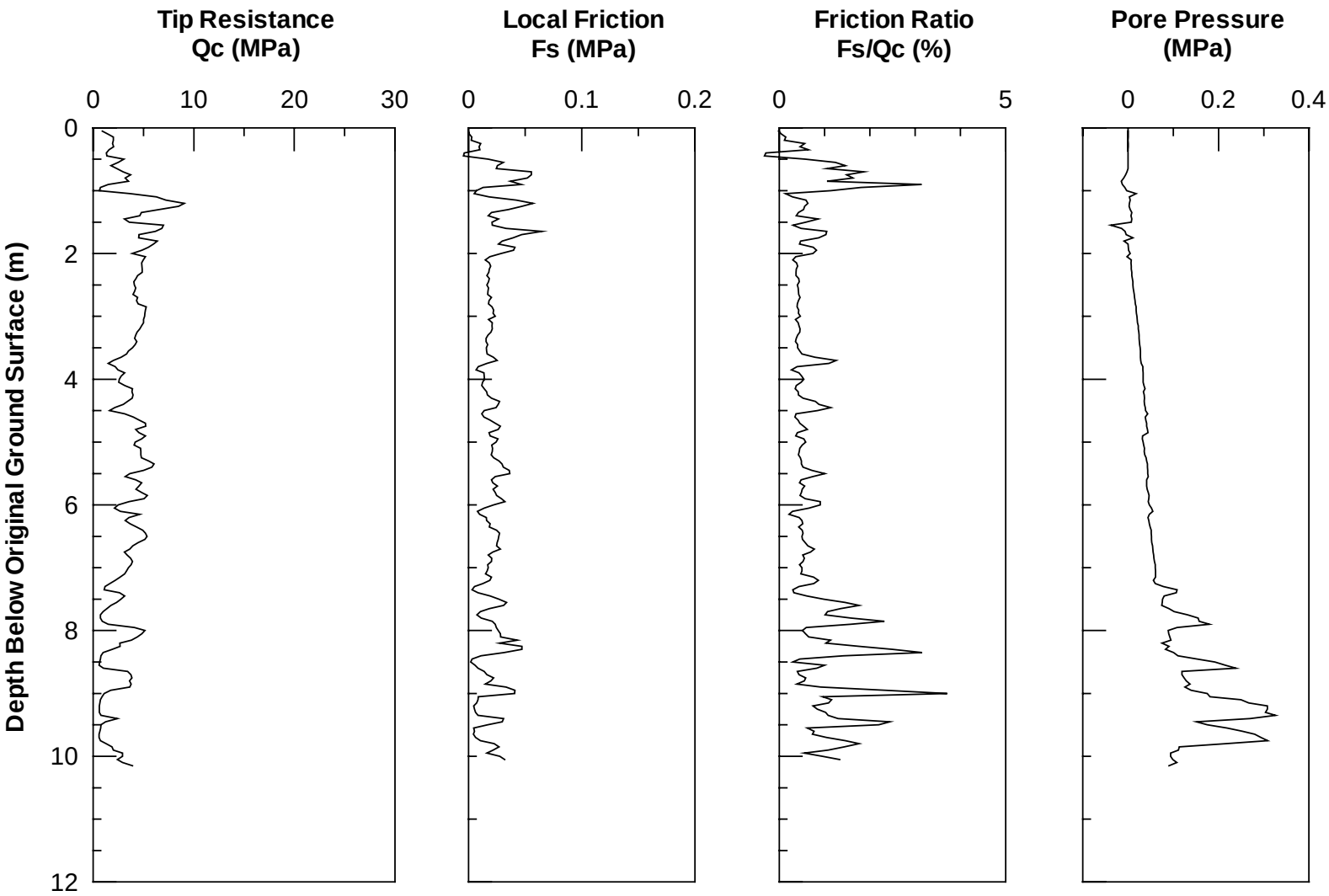

Figure 4.36 Pre-treatment CPT10 Logs for 4-Pile Group/0.6m CISS Pile Test Area (2-08-99)

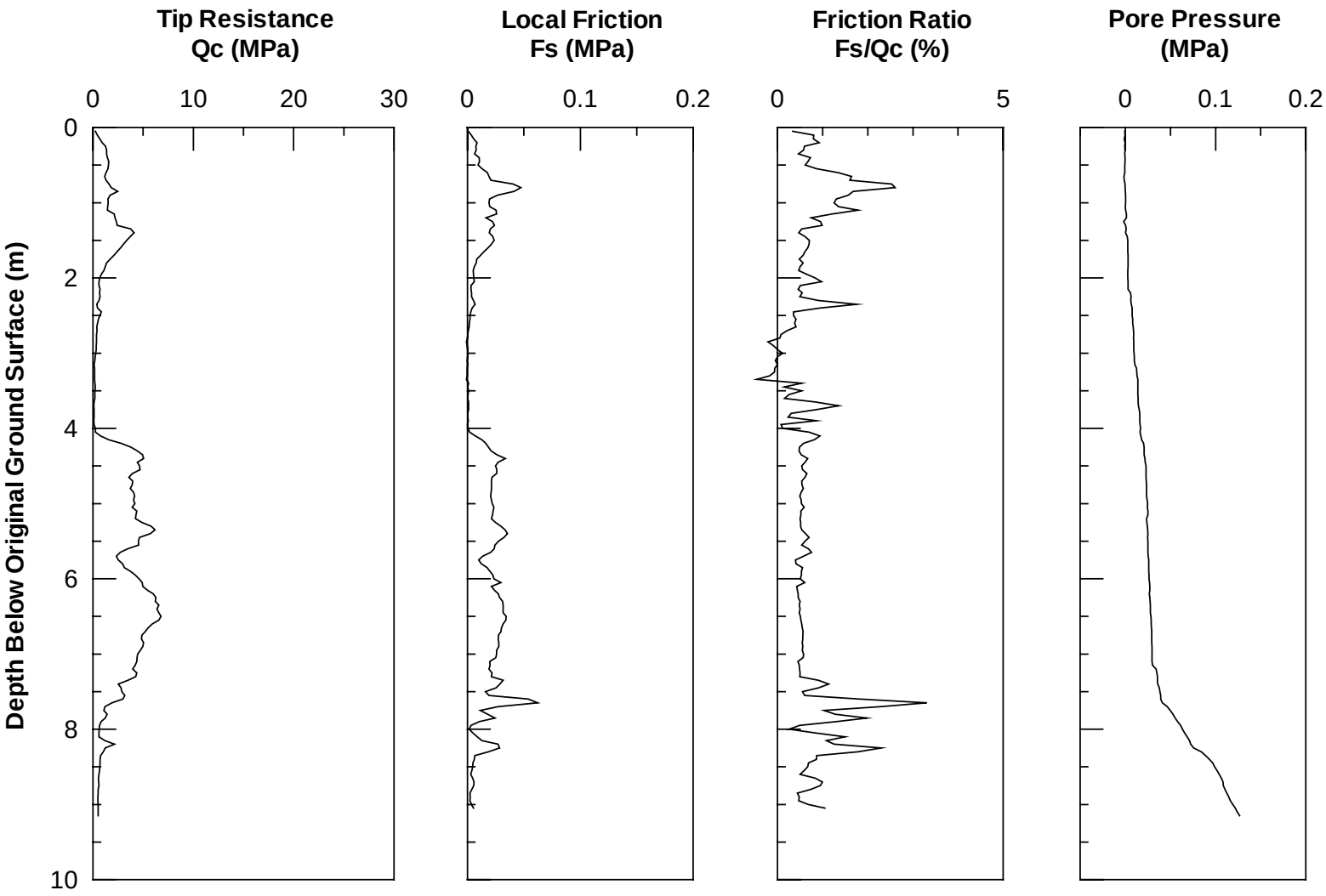

Figure 4.37 Pre-treatment CPT12 Logs for 4-Pile Group/0.6m CISS Pile Test Area (2-08-99)

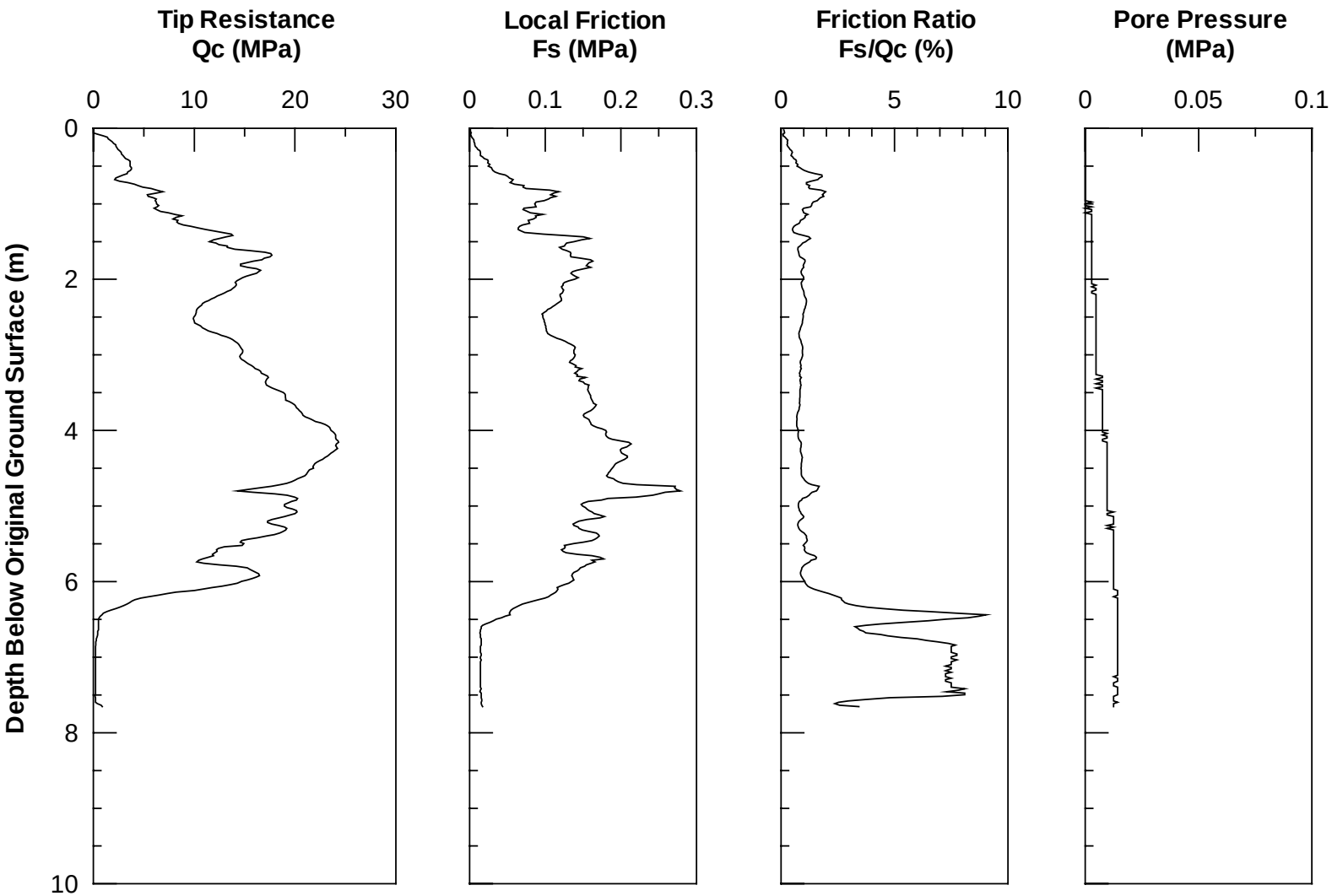

Figure 4.38 Post-treatment CPT1 Logs for 4-Pile Group/0.6m CISS Pile Test Area (2-16-99)

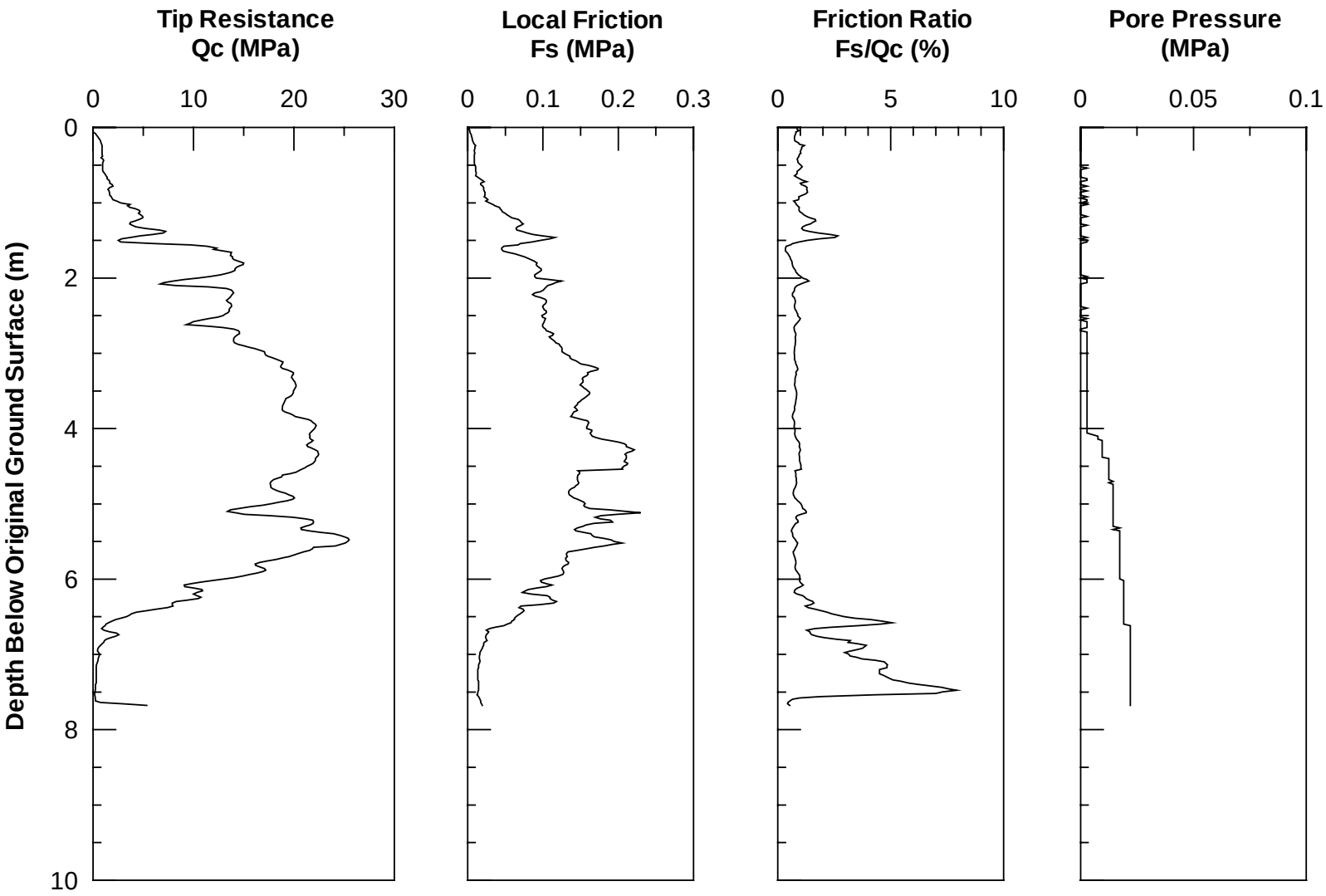

Figure 4.39 Post-treatment CPT2 Logs for 4-Pile Group/0.6m CISS Pile Test Area (2-16-99)

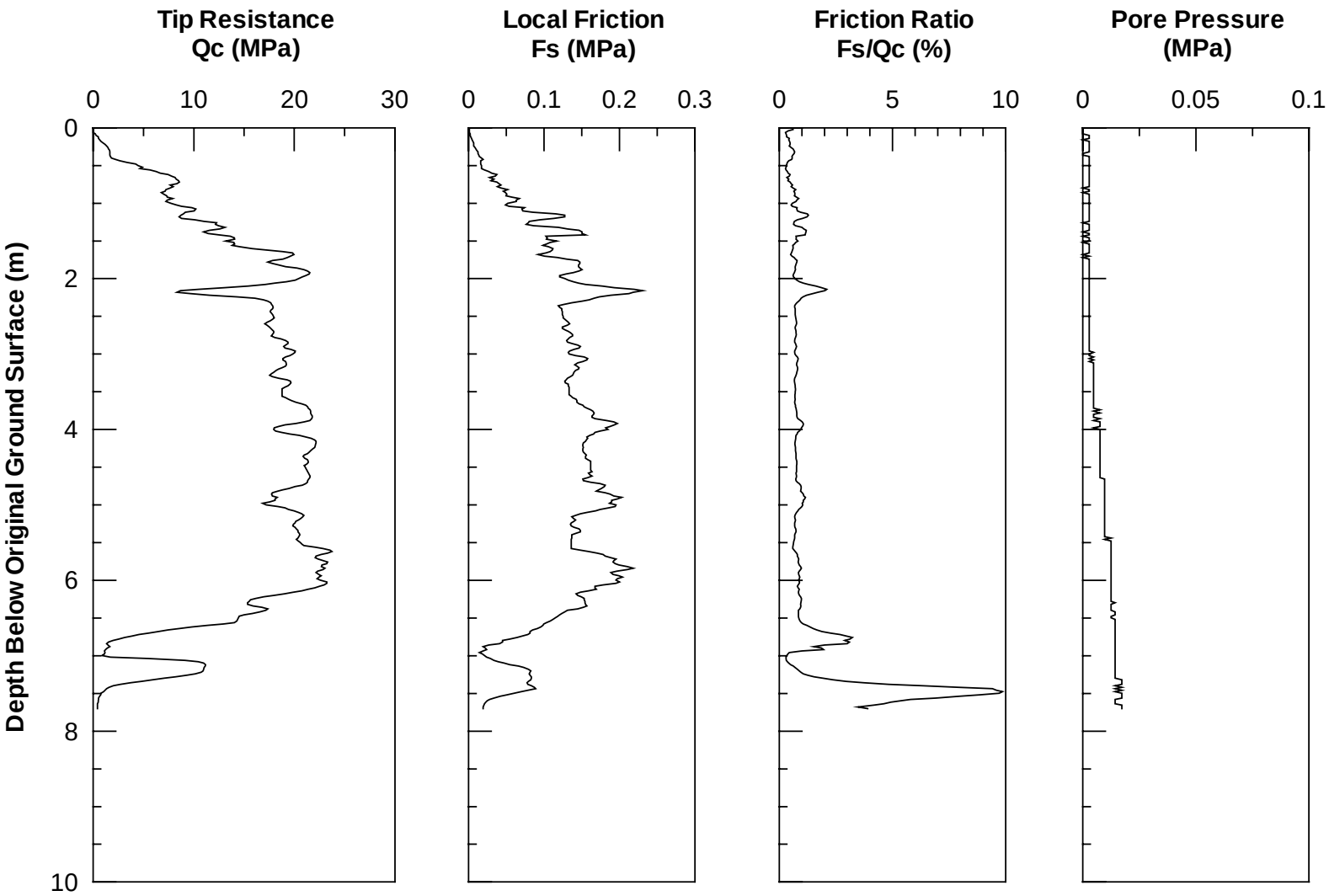

Figure 4.40 Post-treatment CPT3 Logs for 4-Pile Group/0.6m CISS Pile Test Area (2-16-99)

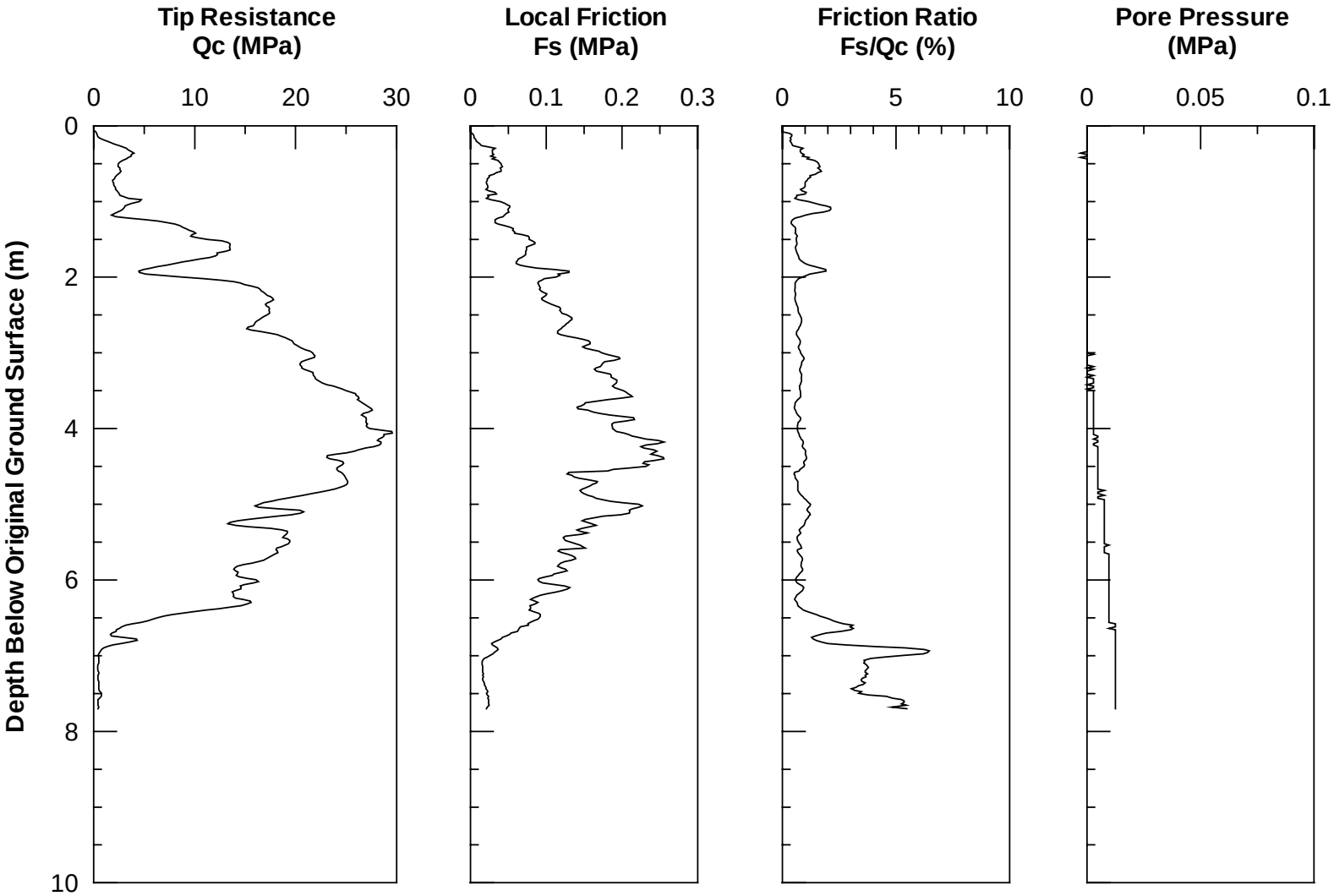

Figure 4.41 Post-treatment CPT4 Logs for 4-Pile Group/0.6m CISS Pile Test Area (2-16-99)

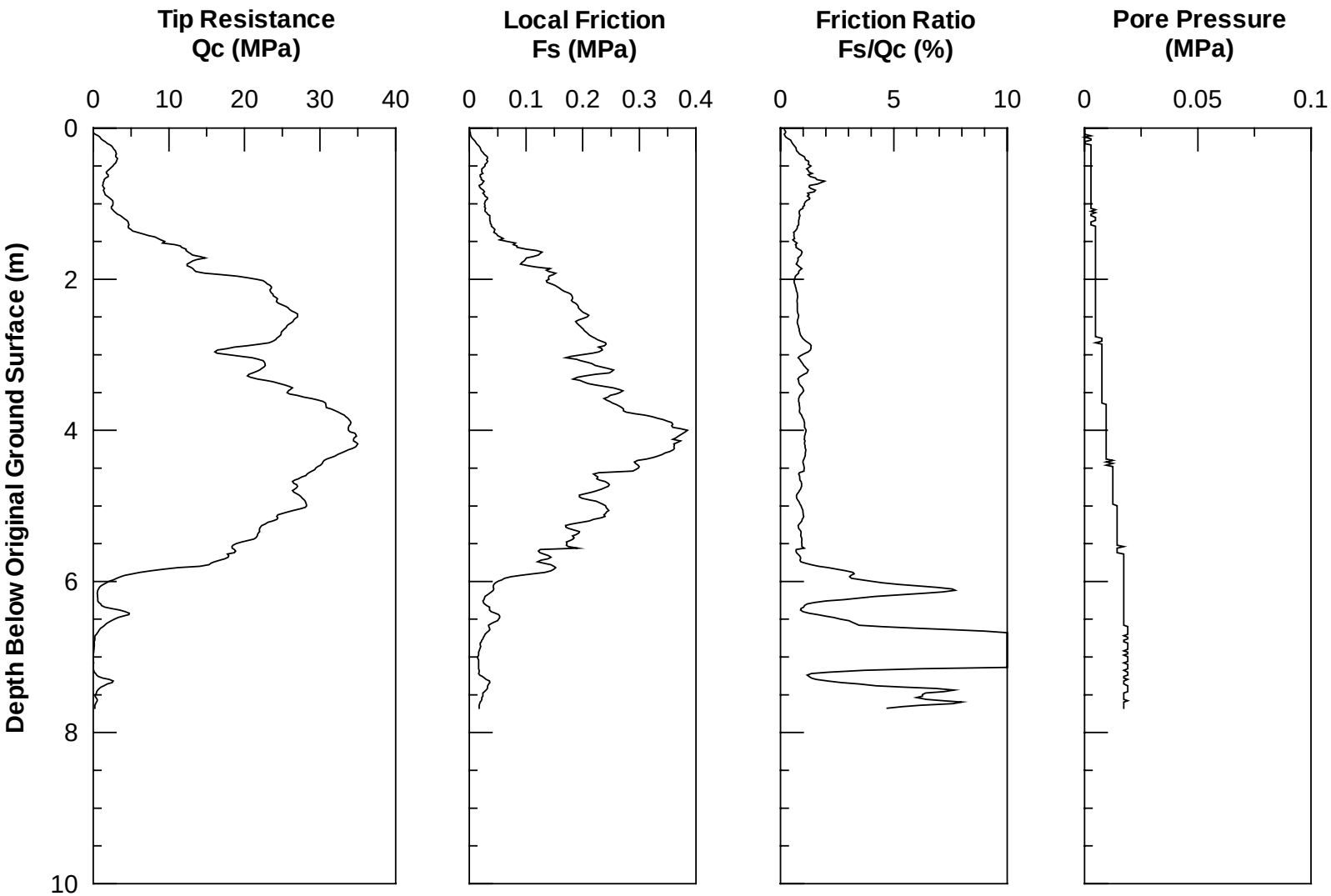

Figure 4.42 Post-treatment CPT5 Logs for 4-Pile Group/0.6m CISS Pile Test Area (2-16-99)

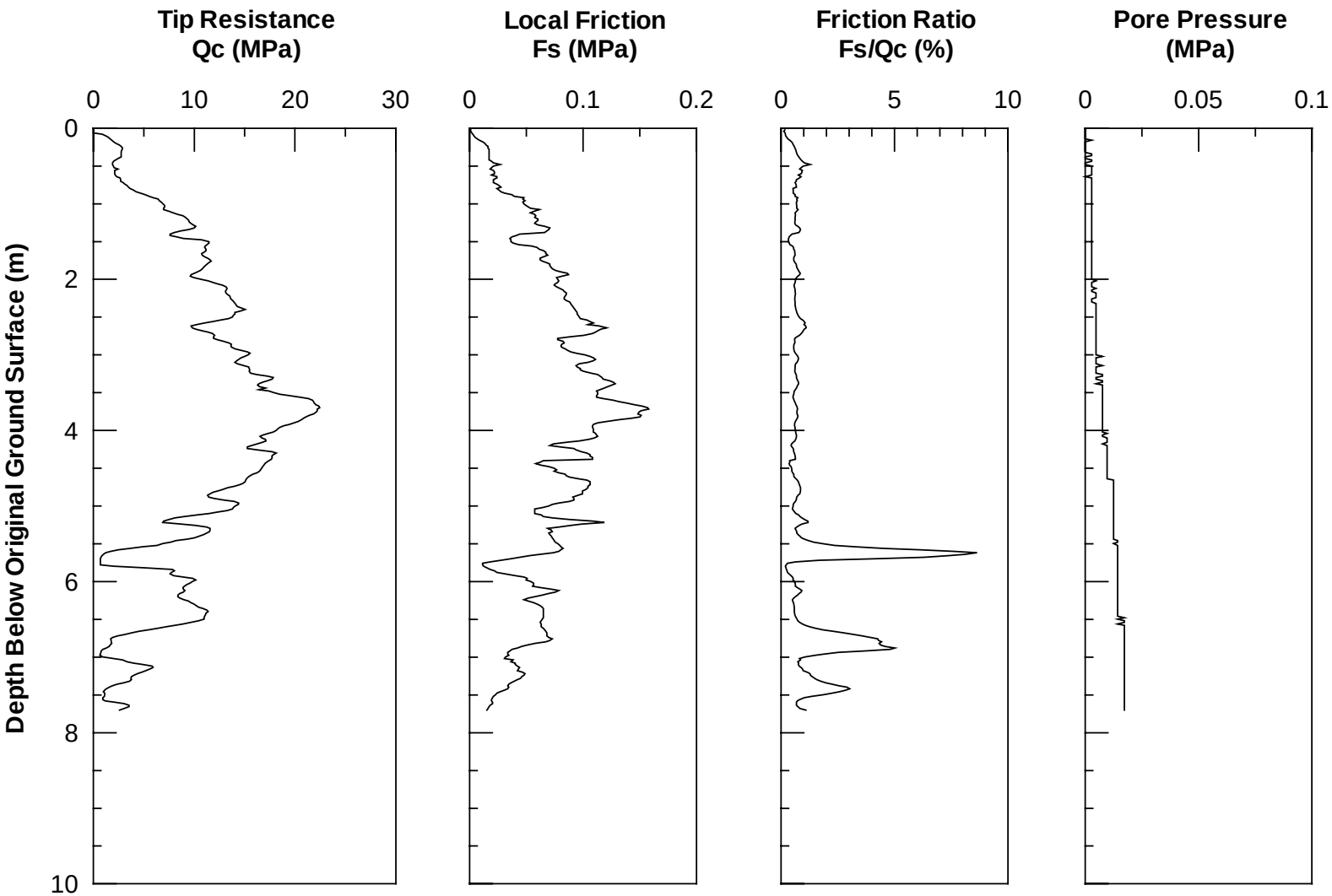

Figure 4.43 Post-treatment CPT6 Logs for 4-Pile Group/0.6m CISS Pile Test Area (2-16-99)

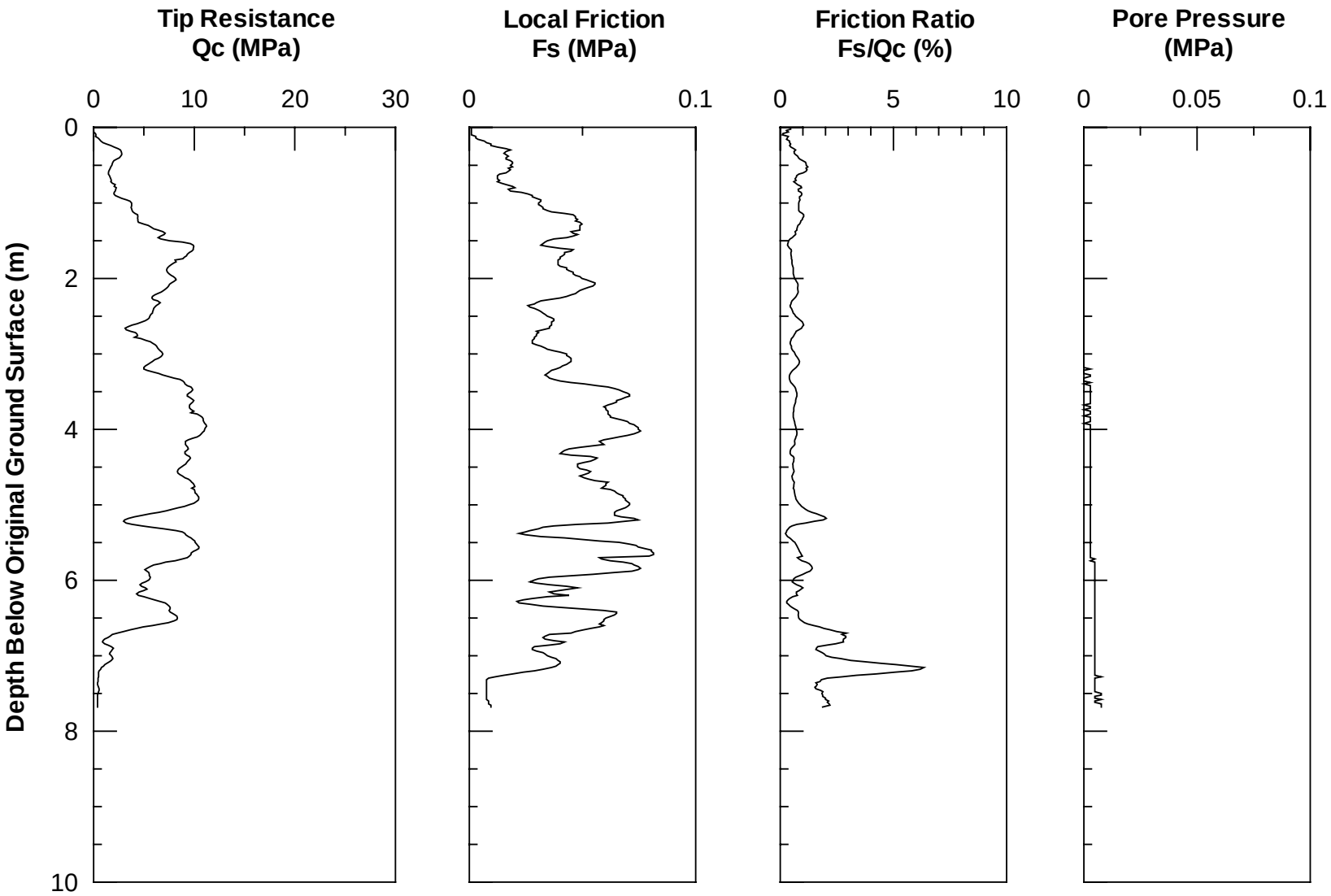

Figure 4.44 Post-treatment CPT7 Logs for 4-Pile Group/0.6m CISS Pile Test Area (2-16-99)

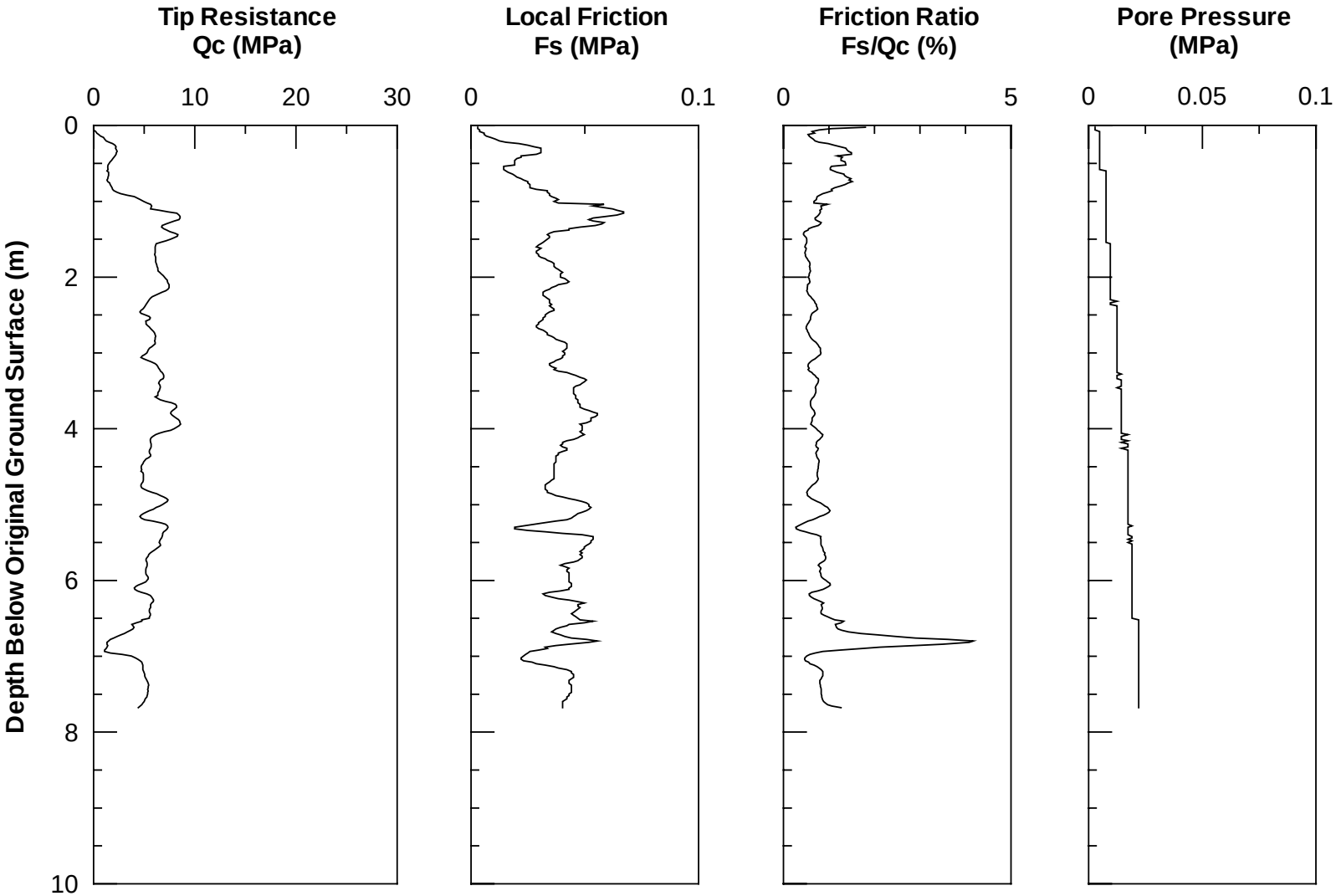

Figure 4.45 Post-treatment CPT8 Logs for 4-Pile Group/0.6m CISS Pile Test Area (2-16-99)

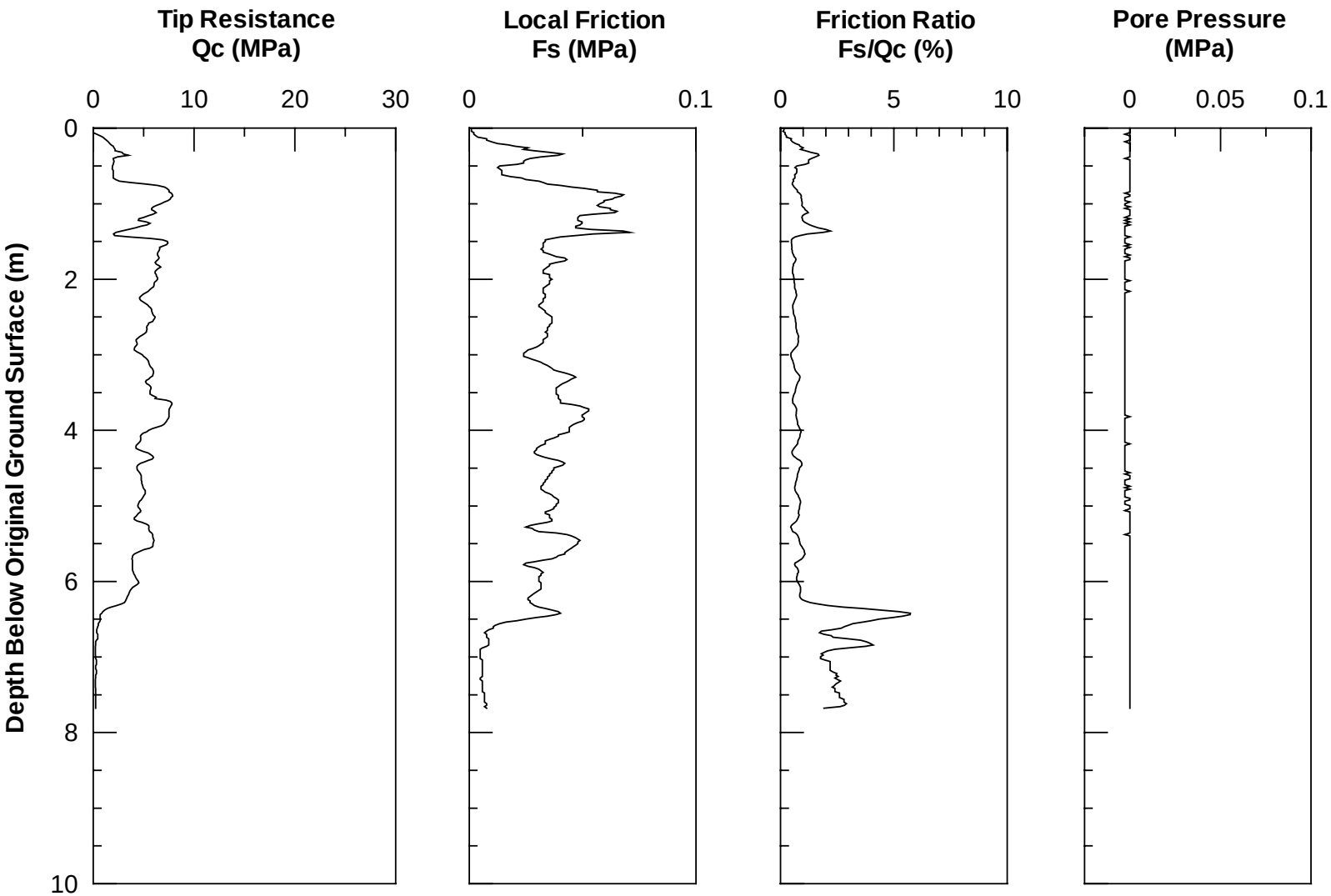

Figure 4.46 Post-treatment CPT9 Logs for 4-Pile Group/0.6m CISS Pile Test Area (2-16-99)

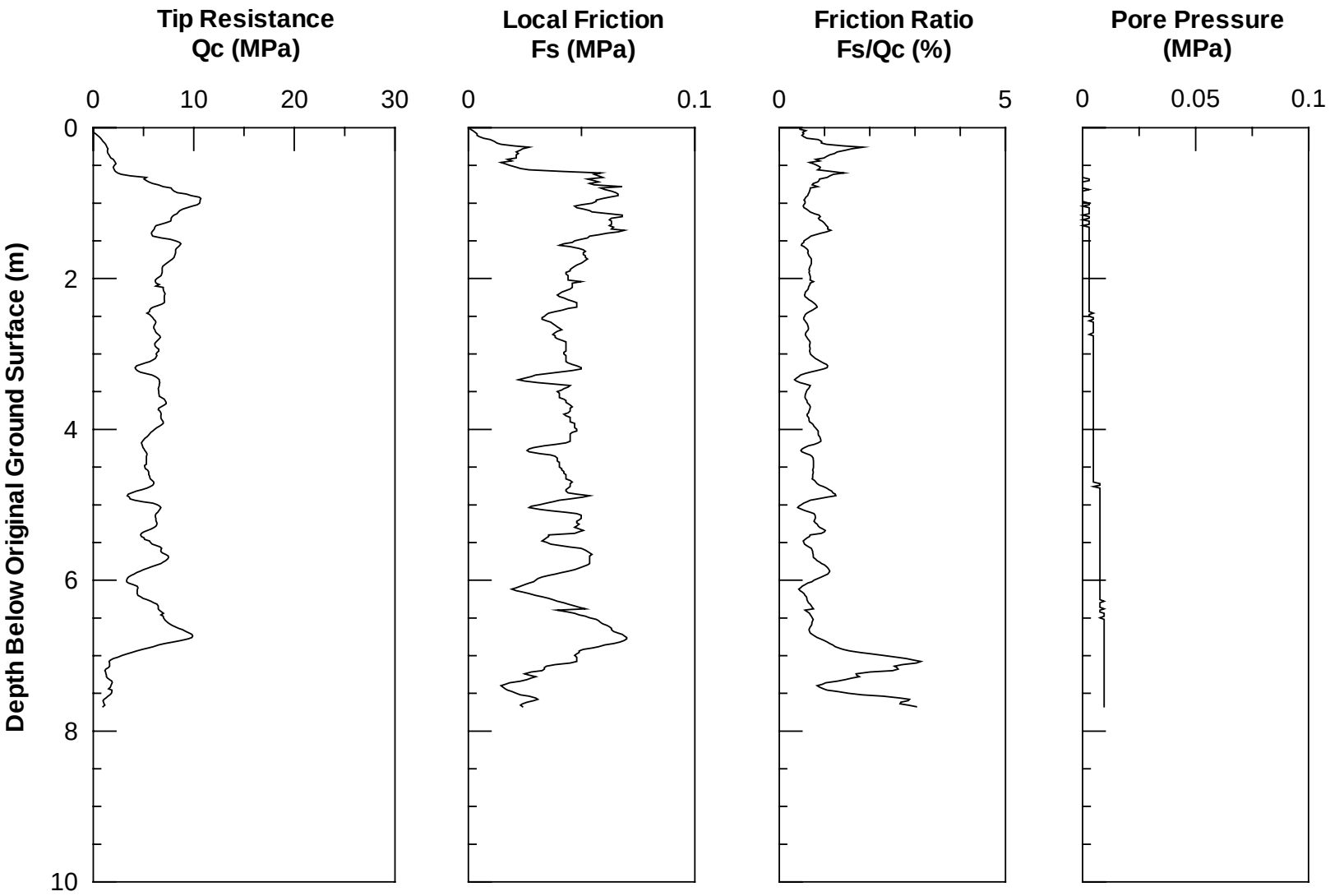

Figure 4.47 Post-treatment CPT10 Logs for 4-Pile Group/0.6m CISS Pile Test Area (2-16-99)

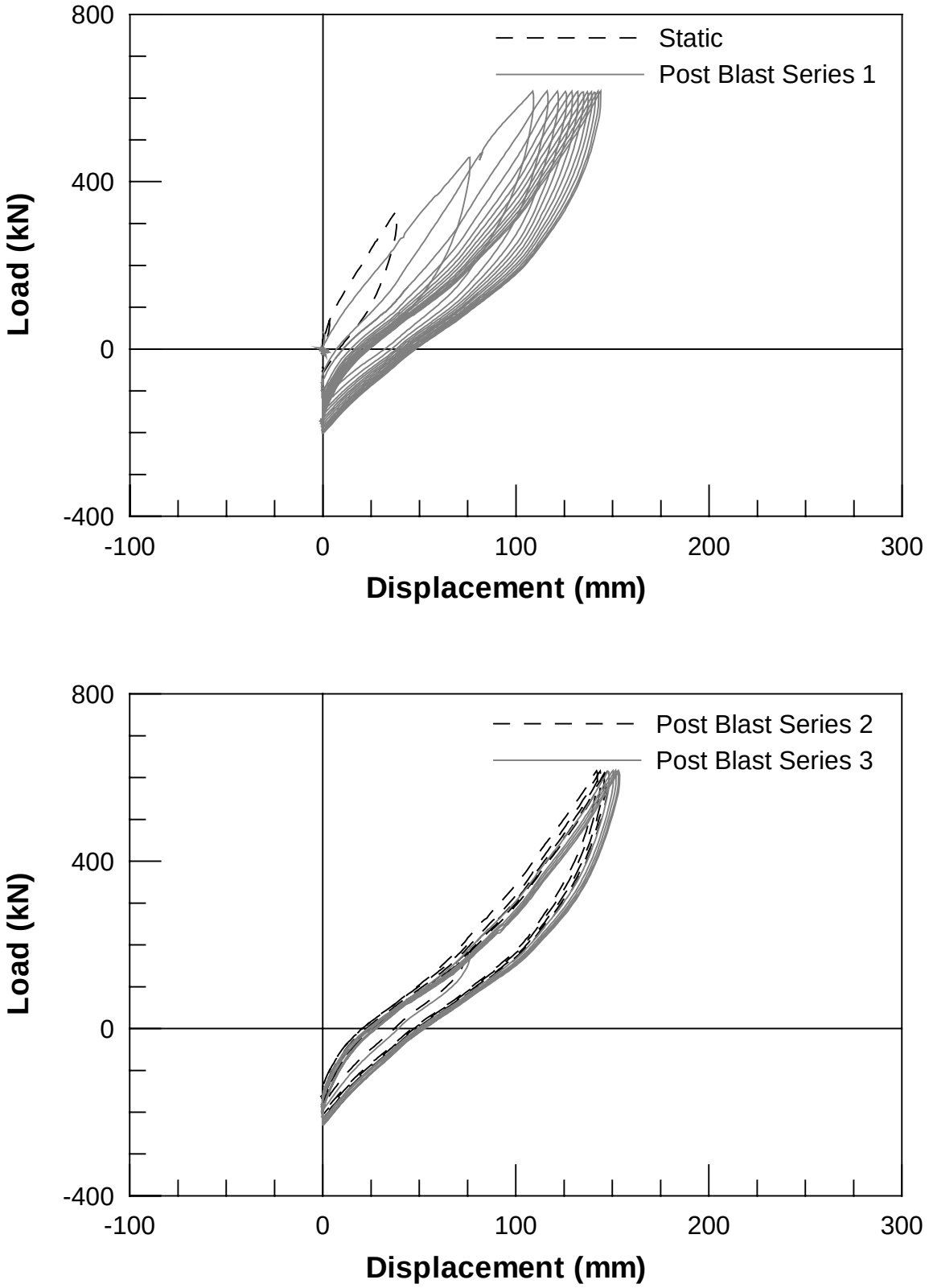

Figure 4.48 4-Pile Group Load vs. Displacement 2nd Blast a) Static and Post Blast Series 1 b) Post Blast Series 2 and 3

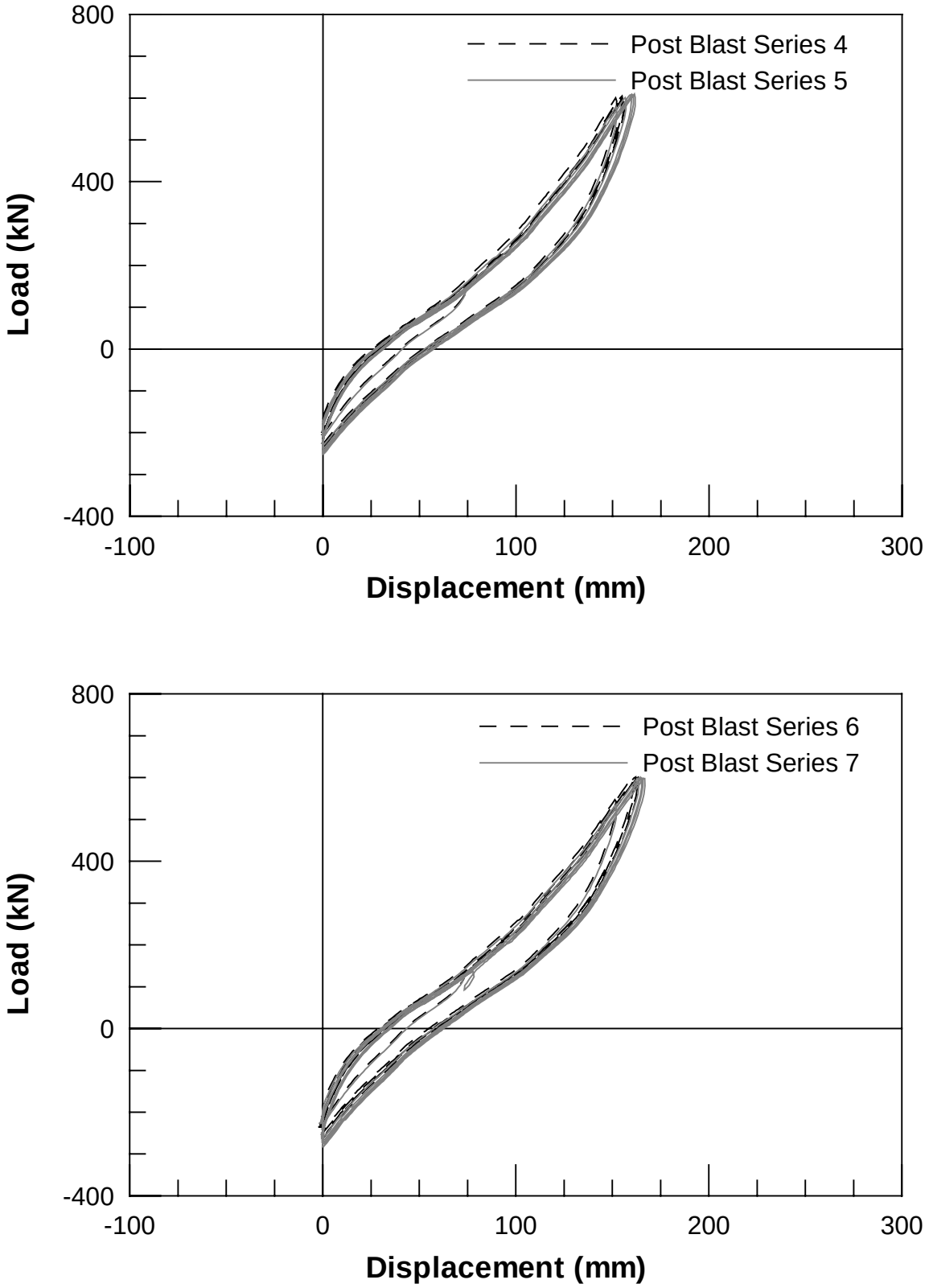

Figure 4.49 4-Pile Group Load vs. Displacement 2nd Blast a) Post Blast Series 4 and 5 b) Post Blast Series 6 and 7

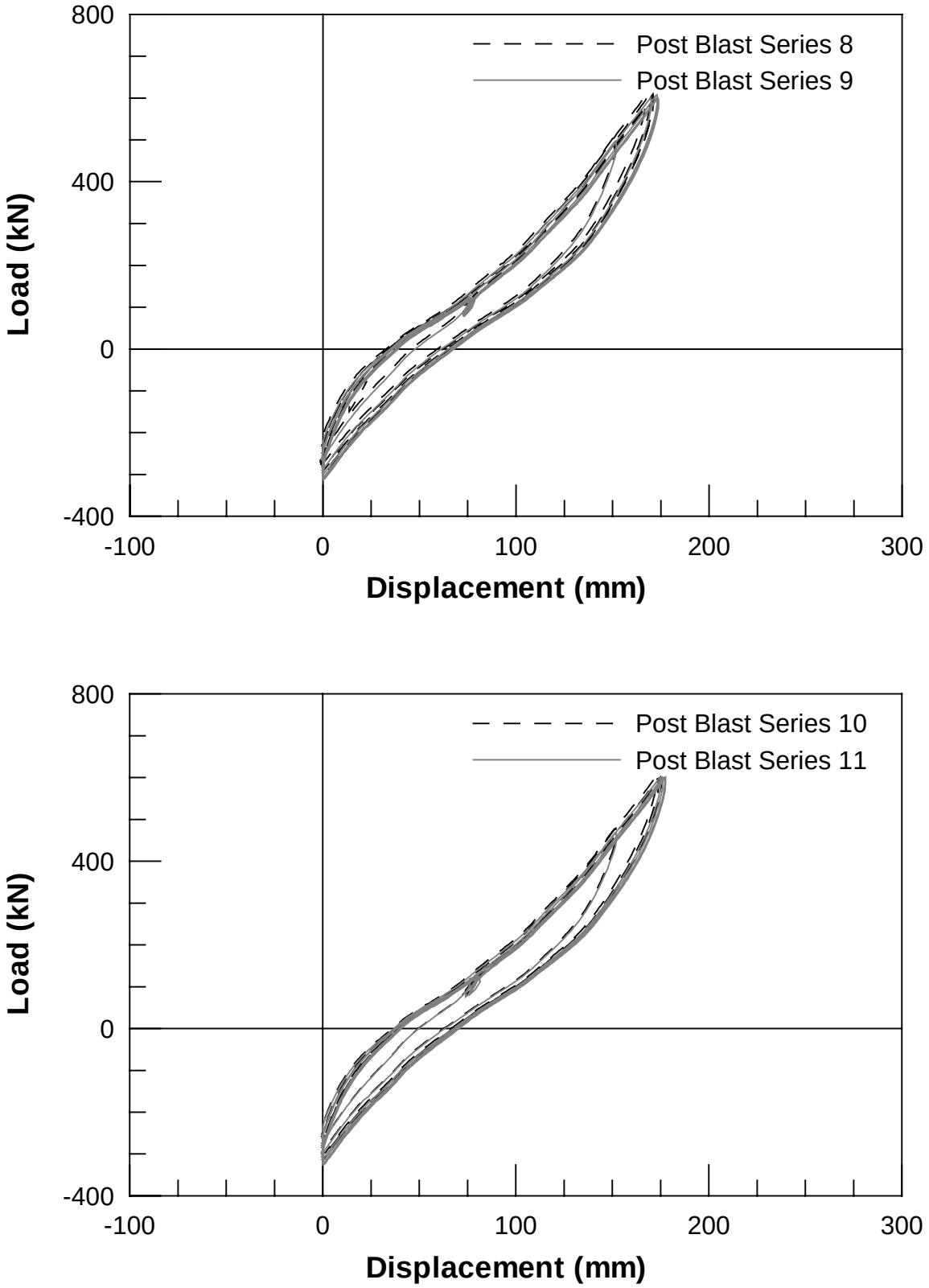

Figure 4.50 4-Pile Group Load vs. Displacement 2nd Blast a) Post Blast Series 8 and 9 b) Post Blast Series 10 and 11

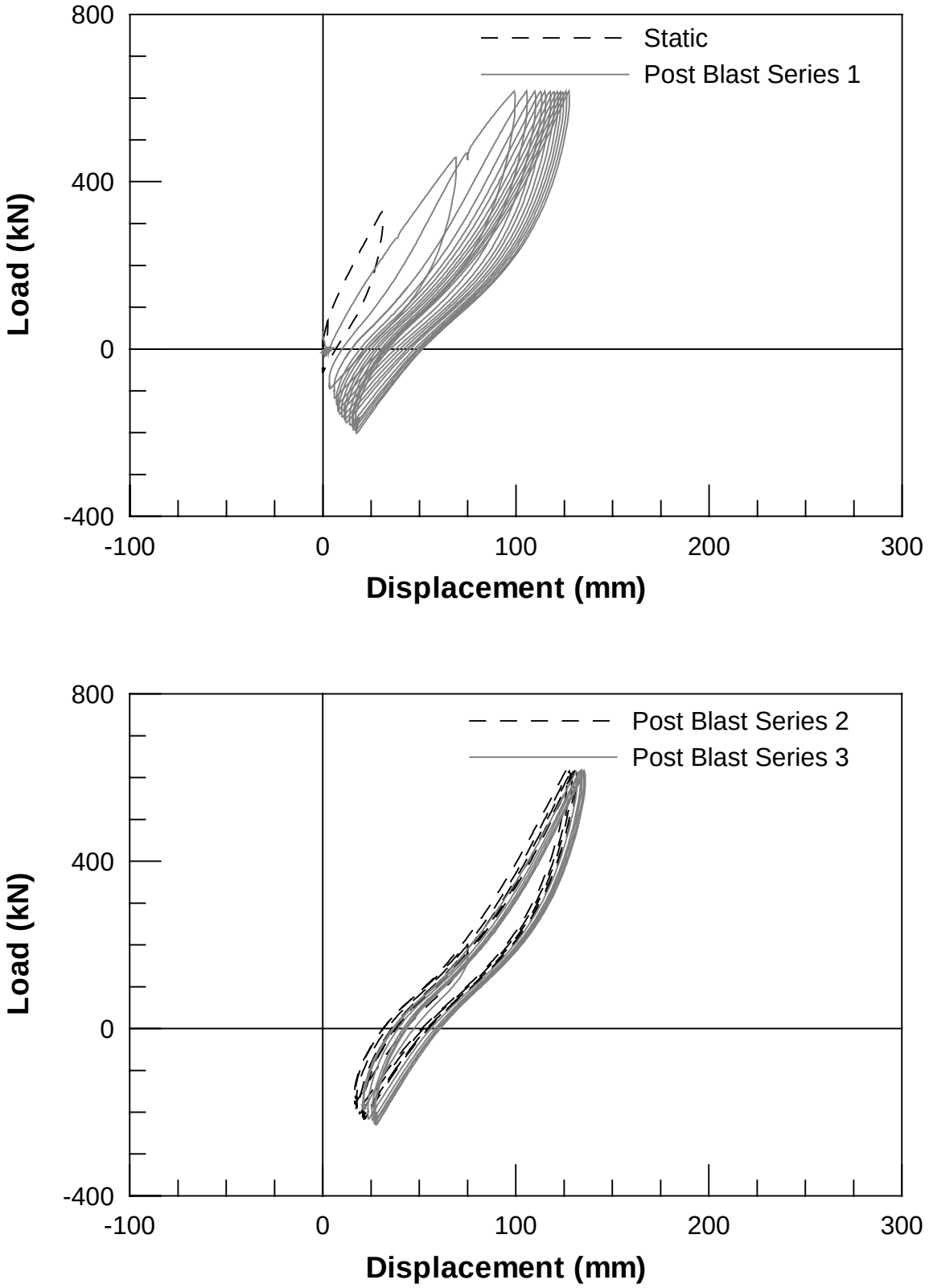

Figure 4.51 0.6m CISS Load vs. Displacement 2nd Blast a) Static and Post Blast Series 1 b) Post Blast Series 2 and 3

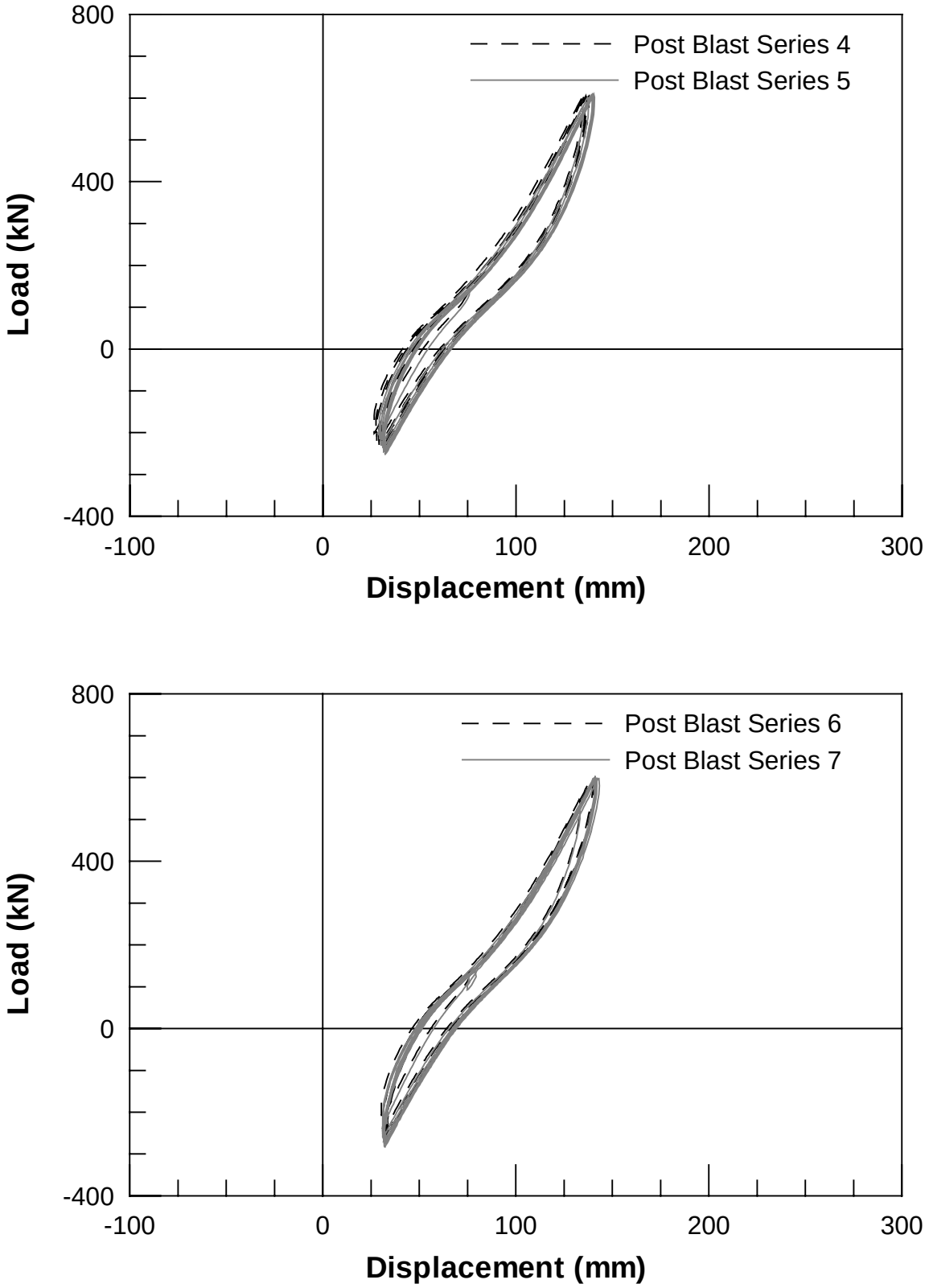

Figure 4.52 0.6m CISS Load vs. Displacement 2nd Blast a) Post Blast Series 4 and 5 b) Post Blast Series 6 and 7

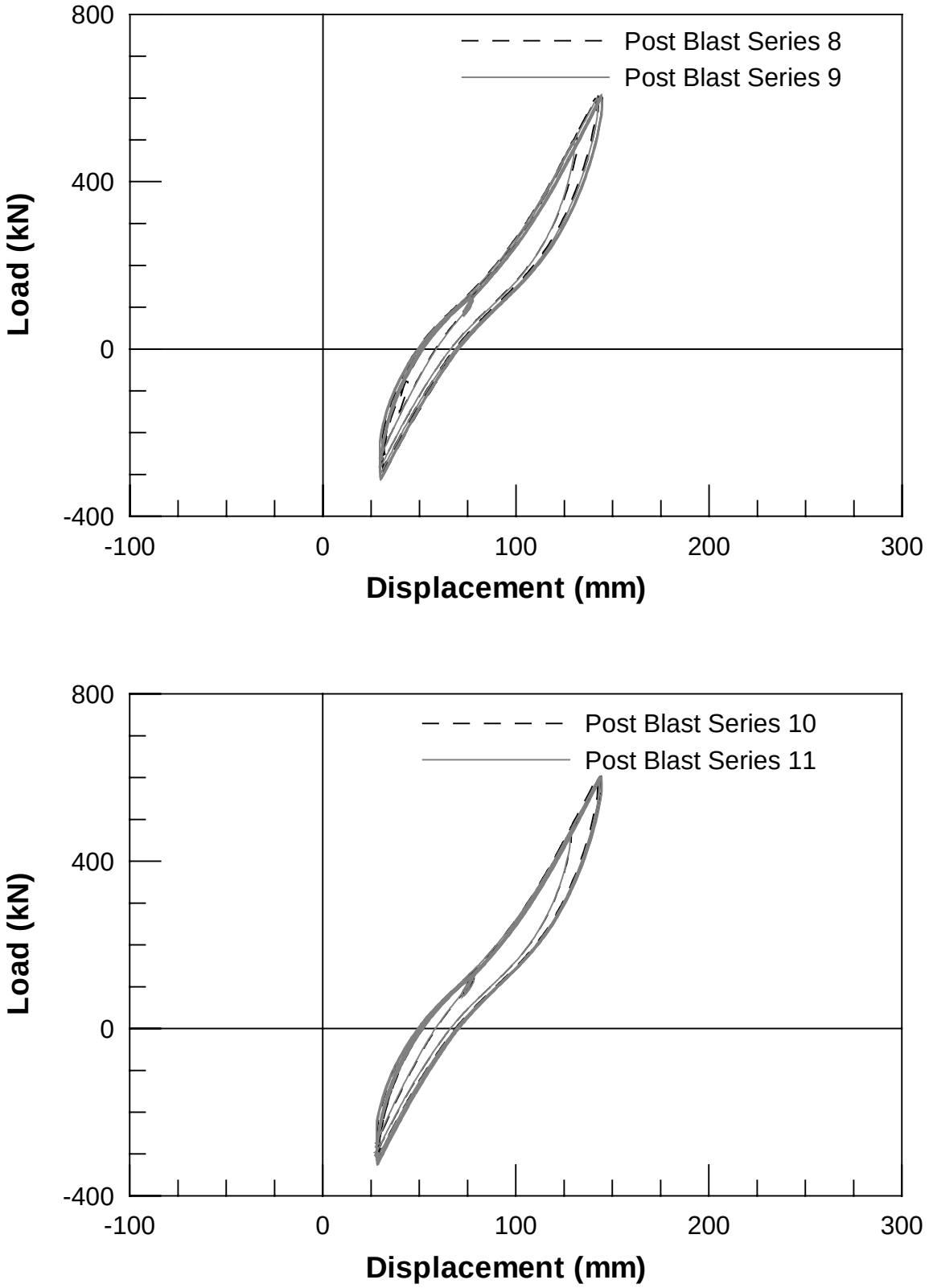

Figure 4.53 0.6m CISS Load vs. Displacement 2nd Blast a) Post Blast Series 8 and 9 b) Post Blast Series 10 and 11

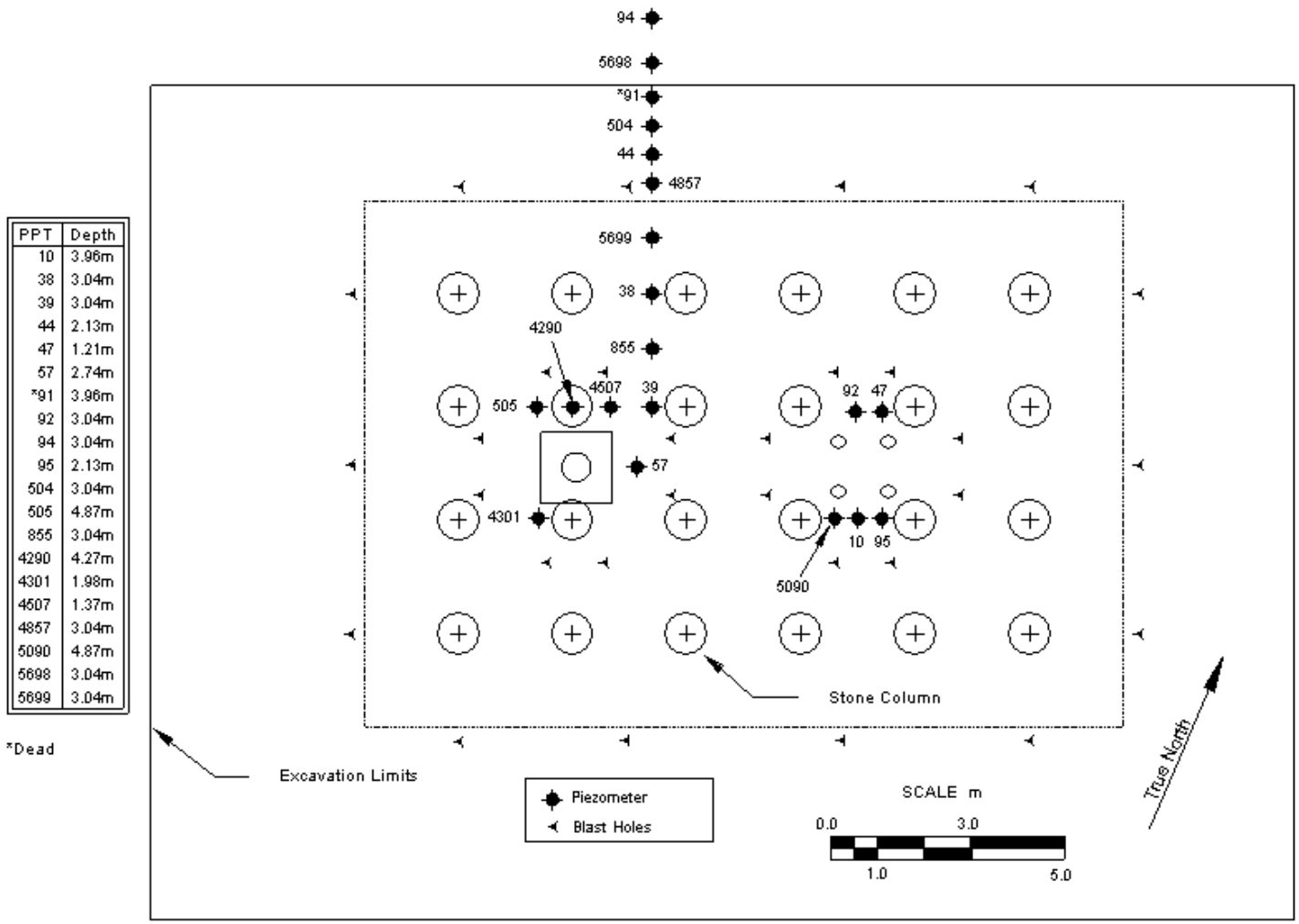

PPT	Depth
10	3.96m
38	3.04m
39	3.04m
44	2.13m
47	1.21m
57	2.74m
*91	3.96m
92	3.04m
94	3.04m
95	2.13m
504	3.04m
505	4.87m
855	3.04m
4290	4.27m
4301	1.98m
4507	1.37m
4857	3.04m
5090	4.87m
5698	3.04m
5699	3.04m

Figure 4.54 Location Map of Pore Pressure Transducers and Explosives for Stone Columns Test

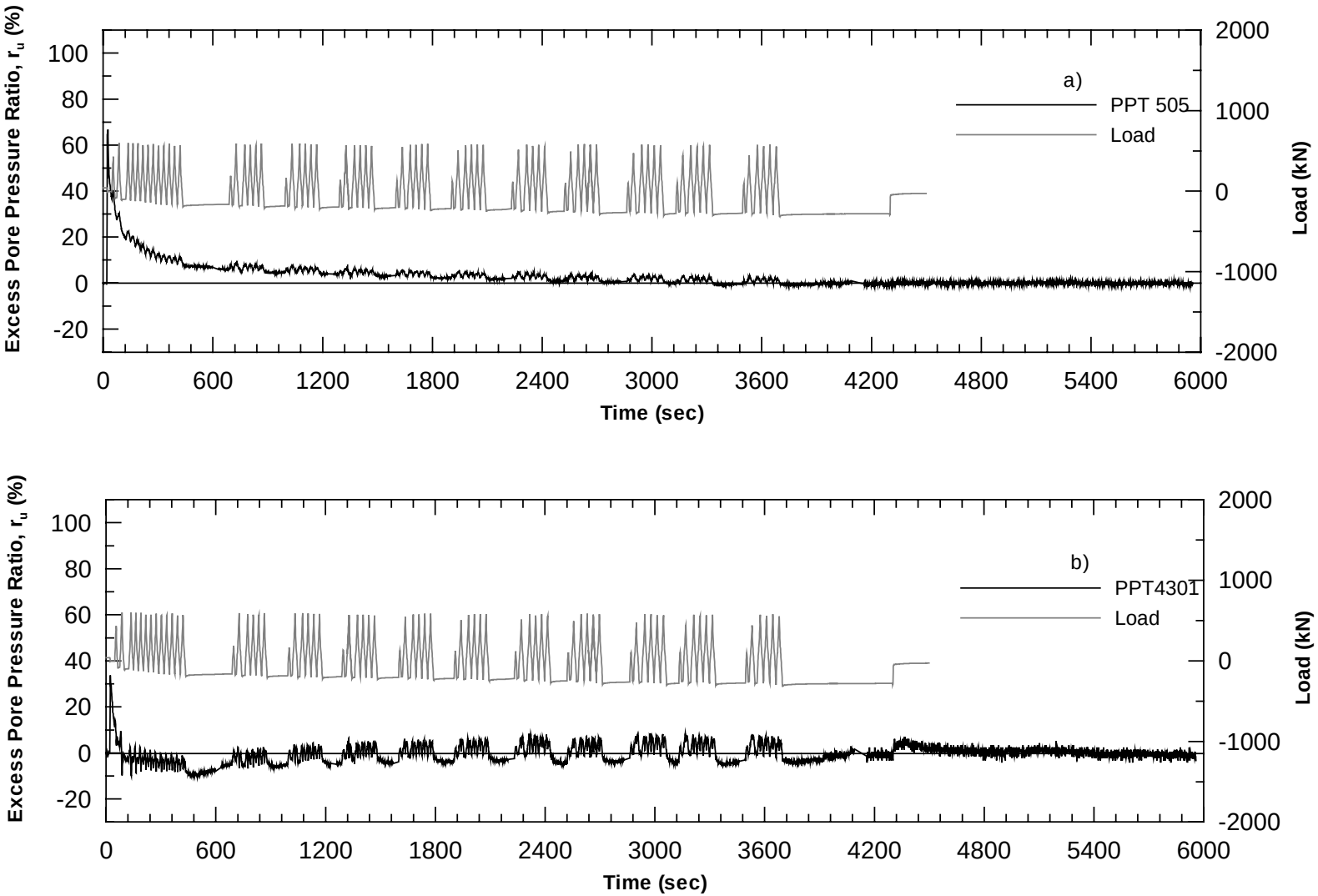

Figure 4.55 Excess Pore Pressure Ratio 4-Pile Group/0.6m CISS Pile 2nd Blast a) PPT505 b)PPT4301

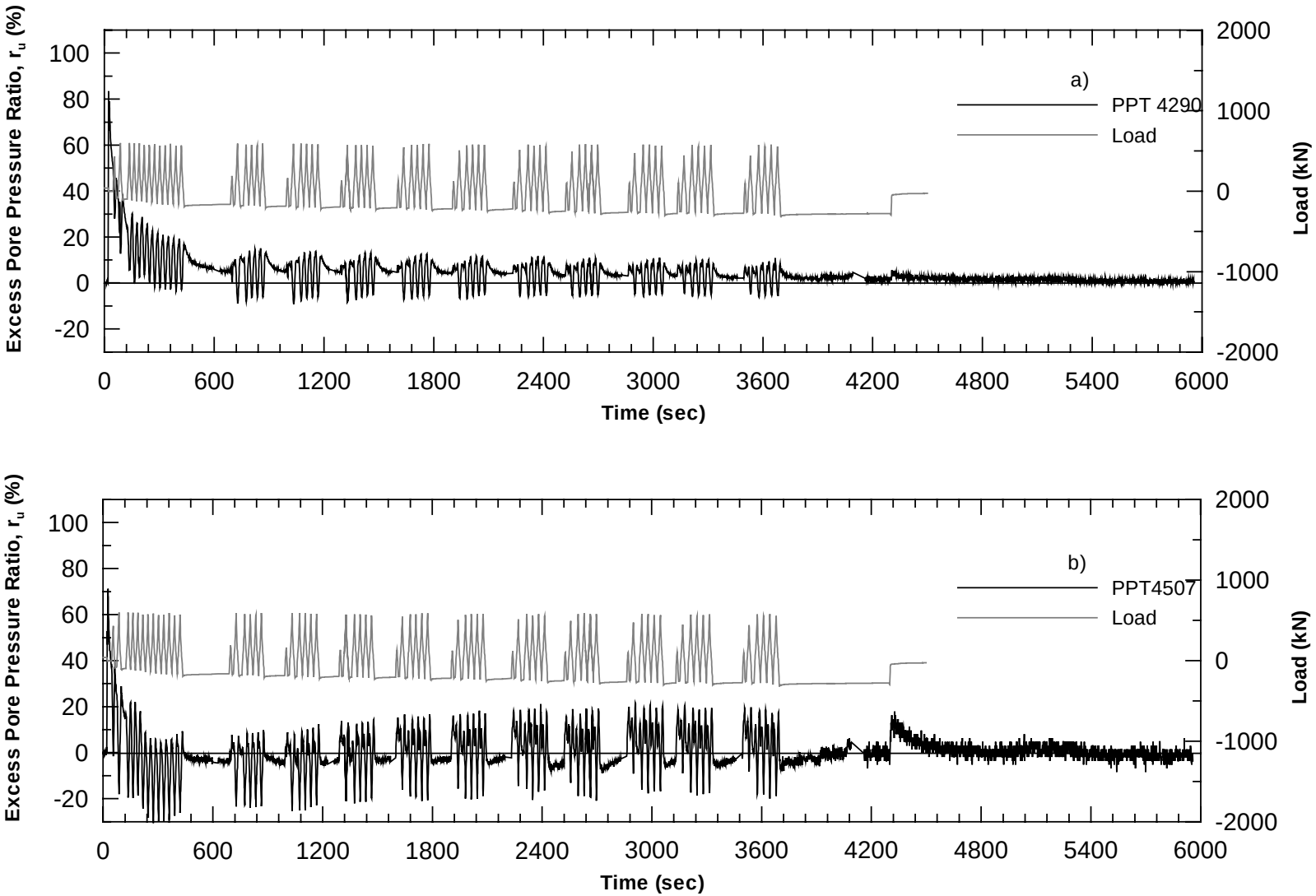

Figure 4.56 Excess Pore Pressure Ratio 4-Pile Group/0.6m CISS Pile 2nd Blast a) PPT4290 b)PPT4507

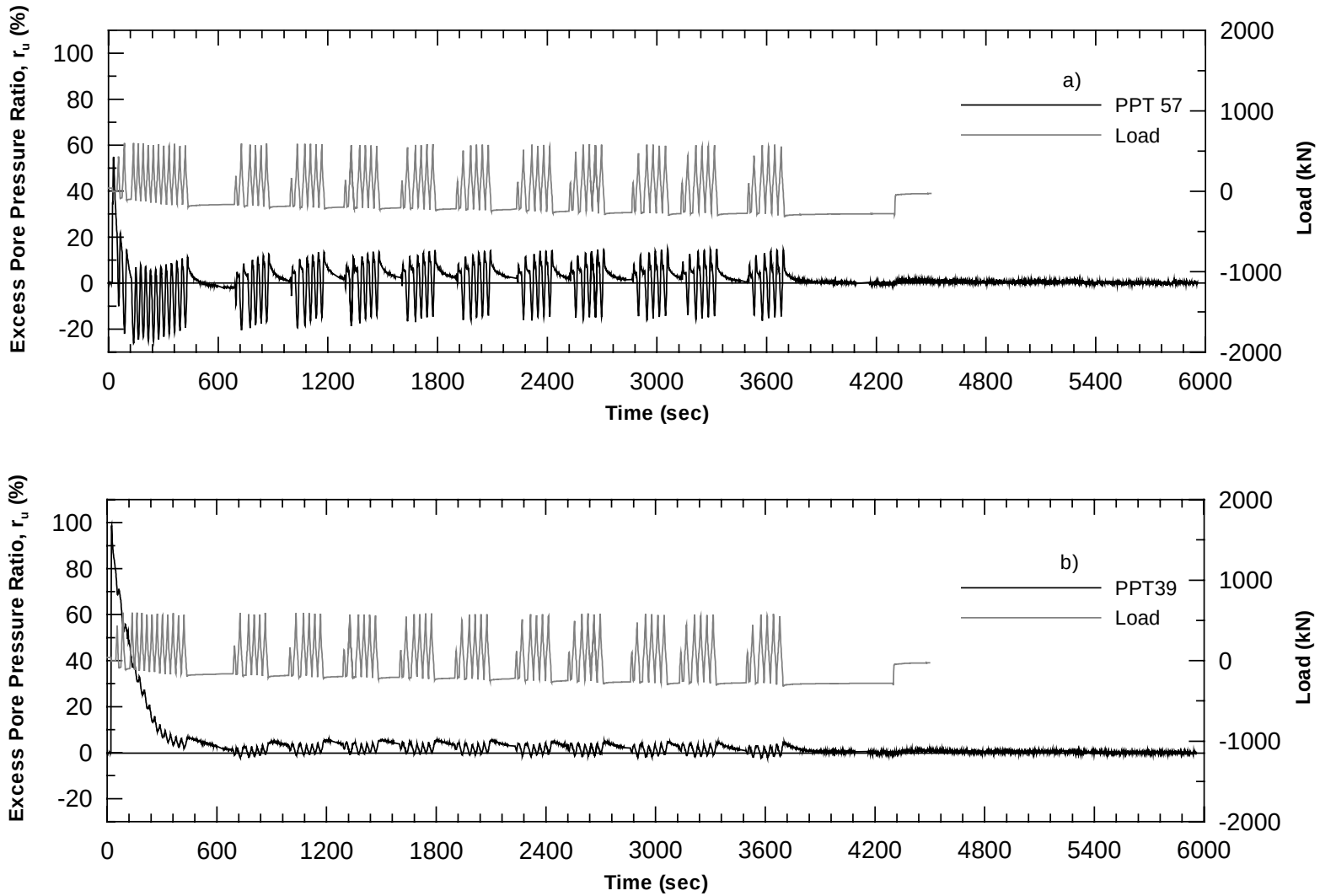

Figure 4.57 Excess Pore Pressure Ratio 4-Pile Group/0.6m CISS Pile 2nd Blast a) PPT57 b)PPT39

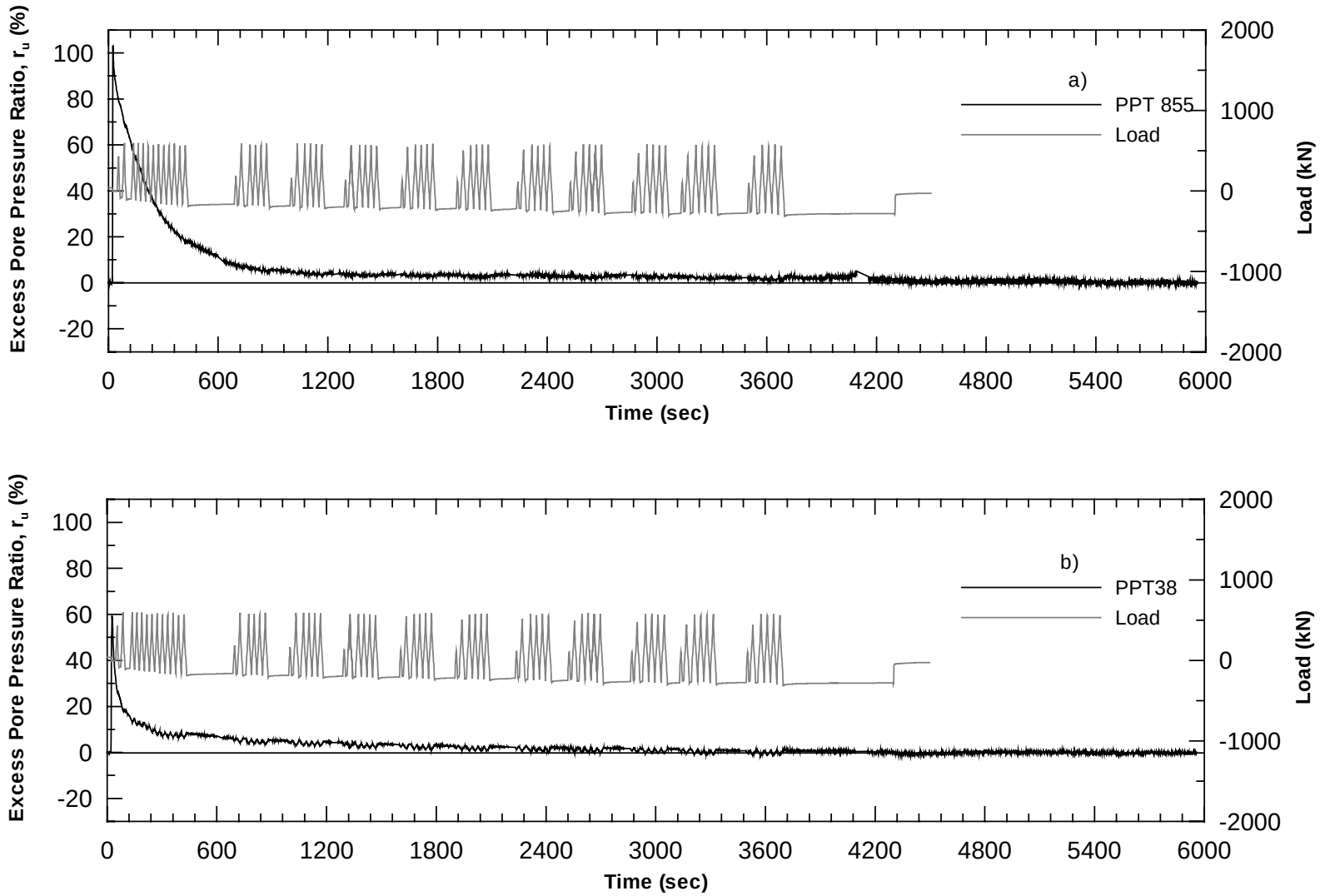

Figure 4.58 Excess Pore Pressure Ratio 4-Pile Group/0.6m CISS Pile 2nd Blast a) PPT855 b)PPT38

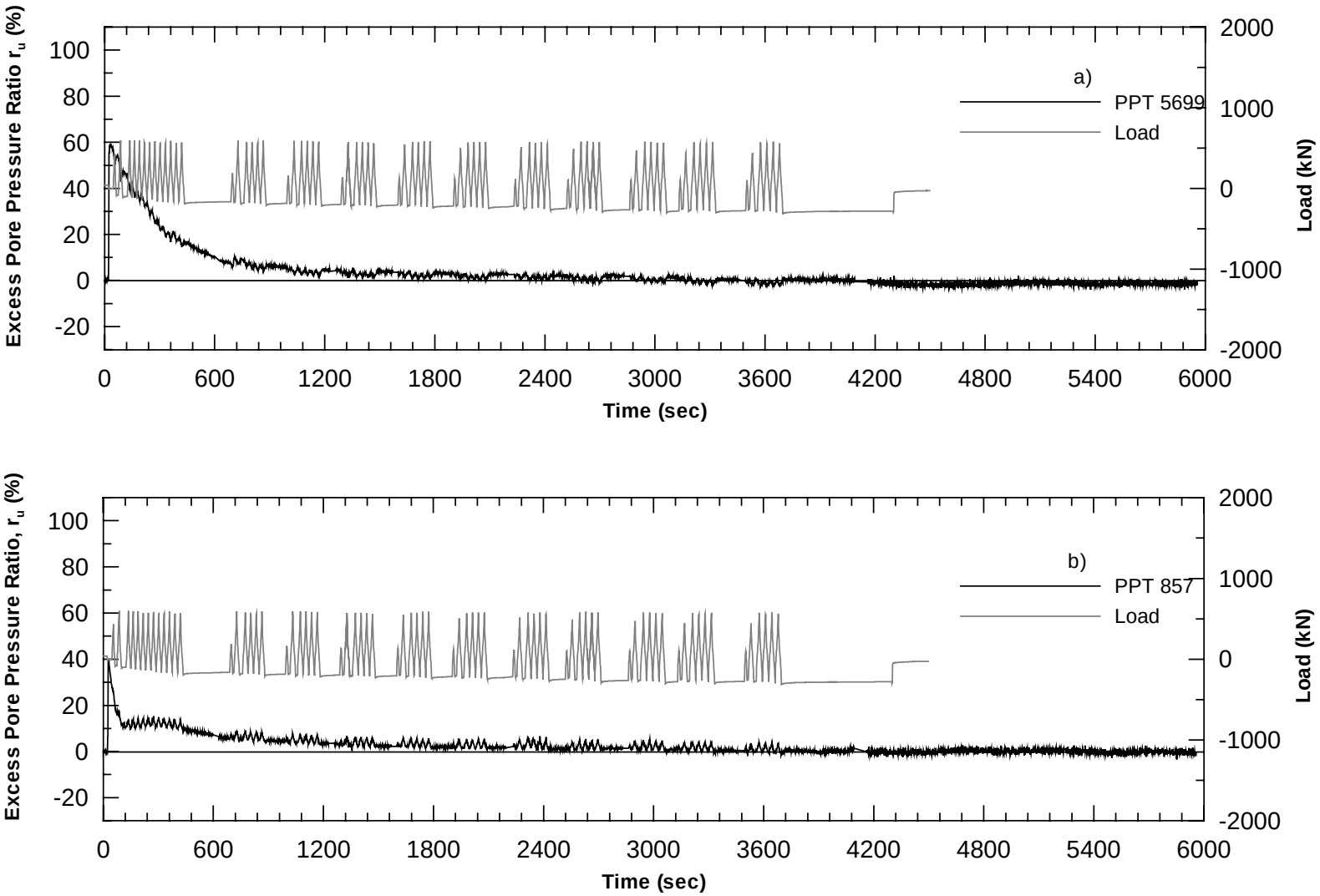

Figure 4.59 Excess Pore Pressure Ratio 4-Pile Group/0.6m CISS Pile 2nd Blast a) PPT5699 b)PPT857

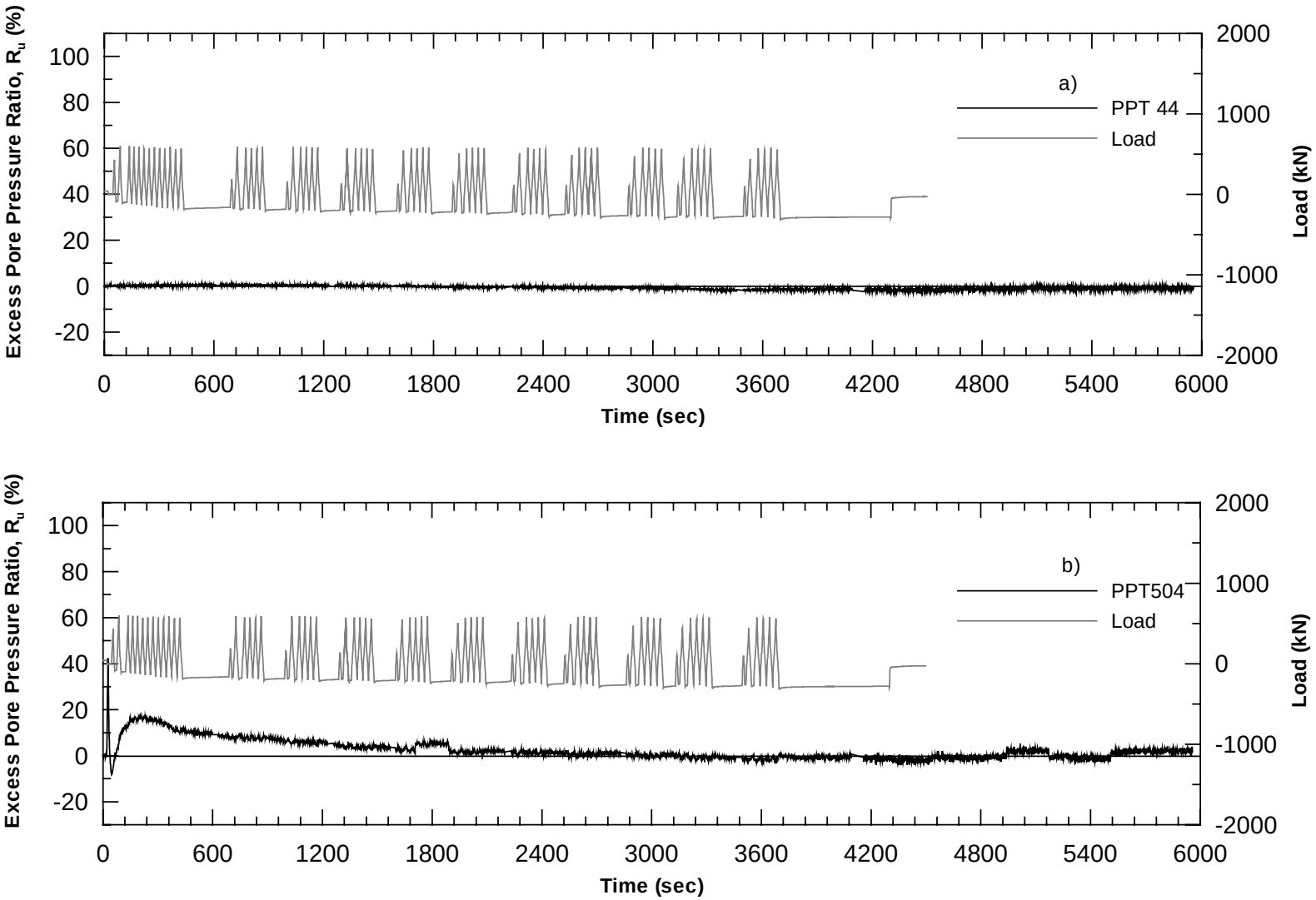

Figure 4.60 Excess Pore Pressure Ratio 4-Pile Group/0.6m CISS Pile 2nd Blast a) PPT44 b)PPT504

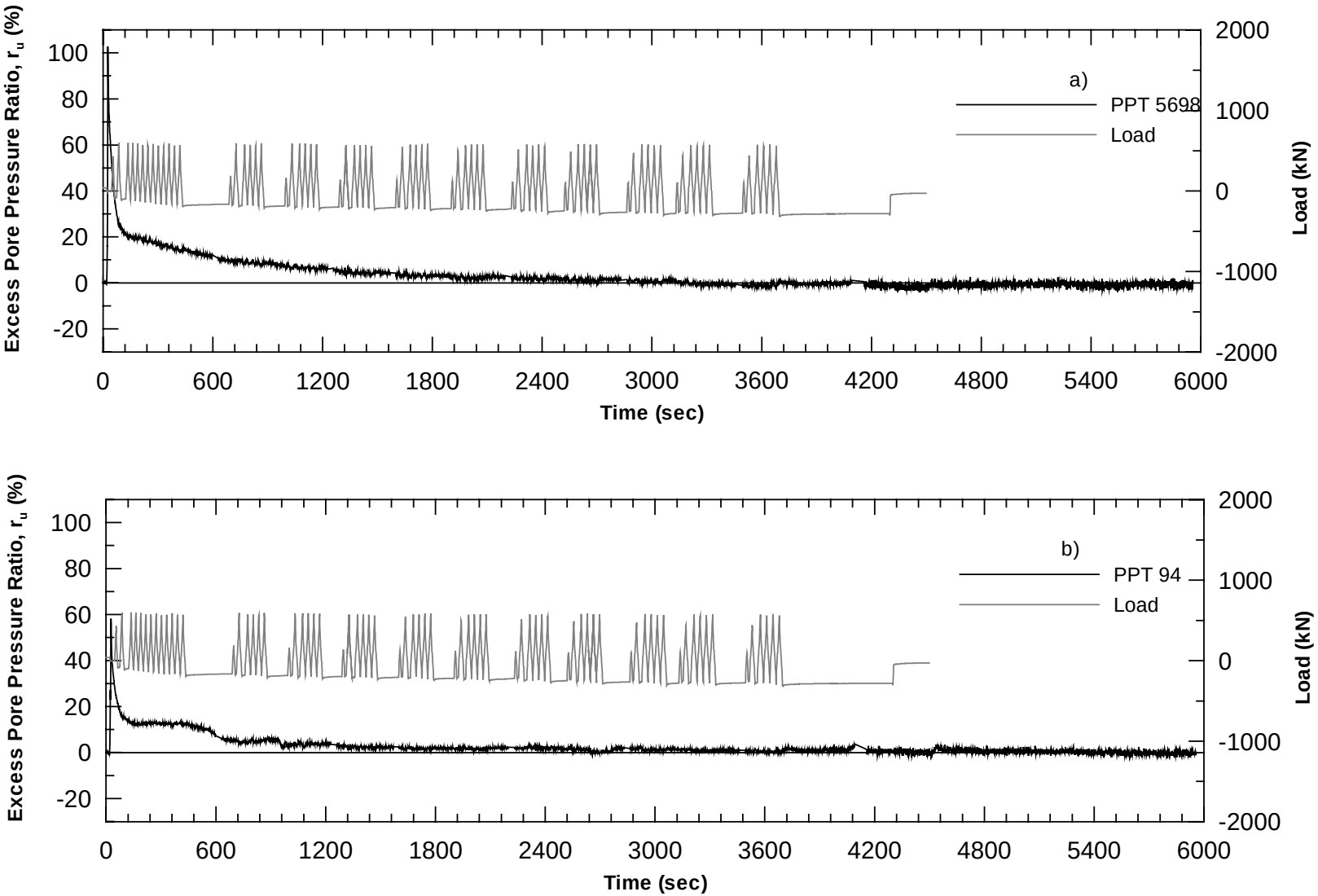

Figure 4.61 Excess Pore Pressure Ratio 4-Pile Group/0.6m CISS Pile 2nd Blast a) PPT5698 b)PPT94

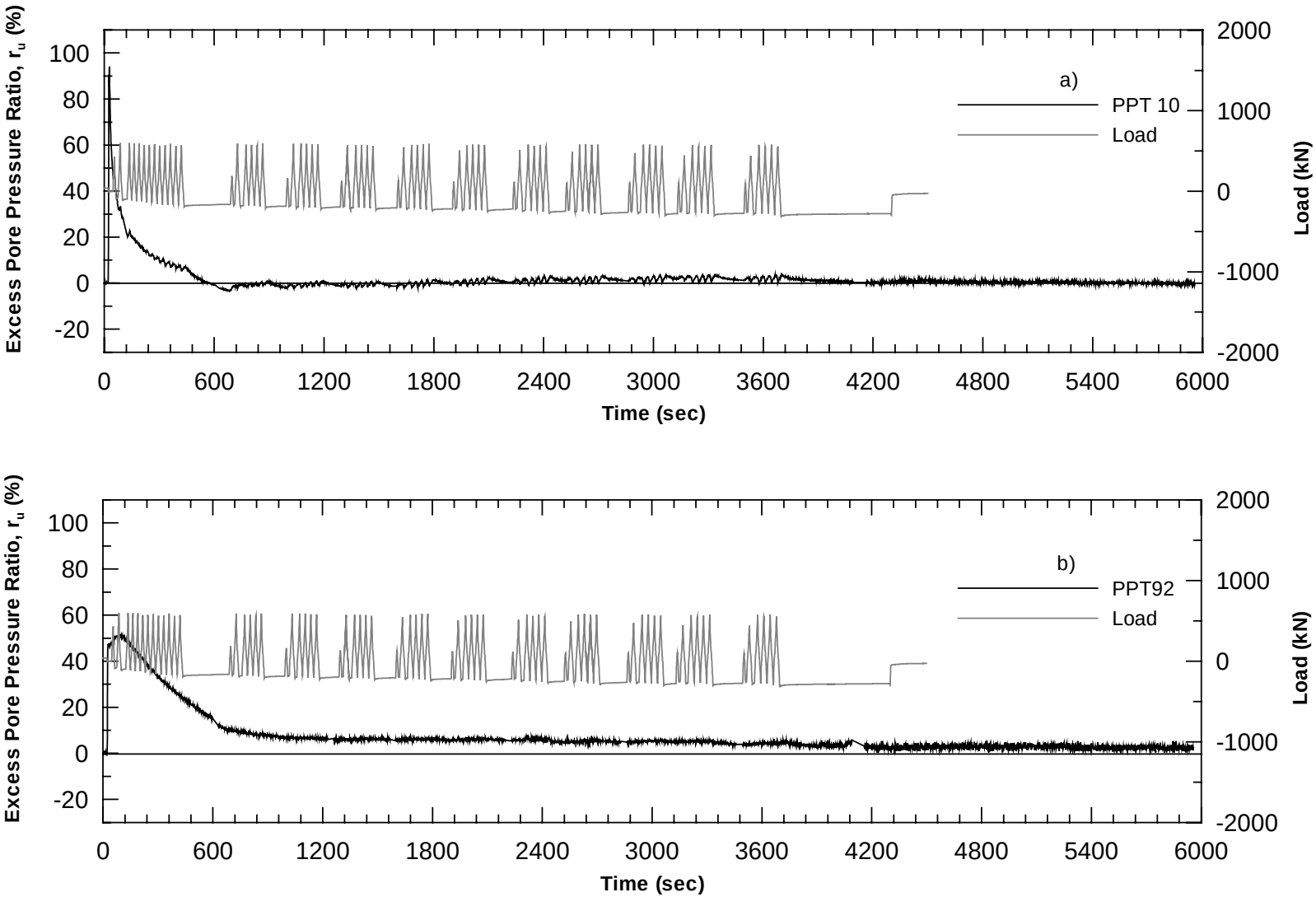

Figure 4.62 Excess Pore Pressure Ratio 4-Pile Group/0.6m CISS Pile 2nd Blast a) PPT10 b)PPT92

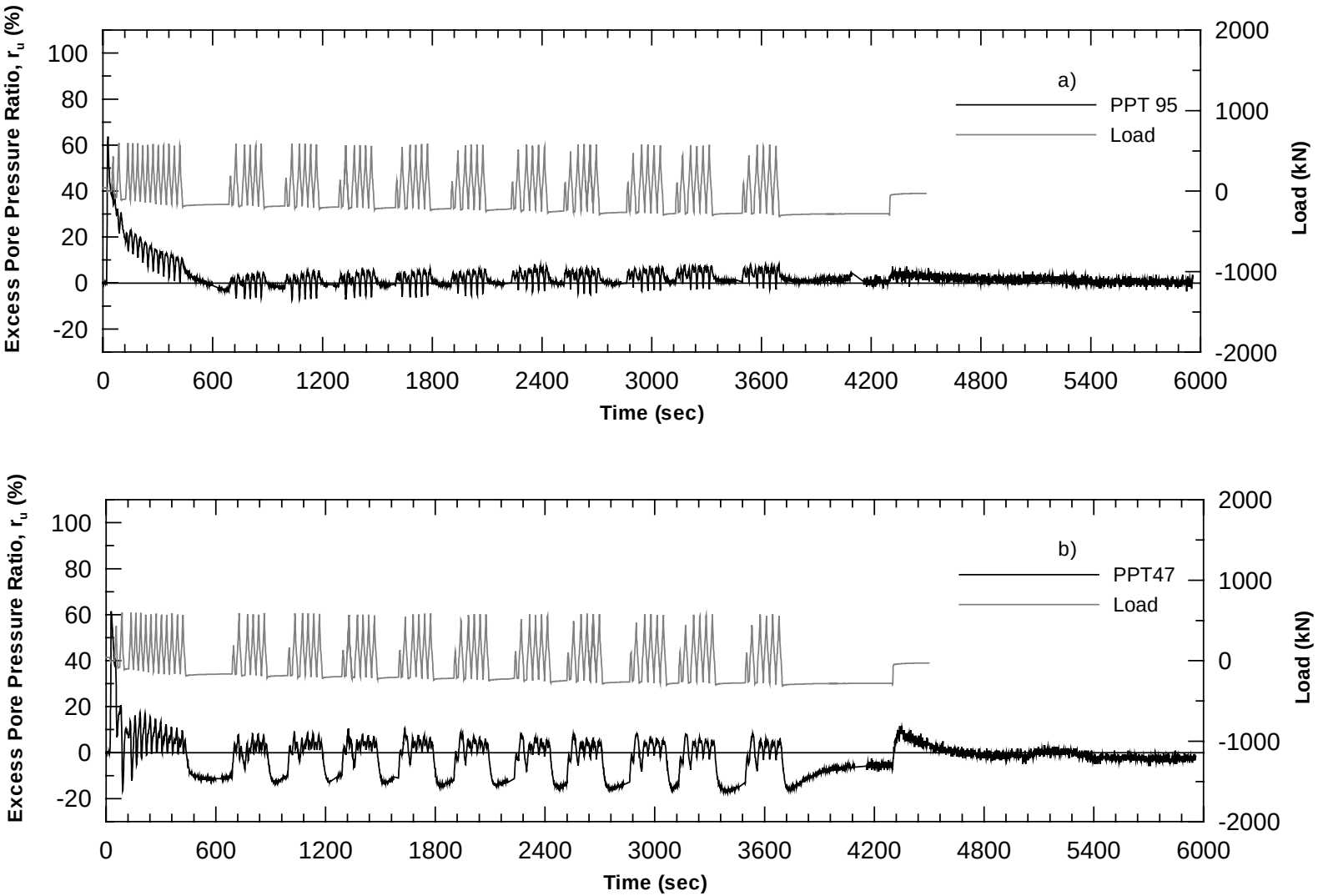

Figure 4.63 Excess Pore Pressure Ratio 4-Pile Group/0.6m CISS Pile 2nd Blast a) PPT95 b)PPT47

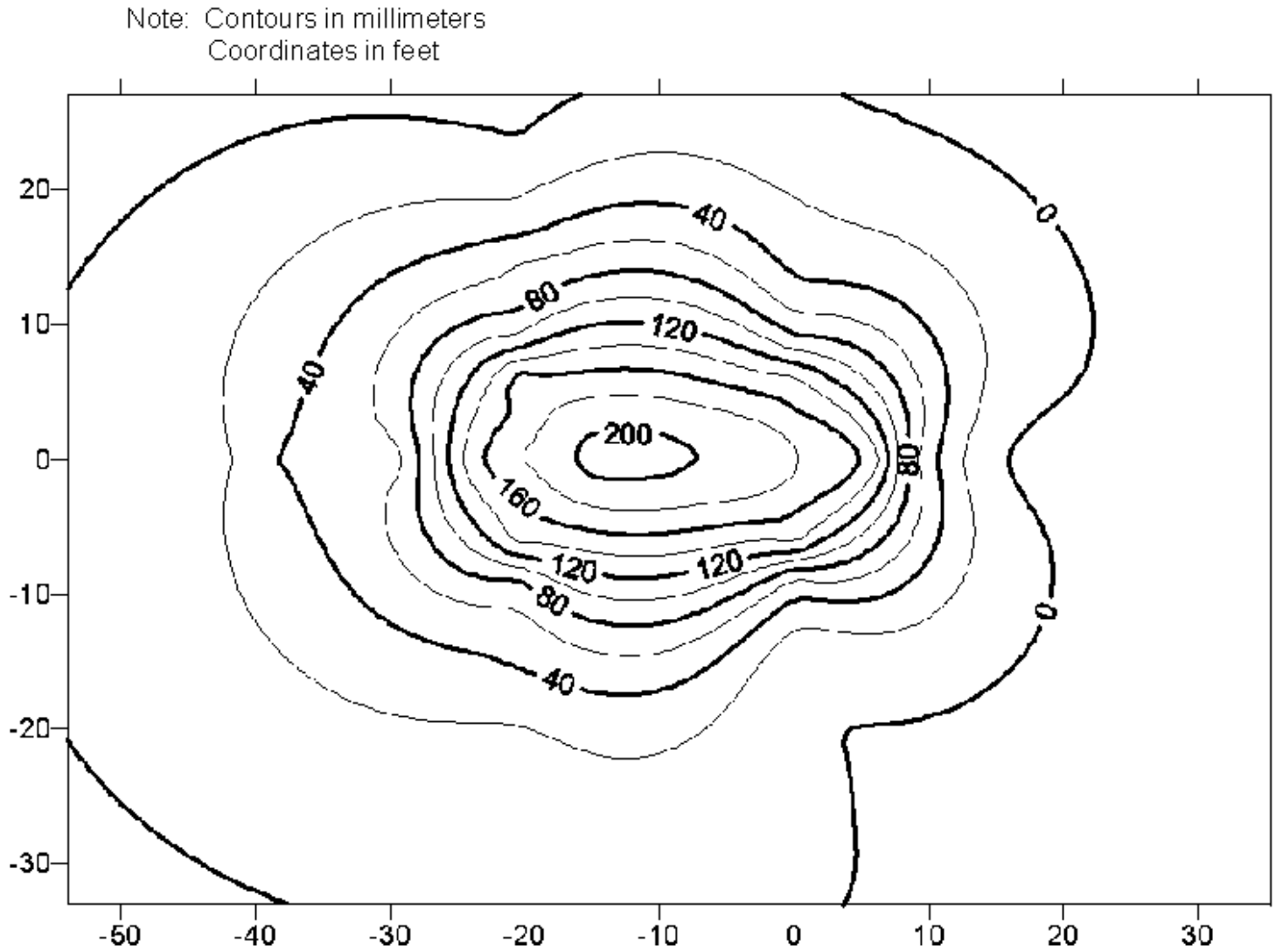

Figure 4.64 Contour of Settlement for 4-Pile Group/0.6m CISS Pile 1st Blast

5 9-PILE GROUP AND 0.9-m CISS PILE TESTS

The 9-pile group and 0.9-m CISS pile tests were performed to further investigate effects of group behavior of closely spaced piles and large diameter piles in liquefied soils. The 9-pile group consisted of 0.32 m outside diameter pipe piles spaced at 3.5 pile diameters driven to a depth of 12 m. The 0.9-m CISS pile consisted of a 0.9-m outside diameter steel shell with an 11-mm wall thickness driven to a depth of 14.8 m, after which soil inside the 0.9-m steel shell was augered out. In all cases, driving was very easy. A rebar cage consisting of thirteen 35.8 mm (#11) bars spaced at 169 mm on center and 15.9 mm (#5) spiral with a 165 mm spacing was then placed inside the steel shell which was then filled with concrete. A 2.2 MN hydraulic actuator placed between the pile group and CISS pile applied lateral loads during testing. Pile instrumentation consisted of strain gages along the depth of the pile and displacement transducers at the pile head. Pore pressure transducers were placed along the sides of the piles and at various distances in front of the piles. Data from the subsurface investigation and in-situ testing are presented along with load and displacement test results, excess pore pressure ratios, and settlement contours resulting from blasting.

5.1 9-Pile Group and 0.9-m CISS Pile Site Characterization

A subsurface investigation was performed at the 9-pile group/0.9-m CISS pile site before foundation testing was conducted. The location of the soil boring BH-3 along with other in-situ tests is shown in Figure 5.1. The soil log from BH-3 is presented in Figure 5.2. The water table at the time of boring was 1.5 m below the original ground surface. The soil profile consists of a loose sand layer extending from the ground surface to a

depth of 8.1 m, which is underlain by a gray clay layer extending from 8.1 m to 9.9 m. Another loose sand layer was found between 9.9 m and 13.1 m. A gray clay extended from 13.1 m to 24.4 m. The soil sample recovered at the bottom of the hole at 24.8 m consisted of silt and silty sand. Low SPT blow counts were observed at this site indicating a susceptibility to liquefaction.

In addition to SPT's, five CPT's were performed at this site before foundation installation (Figures 5.3 through 5.7), one after foundation installation but before lateral load testing (Figure 5.8), and two additional CPT's were performed approximately four months after foundation testing (Figure 5.9 through 5.10). The cone tip resistance from the CPT's performed before foundation installation show values typically between 4 and 7 Mpa in the upper sand layer with little difference in the measured tip resistance after pile installation. The low tip resistance confirms the liquefaction susceptibility of the sand layer.

Shear and compression wave velocity tests were also conducted at the 9-pile group/0.9-m CISS pile site. A seismic CPT test, two down-hole tests, and two suspension logger tests were performed to obtain the shear wave velocity profile. Results of the seismic CPT differ greatly compared to the other shear wave velocity tests. This may be due to the location of CPT3-6 being near the edge of the excavation where the soil density or in-situ stress was significantly greater than toward the middle of the excavation. There is reasonably good agreement between the down-hole and suspension logger tests. The suspension logger was also used to measure compression wave velocity. Velocity profiles for both shear and compression waves are presented in Figure 5.11.

5.2 9-Pile Group and 0.9-m CISS Pile Test Results

A plan view of the test set-up is shown in Figure 5.12, and a profile of the test set-up profile is shown in Figure 5.13. The lateral load for the 9-pile group/0.9-m CISS pile test was applied approximately 1 m above the excavated ground surface. The test procedure and results are described below.

5.2.1 Load-Displacement Results for Test 1

Lateral load testing of the 9-pile group/0.9-m CISS pile commenced on February 18, 1999. The lateral loading consisted of a static test and ten post blast loading series. The lateral load tests were run under displacement control. When either the 9-pile group or 0.9-m CISS pile reached the target displacement, the piles were unloaded until one reached the zero displacement target. The two target displacements for the static test were 3 mm and 38 mm. The 9-pile group reached the target displacement during the static test resulting in the 0.9-m CISS pile displacing less than the 9-pile group. The first post blast series consisted of ten cycles with a target displacement of 37 mm, one cycle at 76 mm, one cycle at 152 mm, and eleven cycles at 228 mm. Approximately 12 minutes elapsed during the first post blast load series. Post blast Series 2 through 10 consist of one 76 mm, one 152 mm, and four 228 mm cycles, and lasted for approximately 4 minutes each. Load versus displacement for the 9-pile group is presented in Figures 5.14 through 5.16. The load-displacement plots for the 0.9-m CISS pile are shown in Figures 5.17 through 5.19. The soil pile system decreased in stiffness during the first five cycles of post blast Series 1. The decrease in stiffness for the last six 228 mm cycles was negligible. After approximately four cycles the soil-pile stiffness of the 9-pile group and

0.9-m CISS pile had decreased to 37% and 25% of the static stiffness respectively. The soil-pile stiffness incrementally increased during post blast Series 2 through 10. Approximately 45% of the static soil pile stiffness was regained by the last load series for the 9-pile group and 40% for the 0.9-m CISS pile. The increase in pile stiffness during the loading series is due to a reduction in pore water pressure with time.

5.2.2 Excess Pore Pressure Response for Test 1

Pore pressure transducers were used to obtain excess pore pressure ratios during the lateral load testing and for approximately one hour after loading stopped. The location and depth below grade of each transducer is shown in Figure 5.20. Pore pressures were measured for approximately two hours after detonation of the down-hole explosives and are shown in Figures 5.21 through 5.33. Transducer data is presented according to location starting with transducers north of the 9-pile group and ending with transducers south of the 0.9-m CISS pile.

A review of excess pore pressure ratios show initial ratios ranging from 70% to over 100% immediately following the blast indicating liquefaction had occurred. Sand boils began forming minutes after detonation of the explosives, providing additional evidence of liquefaction. Large fluctuations in the excess pore pressure ratio near the pile indicate the influence the piles have on the nearby soil, especially at shallow depths where pile displacements are greatest.

Approximately one hour after the blast, excess pore pressure ratios generally ranged from 20% to 50% which correlates well with excess pore pressure ratios at the same time for the 0.6-m CISS and 4-pile group test. However, excess pore pressure ratios adjacent

to the 0.9-m CISS pile at depths of 1.1 and 2.0 meters were as high as 70%. The higher pore pressure ratios near the 0.9-m CISS pile may be a result of pile diameter effects. The excess pore pressure ratios had were close to pre-blast levels after approximately two hours.

5.2.3 Load-Displacement Results for Test 2

The second 9-pile group/0.9-m CISS pile lateral load test occurred on February 19, 1999, one day after the first test. The static test consisted of displacing the piles to 7 mm for five minutes, increasing and to a displacement of 13 mm and holding for eight minutes, increasing and holding a displacement of 19 mm for five minutes, and increasing to and maintaining a final displacement of 26 mm for five minutes. After the 26 mm displacement, the piles returned to a zero displacement and then loaded to a displacement of 38 mm. Approximately 25 minutes elapsed during the static test. The first post blast load series took 14 minutes to execute. The remaining series occurred at 5-minute intervals. The first nine post blast series occurred during the first hour after blasting. The tenth post blast series took place approximately two hours after blasting and the eleventh post blast series occurred 2.5 hours after blasting. Post blast Series 1 consisted of one displacement cycle at 56 mm, on cycle at 128 mm, one cycle at 192 mm, three cycles at 228 mm, one cycle at 278 mm, and four cycles at 300 mm. Post blast Series 2 through 4 onsisted of one 72 mm cycle, one 150 mm cycle, one 228 mm cycle, and three 300 mm cycles. After post blast Series 4 residual displacement of the 0.9-m CISS pile exceed the 72 mm target displacement, therefore post blast Series 5 through 10 did not contain the 72 mm cycle. The eleventh post blast series consisted of one 174 mm

displacement, one 205 mm displacement, one 236 mm displacement, and three 270 mm displacements. Load-displacement data is presented in Figures 5.34 through 5.36 and Figures 5.37 through 5.39 for the 9-pile group/0.9-m CISS pile respectively. The 9-pile group reached the target displacements for the static test while the 0.9-m CISS pile reached the target displacement for the post blast testing. Upon detonation of the explosives, the soil-pile systems began to decrease in stiffness. The soil-pile stiffness at the end of post blast Series 1 was 50% and 30% of the static stiffness for the 9-pile group and 0.9-m CISS pile respectively. Approximately one hour after the blast, the 9-pile group and 0.9-m CISS pile had regained 60% and 50% of the static stiffness. The soil-pile system stiffness increased to approximately 70% and 60% of the static stiffness for the 9-pile group and 0.9-m CISS pile respectively 2.5 hours after the blast. The increase in stiffness between each load series is attributed to the decrease in pore water pressure with time.

5.2.4 Excess Pore Pressure Response for Test 2

The location and depth of pore pressure transducers used to obtain excess pore pressure ratios is presented in Figure 5.20. Figures 5.40 through 5.52 show the variation of excess pore pressure ratio and load with time. Data from the PPT's is presented according to transducer location from north to south. Excess pore pressure ratios generally range between 50% and 100% immediately following the blast and 0% and 20% approximately 70 minutes after blasting. Sand boils began to form approximately three minutes after detonation of the explosives. Generally, pore pressure dissipation between one and two hours after the blast was negligible.

5.3 Blast Induced Settlement

An elevation survey was performed prior to and after blasting in an effort to measure settlement due to blasting. Contours of settlement due to the first and second blast are presented in Figures 5.53 and 5.54. The contours of settlement are in centimeters, while the coordinates from the edge of the excavation are in meters. Settlement of nearly 320 mm was observed after the first test, and an additional 170 mm at the conclusion of the second test.

5.4 Summary

Two series of lateral load tests were performed on a 9-pile group and a 0.9-m CISS pile. Both static and post liquefaction tests were performed. Pile stiffness was observed to decrease after detonation of the explosives due to an increase in pore water pressure. As the pore pressures decreased, pile stiffness increased. The effect of pore-pressure on foundation stiffness is discussed in more detail in Chapters 7 and 8. It was observed that the 0.9-m CISS pile was more stiff during the static test while the 9-pile group was more stiff during the liquefaction testing.

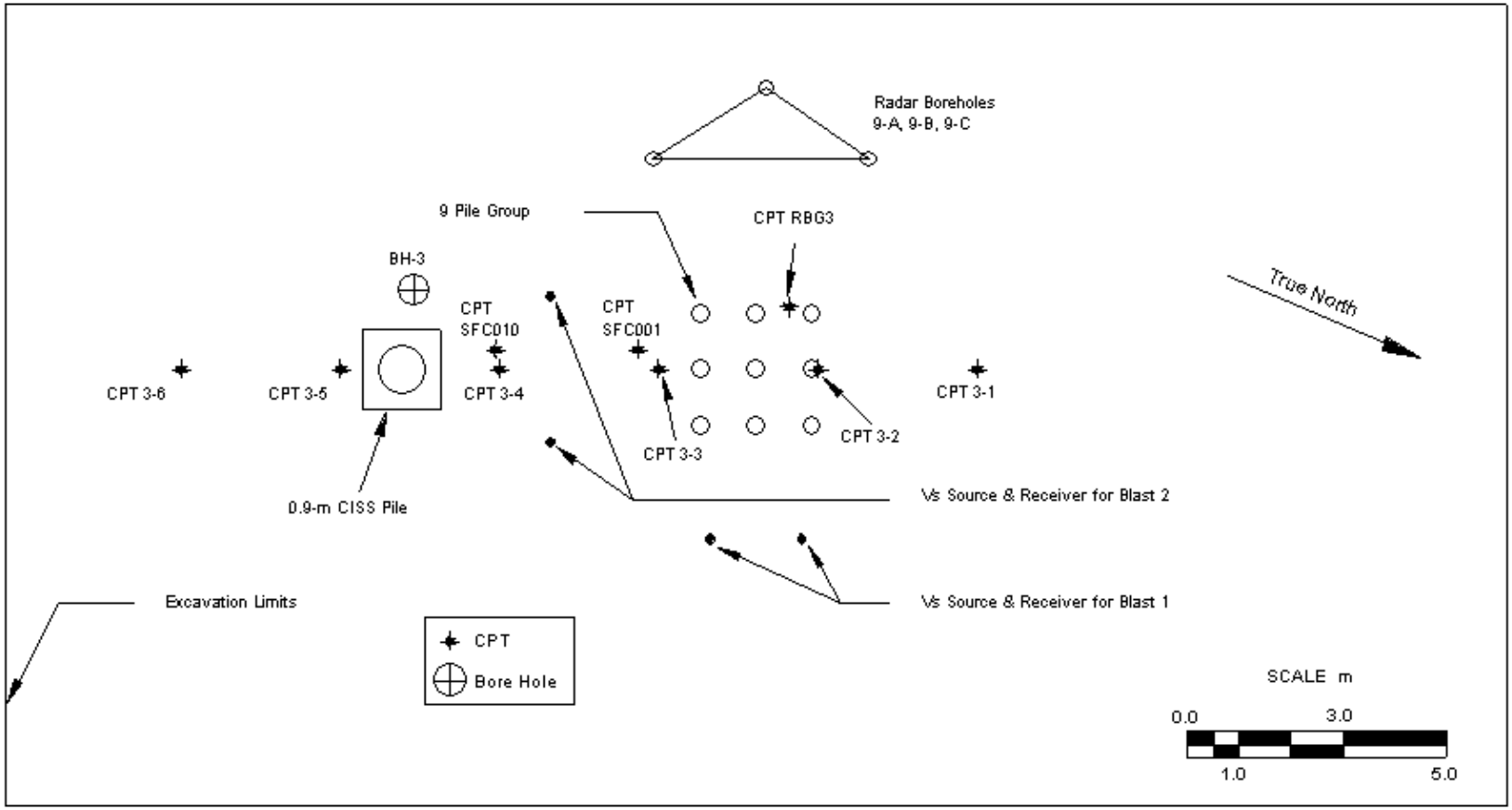

Figure 5.1 Location Map of In-Situ Tests for 9-Pile Group/0.9m CISS Pile Test Area

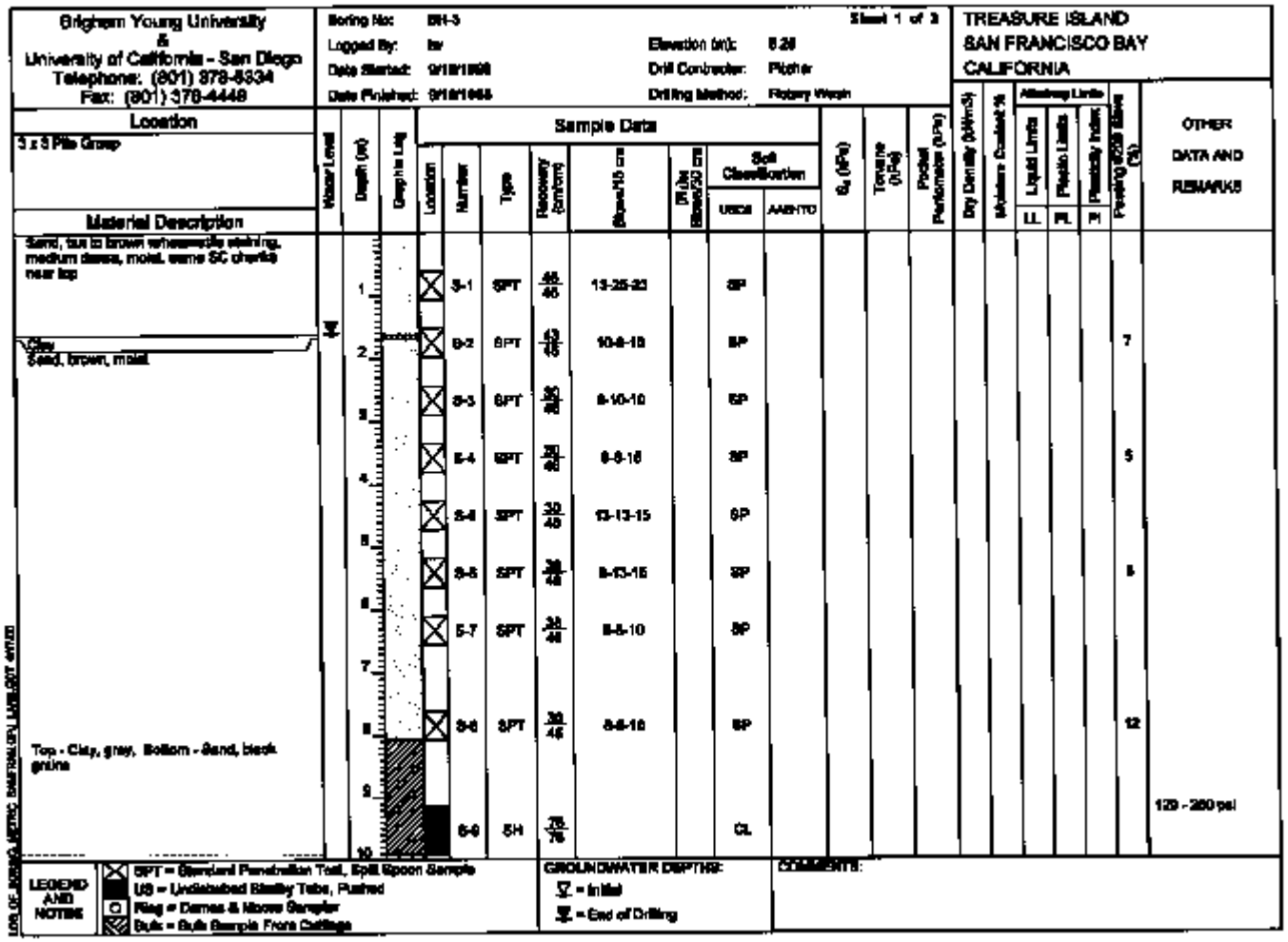

Figure 5.2a Soil Boring Log for the 9-Pile Group/0.9m CISS Pile Test Area

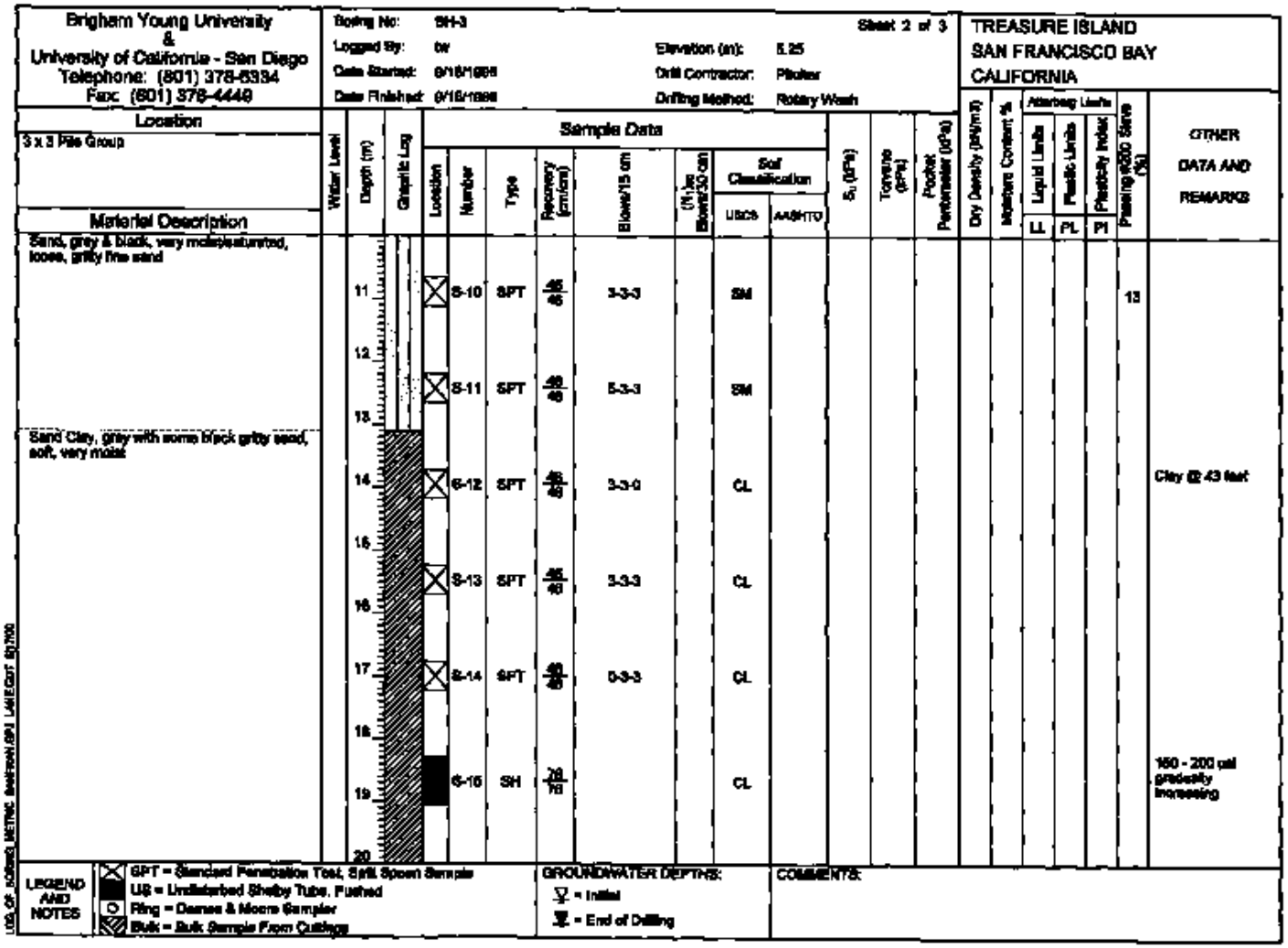

Figure 5.2b Soil Boring Log for the 9-Pile Group/0.9m CISS Pile Test Area

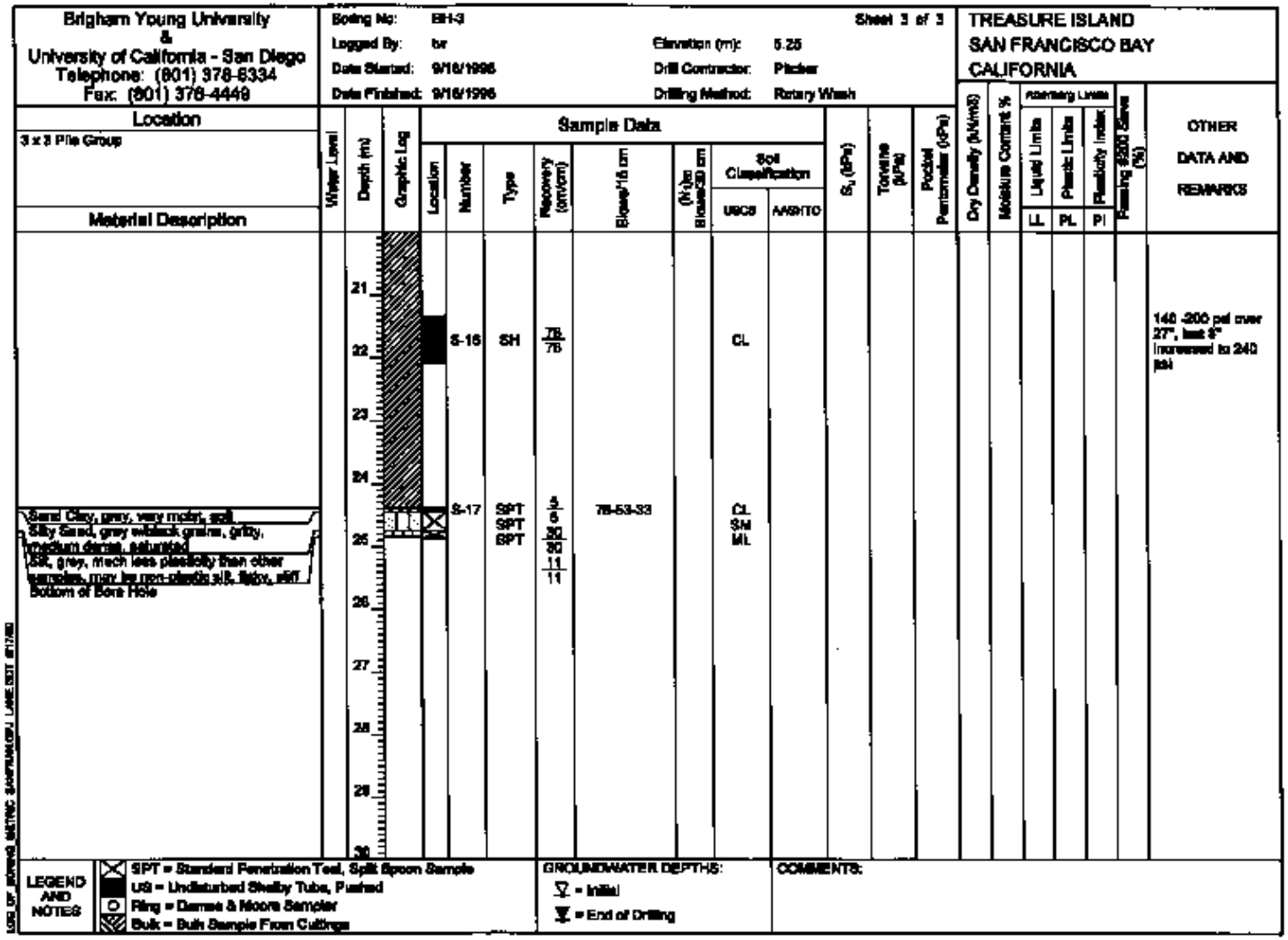

Figure 5.2c Soil Boring Log for the 9-Pile Group/0.9m CISS Pile Test Area

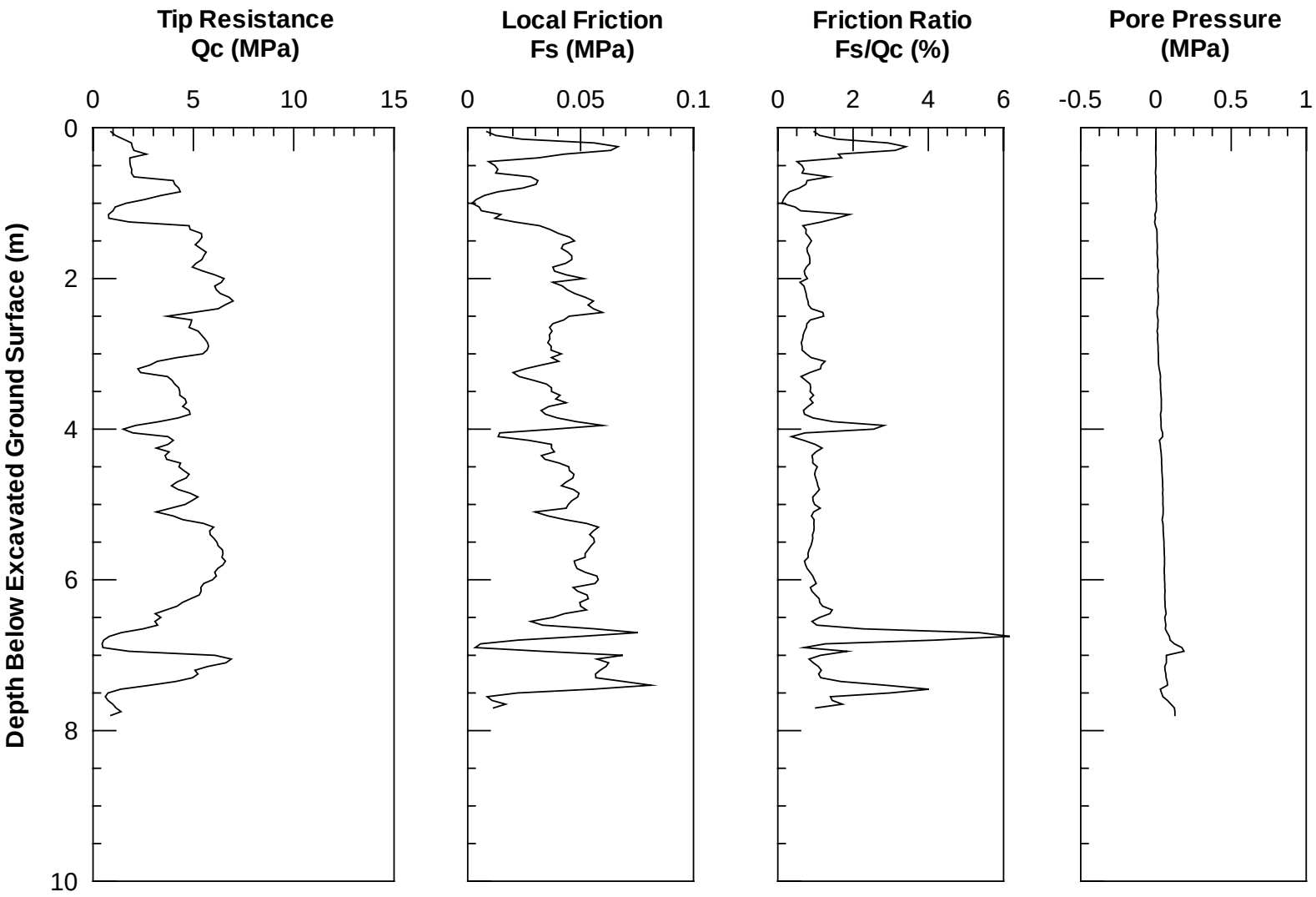

Figure 5.3 CPT3-2 Logs for 9-Pile Group/0.9m CISS Pile Test Area (10-30-98)

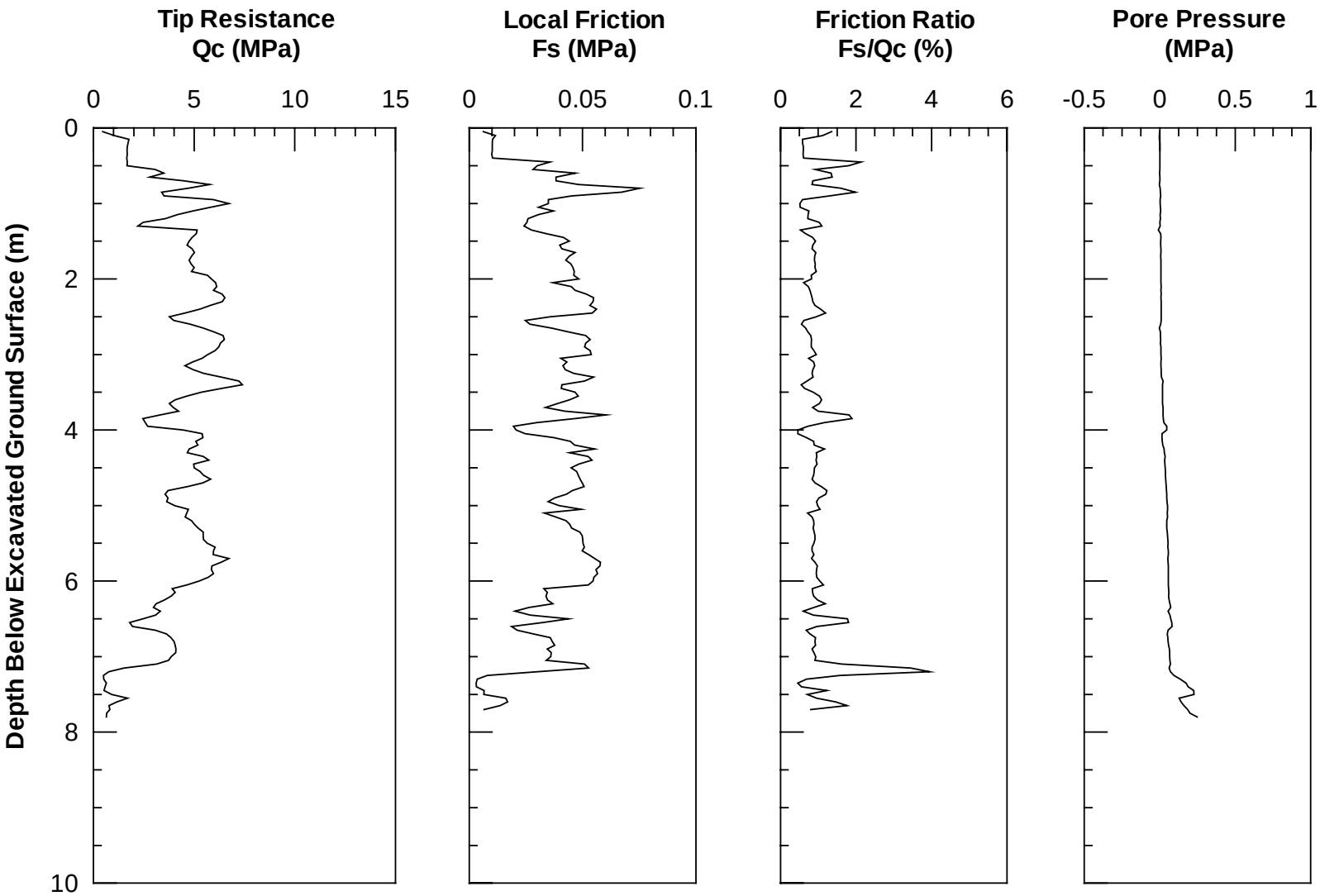

Figure 5.4 CPT3-3 Logs for 9-Pile Group/0.9m CISS Pile Test Area (10-30-98)

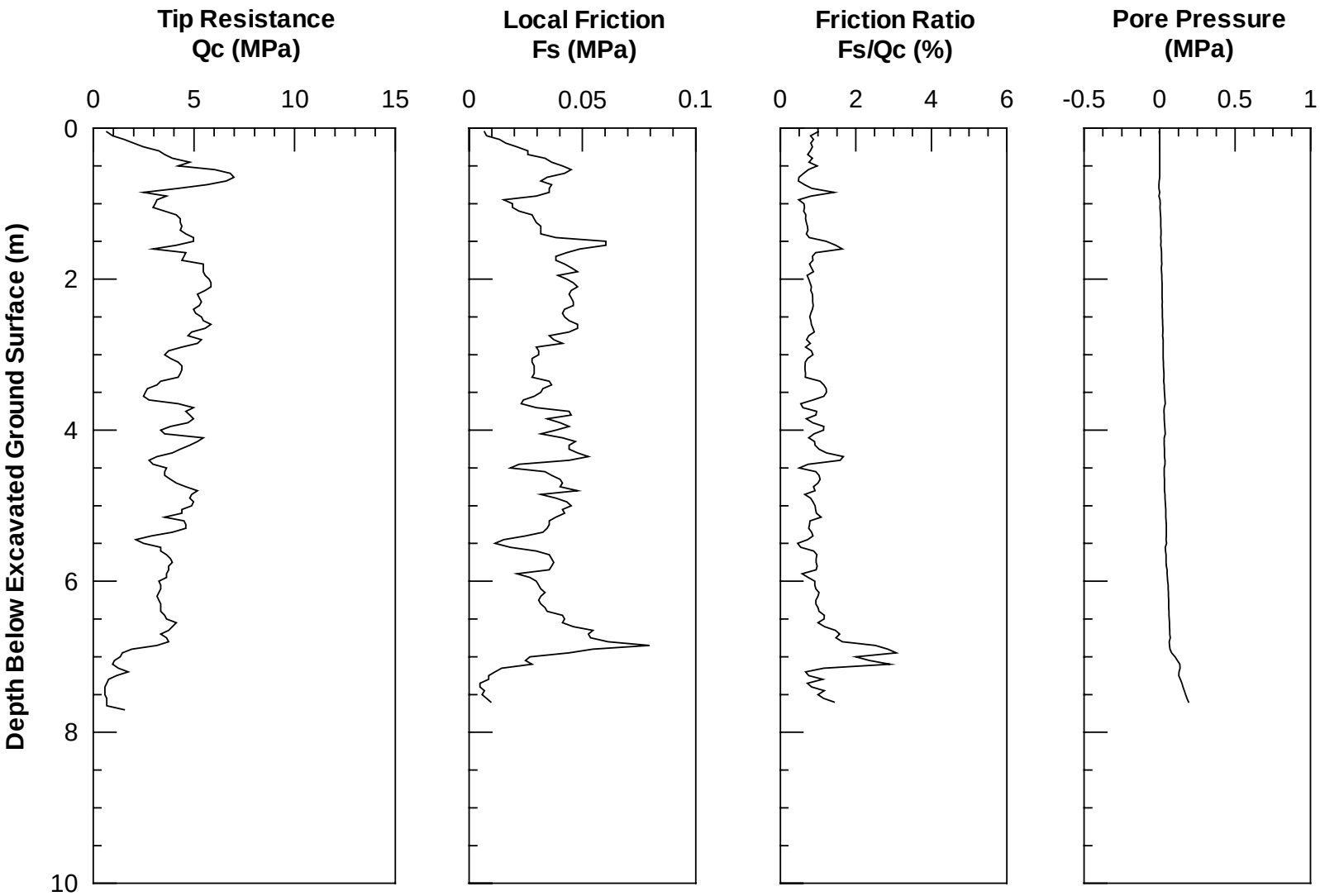

Figure 5.5 CPT3-4 Logs for 9-Pile Group/0.9m CISS Pile Test Area (10-30-98)

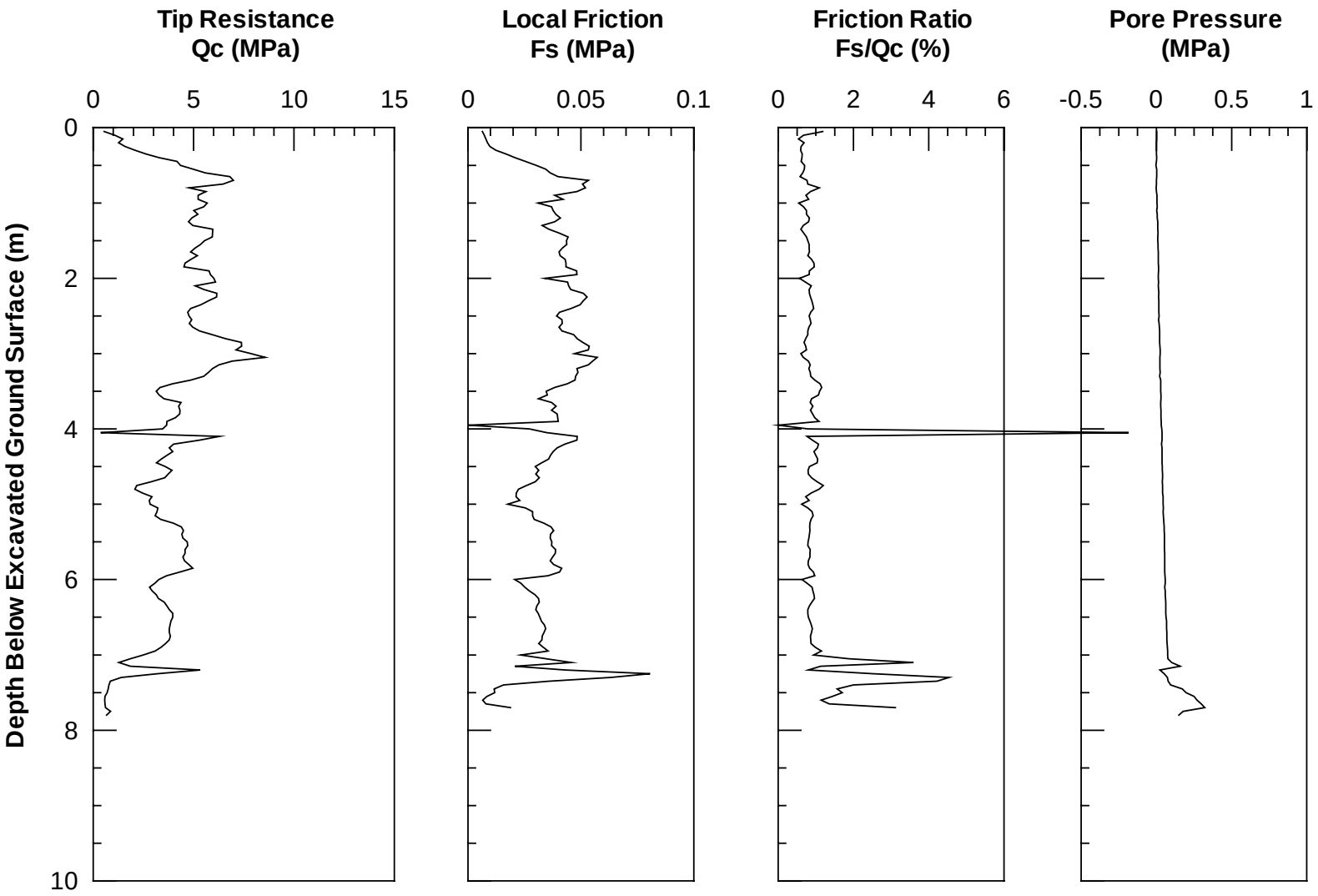

Figure 5.6 CPT3-5 Logs for 9-Pile Group/0.9m CISS Pile Test Area (10-30-98)

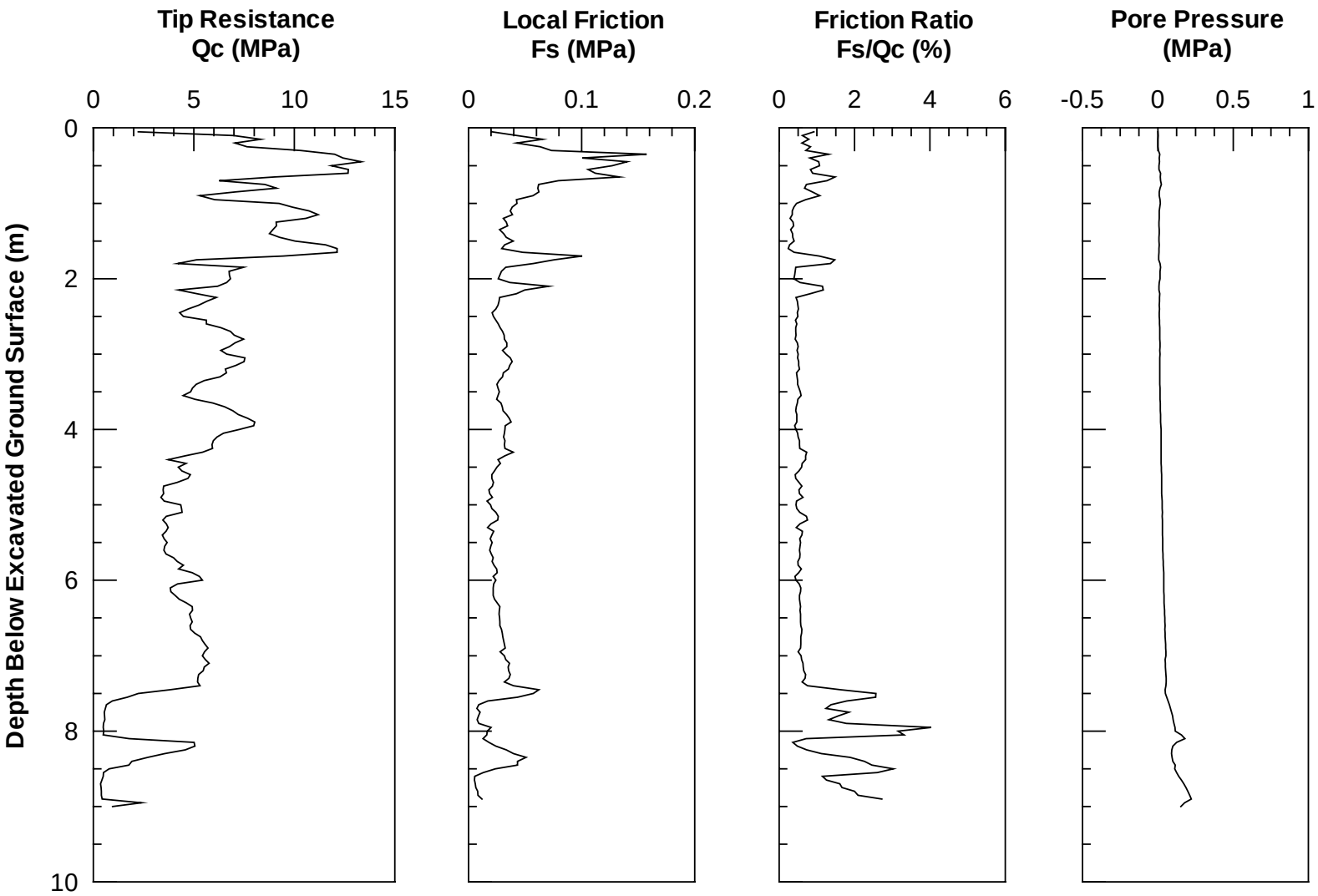

Figure 5.7 CPT3-6 Logs for 9-Pile Group/0.9m CISS Pile Test Area (10-30-98)

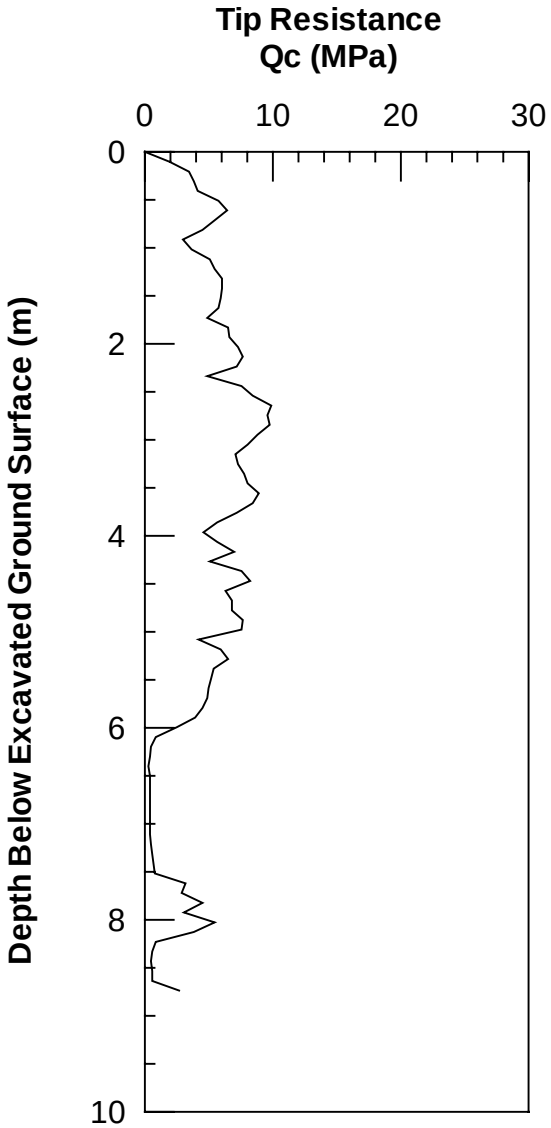

Figure 5.8 CPT RBG3 Logs for 9-Pile Group/0.9m CISS Pile Test Area (1-30-99)

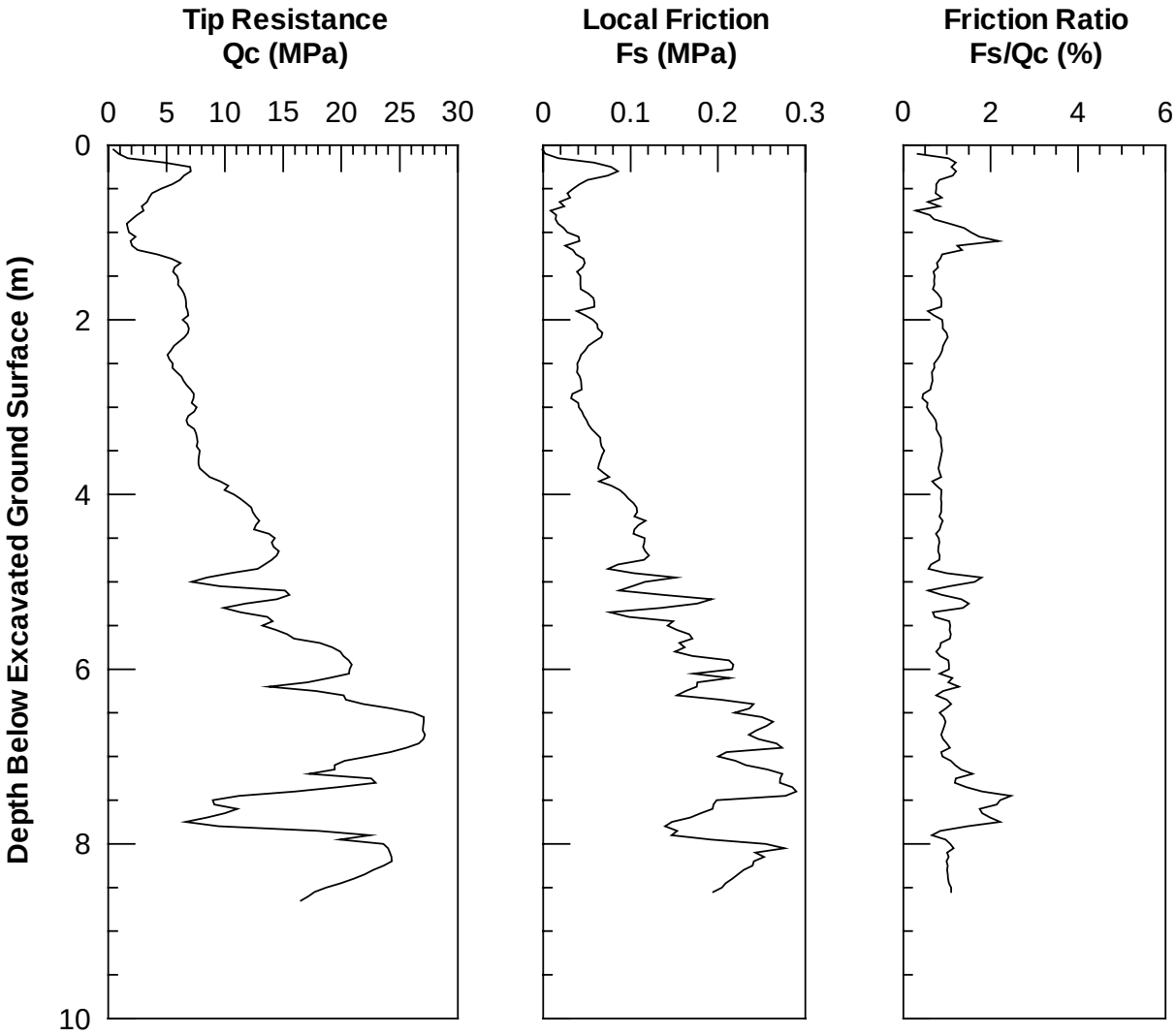

Figure 5.9 CPT SFC001 Logs for 9-Pile Group/0.9m CISS Pile Test Area (6-24-99)

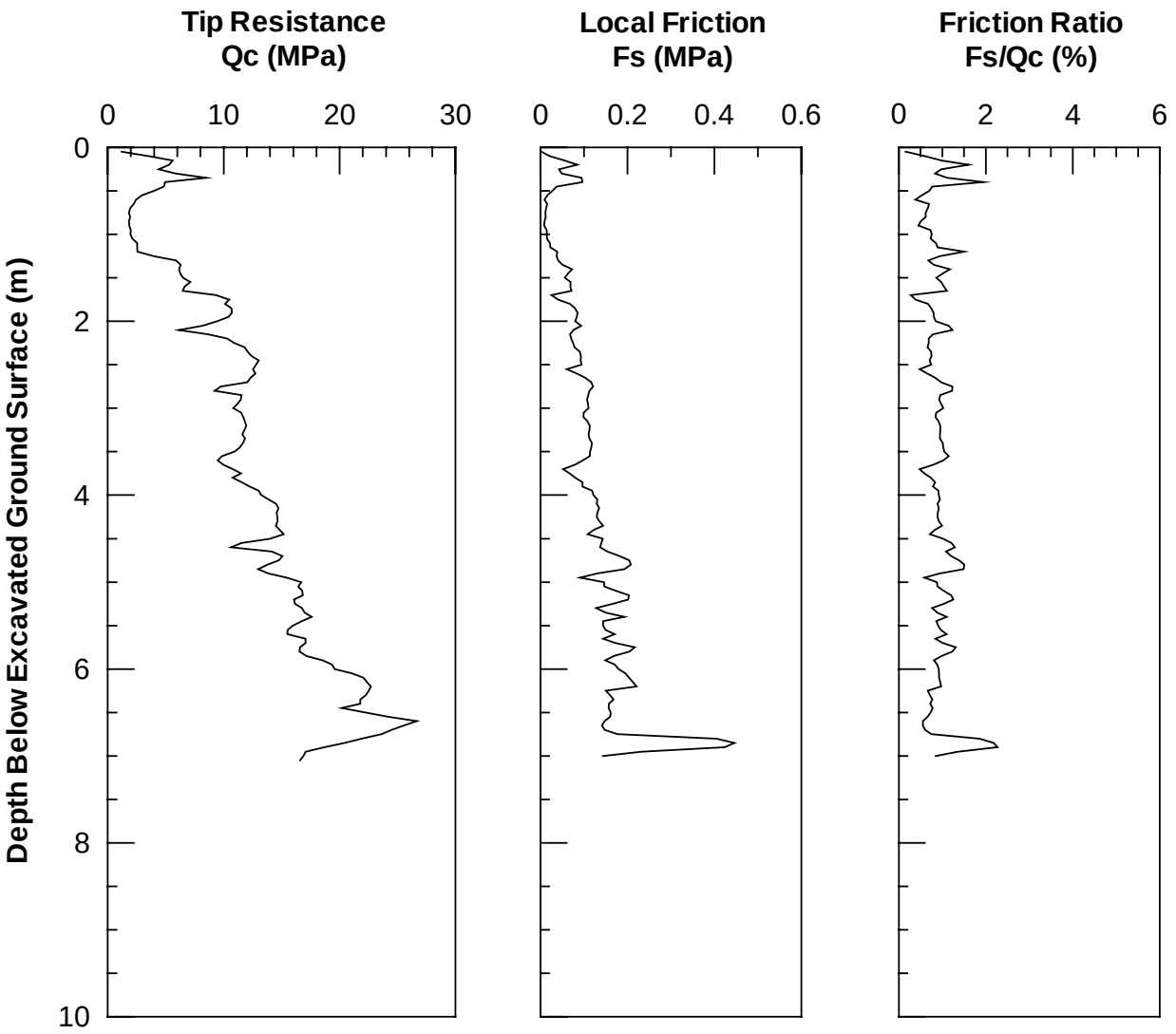

Figure 5.10 CPT SFC010 Logs for 9-Pile Group/0.9m CISS Pile Test Area (6-24-99)

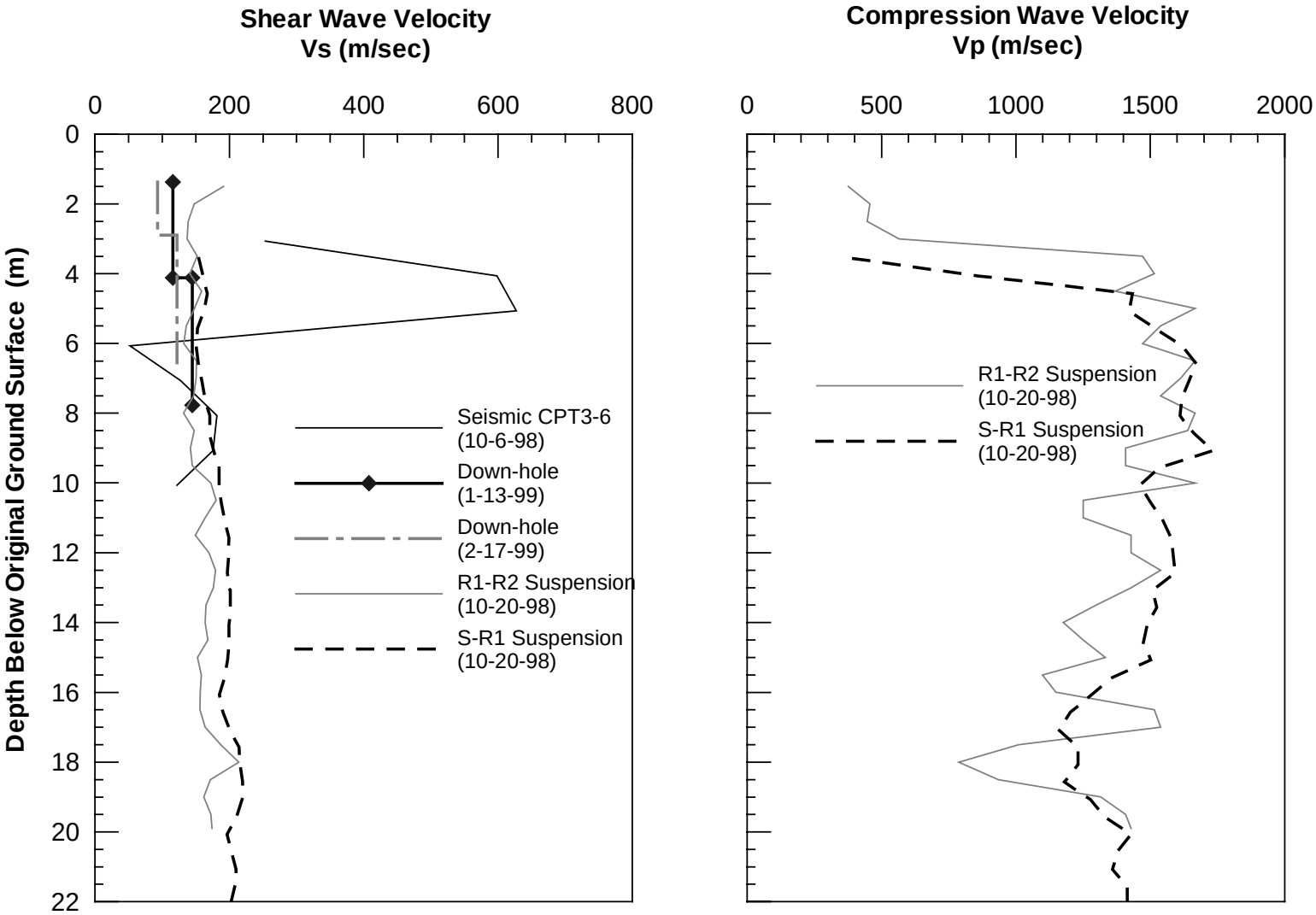

Figure 5.11 9-Pile Group/0.9m CISS Pile Site Pre-blast Velocities a) Shear Wave b) Compression Wave

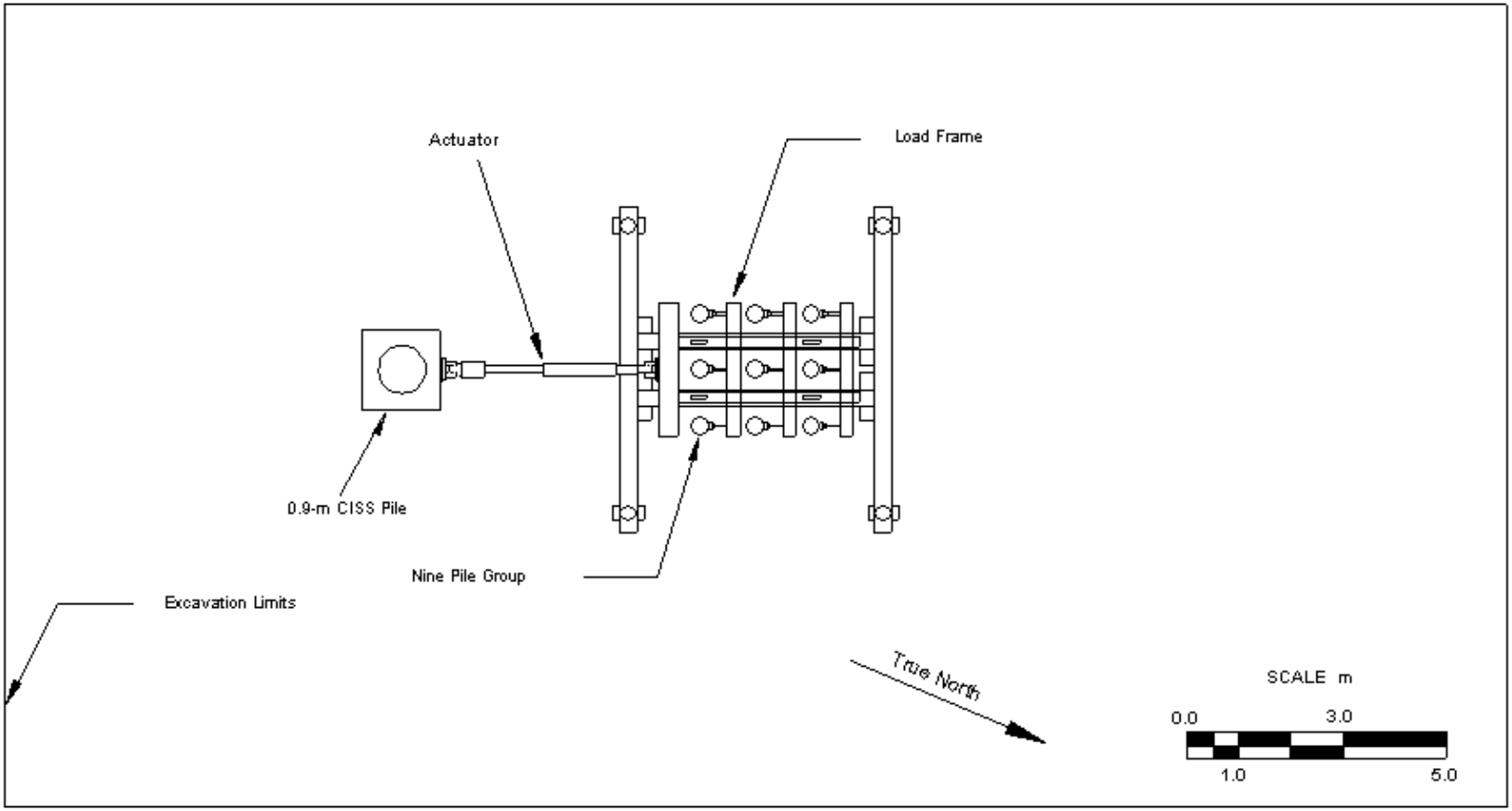

Figure 5.12 Plan View of 9-Pile Group/0.9m CISS Pile Test Set-Up

Figure 5.13 Profile of 9-Pile/0.9-m CISS Pile Test Set-Up

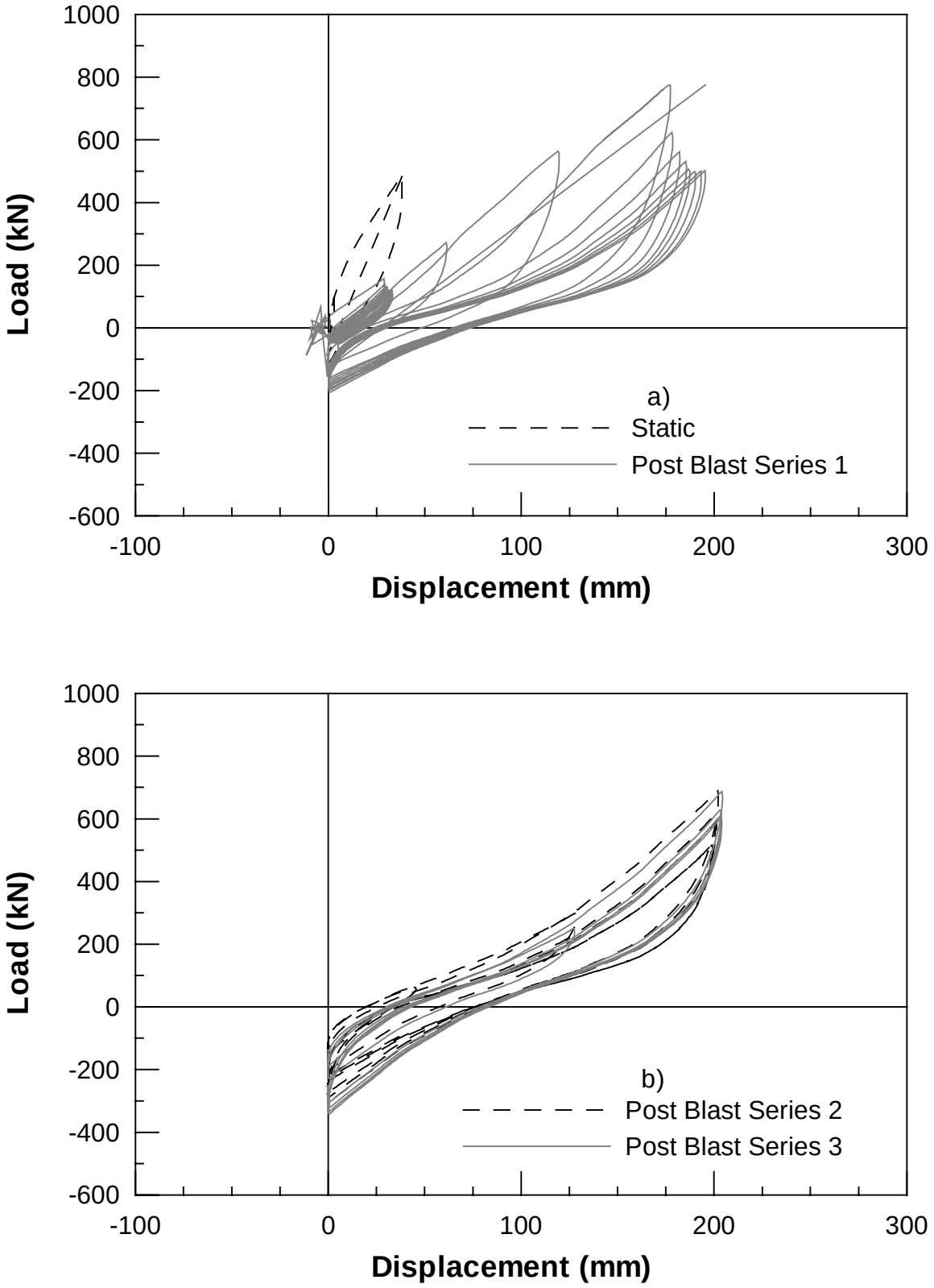

Figure 5.14 Load vs. Displacement for 9-Pile Group a) Static and Post Blast Series 1 b) Post Blast Series 2 and 3

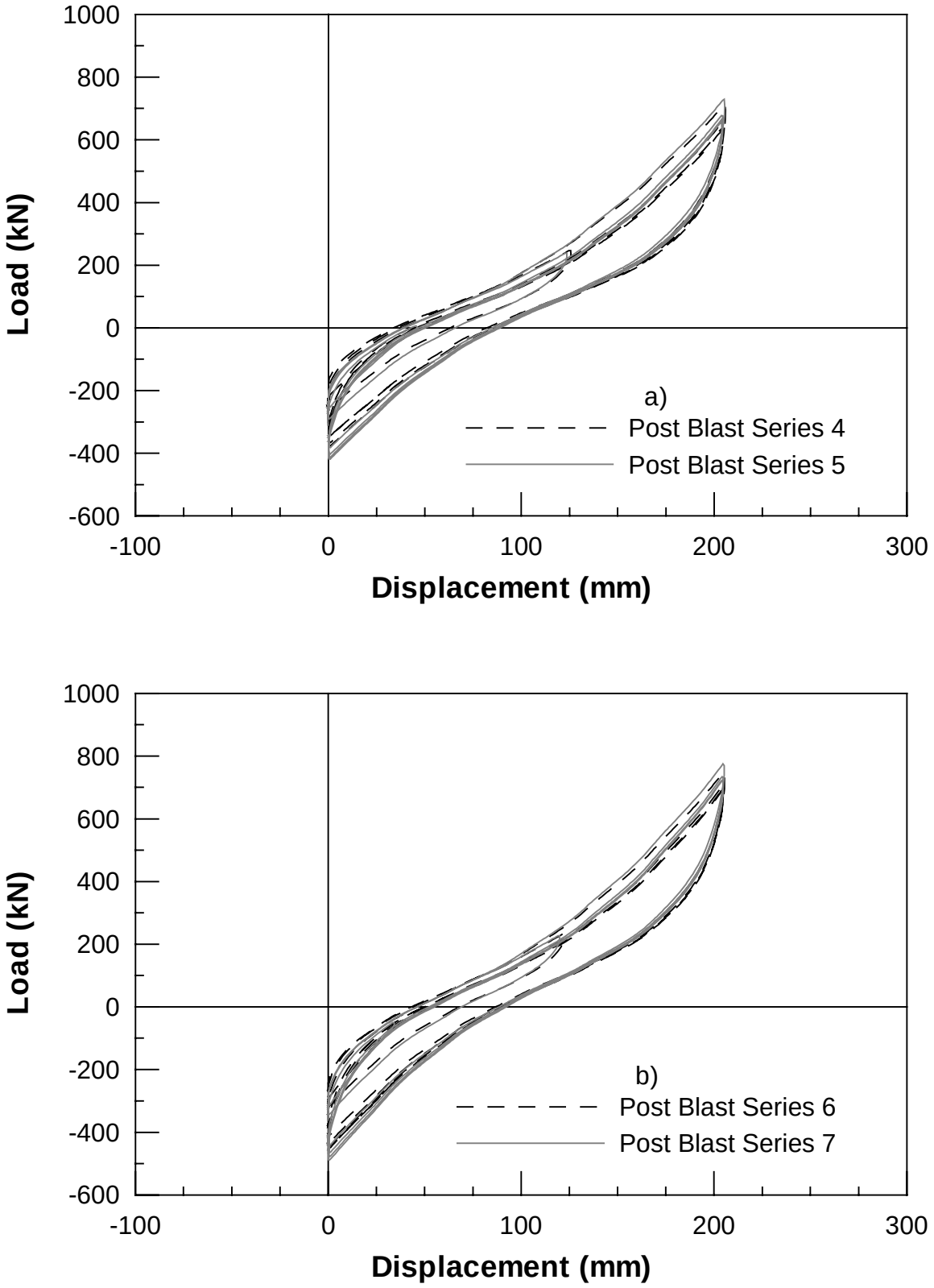

Figure 5.15 Load vs. Displacement for 9-Pile Group a) Post Blast Series 4 and 5 b) Post Blast Series 6 and 7

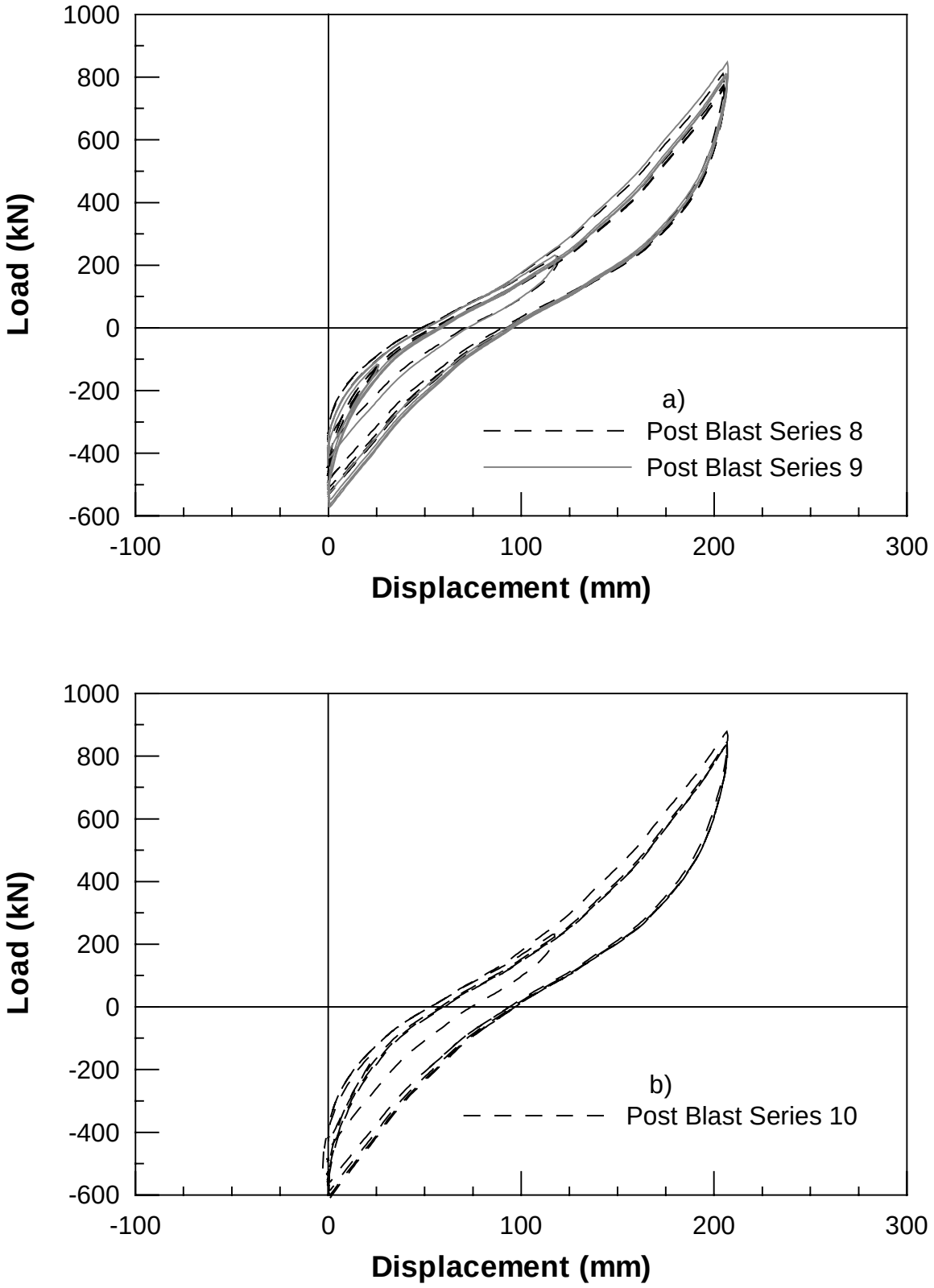

Figure 5.16 Load vs. Displacement for 9-Pile Group a) Post Blast Series 8 and 9 b) Post Blast Series 10

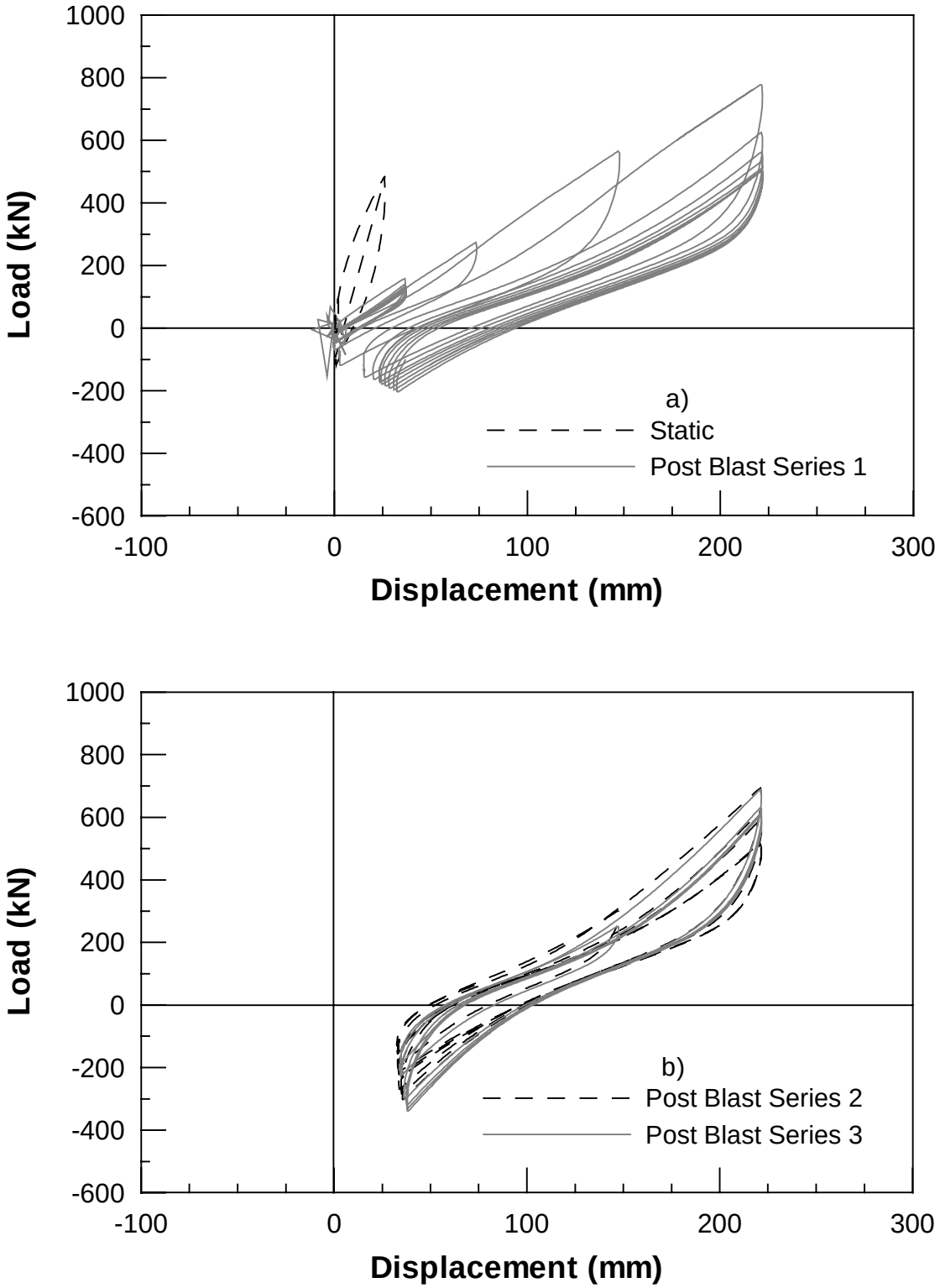

Figure 5.17 Load vs. Displacement for 0.9m CISS Pile a) Static and Post Blast Series 1 b) Post Blast Series 2 and 3

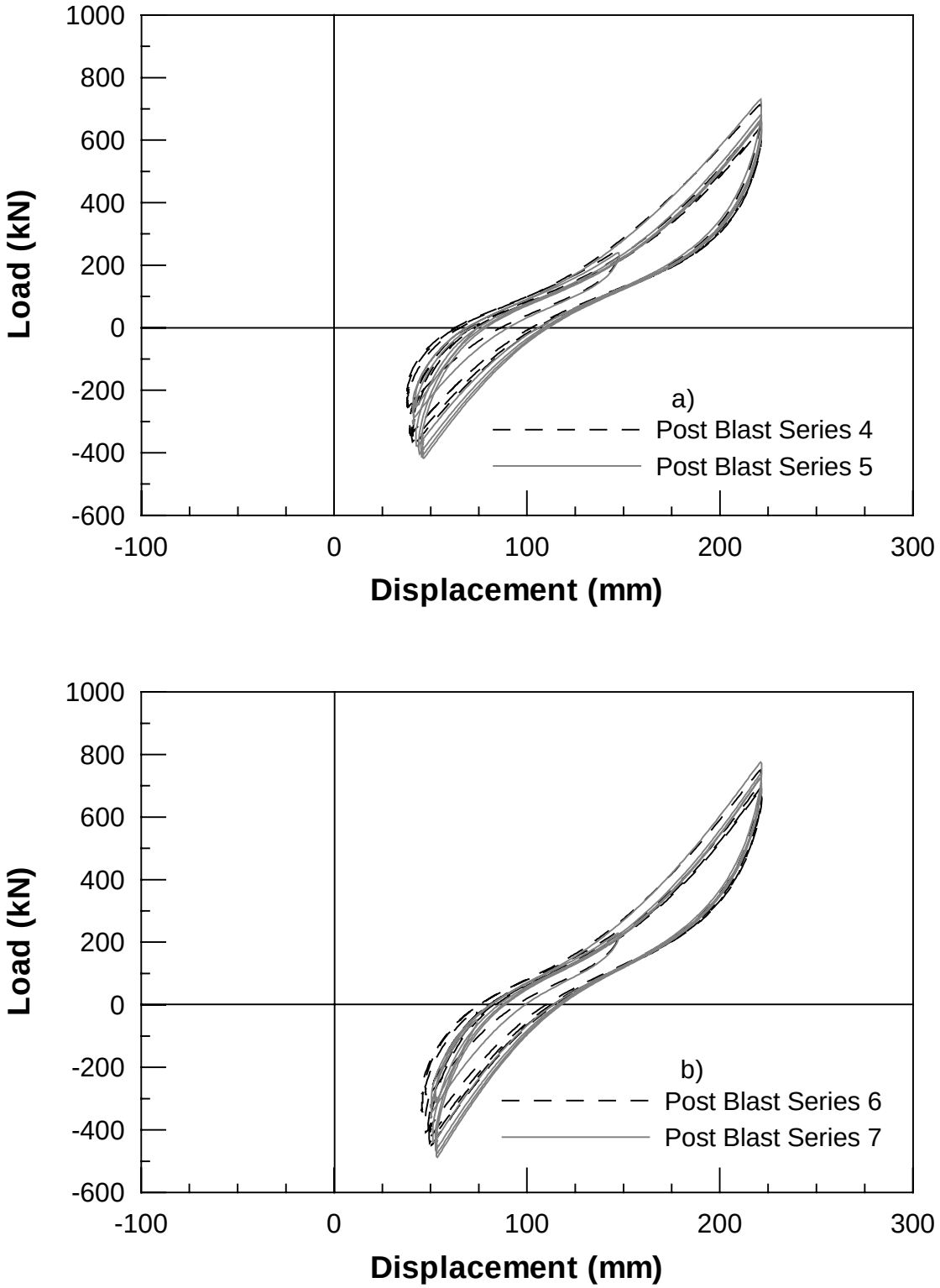

Figure 5.18 Load vs. Displacement for 0.9m CISS Pile a) Post Blast Series 4 and 5 b) Post Blast Series 6 and 7

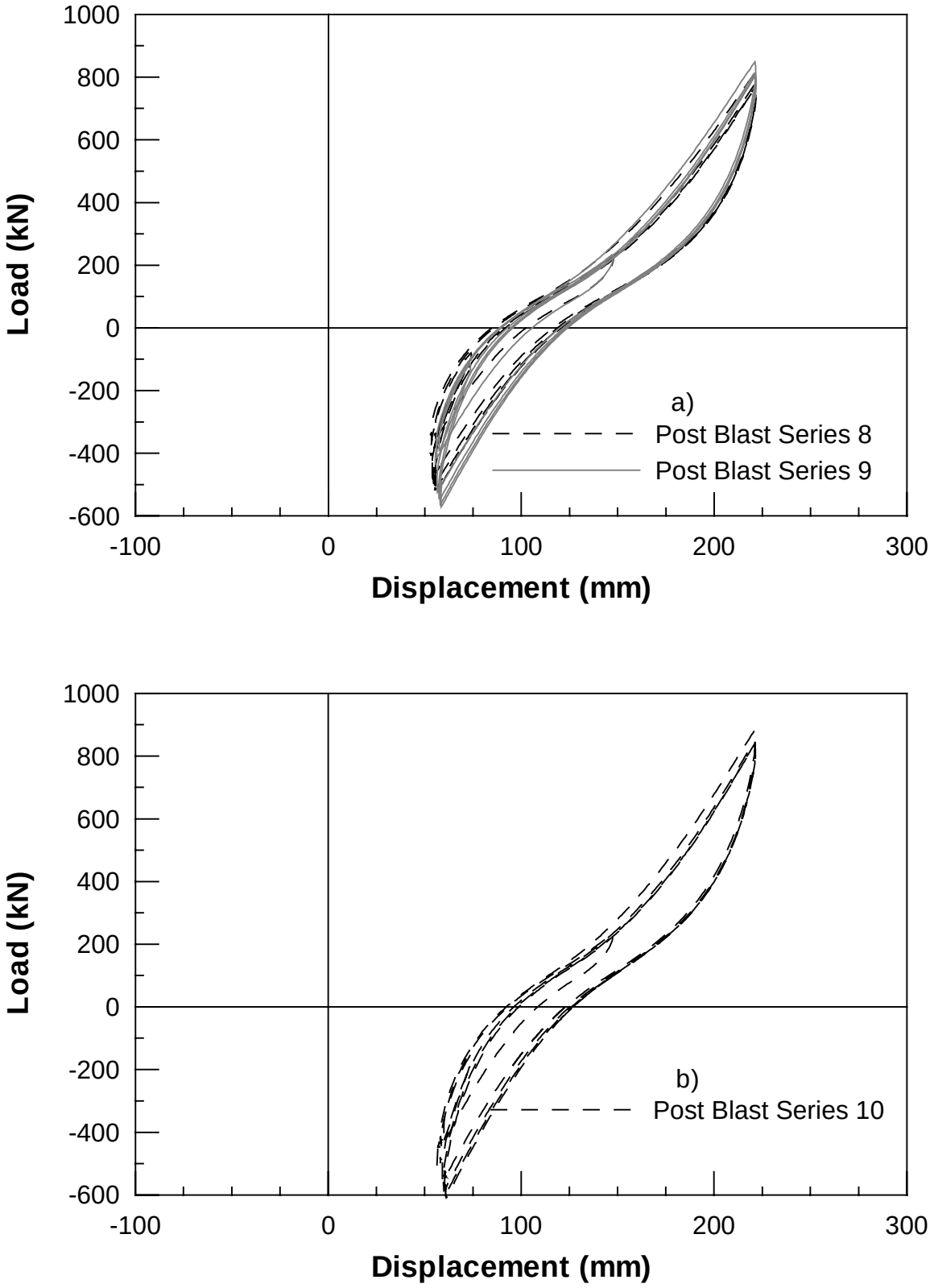

Figure 5.19 Load vs. Displacement for 0.9m CISS Pile a) Post Blast Series 8 and 9 b) Post Blast Series 10

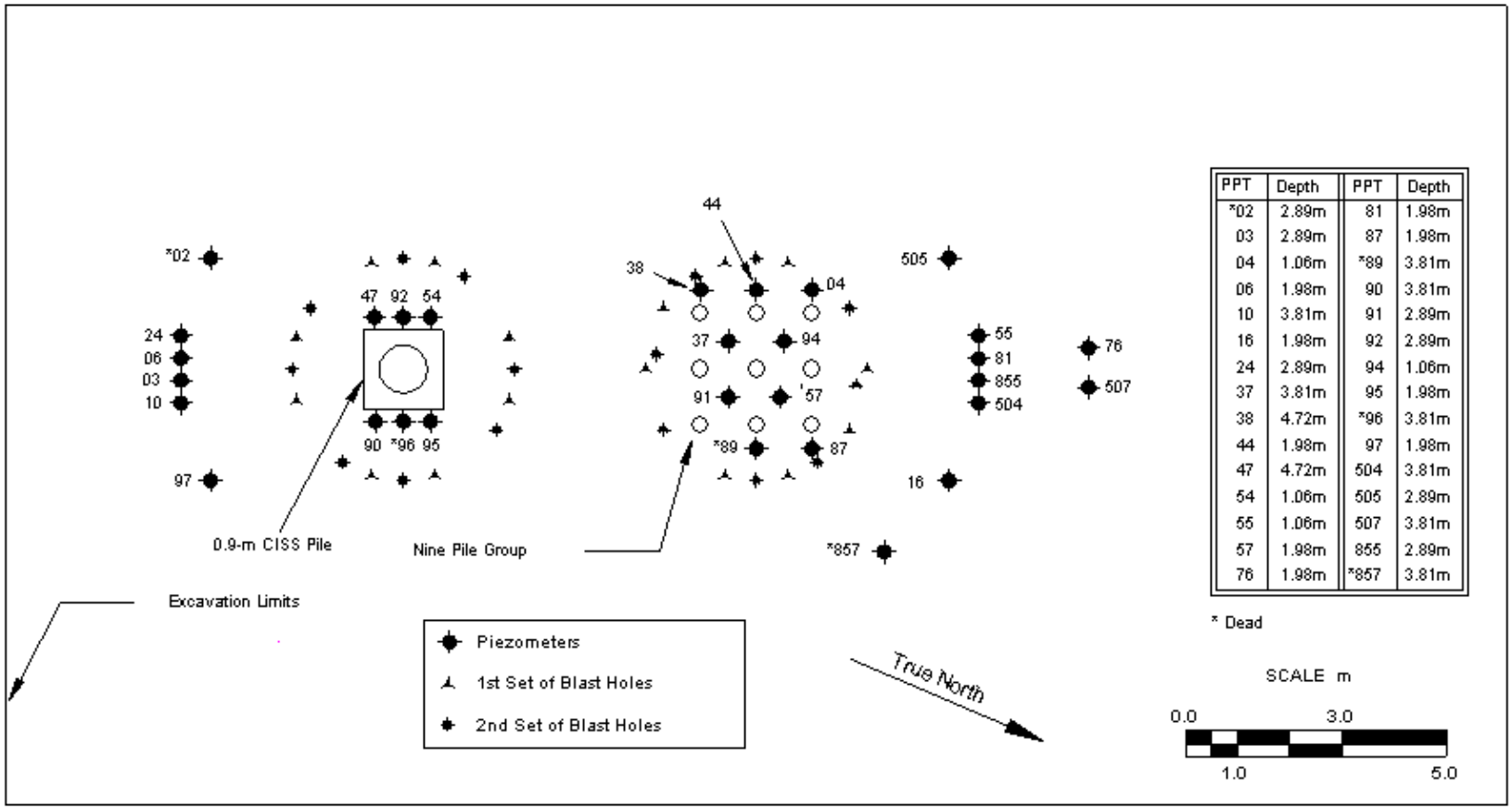

PPT	Depth	PPT	Depth
*02	2.89m	81	1.98m
03	2.89m	87	1.98m
04	1.06m	*89	3.81m
06	1.98m	90	3.81m
10	3.81m	91	2.89m
16	1.98m	92	2.89m
24	2.89m	94	1.06m
37	3.81m	95	1.98m
38	4.72m	*96	3.81m
44	1.98m	97	1.98m
47	4.72m	504	3.81m
54	1.06m	505	2.89m
55	1.06m	507	3.81m
57	1.98m	855	2.89m
76	1.98m	*857	3.81m

* Dead

Figure 5.20 Location Map of Pore Pressure Transducers and Explosives for 9-Pile Group/0.9m CISS Pile Test

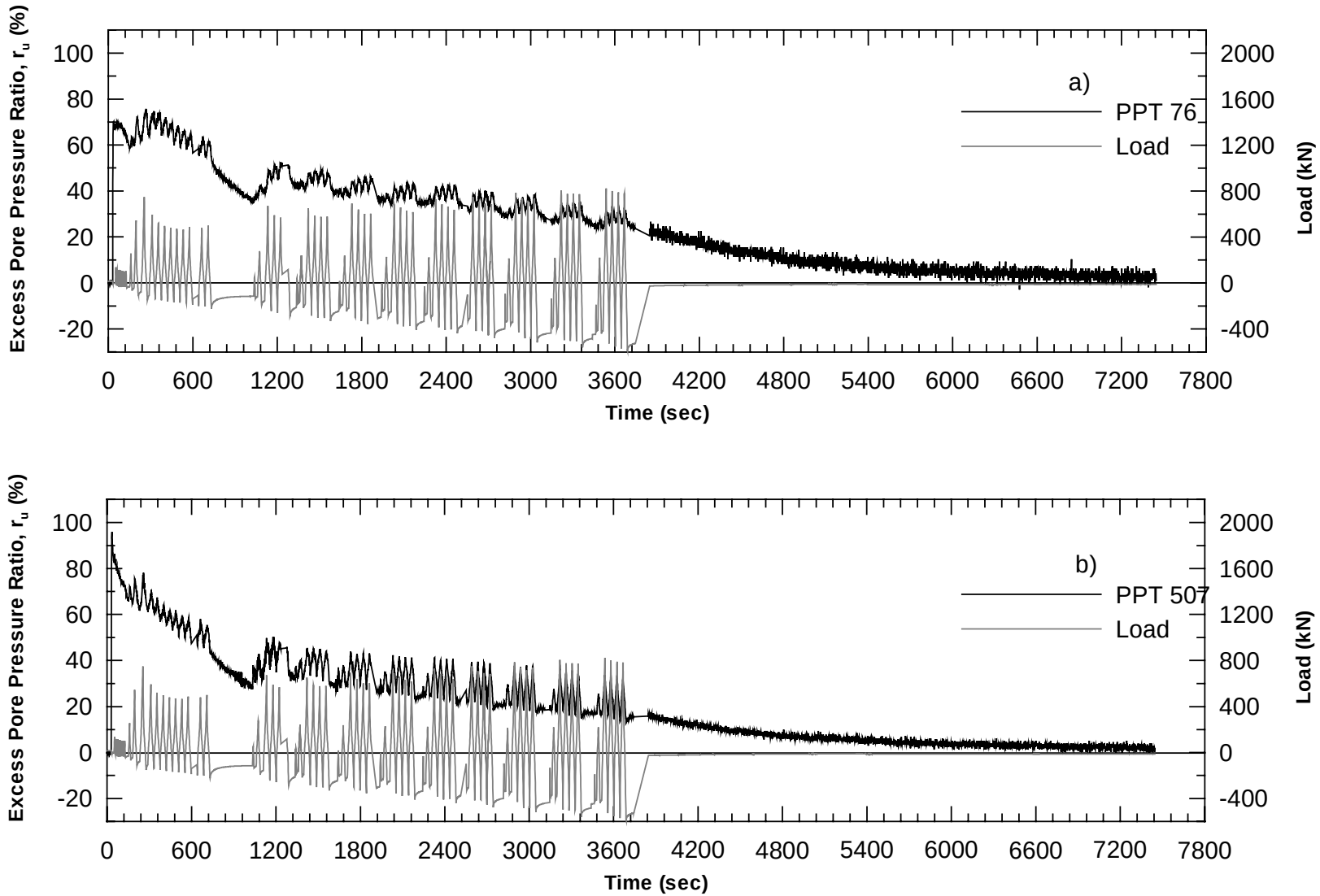

Figure 5.21 Excess Pore Pressure Ratio for 9-Pile Group/0.9m CISS Pile 1st Blast a)PPT76 b)PPT507

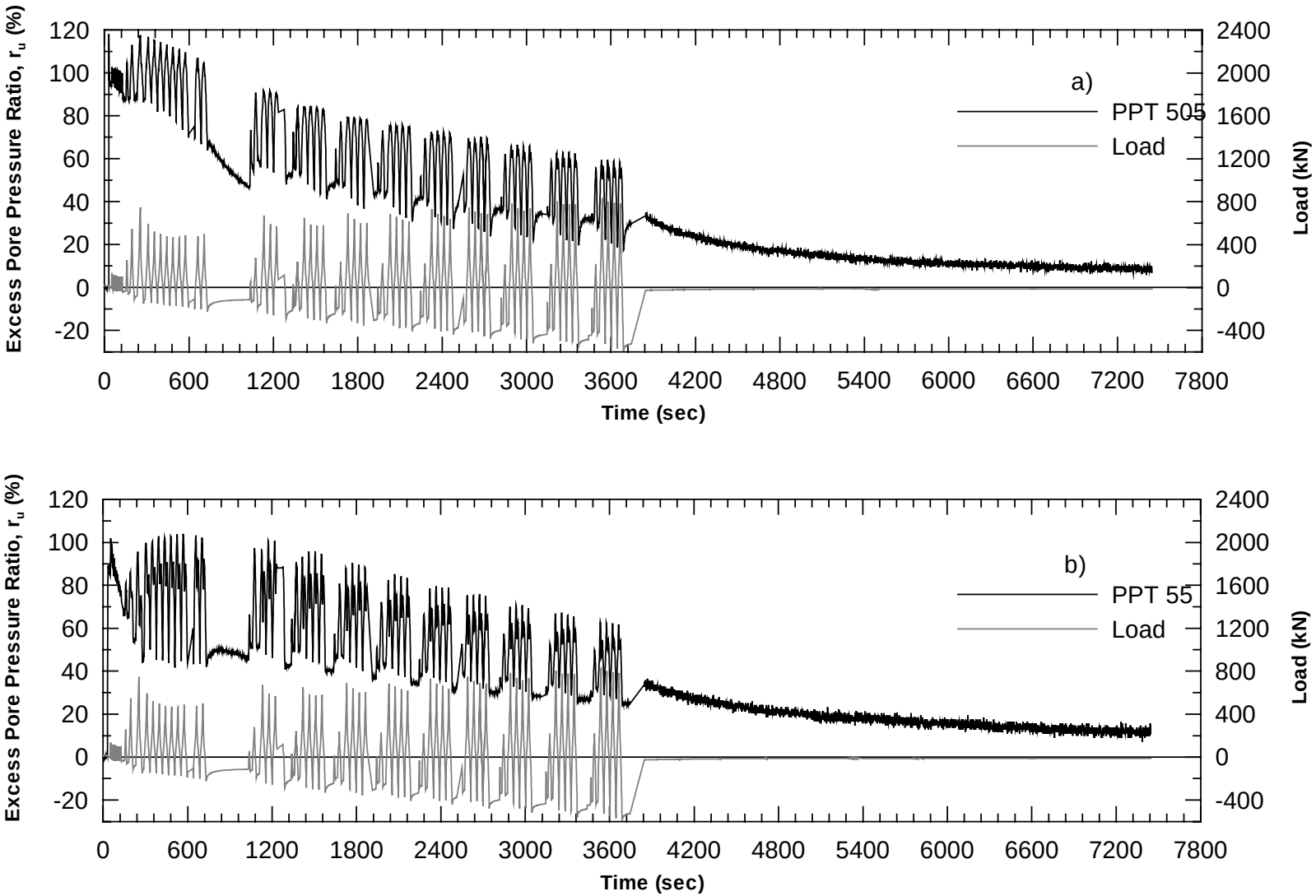

Figure 5.22 Excess Pore Pressure Ratio for 9-Pile Group/0.9m CISS Pile 1 st Blast a)PPT505 b)PPT55

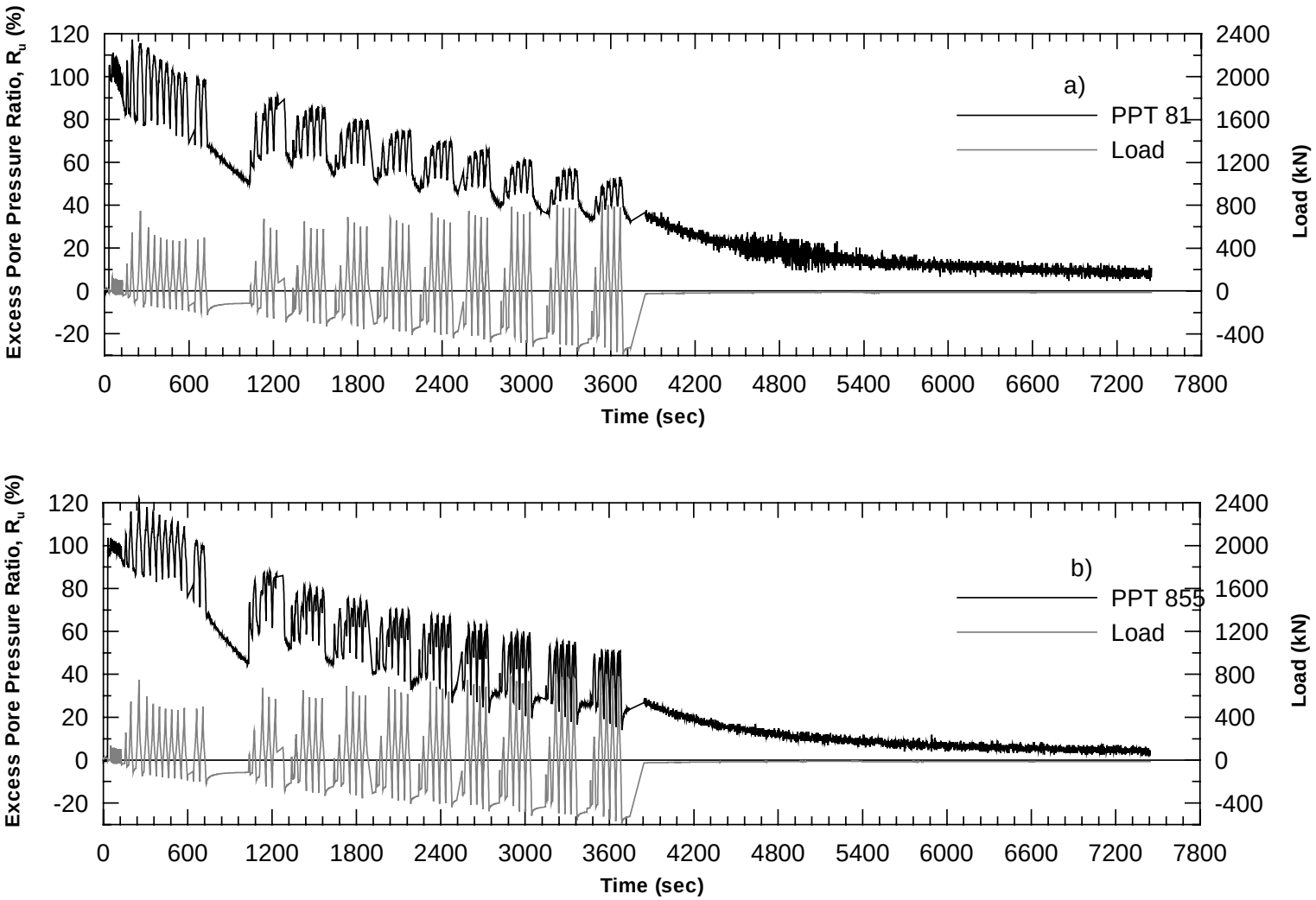

Figure 5.23 Excess Pore Pressure Ratio for 9-Pile Group/0.9m CISS Pile 1 st Blast a)PPT81 b)PPT855

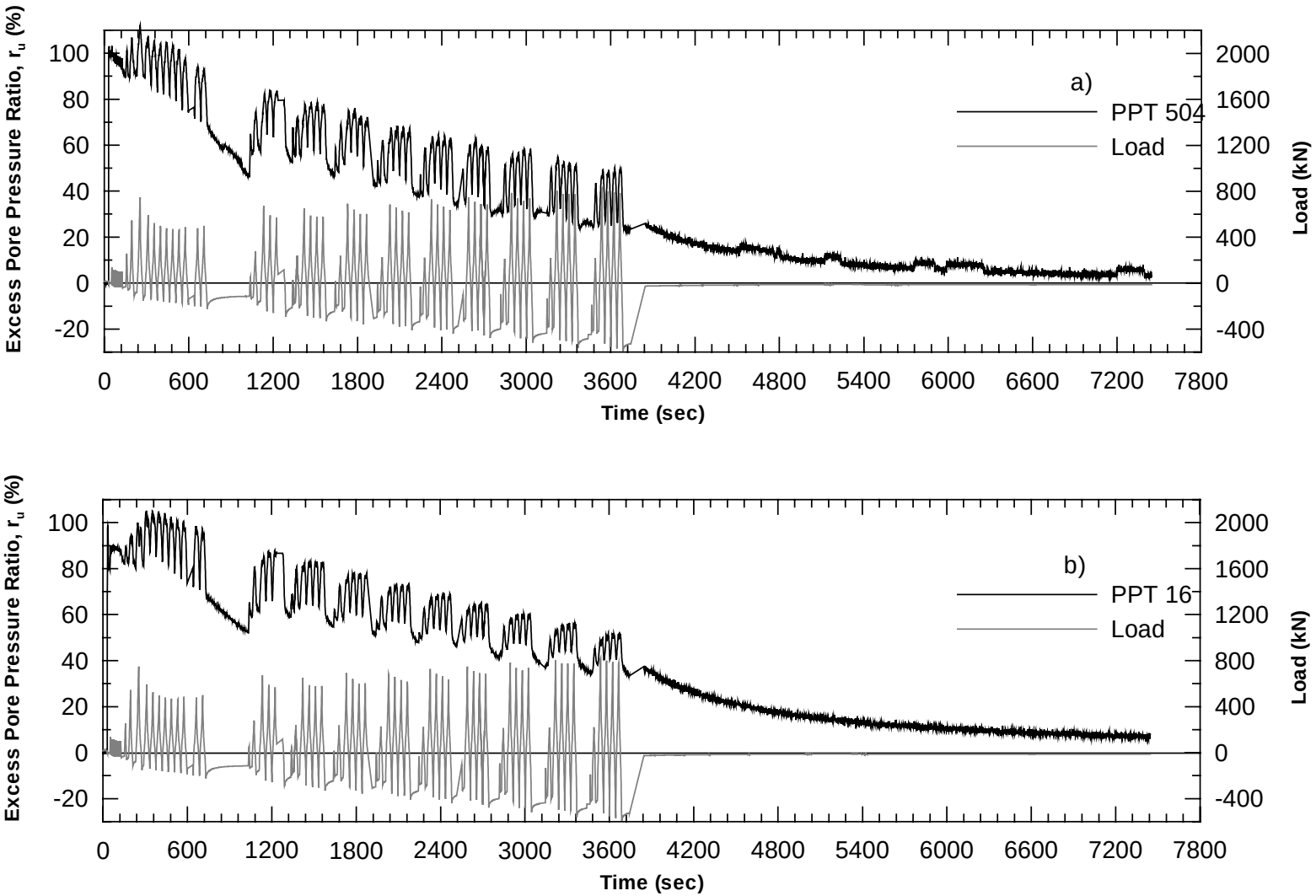

Figure 5.24 Excess Pore Pressure Ratio for 9-Pile Group/0.9m CISS Pile 1 st Blast a)PPT504 b)PPT16

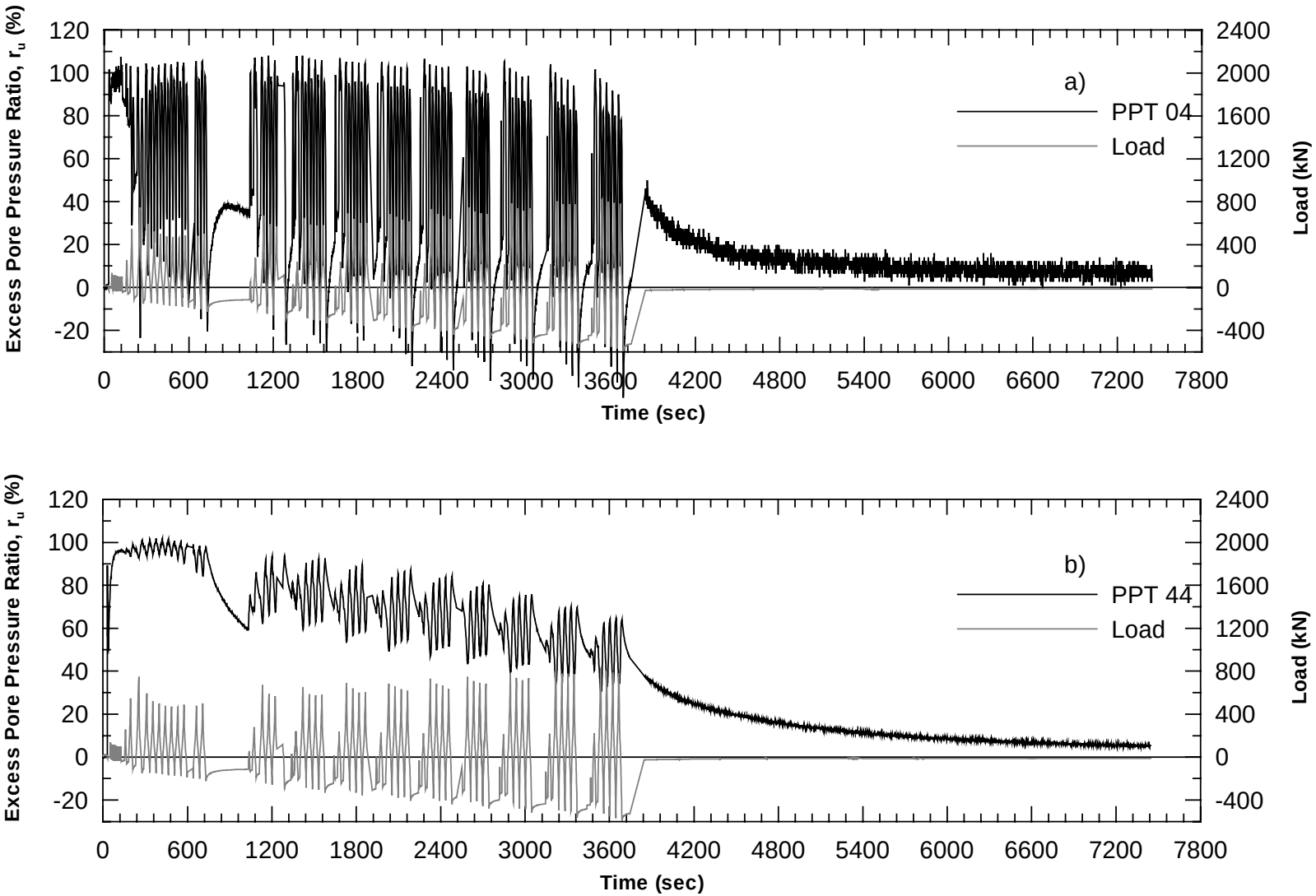

Figure 5.25 Excess Pore Pressure Ratio for 9-Pile Group/0.9m CISS Pile 1 st Blast a)PPT04 b)PPT44

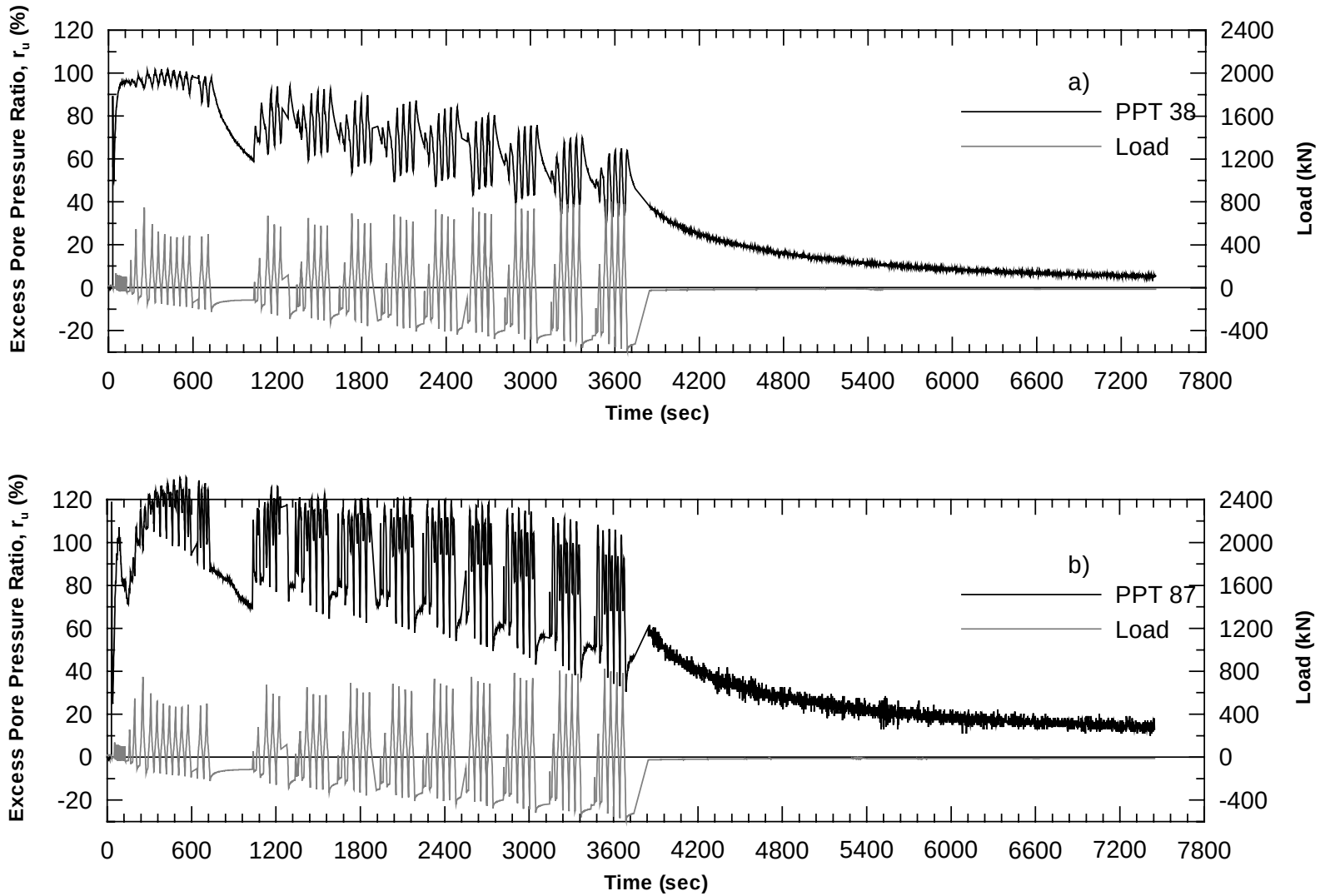

Figure 5.26 Excess Pore Pressure Ratio for 9-Pile Group/0.9m CISS Pile 1 st Blast a)PPT38 b)PPT87

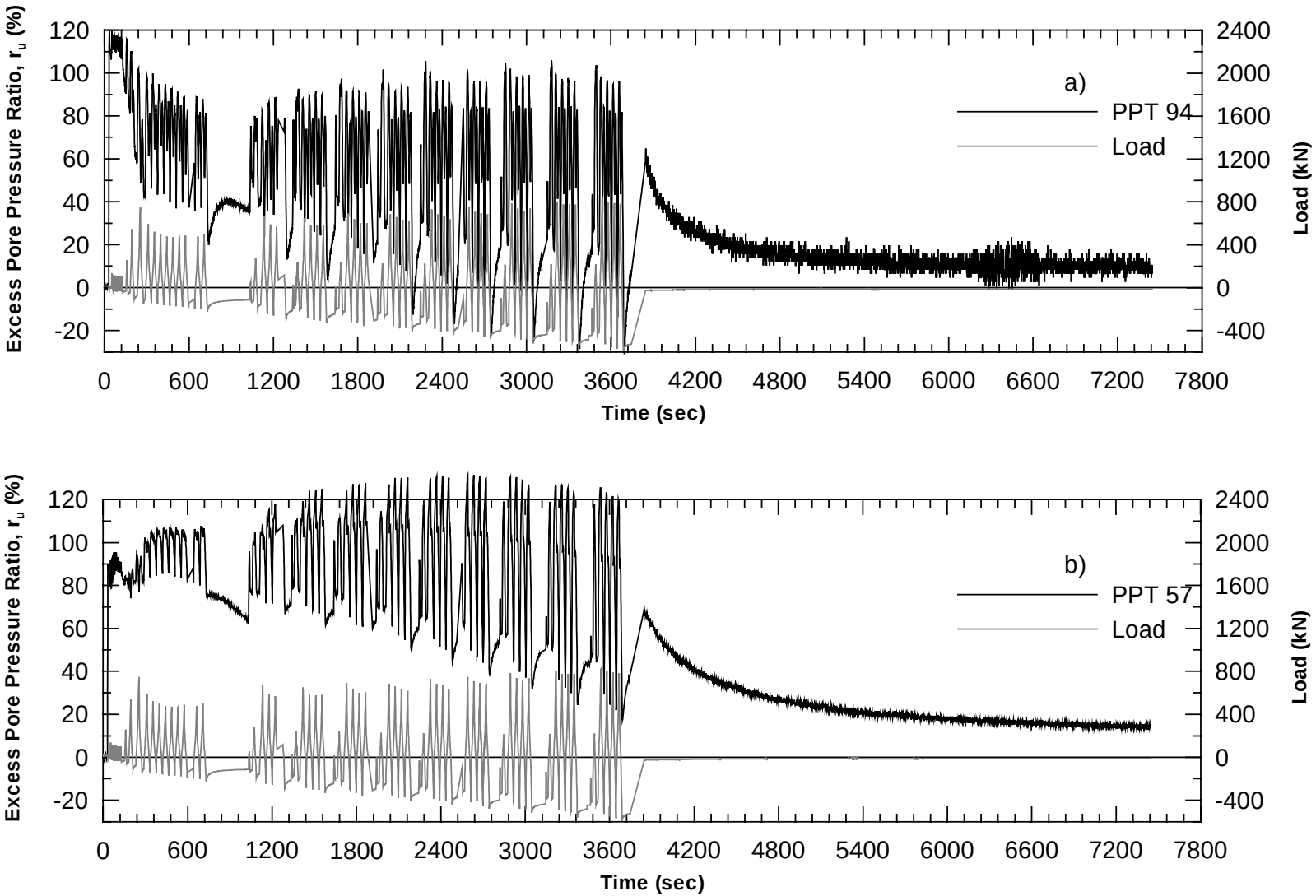

Figure 5.27 Excess Pore Pressure Ratio for 9-Pile Group/0.9m CISS Pile 1 st Blast a)PPT94 b)PPT57

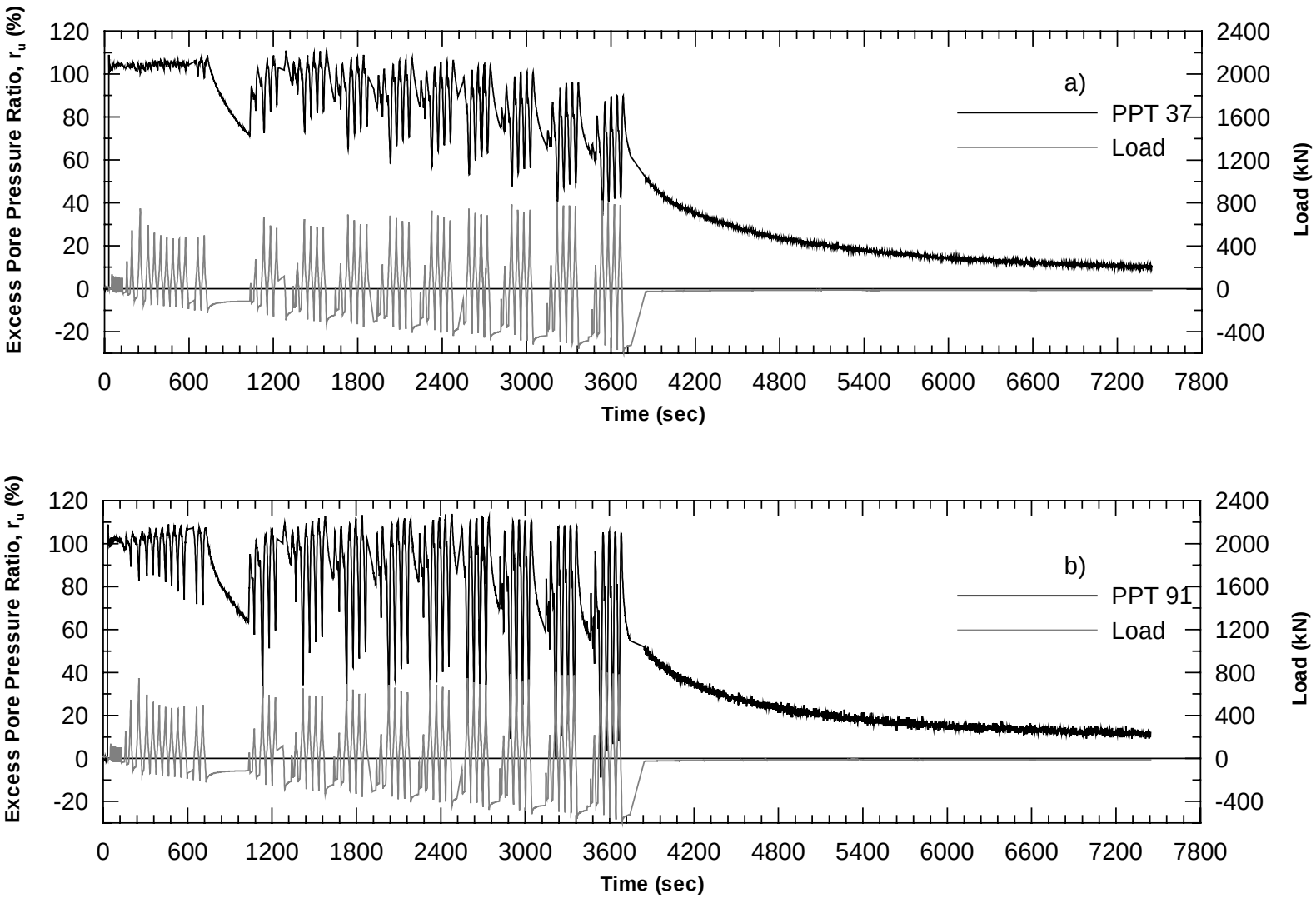

Figure 5.28 Excess Pore Pressure Ratio for 9-Pile Group/0.9m CISS Pile 1 st Blast a)PPT37 b)PPT91

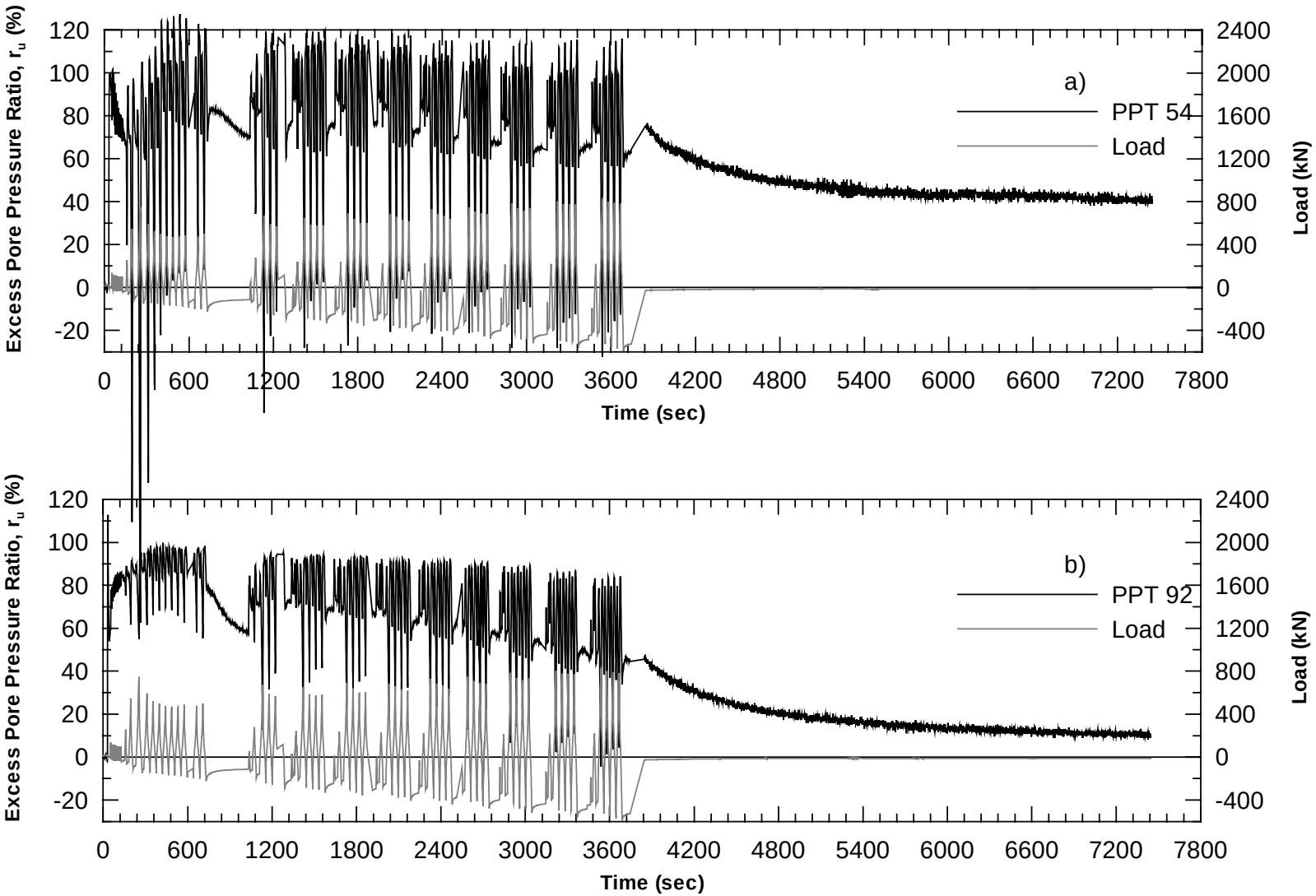

Figure 5.29 Excess Pore Pressure Ratio for 9-Pile Group/0.9m CISS Pile 1 st Blast a)PPT54 b)PPT92

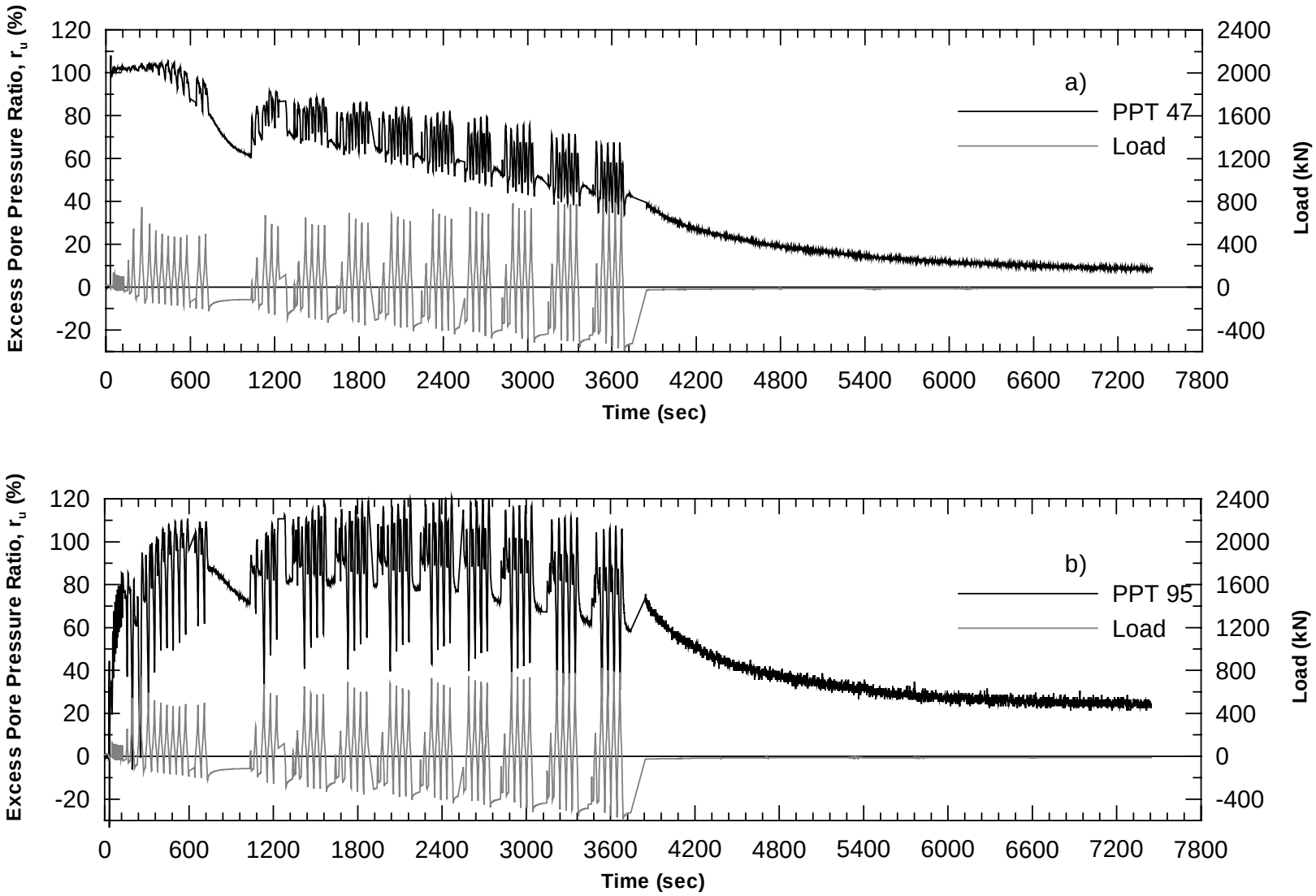

Figure 5.30 Excess Pore Pressure Ratio for 9-Pile Group/0.9m CISS Pile 1 st Blast a)PPT47 b)PPT95

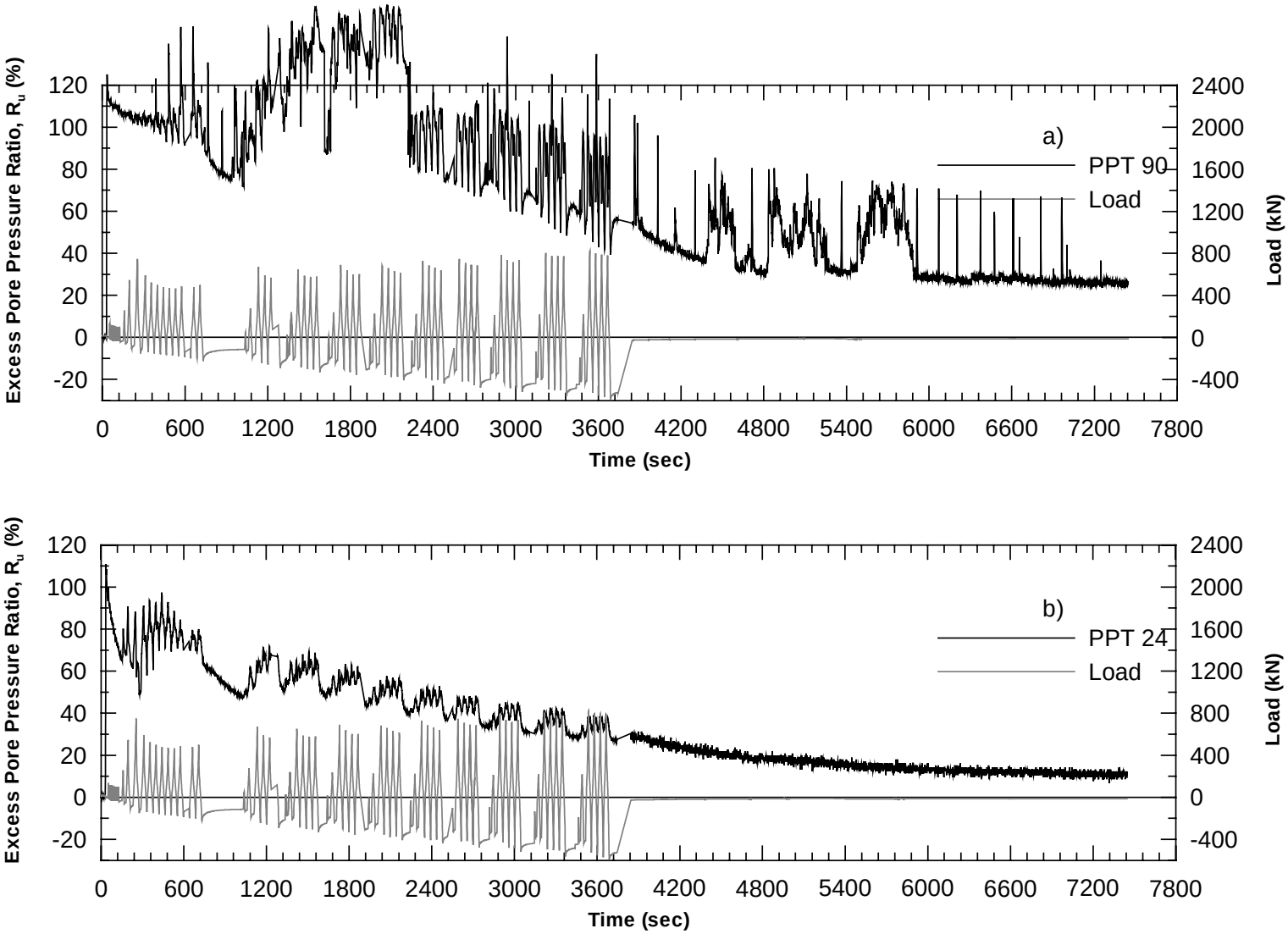

Figure 5.31 Excess Pore Pressure Ratio for 9-Pile Group/0.9m CISS Pile 1 st Blast a)PPT90 b)PPT24

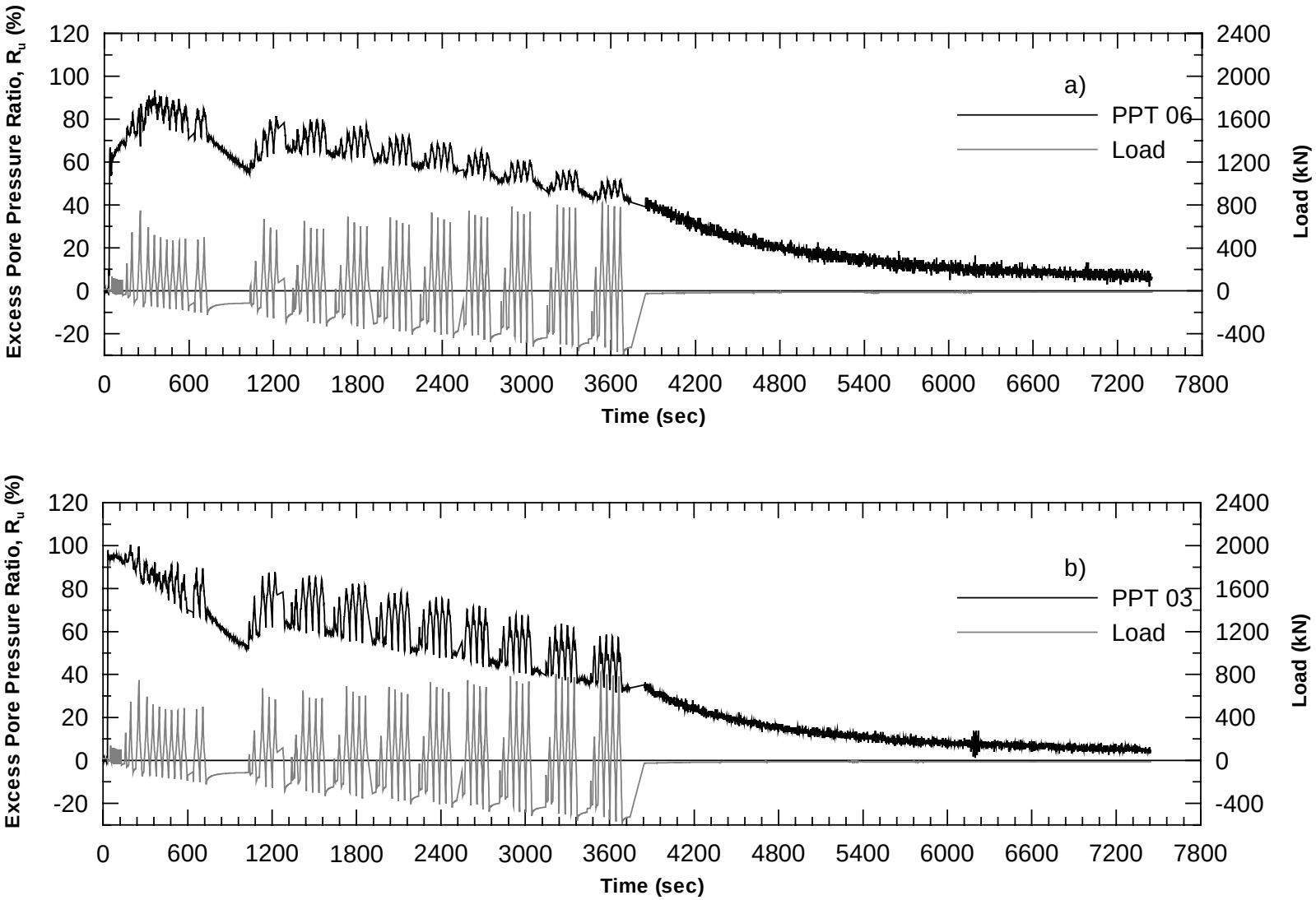

Figure 5.32 Excess Pore Pressure Ratio for 9-Pile Group/0.9m CISS Pile 1 st Blast a)PPT06 b)PPT03

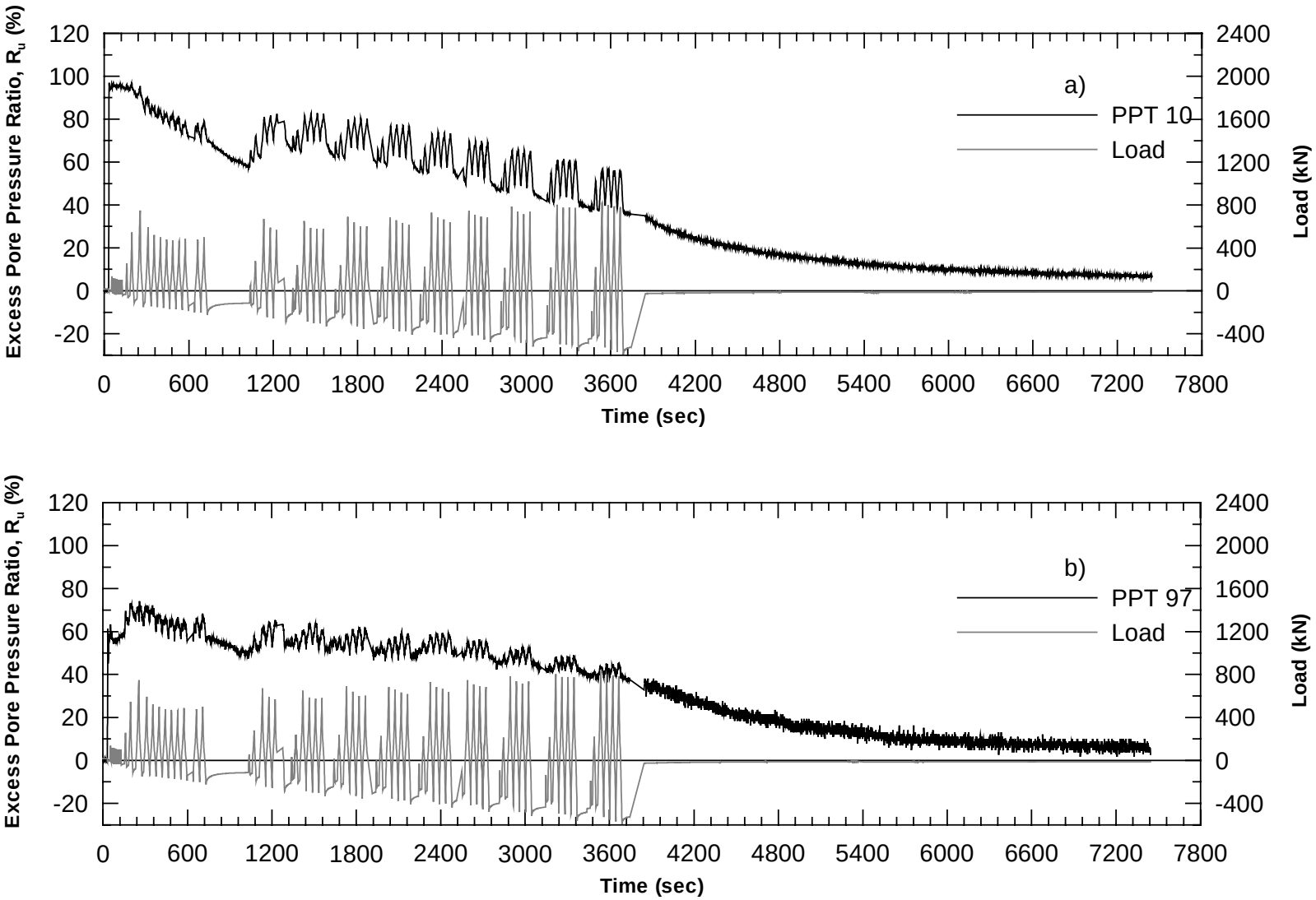

Figure 5.33 Excess Pore Pressure Ratio for 9-Pile Group/0.9m CISS Pile 1 st Blast a)PPT10 b)PPT97

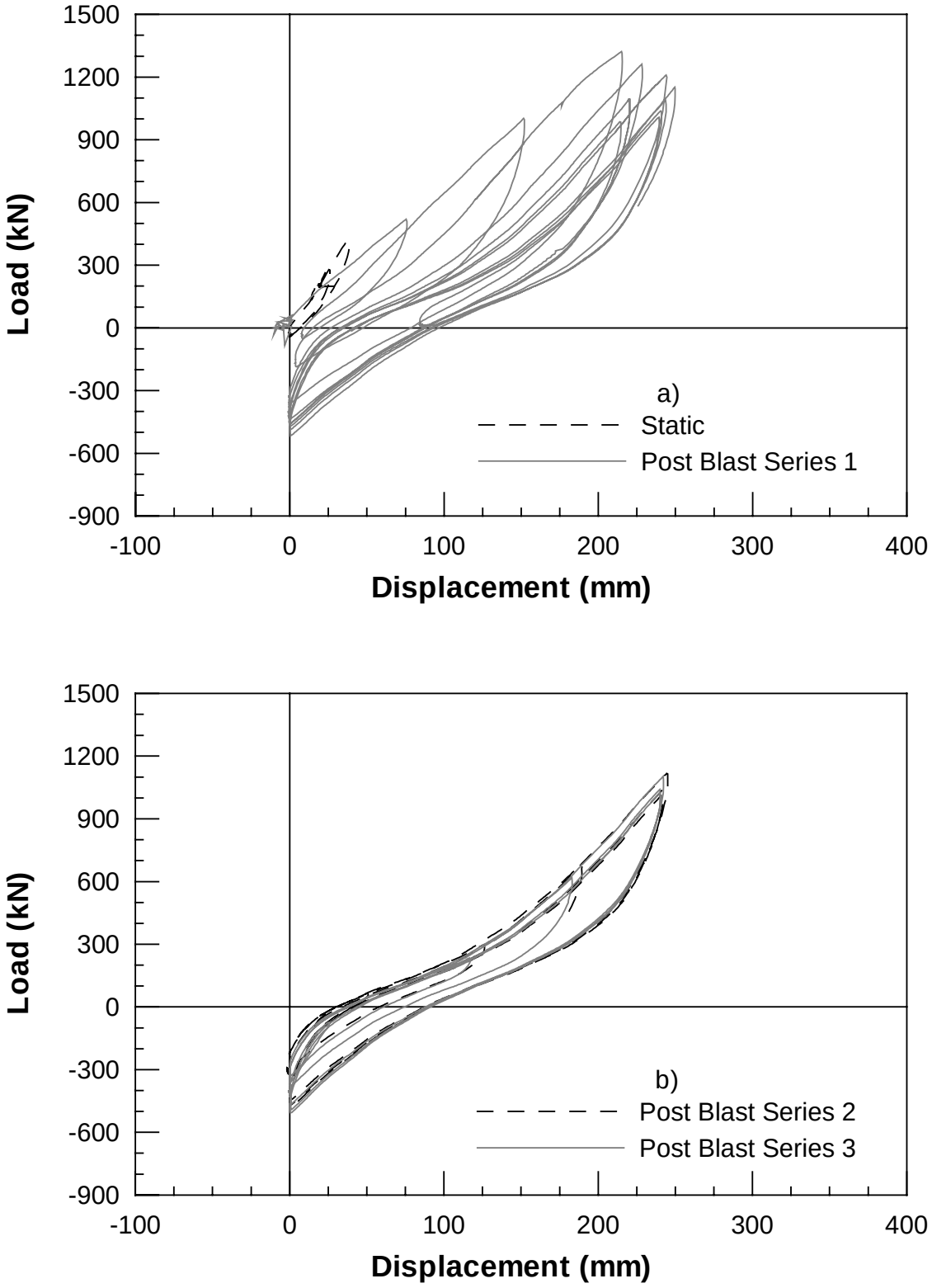

Figure 5.34 Load vs. Displacement 9-Pile Group 2nd Blast a)Static and Post Blast Series 1 b) Post Blast Series 2 and 3

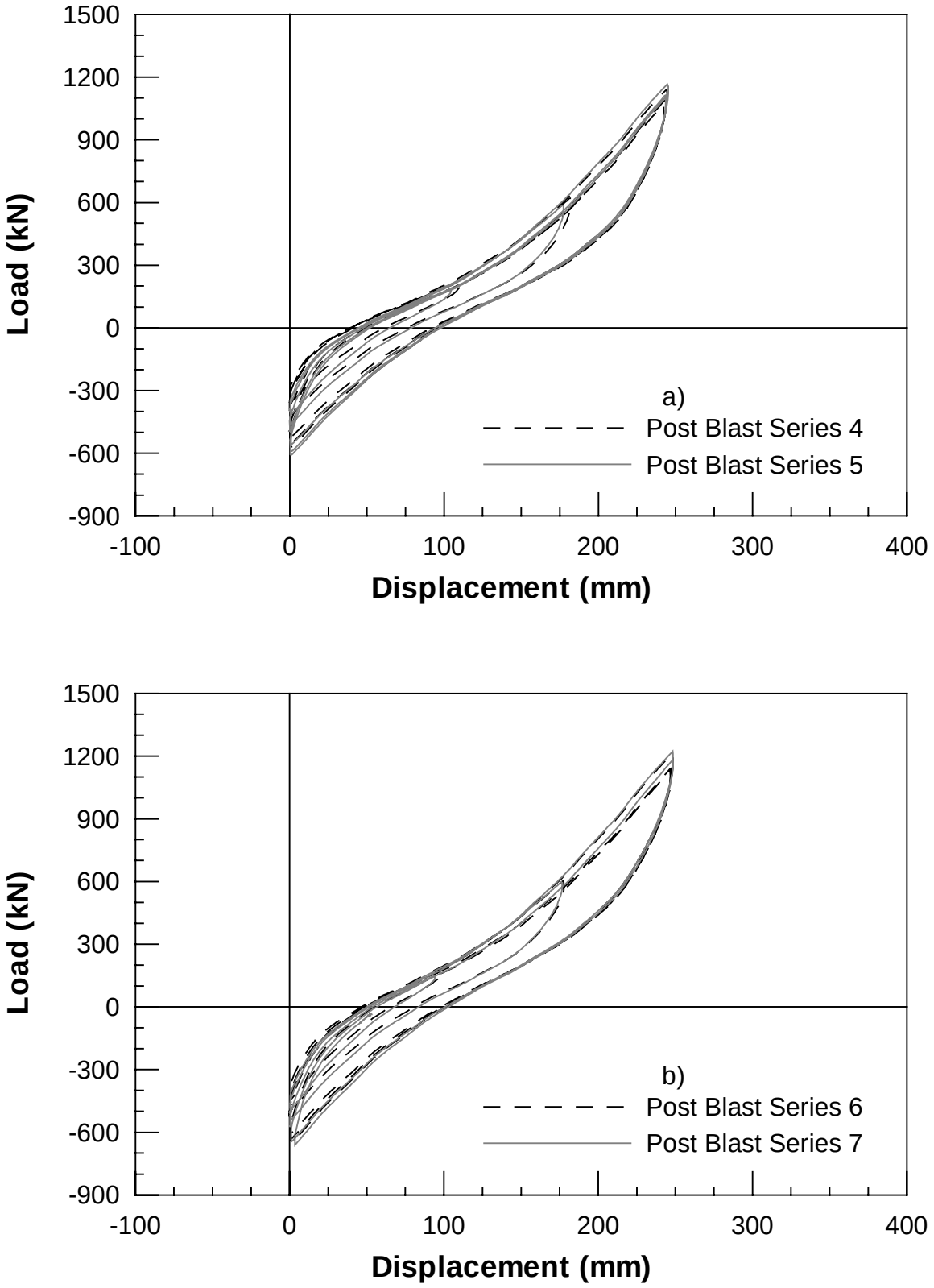

Figure 5.35 Load vs. Displacement 9-Pile Group 2nd Blast a) Post Blast Series 4 and 5 b) Post Blast Series 6 and 7

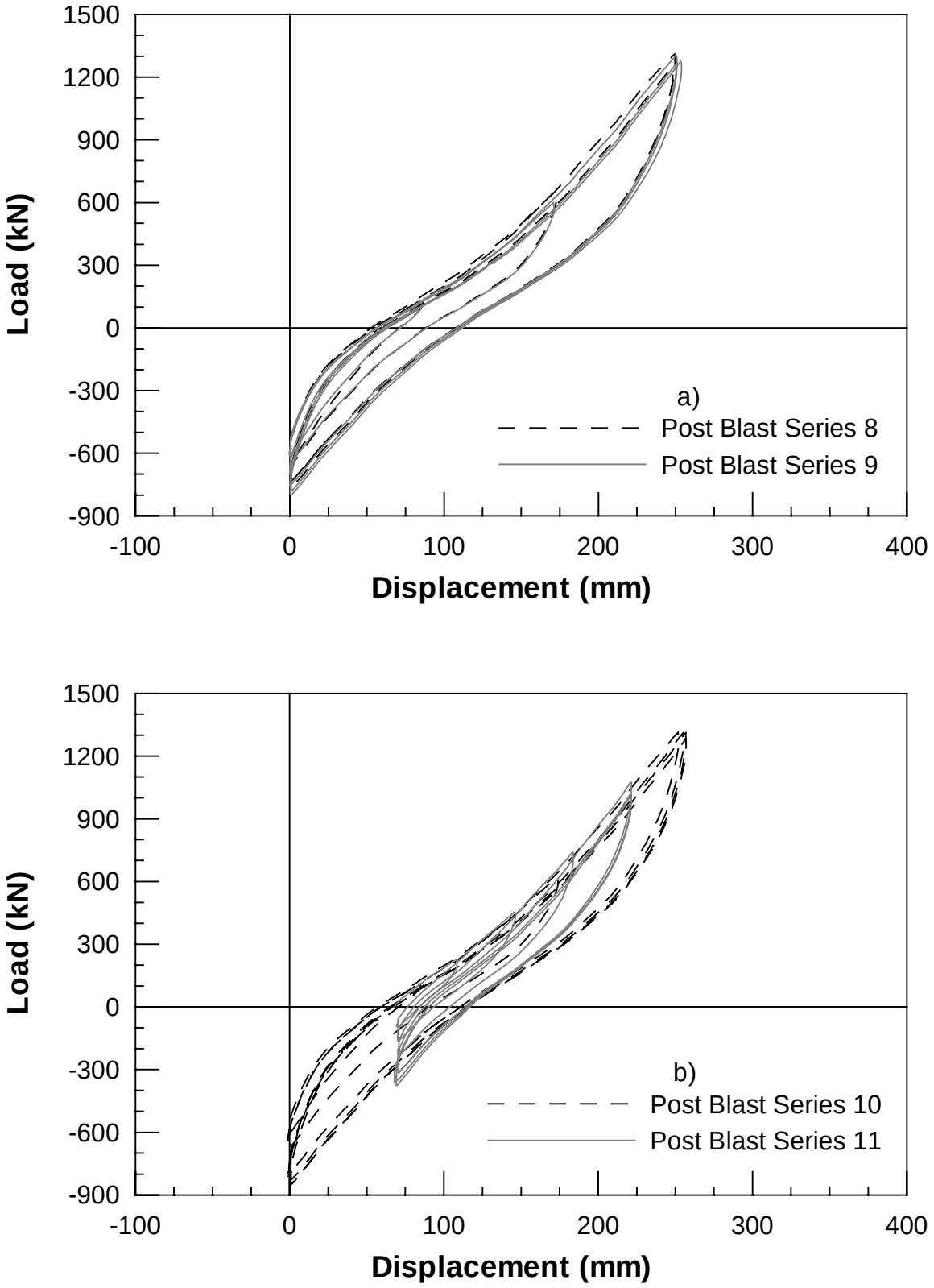

Figure 5.36 Load vs. Displacement 9-Pile Group 2nd Blast a)Post Blast Series 8 and 9 b) Post Blast Series 10 and 11

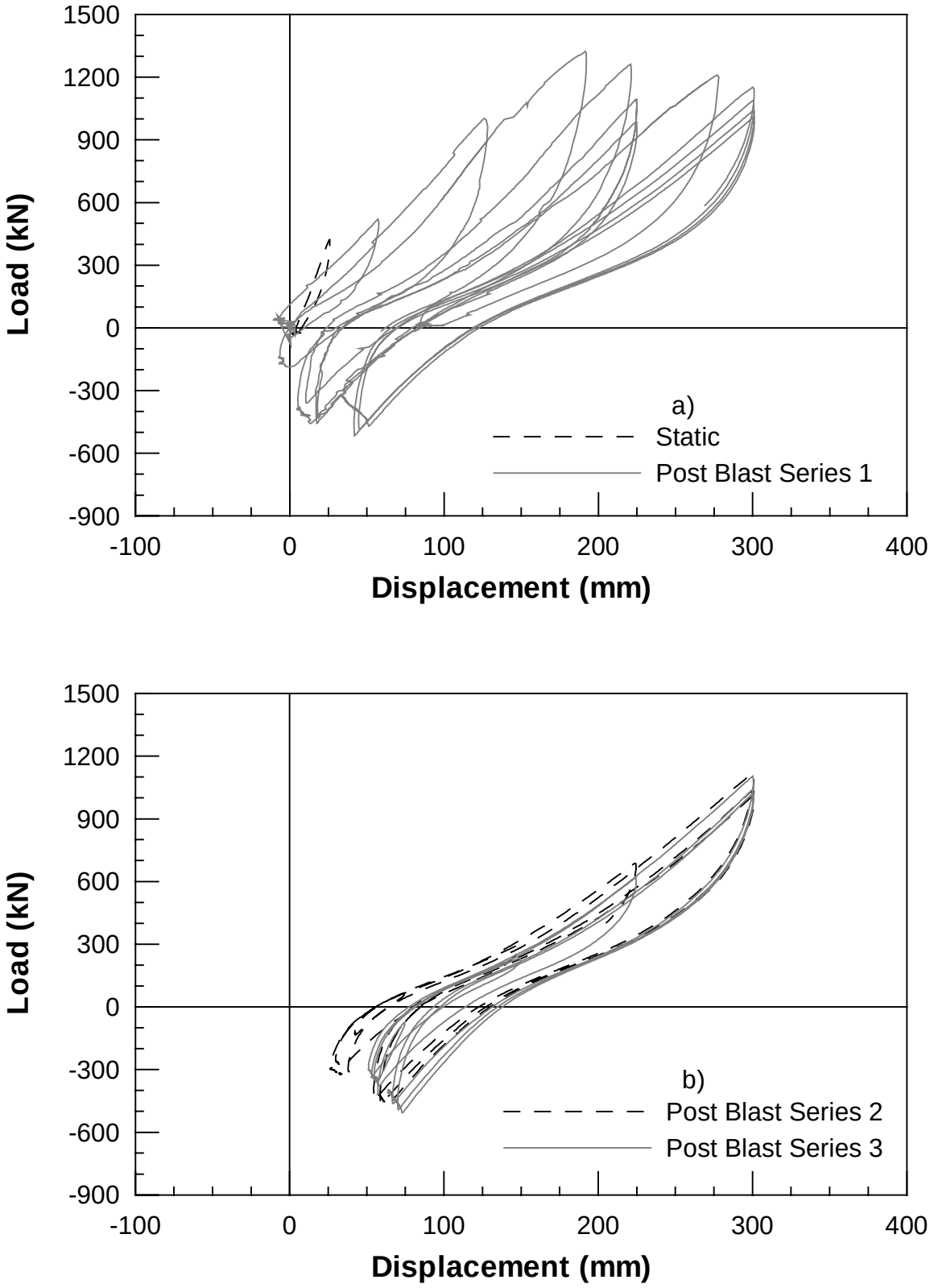

Figure 5.37 Load vs. Displacement for 0.9m CISS Pile 2nd Blast a)Static and Post Blast Series 1 b) Post Blast Series 2 and 3

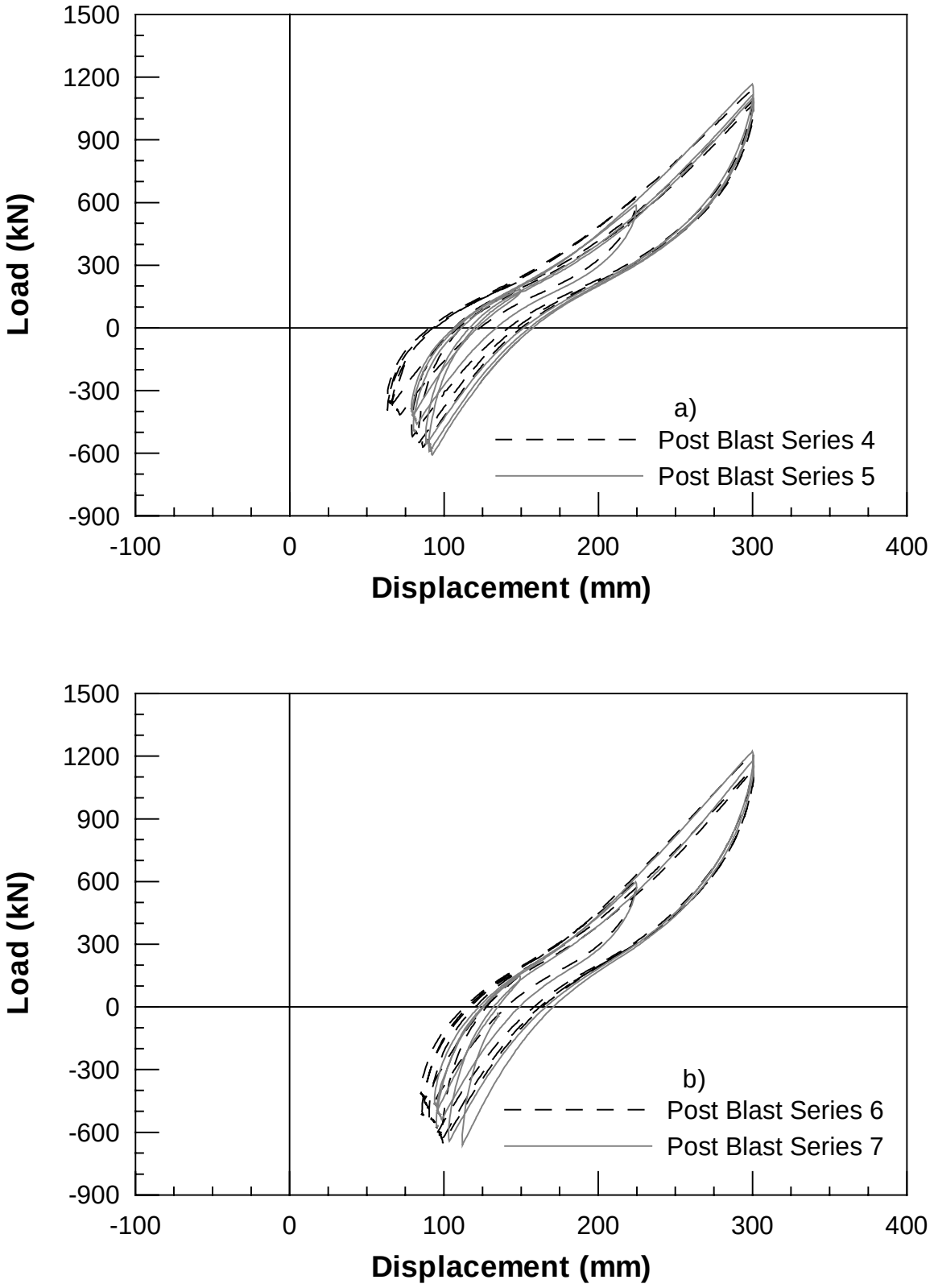

Figure 5.38 Load vs. Displacement for 0.9m CISS pile 2nd Blast a) Post Blast Series 4 and 5 b) Post Blast Series 6 and 7

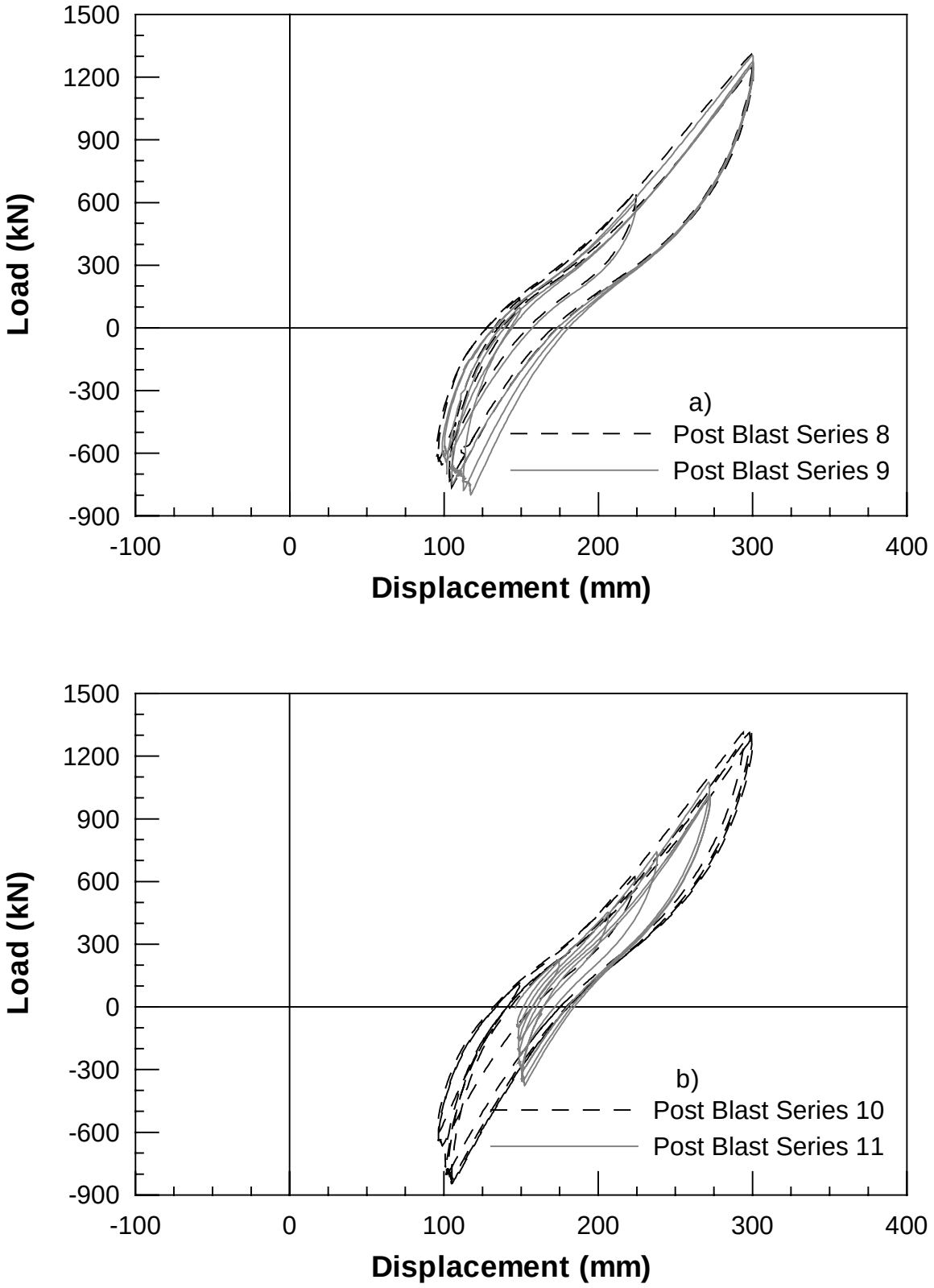

Figure 5.39 Load vs. Displacement for 0.9m CISS pile 2nd Blast a) Post Blast Series 8 and 9 b) Post Blast Series 10 and 11

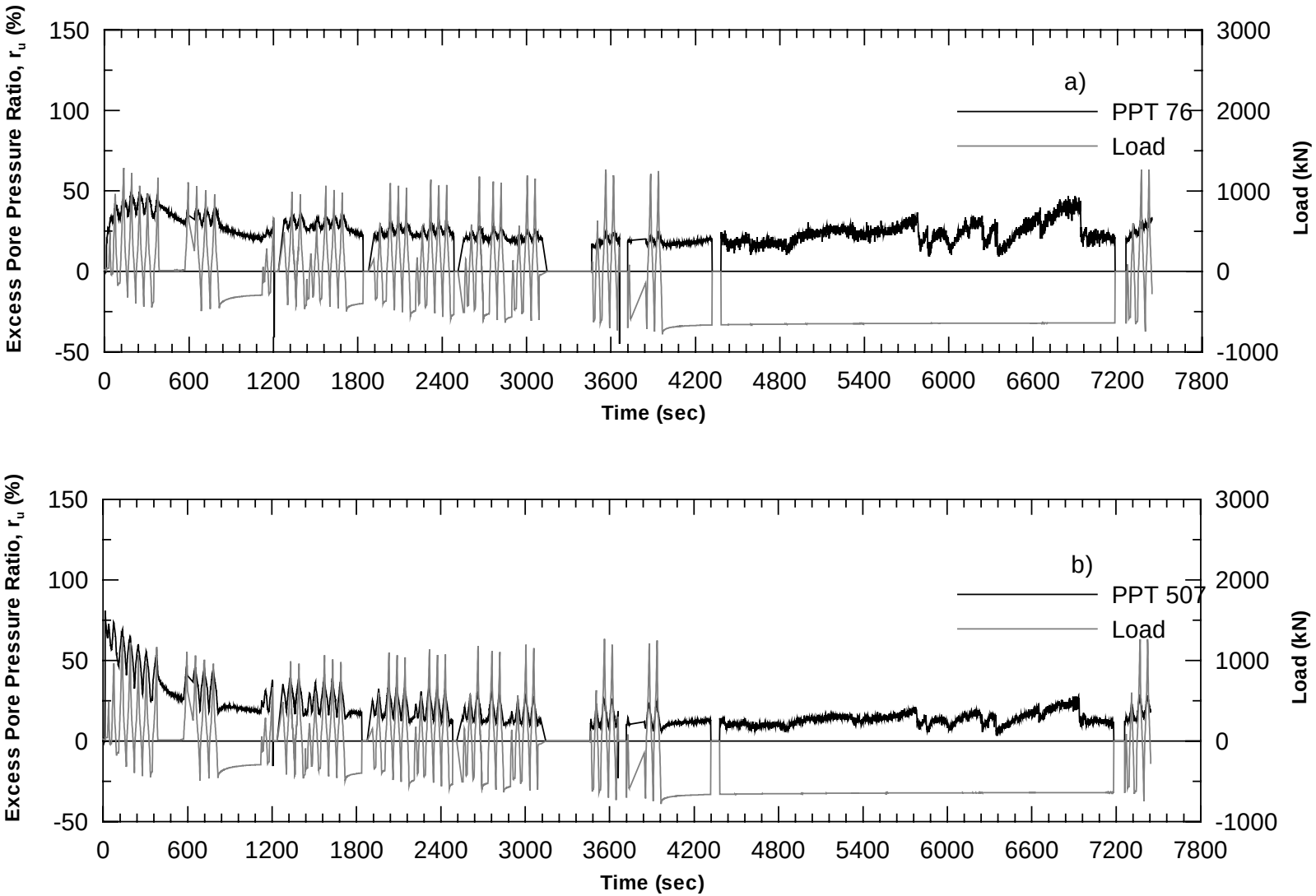

Figure 5.40 Excess Pore Pressure Ratio for 9-Pile Group/0.9m CISS Pile 2 nd Blast a)PPT76 b)PPT507

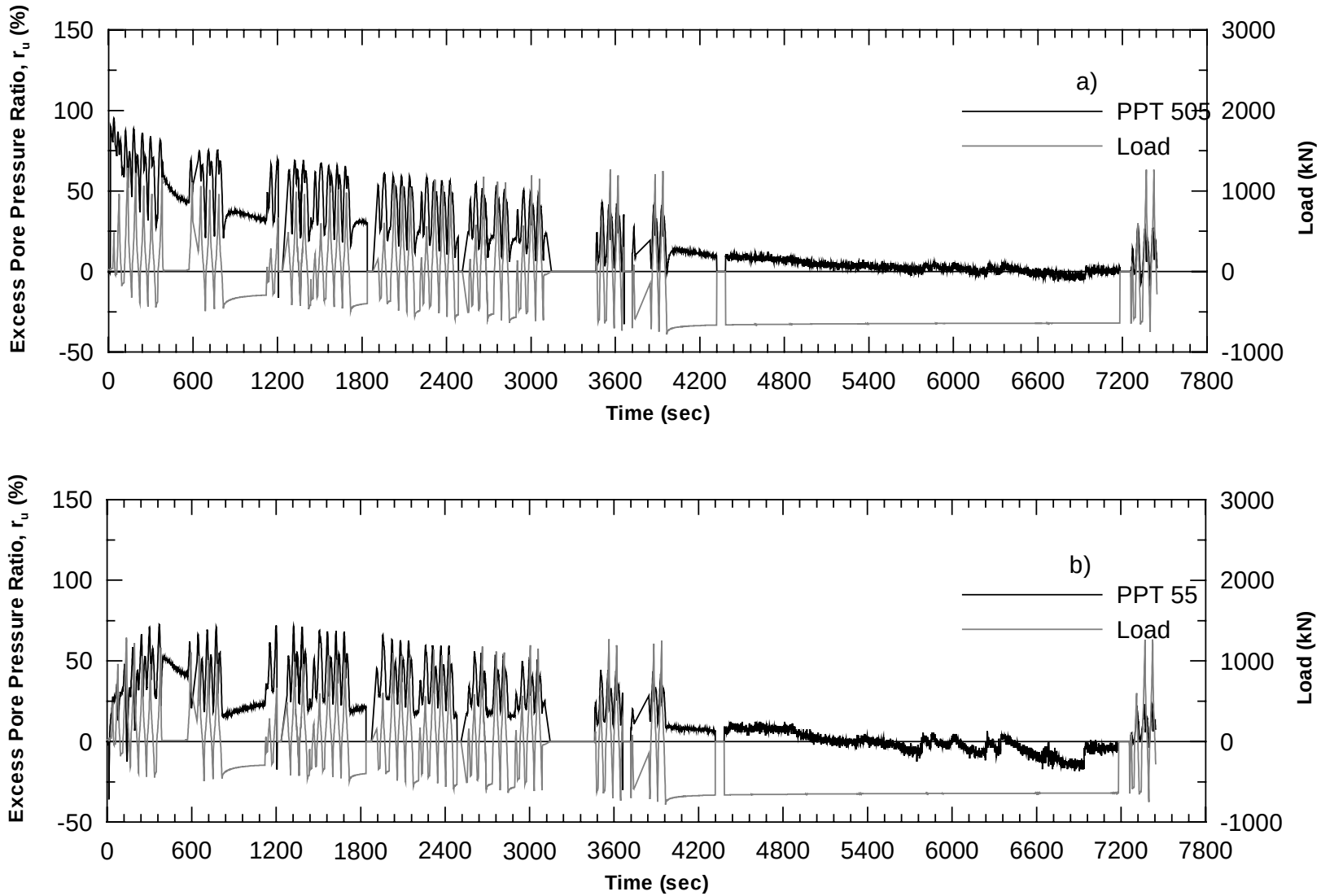

Figure 5.41 Excess Pore Pressure Ratio for 9-Pile Group/0.9m CISS Pile 2 nd Blast a)PPT505 b)PPT55

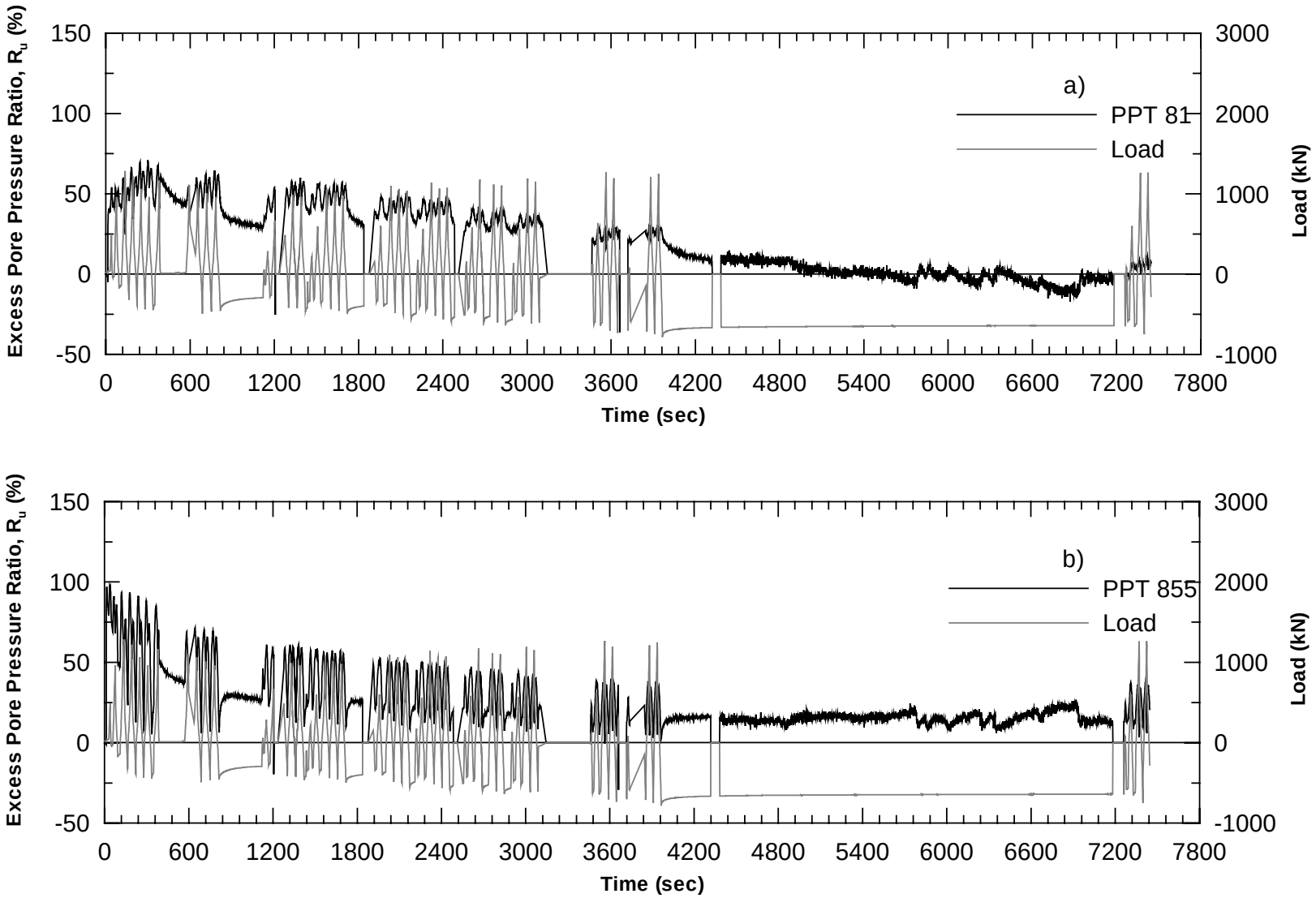

Figure 5.42 Excess Pore Pressure Ratio for 9-Pile Group/0.9m CISS Pile 2 nd Blast a)PPT81 b)PPT855

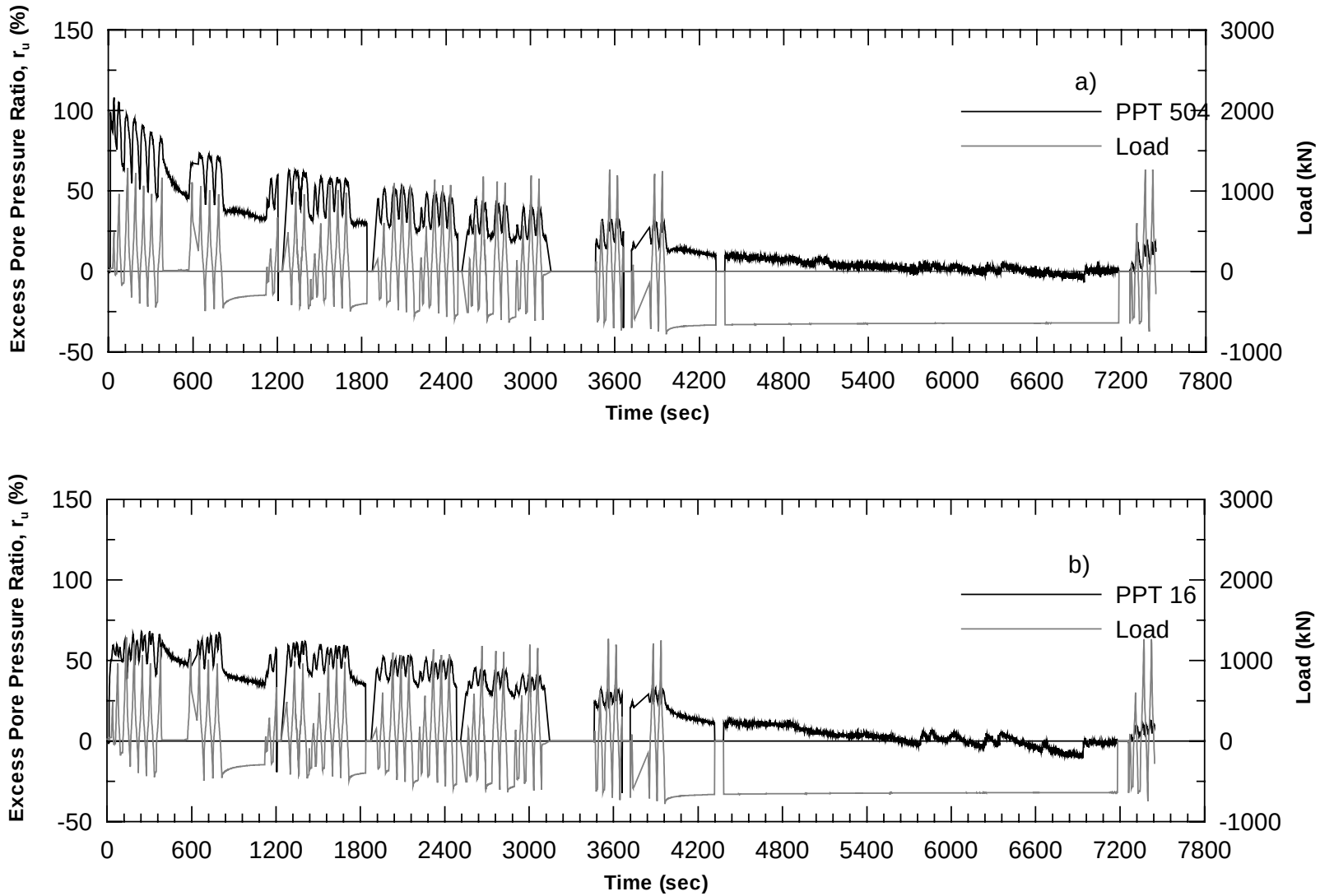

Figure 5.43 Excess Pore Pressure Ratio for 9-Pile Group/0.9m CISS Pile 2 nd Blast a)PPT504 b)PPT16

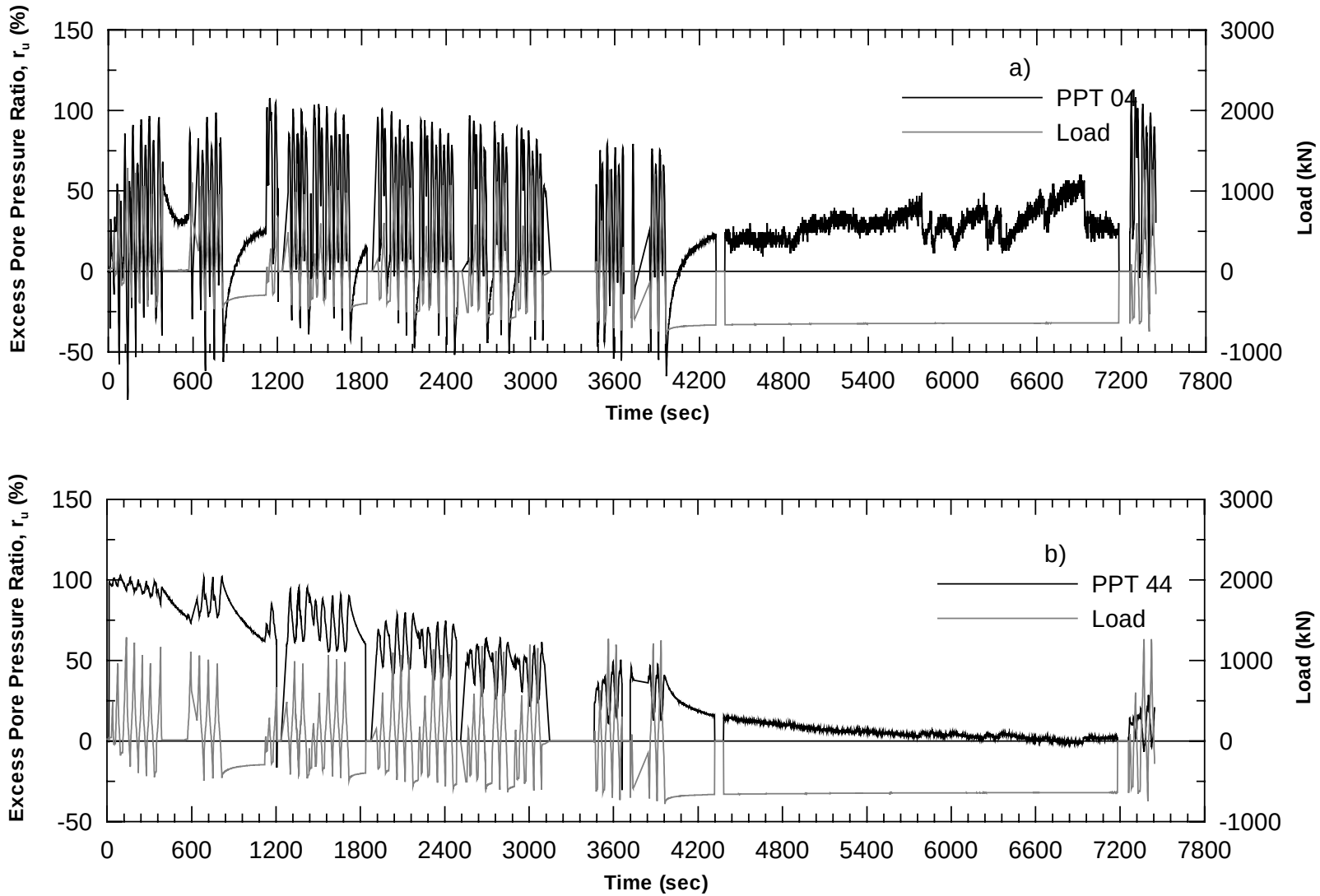

Figure 5.44 Excess Pore Pressure Ratio for 9-Pile Group/0.9m CISS Pile 2 nd Blast a)PPT04 b)PPT44

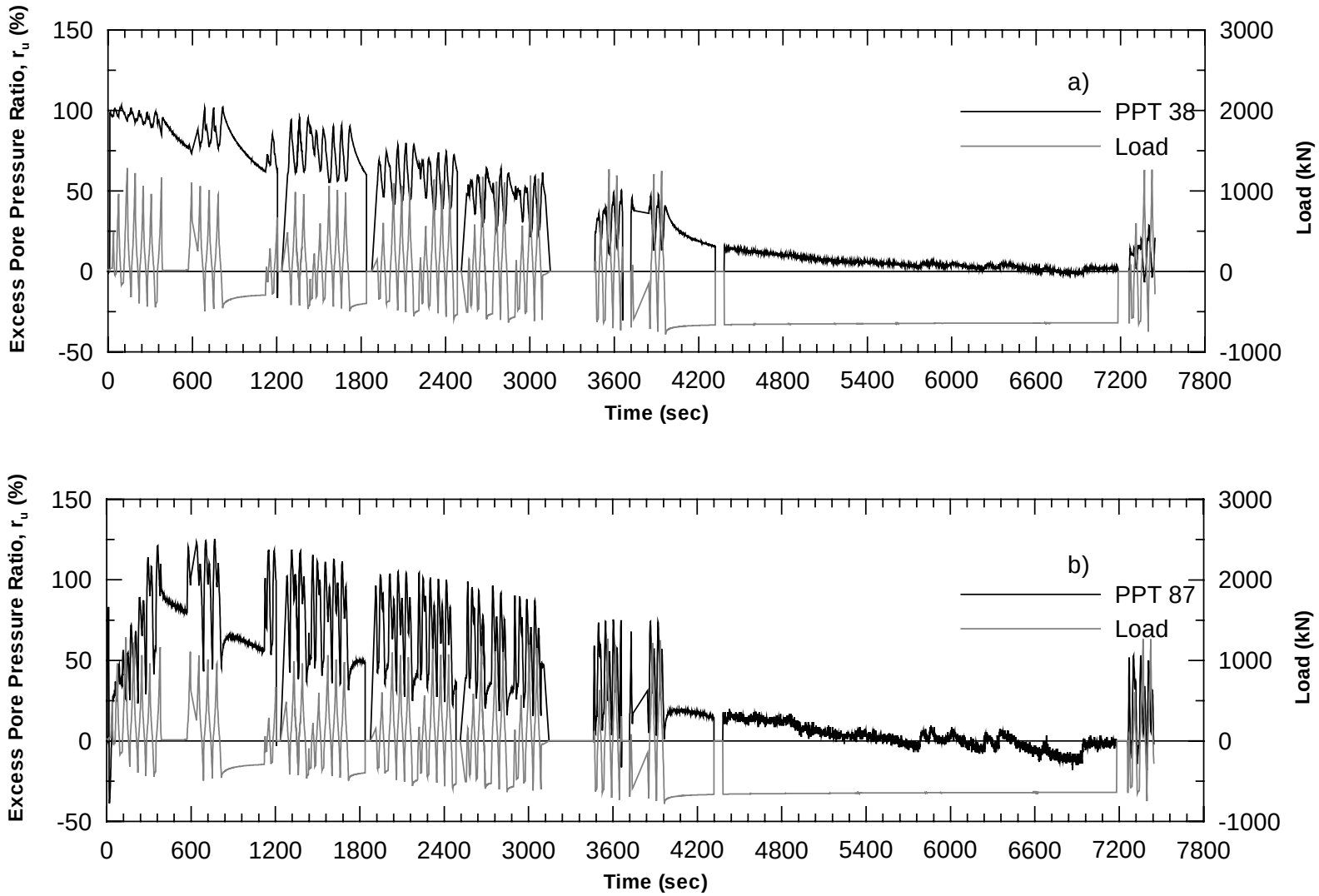

Figure 5.45 Excess Pore Pressure Ratio for 9-Pile Group/0.9m CISS Pile 2 nd Blast a)PPT38 b)PPT87

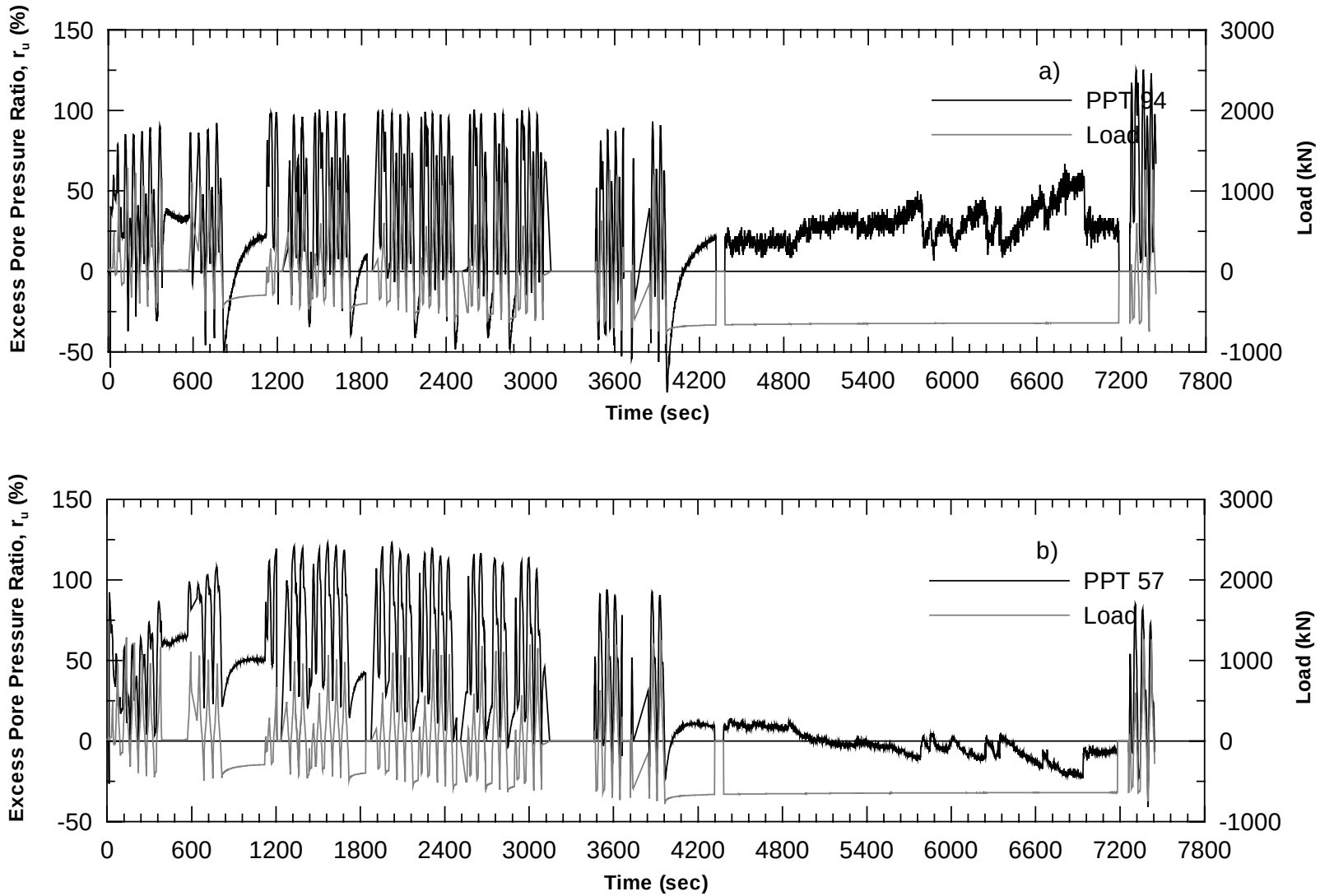

Figure 5.46 Excess Pore Pressure Ratio for 9-Pile Group/0.9m CISS Pile 2 nd Blast a)PPT94 b)PPT57

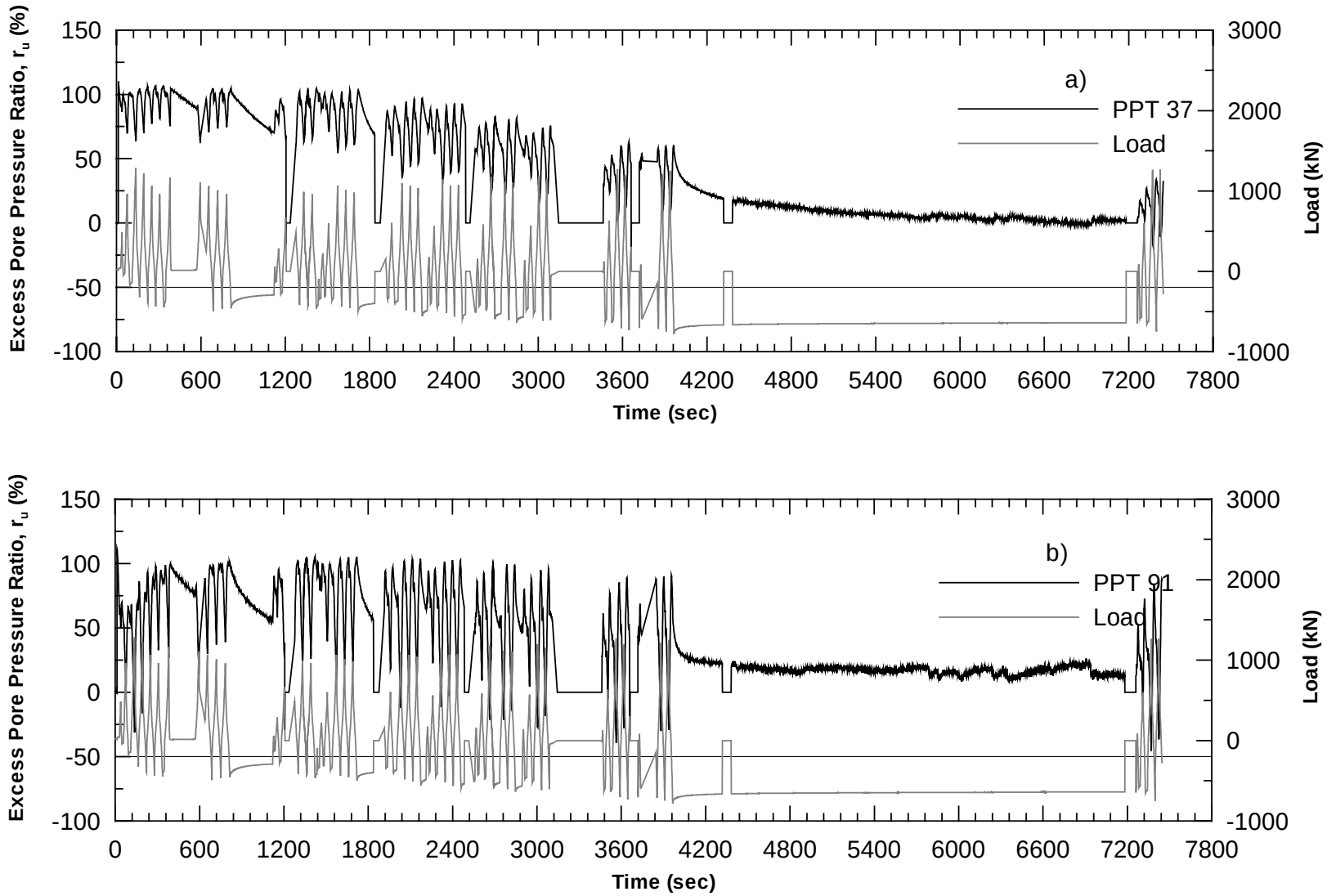

Figure 5.47 Excess Pore Pressure Ratio for 9-Pile Group/0.9m CISS Pile 2 nd Blast a)PPT37 b)PPT91

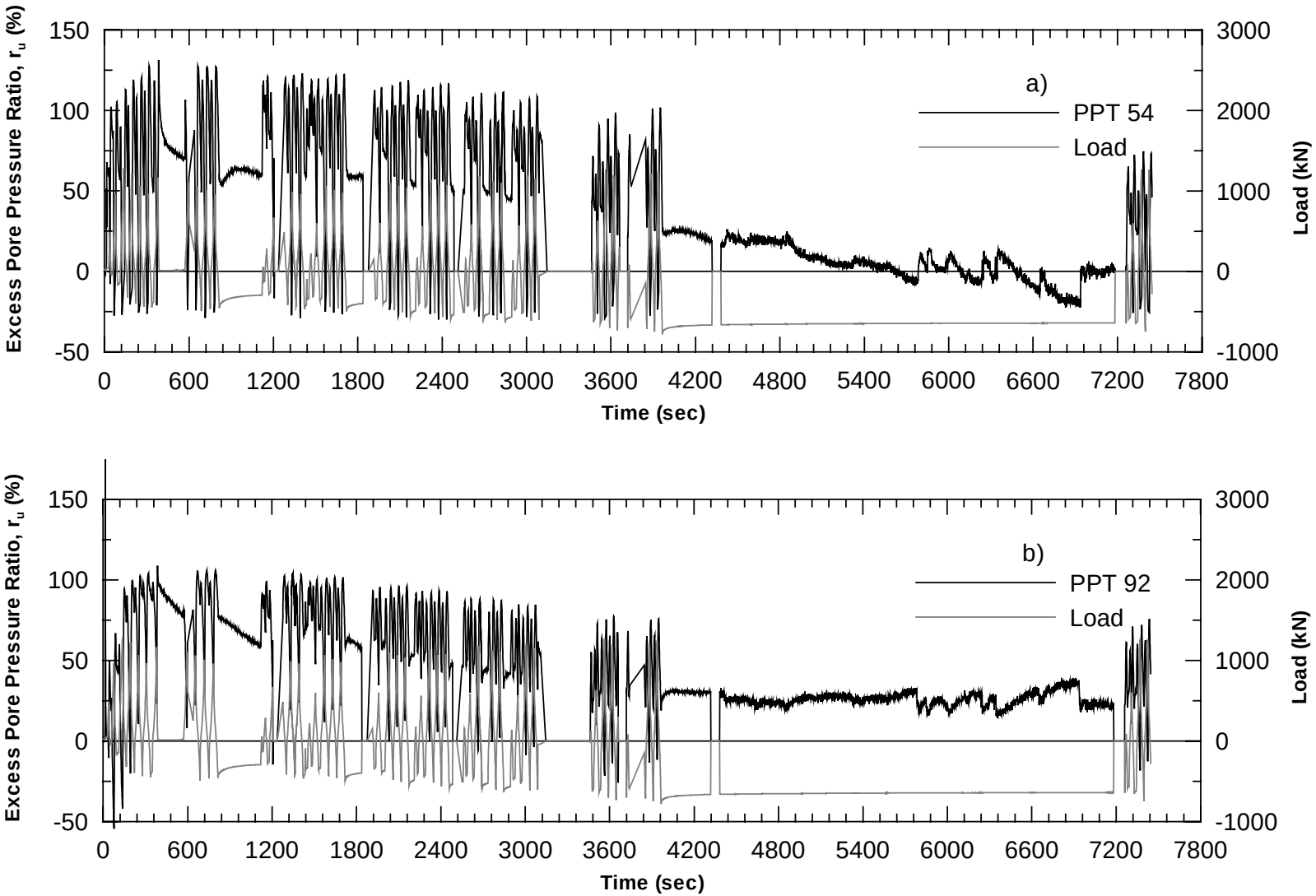

Figure 5.48 Excess Pore Pressure Ratio for 9-Pile Group/0.9m CISS Pile 2 nd Blast a)PPT54 b)PPT92

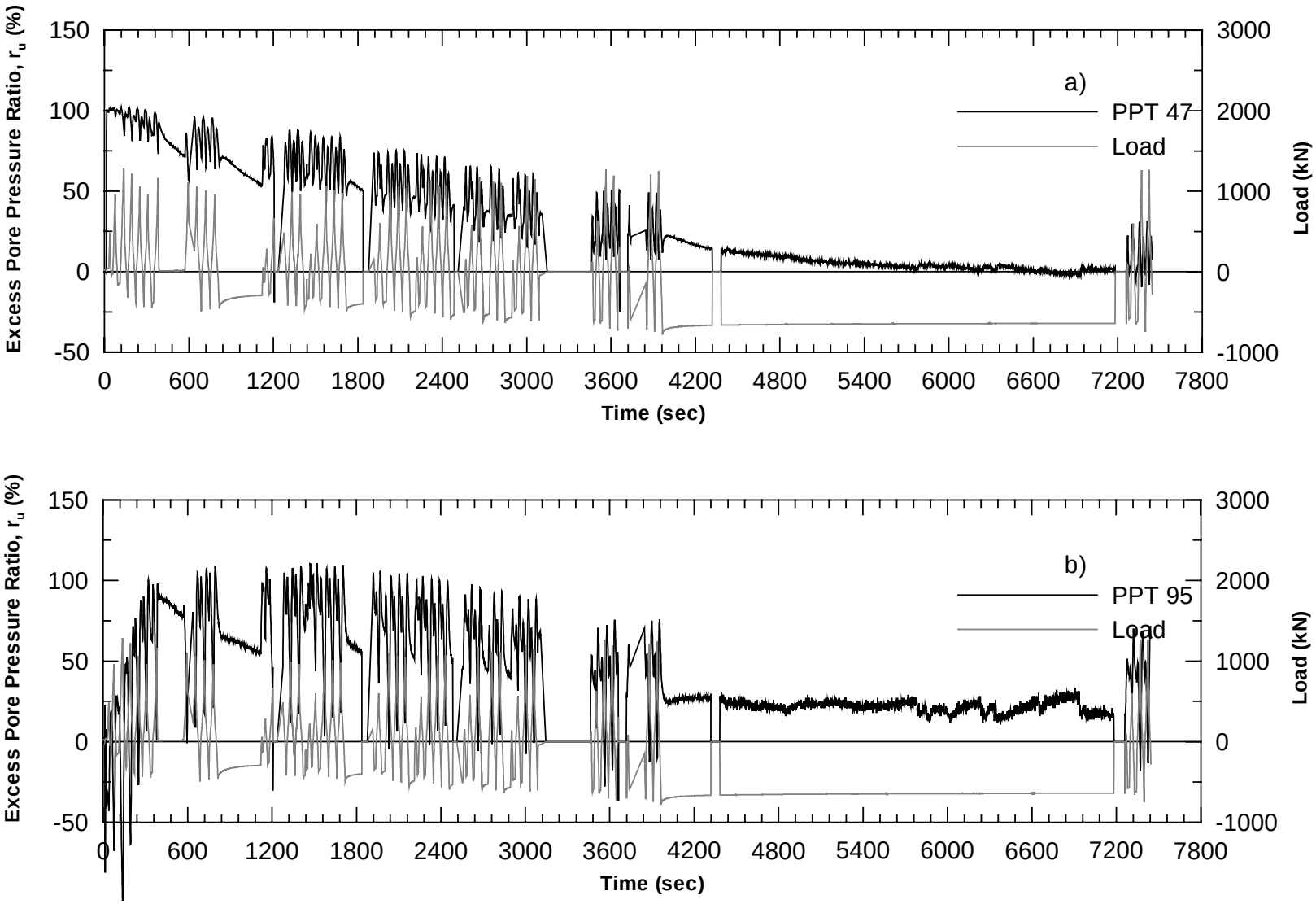

Figure 5.49 Excess Pore Pressure Ratio for 9-Pile Group/0.9m CISS Pile 2 nd Blast a)PPT47 b)PPT95

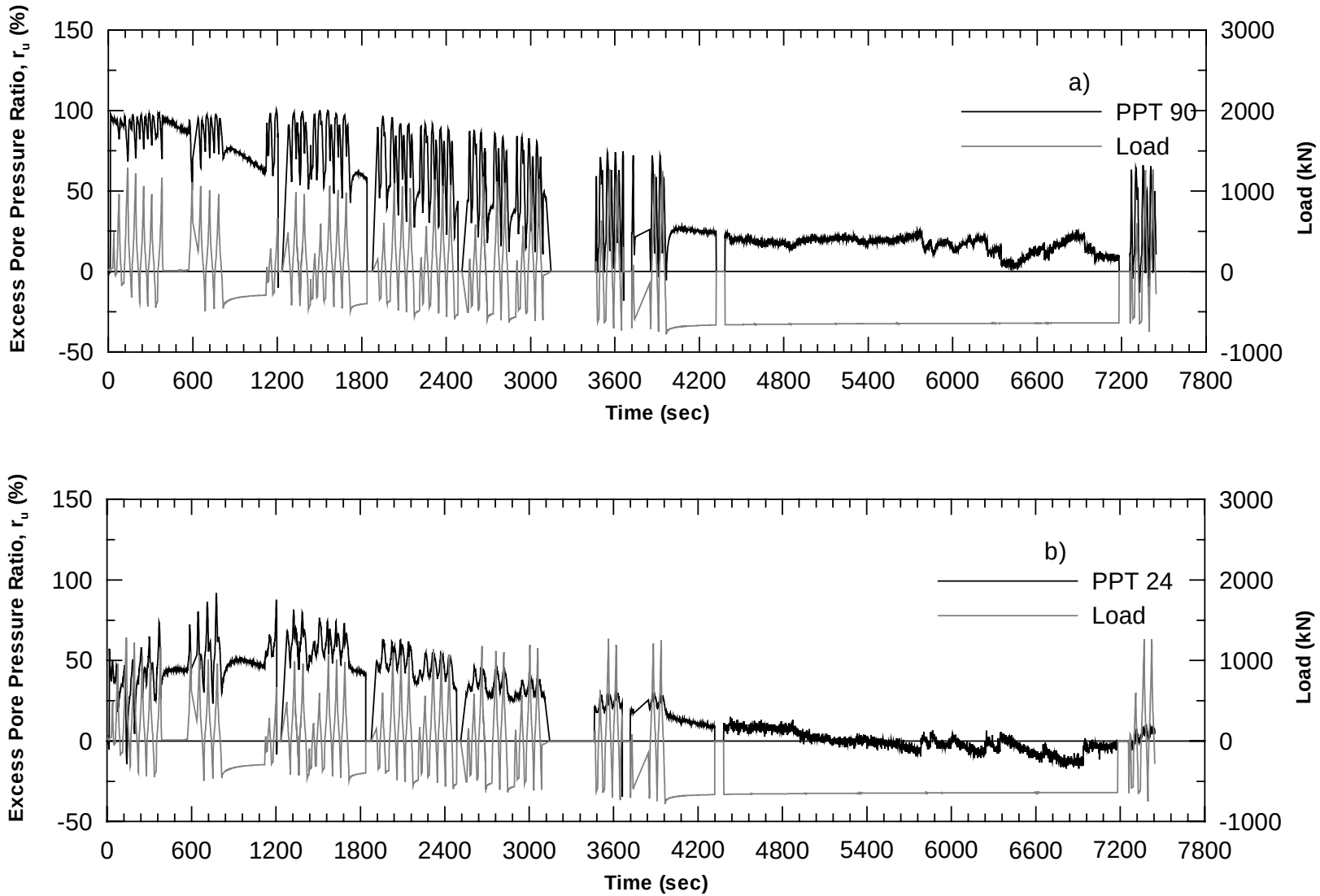

Figure 5.50 Excess Pore Pressure Ratio for 9-Pile Group/0.9m CISS Pile 2 nd Blast a)PPT90 b)PPT24

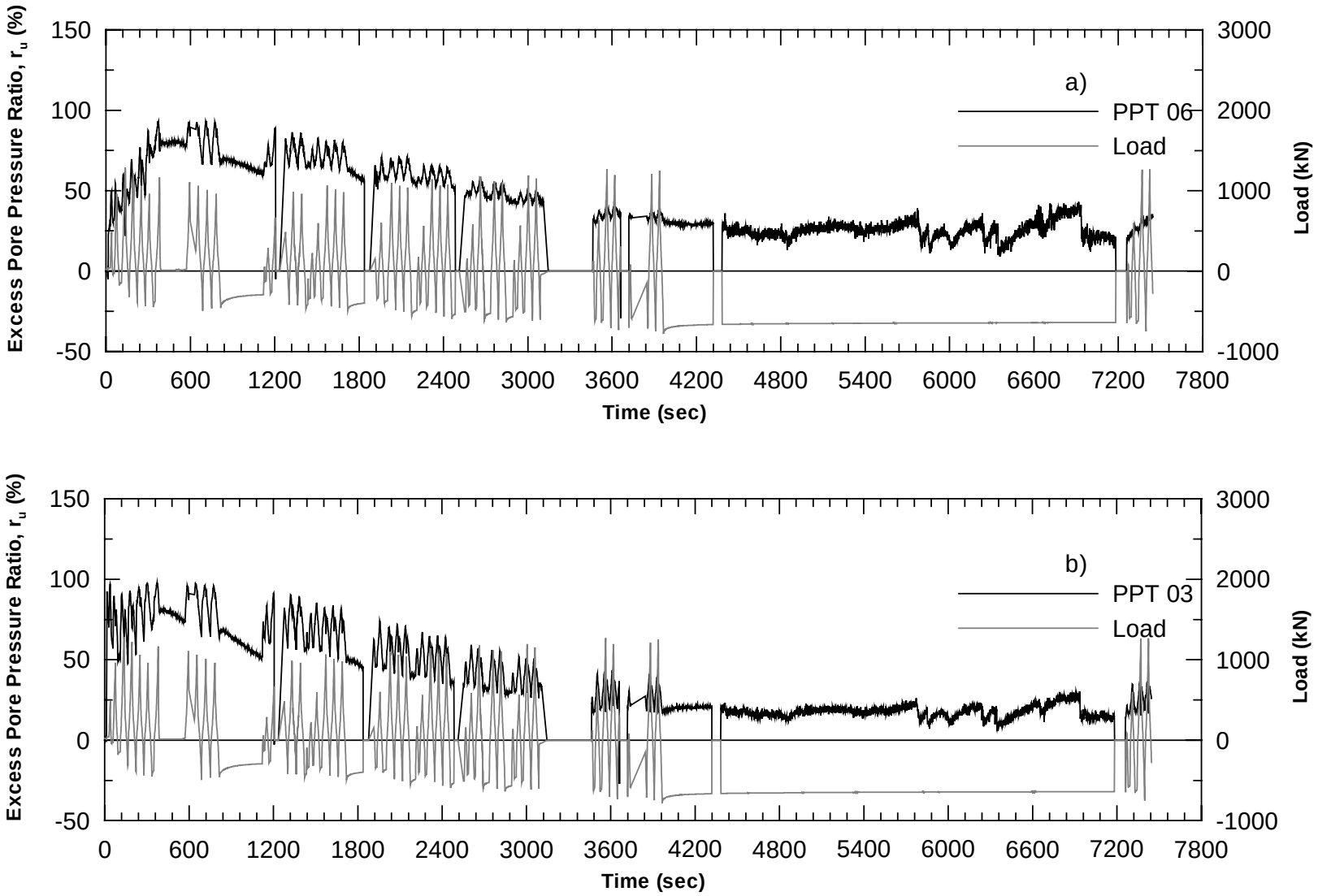

Figure 5.51 Excess Pore Pressure Ratio for 9-Pile Group/0.9m CISS Pile 2 nd Blast a)PPT06 b)PPT03

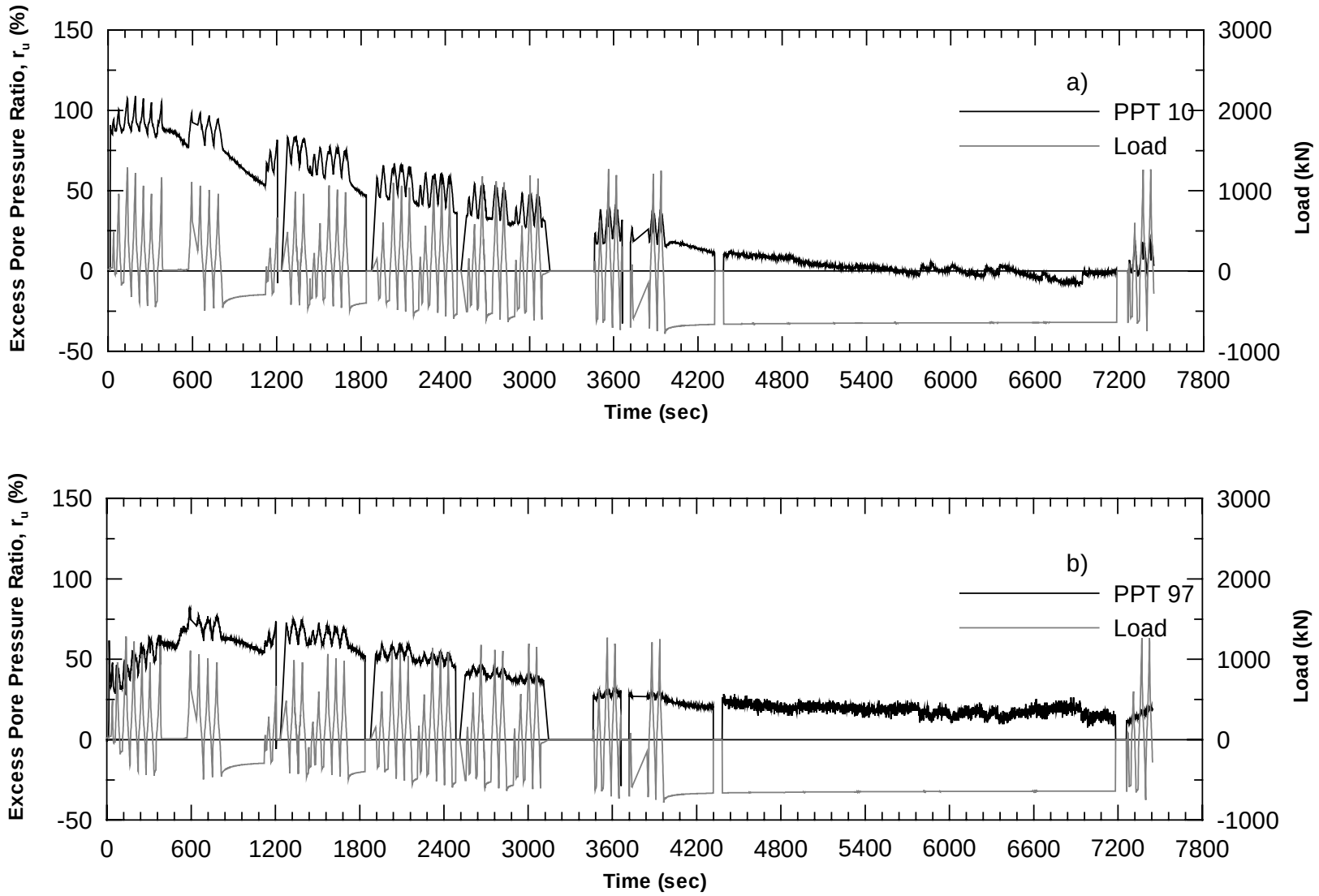

Figure 5.52 Excess Pore Pressure Ratio for 9-Pile Group/0.9m CISS Pile 2 nd Blast a)PPT10 b)PPT97

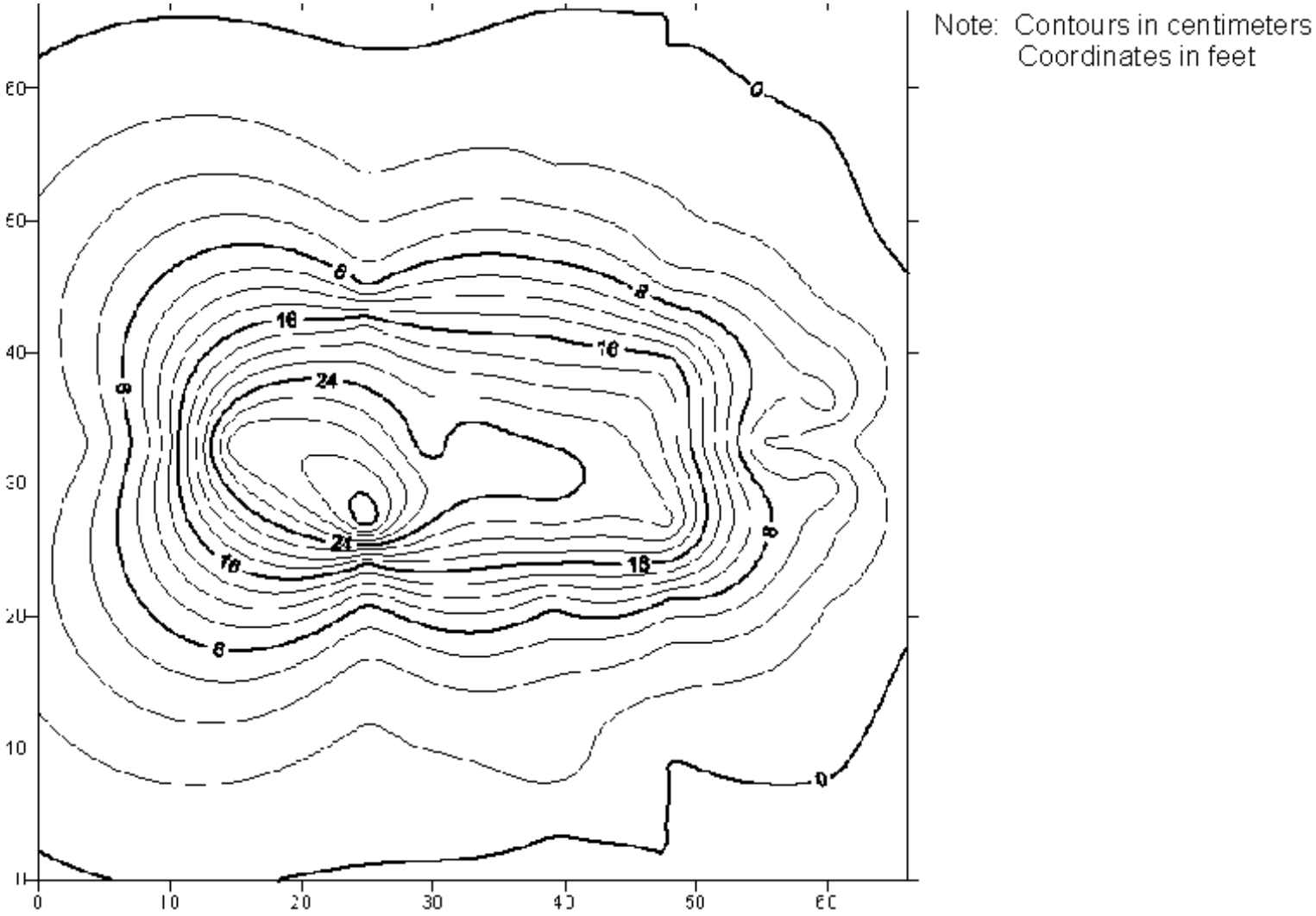

Figure 5.53 Contour of Settlement for 9 Pile-Group/0.9m CISS Pile 1 st Blast

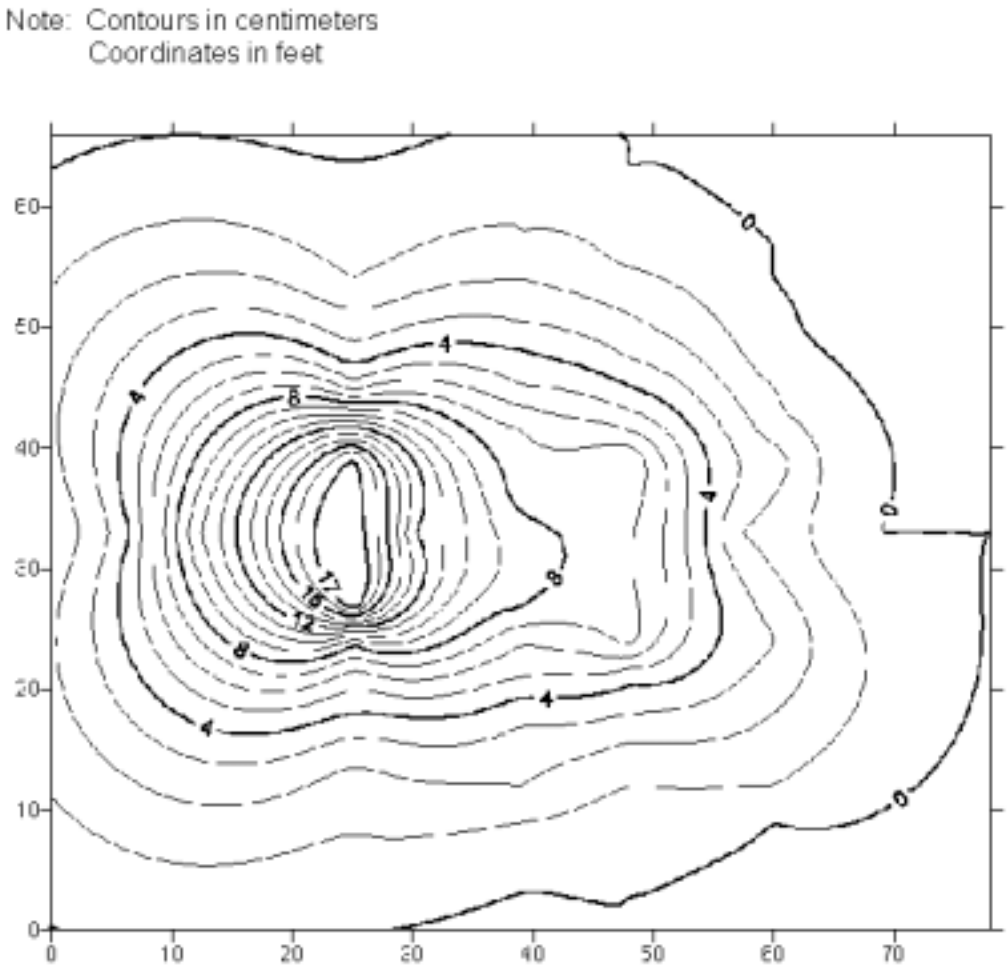

Figure 5.54 Contour of Settlement for 9 Pile-Group/0.9m CISS Pile 2 ndBlast

6 VERTICAL DRAIN PIPE TESTING

6.1 Objectives of Vertical Drain Pipe Testing

The synthetic drains known as E-Quake™ drains are perforated vertical drain pipes which are designed to relieve excess pore pressures during an earthquake and thereby prevent liquefaction. These drains were developed and patented by Geotechnics America, Inc. The concept of using vertical gravel drains for liquefaction mitigation was pioneered by Seed and Booker (1977). They developed design charts that could be used to determine drain diameter and spacing. Although gravel drains or stone columns have been utilized at many sites for liquefaction mitigation, most designers have relied on the densification provided by stone columns rather than the drainage. E-Quake drains can be installed more rapidly and at a fraction of the cost of stone columns but very little data is available regarding the densification which would be produced and the effectiveness of drains in reducing pore pressures and associated ground settlement.

Because the pilot liquefaction study had demonstrated that controlled blasting could produce liquefaction in a volume of sand in the field, a test program was developed to evaluate the performance of the drains using similar techniques. Drains were installed at the pilot liquefaction site after the first two blast tests and a third blast test was performed for comparison. In addition, drains were installed in a virgin test area immediately adjacent to the pilot liquefaction test site. This second test area provided the opportunity to make a direct comparison of the pore pressure behavior with drains in place relative to the behavior at the pilot liquefaction site without drains.

6.2 Site Characterization

To compare the soil properties at the drain site with the pilot liquefaction site, geotechnical investigations were also carried out at the E-Quake drain site as part of this study. The soil profile consisted of hydraulically placed fill and native shoal sands to a depth to 4.2 m. Silty sand and Young Bay Mud underlie the sand. The interpreted soil profile at the E-Quake drain test area is shown in Fig. 6.1 based on the results of all the field and laboratory testing. The excavated ground surface was about 1 m below the original ground surface and the water table was approximately 0.15 m below the excavated ground surface during testing. The sand typically classified as SP-SM material according to the Unified Soil Classification system and generally had a D_{50} between 0.2 and 0.3 mm.

In-situ tests included standard penetration tests (SPT) and cone penetration tests (CPT). The locations of the test holes are shown in relation to the blast holes in Fig. 6.2. The standard penetration resistance and cone resistance values were normalized to an overburden pressure of one atmosphere (q_{c1}) using procedures outlined by Youd and Idriss (2001). The $(N_1)_{60}$ values in the sand typically ranged from 7 to 16 in the cleaner sand layer but dropped to about 6 in the silty sand as shown in Fig. 6.1. Six CPT tests were performed across the test site and the average normalized cone resistance (q_{c1}) profile is shown along with mean ± one standard deviation bounds in Fig. 6.1. The average cone resistance was typically about 14 Mpa in the upper meter of the profile but dropped to between 6 to 9 MPa in the upper sand layer and 4 to 6 Mpa in the underlying silty sand layer. The relative density (D_r) based on the SPT was computed using the equation

$$D_r = \left[\frac{(N_1)_{60}}{40} \right]^{0.5} \tag{6.1}$$

developed by Kulhawy and Mayne (1990). The relative density based on the CPT was computed using the equation

$$D_r = \left[\frac{\left(\frac{q_{c1}}{p_a} \right)}{305} \right]^{0.5} \tag{6.2}$$

developed by Kulhawy and Mayne (1990) where p_a is atmospheric pressure and the sand is assumed to be normally consolidated. The relative density computed using equations 6.1 and 6.2 is plotted versus depth in Fig. 6.1. The estimated D_r was typically between 40 and 60 percent in the clean sand layers and dropped to about 30 percent in the silty sands.

A comparison of the interpreted relative density based on the average normalized cone penetration resistance for the pilot liquefaction site and the drain site is also provided in Fig. 6.1. The curves are generally very similar and indicate that the liquefaction susceptibility of the drain site is at least as high as that for the pilot liquefaction site.

6.3 Drain Properties and Installation Procedures

The corrugated ADS drain pipes used during this study had an inside diameter of 10.2 cm (4 in) and a flow area of 81.7 cm^2 (12.6 in^2). The corrugation on the drains were 9.5 mm (0.38 in) deep, so the outside diameter was 120.7 mm (4.75 in). Three horizontal slots, approximately 25 mm (l inch) long , were cut into each corrugation. This gave these drains an orifice area of 40.2

cm^2/m (1.9 in^2/ft). A standard ADS filter fabric or "sock" was typically placed around the drains to prevent infiltration of sand. The fabric had a permittivity of 0.33 cubic meters of water per second per square meter of fabric per meter of head and an AOS that corresponds to a #50 sieve. Based on the median grain size determined during the geotechnical investigation this filter fabric met the filter criteria listed by both Carrol (1983) and Giroud (1982).

The drains were installed to manner similar to that for PVC drains. The drain pipes were attached to an anchor plate and pushed to the target depth using a mandrel. The mandrel was installed with a converted CAT 235 excavator with a 149 kW (200 hp) engine. A downward for of 133.4 kN (30,000 lbs) could be applied to the mandrel along with a vibratory energy of 113 J (1000 in-lbs) produced by an eccentric mass. The drains could be installed to the design depth of 7.6 m in about 3 minutes.

6.4 Drain Tests at Pilot Liquefaction Site

As shown in Fig. 6.3, four clusters of seven drains and two clusters of seven wick drains were installed at various spacings at the pilot liquefaction site. Although no measurements were made during installation, visual observations indicated that installations induced settlements at the center of the drain clusters ranged from 150 to 300 mm.

The charges were detonated on December 16, 1998, 54 days after the first blast test. Because a considerable amount of time had elapsed since the first two blasts, the soil had likely consolidated into a denser state, but no CPT tests were performed immediately prior to blasting due to mobility problems in the test area. Although a maximum settlement of approximately 100 mm had occurred following each of the first two blasts, settlement for the third blast in the test

area was less than 3 mm. The average pore pressure ratio (R_u) time histories recorded by transducers at a depth of 2.7 m for the first blast (without drains) and the third blast (with drains) are provided in Fig. 6.4. Considering that the R_u time histories for the first two blasts at the pilot liquefaction site were very similar and nearly identical in some cases, the drains appear to have reduced the maximum R_u value and increased the rate of dissipation. However, the lower R_u values for this third blast could be a result of reduced compressibility of the soil produced by densification from the first two blasts. To provide more conclusive results another test was necessary at a virgin test site.

6.5 Drain Tests at Vertical Drain Site

As indicated previously the drain test site was located immediately adjacent to the pilot liquefaction site. The top meter of sand was excavated in an area about 15 m wide and 20 m long to match the conditions at the pilot liquefaction site.

6.5.1 Drain Installation and Test Layout

Figure 6.5 shows the layout of the drains and transducers as well as the location of the blast charges. The drains were installed by Geotechnics America in clusters of seven drains each, arranged so that six of the drains formed the corners of a hexagon while the seventh was placed directly in the center. This layout duplicated the triangular spacing that is normally employed over a much larger area. Theoretically, the drain at the center of the cluster would behave the same as a typical drain in a large group of drains since it was surrounded on all sides by drains. Wick drain clusters were installed along with the E-Quake drains for comparison purposes.

The two clusters of wick drains were installed on February 10, 2001. The six clusters of E~Quake™ drains were installed on February 11, 17, and 18, 2001. Each cluster was installed with the attributes listed in Figure 6.5, which indicate drain type, drain spacing, use of a filter fabric, and relative amount of vibration energy during installation. (For clarification purposes during the discussion in this chapter these attributes, listed in this order, will be placed in parenthesis when a certain cluster is discussed.) By varying these properties, the performance of the drains could be observed in slightly different situations during the first blast. However this also added other sources of variability to the results.

In addition to the seven drain clusters, two auxiliary drains were installed on the east side of the north blast zone. One of the concerns regarding the drains was that the blast pressures would cause the drains to collapse and render the drains inoperable. To ensure that the drains stayed open, wood strips (9.8 cm x 1.3 cm) were placed into the drains. These two drains did not have the wood installed and were used to see if the precaution was really necessary.

6.5.1.1 Transducers

A total of seventeen pore pressure transducers were installed into the ground and three more were lowered down the center drain of Cluster 1 (E~Q drain, 1.2 m, filter, normal vibration), Cluster 6 (E~Q drain, 0.9 m, filter, increased vibration), and Cluster 8 (E~Q drain, 1.2 m, no filter, max. vibration). The three transducers that were lowered down the center drain of three clusters were intended to provide information about change in hydraulic head at the drain itself. This data could be used along with the data from transducers in the soil to evaluate gradients toward the drain. These three transducers were placed 2.9 m (9.5 ft) below the water table.

The transducers that were placed into the ground were laid out strategically so as to provide the best possible measurement of pore water pressures and dissipation with the limited number of available transducers. Twelve of the seventeen were placed within the drain clusters and the other five were placed in the area without drains located in the northeast corner of the site. Each transducer that was placed near the E-Quake™ drains was installed equidistant from three individual drains so it would be located at the spot that was the furthest away from any of the drains. This represented the worst-case scenario within the clusters. Those transducers placed in the non-treated area were installed in a similar layout, to maintain consistency between the transducers. The depth of each transducer below the ground water table is listed is Fig. 6.5.

6.5.1.2 Vibration during Installation

A blast seismograph was used to measure the peak particle velocity for each 15 second interval during insertion of the drains into the ground. The vibrations were measured at the ground surface at distances of 3.0, 6.1, and 12.2 m (10, 20 and 40 ft) away from the finned mandrel as the drains were being installed with a vibratory push. The vibrations were the strongest at a distance of 3.0 m and attenuated rapidly with distance as shown in Fig. 6.6. The peak particle velocities at a distance of 3.0 m ranged from 6.5 to 11.7 mm/sec. The best-fit line for the peak particle velocity (PPV) in mm/sec is given by the equation

$$PPV = 22.65 \; x^{-0.90} \tag{6.3}$$

where x is the distance in meters from the insertion point. This equation has an r^2 value of 0.82.

The highest velocity was measured within the first thirty seconds while the tip of the mandrel was not very deep into the soil profile. The vibrations recorded at the surface generally decreased as the mandrel went deeper into the ground. All of these velocities were quite low and

attenuated rapidly; however, the area immediately around the drain was significantly affected. In fact, the vibrations were sufficient to cause liquefaction and water was observed flowing out of neighboring drains.

6.5.1.3 Settlements during Installation

Significant settlement craters developed around each drain cluster during installation. This settlement was monitored at each cluster and the results are summarized in Fig. 6.7. The installation of wick drains caused practically no settlement. The clusters of E~Quake™ drains installed with vibration and the finned mandrel (1, 3, 6, 7, 8) experienced considerably more settlement than the drains installed without vibration. Closest to the center of the cluster, the settlement from the drains installed without vibration ranged from 6 to 15 cm (2.4 to 5.9 in) less than those drains installed with vibration. In fact, at Cluster 7 (E~Q drain, 1.2 m, filter, increased vibration) and Cluster 8 (E~Q drain, 1.2 m, no filter, max. vibration) the maximum settlements were twice as large as the maximum settlement of Cluster 4 (E~Q drain, 1.2 m, filter, no vibration), where no vibration was employed. Assuming a soil profile with an average unit weight of 20.1 kN/m^3 (128 pcf) and an average height of 6.5 m (21.3 ft) the observed settlement results in a 3-4% increase in unit weight or a volumetric strain of 1.4 to 2.8% within the soil profile. Fig. 6.8 shows contours of installation induced settlement around the various clusters at the test site.

6.5.1.4 CPT Test After Treatment

A CPT sounding was performed between the drains in Cluster 8 (see Fig. 6.5) to evaluate the change in penetration resistance produced by the installation of the drains. This test was performed on February 25, 1999, about a week after the drains were installed at the site and

immediately preceding the blast. Fig. 6.9 shows the cone resistance versus depth for the CPT performed after treatment along with the average cone resistance versus depth prior to treatment. The CPT results indicate that the installation of the drains did increase the cone tip resistance by about 15 to 25% along the length of the drain.

The results of the settlement monitoring and the CPT testing both confirm that the installation of the E-Quake™ drains increased the density of the sand at this test site. Thus, the densification during installation of the drains themselves can add to the liquefaction mitigation provided by drainage. By densifying the soil, the potential for liquefaction is reduced and if liquefaction should still occur, the settlement and strength loss would be less severe. In addition, densification reduces the compressibility of the sand, which allows excess pore pressure to dissipate more rapidly.

6.5.2 Test Blast

In preparation for the test blast, the settlement craters that had developed during installation were backfilled with uncompacted sand to provide a level surface. In addition, different dyes were placed in three drains to help identify the source of water following the blast. The blast test was set off on February 25, 1999 about one week after drain installation. The detonation consisted of eight separate blasts (two charges at a time) and spanned a period of four seconds. Immediately following the eighth explosion a low pop was heard, almost like a ninth explosion, and a large quantity of water was shot about 3 m into the air out of the south auxiliary drain. This auxillary drain was located in the untreated area on the northeast side of the test area as shown in Fig. 6.5.

Following the water spout, a plume of smoke emerged from the drain for about seven seconds suggesting that the drain had become hydraulically linked with the blast holes potentially through a horizontal seam. As the smoke died away, a mixture of water and soil, as shown in Figure 6.10, began to flow out of that same drain at a rate of about 40 liters/minute (10 gallons/minute) or more and continued to flow for over ten minutes. There was a sufficient flow to exceed the flow capacity of the perforations and overtop the drain, which protruded approximately 0.3 m above the ground surface.

The portion of the wick drains protruding out of the ground had been supported so they stood upright. Ten seconds after the blast, water was also observed climbing the wick drain until it reached a height of 0.6 m. Within a minute after the final explosion, the dyed water was observed at the surface, as shown in Fig. 6.11, and was flowing out of every drain in which it was placed. In contrast to the observations at the pilot liquefaction site, no sand boils were observed.

These observations indicate that water was finding its way to the surface through the pathways provided by the drains rather than creating sand boils at blast holes or other points of weakness as in the test at the pilot liquefaction site. This result also suggests that the pressures were being dissipated horizontally to the drains faster than in any other direction. These initial observations indicate that the drains worked as intended.

6.5.2.1 Sand Infiltration of Drains

Before and after the blast the depth of each drain was measured to discover how much sand, if any, had accumulated in the drains during the blast. The maximum, minimum, and average infiltration of sand within the seven drains of a given cluster is shown in Table 6.1. On average, 1.5 m (4.9 ft) of sand had filled up the base of the drain, decreasing the average length by 23%.

However, there were significant variations in the thickness of sand infiltration among the individual drains.

Table 6.1 Sand infiltration into E~Quake™ drains after blasting

	Max [m (ft)]	Min [m (ft)]	Ave [m (ft)]
Cluster 1: filter fabric	4.57 (15.00)	0.15 (0.50)	1.25 (4.10)
Cluster 3: filter fabric	0.66 (2.17)	0.08 (0.25)	0.31 (1.01)
Cluster 4: filter fabric	3.28 (10.75)	0.13 (0.42)	0.61 (1.99)
Cluster 6: filter fabric	3.96 (13.00)	0.10 (0.33)	0.96 (3.15)
Cluster 7: filter fabric	3.96 (13.00)	0.15 (0.50)	2.01 (6.60)
Cluster 8: no filter fabric	6.12 (20.08)	0.25 (0.83)	2.36 (7.75)
Auxilliary: no filter fabric	7.06 (23.17)	6.65 (21.83)	6.86 (22.50)

Each of the clusters installed with filter fabric (sock) had less sand infiltration, on average, in the drains than the one cluster installed without a sock. However, four out of five of those clusters had at least one drain that filled with 3.0 m (10 ft) of sand. Of the nine drains that were installed without socks, three of them filled up with at least 6.1 m (20 ft) of sand which represents 80% of the length of the drain. Only two of the nine drains didn't have at least 1.5 m (5 ft) of sand enter the drain. Although the filter fabric met filter criteria, sand could have infiltrated the drain through the opening at the bottom where the sock was removed to attach the anchor.

6.5.2.2 Blast Induced Settlement

Settlement in Untreated versus Treated Areas at E-Quake Drain Site. Prior to the detonation of the explosives, a grid of 110 elevation stakes was laid out to define the settlement contours across the site. A color contour map of the blast- induced ground settlement in presented in Fig. 6.12. Although the maximum settlement was located between the two blast

zones in Cluster 6, the majority of the settlement occurred in the non-treated area in the northeast corner of the site. All of the elevation stakes that measured a settlement of at least 3.5 cm (l.4 in) were located within the north blast zone. The maximum settlement of 10.9 cm (4.3 in) was measured within Cluster 6 (E~Q drain, 0.9 m, filter, increased vibration) which was one of the clusters that experienced a settlement of more than 20 cm (7.9 in) during installation. The other two clusters that had similar large settlements during installation, Cluster 7 (E~Q drain, 1.2 m, filter, increased vibration) and Cluster 8 (E~Q drain, 1.2 m, no filter, max. vibration), were on the perimeter of the non-treated area but still had settlements as great as 7.6 cm (3.0 in) due to the blast.

This is initially contrary to what would have been expected. Intuitively, these three drain clusters that had the most settlement during installation might have been expected to have the least settlement following blasting. However, because these three clusters developed the largest craters during installation they also required the most backfilling to level them out. This backfill, consisting of sand from the site, was placed by hand and was not mechanically compacted in any way. Therefore, the settlement that occurred around these northern clusters may be primarily attributed to settlement of the loose backfill material. This is supported by how rapidly the settlement decreases at the outside edge of the drain clusters.

The presence of the drains had a definite effect on the settlement during the blast. However the drainage provided by the drains may be more accountable for the effects than the densification during installation. If the installation induced settlements were responsible for the reduction in settlement at the site then there should have been a difference between the settlements around Cluster 1 installed with the finned mandrel and a vibratory push (19.5 cm maximum installation settlement) and Cluster 4 installed with the basic mandrel and a static push

(13.1 cm maximum installation settlement). Instead, the blast-induced settlement was nearly identical at 3.0 cm at Cluster 4 and 3.4 cm at Cluster 1. Additionally, the area around the wick drains, which didn't experience any significant settlement during the installation process, experienced the lowest settlement during the blast.

Settlement at Vertical Pipe Drain Site versus Pilot Liquefaction Site. A comparison with settlement measured at the pilot liquefaction site also indicates that the presence of the E~Quake™ drains reduced the settlement due to blasting. The maximum settlement at the pilot liquefaction site was 9.5 cm (3.7 in). This maximum settlement was located at the intersection of the two blast zones and decreased in concentric rings as shown in the previous chapter.

The settlement that occurred in the non-treated area of the E~Quake™ Drain site was similar in magnitude and shape to that experienced at the pilot liquefaction site. If we assume that the settlement that occurred in Cluster 6 was largely due to loosely compacted fill, the maximum settlement on the site occurred in the non-treated area. A settlement of 9.8 cm (3.9 in) was recorded near the center of the untreated zone during the E-Quake drain test which is nearly identical to that recorded during the pilot liquefaction test. In addition, the amount of settlement decreased in concentric rings to the north and to the east as shown in Fig. 6.12.

The same concentric settlement pattern did not continue to the south or to the west likely due to the presence of the drains in those areas. The settlement that occurred in the south half of the E~Quake™ Drain site, where more drain clusters were located, ranged between 2 and 4 cm). This is 20-40% of the settlement that occurred in non-treated areas or at the pilot liquefaction site and represents a significant reduction in blast induced settlement.

6.5.2.3 Pore Pressure Response

The extreme pressures generated in less than a second by the blasting process made it impossible for the drains to prevent initial liquefaction. However, in an earthquake where excess pore pressure develops over tens of seconds the drains would have time to be more effective. Therefore, for this investigation the primary concern was not so much the initial magnitude of the pore pressure but the rate at which the pressures dissipate with time.

As indicated previously, the pore pressure transducers were primarily installed at depths of 2.7 and 4.6 m in the treated and untreated zones so comparisons will be limited to these depths. Figs. 6.13 and 6.14 illustrate the average dissipation curve at depths of 2.7 m and 4.6 m, respectively for four test situations: (1) the pilot liquefaction site during the first blast without drains, (2) the pilot liquefaction site during the third blast with drains and blast densification, (3) the treated area of the E~Quake™ Drain site, and (4) the non-treated area of the E~Quake™ Drain site. The effect of the drains is well defined in these figures as the pore pressure ratios in the drained areas are consistently less at a given time than those in the non-treated areas.

The rate of dissipation is different for each of the four test situations. At a depth of 2.7 m (9 ft), as shown in Fig. 6.13, the pore pressure ratios are consistently the highest for the untreated soil during the first blast at the pilot liquefaction site. The R_u values are above 60 percent for about 400 seconds. The curve for the untreated area at the E-Quake drain site is the next highest curve; however the shape is quite different from that observed at the pilot liquefaction site. There is a rapid drop off in R_u to about 60 percent in the first 100 seconds which is followed by a more gradual rate of dissipation. The rapid drop in R_u is likely due to the drainage provided by the flow from the auxiliary drain as well as the drains which were located around the perimeter of the untreated area. In hindsight it would have been desirable to have an untreated zone which

was further from any drains at all. The change to a more gradual rate of dissipation may be due to a build-up of sand in the drain aas will be investigated subsequently.

The curve with the next lowest R_u values is that for the treated area at the pilot liquefaction site after the third blast. At this location, the maximum average R_u only reached 63 percent. This lower initial R_u is likely a result of the densification produced by the previous blasts at the site. The dissipation is clearly faster than that for the untreated sand in the first blast at the pilot liquefaction site but slower than in the treated area at the E-Quake drain site. The dissipation rate may be somewhat slower than at the E-Quake drain site because far fewer drains were placed in this area. The lowest R_u values were measured in the areas treated with drains at the E-Quake Drain site. The Ru vs time curve drops very rapidly to a value of about 15 percent in about 60 seconds but then begins to increase again and peaks at a value of about 30 percent before gradually dissipating again. This increase in Ru may also be a result of clogging in the drains due to sand infiltration.

At a depth of 4.6 m, as shown in Fig. 6.14, the areas with drains once again exhibited more rapid pore pressure dissipation than the areas without drains. However, in both cases the rate of dissipation was slower at the E-Quake drain site than at the pilot liquefaction site. The delayed response in dissipation at the E-Quake site suggests the transducers were located in lower permeability soils at this site relative to the pilot liquefaction site.

No consistent trends could be observed in the dissipation rate based on the settlement produced by the drain installation or the drain spacing. In fact, the dissipation rate for the wick drains was about the same as the average rate in the E-Quake drain clusters.

6.6 Analysis of Drain Test Results

A computer analysis of the drain test results was performed to provide insight into the behavior of the drains and to evaluate the behavior of a simple computer model to match the measured pore pressure response.

6.6.1 Description of Computer Model and Input Parameters

The computer analysis was performed using the finite element program, FEQDrain, developed by Pestana et al (1997). This program models transient fluid flow in a porous medium and can account for the head losses associated with flow in a vertical drain pipe or a gravel drain (stone column). The program models pore pressure generation due to earthquake shaking using procedures suggested by Seed et al. (1975). Pore pressure dissipation is governed by the hydraulic conductivity and the compressibility of the soil, which varies with excess pore pressure ratio. The numerical model for the drained case assumes that drains are placed in a grid pattern in plan view. Therefore, the flow to a given drain within the grid can be modeled as an axi-symmetric problem with impervious (no flow) boundaries halfway between adjacent drains and at the base.

The input for FEQDrain is rather simple and can be broken into three general categories: soil properties and geometry, earthquake loading conditions and time integration parameters, and drain properties. The program assumes that the soil layers are perfectly horizontal and infinite in all horizontal directions. The axi-symmetric finite element mesh is defined by vertical and radial increments. The number of radial increments remains constant for the entire mesh, but the number and thickness of the vertical increments varies between soil layers.

6.6.1.1 Required Soil Properties and Geometry

Required soil information includes the soil layer thickness, soil type, unit weight, radial and vertical hydraulic conductivity, modulus of compressibility, relative density, number of cycles to liquefaction, pore pressure generation ratio and the water table depth.

The soil layer thickness, soil type, water table depth and relative density were obtained based on the results of the CPT soundings at the site. A first approximation of the horizontal hydraulic conductivity was made based on measurements made by the US Navy using water wells on Treasure Island. The average value was 3.53×10^{-5} m/sec (1.16×10^{-4} ft/sec) (Faris, Personal Communication) was typically used for the clean sand layers. The horizontal hydraulic conductivity for the silty sand layers was chosen to be about one-fourth the value of the clean sand based on correlations with soil type. However, hydraulic conductivity values are known to vary by two orders of magnitude within a given soil gradation type and variations from these mean values were expected.

The modulus of compressibility was selected based on the material type and relative density of the soil using typical values provide by Pestana et al (1997). The number of cycles required to cause liquefaction was made slightly less than the number of cycles associated with the blast when liquefaction was observed. Finally, the pore pressure generation ratio was taken as 0.7 based on recommendations by Seed et al. (1975).

6.6.1.2 Earthquake Loading Conditions and Time Integration Parameters

The shaking produced by an earthquake is simplified into a series of uniform cyclic loads with a given duration. Correlations with earthquake magnitude can be used to determine the number of equivalent cycles and the expected duration. The user also specifies times at which

results are desired. The number of equivalent cycles produced by the blasting was taken as 12 with and the duration of shaking of three seconds.

In trying to describe the shaking effects of an explosion in earthquake terms, the input parameters for number of cycles to cause liquefaction and number of equivalent cycles in the event had the potential for error. However these parameters only had an effect on the maximum generated pore pressure. Once this was established, alterations were no longer made to these values. For this analysis the importance of these two input parameters was the ratio between the two and not the actual value of each. For this reason the values used in this analysis were arbitrary and were not based on any measured soil characteristics. The blast was so intense that it caused all but the upper meter of material to liquefy, therefore the same nl value was used for all the soil layers in the calibrated model except for the top layer where liquefaction did not occur.

6.6.1.3 Drain Geometry and Drainage Properties

FEQDrain provides four different options for drainage:(1) no drain, (2) perfect drain without any head loss, (3) constant hydraulic conductivity drain (gravel drain),(4) and composite drain (E-Quake drain). When a drain is involved, the drain diameter and spacing are required. If a gravel drain is specified, a hydraulic conductivity is required along with head loss coefficients. If a composite drain is used, details regarding the perforation area, filter fabric permittivity and head loss coefficients are required. Head loss is generally modeled using equations developed by Onoue (1988).

The E-Quake drain parameters were provided by GeoTechnics America and were all values that had a high degree of reliability. The radius of the drain was 6.0 cm (2.36 in) which

corresponded to a drain area of 114.3 cm^2 . The radius of the area of influence was 0.6 m (2 ft) which represented a drain spacing of 1.2 m (4 ft).

The permittivity of the filter fabric around the E~Quake™ drain was 0.08 /sec. The constant for head loss through the perforations was 1 and the area of openings per unit length in the perforated pipe was 0.004 m^2/m. The hydraulic gradient in the vertical direction inside the pipe, i_z is given by the equation

$$i_z = 0.5\ (Q_d(z,t))^2. \qquad (6.4)$$

where Q_d (z,t) is the vertical flow inside the drain at depth z and time t.

The "reservoir" in the drain consisted of the area between the static water table and the ground surface within the drain. This volume was insignificant, however the values were still input into the program. The hydraulic gradient in the vertical direction inside the reservoir, i_{zres} was defined by the equation

$$i_{zres} = 0.37\ (Q_d(z,t))^2. \qquad (6.5)$$

6.6.2 Analysis of Pilot Liquefaction Test Results

The computer analysis of this test had two objectives. First, the analysis was used to determine if the computer program could provide acceptable estimates of the measured pore pressure response. Secondly, the pilot test results provided an opportunity to develop a calibrated soil model for the test site. The calibrated model would then serve as a starting point for modeling the blast at the E-Quake drain site where vertical drains were employed.

Initial estimates of the soil layering and soil properties are shown in Fig. 6.15. Using this soil model in FEQDrain, time histories of R_u were computed for six depths that corresponded with pore pressure transducers located at the center of the East Blast Zone. The time histories at

these transducers were also found to be close to the average values of all the transducers at each depth. The results from the first modeled scenario indicated that, according to FEQDrain, the modeled soil parameters did not match the soil characteristics in the field.

6.6.2.1 Model Calibration

Calibration of the numerical model was performed by systematically adjusting the input parameters until the computed values from the analysis matched the measured values from the testing. A reasonably successful, calibrated model was developed by learning from the changes made to the input parameters in successive iterations. Although not an exact match, the calibrated model produced results close to those measured in the field at depths of 0.9, 1.8, 2.7, 3.7, 4.6 and 5.5 m, as seen in Fig. 6.16. The soil layering and soil properties used in the calibrated soil model are also shown in Fig. 6.15 along with the initial soil model.

Since the input values for relative density and total unit weight were obtained through a correlation with measured CPT data, these values were not altered during the calibration phase. The number of soil layers and their individual thicknesses were also obtained using the CPT data. These parameters remained fairly constant during the calibration, however two changes were made in the process. The first was to lower the contact between the third and fourth layers because the measured values from the transducer at a depth of 4.6 m behaved as if was in a cleaner sand layer. The second change was to split the first layer into two separate, but similar, layers. The measured values from the transducers at 0.9 and 1.8 m were dramatically different, so the layer was divided to be able to account for that difference.

Some minor alterations were made to the earthquake parameters. This included the number of cycles to cause liquefaction (nl) and the number of equivalent cycles (nq) in the “earthquake.” However, the majority of the alterations during calibration were made to those input parameters

that came from educated guesses, such as the modulus of compressibility, and the hydraulic conductivity of the soil. A brief discussion of the changes is provided below.

Modulus of Compressibility Some minor changes were made in individual soil layers, but the modulus of compressibility values in the calibrated model were within ±20% of the values used in the initial modeled scenario. The calibrated modulus of compressibility fell within the range suggested in the FEQDrain literature (Pestana et al, 1997).

Hydraulic Conductivity The majority of the alterations used in calibrating the model were made to the conductivity. The calibrated model has both vertical and horizontal hydraulic conductivities that are significantly different from the original modeled scenario which is not unanticipated. In a scenario with no drainage and no flow boundaries at the radial perimeter, horizontal hydraulic conductivity has little to no effect on the computed results. An attempt was made to keep the values for the horizontal hydraulic conductivity reasonable, but the alterations focused on the vertical hydraulic conductivity.

The vertical hydraulic conductivity provided by the U.S. Navy significantly underestimated the vertical hydraulic conductivity of the soil according to FEQDrain. The calibrated model required vertical hydraulic conductivities that were 4 to 20 times greater than the original modeled values. Even with that increase, the final values were still within the reasonable range for sands (Das, 1994). The problem with the hydraulic conductivity values obtained in this phase of the analysis is that there is a good chance that they are higher than what existed in the field. This discrepancy develops because FEQDrain does not account for radial drainage. In the event of an earthquake a relatively wide area will experience similar shaking levels and excess pore pressures. As a result, radial drainage and accompanying pressure dissipation will not be a

factor and the assumption of a no flow radial boundary, made in FEQDrain, is valid. However; in this blasting experiment the shaking and excess pore pressure generation is localized around the blast points. Drainage and pressure dissipation can also occur radially, away from the blast zones. Therefore, to account for the radial drainage with a model that does not consider radial drainage, the vertical hydraulic conductivity must be artificially increased.

Although the values of hydraulic conductivity used in the model are likely to be artificially high, these values do account for the observed rate of dissipation. Therefore, if similar values are used in the FEQDrain analysis of the E-quake drain test site there might still be a basis for comparison.

6.6.3 Analysis of Vertical Pipe Drain Site

The objective of this analysis was to develop a calibrated model that included E~Quake™ drains. Theoretically, the only changes in the model calibrated for the pilot liquefaction site would be to the horizontal hydraulic conductivity and the drain properties. The computed R_u versus time (dissipation curves) were compared to the average of the measured pore pressure transducers at two depths. The average pore pressure dissipation curve at a depth of 2.7 m was developed based on two transducers within E~Quake™ drain clusters. However, this curve was very similar to the average curve for the transducers in the wick drain clusters. At a depth of 4.6 m an average dissipation curve was developed using data recorded by five transducers.

In the first attempt to model the pore pressure response at the E~Quake drain site , the soil model developed for the pilot liquefaction site was used without any modification and the properties of the composite drains were added to the model. Using this approach FEQDrain significantly overestimated the rate of dissipation observed in the field. FEQDrain calculated

that the maximum R_u would be less than 0.3 at both depths of 2.7 and 4.6 m and that by 600 seconds the excess pore pressure would be completely dissipated.

Subsequently, efforts were made to adjust the horizontal hydraulic conductivity until a match was obtained with the measured curve shapes. However, it proved impossible to develop a single model that could match the entire measured R_u versus time curve. This result suggests that either the computer model is inappropriate or that some change has occurred in the physical system at some point during the dissipation of pore pressure that is not adequately modeled. Based on our previous review of the test results the second alternative appears to be the most likely because there appears to be a distinct change in the pore pressure response in the Ru time histories.

To account for the measured behavior two different models were created. In the first model the drains were assumed to be fully operative and the drain behavior was modeled with the composite drain option in the program. In the second model the drain was assumed to be partially filled with sand and the drain behavior was modeled as a gravel drain or constant hydraulic conductivity drain.

Case 1 Composite Drain model. With the drains in the soil profile the principle direction for drainage was radial rather than vertical. While calibrating the pilot liquefaction site model, adjustments made to the horizontal hydraulic conductivity had no effect on the computed response. Therefore, the horizontal hydraulic conductivity in that model was poorly constrained. During the calibration of the composite drain model the horizontal hydraulic conductivity was varied in an effort to obtain a match with the measured response. After a number of trials, a model was successfully calibrated to the first 40 seconds of the average R_u time history recorded at a depth of 2.7 m (9 ft). The soil profile and properties used in the analysis are shown in

comparison with those for the pilot liquefaction model in Fig. 6.17. The only major difference between the soil profiles is the reduction in the hydraulic conductivities. The horizontal and vertical hydraulic conductivities of the first and second layers were set equal to each other and were reduced to the value provided by the U.S. Navy for Treasure Island (Faris, 1999). For layers 3, 4, and 5, the horizontal hydraulic conductivity is 10 times greater than the vertical hydraulic conductivity and both are reduced from the values developed for the pilot liquefaction site model. Nevertheless, the hydraulic conductivity values are still within the typical ranges for the soil gradations involved (Das, 1994).

Fig. 6.18 shows the computed R_u time history in comparison with the measured time history and the match is very good for the first 40 seconds of the record. After this time, the measured curve moves upwards while the computed curve continues downward. This may represent the point where the infiltration of sand in the drain begins to impede the effectiveness of the drain. No acceptable agreement with the measured curve could be obtained at a depth of 4.6 m. The computer predicts a curve similar to that for the 2.6 m depth; however, the measured dissipation rate is far slower. Infiltration of sand would have occurred more quickly at this greater depth and this could account for this discrepancy.

Case 2-Constant Hydraulic Conductivity Drain Model. In order to support the theory that the infiltration of sand into the E~Quake™ drain resulted in a slower rate of pore pressure dissipation, a different approach was taken for calibration. Rather than using a composite drain with a hollow center, the drain was modeled as a constant hydraulic conductivity drain. This option models a sand or gravel drain with a horizontal and vertical hydraulic conductivity that is much greater than the surrounding soils. Thirteen modeled scenarios were used to develop the final calibrated model.

The soil profile and properties used in the analysis are presented in Fig. 6.19 in comparison with similar data for the pilot liquefaction site. As seen in Fig. 6.19, only some minor changes from the pilot liquefaction soil profile were made for this case. The hydraulic conductivity of the first and second layers was slightly increased and the hydraulic conductivity of the third layer was slightly decreased. The majority of the changes made in the different scenarios during calibration were to the hydraulic conductivities within the drain.

The computed R_u time histories at 2.7 m and 4.6 m depths are compared with the measured time histories in Fig. 6.20. A relatively good match was made with the measured pore pressure response at a depth of 2.7 m (9 ft) after about 600 seconds and a nearly identical match was made with the data at a depth of 4.6 m (15 ft) from the start of the test. These results indicate that the E~Quake™ drains were not performing as designed. The results from this analysis suggest that the E~Quake™ drains performed more as constant hydraulic conductivity (stone column) drains than as hollow, composite drains. Again this data supports the theory that the infiltration of sand played a major role in the performance of the E~Quake™ drains. The reduction in flow volume in the drains may also explain why the wick drains performed as well as the E~Quake™ drains.

6.7 Results and Conclusions Based on Drain Testing and Analysis

6.7.1 Conclusions Regarding Settlement Mitigation Due to Drainage

1. Settlement due to blast induced excess pore pressures was significantly reduced due to the installation of vertical drains. The settlement at the E~Quake™ Drain site due to blasting was typically 2-3 cm (~ 1 in) or less in the areas where clusters of drains had been installed. However, in the area of the site without drains, the maximum settlement was approximately

10 cm (4 in), which was identical to the settlement measured after the first blast at the Pilot Liquefaction site.

2. The reduction in settlement within the drain clusters was likely due to the drainage properties rather than the densification effects from installation. This conclusion is drawn because the blast-induced settlement recorded around the clusters with little installation-induced settlement was the same as the settlement around the clusters with high installation-induced settlement.
3. Higher settlement measured at some of the drain clusters (Nos. 6, 7, & 8) is likely due to settlement of the loose backfill used to level the site rather than settlement of the underlying sand.

6.7.2 Conclusions Regarding Pore Pressure Response

1. Because of the extremely rapid increase in pressure produced by blasting, the drains did not

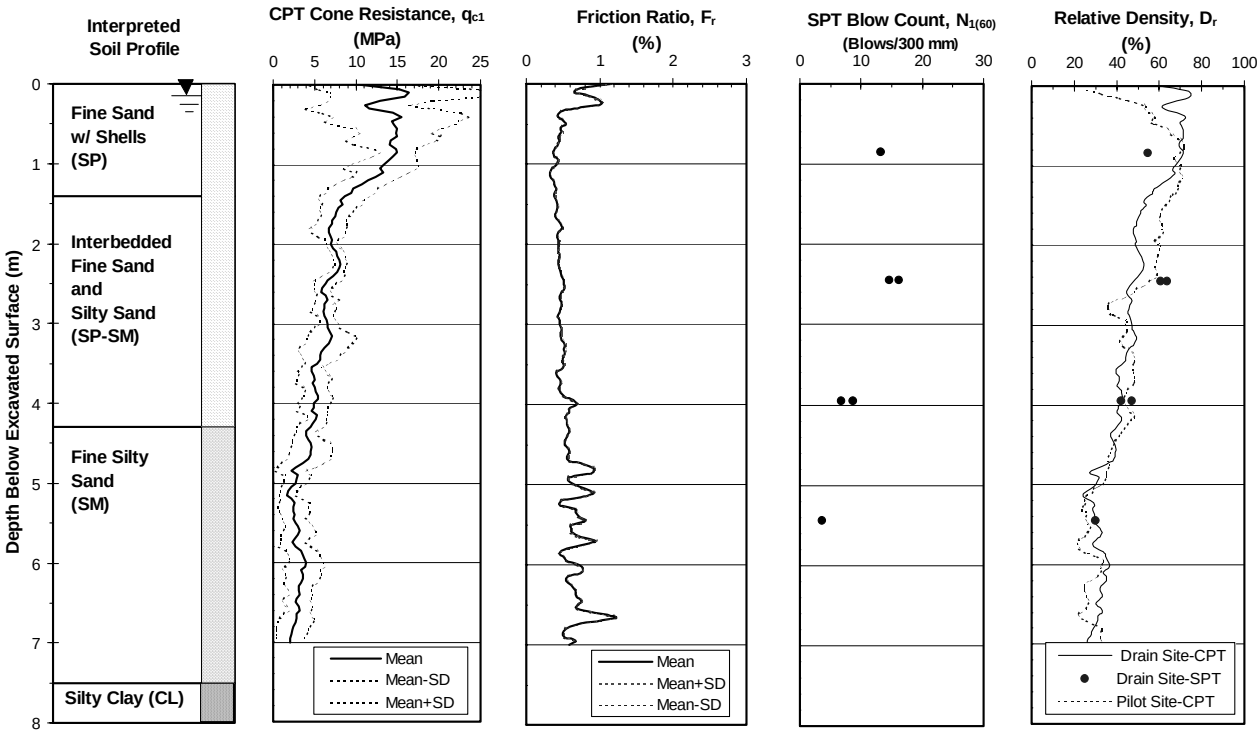

prevent the build-up of excess pore water pressure as they might be expected to during an earthquake.

In all cases, the rate of dissipation was significantly increased in zones treated with vertical drains relative to untreated zones.

2. Immediately following blasting, measured pressures dropped very rapidly indicating that the drains were functioning properly. Subsequently, higher pore pressures built up around the drains presumably due to the reduced hydraulic conductivity in the drains resulting from sand infiltration. Once the pressure was sufficient to drive the water through the sand within the drain, dissipation began again, but the rate of dissipation was much slower.
3. Drain performance was significantly impeded due to infiltration of sand into the drains following blasting. Improved methods for preventing infiltration at the bottom of the drain are necessary to increase drain efficiency.

6.7.3 Conclusions based on Computer Model Analysis of Measured Response

1. The FEQDrain program could produce computed pore pressure versus time curves that matched the measured response at a vertical transducer array for the first blast at the pilot liquefaction site.. This represented an untreated, non-drained situation. However, the values used for the vertical permeability may have been artificially high. This was due to conditions unique to the limited extent of liquefaction during the testing and the fact that the program could not model radial drainage without a drain in place.
2. Two calibrated models were needed to match the measured pore pressure response observed for the E~Quake™ Drain site. The first calibrated model incorporated the use of E~Quake™ drains and typically matched the first 40 seconds of the measured results. The second

calibrated model incorporated the use of vertical drains with a constant hydraulic conductivity and matched the measured results from about 400 seconds to the end of the test. The need for these two separate models support the theory that sand infiltration altered the drainage capacity of the E~Quake™ drains.

3. The results of these calibration studies suggest that accurate estimates of pore pressure response using FEQDrain will be very sensitive to an accurate selection of (a) the number of cycles required to cause liquefaction relative to that produced by an earthquake, (b) the hydraulic conductivity, and (c) the modulus of compressibility. Unfortunately, these parameters may vary significantly for a given soil type. In-situ measurements of these properties are therefore desirable for a given site.

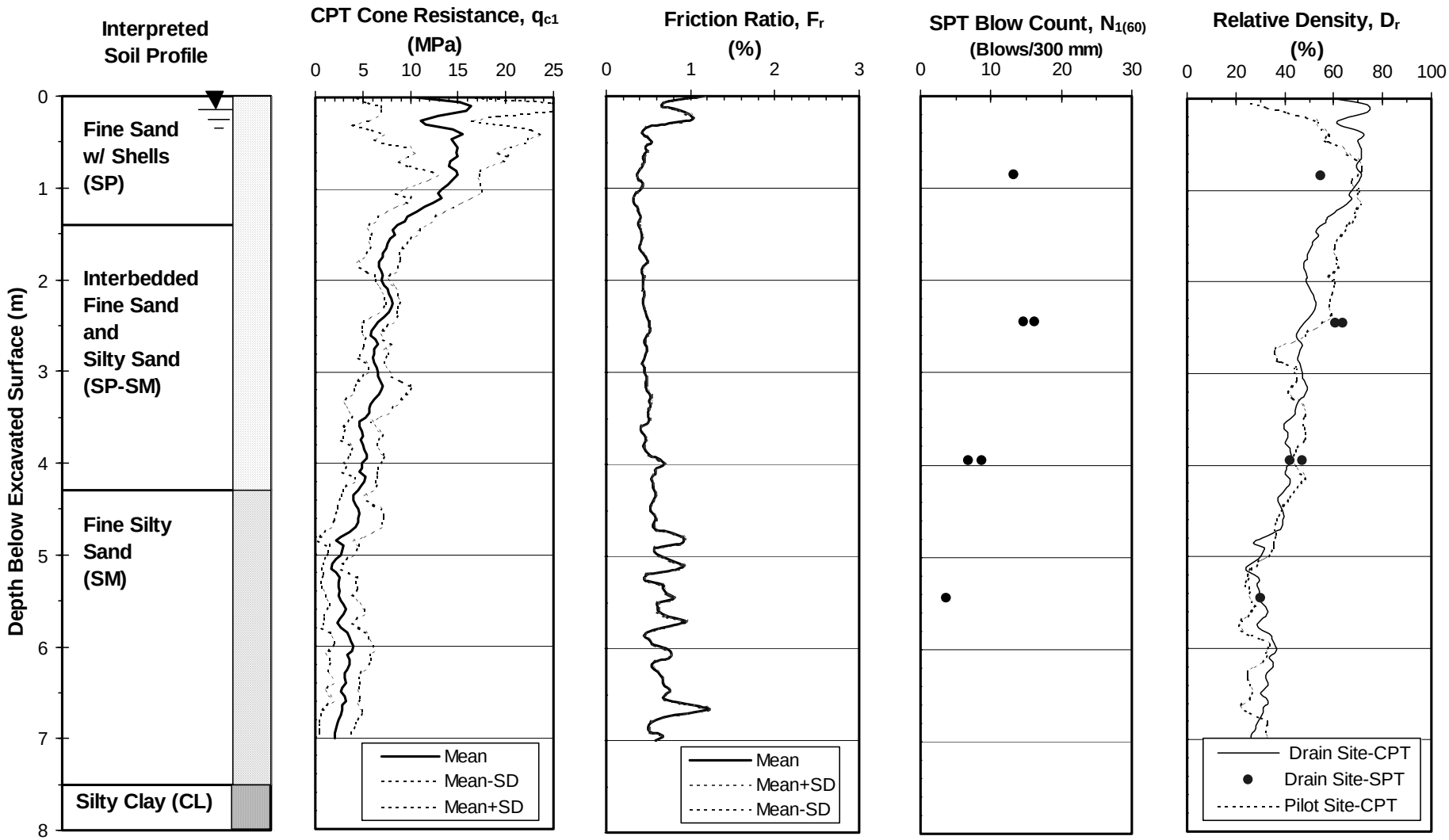

Figure 6.1 Summary of idealized soil profile and in-situ tests along with interpreted relative density.

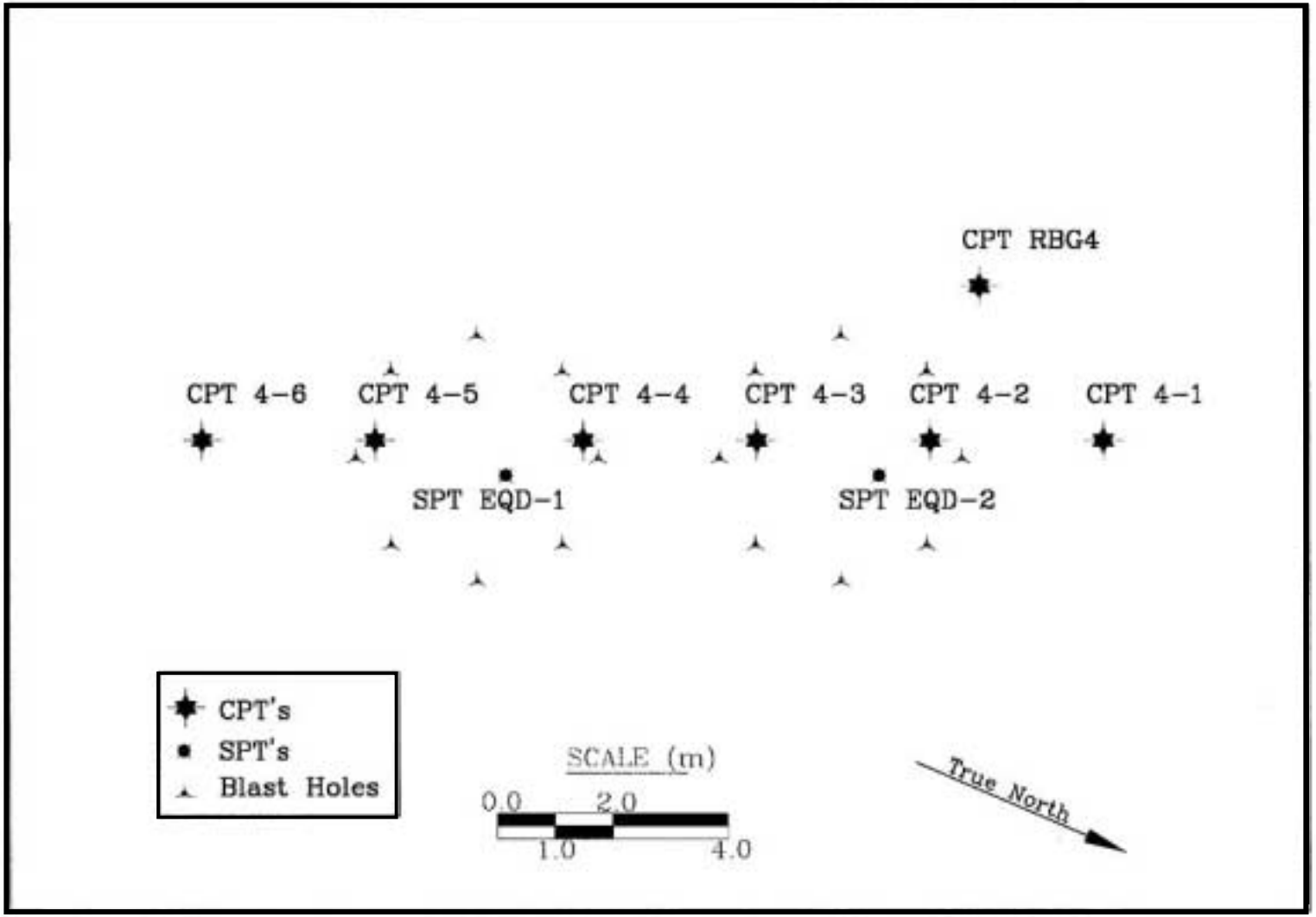

Figure 6.2 Plan view of E-Quake drain test site showing location of CPT and SPT holes relative to the blast hole locations.

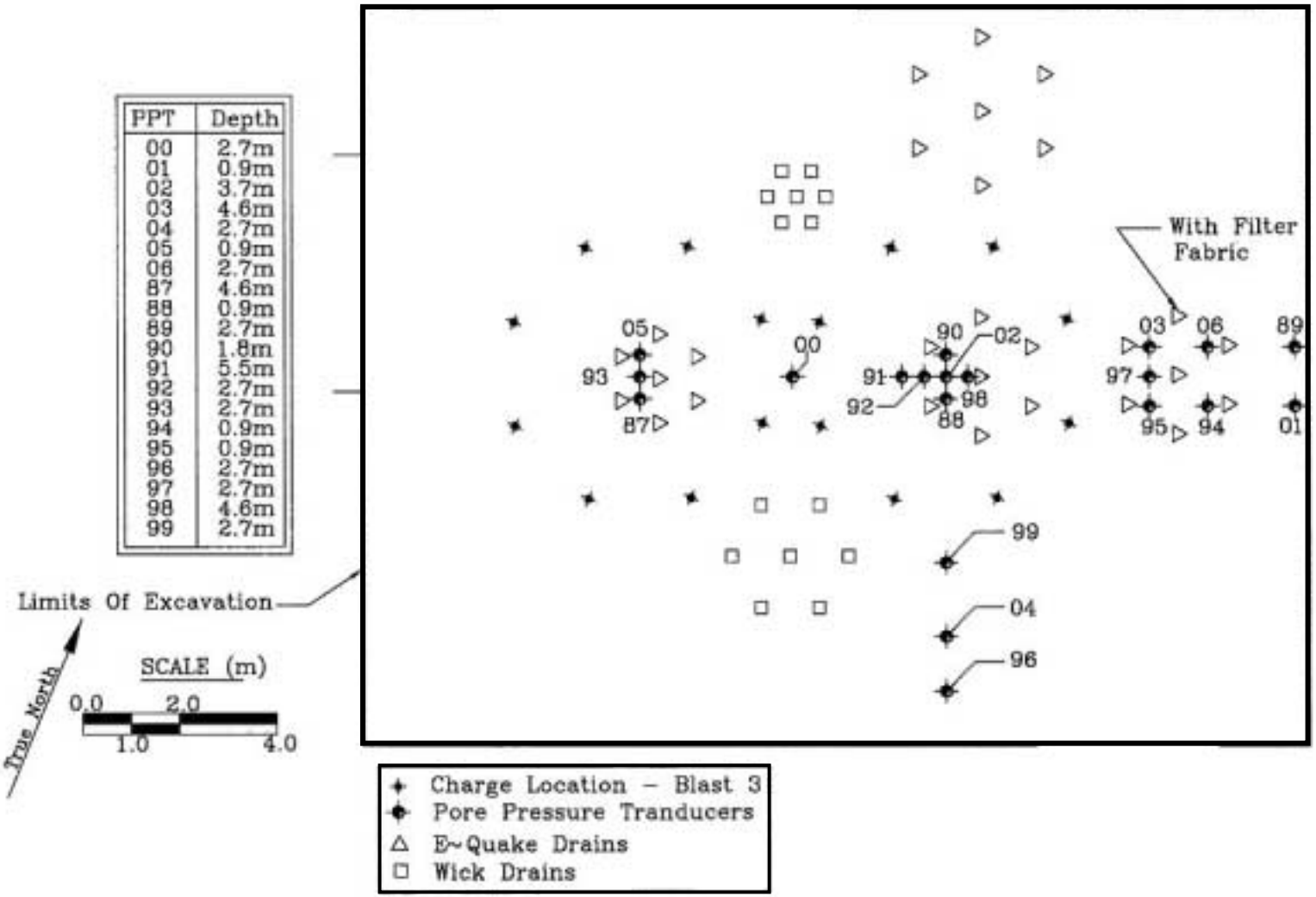

Figure 6.3 Plan view of pilot liquefaction test site showing location of E-Quake drain and wick drain clusters relative to the transducers and blast holes.

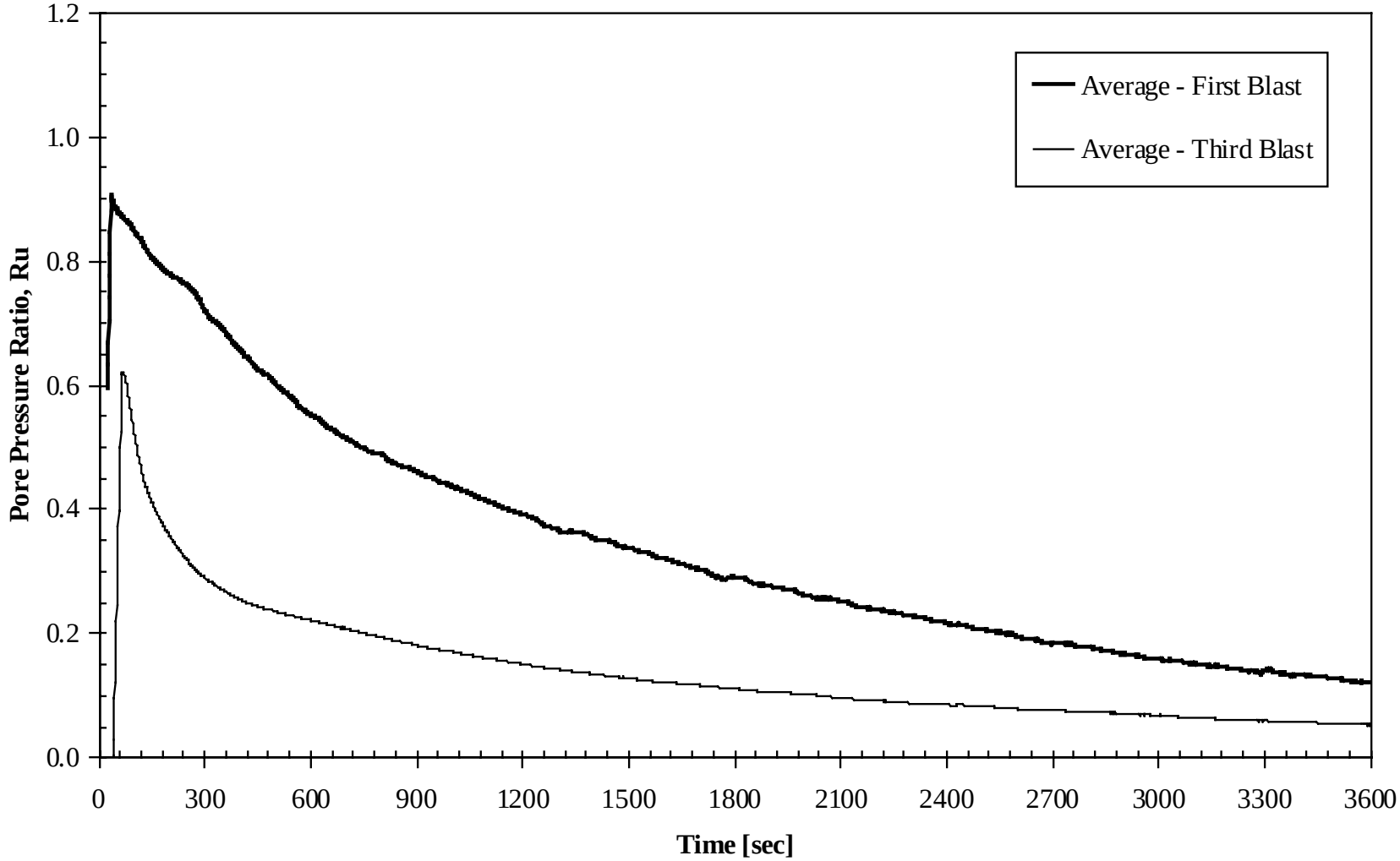

Figure 6.4 Average results from the first and third blasts recorded by the pore pressure transducers at a depth of 2.7m (9 ft).

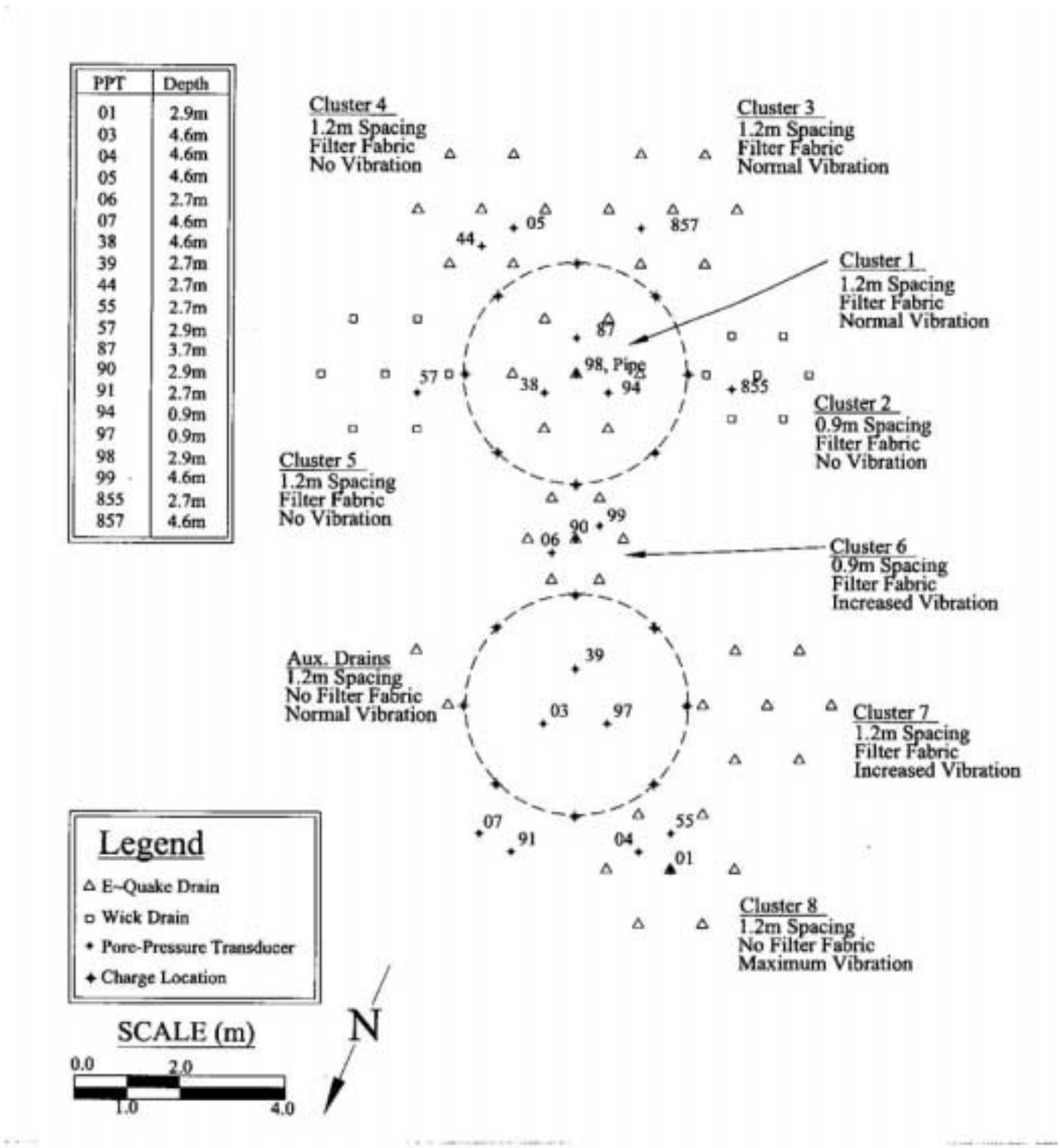

Figure 6.5 Plam view of E-Quake drain test site showing location of E-Quake drain and wick drain clusters relative to transducers and blast holes.

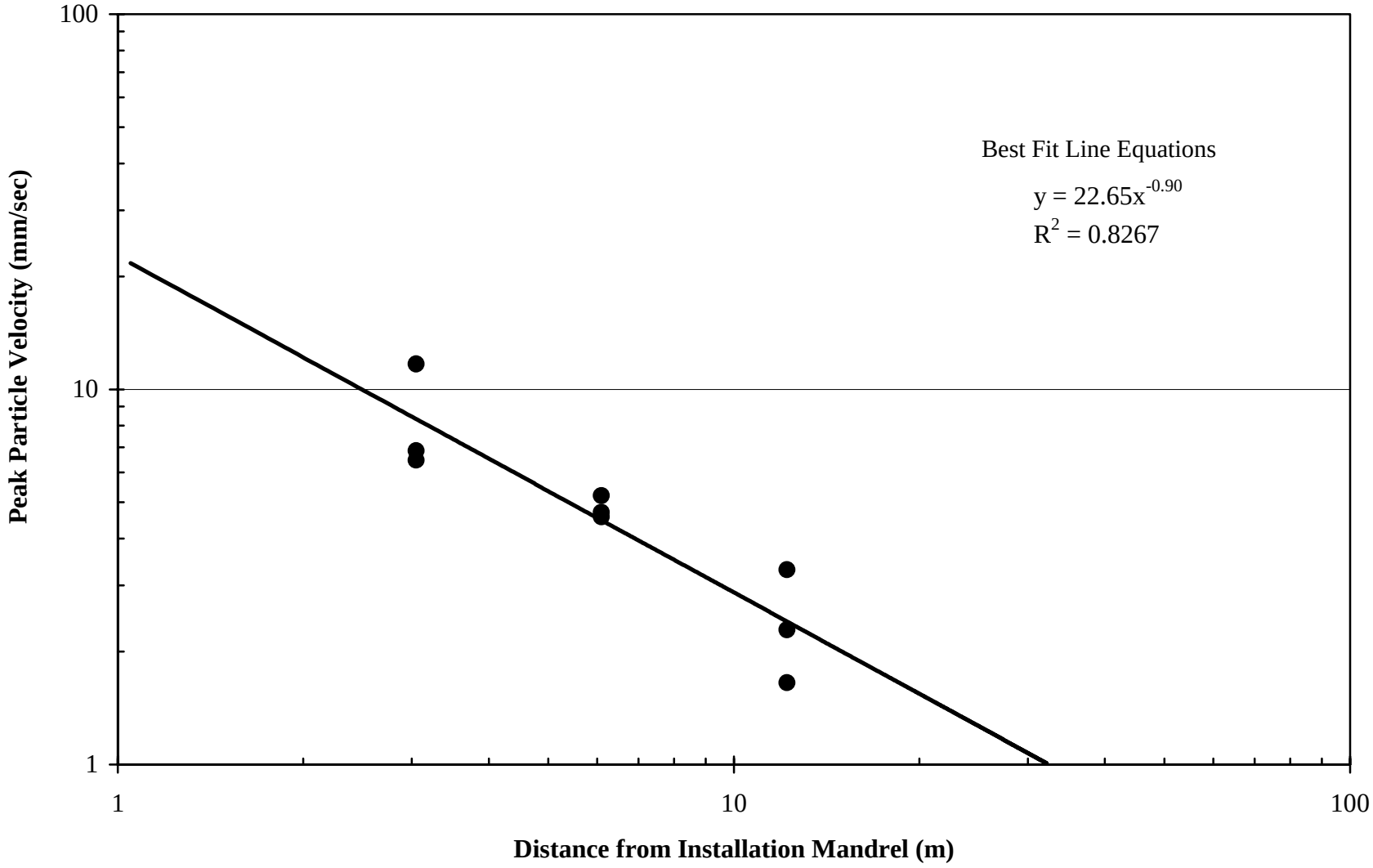

Figure 6.6 Vibration attenuation measured during installation of E-Quake drains.

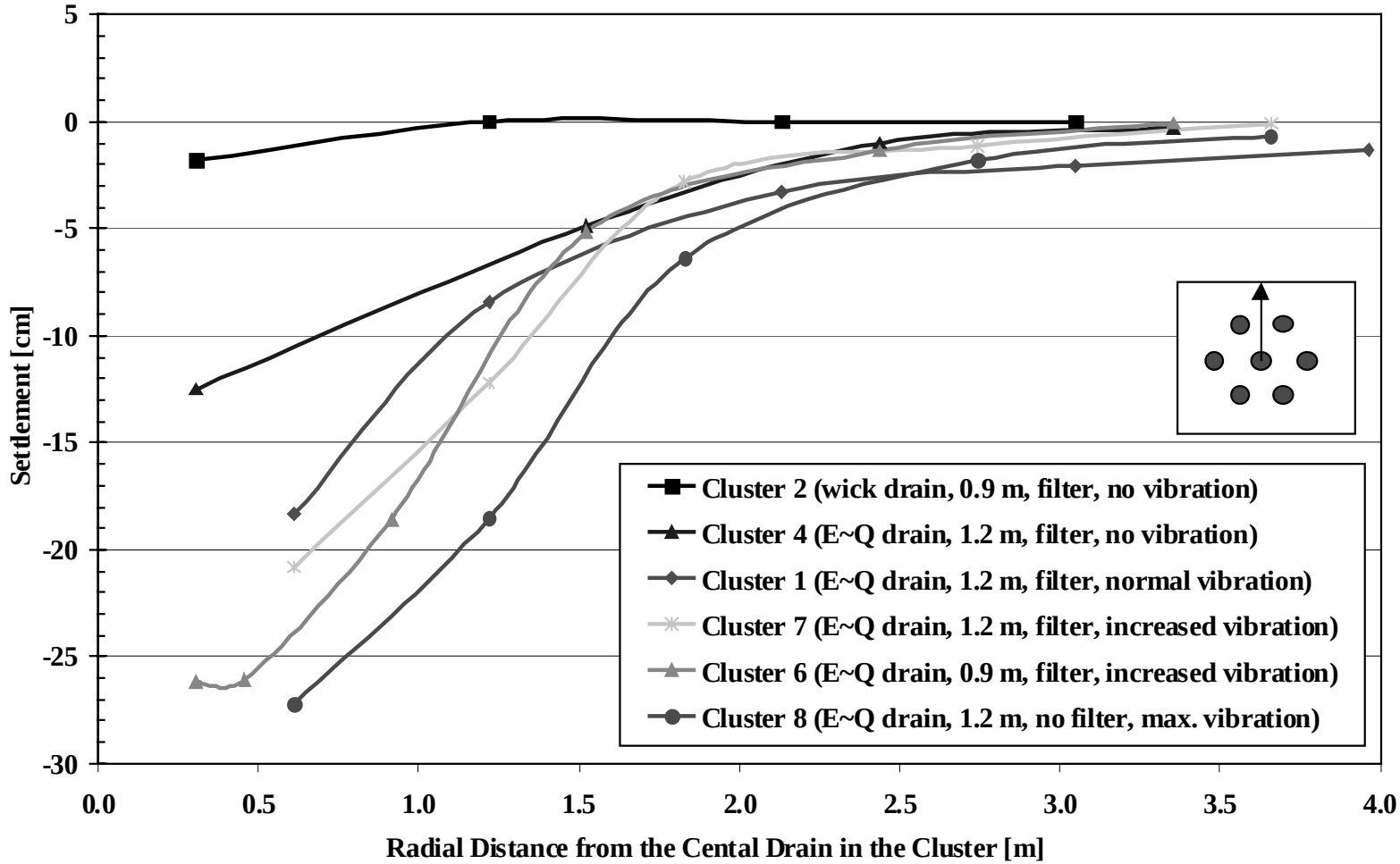

Figure 6.7 Installation-induced settlement profiles for each drain cluster at E-Quake drain site.

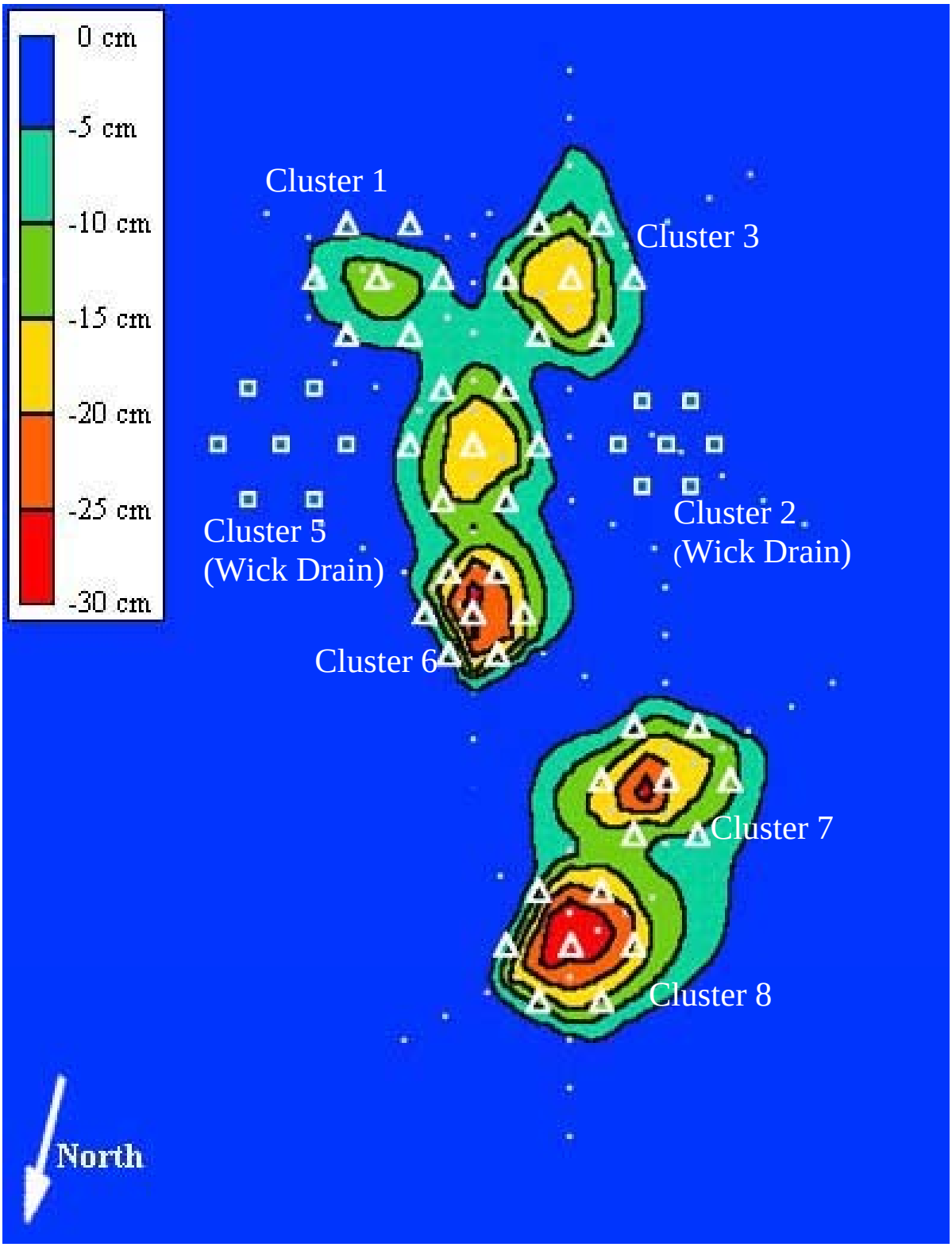

Figure 6.8 Plan view of ground settlement due to installation of E-Quake and wick drains a the E-Quake drain site. (White triangles denote E-Quake drain locations, the white squares denote wick drain locations and the gray dots denote elevation stakes.)

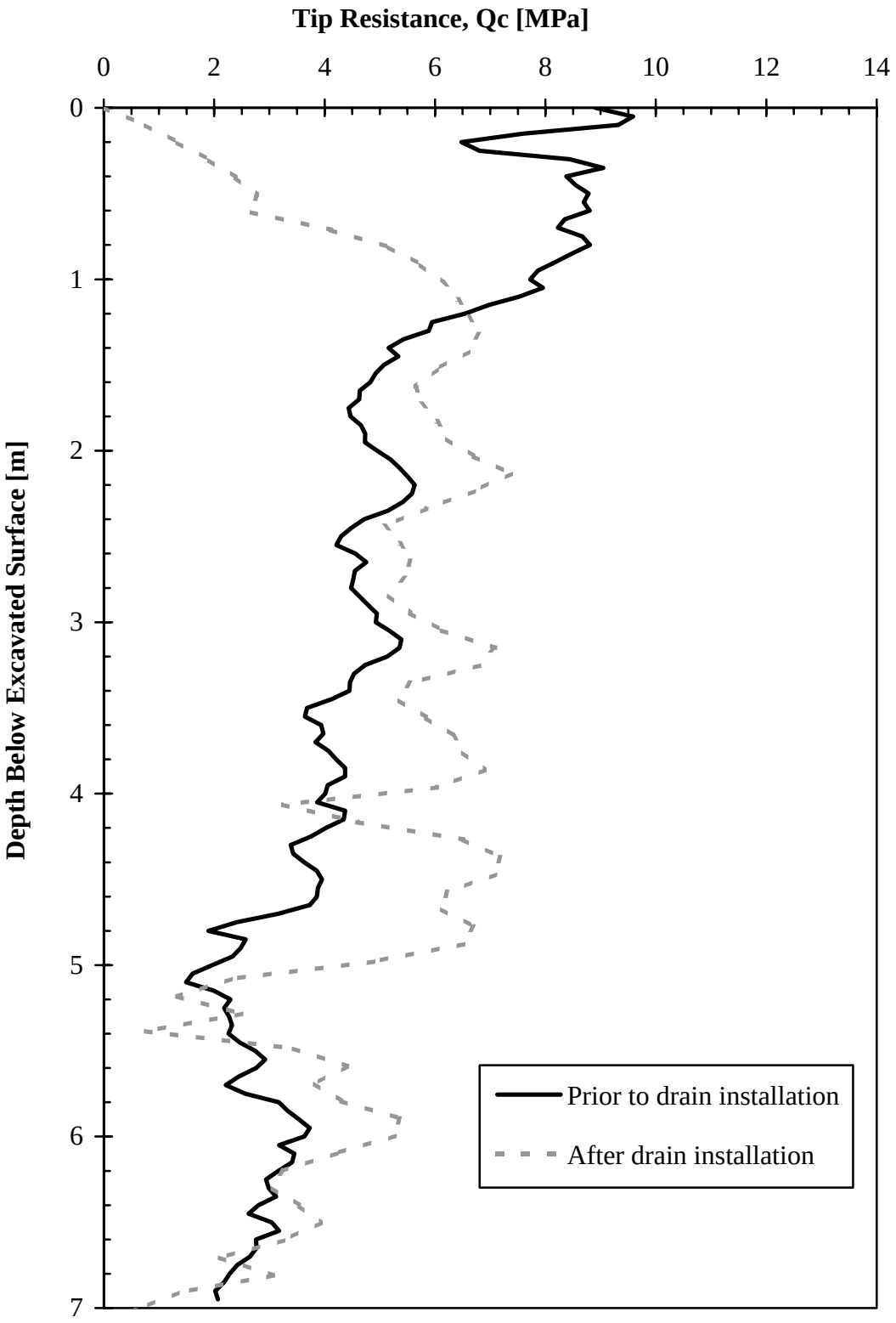

Figure 6.9 Comparison of measure cone tip resistance, q_c, prior to and one week following installation of E-Quake drains.

Figure 6.10 High rate of flow out of south auxiliary drain shortly after blasting occurred.

Figure 6.11 Water dyed blue flowing out of the center drain of Cluster 8 (E~Q drain, 1.2 m, no filter, max. vibration).

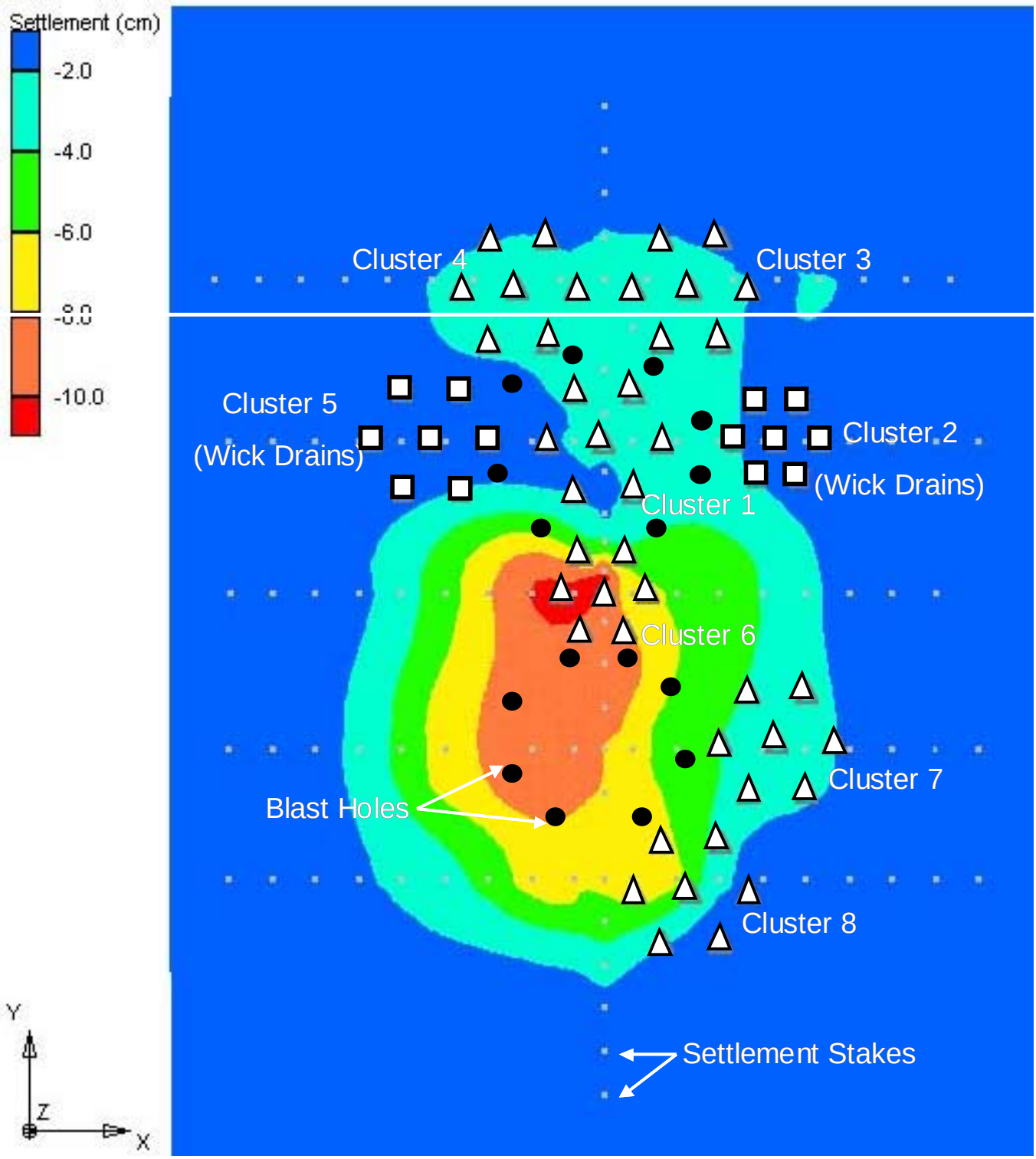

Figure 6.12 Contours of ground settlement due to blasting at the E-Quake drain site. (Triangles indicate E-Quake drain locations and squares indicate wick drain locations.)

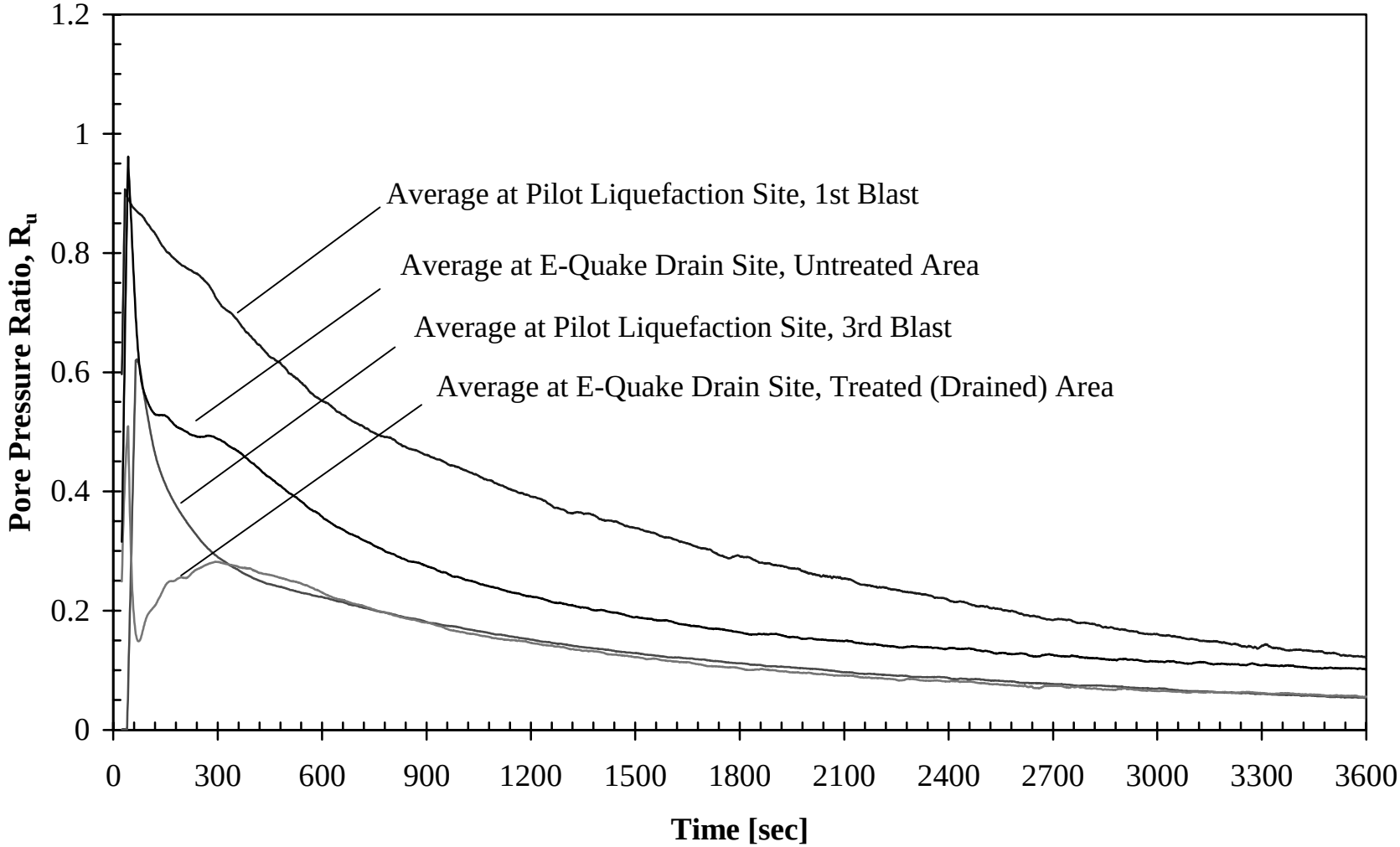

Figure 6.13 Comparison of dissipation rates measured by transducers at a depth of 2.7 m (9 ft) at pilot liquefaction and E-Quake drain sites.

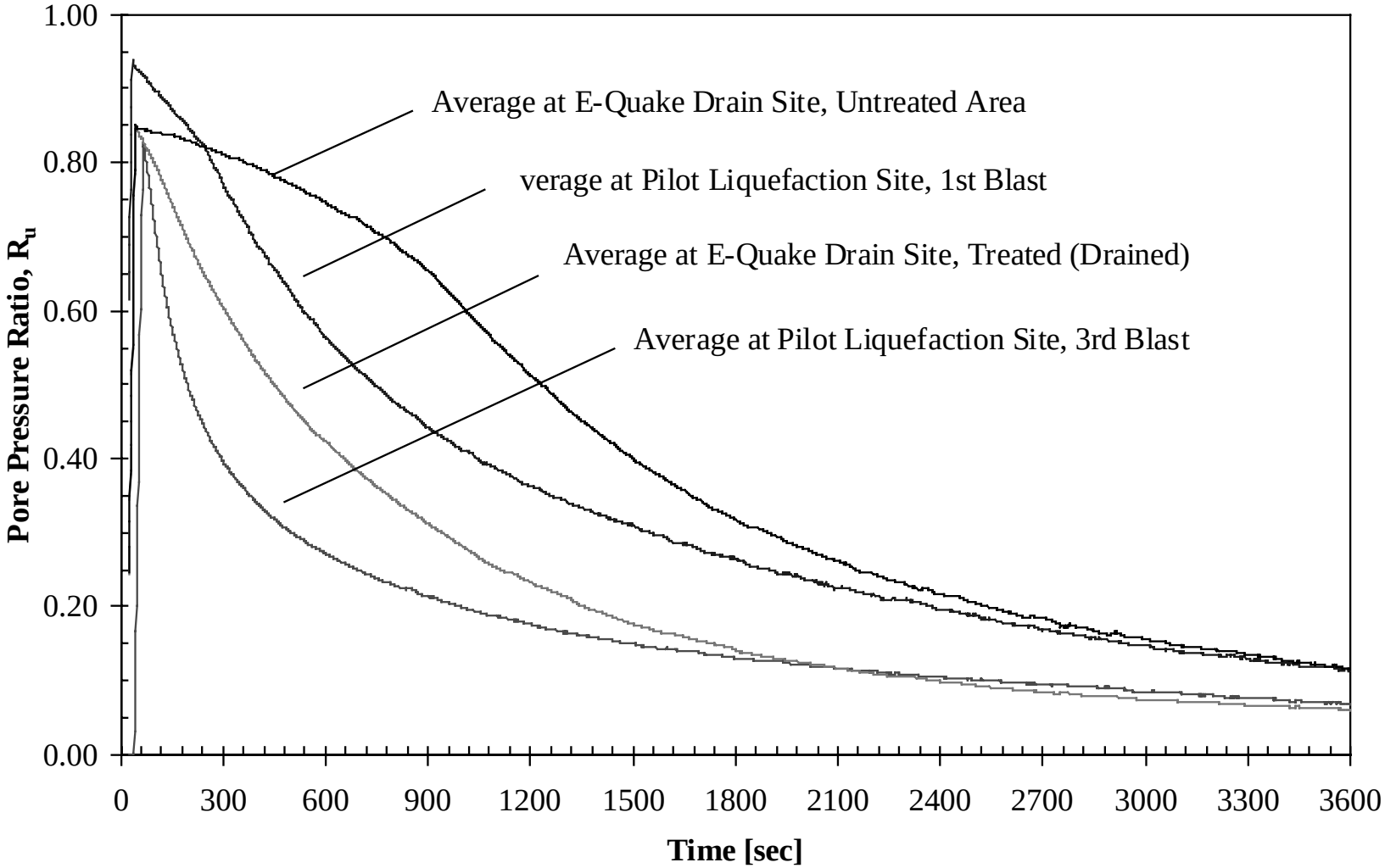

Figure 6.14 Comparison of dissipation rates measured by transducers at a depth of 4.6 m (15 ft) at pilot liquefaction and E-Quake drain sites.

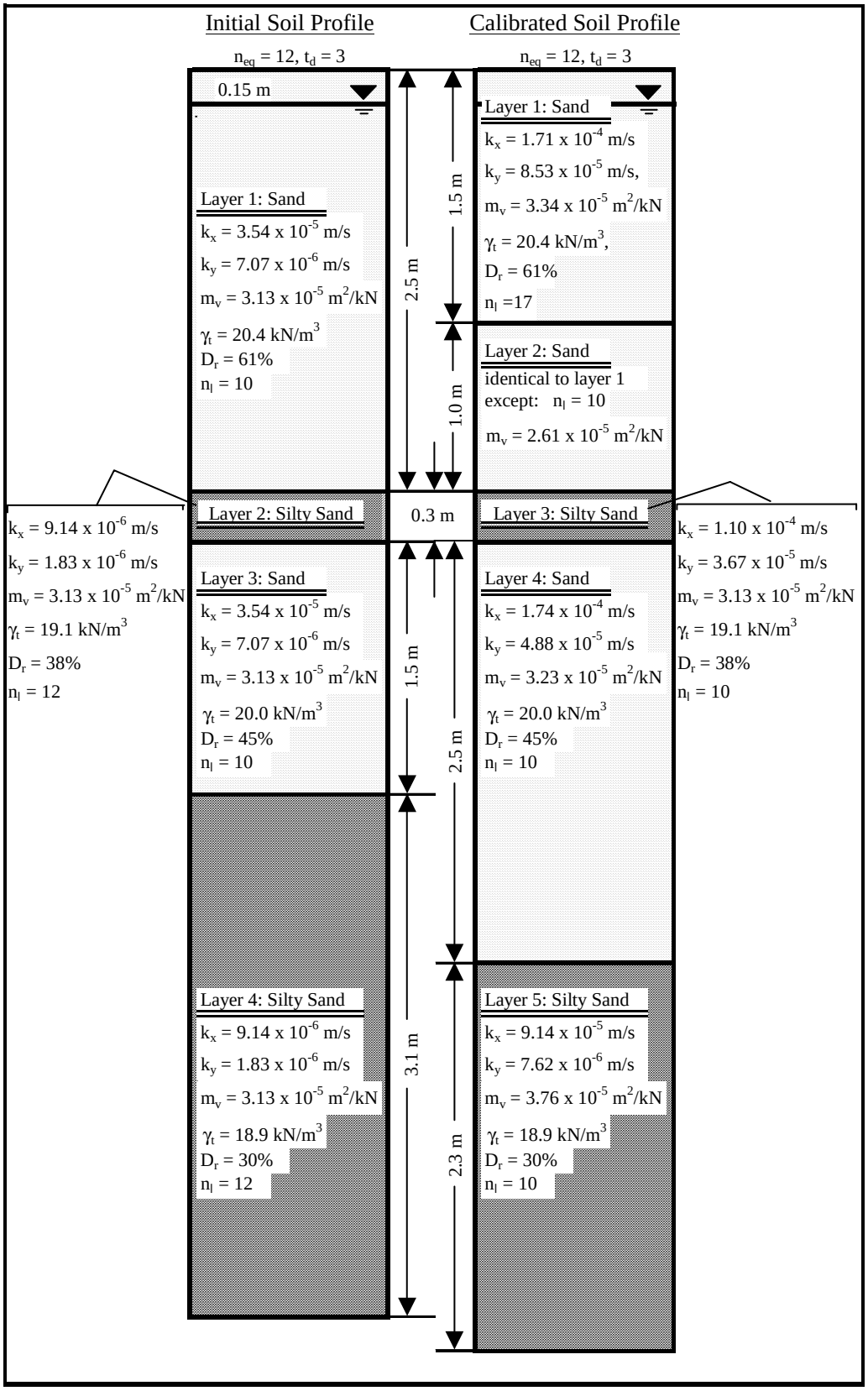

Figure 6.15 Soil profiles and properties used in numerical model for pilot liquefaction site.

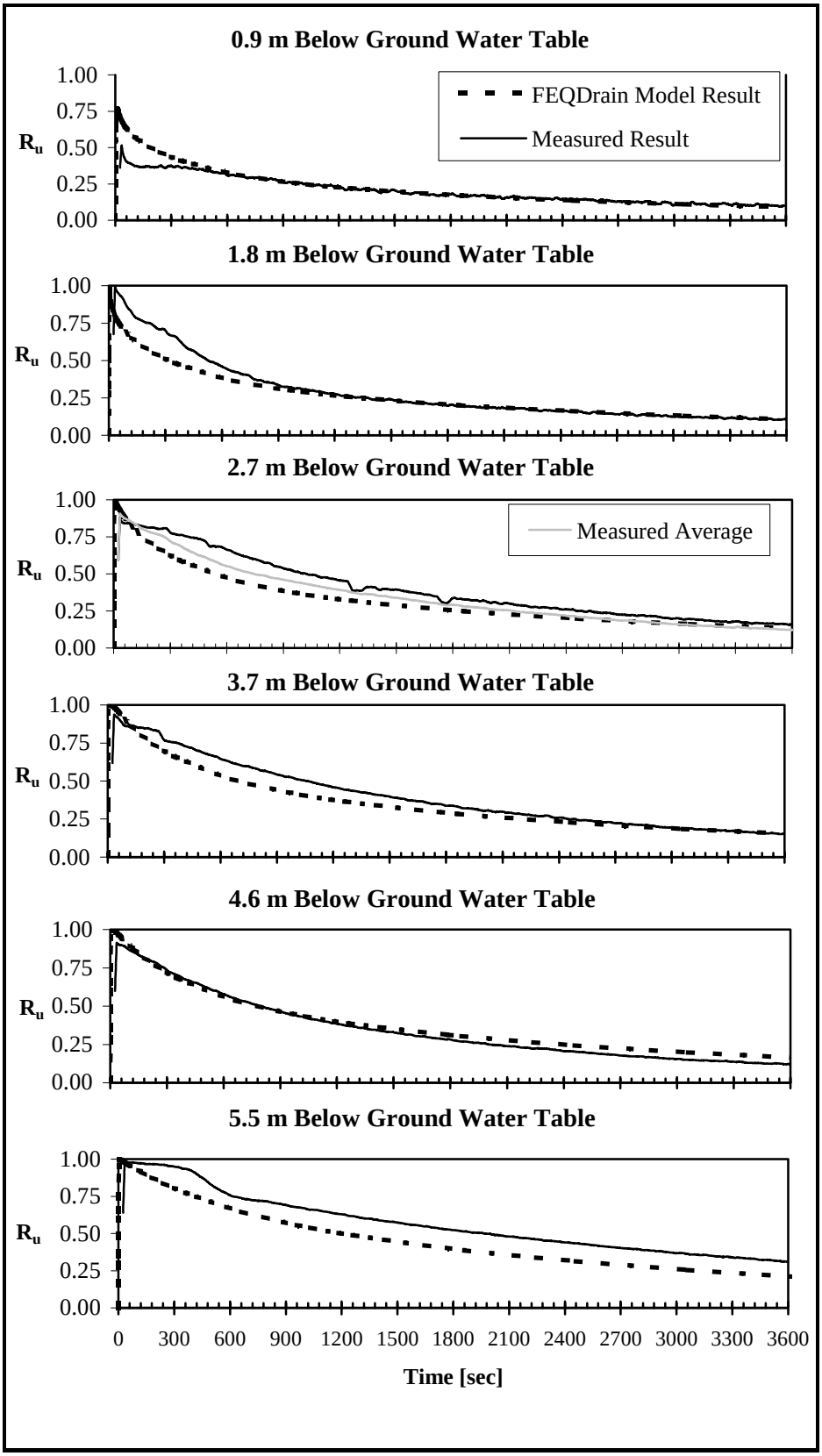

Figure 6.16 Comparison of measured and computed R_u time histories at pilot liquefaction site.

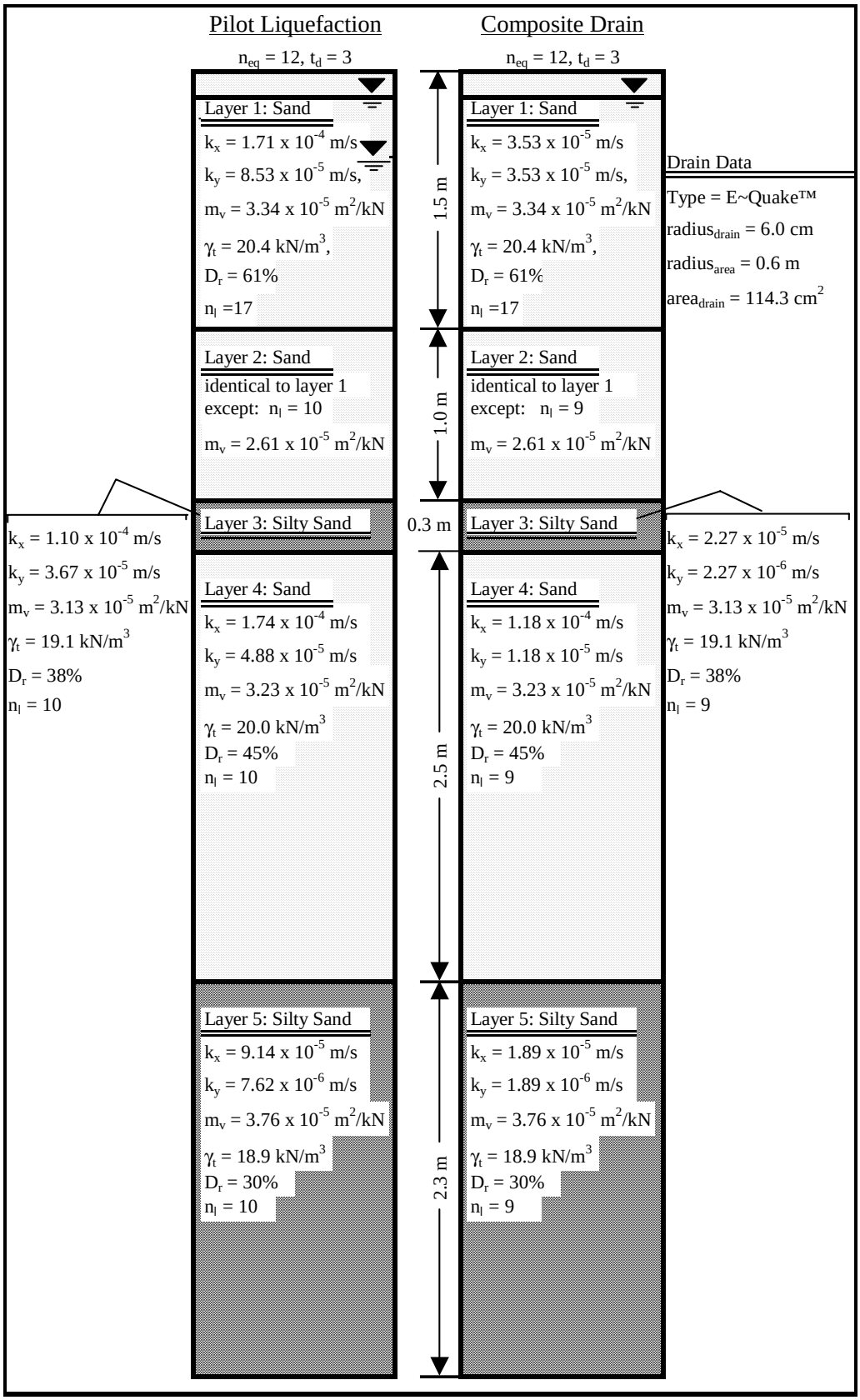

Figure 6.17 Soil profiles and properties for pilot liquefaction and composite drain models used in FEQDrain computer program.

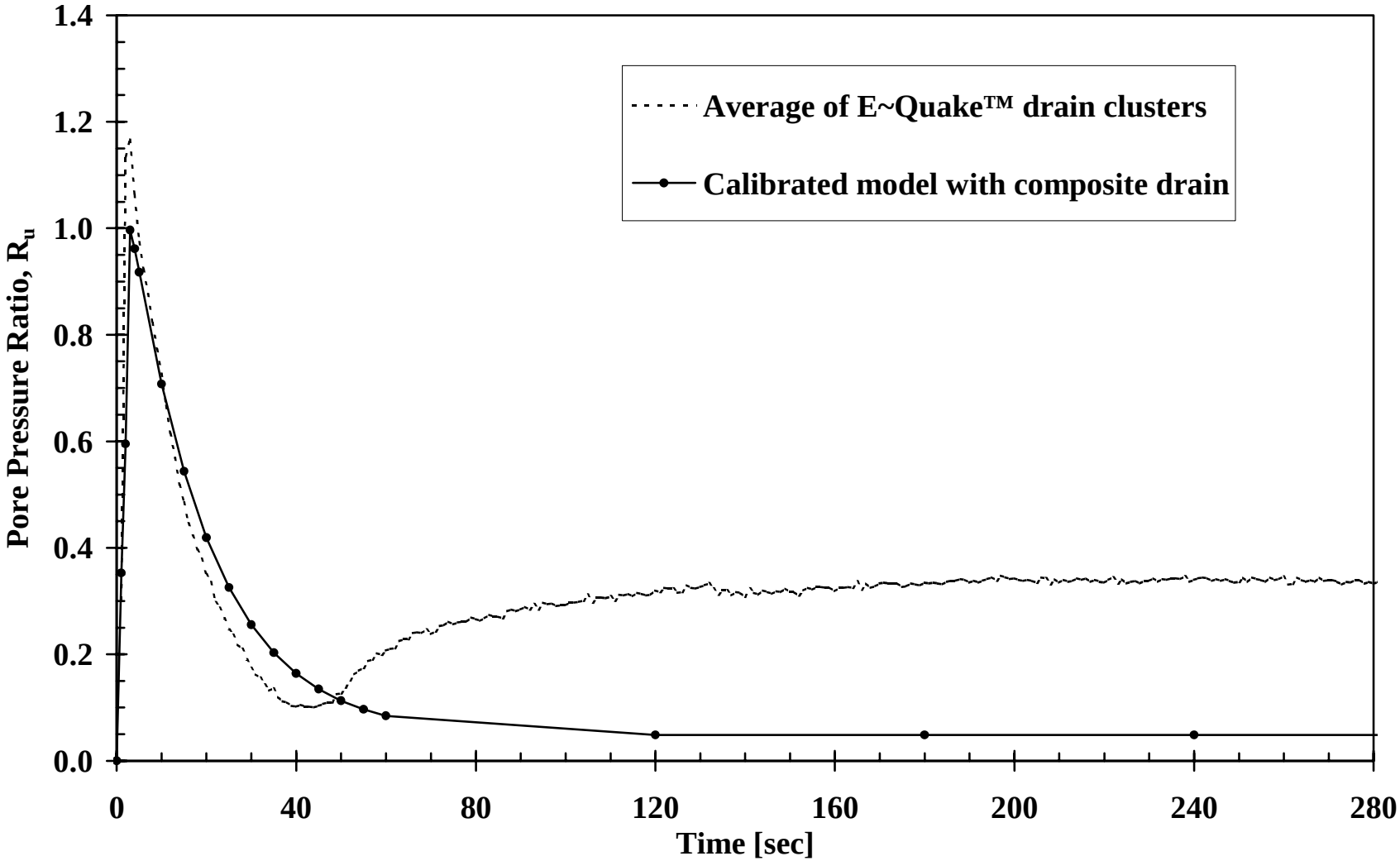

Figure 6.18 Comparison of measured and computed R_u time histories for composite drain model at E-Quake drain site.

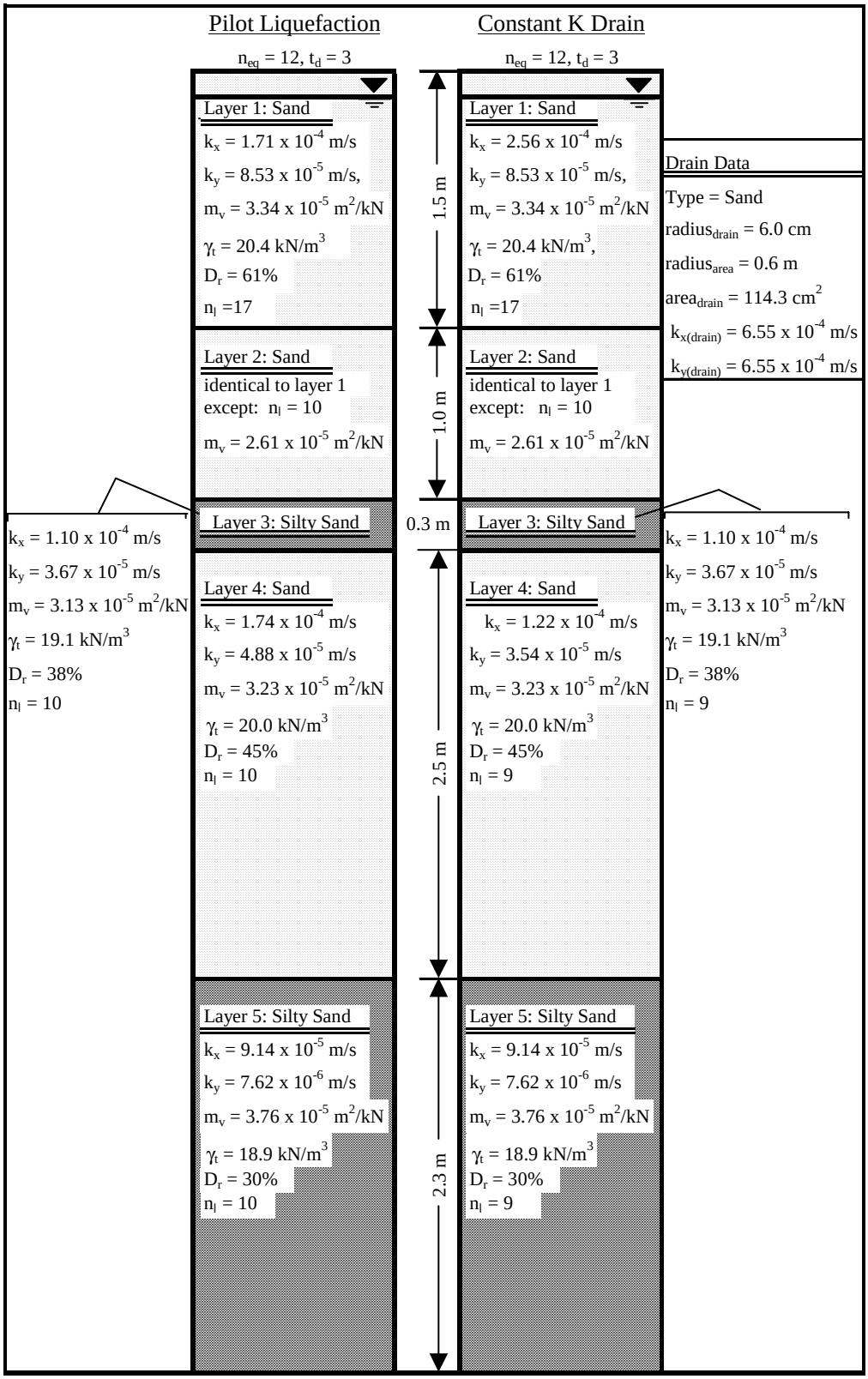

Figure 6.19 Soil profiles and properties for pilot liquefaction and constant hydraulic conductivity drain models used in FEQDrain computer program.

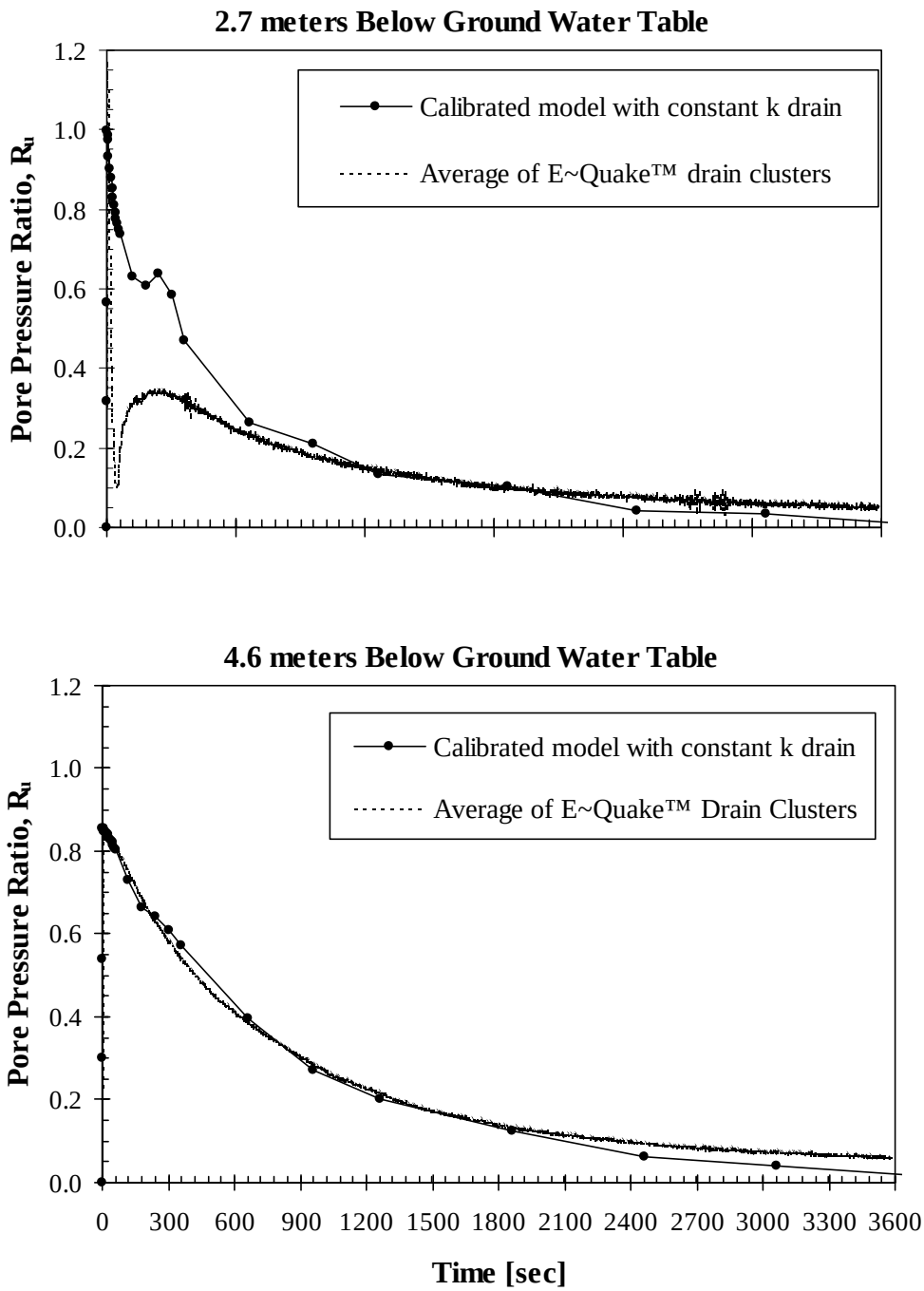

Figure 6.20 Comparison of measured and computed R_u time histories using constant hydraulic conductivity drains at E-Quake drain site.

7 ANALYSIS OF CISS PILES

P-y curves represent the soil resisting force per unit length of pile as a function of soil displacement and are typically used to model soil behavior in soil-pile interaction problems. A number of full-scale tests have been conducted where *p-y* curves were back-calculated from strain gauge data for non-liquefied soils (i.e. Matlock 1970, Reese *et al.* 1974, and Reese *et al.* 1975). *P-y* curves have also been back-calculated recently for liquefied soils using model test results (i.e. Wilson *et al.* 2000 and Adachi *et al*. 2000). However, *p-y* curves for liquefied soils based on full-scale tests have not been reported. This chapter presents the *p-y* curves back-calculated from the full-scale tests for the CISS piles after a brief explanation of the methodology used for the calculations. In addition, a more detailed review and discussion of the pore pressure data is presented which assists in interpreting the soil behavior and *p-y* response.

Studies using small scale centrifuge and shake table tests to investigate soil-pile interaction in liquefiable soils have previously been conducted; however, practitioners have been hesitant to accept the validity of these test results without full-scale testing to provide verification. Additionally, published results of back-calculated *p-y* curves from these tests are rare, leaving a void in understanding concerning how much resistance can be expected during liquefaction. A recent study where *p-y* curves were back-calculated from centrifuge tests were reported by Wilson *et al*. (2000). This chapter presents a comparison between the *p-y* curves back-calculated from the Treasure Island tests with the *p-y* curves back-calculated from the centrifuge test.

When analyzing pile response in liquefied sands, many engineers use simplistic methods for estimating the soil response. Simplified methods for estimating liquefied

soil behavior have been suggested by Liu and Dobry (1995) and Wang and Reese (1998). These methods incorporate the use of standard non-liquefied soil *p-y* curves which are modified to account for the reduced resistance provided by liquefied sand. This chapter presents the *p-y* curves calculated using these simple methods compared to the back-calculated *p-y* curves from the 0.6-m and 0.9-m diameter CISS pile tests. Additionally, the modified *p-y* curves are used to predict the measured test results from Treasure Island. Based on comparisons between the various *p-y* curves and subsequent analyses using those curves, implications for the design of piles and pile supported structures at sites where liquefaction is a potential seismic hazard are discussed.

7.1 Methodology for Back-Calculating p-y Curves

Basic beam theory was used to back-calculate the lateral soil resistance which developed along the length of the CISS piles, as well as the associated soil displacements, during the cyclic loading tests. Strain gauges attached to the CISS piles were utilized extensively to back-calculate the *p-y* curves. The first step taken was to calculate the curvature along the length of the pile. The curvature data is essential in back-calculating both the soil displacement as well as the soil reaction. The following equation shows the relation between measured strain and curvature:

$$\phi = \frac{\varepsilon_n - \varepsilon_s}{h} \tag{7.1}$$

where ϕ is curvature, ε is strain with n and s representing locations on opposite sides of the pile, and h is the distance between strain gauges at a specified depth. Once the curvatures were calculated, both soil displacement and soil reaction could be estimated.

7.1.1 Soil Displacement

Soil displacements were estimated using the following procedure. A polynomial interpolation function was fit to the curvature data, then integrated along the length of the pile twice to obtain the pile displaced shape as shown in the following equation:

$$y = \int \left(\int \phi(z) dz \right) dz \tag{7.2}$$

where y is the pile displacement and ϕ is a polynomial function that was fit to the discrete curvature data. For the purpose of calculating the *p-y* curves, the calculated pile displacement was assumed to be equal to the soil displacement.

7.1.2 Moment Curvature Analyses

In order to estimate the soil resistance developed during lateral load testing, the moment along the length of the pile was required. Moments were calculated using a moment-curvature relationship for the CISS pile cross sections. A number of moment-curvature analyses were performed to quantify the effect of bonding between the steel shell and concrete on the stiffness of the pile. This was accomplished using a computer program developed at the University of California, San Diego (Smith *et al.*, 1994). A comparison was made between the moment calculated by multiplying the lateral force from the actuator by the distance from the load point to the ground surface, and the moment obtained by multiplying the pile stiffness from the moment-curvature analysis by the pile curvature. This comparison indicated that the use of full bonding between steel shell and concrete adequately modeled the pile behavior during the tests.

A review of the curvature data indicates that both piles remained in the elastic range during the cyclic loading after the first blast. Maximum curvatures were 4.65E-03

radians per meter (rad/m) and 3.94E-03 rad/m for the 0.6-m and 0.9-m CISS piles, respectively. The moment curvature relationship for the 0.6-m and 0.9-m CISS pile is shown in Figure 7.1. In addition, the maximum curvature measured during testing is shown along with the pile stiffness used to calculate the moments.

7.1.3 Soil Reaction

Having obtained the moments along the length of the pile, the soil resistance was back-calculated by double differentiating the moment data with respect to depth using the following relationship:

$$p = \frac{d^2}{dz^2} M(z) \tag{7.3}$$

where p is the soil reaction per unit length of pile, z is depth, and M is moment.

Three numerical methods were tried when back-calculating the soil reaction from the moment data. These methods included the weighted residual method (Wilson, 1998), finite difference formulas from quadratic interpolation, and differentiating polynomial interpolation functions. The relative benefit of one numerical method over another appears to be dependent on the data set being differentiated.

Figure 7.2 presents moment data obtained from the 0.6-m CISS pile test with a fitted polynomial interpolation function as well as the soil reaction back-calculated using the three numerical methods previously mentioned. A review of Figure 7.2 shows the polynomial interpolation function provides a good fit to the moment data. A comparison of the back-calculated soil reactions show significant difference according to the numerical technique used. There are oscillations in the soil reactions computed using the

weighted residual and finite difference formulas in the upper section of the pile. The calculated shear versus depth shows that changes in slope from point to point in the moment data result in oscillations in the calculated shear. These oscillations are magnified even further upon differentiating a second time. The three methods are in reasonable agreement below a depth of 4 m where the number of data points decreases. Based on results such as those shown in Figure 7.2, polynomial interpolation functions fitted to the moment data appeared to provide the most reasonable estimate of soil resistance for the data acquired from the Treasure Island CISS pile tests.

7.1.4 Modification to Curvature Data

During the lateral load testing of the 0.6-m and 0.9-m CISS piles, a permanent offset in displacement occurred along the length of the pile. The offset appears to be the result of gaps behind the pile being filled during loading. Therefore, as the pile was being unloaded the soil behind the pile provided resistance prior to the pile reaching the point of zero displacement. As a result, at zero load there was some curvature along the length of the piles. When back-calculating the *p-y* curves, the curvature along the pile at zero load was subtracted from the curvature profile at subsequent loads. This modification allowed for implementing the back-calculated *p-y* curves in simple push-over type analyses independent of previous loading history.

7.2 0.6-m CISS Pile p-y Curves

P-y curves were back-calculated for the 0.6-m CISS pile for the pre-blast load test, as well as for the loading portion of six post-blast cycles representative of various

stages of pore pressure dissipation. The back-calculated *p-y* curves are presented and discussed in the following section.

7.2.1 Pre-Blast p-y Curves

A comparison of *p-y* curves back-calculated from the pre-blast load test with *p-y* curves obtained using the API criteria are presented in Figure 7.3. There is a significant difference between the back-calculated *p-y* curve at a depth of 0.2 meters (below the ground surface) compared with the API curve. The back-calculated *p-y* curve has a greater initial stiffness and a greater ultimate resistance. The difference is likely due to the design equations being directly proportional to the effective overburden pressure while neglecting the effects of cohesion and cementation, which may have been present. At depths greater than 0.2 meters, the initial stiffness and ultimate resistance of the back-calculated *p-y* curves generally compares well with the API curves.

The API and back-calculated *p-y* curves were implemented in a lateral load analysis to compare measured and predicted pile response and is shown in Figure 7.4. Although there are differences between the back-calculated and API *p-y* curves, both sets of *p-y* curves provide a reasonable estimate of the load versus displacement response at the pile head, as shown in Figure 7.4a. A comparison of moment versus depth at three load levels shows that the API *p-y* curves tend to overestimate the maximum moment. The moments predicted using the back-calculated *p-y* curves compare well with the measured results, as expected. A good comparison between predicted and measured results indicate the back-calculated *p-y* curves reasonably estimate the soil response. Although there are differences between the back-calculated and API *p-y* curves, the API

curves appear to provide a reasonable estimate of pile behavior under drained lateral loading conditions.

7.2.2 Excess Pore Pressure Ratio's Adjacent to 0.6-m CISS Pile

Excess pore pressure ratios at various depths adjacent to the 0.6-m CISS pile for six load series are presented in Figure 7.5. These pore pressure ratios are from the point in time where there was zero load on the pile, just prior to the cycle for which the *p-y* curve was back-calculated. This figure shows that the blasting was more effective in increasing the pore pressure ratios at the blast level (3.0 meters) and deeper. The maximum excess pore pressure ratio occurred at approximately 4.0 meters below the ground surface. The excess pore pressure ratios show that pore pressures dissipated at a faster rate at the greater depths. The faster dissipation of pore pressures at greater depths has also been noted in some centrifuge and shake table tests. The average pore pressure ratio for each load series where *p-y* curves were back-calculated are 83%, 73%, 62%, 53%, 41%, and 35% for load Series 1, 2, 4, 6, 8, and 10 respectively.

7.2.3 Post-Blast p-y Curves

P-y curves were back-calculated for representative cycles of post-blast loading Series 1, 2, 4, 6, 8, and 10 to investigate the soil and pile response at different excess pore pressure ratios. The representative cycles are shown in relation to the entire series in Figures 7.6 through 7.8. The back calculated *p-y* curves are presented in Figure 7.9

During the first loading series when the average excess pore pressure ratio adjacent to the pile was 83%, the *p-y* curves initially show no resistance at displacement levels as great as 50 mm for the 7th cycle at the 225-mm displacement level. The pile

displacement necessary for the soil to provide some resistance decreases with depth to almost zero below 5.3 m. There were two possible contributing factors to this zone of zero resistance: the formation of a gap and cyclic degradation of the soil. These two effects are shown in Figure 7.10 through a comparison of *p-y* curves back-calculated for the initial 75 mm pile head displacement cycle after the blast and subsequent loading cycles with a maximum pile head displacement of 225 mm. Gapping at the ground surface was noticed prior to the formation of sand boils, but once water began flowing out of the ground, gapping could not be observed and gapping was not a parameter measured during testing.

After *p-y* curves were back-calculated for representative cycles in each load series, an analysis was performed to verify that the back-calculated *p-y* curves can be used to reasonably model the pile response. Results of the analysis and test results for the first load series are compared in Figure 7.11. This was an important step in the process of back-calculating the *p-y* curves since it was observed that various techniques for differentiating the moment data can result in large variations in soil resistance.

7.3 0.9-m CISS Pile p-y Curves

7.3.1 Pre-Blast p-y Curves

A comparison of *p-y* curves back-calculated from the pre-blast load test with *p-y* curves obtained using the API criteria are presented in Figure 7.12. As with the *p-y* curves back-calculated from the 0.6-m CISS pile test, there is a significant difference between the back-calculated *p-y* curve at a depth of 0.2 meters below the ground surface compared with the API curve. The back-calculated curve has a greater initial stiffness

and a greater ultimate resistance. At depths greater than 0.2 meters, the initial stiffness of the back-calculated *p-y* curves generally compares well with the API curves. At depths greater than 2.3 meters, the differences between the API and back-calculated *p-y* curves increases with the API *p-y* curves providing greater resistance.

The API and back-calculated *p-y* curves were implemented in a lateral load analysis to compare measured and predicted pile response and is shown in Figure 7.13. Similar to the 0.6-m CISS pile analysis, the API *p-y* curves provided reasonable estimates of the load-displacement and moment-depth response of the pile. As expected, the analysis with the back-calculated *p-y* curves results in a good comparison between measured and computed pile response. From a designers viewpoint, the standard *p-y* curves appear to be adequate for static analyses of CISS piles, at least up to 0.9 m in diameter as tested at Treasure Island.

7.3.2 Excess Pore Pressure Ratio's for 0.9-m CISS Pile

Excess pore pressure ratios at depths up to 4.6 m below the ground surface adjacent to the pile are presented in Figure 7.14. The pore pressure ratios are from the time when zero load was applied to the pile, just prior to the cycle for which the *p-y* curves were back-calculated. Immediately, it can be seen that blasting was more effective at inducing liquefaction at the 0.9-m CISS pile site. Excess pore pressure ratios of 100% were recorded at depths near 1.0 and 2.0 meters for a significant portion of the testing. This may be due to a higher groundwater table and the effect pile diameter had on the pore water pressure near the pile. Similar to the 0.6-m CISS pile site, the pore pressures dissipated more rapidly at greater depths. The average excess pore pressure

ratio for loading Series 1, 2, 4, 6, 8, and 10 are 97%, 95%, 93%, 90%, 88%, and 81% respectively.

The decrease in excess pore pressure during testing was less severe for the 0.9-m CISS pile test when compared to data from the 0.6-m CISS pile. At the end of lateral load testing, the average excess pore pressure ratio for the 0.9-m CISS pile test was approximately twice that at the end of the 0.6-m CISS pile test. Pore pressures generally dissipated between each loading series, with the exception near the ground surface where the excess pore pressure ratio remained near 100% during most of the testing.

7.3.3 Post-Blast p-y Curves

P-y curves were back-calculated for representative cycles during post blast-Series 1, 2, 4, 6, 8, and 10 to investigate the soil and pile response at the different excess pore pressure ratios. Figure 7.15 through 7.17 presents the load versus displacement data indicating the cycle for which the *p-y* curves were back-calculated. The back-calculated p-y curves are shown in Figure 7.18.

A review of the back-calculated *p-y* curves show a general increase in soil stiffness for each loading series, although the average excess pore pressure adjacent to the pile does not consistently and significantly decrease between each series. Figure 7.19 shows the excess pore pressure ratio adjacent to, and at a distance of 4.2 meters, from the 0.9-m CISS pile with time with a line indicating an envelope of the peak excess pore pressure ratio. A review of pore pressure data adjacent to, and at a distance of 4.2 meters from, the pile shows a more dramatic decrease in excess pore pressure between successive displacement cycles at the 4.2-meter distance. It appears that the pile significantly retarded the dissipation of pore water pressures at close distances. The soil

at greater distances from the pile may be providing the increased resistance due to the more rapid dissipation of excess pore pressures and subsequent increase in strength. At the lower displacement levels when the *p-y* curves provide little resistance, it is difficult to see a definite trend in the *p-y* stiffness between the loading series. As the pile displacement increases the general trend of increasing stiffness with each subsequent loading series prevails.

After *p-y* curves were back-calculated for each load series, an analysis was performed to verify that the back-calculated *p-y* curves provide a reasonable estimate of the pile response. Results of the analysis compared to measured test results are presented in Figure 7.20.

7.4 Comparison of 0.6-m and 0.9-m CISS Pile p-y Curves

A comparison between the *p-y* curves back-calculated from the 0.6-m and 0.9-m CISS pile tests provides insight into the effect of diameter on the *p-y* curve. Figure 7.21 shows the *p-y* curves back-calculated for post-blast Series 1 for both CISS piles. At a depth of 0.2 and 1.5 meters, the *p-y* curves are very similar. This, in part, is likely due to the excess pore pressure ratio at these shallow depths being greater for the 0.9-m CISS pile test than they were for the 0.6-m CISS pile test. At greater depths where pore pressure ratios for both tests ranged between 90 and 100%, the 0.9-m CISS pile *p-y* curves provide more resistance. Another significant difference between the *p-y* curves is that at depths of 2.3 meters and greater, it takes less displacement for the soil to provide resistance to the 0.9-m CISS pile compared to the *p-y* response for the 0.6-m CISS pile. For example, at a depth of 2.3 meters the soil began providing resistance to pile movement after 40 mm of displacement for the 0.6-m CISS pile test; whereas, only 20

mm of displacement were required for the soil to provide resistance for the 0.9-m CISS pile test. These results indicate that there may have been less gapping or that it takes less pile movement for larger diameter piles to induce a phase transformation resulting in dilatent soil behavior. The effect of pile diameter is further investigated in a detailed review of the pore pressure data.

7.5 Excess Pore Pressure Response

Immediately after detonation of the explosives, excess pore pressure ratios varied between 70% and 100% adjacent to the piles. A detailed review of excess pore pressure ratios provides information which reveals the nature of soil behavior in response to the laterally loaded piles. Specifically, the excess pore pressure ratios in front of the piles indicate that liquefied soils may provide significant resistance to pile movement as a result of a phase transformation and subsequent dilatent behavior.

Excess pore pressure ratios within 1.0 meter directly in front of the pipe pile and at a distance of 4.2 meters from the pile center are shown in Figure 7.22. Excess pore pressure ratios within 1 meter from the pile for the first load cycle with a maximum pile head displacement of 75 mm, increase until loading stops, and then decreases as the load is reduced. Subsequent cycles with maximum displacements of 150 mm or greater show an initial increase in excess pore pressure as the pile is pushed toward the piezometer. However, with continued pile displacement, the excess pore pressures begin to reduce until the peak pile displacement is reached. The reduction in excess pore pressure is the result of a phase transformation where the soil changes from contractive to dilative in behavior. As the pile is unloaded, excess pore pressures begin to increase initially and finally decrease again as the pile continues to be unloaded. At a distance of 4.2 meters

from the pipe pile, dilative behavior is not evident. This indicates that the 0.3-m pipe pile did not typically cause strains of large enough magnitude to cause a phase transformation at this distance.

Piezometers in front of the CISS piles were located 4.2 meters from the pile centers. In order to minimize soil disturbance in the loading zone, piezometers within 1 meter in front of the CISS piles were not installed. A detailed view of the excess pore pressure response for the CISS piles are shown in Figure 7.23 and 7.24. Again, the excess pore pressures ratios follow the same pattern as observed during the 0.3-m pipe pile test where the pore pressures initially increase as the pile is displaced toward the piezometer and then decrease as a result of a phase transformation. Dilative behavior was not noticeable at small pile displacements, as observed initially in Figure 7.23, and at greater depths shown in Figure 7.24. The dilative behavior is also less noticeable with each successive 225-mm displacement cycle indicating that a gap may have formed; therefore, the soil would experience less strain during subsequent cycles. The decrease in excess pore pressure resulting from a phase transformation is more apparent at a distance of 4.2 meter from the CISS pile tests compared to the 0.3-m pipe pile test indicating that as pile diameter increases, the zone of liquefied soil resisting pile movement increases.

The observed excess pore pressure response provides evidence that a phase transformation occurred directly in front of the laterally loaded piles in liquefied sand. The occurrence of a phase transformation of liquefied sand appears to be a significant factor in the soil providing resistance to laterally loaded piles. Previous research (e.g. Dobry and Abdoun, 1998) has shown that a phase transformation of liquefied sands reduces the displacements associated with lateral spreading as a result of increased

capacity of the soil to resist shear stresses. Similarly, a phase transformation will allow liquefied soils to provide increased resistance to foundation displacements. Previous work presented by Dobry and Abdoun (1998) and Kutter and Wilson (1999) explain that the phase transformation of liquefied sands is a result of acceleration spikes. Data from the full-scale lateral load tests show that the inertial loading of deep foundations also causes a phase transformation in liquefied sand. The observance of this dilative behavior in response to foundation movement is important in verifying models used to predict soil-pile interaction in liquefied sands.

In addition to observing the phase transformation in the liquefied sands, the excess pore pressure data provides information which assists in assessing our fundamental knowledge concerning liquefied soil behavior in response to cyclic pile movement. A detailed view of one loading cycle of the 0.3-m diameter pipe pile is shown in Figure 7.25 with a description of the fundamental soil behavior on the granular level. The loading cycle has been described at 5 points. Prior to cyclic loading the excess pore pressure ratio directly in front of the pile is approximately 90%, and the contact pressure between individual sand grains is very small at this point. As the pile is pushed into the soil, the soil begins to contract resulting in an increase in excess pore pressure and an even smaller contact pressure between sand grains. With increased pile displacement, the soil can not contract any longer, and the grains begin to slide up and over one another. During this phase of loading, the contact pressure between the sand grains increases and accounts for the resistance provided to pile movement. This dilative behavior continues until the maximum lateral load is reached. During the dilation phase, the slope of the loading curve begins to increase indicating the soil is providing increased

lateral resistance. When the pile is unloaded, the sand grains begin to slide back to a more stable configuration resulting in a reduction of pore volume and a subsequent increase in excess pore pressure. As the pile continues to be unloaded, the pore pressure begins to reduce again. The pore pressure reduction is a result of water draining from the soil matrix with the rate of drainage dependent on the hydraulic conductivity of the soil.

7.6 Centrifuge p-y Curves

A comparison of *p-y* curves back-calculated from centrifuge and full-scale tests are an essential part of validating small-scale testing methods. Wilson *et el.* (2000) presented back-calculated *p-y* curves in liquefying sand for a 0.67-m diameter pile based on centrifuge test results. The *p-y* curves back-calculated from the full-scale tests at Treasure Island are compared to the centrifuge and API *p-y* curves in Figure 7.26 at a depth of three pile diameters (1.8 meters). For purposed of comparison, the centrifuge *p-y* curves were slightly modified by adjusting the displacement so that both sets of *p-y* curves provided zero soil resistance at zero displacement.

A review of Figure 7.26 shows that both the centrifuge and full-scale *p-y* curves have the same basic shape with the slope of the *p-y* curve increasing with displacement. Both *p-y* curves show that liquefied soils can and do provide significant resistance to laterally loaded piles when compared to the estimated resistance using the standard API sand *p-y* curve. The significant difference between the two *p-y* curves is the level of displacement required to develop the soil resistance. It can be seen that the *p-y* curves back-calculated from the centrifuge test provide significantly more resistance compared to the full-scale *p-y* curves at the same displacement level. One of the possible reasons for the difference between the centrifuge and full-scale *p-y* curves is the difference in the

rate of pile loading. The centrifuge test was a dynamic test with the inertial loading of the pile occurring at a frequency of about 1 Hz (with the velocity of the pile movement in relation to the soil being as great as 300 mm/sec); whereas, the Treasure Island tests were conducted at a rate of about 0.04 Hz (with the velocity of the pile in relation to the soil being approximately 10 mm/sec). Therefore, if the soil provides a viscous reaction to the pile movement as suggested by Kagawa *et al*. (1995) and Yao and Kobayashi (1992), the centrifuge *p-y* curves should provide more resistance when compared to the Treasure Island *p-y* curves.

Soil properties may also be a reason for the difference in observed behavior. A fine, uniform, Nevada sand (C_u = 1.5, D_{50} = 0.15 mm) was used for the centrifuge testing; however, due to the centrifugal acceleration, the D_{50} would increase from 0.15 mm , which is a fine sand, to 4.5 mm in grain size which is a coarse sand. The smallest grain size for a gravel particle is 4.75 mm; therefore, almost 50% of the soil in the centrifuge test would be considered gravel due to scaling effects.

Another possible reason for the difference between the *p-y* curves is the formation of a gap during the full-scale tests. During the full-scale test, a gap between the pile and soil was noticed prior to the formation of sand boils, and is partially responsible for the zone of zero soil resistance at displacements as great as 50 mm near the ground surface. The occurrence of gapping is not apparent in the *p-y* curves back-calculated from the centrifuge test. Gapping may not have occurred during the centrifuge tests due to the pile being fully cycled as opposed to the half cycle loading performed during the Treasure Island Test. It was observed during the Treasure Island testing that soil had filled in some gaps behind the pile and significant force was required to pull the pile back towards

the initial position. In addition, the Treasure Island tests displaced the pile and soil through significantly larger displacements likely resulting in greater degradation of the soil.

Although there are differences between the full-scale and centrifuge *p-y* curves, the similarities between *p-y* shape and magnitude of soil resistance provide some validation of the centrifuge studies. The results presented in this section indicate that more full-scale and model tests are warranted to further clarify and quantify the factors controlling the *p-y* response in liquefied sand. Potential key factors effecting the *p-y* response brought to light through comparison of the full-scale and centrifuge *p-y* curves are the effects of viscous damping of the liquefied soil, the effect of soil particle size on soil behavior, displacement level and subsequent degradation of the *p-y* response, and the potential for gapping to occur in soils susceptible to liquefaction.

7.7 Modified p-y Curves

Currently, the state of practice in geotechnical engineering is to use a simple pushover analyses to estimate the capacity and response of laterally loaded piles. A number of software packages based on the finite difference or finite element method with the soil response represented by non-linear springs are typically used (e.g. LPILE and FLPIER). These programs incorporate standard methods for calculating *p-y* curves. However, a standard *p-y* model for liquefied sands has not been generally adopted by the profession for pushover type analyses. Therefore, researchers have proposed methods to modify the standard non-liquefied *p-y* curves to account for the reduced resistance provided by the liquefied sand. These procedures are briefly described along with a presentation of the modified *p-y* curves compared to the back-calculated *p-y* curves.

One simple method which has been used to account for the reduced resistance provided by liquefied sands is to multiply the API (1993) or Reese *et al*. (1974) sand *p-y* curve by a reduction factor (*p*-multiplier). This method was proposed by Liu and Dobry (1995) along with suggestions for calculating *p*-multiplier as a function of the excess pore pressure ratio. Wilson (1998) also proposed *p*-multipliers based on the initial relative density of the liquefiable sand. Based on the research conducted by Liu and Dobry (1995) and Abdoun et al. (1996), a *p*-multiplier of 0.1 was used to modify the standard API *p-y* curves for comparison with the *p-y* curves back-calculated from the Treasure Island testing. The recommendations proposed by Wilson (1998) based on centrifuge test results suggest using a *p*-multiplier between 0.25 and 0.35 for sands with a relative density of 55%. Since the liquefiable sands at Treasure Island typically had a D_r of 50%, a *p*-multiplier of 0.30 was also applied to the API curves for comparison with the back-calculated *p-y* curves.

Soft clay *p-y* curves have also been used to analyze piles in liquefied sands. This method has been proposed by Wang and Reese (1998). The soft clay *p-y* curve is in part defined by the shear strength of the soil. The residual shear strength of liquefied sand may be estimated using a correlation with $N_{1(60)c\text{-}s}$ proposed by Seed and Harder (1990). The average corrected blow count in the liquefied zone at Treasure Island was approximately 12 blows per foot which corresponds to a lower bound residual shear strength of 8 kPa. A comparison of the back-calculated *p-y* curves with the modified API and soft clay *p-y* curves are shown in Figures 7.27 and 7.28 for the 0.6-m and 0.9-m CISS piles, respectively.

A review of Figures 7.27 and 7.28 shows that the shape of the back-calculated *p-y* curves are significantly different than the *p-y* curves calculated using the simplified methods. The back-calculated *p-y* curves shown in these figures are for the 7th 225-mm and 11th 221-mm displacement cycle for the 0.6-m and 0.9-m CISS piles, respectively. These cycles were selected as being representative of the steady state condition after the soil structure had been broken down. The back-calculated *p-y* curves provide little to no resistance initially (zero slope/no stiffness) and increase in resistance with displacement. However, the modified *p-y* curves have a steep slope (stiff) initially which decreases to zero (no stiffness) at the ultimate soil resistance. It should be noted that near the ground surface, the soil was displaced up to 150 mm and an ultimate soil resistance was not reached. However, the ultimate resistance calculated using the modified *p-y* curves occurred at relatively small displacements (typically less than 10 mm).

The *p-y* curves in Figures 7.27 and 7.28 also show that using a *p*-multiplier of 0.1 or using the soft clay *p-y* curves with the lower bound residual strength result in similar *p-y* curves. With increased depth, the soft clay *p-y* curves have a limited ultimate resistance which is equal to the smaller value obtained using the following two equations:

$$p_u = \left(3 + \frac{\gamma'}{c} z + \frac{J}{b} z\right) cb \qquad \text{(Eq. 7.4)}$$

$$p_u = 9cb \qquad \text{(Eq. 7.5)}$$

where p_u is the ultimate soil resistance, γ' is the effective unit weigh of the soil, c is the soil shear strength, J is a value assumed to be 0.5 for soft clay based on results of pile tests, and b is pile diameter. The ultimate soil resistance continually increases with depth when using Eq. 7.4; therefore, at a critical depth Eq. 7.5 limits the ultimate resistance

provided by the clay *p-y* curve. However, there are no limitations with depth on the ultimate resistance provided by sands. Analyses using the modified and back-calculated *p-y* curves are presented and discussed in the following section.

7.8 Simplified Analyses

Four lateral load analyses for each CISS pile were performed using simplified procedures for estimating the soil response. The analyses consisted of using *p*-multipliers of 0.1 and 0.3 with the API sand *p-y* curve, using the soft clay *p-y* curve with the ultimate resistance defined by the lower bound residual strength of the liquefied soil (S_u = 8 kPa), and assuming the soil provided no resistance to pile movement. The results of these analyses are presented below.

7.8.1 0.6-m CISS Pile Analyses

Figure 7.29 presents the lateral load-displacement results for each simple pushover type analysis. Over the first 50 mm of pile head displacement, the assumption that the soil provides no lateral resistance resulted in a good comparison with results when using the back-calculated *p-y* curves. The pile head load displacement obtained using the back-calculated *p-y* curves overlays the measured test results. Figure 7.30 presents the ratio of predicted pile response (pile head displacement, maximum moment, and depth to maximum moment) to the pile response obtained using the back-calculated *p-y* curves for each of the simplified analyses. At a load of approximately 260 kN, assuming the soil provides zero lateral resistance results in overestimating the pile head displacement by as much as 2.5 times (Figure 7.30a). Figure 7.30b shows that the maximum moment is overestimated by as much as 2.3 times. The depth at which the

maximum moment occurs was overestimated slightly at small loads and by as much as 1.5 times at a load of 260 kN, assuming no soil resistance (Figure 7.30c).

When using the API sand *p-y* curve with a *p*-multiplier of 0.1, the pile head load-displacement response was too stiff up to 100 mm of displacement. The soft clay *p-y* curve with a residual strength of 8 kPa also resulted in a prediction that was too stiff up to about 125 mm of pile head displacement. When using the API *p-y* curves with a *p*-multiplier of 0.3, the predicted load-displacement response was too stiff up to displacements of 160 mm. As presented in Figure 7.27, the modified *p-y* curves provide significantly more resistance at small displacements compared to the back-calculated *p-y* curves from the full-scale test. Therefore a more stiff pile head load-displacement response is expected at small displacements. Additionally, when using the modified *p-y* curves, the soil yeilds at small displacements, whereas the back-calculated *p-y* curves continue to provide increased resistance with continued displacement. Therefore, the load-displacement response obtained using the modified *p-y* curves eventually results in predicting more displacement than would actually occur at larger loads.

The ratio of pile response (pile head displacement, maximum moment, and depth to maximum moment) using the modified *p-y* curves to the pile response obtained when using the back-calculated *p-y* curves (Figure 7.30) shows that the pile head displacement, maximum moment, and predicted depth of maximum moment are typically underestimated at relatively small loads and overestimated at large loads. When considering the four methods used, the best response on average is obtained by either the modified API *p-y* curve with a *p*-multiplier of 0.1, or when using the soft clay *p-y* curves with the lower bound residual strength of 8 kPa. As observed from Figure 7.29 and 7.30,

when using a *p*-multiplier of 0.3 with the Treasure Island test results, the pile response is typically underestimated.

In an effort to further illustrate the effect of using modified *p-y* curves to model soil-pile interaction in liquefied sands, a series of analyses were performed where the height of loading above the ground surface was varied. The *p-y* curves used in the previous analyses were employed in these analyses, and it was assumed that the pile response obtained using the back-calculated *p-y* curves resulted in the response that would be measured in the field. Therefore, the ratios of pile response shown in Figure 7.31 through 7.33 are referenced to the response obtained using the back-calculated *p-y* curves. These figures show the pile response ratio versus the predicted ground line displacement obtained from each analysis, so although two analyses may have the same ground line displacement, the applied lateral load varies significantly. It can be observed in Figure 7.31 that as the height loading above the ground surface increases, the variation in pile head displacement ratio decreases. When the height of loading was 1.6 pile diameters (1.6D), above the ground surface, the height of loading during the full-scale tests, Figure 7.31c shows the pile head displacement ratio varying from 0.5 to 1.4 over a groundline displacement range of 15 to 175 mm. When the height of loading above the ground surface was 20D, the pile head displacement ratio varied between 0.25 to 1.25 over the same displacement range.

The maximum moment ratios obtained from analyses using the modified *p-y* curves are shown in Figure 7.32. Again the trend is for the variation in the maximum moment ratio to reduce as the height of loading above the ground surface increases, indicating that results from the modified *p-y* curve analyses more closely match results

obtained using the back-calculated *p-y* curves. On the contrary, a review of Figure 7.33 shows that the predicted depth of maximum moment tends to decrease in accuracy as the height of loading above the ground surface increases.

Figures 7.31 through 7.33 highlight the magnitude of error that could be expected when using modified *p-y* curves to analyze piles in liquefied soils. When assuming the soil does not provide lateral resistance, the predicted pile head displacement matched the response obtained using the back-calculated *p-y* curves well for displacements up to 50 mm. As displacements increased, the predicted pile head displacement was dramatically overestimated. The modified *p-y* curves vary in accuracy over the displacement range of the analyses, underestimating pile behavior initially and overestimating pile behavior at large ground line displacements

7.8.2 0.9-m CISS Pile Analyses

Analyses similar to those presented for the 0.6-m CISS pile were also performed for the 0.9-m CISS pile. Figure 7.34 shows the pile head load-displacement results for analyses using modified sand and clay *p-y* curves as well as the back-calculated *p-y* curves and a case where the soil is assumed to provide no lateral resistance. The load-displacement results obtained using the back-calculated *p-y* curves overlay the pile response measured during testing. Again, the modified *p-y* curves tend to underestimate the pile behavior at the smaller displacements and overestimate the behavior at the larger displacements. Figure 7.34 also shows that when assuming the soil provides no lateral resistance, a good estimate of pile behavior is obtained for pile head displacements less than 50 mm.

Figure 7.35 presents the ratio of predicted pile head displacement, maximum moment, and depth to maximum moment to the pile response computed using the back-calculated *p-y* curves. Similar to the 0.6-m CISS case, the zero soil resistance assumption results in overestimates of pile head displacement, maximum moment, and depth to maximum moment. However, the overestimate is not as significant as it was for the 0.6-m CISS pile case. At the maximum test load, the pile head displacement was overestimated by 1.5 times; whereas, the pile head displacement was overestimated by as much a 2.5 times for the 0.6-m CISS pile test. On average, the soft clay and sand *p-y* curves with a *p*-multiplier of 0.1 provided the best estimate of pile performance when using modified *p-y* curves. Although the modified *p-y* curves typically overestimate pile head displacement and maximum moment at large loads and displacement, the soft clay and sand *p-y* curve with a p-multiplier of 0.1 did not significantly overestimate the depth to maximum moment for loads greater than 150 to 200 kN.

A series of analyses for the 0.9-m CISS pile were also performed with the lateral load being applied at different heights above the ground surface. The ratio of predicted pile response (pile head displacement, maximum moment, and depth to maximum moment) to pile response obtained using the back-calculated *p-y* curves are shown in Figures 7.36 through 7.38. The pile response obtained using the back-calculated *p-y* curves were assumed to be equivalent to a measured field response. The analyses were performed for loads applied at height of 1 pile diameter (1D, height of load during full-scale tests), 10D and 20D. Similar to the 0.6-m CISS pile analyses, as the load point increased in distance from the ground surface, the predicted pile head displacements and maximum moments compared well with results obtained using the back-calculated *p-y*

curves. However, the predictions of the depth of maximum moment decreased in accuracy with increased height of loading.

7.9 Considerations for Design of Deep Foundations in Liquefied Sand

Comparisons between the back-calculated centrifuge and full-scale *p-y* curves, as well as the comparisons between pile response obtained using the modified and back-calculated *p-y* curves, provide information that can be implemented in the analysis and design of piles and pile supported structures founded in liquefiable soils. Though developed specifically from data on CISS piles presented in this chapter, these considerations would apply to other types of deep foundations as well. Additionally, the comparison between the centrifuge and full-scale *p-y* curves indicate that the full-scale *p-y* curves provide a lower bound soil response for sands with a relative density of approximately 50%. Therefore, the full-scale *p-y* curves can be directly implemented in certain cases if a lower bound soil response is deemed appropriate. The comparisons between the pile response obtained using the modified and back-calculated *p-y* curves provide engineers with a better understanding of the limitations of these methods. Therefore, the use of the modified *p-y* curves should be used with caution. With the understanding obtained from these comparisons, a simplified design methodology is outlined below, and the shortcomings of this simplified procedure are discussed.

Any simplified pushover type analysis should incorporate analyses for the liquefied case as well as for the case when the soil does not liquefy. Depending on the thickness of the liquefiable zone as well as the relative stiffness between the liquefiable and non-liquefiable underlying layer, plastic hinging may not be a concern after the onset of liquefaction. At Treasure Island, the liquefiable layer was directly underlain by soft

clay that did not differ greatly in stiffness from the liquefying sand. Therefore, there was not a dramatic increase in curvature/moment at the interface of these two layers. Although ground line displacements for the first series of tests were as great as 150 mm, the pile did not form any plastic hinges. However, if the liquefiable sand was underlain by stiff soil, the maximum pile stresses would likely occur at the interface of the two layers and a plastic hinge would have developed at that location. The reasoning for performing an analysis for the non-liquefied case is based on recent large scale shake table tests (Cubrinovski et al. 1999, Mizuno et al. 2000, Tamura et al. 2000, and Yasuda et al. 2000) that show large inertial loads occuring prior to the onset of liquefaction resulting in plastic hinging in the pile during the early stages of an earthquake. Therefore, an analysis accounting for the non-liquefied soil response is also necessary.

As stated previously, the *p-y* curves obtained from the full-scale tests appear to provide a lower bound estimate of the soil response for sands with a relative density of approximately 50%. In addition, these *p-y* curves incorporate the effects of gapping that occurred during the Treasure Island tests. Therefore, if a lower bound soil response is deemed appropriate for estimating pile and structural response to lateral loading, the *p-y* curves back-calculated from the full-scale tests may be implemented. Two key limitations for directly implementing the *p-y* curves back-calculated from the full-scale tests include: 1) the full-scale *p-y* curves were back-calculated to a maximum depth of between 6 to 7 meters below the ground surface, and 2) the *p-y* curves were obtained for 0.6-m and 0.9-m diameter piles. At depths near 6 to 7 meters, the full-scale back-calculated *p-y* curves compare favorably with the API sand *p-y* curve when using a p-multiplier of 0.1 (Figures 7.27 and 7.28). At these depths, pile displacements are

typically small, therefore actual resistance values significantly greater than the modified API *p-y* curves are not as likely as observed at large displacements at shallower depths. Therefore, when analyzing piles at a liquefiable site with zones of liquefiable soils that extend beyond 6 to 7 meters in depth, modifying the API sand *p-y* curve with a *p*-multiplier of 0.1 seems appropriate. More testing with larger diameter piles would be useful for clarifying the relationship between the *p-y* response and pile diameter. Although the comparison between the pile response using the modified and back-calculated *p-y* curves highlighted the inadequacy of these methods, understanding that the simplified methods will likely provide too much resistance at small displacements and too little resistance at large displacements allows the engineer to make use of these methods effectively if they are deemed to provide a response that results in a safe pile and structural design.

One of the difficulties in performing any pushover type analysis is in determining the appropriate inertial load to apply to the pile. Also, a typical pushover analysis neglects kinematic loading from the soil. A pseudo-static procedure for the analysis of piles proposed by Tabesh and Poulos (2001) suggest using the spectral acceleration obtained from a site response analysis to estimate the applied lateral load from the structure. In estimating the superstructure period, the effect of pile head stiffness should be taken into account. In addition to estimating the inertial loading, the pseudo-static procedure includes applying a kinematic load to the piles obtained through a site response analysis. The kinematic loading suggested in this procedure is obtained by taking the maximum soil displacements obtained from the site response analysis, even though these displacements occur at different times, and applying them in conjunction with the inertial

load to obtain the maximum pile response. When incorporating this methodology for the design of piles in liquefiable soils, the inertial load obtained from the response spectra may be a result of accelerations prior to the onset of liquefaction. Previous studies (Miyamoto et al. 1992, Kobayashi et al. 1992, and Mori et al. 1992) have shown that the liquefied soils dampen out higher frequency motion; therefore, inertial loads may drastically reduce after the onset of liquefaction. In light of this recent research, inertial loads obtained using the peak pseudo acceleraction may be excessively large. Additionally, kinematic loadings obtained using the pseudo-static procedure may be a combination of loadings obtained prior to or after the onset of liquefaction.

In summary, there are two simple approaches to analyzing piles in liquefied soils. One method is to perform a pushover type analysis. Since large inertial loads may be of critical concern prior to or after the onset of liquefaction, both cases should be assessed. One of the drawbacks is that this method neglects the effects of kinematic loading. These effects may be relatively small compared to the inertial loading applied by the structure, but there is no rule of thumb available to determine when that may be the case. The second simple procedure is an extension of the pushover type analysis where the kinematic loading is applied in conjunction with the inertial load. The drawback with this method is that the inertial and kinematic loads are peak values and may be excessive for the case of liquefaction. Therefore, if engineering judgement suggests the results from the pushover or pseudo-static procedure are unreasonable, dynamic analyses resulting in more appropriate inertial and kinematic loadings may be warranted.

7.10 Summary

P-y curves were back calculated for the 0.6-m and 0.9-m CISS piles for pre-blast and post-blast cycles. The *p-y* curves back-calculated from the pre-blast testing have a shape similar to standard *p-y* curves where the soil stiffness degrades with displacement. The standard and back-calculated *p-y* curves generally compared well. Comparisons of measured and predicted results show that the standard *p-y* curves provide adequate estimates of lateral pile behavior.

The back-calculated curves for the post-blast testing show little to no resistance at displacements as great as 50 millimeters near the ground surface when excess pore pressure ratios ranged between 70 and 100%. Soil resistance was observed to increase over the entire displacement range with the shape of the *p-y* curves being concave up. This *p-y* shape is dramatically different from standard *p-y* curves, but is consistent with back-calculated *p-y* curves from centrifuge testing (Wilson *et al.* 2000). The back-calculated *p-y* curves also agree with previous testing showing increased resistance as the excess pore pressures decreased. Observance of increased resistance between loading series was noted even when the excess pore pressure ratio adjacent to the pile did not decrease significantly. The increased soil resistance is attributed the more rapid decrease in pore pressures at greater distances from the pile.

The use of controlled blasting to induce liquefaction and subsequent lateral load testing is an effective method for increasing our understanding of soil-pile interaction and fundamental soil behavior in liquefied sands. Excess pore pressure data obtained from these full-scale tests together with loading data indicate that pile displacement can induce a phase transformation in liquefied soils. As the foundation diameter increases, the zone

of soil providing resistance also appears to increase. Both tests indicated gapping at liquefiable sites can be a factor in pile-soil interaction. The ability of a liquefied sand to undergo a phase transformation appears to be a key factor in assessing the capacity of the soil to resist pile movement.

The *p-y* curves back-calculated from the full-scale tests were compared to *p-y* curves back-calculated from a centrifuge model test. This comparison showed that the full-scale *p-y* curves provide less resistance to pile movement. Some reasons for the differences in the back-calculated *p-y* curves include the rate of loading, the effect of gapping that was observed at Treasure Island, and the effect of degradation at large displacement levels. Based on a review of the small amount of data available concerning liquefied soil response, the full-scale *p-y* curves appear to provide a lower bound estimate of the *p-y* relationship for liquefied sands having a relative density of 50%.

The full-scale *p-y* curves were also compared to standard *p-y* curves that had been modified to account for the liquefied soil response. These comparisons showed that the modified *p-y* curves are significantly more stiff than the back-calculated *p-y* curves at small displacements. Additionally, the modified *p-y* curves reach an ultimate resistance at relatively small displacements; whereas, the back-calculated *p-y* curves continue to increase in resistance throughout the loading of the pile.

Lateral load analyses of the 0.6-m and 0.9-m CISS piles were performed with the back-calculated *p-y* and modified *p-y* curves. These analyses highlight the limitations or inadequacies of using modified *p-y* curves to analyze laterally loaded piles. The modified p-y curves typically result in underestimating pile head displacement, maximum moment, and depth to maximum moment at small displacements, and overestimating these

responses at large displacements. Understanding these inadequacies will allow engineers to make more rational decisions when performing analyses.

Some basic recommendations were provided for analyzing laterally loaded piles in liquefied soil based on comparisons of centrifuge, modified, and back-calculated *p-y* curves, as well as comparisons between analyses using the modified and back-calculated *p-y* curves. It was suggested that the back-calculated *p-y* curve from the full-scale tests could be implemented directly in analyses of 0.6-m and 0.9-m diameter piles if the lower bound soil response is deemed appropriate for the proper design of the piles and structure. One of the difficulties when performing lateral load analyses in liquefiable soils is choosing the appropriate lateral inertial load applied to the pile foundation. A pushover analysis typically used when analyzing laterally loaded piles has a drawback in that kinematic loading is neglected. A pseudo-static design methodology was briefly discussed which provides recommendations for obtaining the lateral inertial load as well as accounting for kinematic loading of the foundation. However, this method may result in excessively large loading of pile. Engineering judgement should be used to assess the analysis method as well as the results obtained from the analysis. When analysis results from the simplified methods appear unreasonable, a more complex dynamic time history analysis may be warranted.

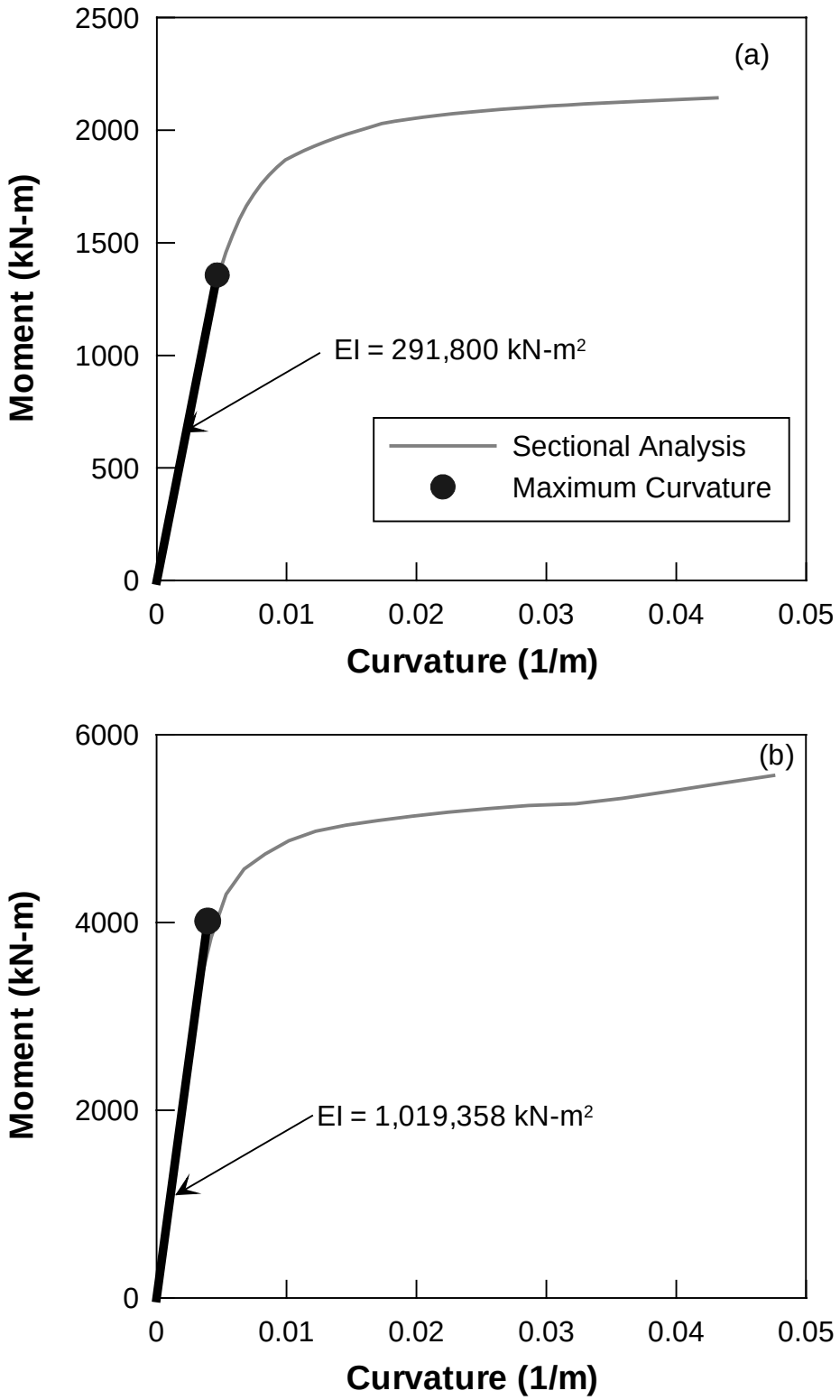

Figure 7.1 Moment Curvature Relationship for the a) 0.6-m CISS Pile b) 0.9-m CISS Pile

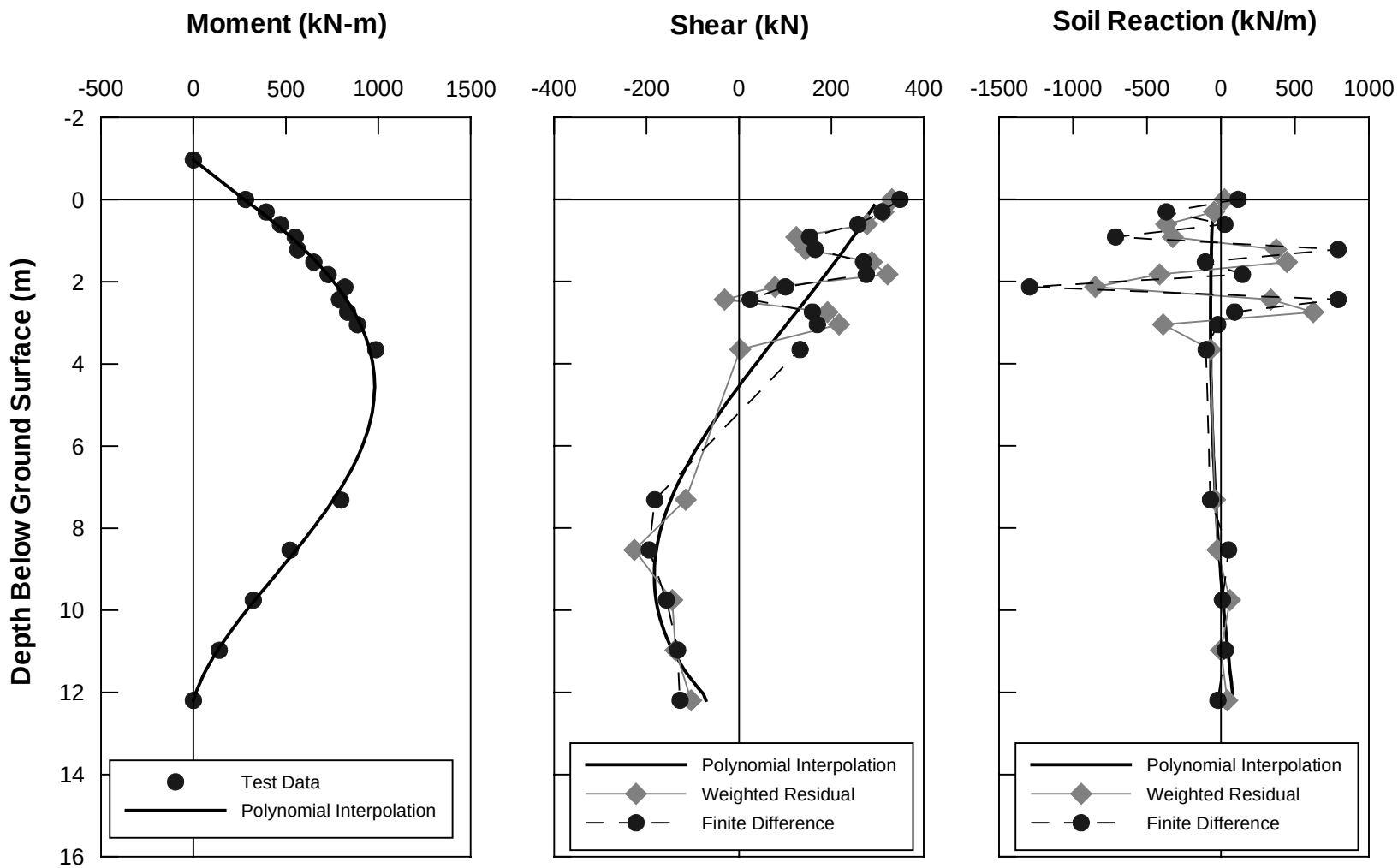

Figure 7.2 Comparison of Numerical Differentiation Methods for Back-Calculating Soil Resistance for the 0.6-m CISS Pile

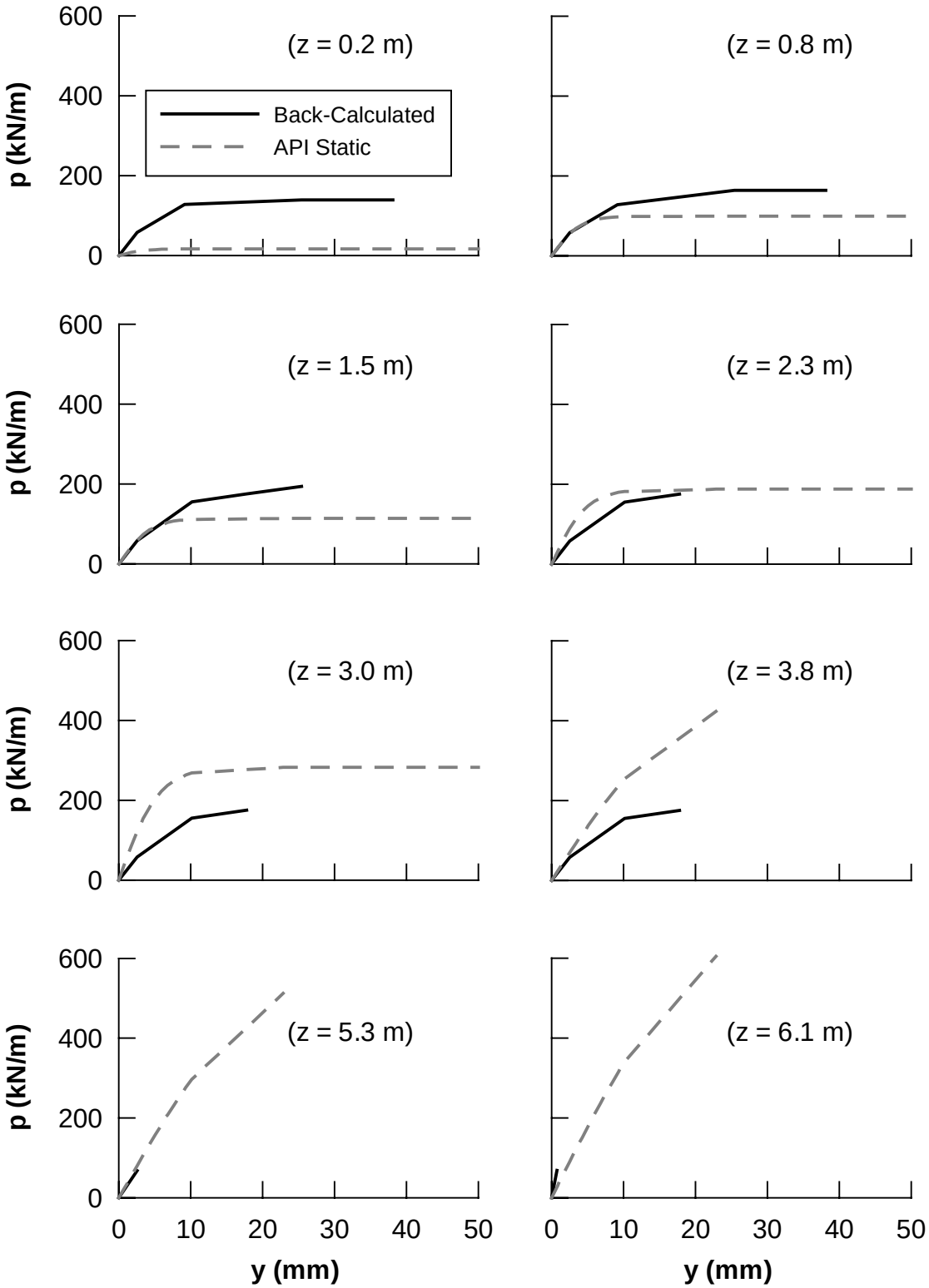

Figure 7.3 Back-Calculated and API p-y Curves for the 0.6-m CISS Pile Pre-Blast Load Test

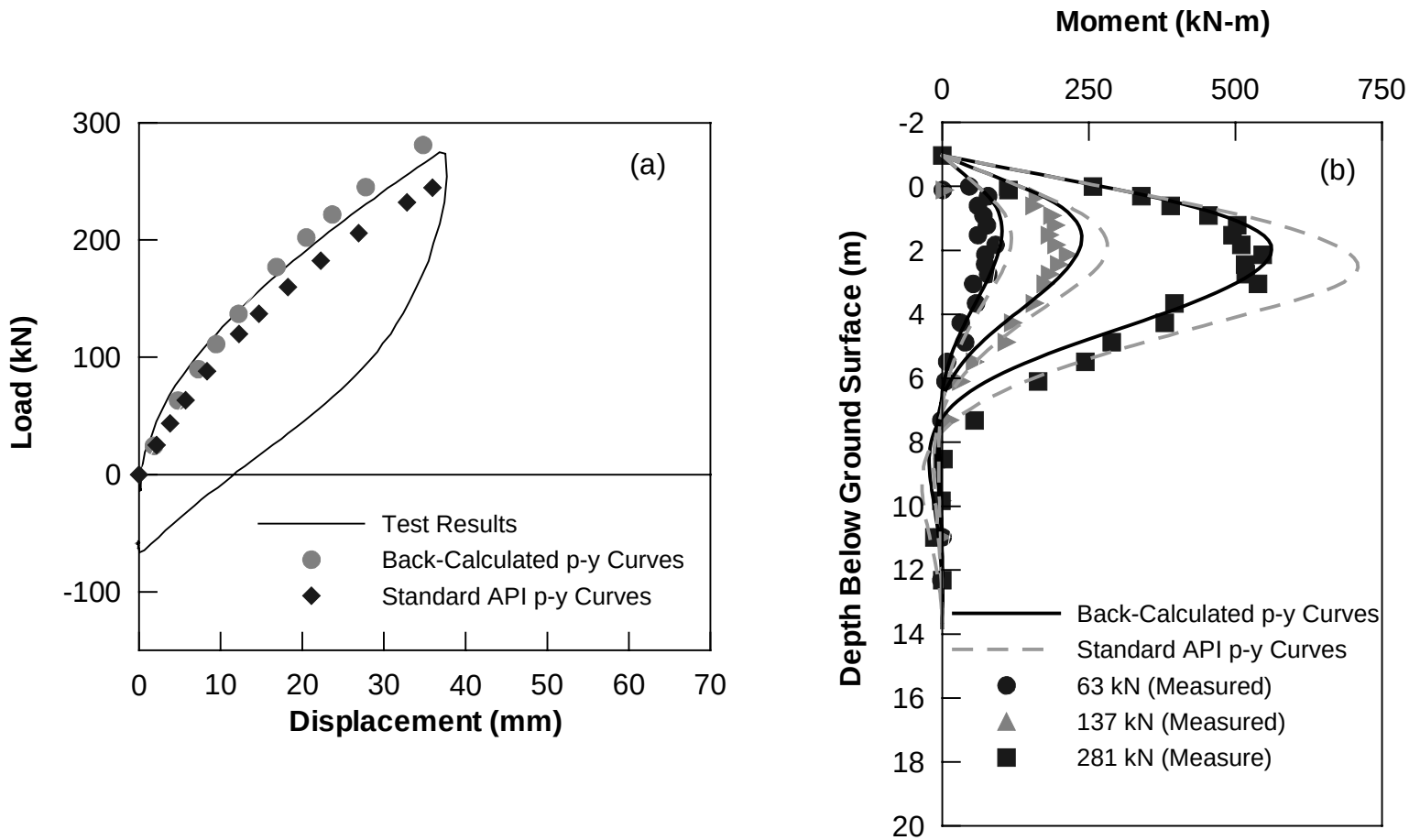

Figure 7.4 Comparison of Test Results and Analysis using Back-Calculated and Standard API p-y Curves for the 0.6-m CISS Pile Pre-Blast Test a) Load vs. Displacement b) Moment vs. Depth

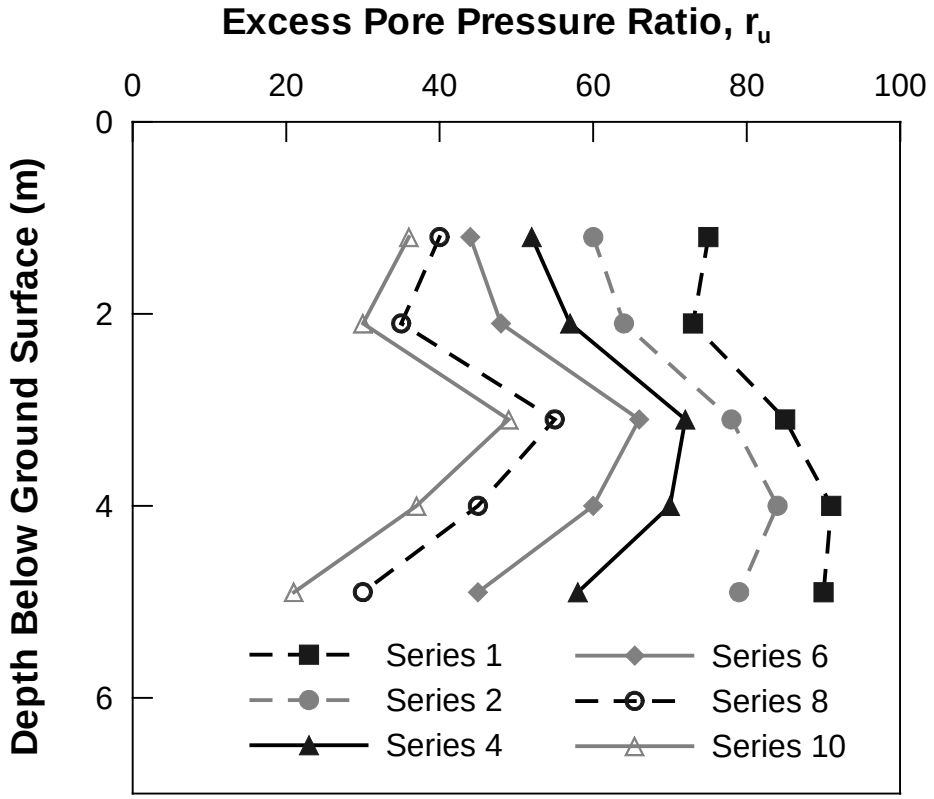

Figure 7.5 Excess Pore Pressure Ratio vs. Depth Adjacent to the 0.6-m CISS Pile

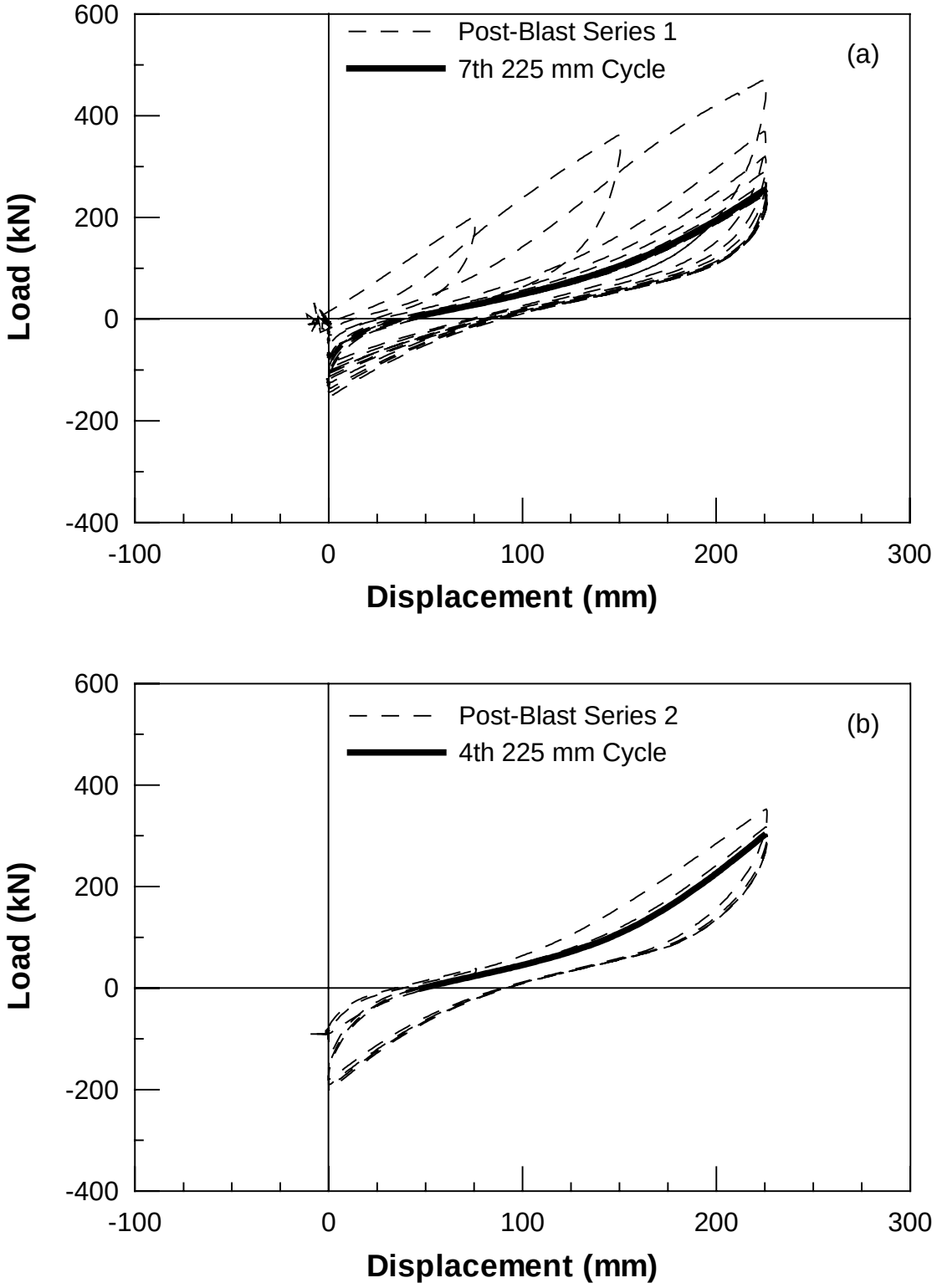

Figure 7.6 Load vs. Displacement for 0.6-m CISS pile a) Post-Blast Series 1 b) Post Blast Series 2

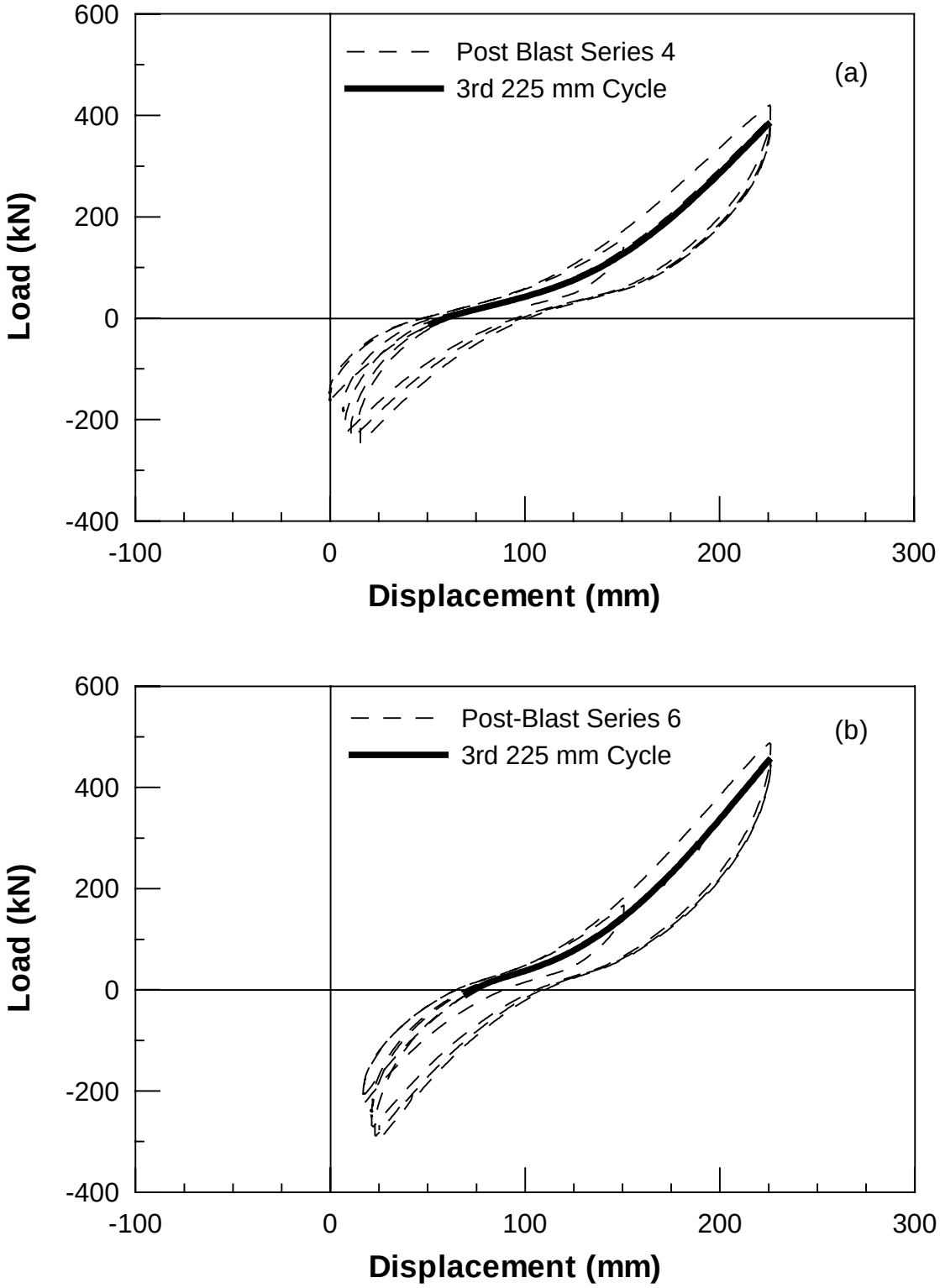

Figure 7.7 Load vs. Displacement for the 0.6-m CISS Pile a) Post-Blast Series 4 b) Post-Blast Series 6

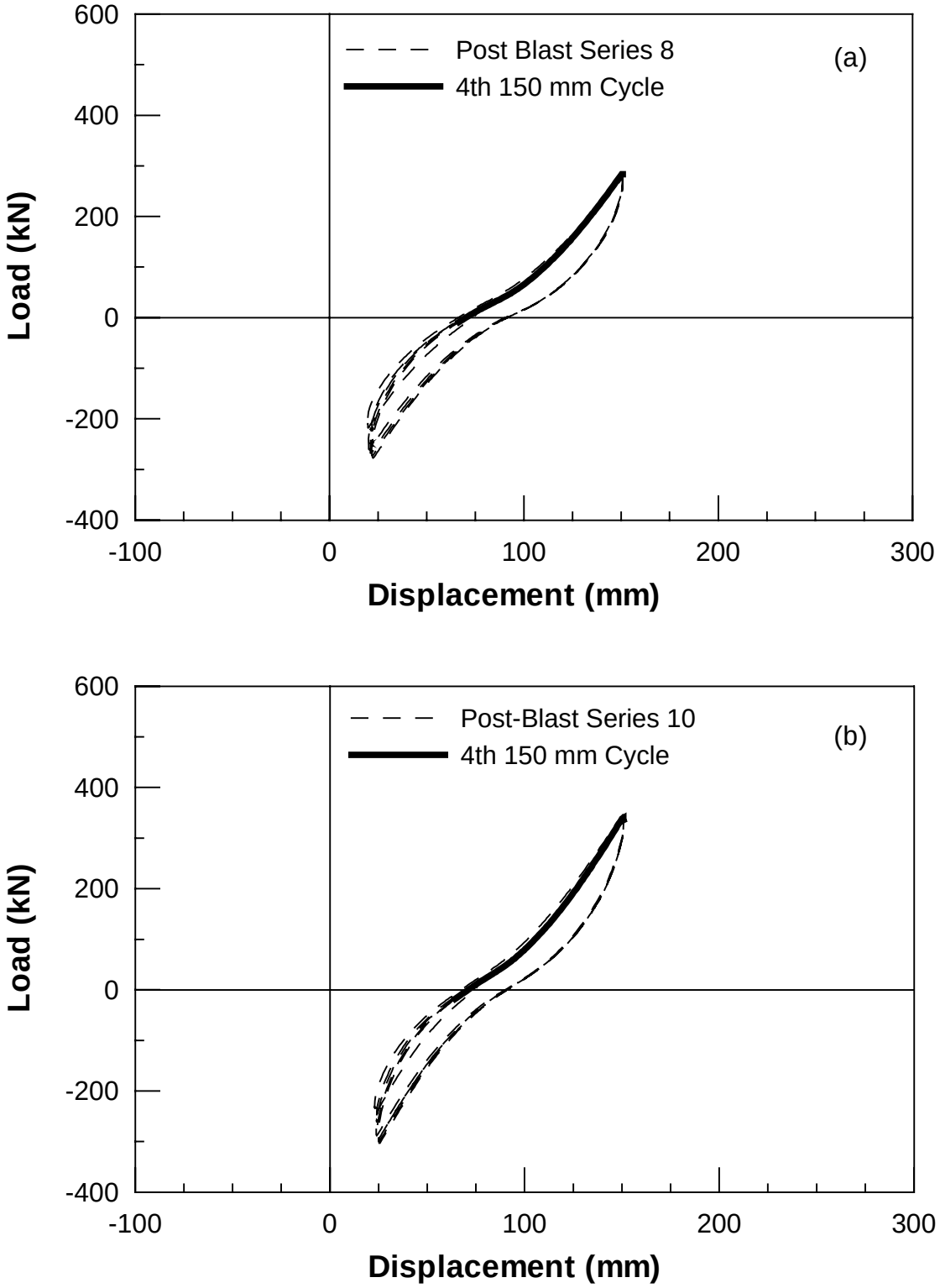

Figure 7.8 Load vs. Displacement for the 0.6-m CISS Pile a) Post-Blast Series 8 b) Post-Blast Series 10

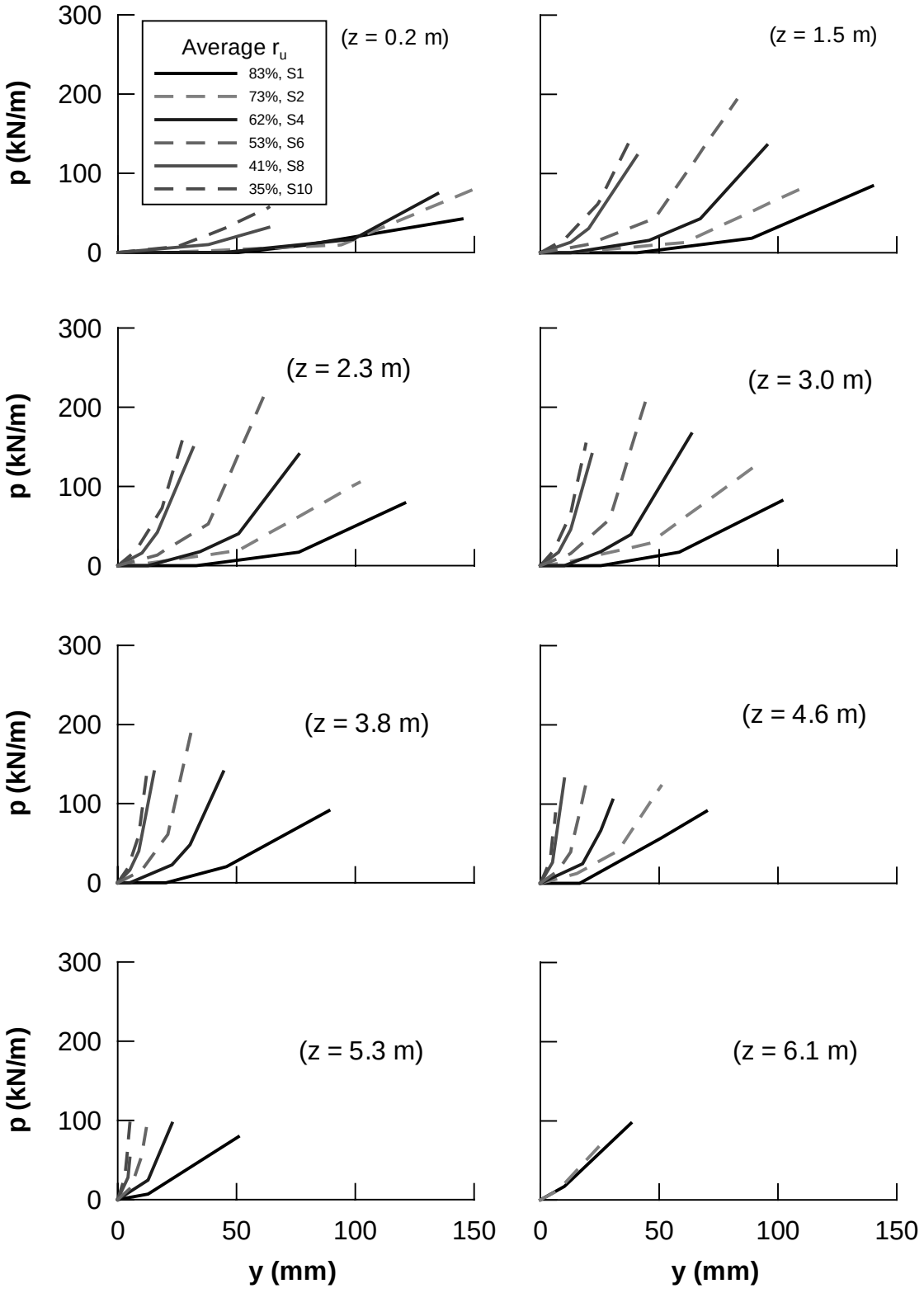

Figure 7.9 Back-Calculated p-y curves for 0.6-m CISS Pile for Average Excess Pore Pressure Ratios Ranging between 83% and 35%

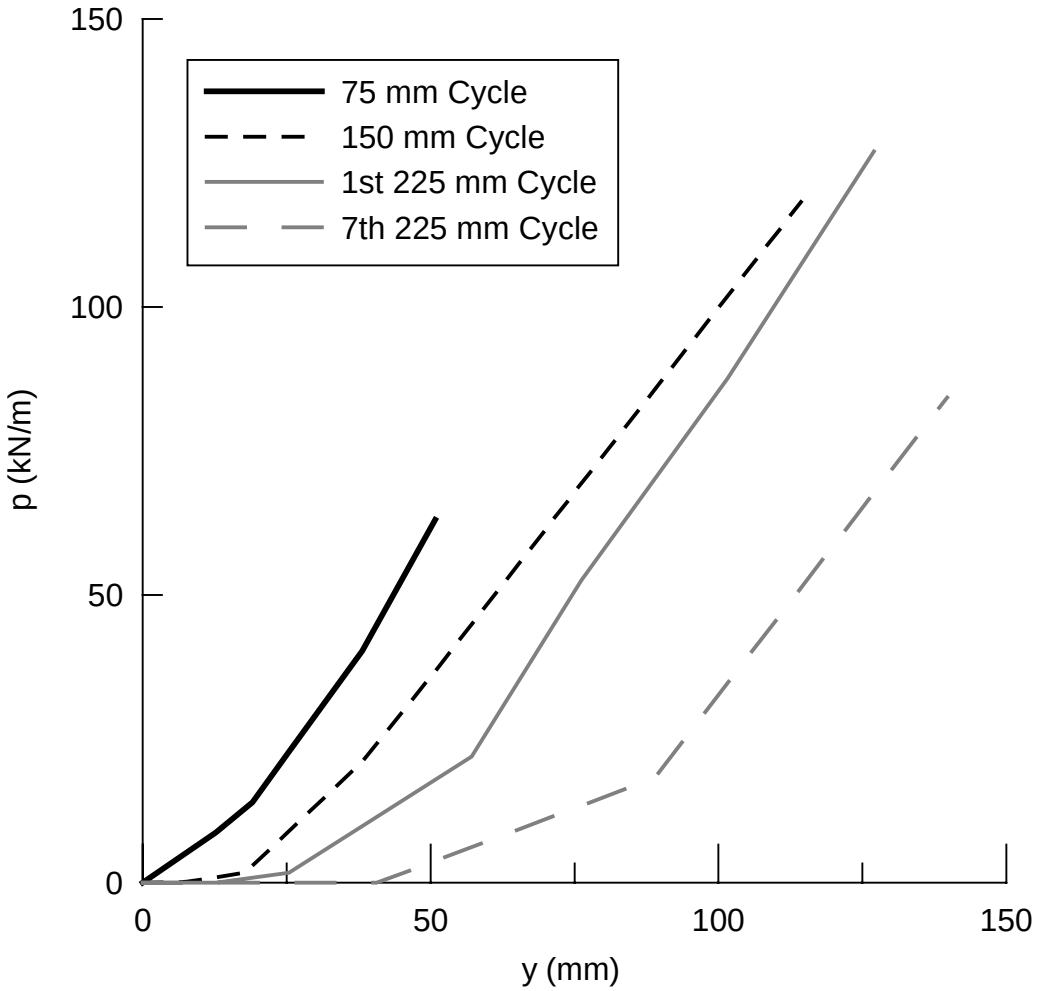

Figure 7.10 Degradation of Post-Blast p-y Curve for 0.6-m CISS Pile Test

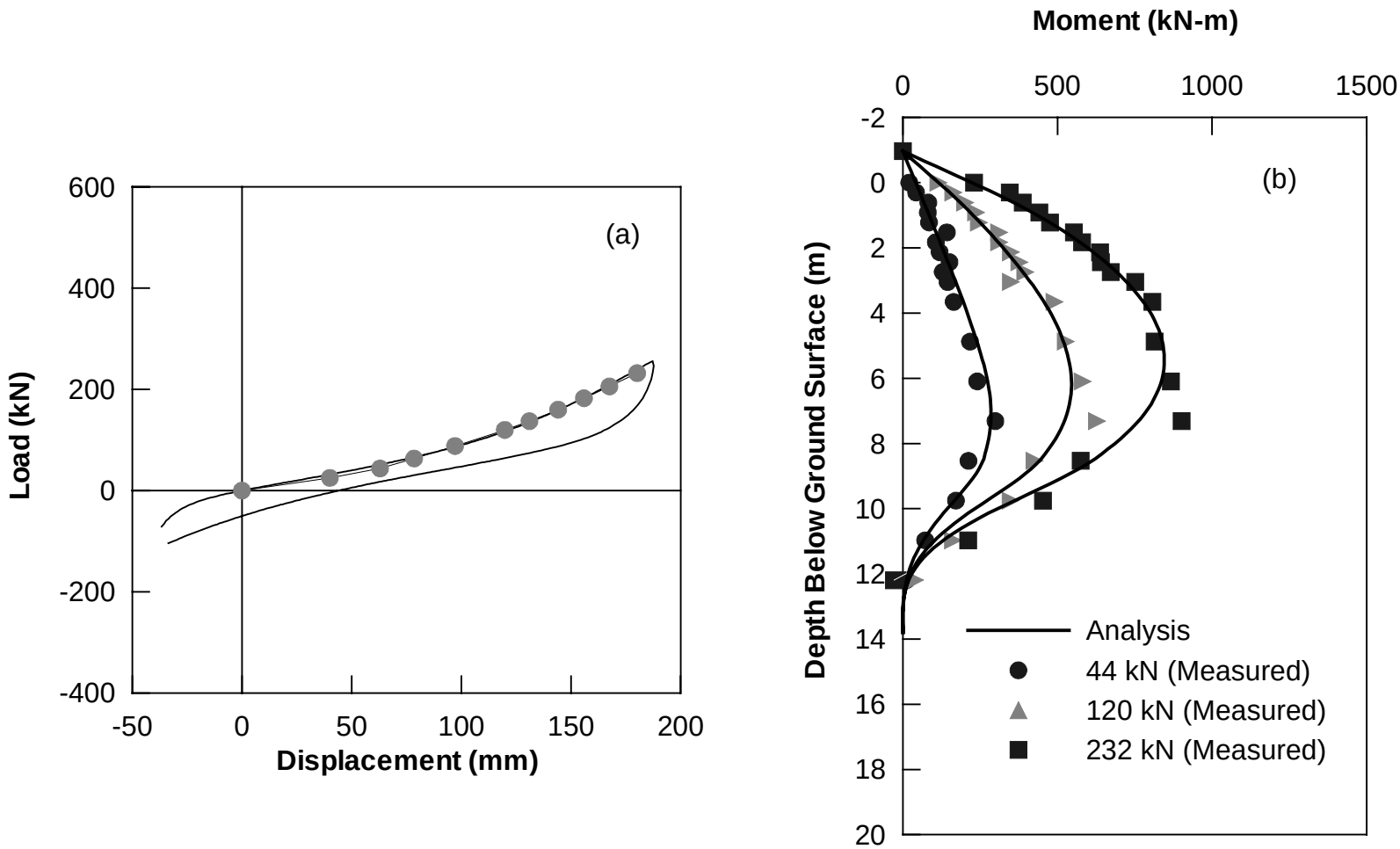

Figure 7.11 Comparison of Test Results and Analysis using Back-Calculated p-y Curves for the 0.6-m CISS Pile Post-Blast Series 1 a) Load vs. Displacement b) Moment vs. Depth

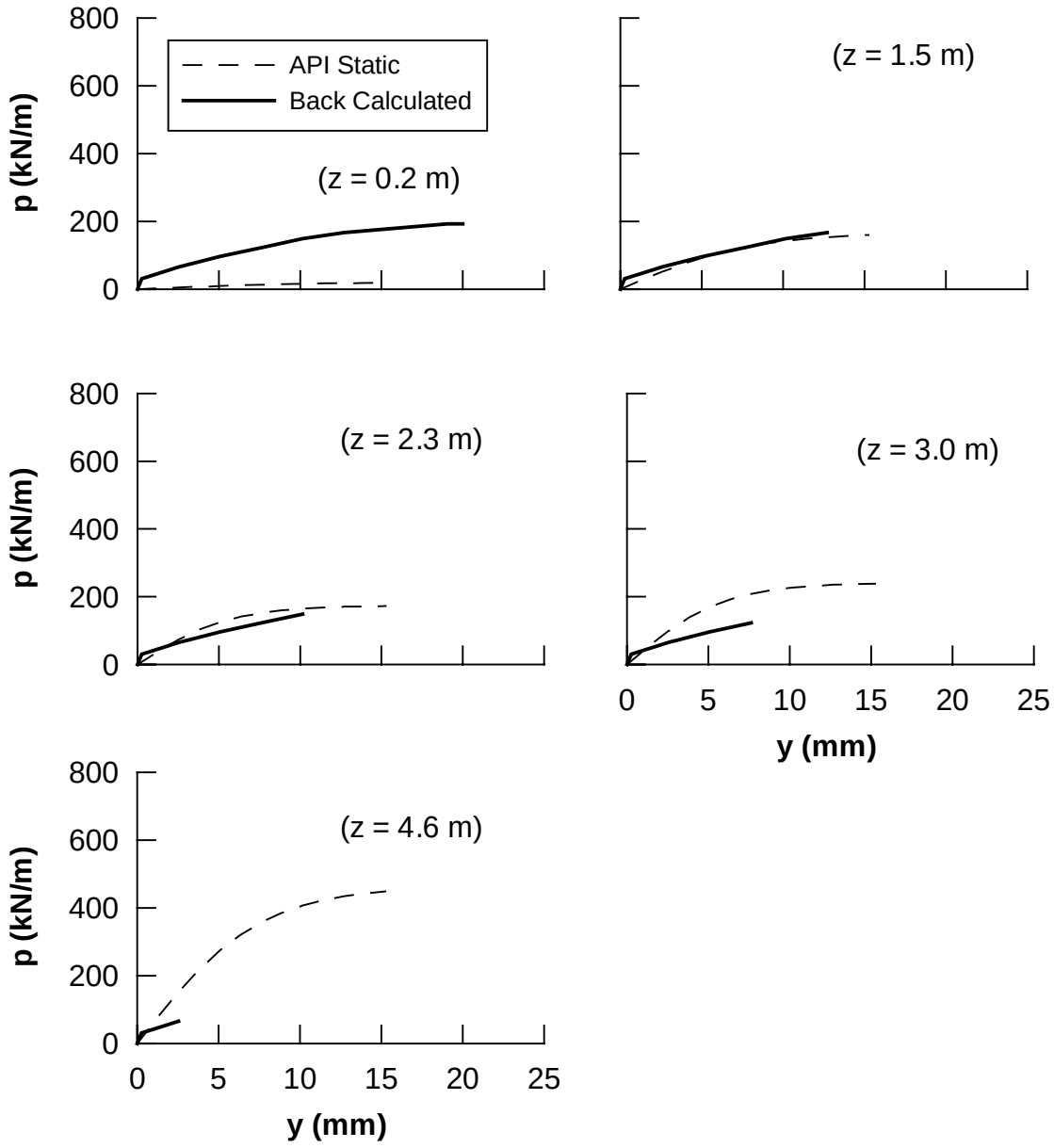

Figure 7.12 Back-Calculated and API Pre-Blast p-y curves for the 0.9-m CISS Pile Test

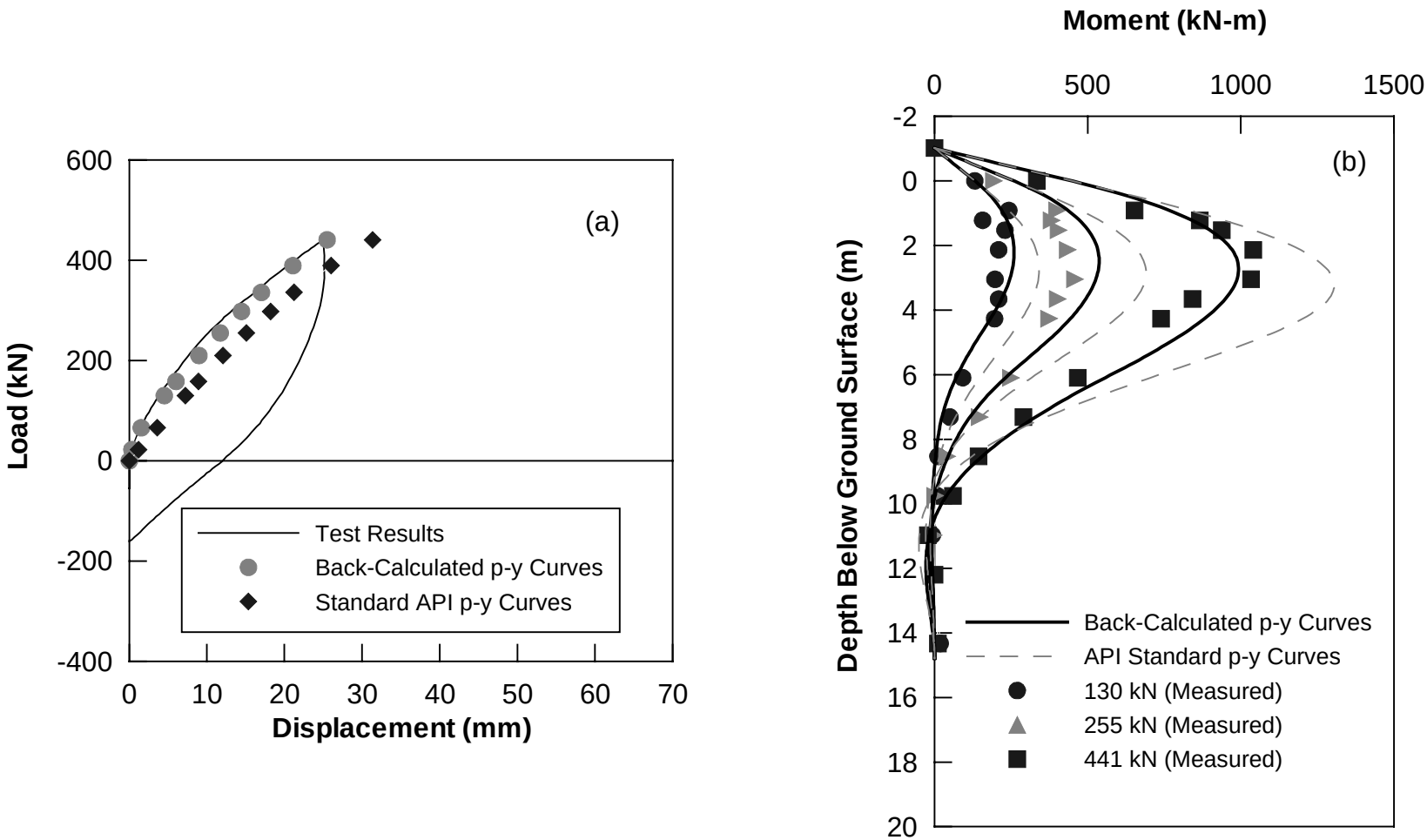

Figure 7.13 Comparison of Pre-Blast Test Results and Analysis using Back-Calculated and API p-y Curves for the 0.9-m CISS Pile Test a) Load vs. Displacement b) Moment vs. Depth

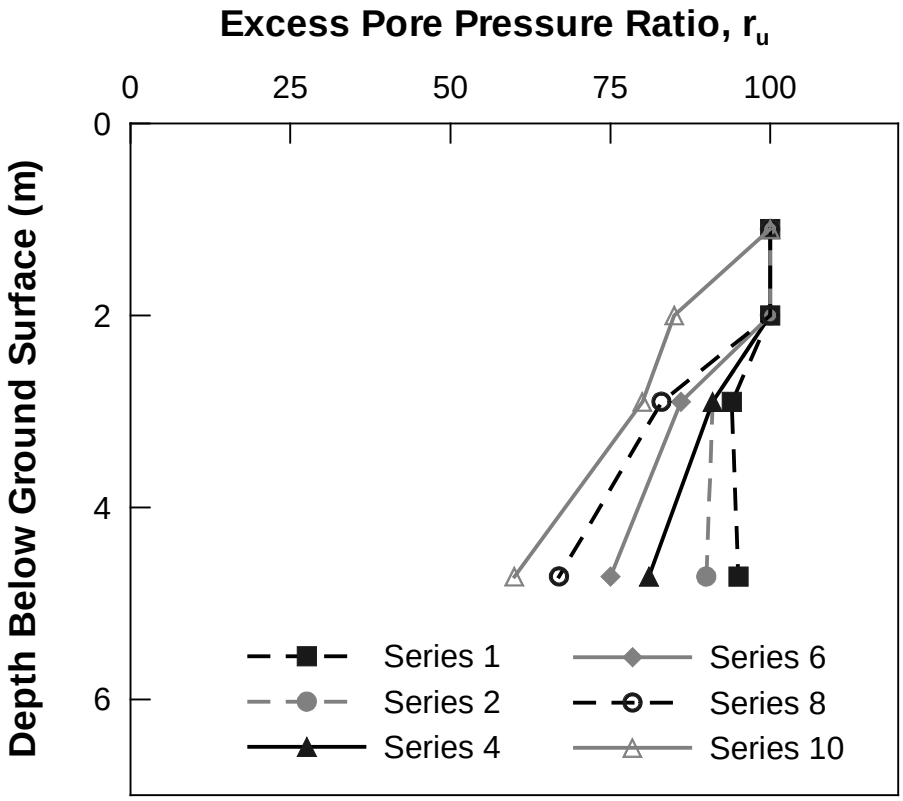

Figure 7.14 Excess Pore Pressure Ratio vs. Depth Adjacent to the 0.9-m CISS Pile

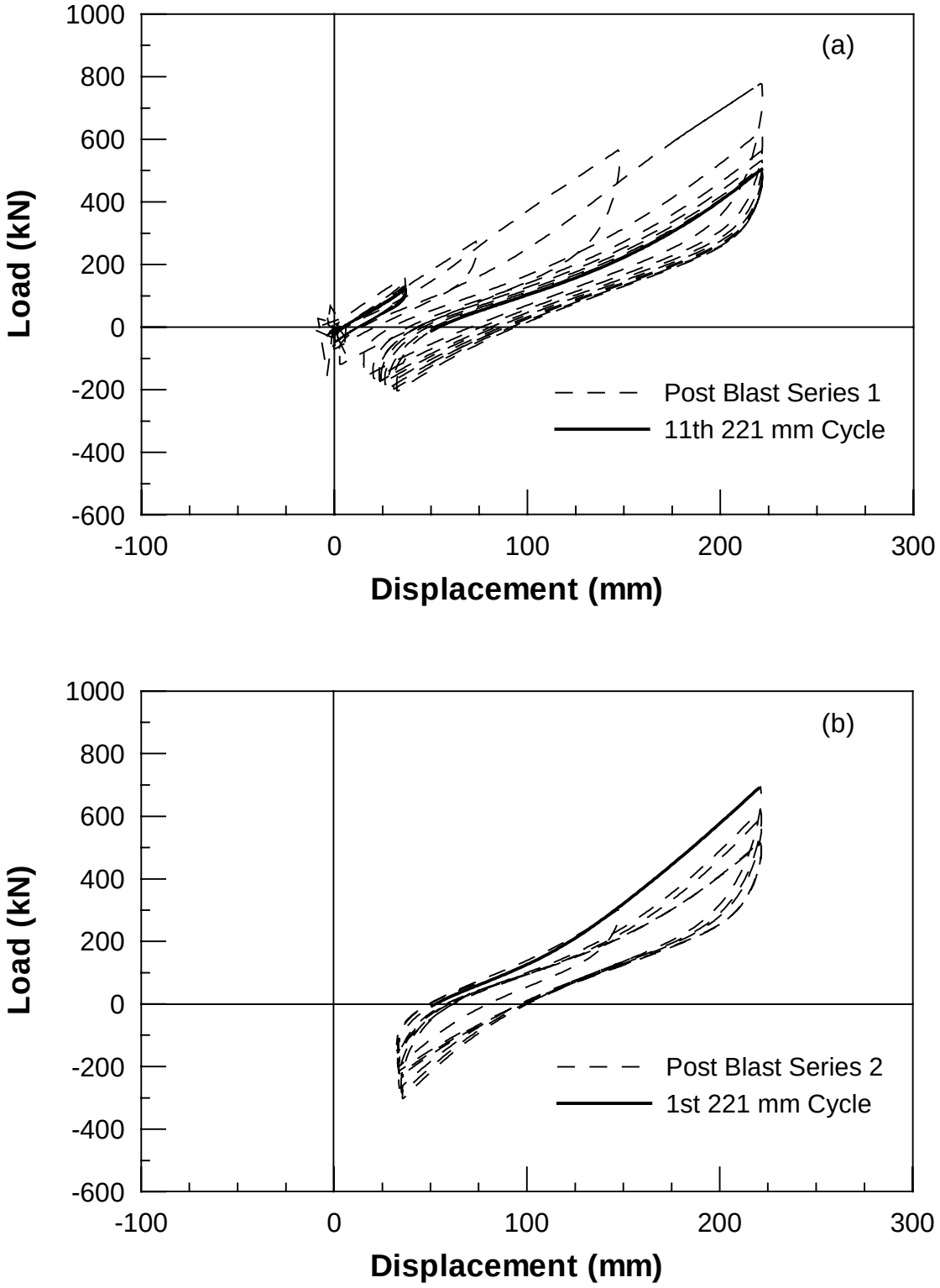

Figure 7.15 Load vs Displacement for the 0.9-m CISS Pile a) Post-Blast Series 1 b) Post-Blast Series 2

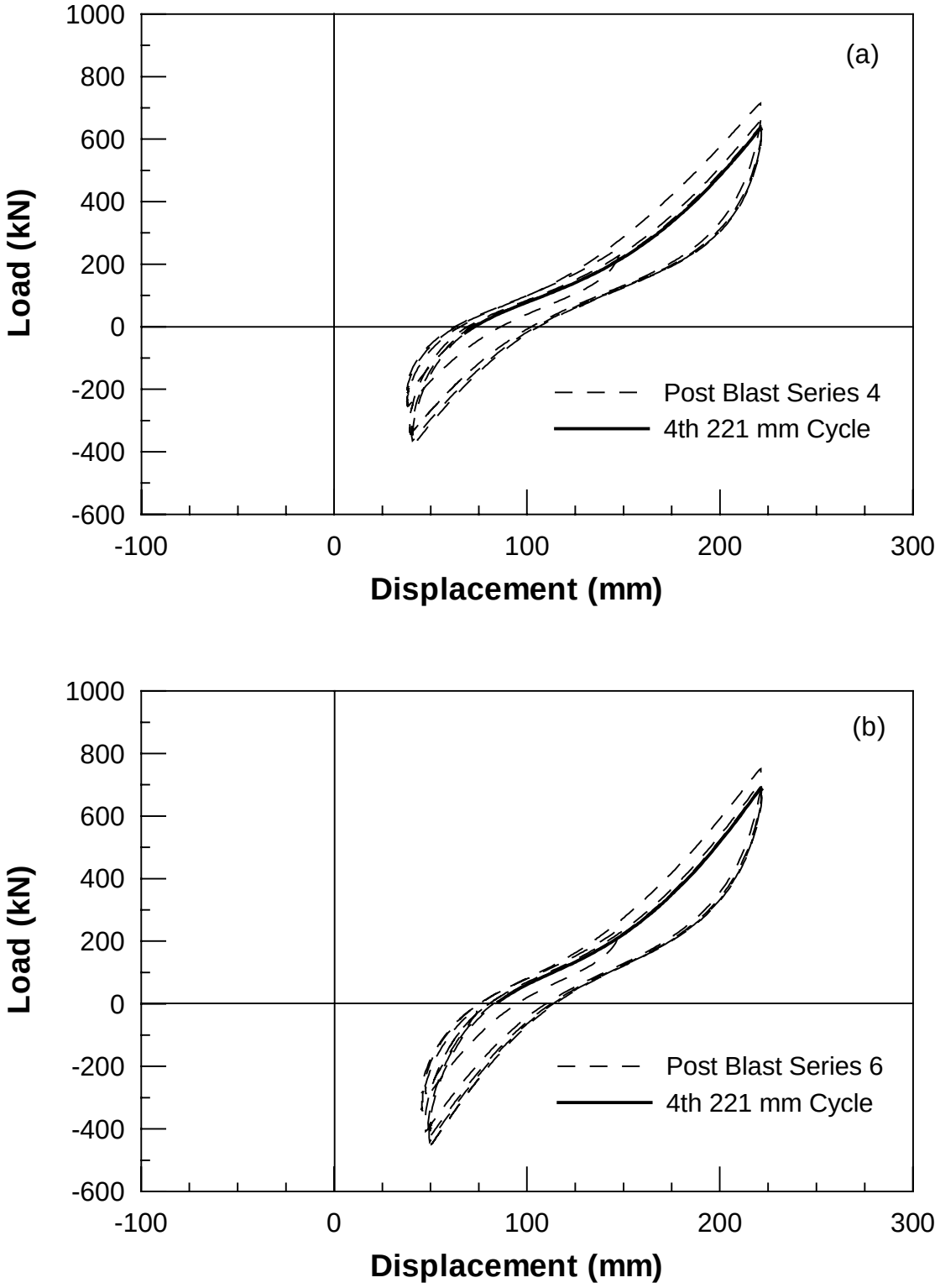

Figure 7.16 Load vs Displacement for 0.9-m CISS Pile a) Post-Blast Series 4 b) Post-Blast Series 6

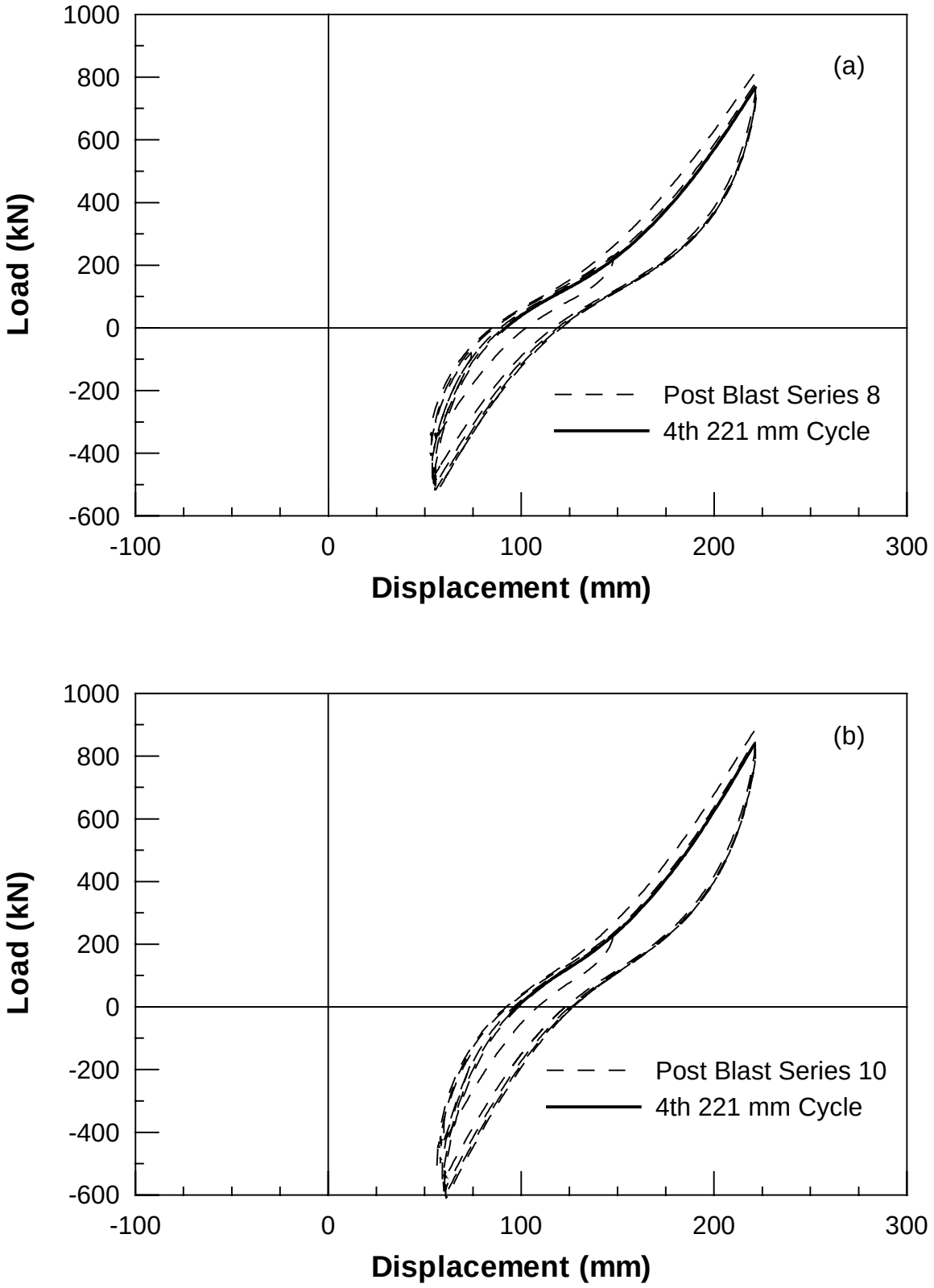

Figure 7.17 Load vs Displacement for the 0.9-m CISS Pile a) Post-Blast Series 8 b) Post-Blast Series 10

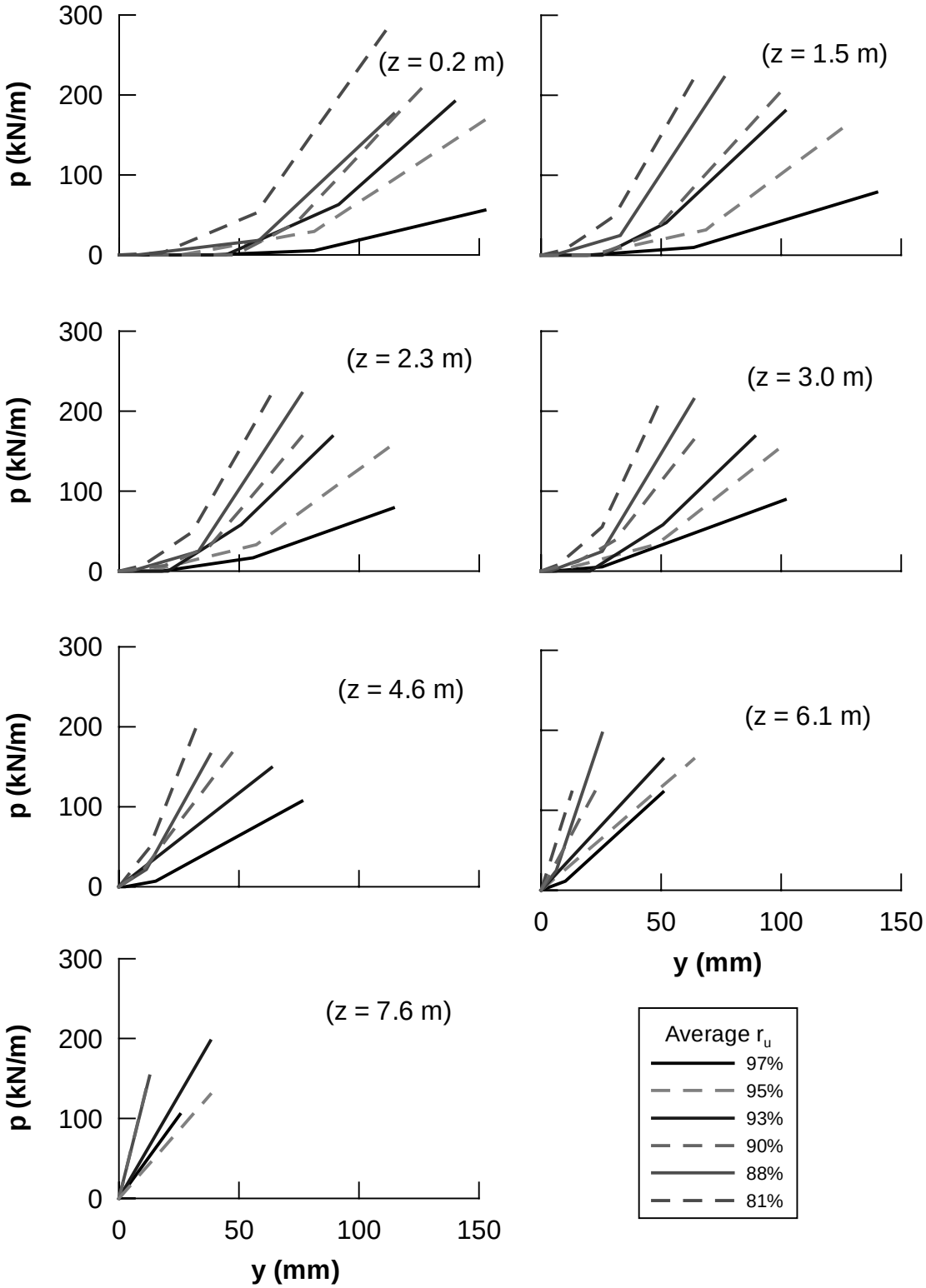

Figure 7.18 Back-Calculated p-y curves for 0.9-m CISS Pile Test at Average Excess Pore Pressure Ratios Ranging between 97% and 74%

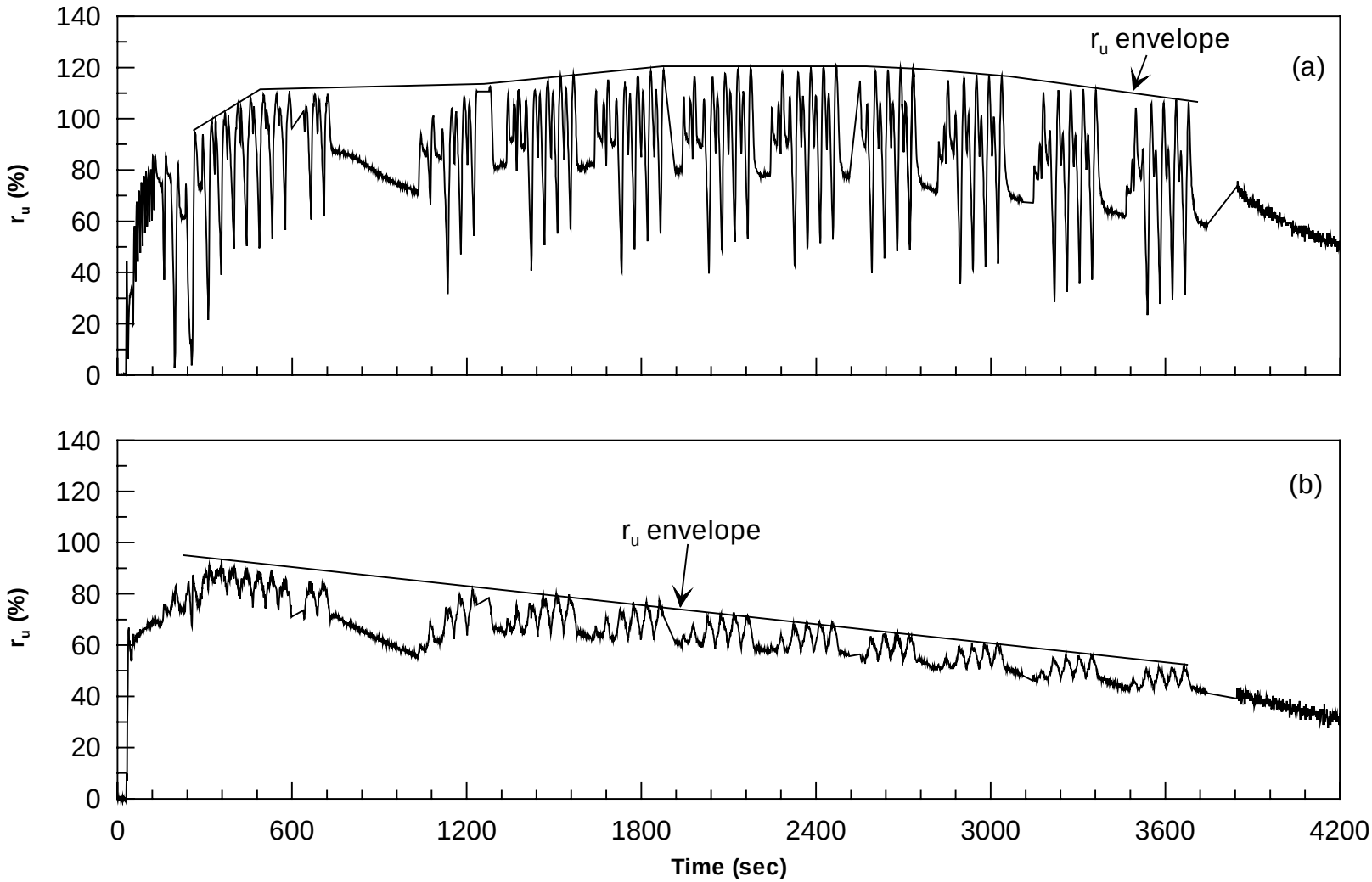

Figure 7.19 Excess Pore Pressure Ratio a) Adjacent to the 0.9-m CISS Pile b) 4.2 meters from the CISS Pile

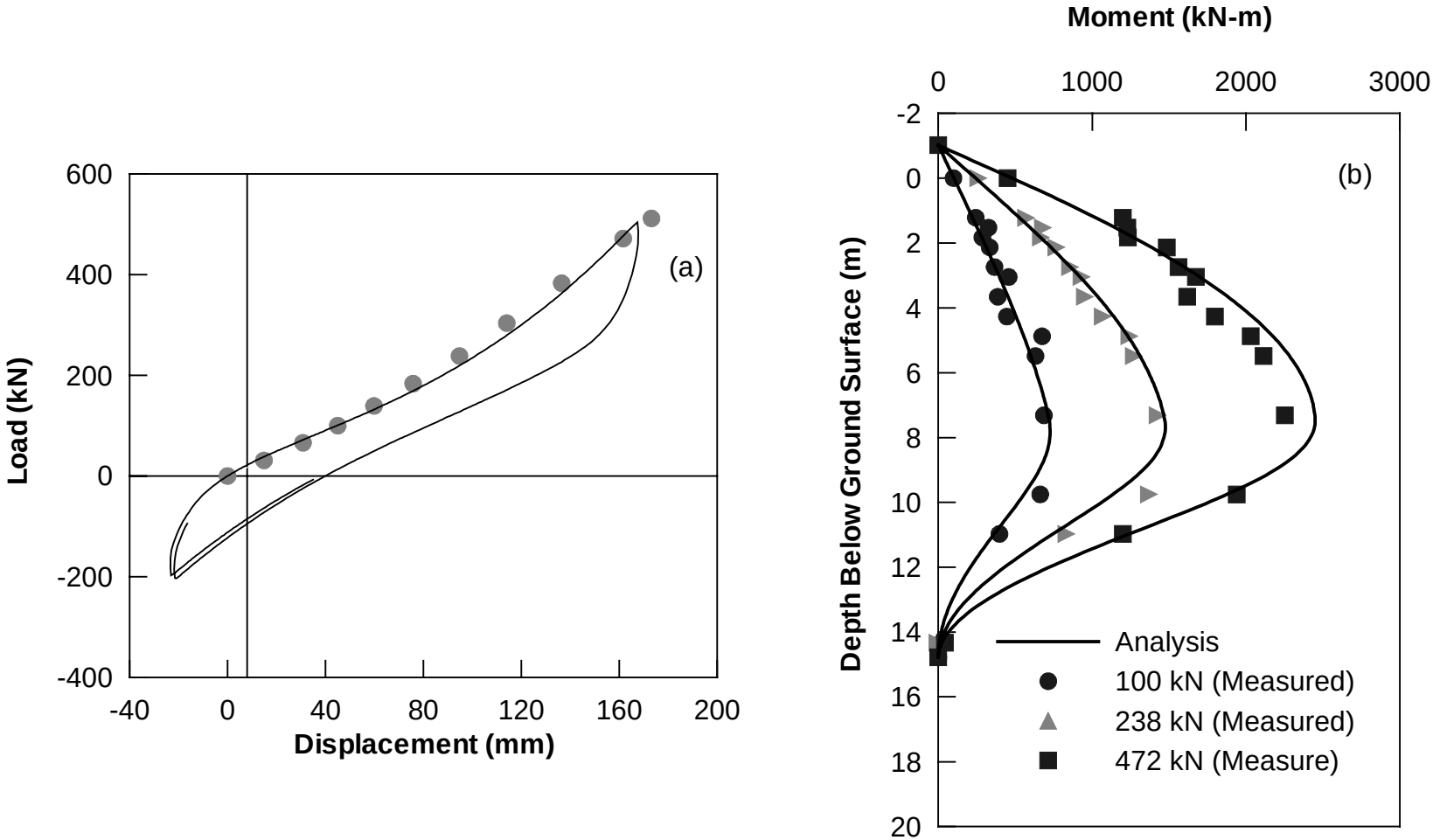

Figure 7.20 Comparison of Test Results and Analysis using Back-Calculated p-y Curves for the 0.9-m CISS Pile for Post-Blast Series 1 a) Load vs. Displacement b) Moment vs. Depth

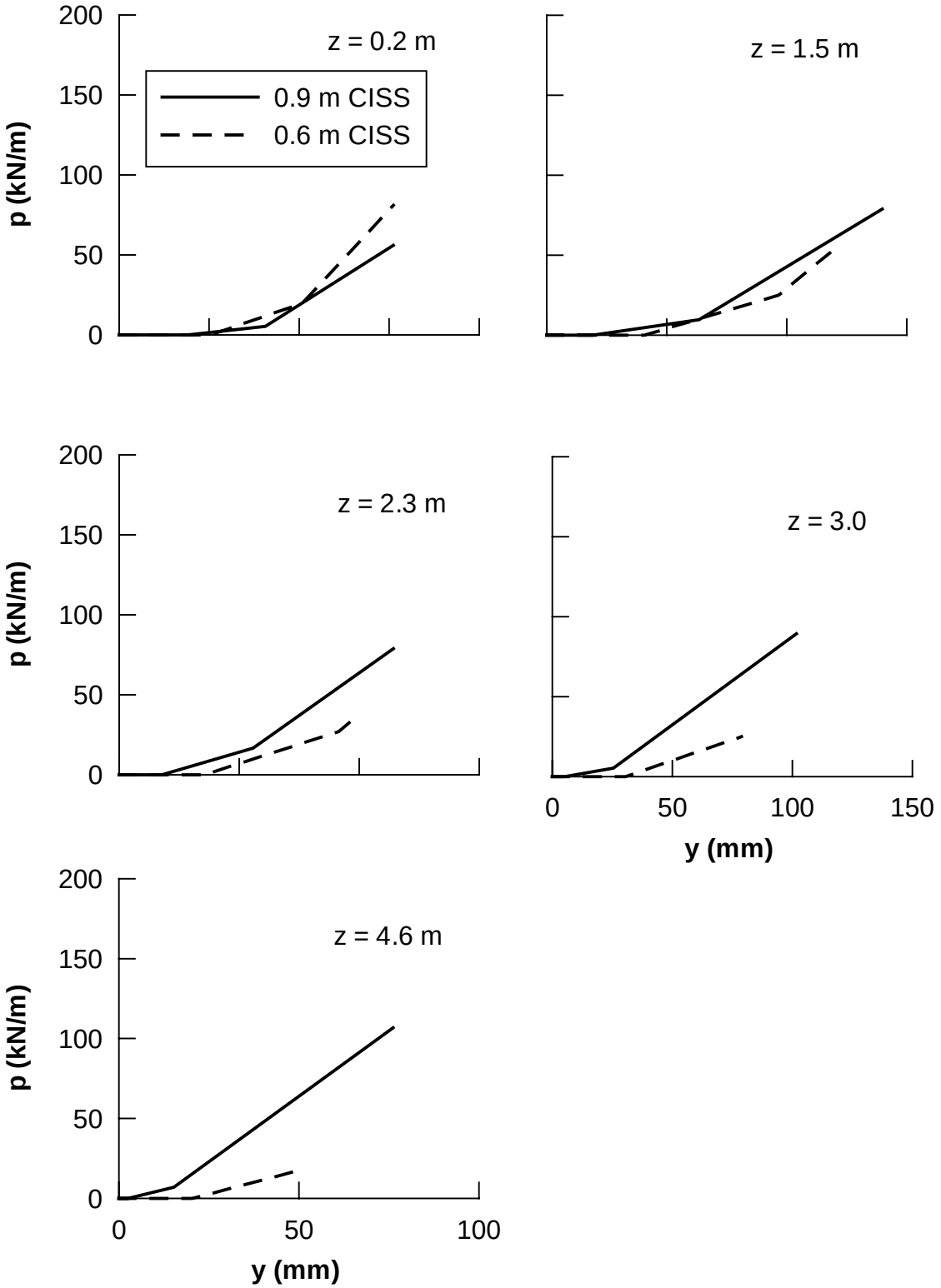

Figure 7.21Comparison of 0.6-m and 0.9-m CISS Pile Back-Calculated p-y Curves for Post-Blast Series 1

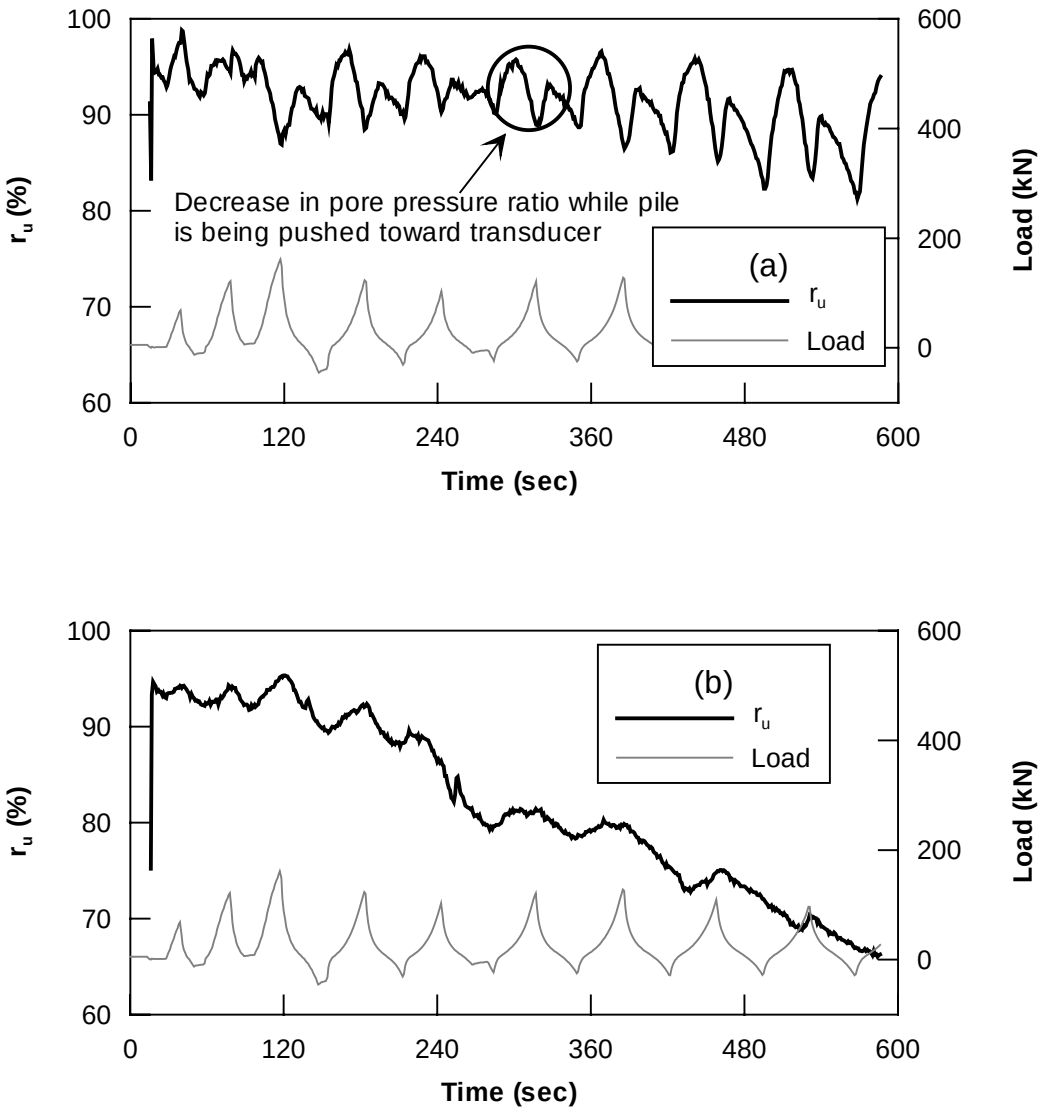

Figure 7.22 Excess Pore Pressure Ratio a) within 1 meter from pipe pile b) 4.2 meters from pipe pile

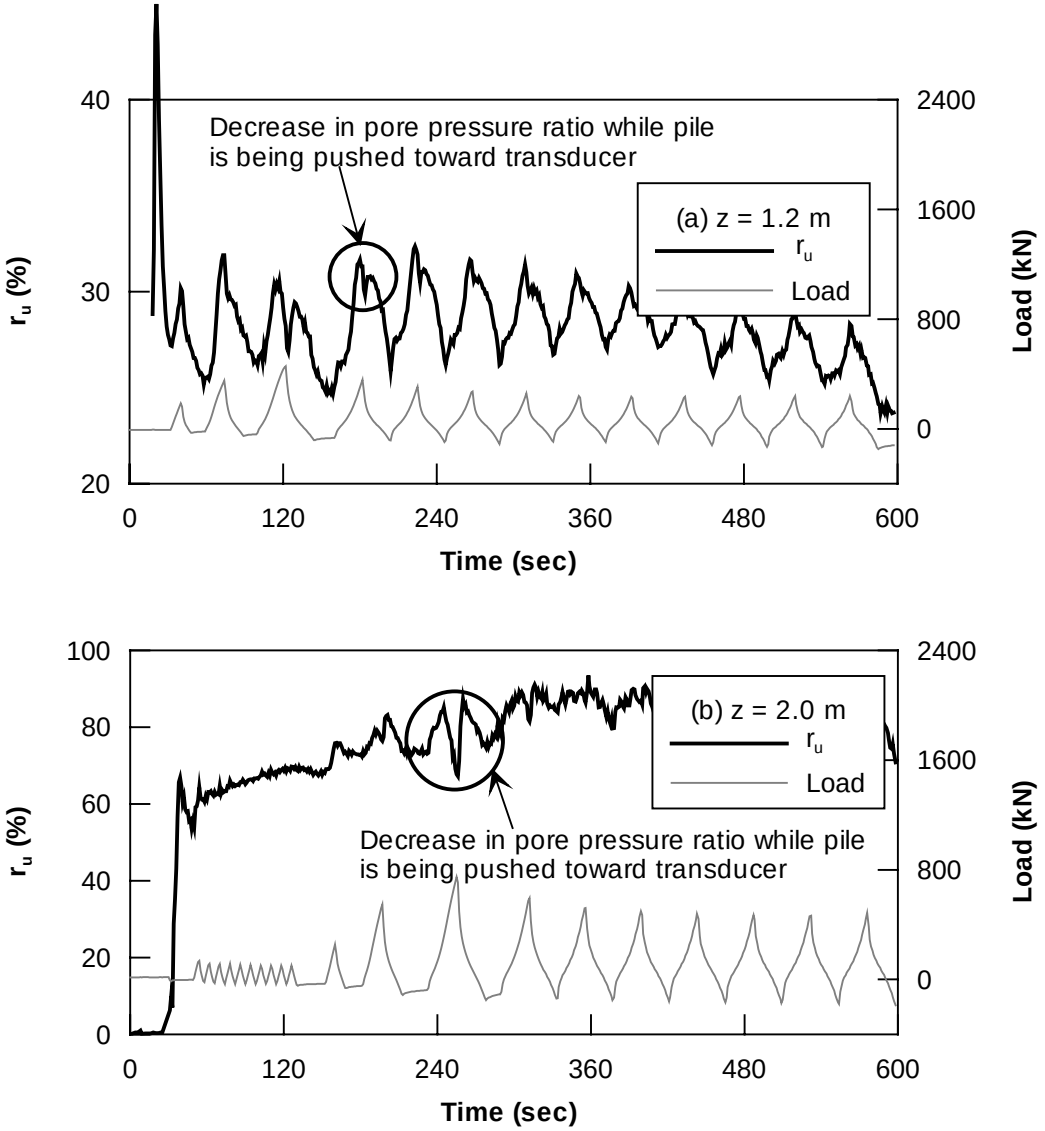

Figure 7.23 Excess Pore Pressure Ratio versus Time in Front of CISS Piles a) 4.2 m from the 0.6-m CISS Pile b) 4.2 m from the 0.9-m CISS Pile

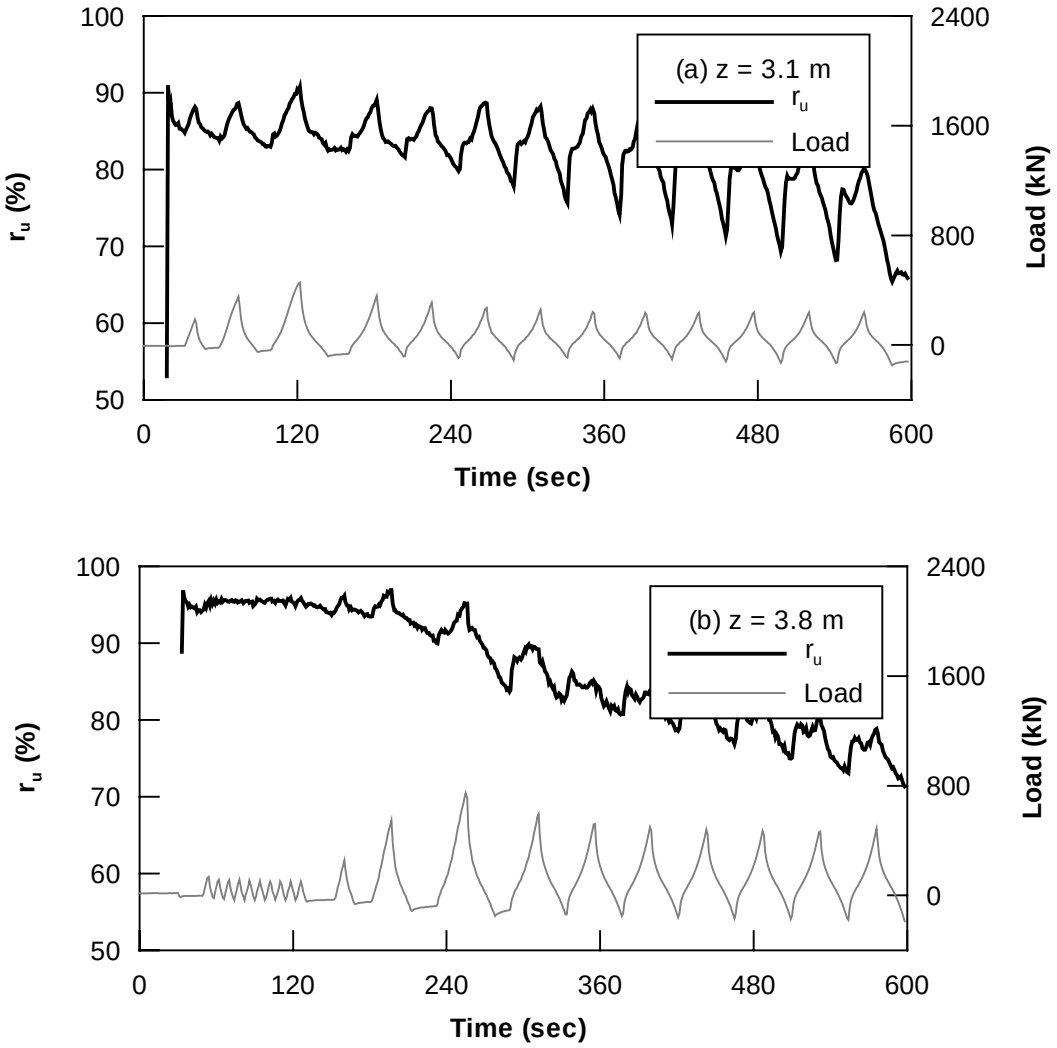

Figure 7.24 Excess Pore Pressure Ratio 4.2 m from a) the 0.6-m CISS Pile b) the 0.9-m CISS Pile

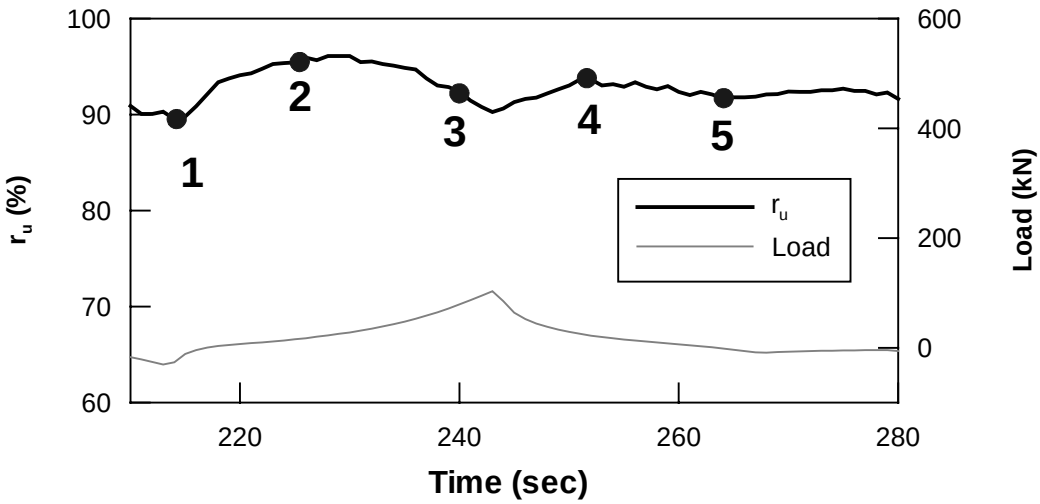

		Δ Volume	Δ U	Description
1	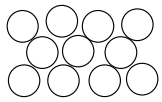	0	0	Initial Condition Zero Load - Zero Displacement
2	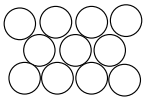	↓	↑	Pile pushed into soil causing loose soil to densify
3	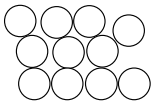	↑	↓	Continued displacement of pile into soil - Soil changes from contractive to dilative in behavior
4	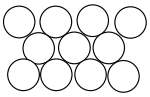	↓	↑	Unloading of pile - Soil particles settle and move into more stable configuration
5	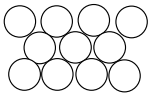	↓	↓	Loading of pile stops - soil continues to settle as pore pressures dissipate at rate dependent on hydraulic conductivity of soil until steady state reached or until pile loaded and cycle repeats

Figure 7.25 Detailed Excess Pore Pressure Response for the 0.3-m Pipe Pile and Corresponding Description of Soil Behavior

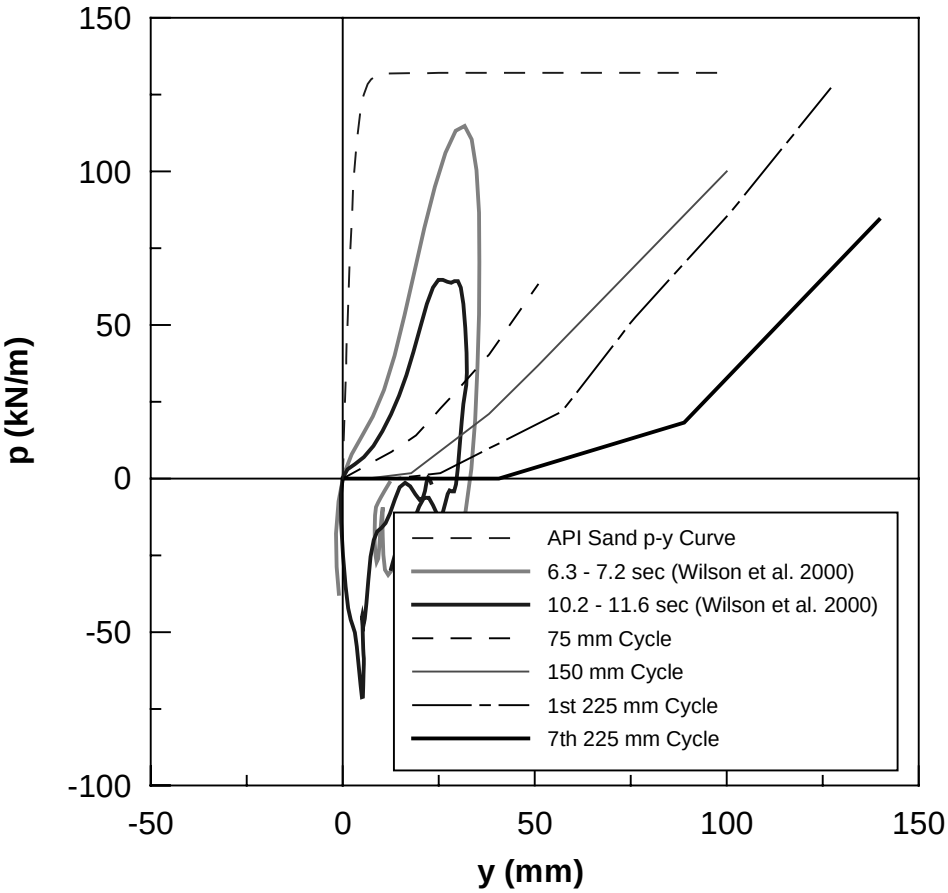

Figure 7.26 Comparison of p-y Curves from API, Centrifuge Testing, and Full-Scale Tests at Treasure Island at a depth of 1.8 meters

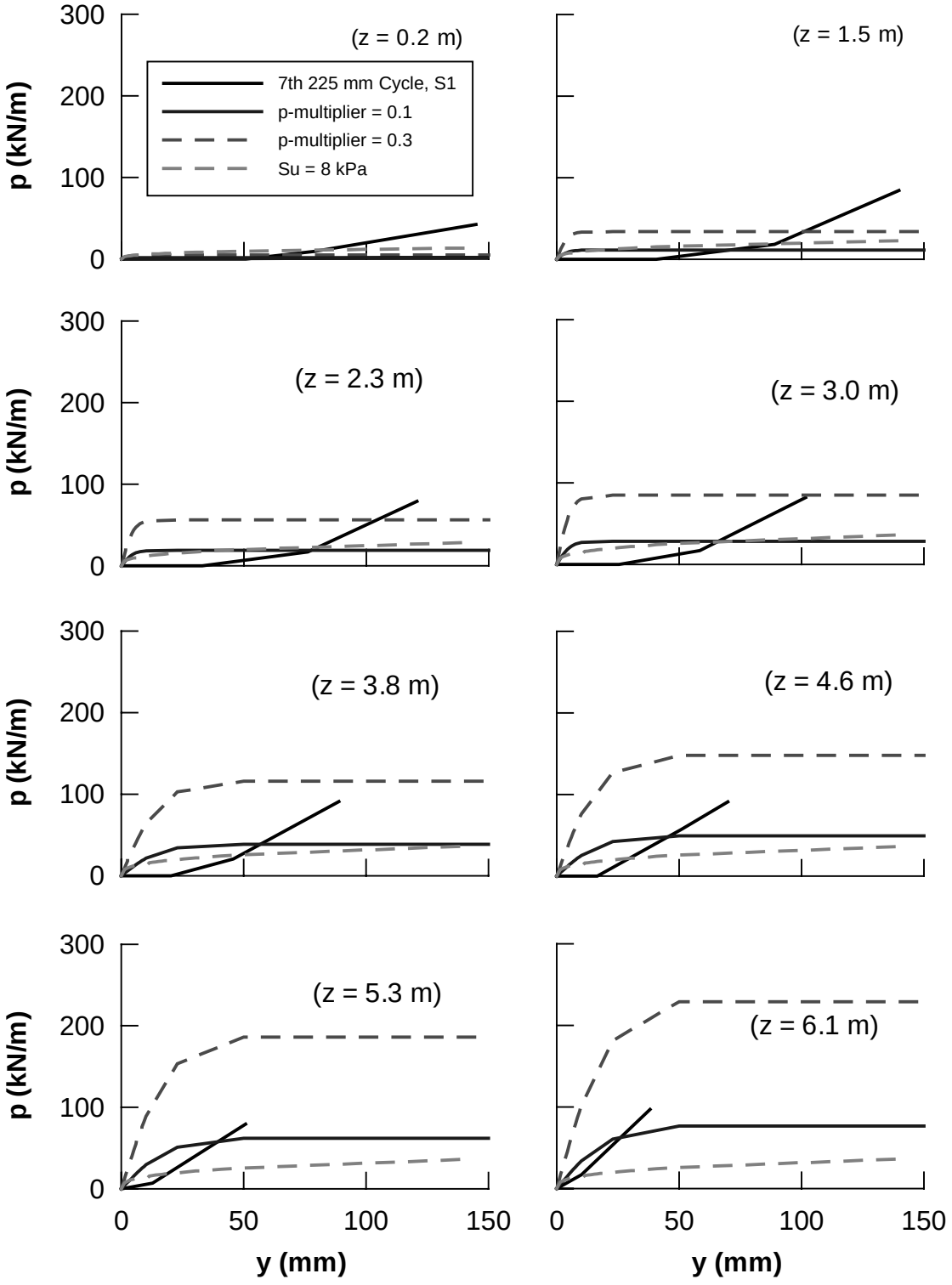

Figure 7.27 Comparison of Back-Calculated p-y curves from the 7th 225-mm Displacement Cycle for Load Series 1 of the 0.6-m CISS Pile Test with Modified API Sand and soft clay p-y Curves

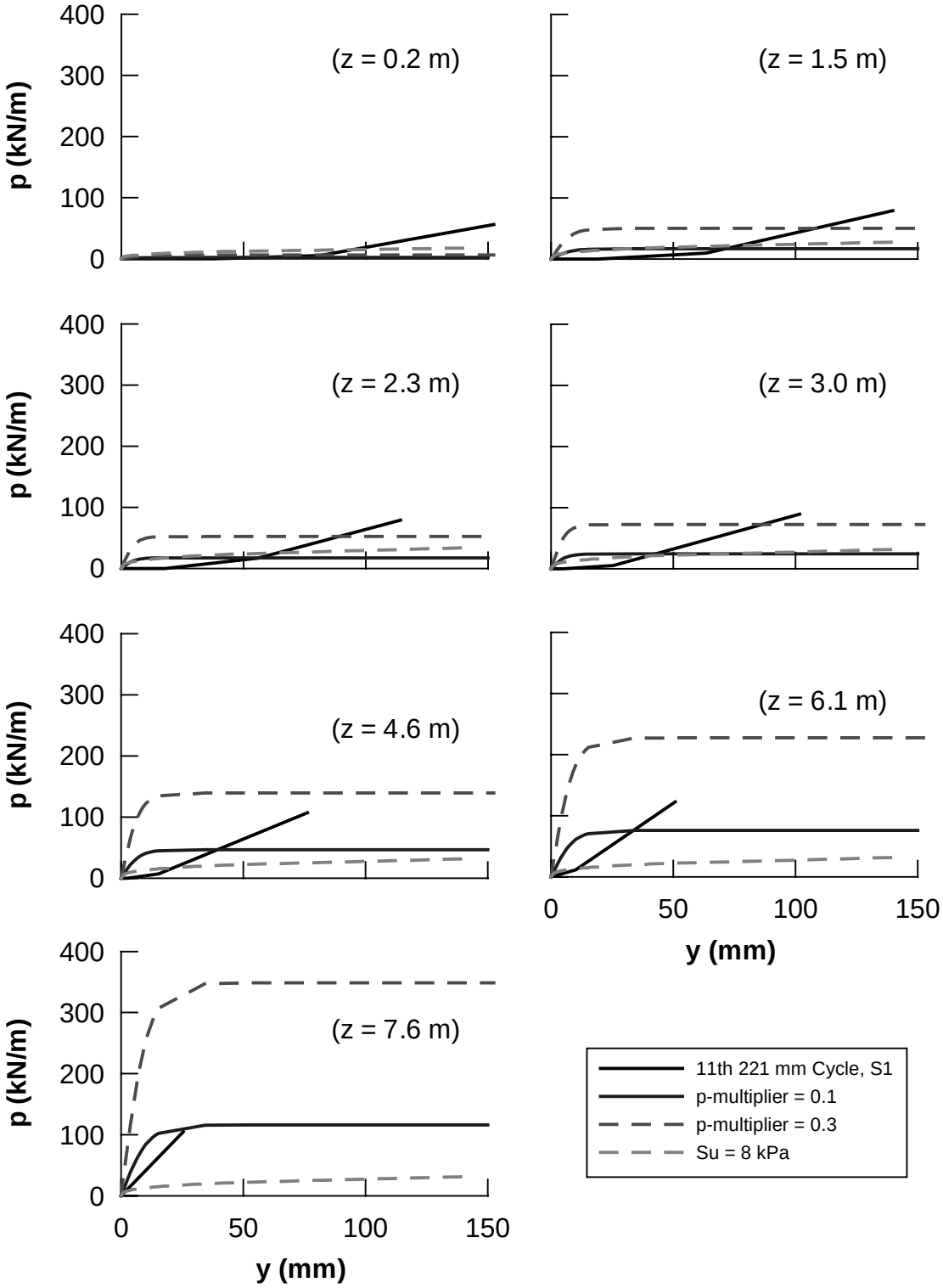

Figure 7.28 Comparison of Back-Calculated p-y curves from the 11th 221-mm Displacement Cycle for Load Series 1 of the 0.9-m CISS Pile Test with Modified API Sand and soft clay p-y Curves

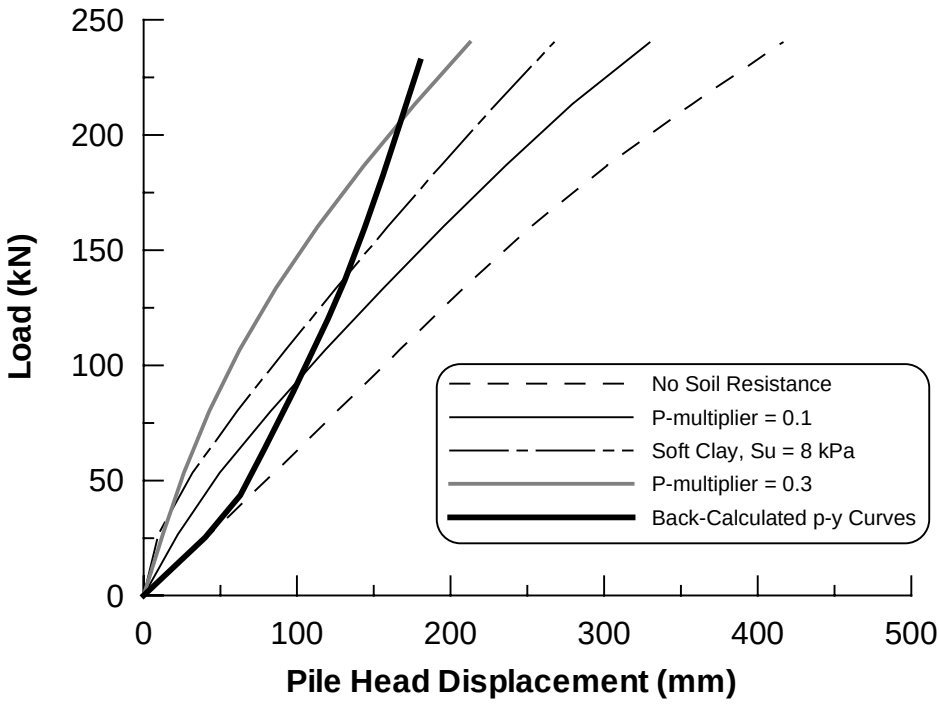

Figure 7.29 Load vs Pile Head Displacement for the 0.6-m CISS Pile from Analyses using Modified and Back-Calculated p-y Curves

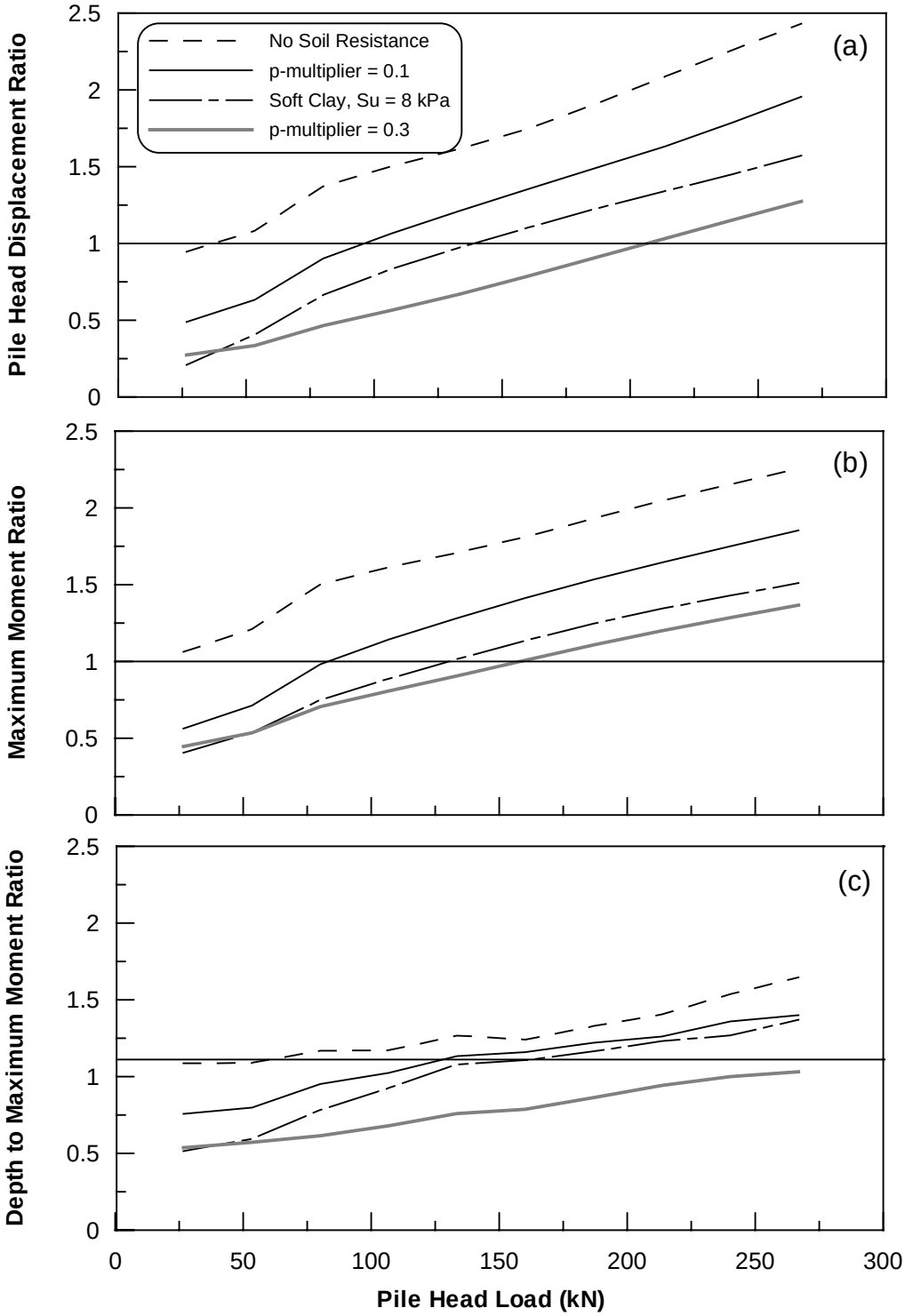

Figure 7.30 Predicted Pile Head Displacement, Maximum Moment, and Depth to Maximum Moment using Modified p-y Curves Compared to Response Obtained using Back-Calculated p-y Curves for the 0.6-m CISS Pile a) Pile Head Displacement b) Maximum Moment c) Depth to Maximum Moment

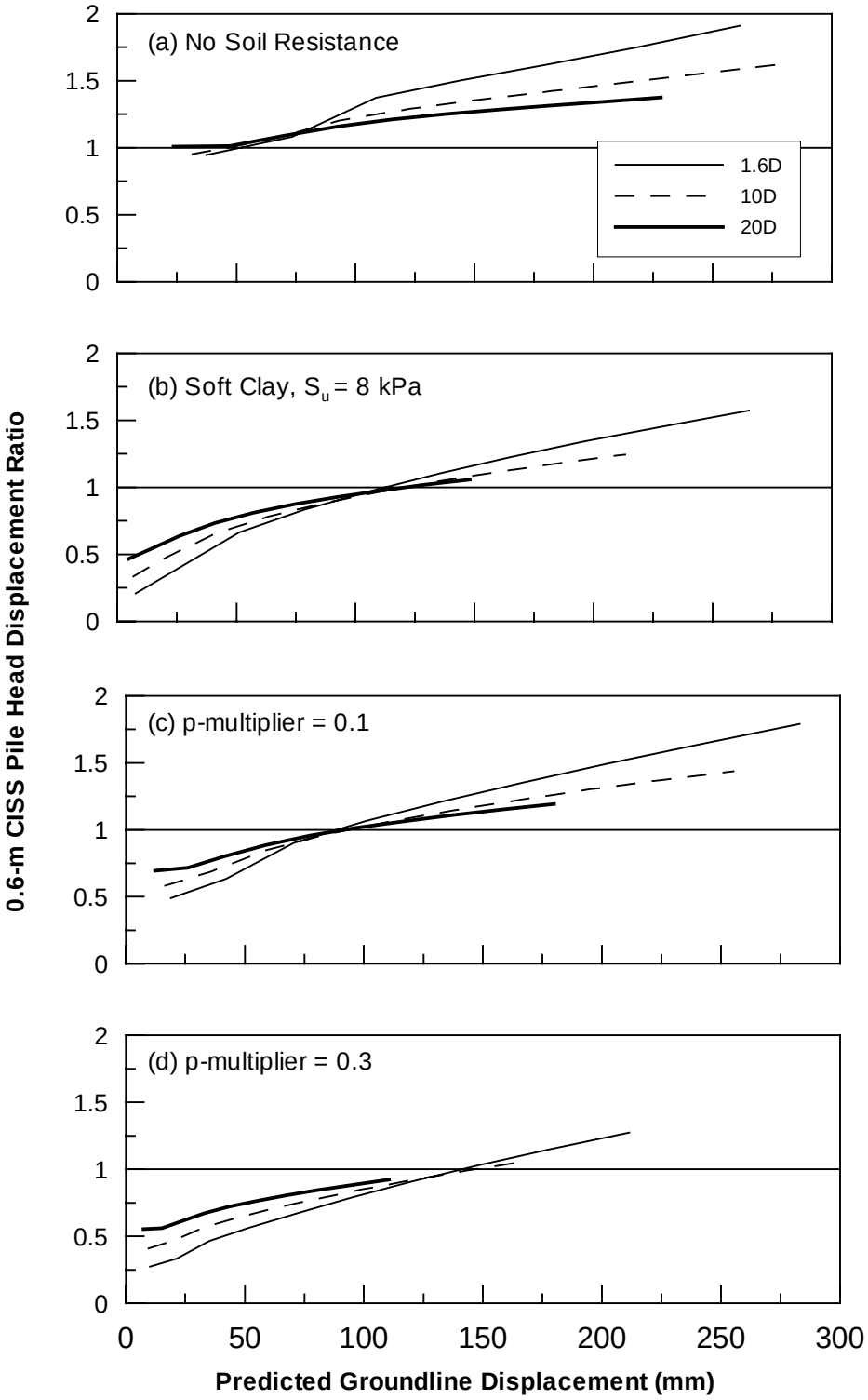

Figure 7.31 Calculated Pile Head Displacement for 0.6-m CISS Pile using a) No Soil Resistance b) Soft Clay p-y Curves c) and d) API Sand p-y Curves Compared to Pile Head Displacement Calculated using Back-Calculated p-y Curves

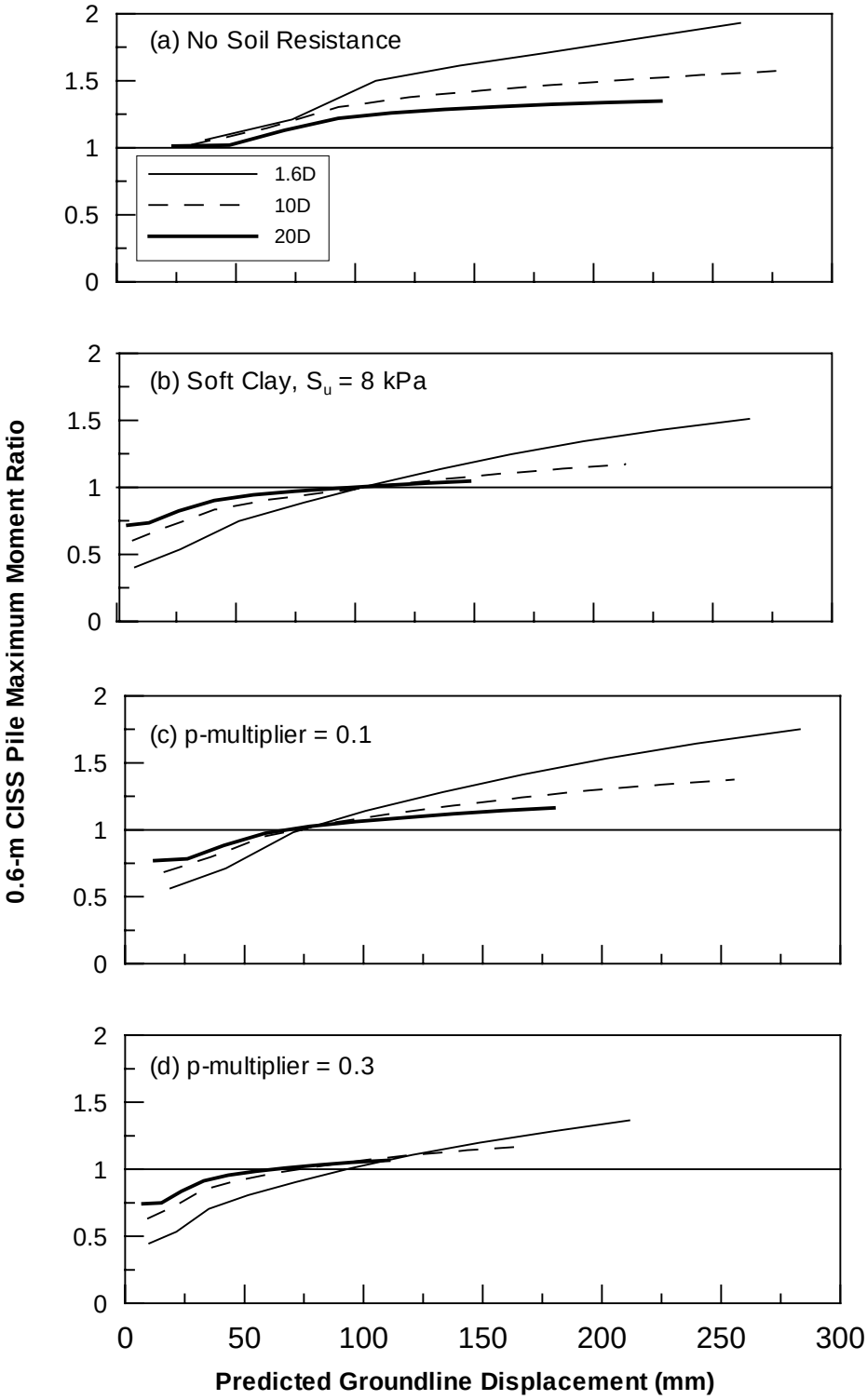

Figure 7.32 Calculated Maximum Moment for 0.6-m CISS Pile using a) No Soil Resistance b) Soft Clay p-y Curves c) and d) API Sand p-y Curves Compared to Maximum Moment Calculated using Back-Calculated p-y Curves

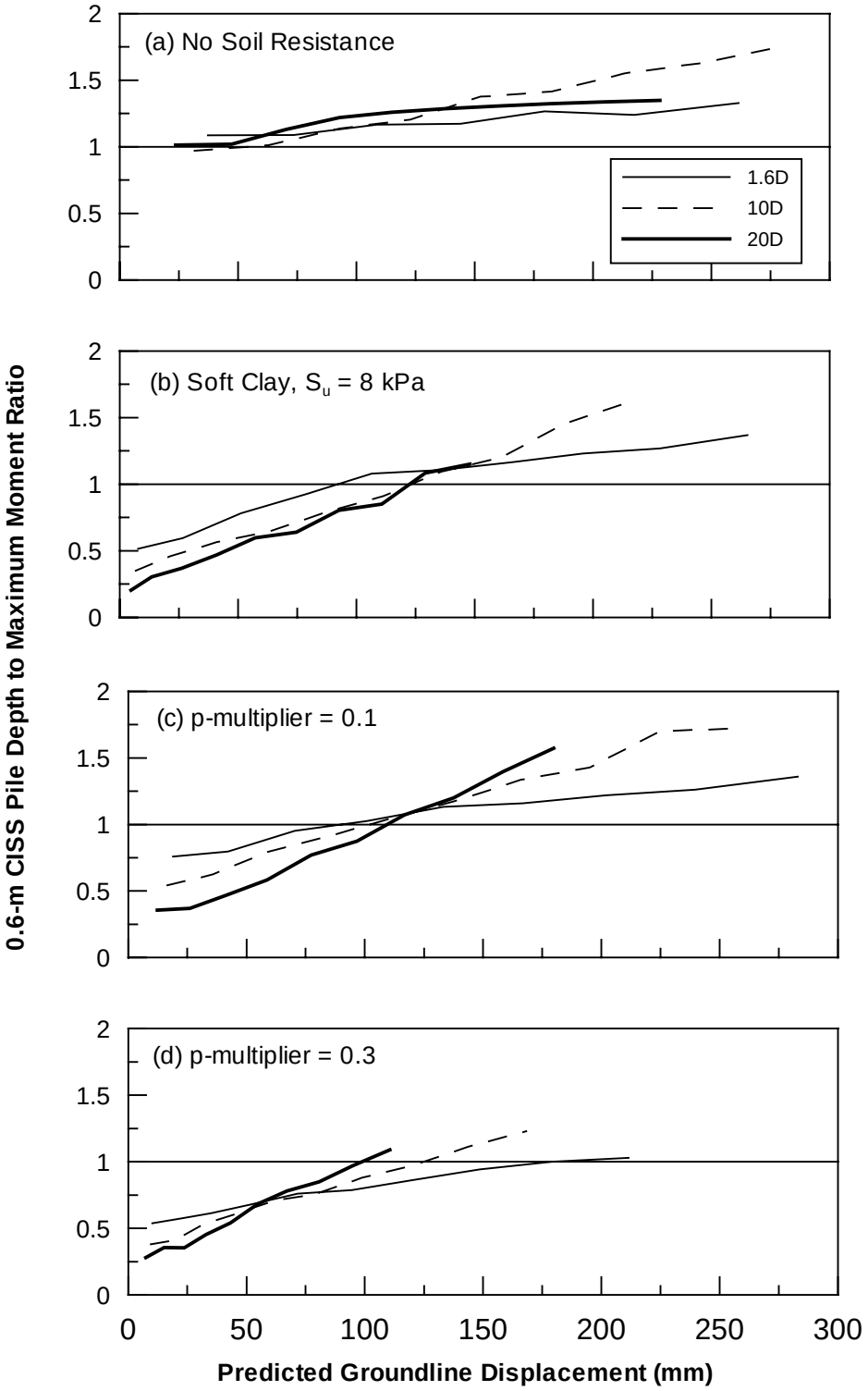

Figure 7.33 Calculated Depth to Maximum Moment for 0.6-m CISS Pile using a) No Soil Resistance b) Soft Clay p-y Curves c) and d) API Sand p-y Curves Compared to Maximum Moment Calculated using Back-Calculated p-y Curves

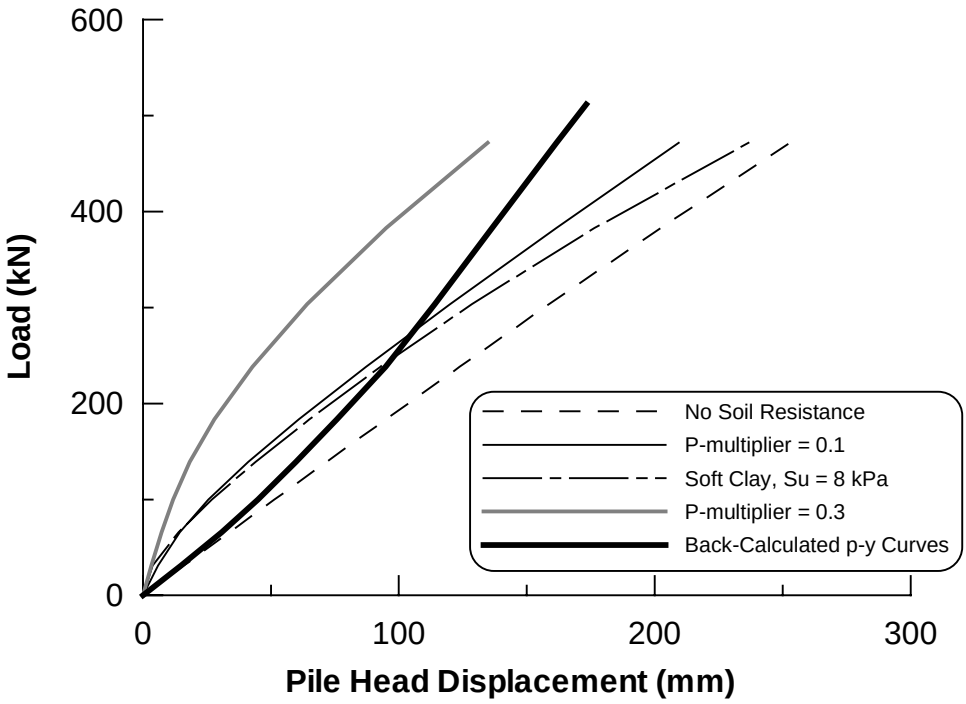

Figure 7.34 Load vs Pile Head Displacement for the 0.9-m CISS Pile from Analyses using Modified and Back-Calculated p-y Curves

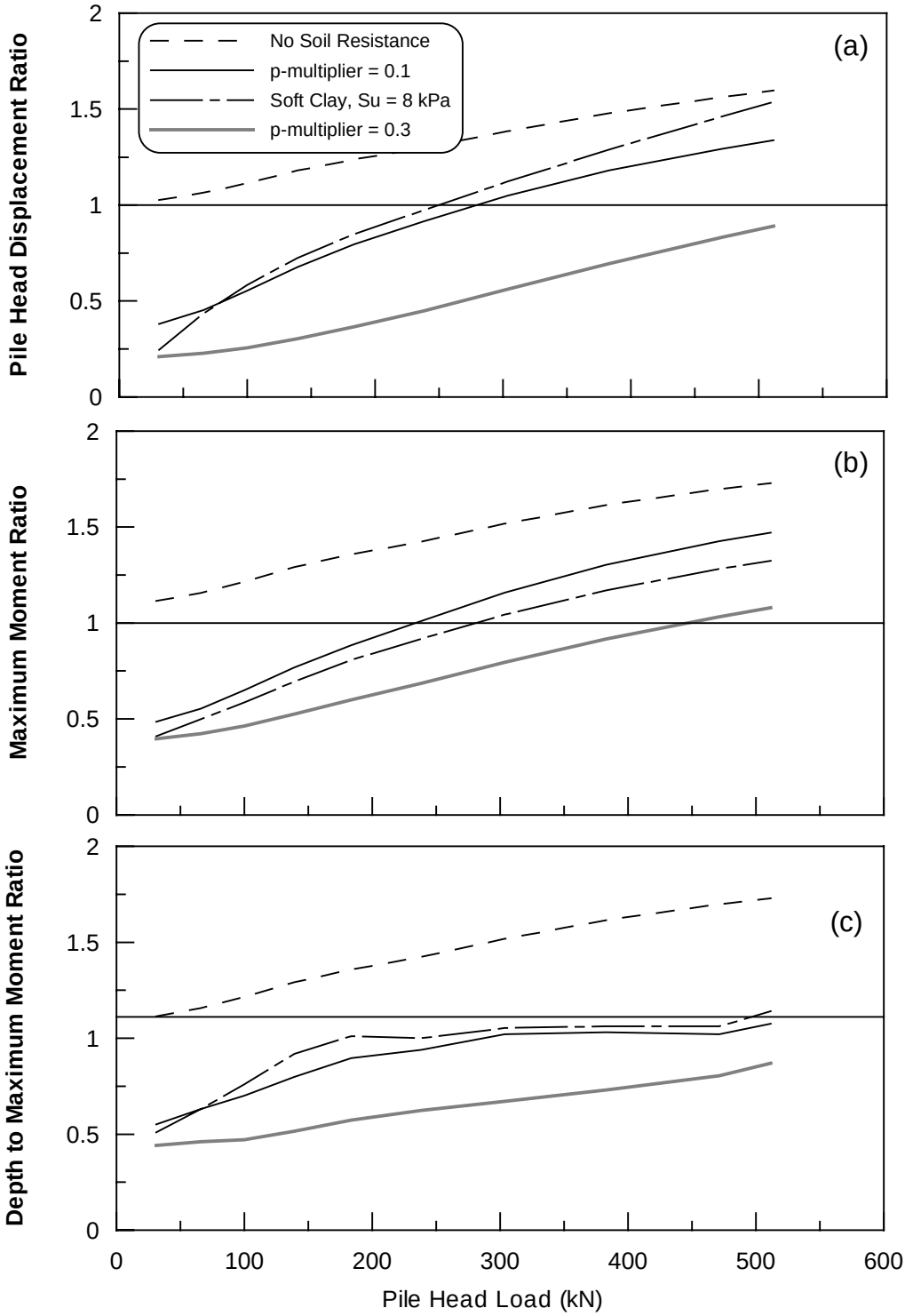

Figure 7.35 Predicted Pile Head Displacement, Maximum Moment, and Depth to Maximum Moment using Modified p-y Curves Compared to Response Obtained using Back-Calculated p-y Curves for the 0.9-m CISS Pile a) Pile Head Displacement b) Maximum Moment c) Depth to Maximum Moment

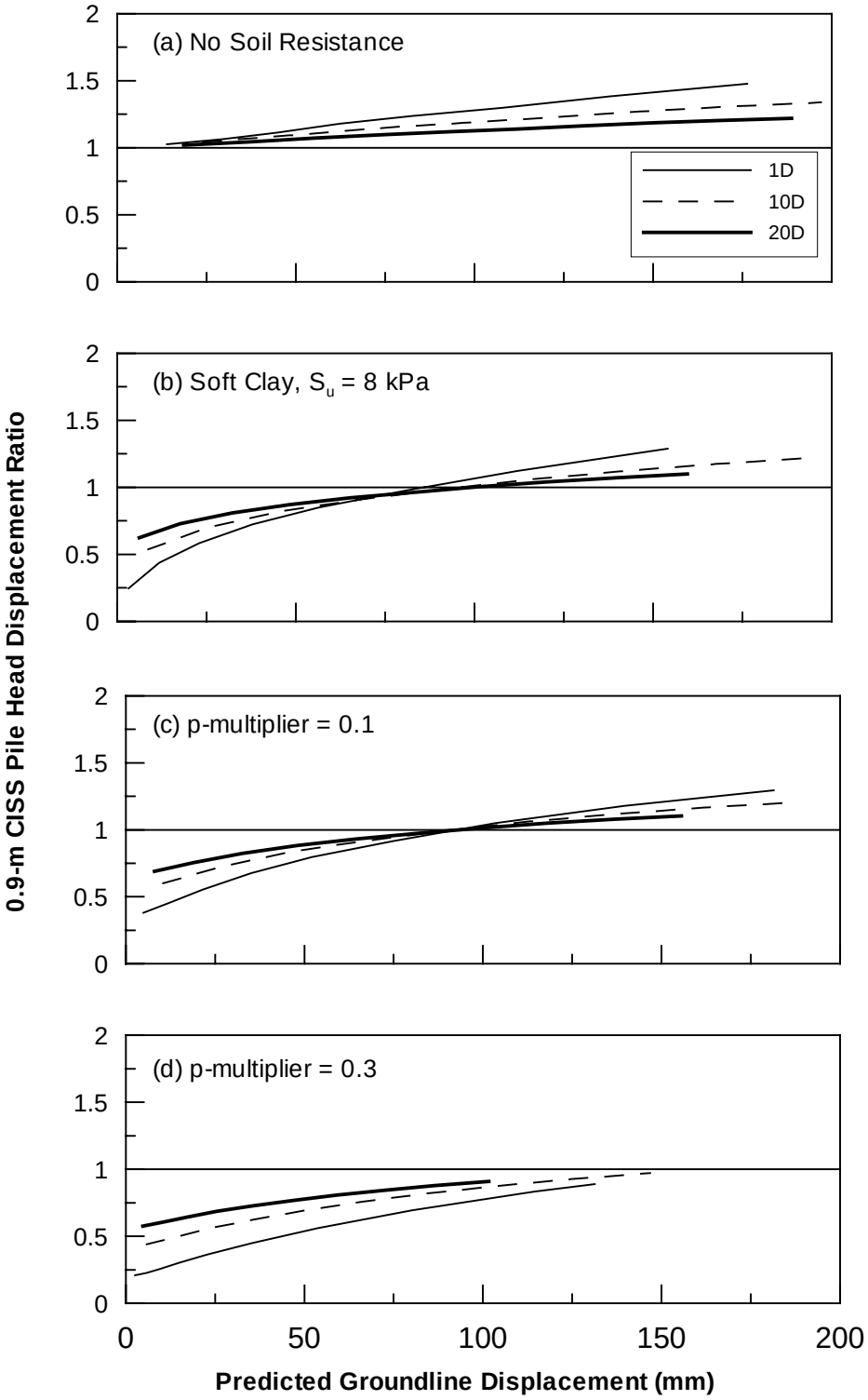

Figure 7.36 Calculated Maximum Moment for 0.9-m CISS Pile using a) No Soil Resistance b) Soft Clay p-y Curves c) and d) API Sand p-y Curves Compared to Maximum Moment Calculated using Back-Calculated p-y Curves

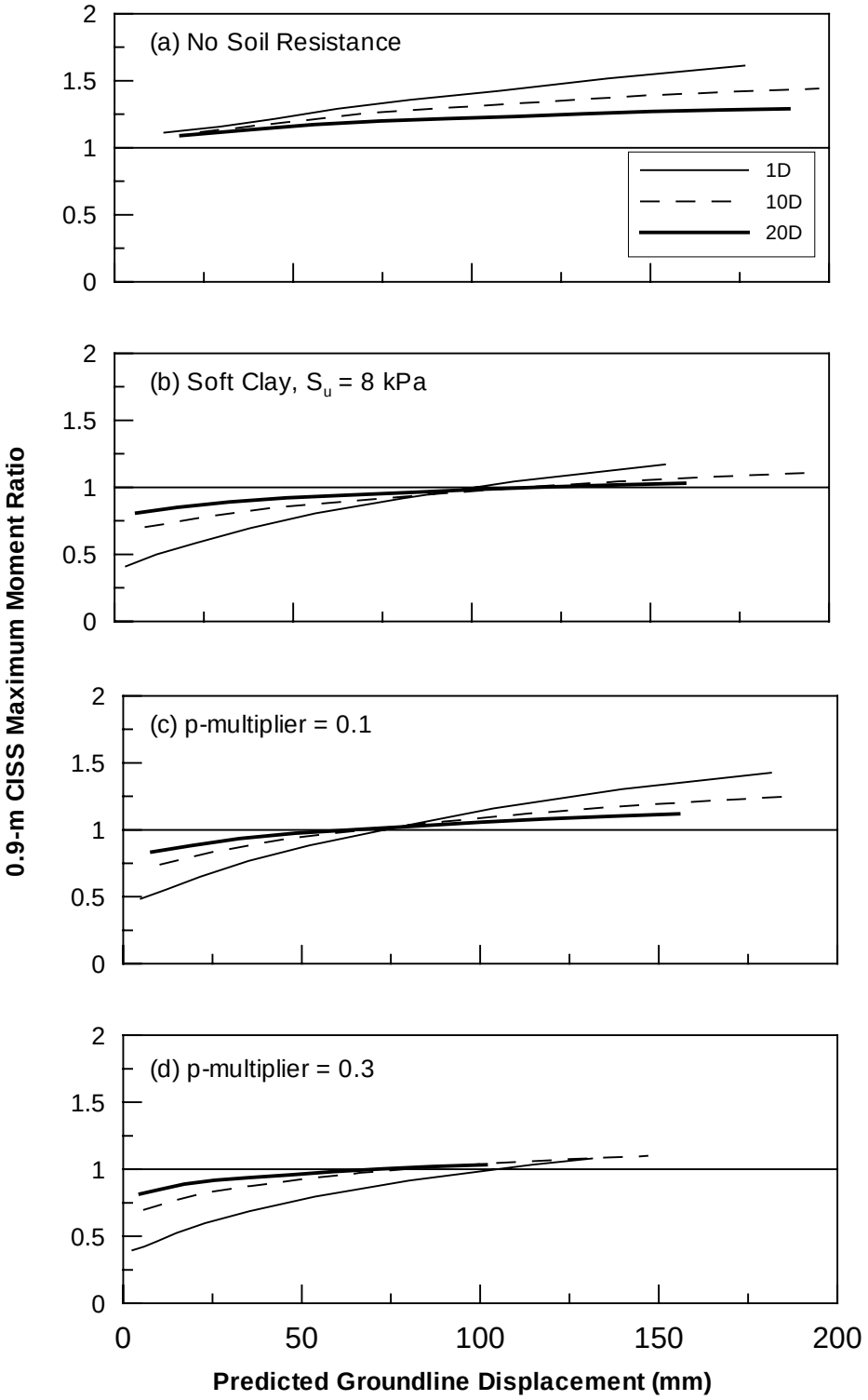

Figure 7.37 Calculated Maximum Moment for 0.9-m CISS Pile using a) No Soil Resistance b) Soft Clay p-y Curves c) and d) API Sand p-y Curves Compared to Maximum Moment Calculated using Back-Calculated p-y Curves

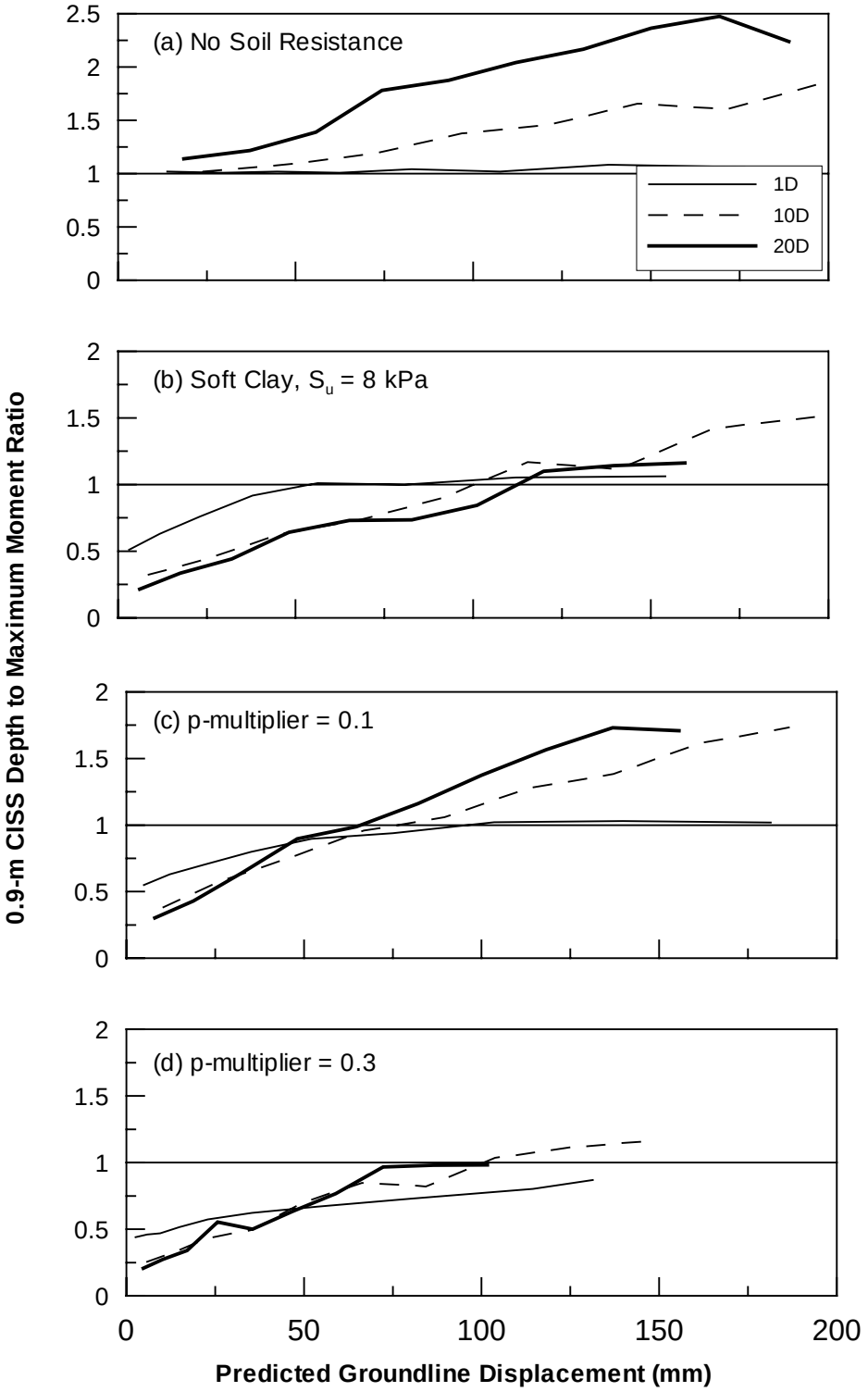

Figure 7.38 Calculated Depth to Maximum Moment for 0.9-m CISS Pile using a) No Soil Resistance b) Soft Clay p-y Curves c) and d) API Sand p-y Curves Compared to Maximum Moment Calculated using Back-Calculated p-y Curves

8 ANALYSIS OF STEEL PIPES AND PILE GROUPS

8.1 Analysis of Single Pile Response for Pre-Blast Load Tests

8.1.1 Summary of Site Conditions and Soil Property Selection

As indicated previously, site-specific geotechnical investigations were carried out as part of this study. The soil profile at the single pile site consists of hydraulically placed fill and native shoal sands to a depth to 6 m. The hydraulic fill generally consists of loose fine sand or silty sand with thin interbeds of lean clay. Silty sand and Young Bay Mud underlie the sand. The interpreted soil profile at the single pile test area is shown in Fig. 8.1 based on the results of all the field and laboratory testing. The excavated ground surface was about 1 m below the original ground surface and the water table was typically 0.5 m below the excavated ground surface during testing The average horizontal hydraulic conductivity of the sand was 3.5×10^{-3} cm/sec (Faris, personal communication). The sand typically classified as SP-SM material according to the Unified Soil Classification system and generally has a D_{50} between 0.2 and 0.3 mm.

A number of in-situ tests were performed at the site including standard penetration testing (SPT), cone penetration testing (CPT), dilatometer testing (DMT), cone-pressuremeter testing (PMT), and shear wave velocity logging. The standard penetration resistance and cone resistance values were normalized to an overburden pressure of one atmosphere (q_{c1}) using procedures outlined by the Youd and Idriss (2001). The $(N_1)_{60}$ values in the sand typically ranged from 7 to 16 as shown in Fig. 8.1. Six CPT tests were performed across the test site and the average normalized cone resistance (q_{c1}) profile is shown along with mean ± one standard

deviation bounds in Fig. 8.1. The average cone resistance typically ranged from 6 to 9 MPa in the upper sand layer and 4 to 6 Mpa in the underlying silty sand layer. The relative density (D_r) based on the SPT was computed using the equation

$$D_r = \left[\frac{(N_1)_{60}}{40} \right]^{0.5} \tag{8.1}$$

developed by Kulhawy and Mayne (1990). The relative density based on the CPT was computed using the equation

$$D_r = \left[\frac{\left(\frac{q_{c1}}{p_a} \right)}{305} \right]^{0.5} \tag{8.2}$$

developed by Kulhawy and Mayne (1990) where p_a is atmospheric pressure and the sand is assumed to be normally consolidated. The relative density computed using equations 8.1 and 8.2 is plotted versus depth in Fig. 8.1 and the agreement is very good. The estimated D_r was typically between 40 and 60 percent in the clean sand layers and dropped to about 30 percent in the silty sands.

One DMT sounding was made and the interpreted horizontal earth pressure coefficient (K_o) is plotted along with the Dilatometer modulus (E_D) as a function of depth in Fig. 8.2. Both The K_o and E_D values drop rapidly near the surface to a relatively constant value below 1.5 m. K_o stabilizes at about 0.6 and E_D averages 16 ± 4 MPa. These results are in good agreement with tests reported by De Alba et al. (1994). Four cone PMT tests were also performed at approximately one-meter depth intervals. The limit pressure (p_l), initial pressuremeter modulus

(E_m), and re-load pressuremeter modulus (E_r) are shown in Fig. 8.2 as a function of depth. All parameters show a small increase to a depth of 1.7 m but then remain relatively constant at greater depths. Shear wave velocity was measured using both a conventional downhole approach and two seismic cone tests. The velocity profiles are also shown in Fig. 8.2 and the agreement between the methods is generally very good. The velocity is also relatively constant with depth and the average value is about 125 m/sec. All the in-situ tests confirm that the properties of the sand are relatively uniform with depth.

The angle of internal friction in the sands was estimated using two correlations, the API method and the Bolton method. For the API method, the friction angle (ϕ) can be give in terms of the relative density by the equation

$$\phi = 16D_r^{\ 2} + 0.17D_r + 28.4 \tag{8.3}$$

where relative density is a fraction. For the Bolton (1986) method, with quartz sands, the triaxial compression friction angle (ϕ_{tc}) is given by the equation

$$\phi_{tc} = \phi_{cv} + 3I_{rd} \tag{8.4}$$

where ϕ_{cv} is the critical void ratio friction angle. Bolton (1986) recommends a value of 31 to 33 degrees for ϕ_{cv} in quartz sands with some silt and we have assumed a value of 32 degrees in this study. I_{rd} is given by the equation

$$I_{rd} = D_r\left[10 + \ln[100(\frac{p_f}{p_a})]\right] - 1 \tag{8.5}$$

where p_f is the mean effective stress at failure. Horizontal pressures at the failure state were estimate using Rankine values for active and passive pressures. The friction angle versus depth profiles computed using these two methods are shown in Fig. 8.1 and there is a substantial difference between the two estimates. The friction angles estimated using the Bolton approach

are typically about five or six degrees higher than the API values. The friction angles estimated using the API approach are more typical of what would be used in engineering practice and typically range from 30 to 33 degrees.

8.1.2 Test Pile Properties and Instrumentation

As indicated previously, the single pile test involved a single steel pipe pile reacted against an H pile. The steel pipe pile had an outside diameter of 324 mm (12.75), a wall thickness of 9.5 mm (0.375 in), and was driven open-ended to a depth of 11.5 m below the excavated ground surface. The pile plugged at a depth of 5.5 m when it reached the looser silty sand layer. The steel pipe conformed to ASTM A252 Grade 3 specifications. Tests performed by the supplier, Geneva Steel, on 192 specimens indicate a mean yield strength of 404,592 kN/m^2 (58,700 psi) based on a 0.2% offset criteria with a standard deviation of 15,168 kN/m^2 (2200 psi). The moment of inertia of the pipe was 1.16 x 10^8 mm^4 (279 in^4). An angle iron was welded to both sides of the pile in the direction of loading to protect the strain gauges, which increased the moment of inertia to 1.43 x 10^8 mm^4 (344 in^4).

The H-pile, which was also driven to a depth of 11.5 m, was an HP12x53 section (306 mm wide flange with a depth of 299 mm) with a moment of inertia of 1.64 x10^8 mm^4 (393 in^4) that increased to 1.89 mm^4 (452.4 in^4) when the angle irons were attached. Therefore, the H-pile while having about the same width as the pipe pile had a moment of inertia that was about 30% larger. Although a plug likely developed between the flanges of the H-pile as it was driven, there was little evidence observable from the ground surface. The sand above the plug apparently caved into the space between the flanges, creating a relatively small depression around the pile prior to testing.

Electrical resistance strain gauge pairs were placed on the outside face of both piles at 0.38 m (1.25 ft) intervals from a depth of 0.3 to 2.6 m (1 ft to 8.5 ft) and then at 0.76 m (2.5 ft) intervals to a depth of 9.45 m (31 ft). One additional gauge was placed at depth of 11 m (36 ft).

The load was applied at a height of 0.69 m above the ground surface using a 2200 kN (250 ton) capacity hydraulic actuator with a stroke of ± 0.6 m. The actuator was controlled with an electromechanical servo-valve and the electric hydraulic pump drove the actuator at a rate of 19 mm/sec. Load cells were attached to the actuator to measure the applied force and string potentiometers were used to measure absolute displacement as described previously. The test piles were spaced approximately 6.1 m apart center to center and the actuator was attached to each pile with a pinned connection to create a free-head end condition.

8.1.3 Measured Response

The virgin load-displacement curves for the pipe pile and H-pile are shown in Figs. 8.3 for comparison purposes. The maximum displacement of the pipe pile was set at 38 mm and the actuator moved at a rate of 19 mm/sec so the maximum displacement on an individual pile developed in about 4 seconds. Although the H-pile had a 30% higher moment of inertia then the pipe pile, the H-pile deflected 27% more at the maximum load. This is likely due to the loose sand between the flanges of the H-pile near the ground surface resulting from the formation of a plug as the pile was driven. The poor performance of the H-pile in this test program points out the potential for unsatisfactory lateral resistance for this pile type when soil plugs develop.

Data obtained from the strain gages were used to calculate the bending moment (M) for the pre-blast tests using the equation

$$M = \frac{EI \cdot \left(\varepsilon_T - \varepsilon_c\right)}{h} \tag{8.6}$$

where ε_T is the tensile strain, ε_C is the compressive strain, and h is the horizontal distance between gauges spaced at equal but opposite distances from the neutral axis. This approach cancels out any contribution due to axial strain, leaving only strains due to bending. In this case where displacements are low and the piles are behaving linearly, E was assumed to be constant at 200 GPa (29 x 10^6 psi). Fig. 8.4 shows the measured bending moment versus depth (below ground surface) curves for both piles at five load levels. The maximum moment typically occurred between 1.5 and 1.8 m below the ground surface. For a given load, the maximum bending moment is somewhat higher for the H pile than for the pipe pile due to the softer soil response around the H pile.

8.1.4 Computed Response

The pre-blast lateral pile response was computed using two different computer programs, namely LPILE plus version 3.0 (Reese et al, 1996) and SWM version 3.2 (Ansour et al. 1994). Both programs use the finite difference method where the pile is represented by a beam with lateral stiffness based on the pile modulus of elasticity and moment of inertia. However, the p-y curves used to define the lateral resistance of the soil per pile length (p) versus the lateral displacement of the pile (y) are developed using two different procedures. Nevertheless, both programs require similar information from the user regarding the sand properties including friction angle (ϕ) and effective unit weight (γ'). In addition, LPILE requires a modulus of lateral subgrade reaction or lateral subgrade modulus (k) and SWM requires the strain at 50% of failure load (ε_{50}). Initially, ϕ was defined using the API correlation while γ' was based on the relative density. The values for the layers used in the analysis are summarized in Tables 8.1. The k values used in the LPILE analysis were determined using the correlation with relative density

Table 8.1 Soil layering and soil properties used in lateral pile analysis with LPILE & SWM for single pile test site using API correlation for friction angle.

Depth Below Excavated Ground		Curve Type	Effective Unit wt.	Cohesion c	Friction Angle, ϕ	Lateral Subgrade Modulus, k	ε_{50}
Top (m)	Bottom (m)		(kN/m^3)	(kPa)	(degrees)	(MN/m^3)	(strain)
0.00	0.51	sand	19.5	0	33	24.4	-
0.51	2.59	sand	11.1	0	33	15.4	-
2.59	4.73	sand	11.1	0	32	13.6	-
4.73	7.49	sand	11.1	0	30	10.8	-
7.49	9.25	soft clay	9.5	19.2	0	-	0.01
9.25	10.16	sand	11.1	0	30	10.8	-
10.16	11.84	soft clay	9.5	19.2	0	-	0.01

shown in Fig 8.5 and are also summarized for each layer in Table 8.1. The ε_{50} values for sand, which are required by SWM in addition to those for clay, were based on default correlations with friction angle used internally by the program.

The load-displacement curves for the pipe pile computed by LPILE and SWM using the API friction angles are shown in Fig. 8.6 along with the measured curve. In both cases, the computed displacement for a given load was significantly higher than the measured displacement with SWM computing somewhat greater displacements than LPILE. The computed maximum moment versus load curves using the API correlations for friction angle are shown in Fig. 8.7 relative to the measured curve. In both cases, the computed bending moment is 20 to 30% higher than the measured moment for a given load. The discrepancy between the measured and computed response using the API based friction angles may be due to the fact that the correlations for p-y curves are typically based on load tests where the load is applied incrementally and held constant at each increment for a 3 to 5 minute interval or until displacement stabilizes. In contrast, the load in the TILT tests was applied in about 4 seconds leading to considerably less displacement.

These rate-of-loading effects on p-y curves are particularly important for seismic loadings and are deserving of additional study. Therefore, the soil strength properties were adjusted until the computed load-displacement curves provided a better match with the measured curve. This investigation found that very good agreement could generally be obtained when the friction angle was estimated using the Bolton correlation. This conclusion was also found to be true for the CISS piles and the pile groups as will be shown subsequently.

As described previously, the friction angles using the Bolton method were typically about 5 to 6 degrees higher than were estimated using the API correlation and considerably higher than would be used by most practicing engineers. In addition, the k values used in the LPILE analyses had to be increased so that they were consistent with the friction angle used in the analyses. Therefore, k values were determined by correlating with the friction angle rather than the relative density as shown in Fig. 8.5. The soil strength properties used in the analyses for the high rate-of-loading conditions are shown in Table 8.2. The friction angle used to provide the best match with SWM was one degree lower than that used for LPILE but the values are still close to what would be estimated using the Bolton correlation.

Table 8.2 Soil layering and soil properties used in lateral pile analysis with LPILE & SWM for single pile test site using Bolton correlation for friction angle.

Depth Below Excavated Ground		Curve Type	Effective Unit wt.	Cohesion c	Friction Angle, ϕ	Lateral Subgrade Modulus, k	ε_{50}
Top (m)	Bottom (m)		(kN/m^3)	(kPa)	(degrees)	(MN/m^3)	(strain)
0.00	0.51	sand	19.5	0	39 (38)	65.0	-
0.51	2.59	sand	11.1	0	39 (38)	37.9	-
2.59	4.73	sand	11.1	0	37 (36)	29.8	-
4.73	7.49	sand	11.1	0	34 (33)	19.0	-
7.49	9.25	soft clay	9.5	19.2	0	-	0.01
9.25	10.16	sand	11.1	0	34 (33)	19.0	-
10.16	11.84	soft clay	9.5	19.2	0	-	0.01

Note: Friction angles in parentheses were used for SWM analysis

The load-displacement curves computed using LPILE and SWM with the higher strength properties are also shown in Fig. 8.6 along with the measured curve. When these higher strength properties are employed, the agreement is very good. The computed bending-moment versus load curves are shown relative to the measured curves in Fig. 8.7 and the agreement is also very good except at the lowest load levels where the lateral soil response is very sensitive to small gaps produced by pile driving and local variations in the sand properties. Finally, the computed bending moment versus depth curves at four load levels are shown relative to the measured curves in Fig. 8.8. Using the Bolton friction angle correlation, the two computer models generally provide a good estimate of the depth to the maximum moment and the overall shape of the bending moment versus depth curves.

The computed load-displacement curves for the H-pile are shown relative to the measured curve in Fig. 8.9. When the same friction angle profile based on the Bolton correlation is used to analyze the H-pile response as was used for the pipe pile, the computed load is significantly higher than the measured load at any given displacement likely due to the loose soil between the flanges. In order to obtain a match with the measured response, the friction angles were estimated using the API correlation which produces a much lower strength profile. The load versus displacement curves computed using LPILE and SWM with the API correlation are also shown in Fig. 8.9 and they provide a reasonable match with the measured response although the computed curves are still somewhat higher.

The bending moment versus load curves computed using LPILE and SWM with API correlation for friction angle are shown in Figure 8.10 along with the measured curve. The computed values are typically 10 to 20% higher than the measured values.

8.2 Analysis of 4-Pile Group Response for Pre-Blast Test Before Improvement

8.2.1 Summary of Site Conditions and Soil Property Selection

The soil profile and the results of the CPT and SPT testing at this site are summarized in Fig. 8.11. Six CPT tests were performed across the test site and the average normalized cone resistance, q_{c1} profile is shown along with mean ± one standard deviation bounds in Fig. 8.11. In addition, the $(N_1)_{60}$ values are shown in Fig. 8.11 and range from 4 to 20. The relative density values interpreted from the SPT and CPT testing are also shown in Fig. 8.11 and the agreement between the two tests is reasonable but not as good as for the single pile site. The relative density obtained from the CPT testing is very similar to that for the single pile site; however, the SPT testing suggests that the relative density at the four-pile group site is somewhat higher than at single pile site in the upper 2 meters of the profile.

Although the test piles were driven open-ended, the piles plugged at a depth of 5.5 meters as they penetrated the silty clay layer. To evaluate the influence of the pile driving on the sand layer, one CPT test was performed inside the four pile group cluster six weeks after the piles were driven. This CPT profile is also shown in Fig. 8.11 for comparison purposes. There appears to be some increase in penetration resistance particularly at the lower end of the profile, but part of the difference could also be natural variation in density. This increase in resistance would, of course, be less significant with distance from the center of the pile group.

Although the relative density at the four-pile group is relative close to that at the single pile site, there are differences between the two sites that make a direct comparison between the single pile and four pile group behavior problematic. First, the water level at the time of testing was 0.5 m (20 in) below the excavated ground surface at the single pile site but only 0.3 m (12

in) below the ground surface at the four-pile group site. In addition, the gray silty clay layer was located at 7.5 m below the excavated ground surface at the single pile site but only at 5.5 m below the ground surface at the four-pile group site. The procedure we employed to deal with these discrepancies will be described subsequently.

8.2.2 Measured Response

The measured total load-displacement curves for the four pile group and the 0.6 m CISS pile are shown in Figure 8.12. Although the foundations moved in opposite directions, they have been plotted in the same direction to facilitate comparisons. The curves are almost identical to one another as was desired. Fig. 8.13 presents the measured average load-displacement curves for the leading row and trailing row piles in the four pile group. The trailing row piles carry slightly less load than the leading row piles, presumably due to group interaction effects, but the difference is less than might be expected based on centrifuge test results (McVay et al, 1995). A possible explanation for this small difference may be that the trailing row piles are moving toward the sand in the center of the pile group which has been densified to some extent by the driving while the leading row piles are moving into soil which has not been densified.

8.2.3 Computed Response

The piles in the four pile group were spaced at 1.07 m (3.29 pile diameters) on centers in both directions. The pipe piles were driven open-ended and had the same properties as defined for the pipe pile at the single pile site. Since the soil profile at the four pile group test site was different than that at the single pile test site, the load-displacement curve provided by the 0.6 m CISS pile was used to develop a calibrated soil model. Once this soil model was developed, the

model was used to compute the load-displacement curve that would have been expected for a 324 mm pipe pile at this site. This curve then served as the single pile curve for comparison purposes. Finally, the p-multipliers for the pile group were back-calculated using the same soil model.

Essentially the same analysis procedure was followed in developing the soil model as was used for the single pile test. The friction angles were estimated using the correlation with relative density proposed by Bolton (1990). In addition, the k values were obtained using the correlation with friction angle shown in Fig. 8.5. The soil profile and soil properties used in the analysis are listed in Table 8.3.

Table 8.3 Soil layering and soil properties used in lateral pile analysis with LPILE & GROUP for four pile group test site using Bolton correlation for friction angle.

Depth Below Excavated Ground		Curve Type	Effective Unit wt.	Cohesion c	Friction Angle, ϕ	Lateral Subgrade Modulus, k	ε_{50}
Top (m)	Bottom (m)		(kN/m^3)	(kPa)	(degrees)	(MN/m^3)	(strain)
0.00	0.30	sand	19.5	0	40	59.6	-
0.30	2.92	sand	11.1	0	39	37.9	-
2.92	5.06	sand	11.1	0	36	27.1	-
5.06	8.10	soft clay	9.5	19.2	0	-	0.01
8.10	12.68	sand	11.1	0	32	10.8	-
12.68	14.41	soft clay	9.5	19.2	0	-	0.01

Apart from the layer thicknesses and water table location the strength parameters are very similar to those at the single pile test site. The load-displacement curve for the 0.6 m CISS was computed with the non-linear option in LPILE and is shown in Fig. 8.12. The agreement with the measured curve is excellent and confirms the appropriateness of the correlations employed. The same soil model was then used to compute the load-displacement curve for a single 324 mm steel pipe pile and the computed curve is shown in Fig. 8.13. The leading and trailing row piles carry somewhat lower loads than the single pile as would be expected due to group interaction effects. Using the same soil model in the computer program GROUP, (Reese and Wang, 1996)

the p-multipliers were back-calculated. A very good match between measured and computed load-displacement curves was obtained using p-multipliers of 0.8 and 0.7 for the leading and trailing row piles, respectively as shown in Fig. 8.13. These p-multipliers are identical to the multipliers obtained by Ruesta and Townsend (1997) for the first two rows of piles in a full-scale four row pile group test in sand.

8.3 Analysis of 4- Pile Group Response for Pre-Blast Test After Improvement

8.3.1 Summary of Site Conditions and Soil Property Selection

After the first test was performed at this site, Hayward-Baker used 0.8 m stone columns to densify the sand around the four pile group and 0.6 m CISS. After the treatment, six CPT tests were performed within the treated area. The soil profile is shown along with the average cone resistance and standard deviation bounds in Fig. 8.14. A comparison with similar curves in Fig. 8.10 indicates that there is a substantial increase in the cone resistance due to the treatment. The relative density profiles and interpreted friction angles using the Bolton correlation are also shown in Fig. 8.14. The relative density in the upper sand layer ranges from 90 to 100% and friction angles typically reach the upper limit of 44 degrees for the Bolton correlation.

8.3.2 Measured Response

The measured total load-displacement curves for the 0.6 m CISS and the four pile group after treatment are shown in Fig. 8.15. In contrast to the pre-treatment case where response was almost identical, for the post-treatment test, the CISS pipe carried about 20% more load than the four pile group for a given displacement. This may be due to variations in the placement of the stone columns around the CISS versus the pile group or simply local variations in the

effectiveness of the treatment due to variations in soil properties. The measured average load-displacement curves for the leading row and trailing row piles are shown in Fig. 8.16. The load carried by the trailing row is 15 to 20% lower than the leading row pile at a given deflection as would be expected due to group interaction effects.

8.3.3 Computed Response

Once again, the response of the 0.6 m CISS was used to establish a soil model which was then kept constant throughout the remaining analyses necessary to develop p-multipliers. Initially, the same analysis procedure was followed in developing the soil model as was used for the single pile test and the four pile group test prior to treatment. Based on the Bolton correlation for relative density the friction angle was essentially 44 degrees throughout the entire treated sand layer. However, even with this relatively high friction angle, the computed load-displacement curve was still softer than the measured curve. Therefore, the friction angle of the layer was progressively increased until a reasonable match was obtained with a friction angle of 47.5 degrees. The higher than expected friction angle is likely due to the fact that the soil profile is now a composite of stone columns in a matrix of densified sand. A summary of the soil profile and soil properties used in the lateral pile load analysis is provided in Table 8.4. The match between the measured load-displacement curve and the curve computed using the non-

Table 8.4 Soil layering and soil properties used in lateral pile analysis with LPILE & GROUP for four pile group test site after stone column treatment using Bolton correlation for friction angle.

Depth Below Excavated Ground		Curve Type	Effective Unit wt. (kN/m^3)	Cohesion c (kPa)	Friction Angle, ϕ (degrees)	Lateral Subgrade Modulus, k (MN/m^3)	ε_{50} (strain)
Top (m)	Bottom (m)						
0.00	0.30	sand	19.5	0	47.5	122.0	-
0.30	2.92	sand	11.6	0	47.5	92.1	-
2.92	5.06	sand	11.6	0	47.5	92.1	-
5.06	8.10	soft clay	9.5	19.2	0	-	0.01
8.10	12.68	sand	11.1	0	32	10.8	-
12.68	14.41	soft clay	9.5	19.2	0	-	0.01

linear reinforced concrete pile model in LPILE is shown in Fig. 8.15. Once again the agreement is very good.

The same soil model was then used to compute the load-displacement curve for a single 0.324 mm steel pipe pile and the computed curve is shown in Fig. 8.16. The leading and trailing row piles carry somewhat lower loads than the single pile as would be expected due to group interaction effects. Using the same soil model in the computer program GROUP, the p-multipliers were back-calculated. A very good match between measured and computed load-displacement curves was obtained using p-multipliers of 0.75 and 0.53 for the leading and trailing row piles, respectively as shown in Fig. 8.16. The leading row p-multiplier is very close to that obtained prior to treatment (p_m=0.80) but the trailing row p-multiplier is somewhat lower. This may indicate that the zone between the piles was not densified to the same degree by the stone columns treatment as the area outside the pile group.

8.4 Analysis of 9-Pile Group Response for Pre-Blast Test

8.4.1 Summary of Site Conditions and Soil Property Selection

The soil profile and the results of the CPT and SPT testing at this site are summarized in Fig. 8.17. Six CPT tests were performed across the test site and the average normalized cone resistance, q_{c1} profile is shown along with mean ± one standard deviation bounds in Fig. 8.17. In addition, the $(N_1)_{60}$ values are shown in Fig. 8.17 and are typically about 10 in the upper clean sand layer and about 7 in the underlying silty sand layer. The relative density values interpreted from the SPT and CPT testing are also shown in Fig. 8.17 and the agreement between the two test methods is very good. In general, the relative density is about 50% in the upper sand layer

and about 40% in the silty sand layer. The soil profile and relative density at this test site is generally quite close to that at the single pile test site. However, the water table during this test was only about 0.1 m below the ground surface compared to 0.5 m below the ground during the single pile test.

Although the test piles were driven open-ended, the piles plugged at about a depth of 5 meters as they moved into a looser sand layer. To evaluate the influence of the pile driving on the sand layer, one CPT test was performed between two of the outer piles in the nine pile group cluster six weeks after the piles were driven. This CPT profile is also shown in Fig. 8.17 for comparison purposes. There appears to be some increase in penetration resistance particularly at the lower end of the sand layer.

8.4.2 Measured Response

Total load-displacement curves for both the 0.9 m CISS pile and the nine pile group are presented in Figure 8.18 for comparison purposes. The CISS pile carries about 30% higher loads for the same displacement as the pile group. The load carried by individual piles in the group was found to be a function of row location as shown in Fig. 8.19(a). The leading row piles carry considerably more load than the middle and trailing row piles. In addition, the trailing row (back row) piles actually carried somewhat more than the middle row piles. This finding is consistent with previous studies on lateral resistance of pile group (Rollins, et al, 1998) and is considered to be a result of overlapping shear zones since the piles are only spaced at 3.5 pile diameters on centers.

The load carried by individual piles in the group was also found to be a function of position within a given row itself. Fig. 8.20 shows the load carried by the left, middle and right

pile in each row during the test. In all cases, the middle pile carried the smallest load in the row at a given displacement while the left and right piles tend to carry similar loads in most cases. This finding is at odds with results with all previous full-scale pile group load tests (Brown, 1997; Brown, 1998; Ruesta & Townsend, 1997; and Rollins, 1998), in which no consistent trends were observed within a row. From a practical standpoint, the middle piles in a row would have the most interaction with adjacent piles and therefore, would be expected to carry less load than the outer piles. In previous testing these effects may have been masked by pile-driving effects which would tend to improve the soil in the middle of a pile group relative to piles on the edge. Since the piles in this study were driven open-ended, pile-driving effects would be minimized in comparison with the previous pile group load tests and the result would be lower resistance in the middle piles.

8.4.3 Computed Response

The pipe piles in the nine pile group were driven open-ended and were spaced at 1.07 m (3.29 pile diameters) on centers in both directions. The pipe piles in the group had the same properties as those described for the pipe pile at the single pile test site. The response of the nine pile group was analyzed using the same approach that has been outlined at the previous sites. By matching the computed response with the measured response of the 0.9 m CISS pile, a calibrated soil model was developed. However, very little modification of the soil properties was required after selecting values for ϕ and k using the Bolton correlation. The soil profile and properties used in the analysis are presented in Table 8.5. The properties are actually quite similar to those adopted for the single pile site.

Table 8.5 Soil layering and soil properties used in lateral pile analysis with LPILE/GROUP and SWM for nine pile group test site using Bolton correlation for friction angle.

Depth Below Excavated Ground		Curve Type	Effective Unit wt.	Cohesion c	Friction Angle, ϕ	Lateral Subgrade Modulus, k	ε_{50}
Top (m)	Bottom (m)		(kN/m^3)	(kPa)	(degrees)	(MN/m^3)	(strain)
0.00	0.10	sand	19.5	0	39 (38)	59.6	-
0.10	2.97	sand	11.1	0	39 (38)	35.2	-
2.97	3.99	sand	11.1	0	37 (36)	35.2	-
3.99	6.00	sand	11.1	0	36 (35)	24.4	-
6.00	7.49	sand	11.1	0	35 (34)	21.7	-
7.49	9.20	soft clay	9.5	19.2	0	-	0.01
9.20	12.73	sand	11.1	0	32 (31)	10.8	-
12.73	14.51	soft clay	9.5	19.2	0	-	0.01

Note: Friction angles in parentheses were used for SWM analysis

The load-displacement curve computed using LPILE for the 0.9 m CISS pile is shown along with the measured curve in Fig. 8.18 and the agreement is relatively good, although less precise than in the previous cases. The same model was then used to compute the response of a single 324 mm pipe pile for the site and the computed curve is shown in Fig. 8.19. Once again the single pile curve is stiffer than the piles in the group because the group interaction effects decrease the resistance of the piles in the group. Lastly, the computer program GROUP was used with the same soil model to back-calculate the appropriate p-multipliers for the various rows. Based on this curve-fitting technique, p-multipliers of 0.8 and 0.4 were selected for the leading row and trailing row piles, respectively. The match between measured and computed load-displacement curves is shown in Fig. 19(b) and the agreement is good. Using these p-mulipliers, the total load-displacement curve for the nine pile group was also computed and that curve is shown in Fig. 8.18 along with the measured curve.

In addition to the analyses using LPILE/GROUP, analyses were performed using the strain wedge program (SWM). SWM computes interaction factors directly for piles within a group. For a nine pile group in a 3x3 arrangement, SWM lumps the pile group behavior into

four pile types. The outer piles in the trailing rows are defined as pile type 1, the middle piles in the trailing rows are pile type 2, the outer piles in the lead row are pile type 3, and the middle pile in the lead row is pile type 4. In performing the analyses with SMW, the friction angles obtained with the Bolton correlation were decreased by 1 degree as was done with the single pile analysis to improve the fit. The default values of ε_{50} were used in all cases. The load-displacement curves computed using SWM for each pile type are compared with the measured load-displacement curves in Fig. 8.21. Generally, the agreement is very good especially considering that no back-calculations were made to account for group effects. The only major discrepancy appears to be for pile type 2 in which the computed load was 30 to 40% higher than the measured load. The total load-displacement curve computed for the pile group using SWM is shown in Fig. 8.18 and the agreement is at least as good as that obtained using the GROUP method with back-calculated p-multipliers.

8.5 Results and Conclusions Relative to Pile Behavior in Non-Liquefied Sand

1. The measured load-displacement curves could only be matched by computer methods (LPILE or SWM) when using a friction angle that was significantly higher (by 5 to 6 degrees) than would normally be anticipated for sands with the observed relative density. However, the increased resistance could be accurately modeled by using the Bolton (1986) correlation between friction angle and relative density along with a correlation between the modulus of subgrade reaction and the friction angle (see Fig. 8.5).

2. The increased resistance may be associated with the speed of the load test which had a duration of only about 4 seconds in contrast to the relatively slow maintained load

test approach in which the load is held constant for 3 to 5 minutes at each load interval. For the rapid load test, the resistance was approximately 20 to 30% higher would have been expected based on widely used correlations with friction angle. This apparent increased resistance would be an important consideration for earthquake loads and should be investigated further.

3. The lateral resistance provided by the pipe pile was 30% higher than that provided by the H-pile even though the moment of inertia of the H-pile was about 30% higher than that of the pipe pile. The reduction in resistance for the H-pile appears to result from plugging of the pile between the flanges during driving which left a loose volume of soil around the top of the pile. Similar poor performance following liquefaction suggests that H-piles would be undesirable for applications where lateral loads and/or liquefaction are important design issues and plugging is expected.

4. The use of the stone columns significantly increased the relative density and lateral resistance of the sand surrounding the pile group. Based on back-analysis of the test results the friction angle of the composite sand-stone column profile was about 48 degrees. This is about 8 to 10 degrees higher than the friction angle for the untreated sand.

5. Group interaction effects led to reduced capacity relative to single pile behavior in all the pile groups tested. Lateral resistance was found to be a function of row location with the leading row piles carrying the largest load and the trailing rows carrying significantly less load as has been observed in previous full-scale tests. Lateral resistance was also found to be a function of position within a row with middle pile in a row

carrying substantially lower load than the outer piles. This result has not been observed in previous full-scale tests.

6. The group interaction factors could be adequately accounted for using p-multipliers in a lateral analysis program such as LPILE or GROUP. A summary of the P-multipliers back-calculated from the results of the all the tests at this site are presented in Table 8.6.

Table 8.6 Summary of P-multipler values based on pile group tests in sand during the TILT project. (Pile spacing is 3.29 pile diameters on centers)

Test Group	**Row 1 (Leading Row)**	**Row 2 (1st Trailing Row)**	**Row 3 (2nd Trailing Row)**
Four Pile Group (Before Treatment)	0.8	0.7	--
Four Pile Group (After Treatment)	0.75	0.53	--
Nine Pile Group	0.8	0.4	0.4

7. The test results indicate that the use of 0.8 as a p-multiplier for leading row piles and 0.4 as a p-multiplier trailing row piles would be appropriate for design purposes with piles having center to center spacing of 3 to 3.5 pile diameters. These results are in very good agreement with recommendations based on centrifuge testing in sand (McVay et al, 1995).

8. The computer program SWM provided a relatively good match between measured and computed lateral resistance for the nine pile group. The program gave an excellent match with all but the interior trailing row pile type.

8.6 Excess Pore Pressure Measurements at Test Sites After Blast

After the explosives were detonated and pore water pressures were elevated, the test piles were subjected to eight to ten series of lateral load cycles over a one hour period, as described in the previous chapters. One of the key parameters affecting the lateral resistance of the piles following the blasting is the excess pore pressure ratio, R_u. Plots of R_u versus time for each transducer have been presented previously. A review of these plots indicates that R_u increases and decreases throughout each load cycle. An average R_u value for each transducer has been calculated for each series of load cycles in each test. Fig. 8.22(a) shows the average R_u value as a function of depth for three of the test sites. In general, the R_u values are highest for the nine pile group area. Apart from the transducer at 1 m depth all of the R_u values were near 100%. At the single pile site, the R_u are about 90% in the upper 3 m but drop to about 80% below 3 m. In contrast, the R_u values at the four pile group site are only 50 to 70% in the upper 3 m but moveabove 80% at greater depths. Because the R_u values are so low at the four pile group site, the results in this report will focus on analyses of the single pile and nine pile groups. Fig. 8.22 (b) compares the average R_u versus depth curves for the first series and last series of load cycles at the nine pile group site. After an hour, the R_u values dropped 15 to 35 percentage points.

8.7 Response of 9-Pile Group Response for Tests after Blasting

8.7.1 Measured Load versus Deflection

Fig. 8.23 shows the load-displacement curves for the left, middle and right piles in each row in the nine pile group after six cycles of loading following blasting. There is almost no difference in the load carried by the piles within a given row. Fig. 8.24(a) and (b) show the average load-displacement curves for the rows in the four pile and nine pile groups, respectively after six cycles of loading. In both cases, there are only very small differences in the load carried by each row as a function of displacement. Fig. 8.25(a) shows the load-displacement curve for the single pile relative to the average load-displacement curves for the three rows in the nine pile group. Although the single pile curve is slightly higher than the three pile group curves as load is applied, the difference is relatively small. The results presented in Figs. 8.23-8.25 strongly suggest that group effects are relatively unimportant for pile groups in liquefied sand. Fig. 8.25(b) shows the average load-displacement curve for the four pile group in comparison with the average load-displacement curve for the nine pile group. Because the R_u values at the four pile group site are substantially lower than at the nine pile group site, the load-displacement curve for the four pile group is much stiffer and exhibits less deflection for a given load.

8.6.2 Measured Bending Moment

Fig. 8.26 shows the bending moment versus depth curves for the single pile before liquefaction and after liquefaction with an applied load of 69 kN in both cases. Although the applied load is the same in both cases, the liquefied soil is much softer which leads to greaterbending of the pile. As a result, the maximum moment occurs at a depth of 3 m after liquefaction rather than a depth of 1.2 m before liquefaction. In addition, the maximum moment is 80% higher after liquefaction than before and significant bending moments develop at depths

where the bending moment was essentially zero prior to liquefaction. This behavior was typical of the results from all of the tests piles.

8.8 Development of p-y Curves

8.8.1 Analysis Procedure

P-y curves are commonly used in computing the lateral resistance of piles. The p value represents the lateral resistance per length of pile provided by the soil, while the y value represents the lateral deflection of the pile. The p-y curves are computed based on the strain measured on either side of the piles during the test. Strain measured along the pile was first processed to determine the pile curvature. In more conventional analyses, the first step would have been to determine the bending moment (with the curvature being implicitly included in subsequent calculations involving the pile's flexural rigidity). However, in order to accommodate the possibility of the pile being loaded past its elastic limit, curvature was explicitly determined first. From beam mechanics, it is known that strain (ε) is proportional to curvature (k) and varies linearly with distance (h) from the neutral axis. A rearrangement of this strain-curvature relationship gives the curvature as

$$k = \frac{\varepsilon}{h} \tag{8.7}$$

Equation 8.7 is equation is based solely on geometry and not material properties; therefore, it is valid for linear as well as non-linear elastic materials. When both sides of a symmetric pile are instrumented, the above equation becomes:

$$k = \frac{\varepsilon_t - \varepsilon_c}{2\,h} \tag{8.8}$$

where “t” and “c” denote tension and compression (with opposite signs), respectively.

After determining curvature, the structural and material properties of the pile were then used to determine moment. This was accomplished using the computer program, UCFyber (version 2.2.3) developed by ZEvent (2000) of Berkeley, California. The program models structural cross sections with user-defined stress-strain material relationships, producing a moment-curvature relationship. The steel stress-strain relationships used in the analyses were based on the results of laboratory testing and manufacturer’s material certifications.

Using the resulting moment-curvature relationship, unique sets of curvature and moment were assigned to nodes distributed along the pile with depth corresponding to the locations of strain gauges. Unfortunately, it became readily apparent that some of the gauges did not function correctly, as seen by sharp discontinuities in the curvature and moment diagrams. This lack of functionality is likely in part attributable to poor splicing in the electrical wiring and possible shock damage from the blasting used to liquefy the subsurface.

In order to compensate for the damaged gauges and limit the loss of precision resulting from excessive spacing between nodes, estimated values of curvature and moment were substituted. These estimates were made using a parabolic Lagrangian interpolation polynomial based on the remaining values.

8.8.2 Deflection Calculations

Early attempts at calculating deflection involved direct integration of polynomials fitted to the curvature data, as well as both central- and end-based finite difference formulations. Both approaches were found to have distinct disadvantages. Direct integration relies on measured boundary conditions to obtain deflection, and as such, forces a particular result to be determined despite possible disagreement with trends in curvature data. Also, low order polynomials tend to smooth out important inflections in the data; whereas high order polynomials easily become ill-conditioned. Finite difference approaches rely upon small intervals between regularly spaced nodes to reduce error. As instrumented, the gauges on the piles were not always regularly spaced, and those spacings (whether regular or not) cannot be considered as being "close." Also, there is again reliance on multiple boundary conditions in order to use finite difference formulations.

As a result of these deficiencies, both direct integration and finite difference formulations were abandoned in favor of the curvature-area method from beam mechanics to calculate deflections along the pile. This method is much less sensitive to the factors that affected the other approaches and relies on fewer boundary conditions. With this method, an unbiased assessment of the goodness of fit between measured and calculated pile head deflections can readily be made. The curvature-area method, which is the more general case of the moment-area method, gives the offset from vertical (y) from point A to B by the equation,

$$y = -\int_A^B x_1 \, k \, \partial x \tag{8.9}$$

where x_1 is the vertical distance between the integration element (dx) and the point of interest (B). Assuming a displacement of zero at the lowermost node (A), subsequent offsets from vertical (y) are equal to the first moment of the area of the curvature diagram between the point

of interest (B) and the lowermost node (A), taken with respect to the point of interest (B). The area of the curvature diagram was approximated by linear segments between nodes. It should be noted that this approach would require modification if deflections were for other than small angles of rotation. The same can be said about the previously mentioned relationship between curvature and strain.

8.8.3 Soil Reaction Calculations

The soil reaction per unit pile length, p, is related to the bending moment by the equation

$$p = \frac{d^2(M(z))}{dz^2} \tag{8.10}$$

where z is the depth and M is the moment. Calculation of soil reaction turns out to be more problematic than calculation of deflection. The cause of this difficulty lies in the double differentiation required to obtain load from moment. Unlike integration, differentiation is a very unforgiving process; small errors in measured versus actual moment, as well as errors associated with approximate numerical methods (such as finite difference approximations), compound and produce greatly errant soil reactions. The significance of this fact has been illustrated by Matlock and Ripperger (1958). In a hypothetical example using a low order central difference equation, Matlock and Ripperger demonstrated how a +1 percent error in the moment at one node could produce a –140 percent error in the subsequently calculated soil reaction. Smoothing the data can help reduce the effect of such errors (a resultant error of only –20 percent in the referenced example); however, care must be taken that real variations in the data are not lost.

In light of this fact, we decided to evaluate soil reaction using a technique similar to the one proposed by Matlock and Ripperger (1958) involving fitting of cubic polynomials to successive sets of five nodes and the differentiating at the midpoint. Rather than using their finite difference

formulation requiring equally spaced nodes, least-square polynomials of the moment data were evaluated and differentiated directly. Inherent in this approach is the treatment of soil reaction in the vicinity of the five nodes as a linear function. Consequently, closer spacing of the nodes would provide a more refined interpretation of the soil reaction along the pile length.

Determining soil reaction near the ground surface and pile tip required special attention when using the fitted polynomial technique. Two artificial nodes were added to the top and bottom of the pile to provide the extra nodes necessary to create fitted polynomials for differentiation. The extra top nodes were spaced similarly to the real nodes located immediately below and assigned values corresponding to the hypothetical extension (i.e., projection) of the moment diagram, which passes through zero at the load point (due to the pile's free-head condition). The slope of the extension is equal to the average slope of the moment diagram from the free-head node to any other nodes located at or above the ground surface since the moment diagram is linear between the free-head and the ground surface because the load intensity along the pile length in this region is zero and shear is constant.

The extra bottom nodes were more problematic. The bending moment near the bottom of the pile, unlike that at the top, cannot be consistently described in terms of a linear or other simple mathematical function. This makes extrapolation of the bending moment to the depths of the artificial nodes difficult. To overcome this difficulty, a modified form of the curvature-area method together with iterative error minimization was used. First, arbitrary values of moment (linearly related with depth) were assigned to the artificial nodes. From this, corresponding soil pressures were computed using the aforementioned cubic polynomial technique. Next, the curvature-area method was applied using the calculated soil pressures in lieu of measured curvature, resulting in back-calculated moments (instead of deflections). The values of the

artificial nodes were then iteratively reselected until the sum of the squares of the error between measured and back-calculated moments was minimized. The accuracy of the soil reactions so calculated can be roughly gauged by comparing the measured pile load to the sum of the net area of the soil reaction along the pile (which, when summing up from a fixed pile tip is generally equal to the shear).

It is important to realize that this approach to developing p-y curves is less biased than other common computational techniques because it relies only upon measured curvature to determine deflections. If double integration is performed with the measured pile head slope and deflection used as integration constants, subsequent comparisons of the measured and computed deflections at the pile head provide no indication of the accuracy of derived p-y curves. The computed and measured deflections at the pile head are forced to be the same by the integration process. However, calculated deflections at depth could be quite different from actual ones. In any case, a more complete assessment of derived p-y curves requires careful comparison of both deflections and bending moments along the complete length of the pile.

8.9 P-y Curves for 9 Pile Group

8.9.1 First Set of Load Cycles

Fig. 8.27 presents p-y plots computed at a ten depths along the length of the east pile in the middle (or center) row of the nine pile group during the first set of load cycles following the first blast. P and y values were computed at each 0.1-second interval throughout the load history which accounts for some of the “noise” in the curves. In each plot, the average R_u value at that depth during the testing interval is also provided. During the first few load cycles significant resistance is observed in the three upper p-y plots; however, after four or five large cycles the

shape of the p-y curves reach a more or less steady-state condition. This steady-state curve likely represents the curve shape that would be expected for a liquefied soil. If the pore pressures had been generated by an earthquake, the degradation in soil resistance would have been produced by the same shear forces that produced the build-up of excess pore pressures. Although the p-y curves appear to stiffen with depth, the lateral deflections become progressively smaller with depth making comparisons somewhat difficult.

The p-y curve providing the largest resistance is at a depth of 0.76 m below the ground surface (Chart B) where the average R_u value is also the lowest (R_u=76%) along the length of the pile. This result, which is consistently observed for all of the instrumented piles in the group, indicates that lateral resistance is strongly dependent on the excess pore pressure ratio. Because the resistance provided with a R_u of 76% may be considerably more than that for a R_u of 100%, care must be taken to obtain p-y curves that are truly representative of a liquefied state ($R_u \approx 100\%$). Otherwise, non-conservative estimates of the lateral soil resistance in the liquefied state might be obtained.

Figs. 8.28 and 8.29 compare the measured versus calculated pile head deflection and pile head load, respectively for the p-y curves shown in Fig. 8.27. The error, which is generally within ± 10%, is typical of the results for the other instrumented piles in the group. Since the pile head deflection was not used as a boundary condition during the development of the p-y curve shapes, this comparison does provide an indication of the goodness-of-fit obtained with the p-y curve interpretations.

Figs. 8.30 through 8.35 provide expanded plots of the p-y curves for the upper six strain gauge locations shown in Fig. 8.27. Each plot also provides the average R_u during the test interval, the relative density at that depth from the CPT, and the vertical effective stress prior to

detonation of the explosives. In contrast to conventional p-y curves, which are concave down, the computed p-y curves in the liquefied soil are concave up. As the pile is loaded and the soil is deformed laterally, the soil dilates causing a drop in excess pore pressure and an increase in lateral resistance.

A review of the curves strongly suggests that the average R_u has more to do with the variation in computed resistance than either relative density or effective stress within this depth range. However, near the ground surface, the low effective stress may be responsible for the fact that the soil resistance is very small. Small vertical offsets in the p-y curves may be attributed to small numerical errors and to the fact that the piles never do return to the undeflected condition after the first push. The pile group tended to drift in the direction of load because the liquefied sand flowed into the space behind the pile as it was loaded. Even if the piles returned to a zero pile head deflection there would still be a residual moment along the length of the pile and a negative force on the pile.

Figs. 8.36 through 8.39 present p-y plots computed at a number of depths along the length of the remaining four instrumented piles in the nine pile group during the first set of load cycles following the first blast. Generally the observed behavior is relatively consistent with observations made regarding the east pile in the middle row of the group.

For each instrumented pile in the nine pile group, a smoothed p-y curve was developed numerically at each depth for the sixth “225 mm push” following the blast. The curves were all adjusted to zero displacement and zero soil resistance when the pile head load was equal to zero. The p-y curves for each pile at each depth are shown together in Fig. 8.40. Although the curve shapes are generally consistent, there is variation from pile to pile which may be attributable to local variation in pore pressure, soil density, pile location within the group and natural variation

in strain gauge readings. At most depths, no consistent trends can be observed in the p-y curves with respect to pile row location. This finding supports the concept that p-multipliers for piles in liquefied soil should be taken as 1.0.

Nevertheless, at a depth of 0.76 m (Chart B), pile group effects are evident in the shape of the p-y curves. At this depth, where the average R_u has dropped to 76%, the leading row piles (N & NE) have the stiffest p-y curves, the middle row piles (E and C) have considerably softer p-y curves, and the back row pile (S) has a p-y curve somewhat softer than the middle row piles. Apparently, as the average R_u drops off and the sand reconsolidates, failure planes may form sufficiently that they overlap with adjacent piles and reduce the resistance of the trailing row piles.

8.9.2 Last Set of Load Cycles

Fig. 8.41 presents p-y plots computed at ten depths along the length of the east pile in the middle (or center) row of the nine pile group during the last set of load cycles following the first blast. P and y values were again computed at each 0.1-second intervals throughout the load history. In each plot, the average R_u value at that depth during the testing interval is also provided. Although the p-y curve near the ground surface remains relatively flat, conceivably due to the presence of a gap in the soil around the pile, the p-y curves at the other depths have stiffened considerably relative to the resistance in the first set of load cycles following the blast. At locations B, C, D, and E, the p-y curves still exhibit a concave upward shape as load is applied; however at greater depths, the curve shapes become stiffer and more linear in shape. In addition, the area within the loops in the p-y curves decreases with depth

Figs. 8.42 and 8.43 compare the measured versus calculated pile head deflection and pile head load, respectively for the p-y curves shown in Fig. 8.41. The error, which is generally within ± 10%, is typical of the results for the other instrumented piles in the group. For this particular pile, the error in the unload cycles is much greater than for the load cycles. Since pile head deflection was not used as a boundary condition during the development of the p-y curve shapes, this comparison does provide an accurate indication of the goodness-of-fit obtained with the p-y curve interpretations.

Figs. 8.44 through 8.49 provide expanded plots of the p-y curves for the upper six strain gauge locations shown in Fig. 8.41. Each plot also provides the average R_u during the test interval, the relative density at that depth from the CPT, and the vertical effective stress prior to detonation of the explosives. Although the average R_u values are considerably lower than during the first set of cycles, the dilation occurring as the pile is loaded still produced a concave upward shape after the significant displacement. Some of this delay in the development of soil resistance with these lower average R_u values may now simply be due to gaps around the pile.

Figs. 8.50 through 8.53 present p-y plots computed at a ten depths along the length of the remaining four instrumented piles in the nine pile group during the last set of load cycles following the first blast. Generally the observed behavior is relatively consistent with observations made regarding the east pile in the middle row of the group.

8.9.3 Effect of Excess Pore Pressure Ratio and Depth on P-Y Curves

Fig. 8.54 shows smoothed and zeroed p-y curves at eight depths for the first and last set of load cycles as interpreted from the east pile in the middle row of the nine pile group. The average R_u values for each curve are also provided in the figure for reference. Although the

curve shapes at the ground surface are nearly identical, at all other depths there is a considerable increase in the stiffness of the p-y curve as the excess pore pressure ratio drops. This is particularly evident for charts E and F where the R_u values change from 100% to 65%. Despite the drop in R_u values, the curve shapes are generally still concave up. However, for the last set of load cycles, the p-y curve shape appears to transition from concave up to concave down between 3.81 and 4.57 m below the ground surface or where the R_u value drops from 66% to 51% (Compare charts F and G).

Figs. 8.55 and 8.56 present summary plots of the smoothed and zeroed p-y curve shapes at various depths for the first and last set of load cycles, respectively in the nine pile group. The family of p-y curves in Fig. 8.55 represents our best estimate of the p-y curves for liquefied soil conditions as a function of depth. In Fig. 8.55 the curves at 0.76 and 1.52 m depth have been excluded because the R_u values at those depths were below 90%. Fig. 8.56 presents a family of p-y curves which would be appropriate for use when R_u values are approximately 65%. In both figures there is a clear trend for the curve shape to become stiffer and begin bending upward at smaller deflections as the depth increases. These results suggest that the p-y curves at R_u values of both 100% and 65% are dependent on depth or initial vertical effective stress.

8.9.4 Validation Using Lateral Response Analysis

To provide some validation of the smoothed and zeroed p-y curves shown in Fig. 8.54, a lateral pile analysis was performed with the computer program LPILE using the p-y curves developed for the liquefied as user-defined p-y curves. Figs. 8.57 through 8.59 show the computed bending moment and deflection versus depth curves along with the measured bending moment versus depth and pile head deflection for three load levels. The match with measured

bending moment is very good for each case and the match with deflection is reasonable, although the computed deflections are somewhat higher than measured particularly at the highest load level. Some of this discrepancy may be attributed to the fact that at the zero load reference point the pile is actually deflected about 25 mm so the comparison are not completely direct. In any event the accuracy of the fit with deflection and moment suggest that the p-y curve shapes are reasonable approximations of the soil behavior.

8.9.5 Comparison With Other Methods for p-y Determination

Other approaches have been proposed for generating p-y curves in liquefied sand. For example Liu and Dobry (2000) suggested that the p-y curve for the API sand be adjusted for liquefied conditions by using a p-mulitiplier of 0.1 to 0.3. Wang and Reese (1998) and others have recommended that the soft clay p-y curve shape be used for liquefied sand with an undrained strength equal to the residual strength obtained from a correlation with SPT $N_{1(60)}$ (Harder and Seed, 1990).

To evaluate the accuracy of these alternative approaches, a series of lateral pile load analyses have been performed using LPILE. Calculations have been performed using the p-multiplier approach with p-multipliers of 0.1 and 0.3 along with the "soft clay" approach using residual strength values equal to the lower-bound value and the mean value. Fig. 8.60 shows the p-y curves for liquefied sand compared with the p-y curve shapes for the various approaches at seven depths. A review of the curves indicates that the shape of the p-y curves for the alternative methods is fundamentally different than the curve shapes derived from the test data. As a result, any match is generally coincidental. For example, the p-multiplier concept provides acceptable soil resistance values at shallow depths but significantly overestimates the resistance at greater

depths. Since centrifuge tests typically involve relative shallow models, this behavior may not have become evident in these tests. In contrast, the "soft clay" approach appears to underpredict soil resistance at shallow depths but gives reasonable values at greater depths.

Fig 8.61 shows the measured load-deflection for a pile in the nine pile group relative to the load-deflection curves estimated using the various p-y curve approaches. Although the p-y curves developed from this study tend to be somewhat conservative in their estimation of pile head deflection, the shape of the curve is accurately reflected. The alternative methods miss the basic shape of the curve. The p-multiplier approach significantly overestimates soil resistance particularly at small deflections. The curves obtained with the soft clay approach appear to bound the measured curve at small deflections but underestimate soil resistance at greater values.

Fig. 8.62 shows the measured bending moment versus depth curves for three load levels along with the computed curves for the p-multiplier approach with p-multipliers of 0, 0.1 and 0.3. At shallow depths, the match with measured moment is acceptable, but at greater depths, the measured moment is significantly higher than predicted using the 0.1 and 0.3 values but much less than estimated using a p-multiplier of 0. These results indicate the difficulty of making reasonable estimates of bending moment using the p-multiplier approach. Agreement at one load level or in one depth range may be possible but consistent matches over a range of load levels is very difficult.

Fig. 8.63 shows the measured bending moment versus depth curves for three load levels along with the computed curves using residual strength values equal zero as well as the mean and lower bound values proposed by Seed and Harder (1990). Although it is possible to obtain a good fit at one load level using this approach with a given strength assumption, it is not possible to achieve the match at all load levels. Fig. 8.63 also demonstrate that assuming no soil

resistance in the liquefied sand leads to significant overestimates of the magnitude of the bending moment and the depth at which the maximum bending moment occurs.

8.10 P-y Curves for Single Pile

Because of problems with one of the data acquisition systems, bending moment data was not recorded for the H pile and half of the strain gauges on the pipe pile during the first few set of load cycles after the first blast. However, strain gauge data was available for strain gauges on one half of the pipe pile from a second acquisition system. Therefore, it was not possible todevelop p-y curves for the H pile from the first test. As discussed previously, the loose sand between the flanges of the H-pile allowed it to deform excessively. The excessive deformation also made it difficult to consistently control the displacement of the pipe pile which made further analysis extremely difficult. At the conclusion of the first test, the H-pile had yielded and rotated to the point that it could no longer be used for the second test. Therefore, p-y curves were only developed for the single pipe pile for the second load cycle.

Fig. 8.64 shows the smoothed and zeroed p-y curves for the pipe pile derived for the first set of load cycles for the single pile test. The average R_u values are shown on the curves at each depth. Because the R_u values are lower for this test site than at the nine pile group test site, the p values are higher than derived for the nine pile group. For example, the p-values at depth of 3.3 and 4.06 (R_u =86% and 80%, respectively) are roughly twice as high as the p-values at similar depths at the nine pile group site where R_u was close to 100%.

8.10.1 Validation Using Lateral Response Analysis

Fig. 8.65 shows the measured load versus deflection curve for the 11th cycle of loading during the first set of load cycles following the second blast along with the curve computed by LPILE using the p-y curves in Fig. 8.64. Once again the computed deflection follows the shape observed in the testing but tends to overestimate the displacement somewhat particularly at the highest load levels. Fig. 8.66 shows a comparison of computed and measured bending moment versus depth curves for the single pile at two load levels. Once again the agreement is generally good throughout the length of the pile.

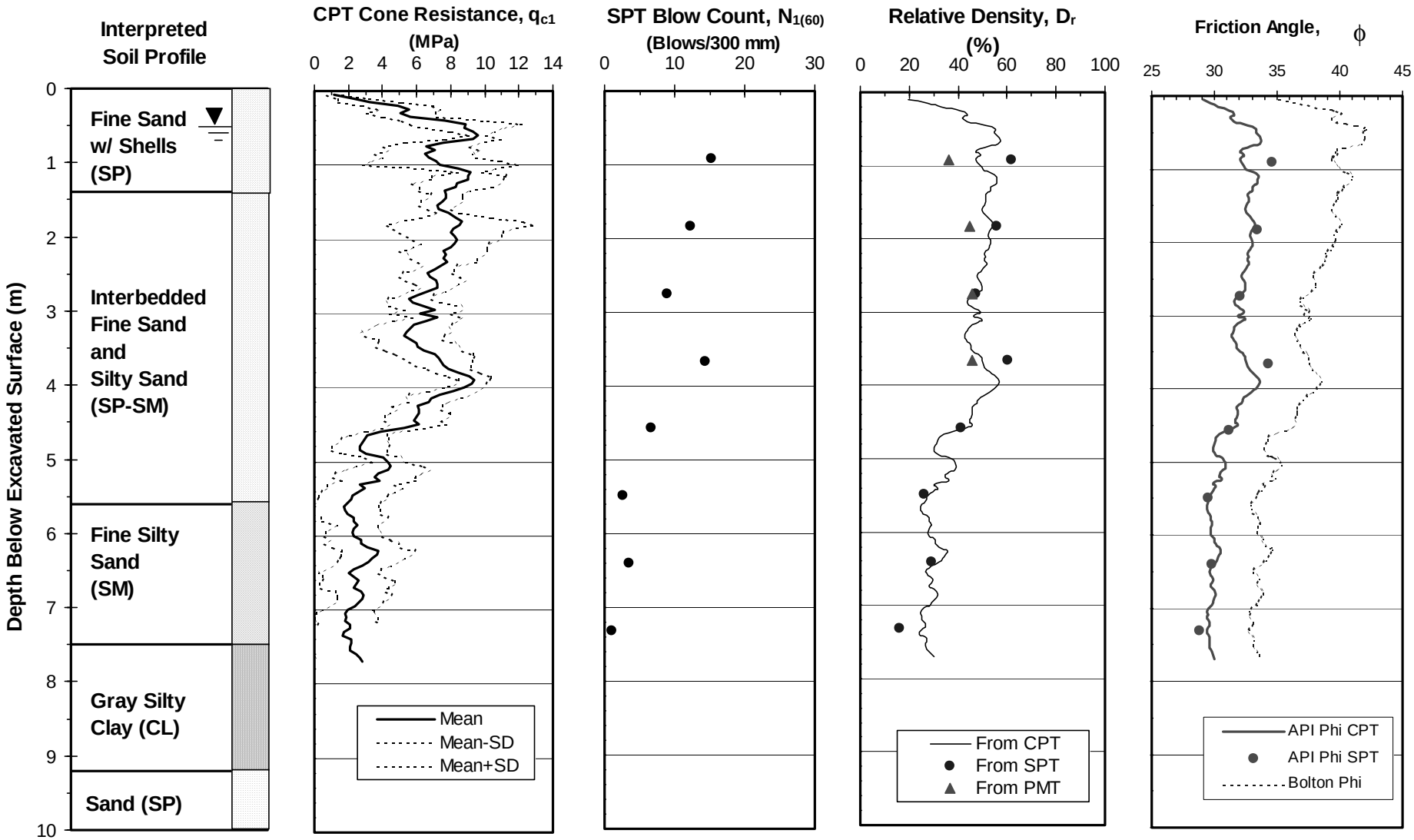

Figure 8.1 Summary of idealized soil profile, in-situ tests along with interpreted relative density and friction angle.

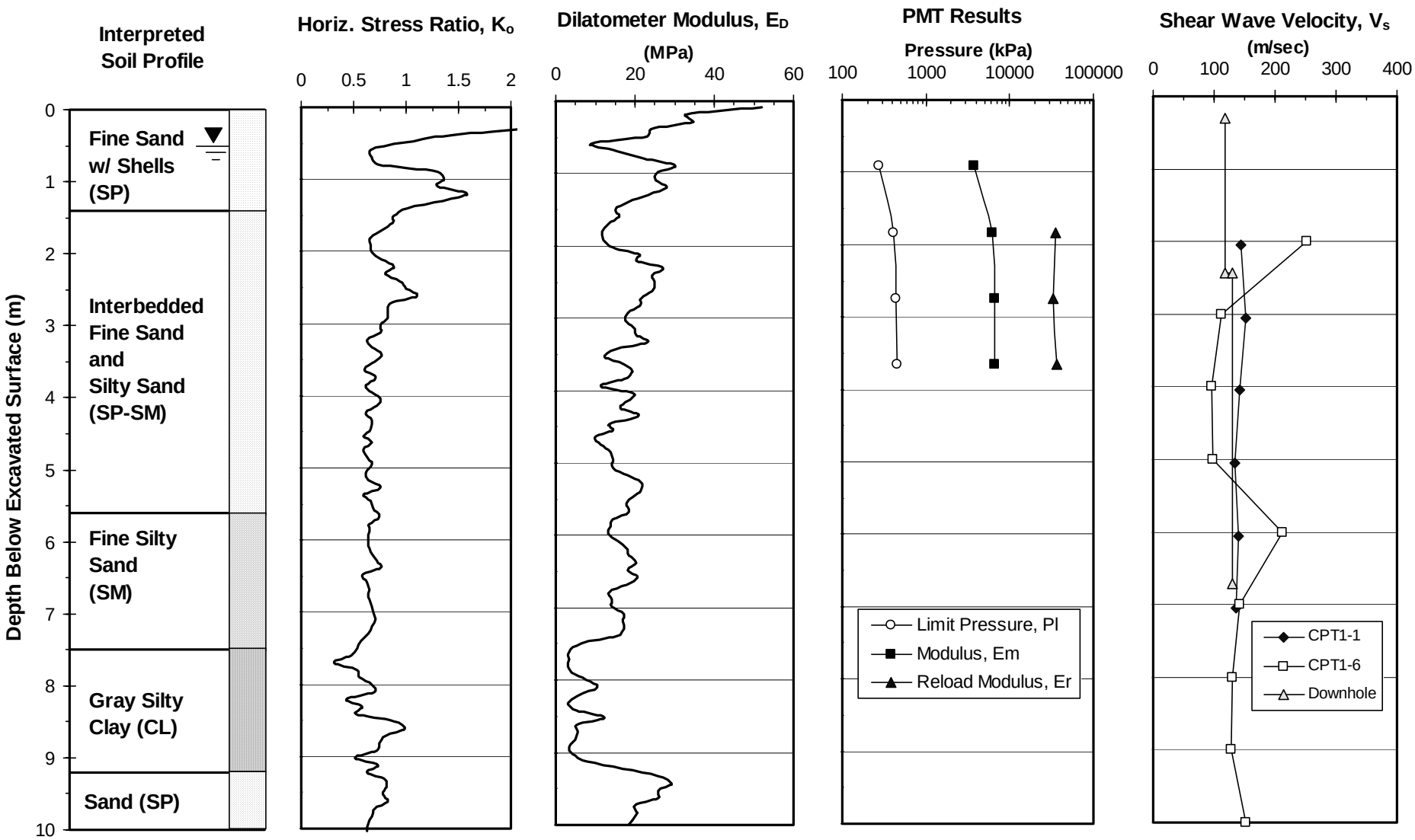

Figure 8.2 Summary of idealized soil profile and results of dilatometer, pressuremeter and shear wave velocity tests.

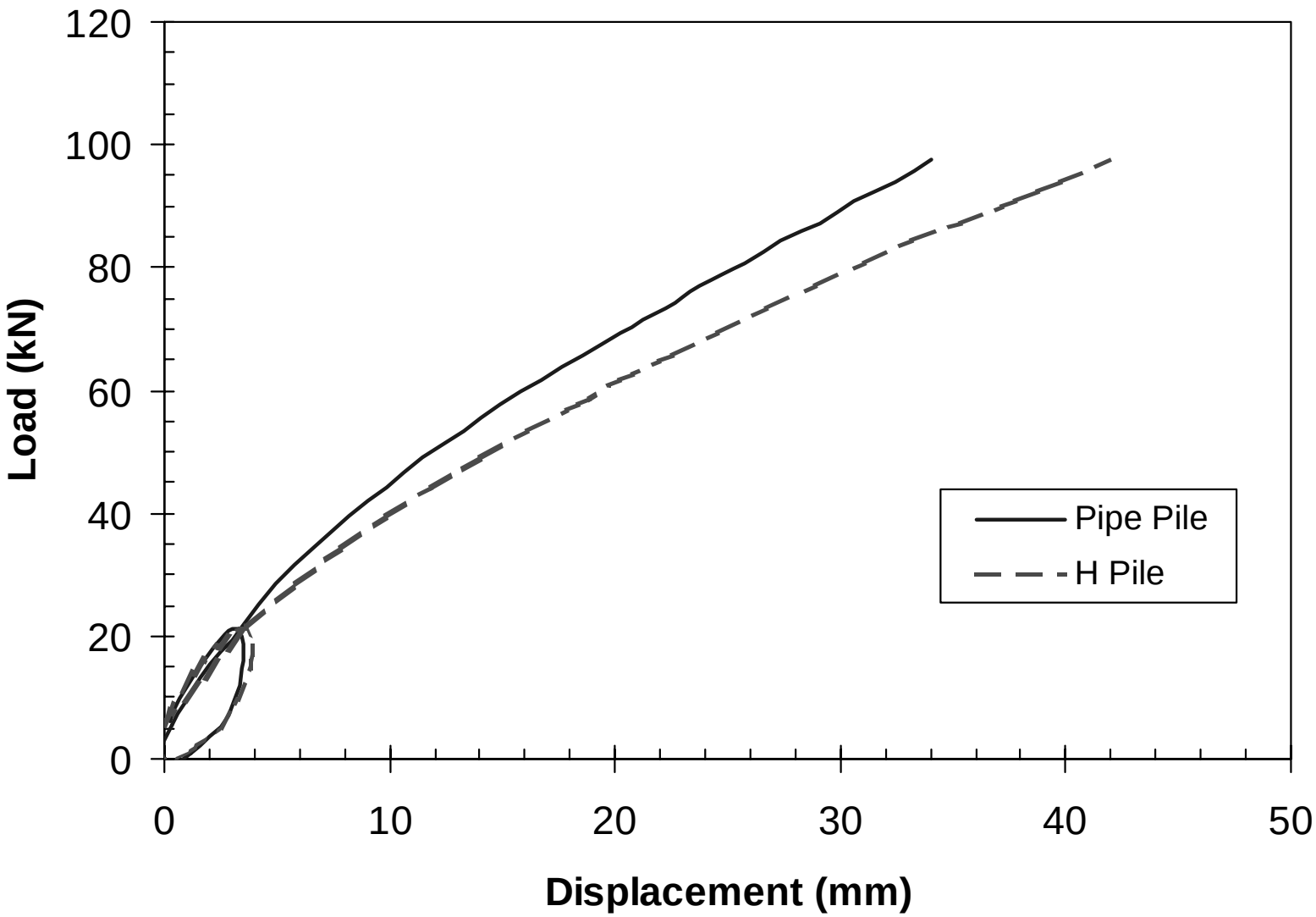

Figure 8.3 Measured load-displacement curves for single pipe and H-piles prior to first test blast.

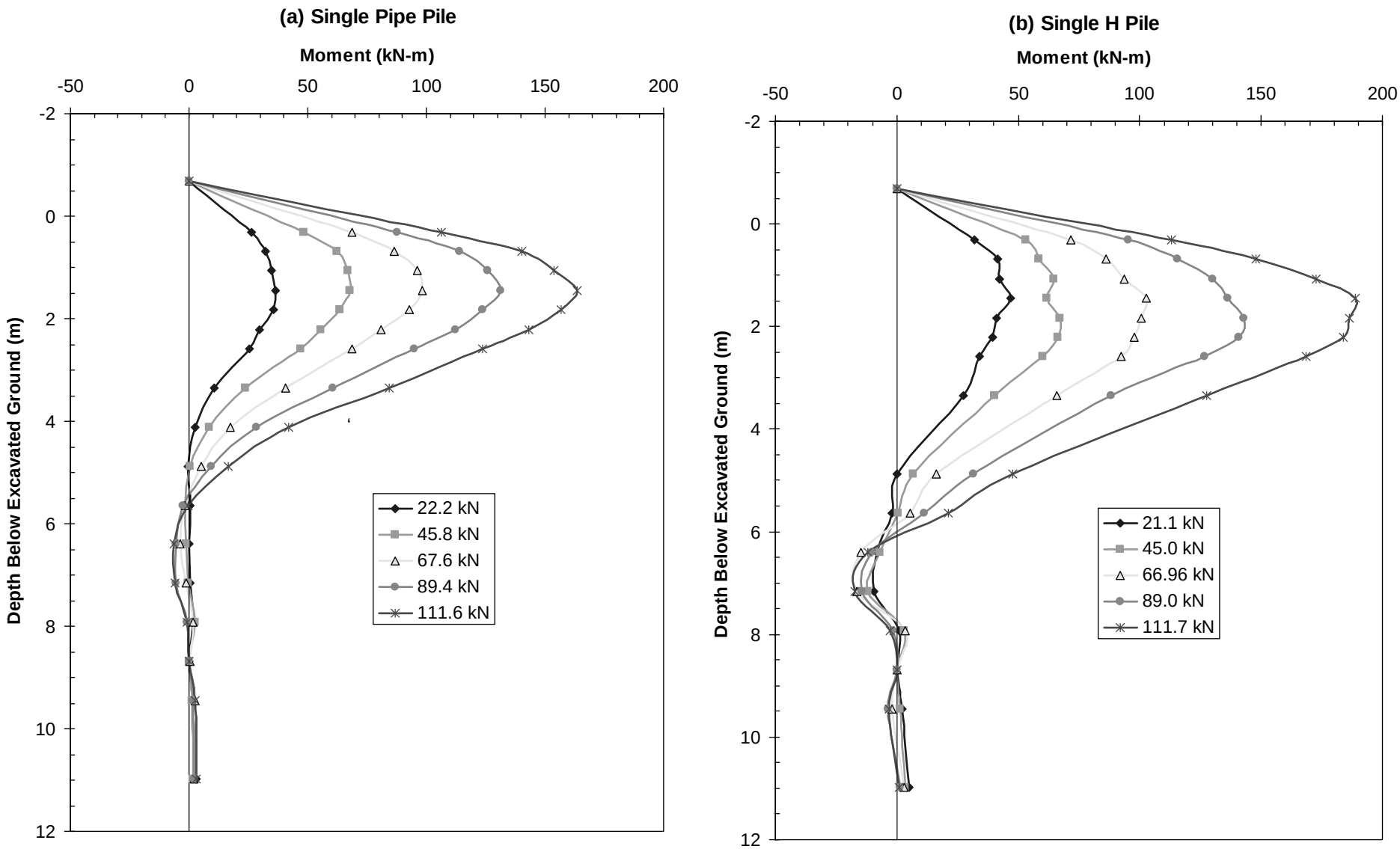

Figure 8.4 Bending moment versus depth curves at five load levels for (a) the single pipe pile and (b) the H pile prior to the first blast.

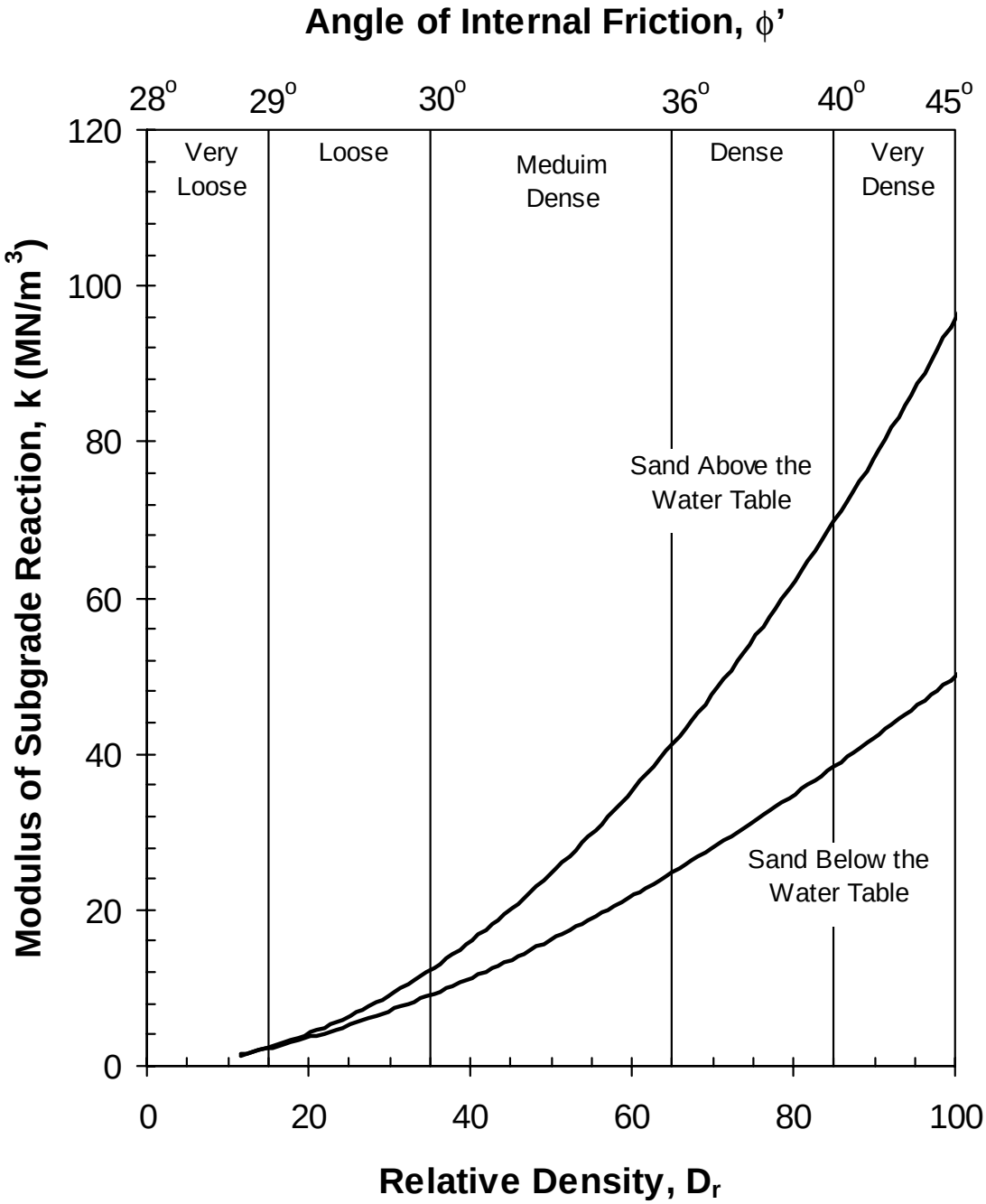

Figure 8.5 Relationship between lateral subgrade modulus and relative density or friction angle.

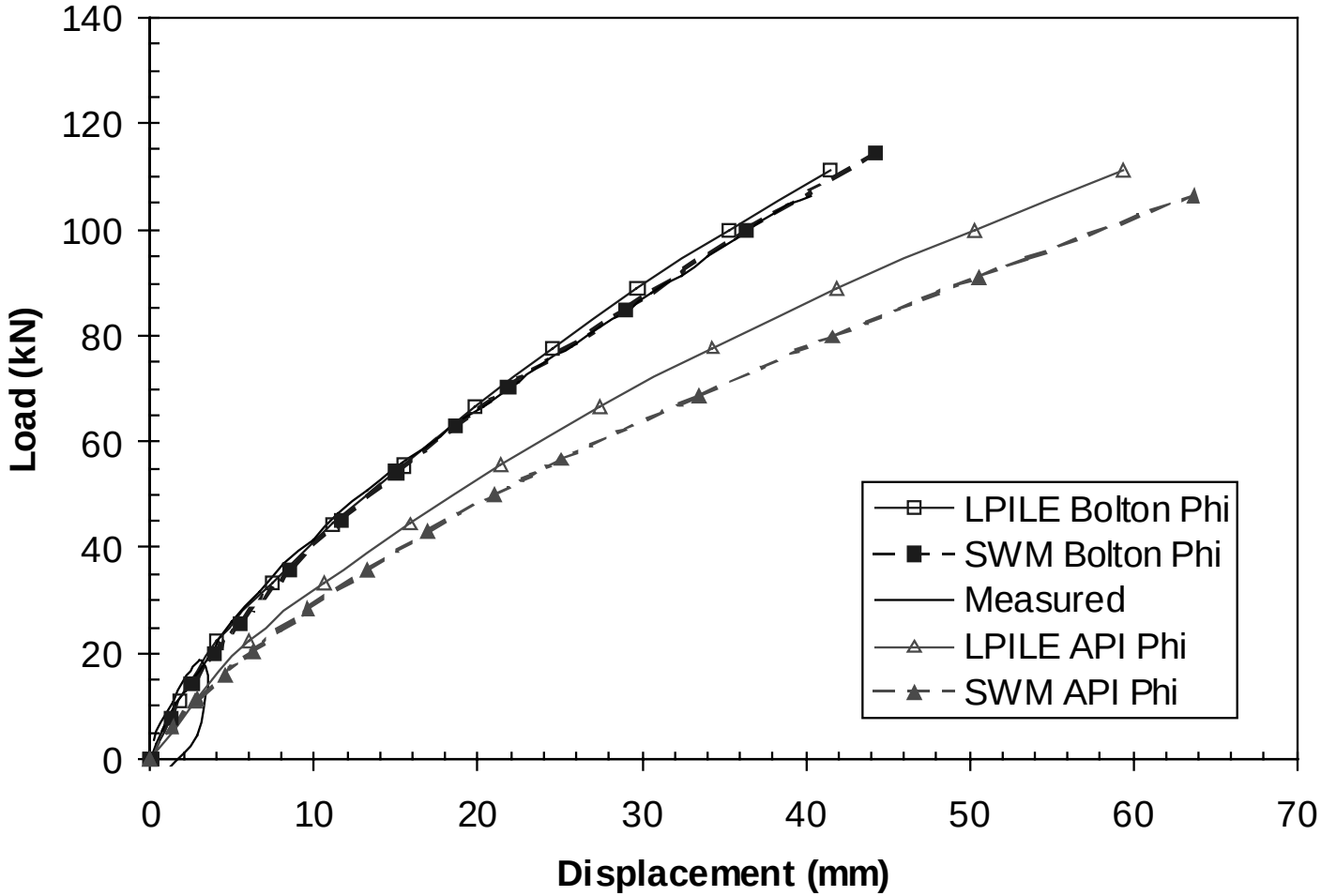

Figure 8.6 Measured load-displacement curve for single pipe pile along with computed curves using LPILE and SWM

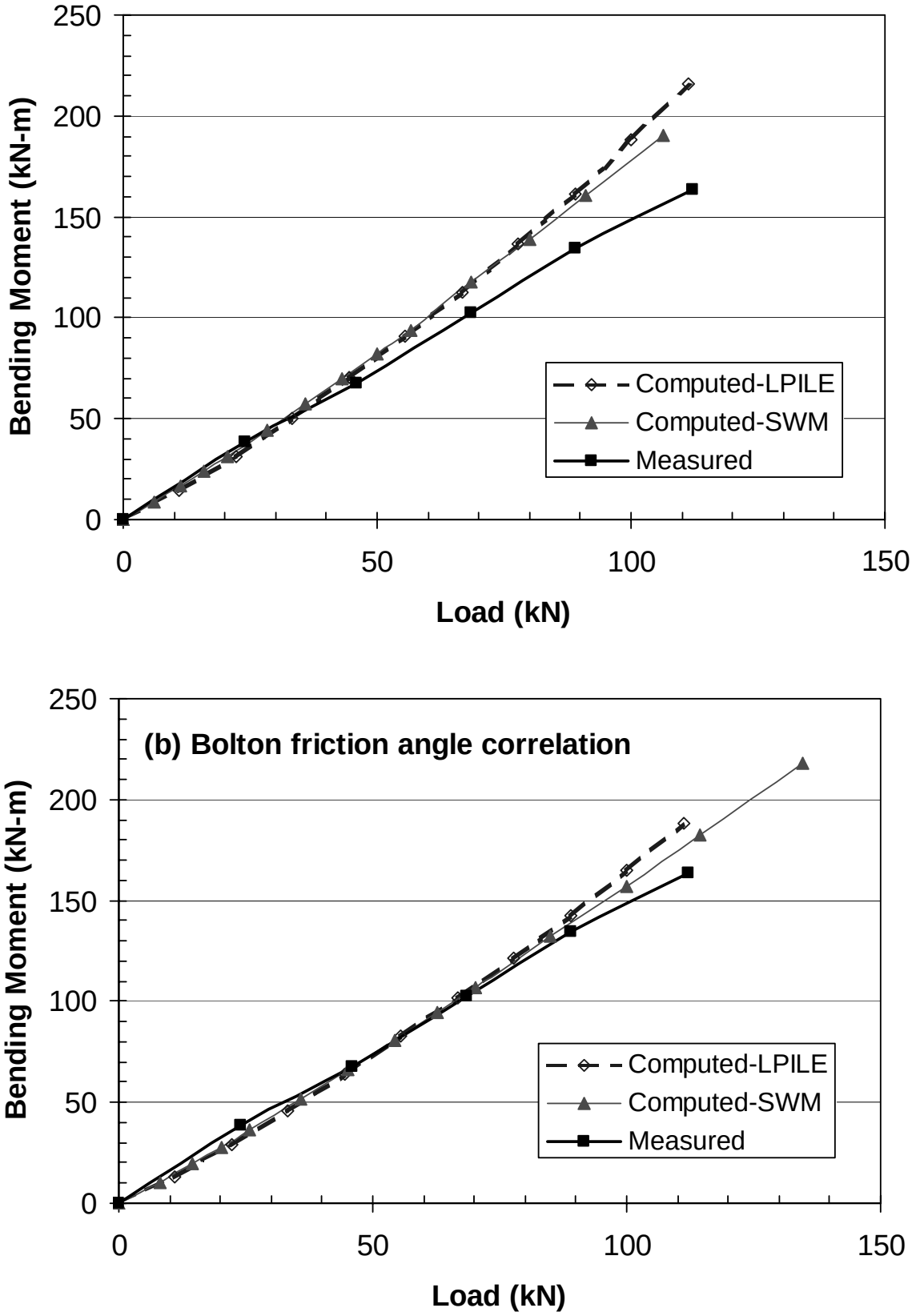

Figure 8.7 Measure bending moment versus load curves along with computed curves using LPILE and SWM with (a) API friction angle and (b) Bolton friction angle correlations.

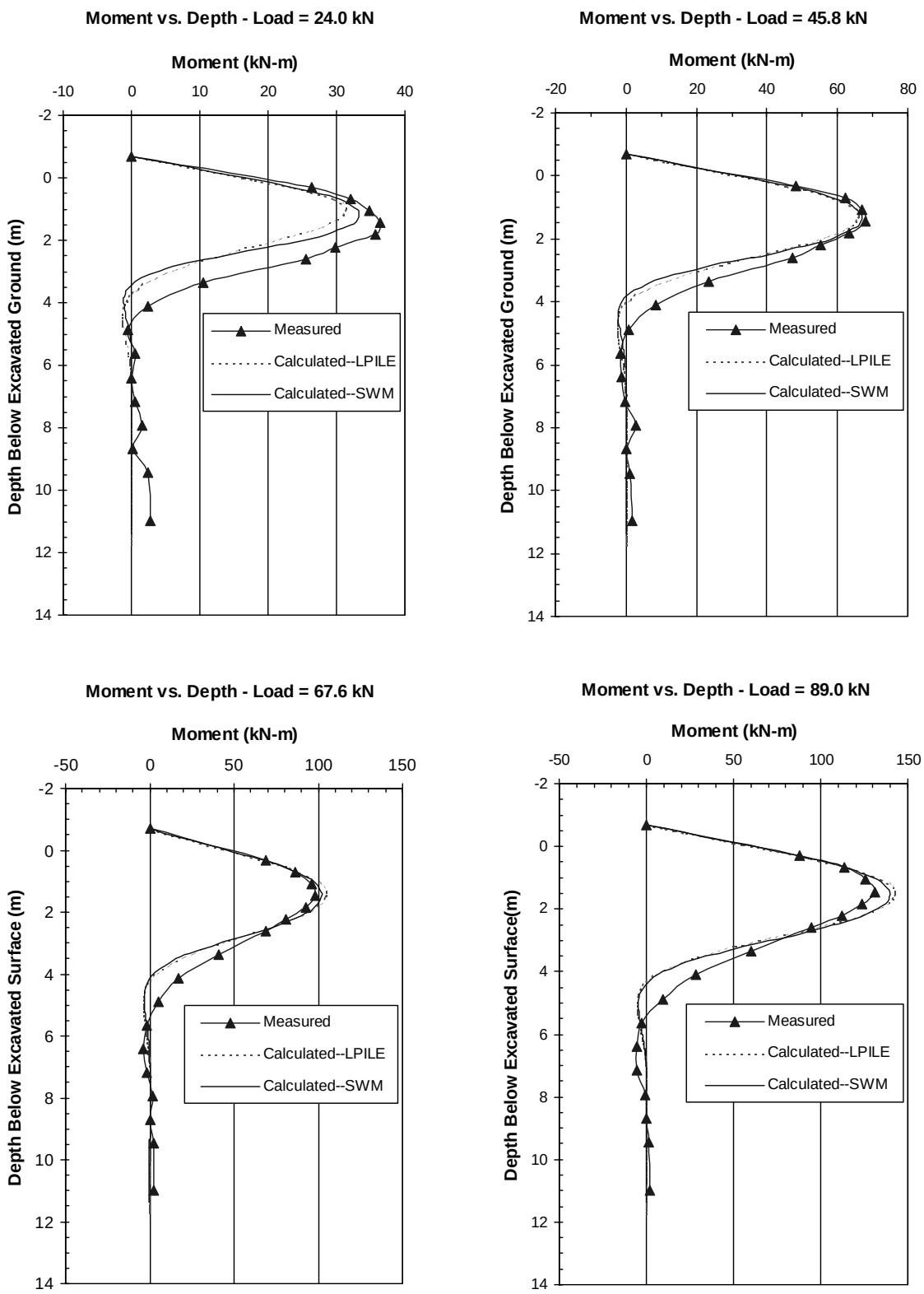

Figure 8.8 Comparison of measured bending moment versus depth curves for the single pipe pile with curves computed using LPILE and SWM with Bolton friction angle at four load levels.

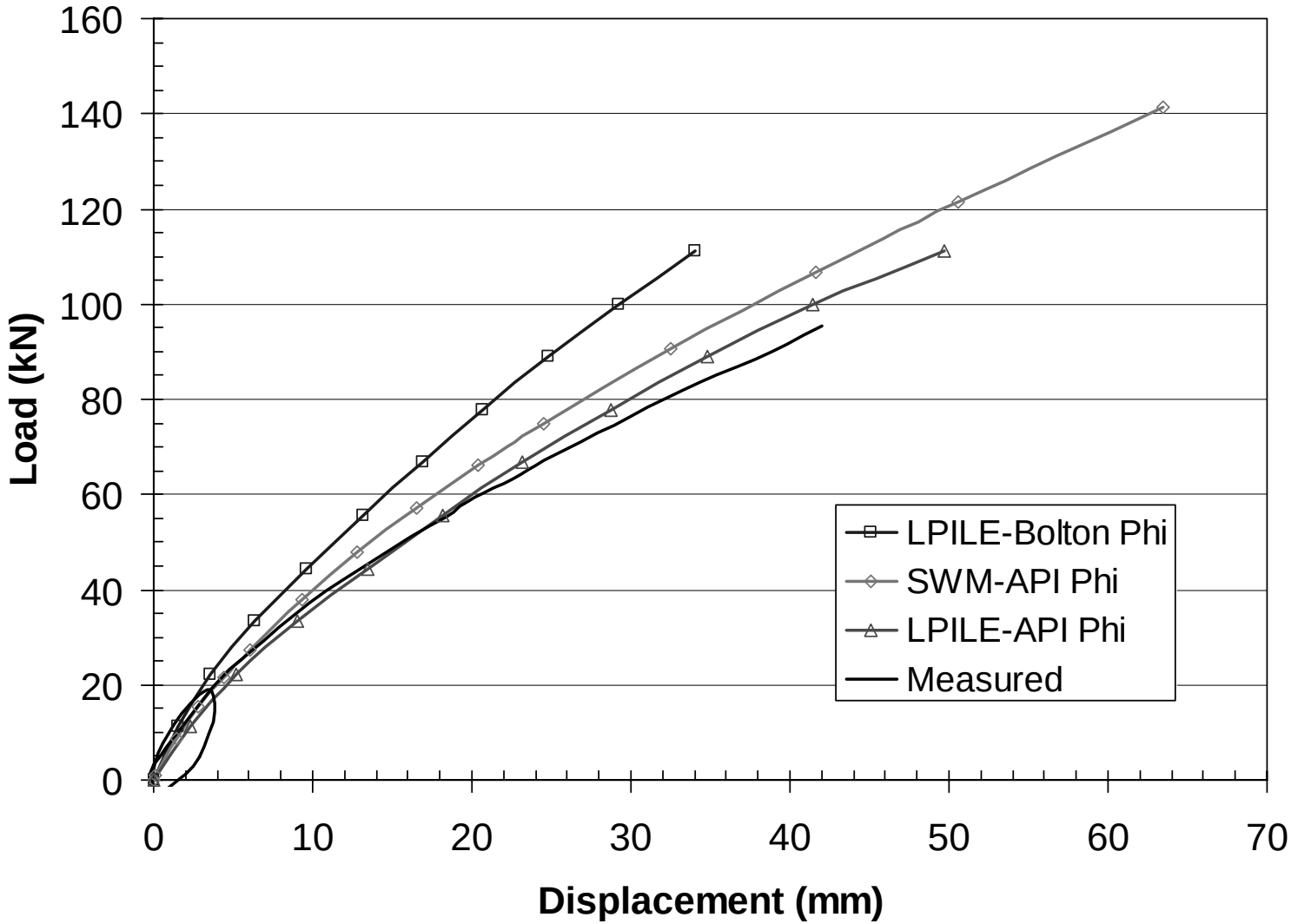

Figure 8.9 Measured load-displacement curve for H-pile along with computed curves using LPILE and SWM.

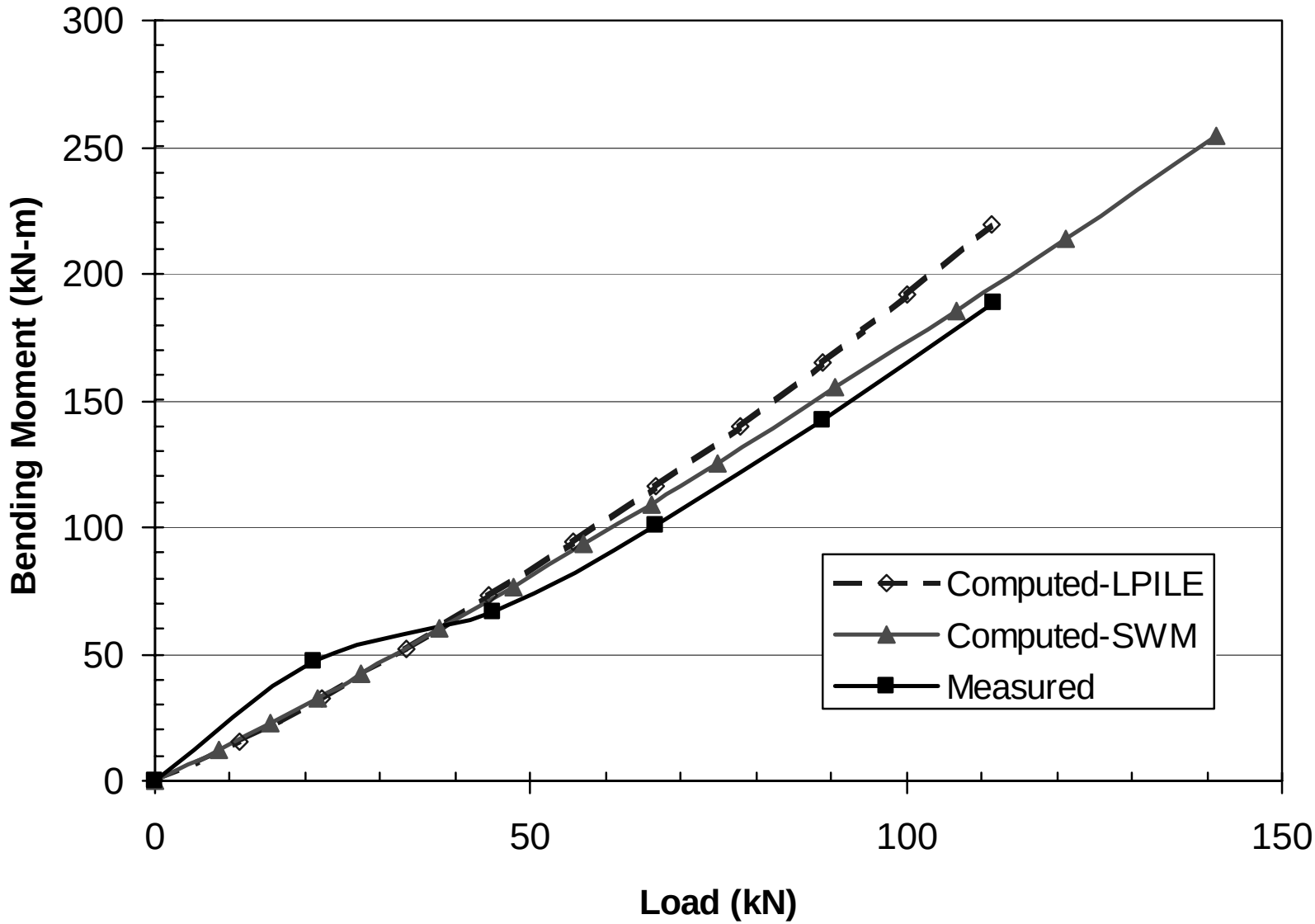

Figure 8.10 Measured bending moment versus load curve along with curves computed using LPILE and SWM using API friction angle correlation.

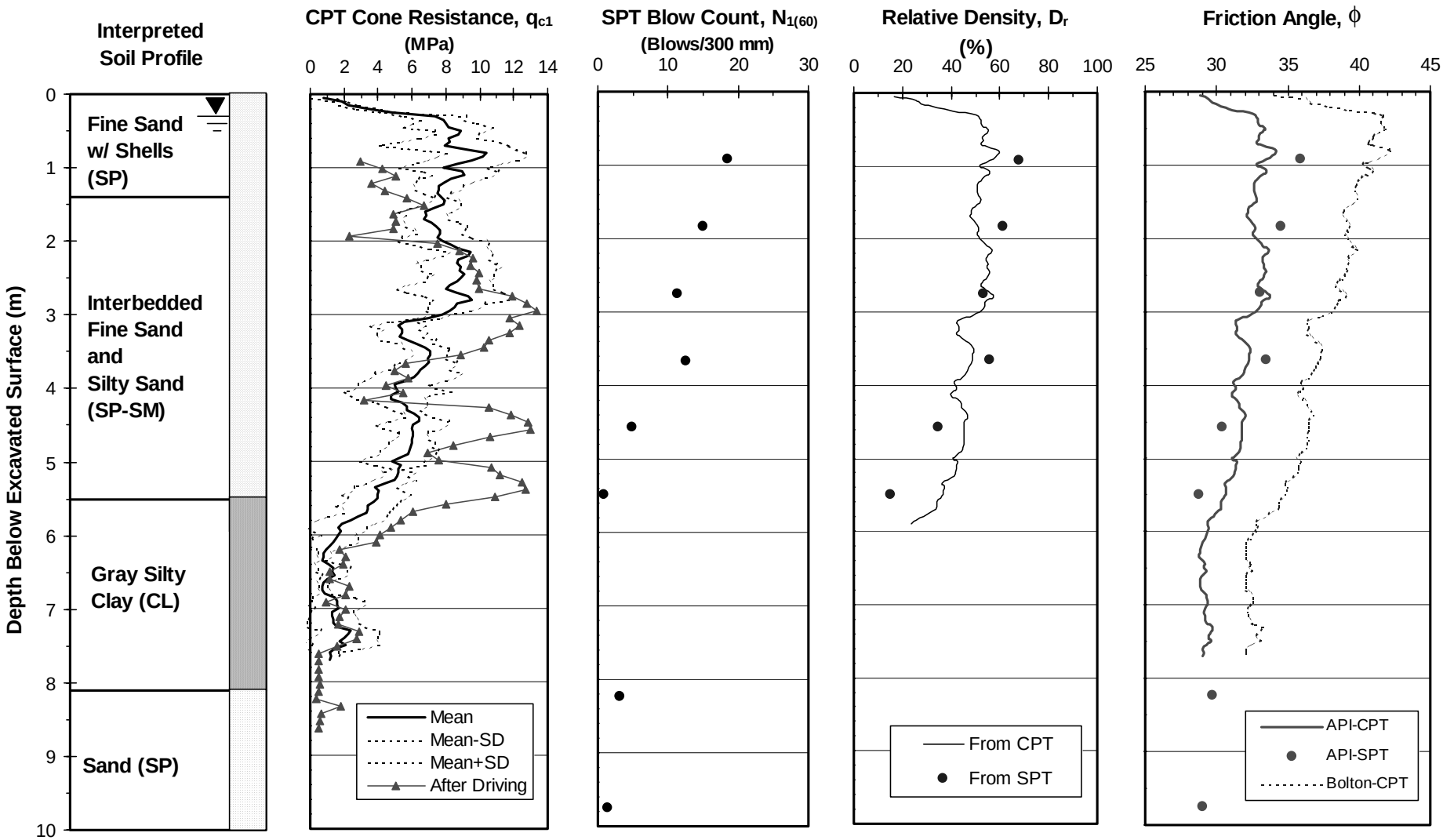

Figure 8.11 Summary of idealized soil profile, in-situ tests along with interpreted relative density and friction angle.

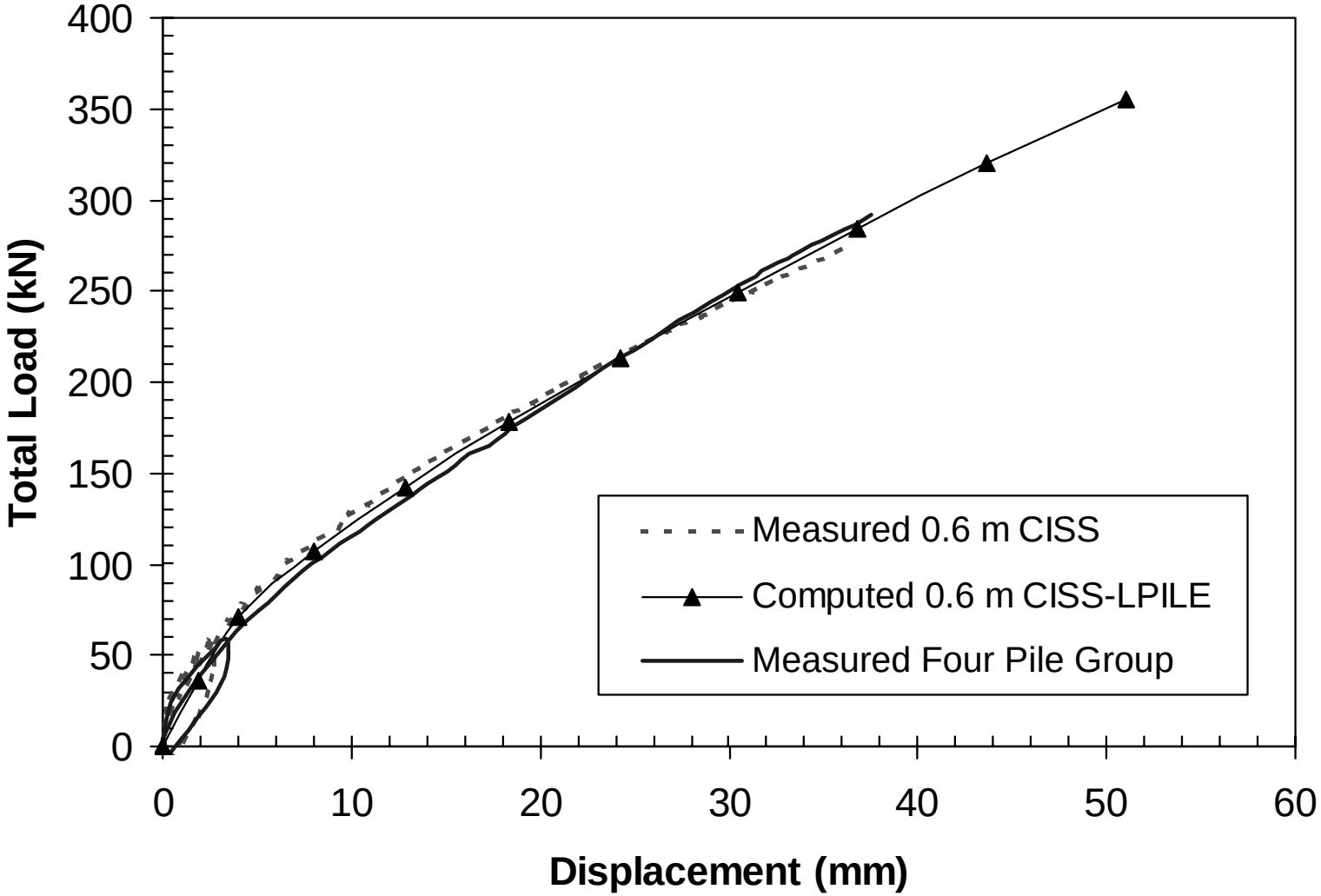

Figure 8.12 Measured total load-displacement curve for 0.6 m CISS and four pile group along with curve computed using LPILE.

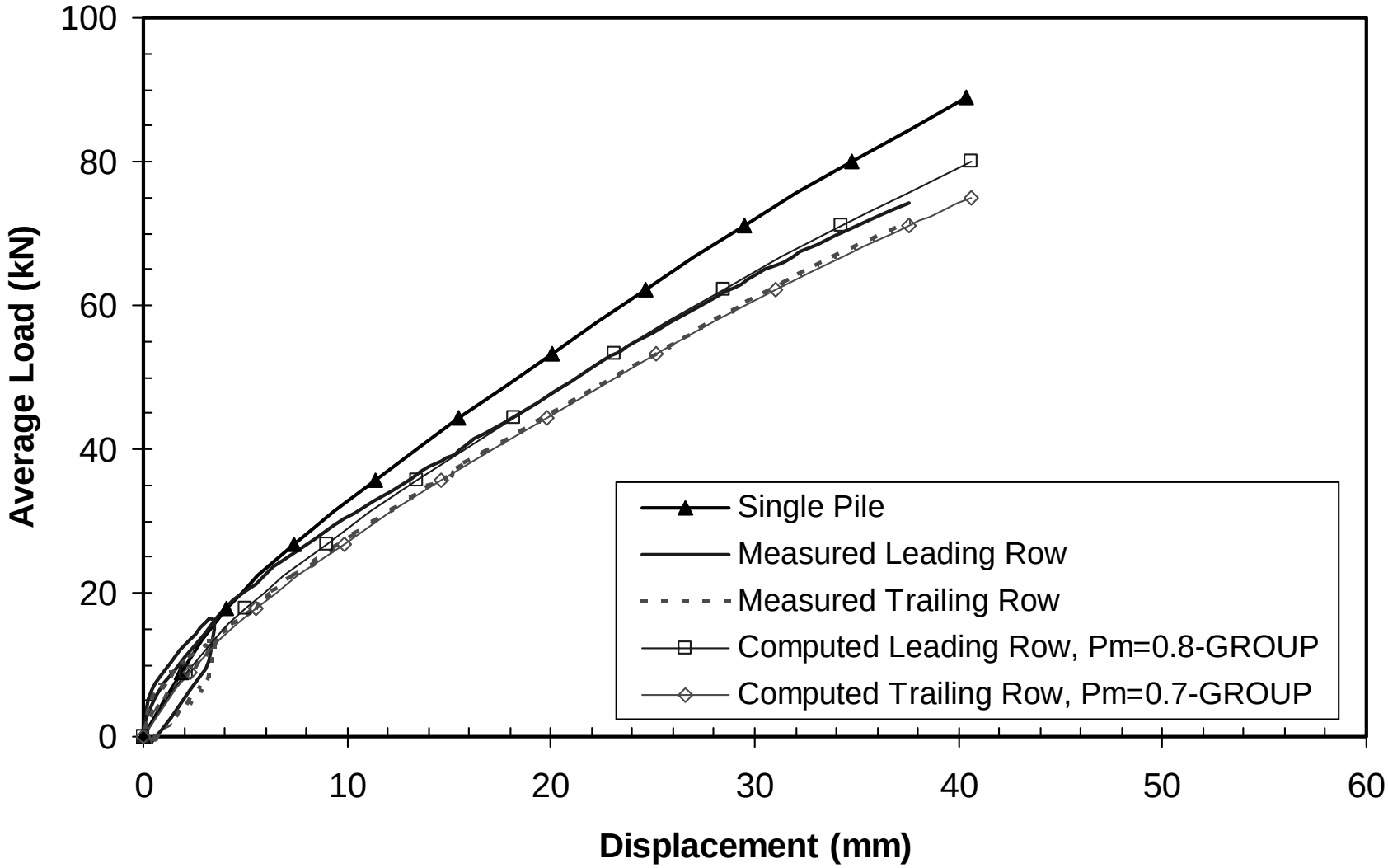

Figure 8.13 Measured average load-displacement curves for the two rows in the four pile group along with curves computed using GROUP with p-multipliers.

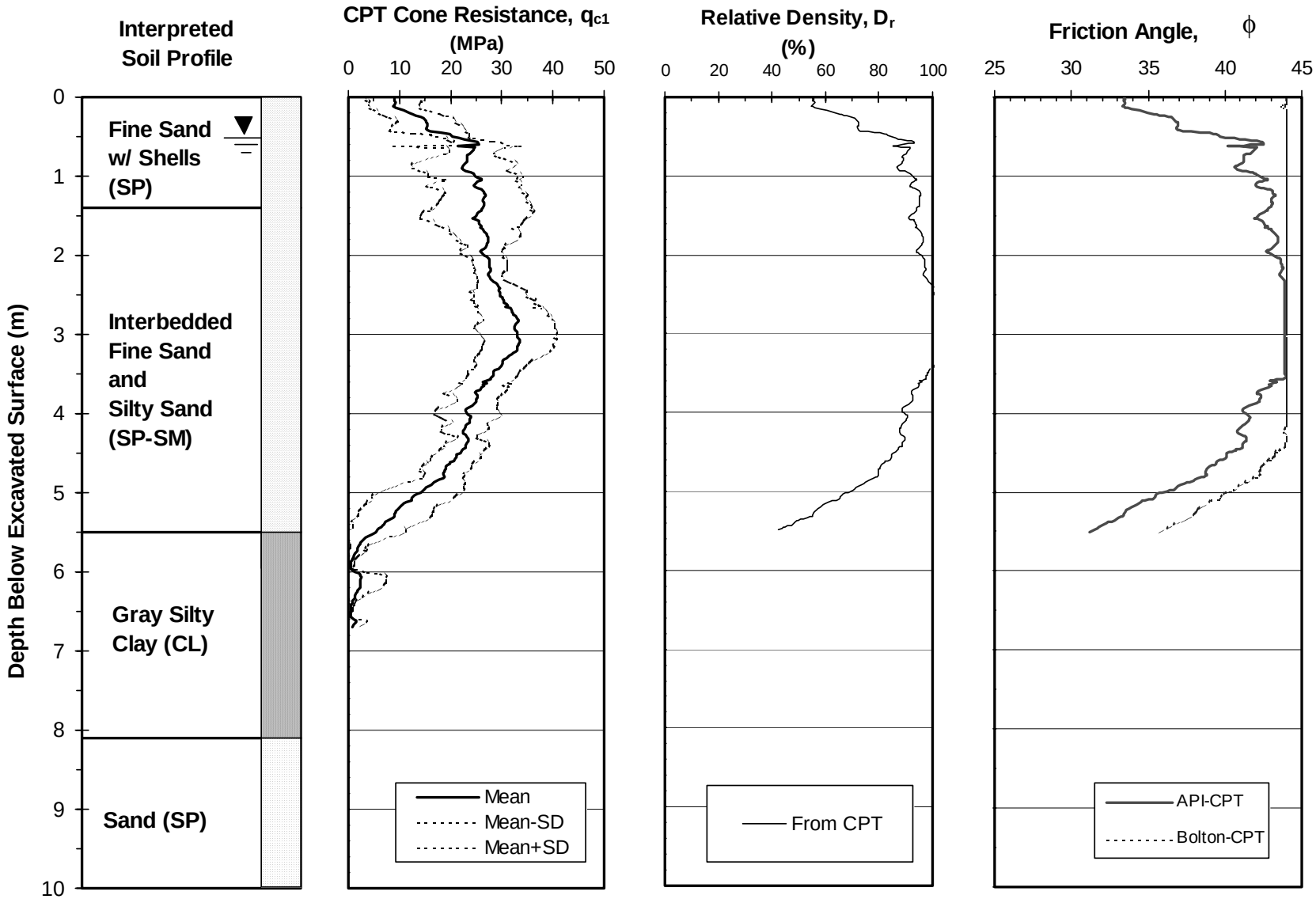

Fig. 8.14 Summary of idealized soil profile, in-situ test along with interpreted relative density and friction angle

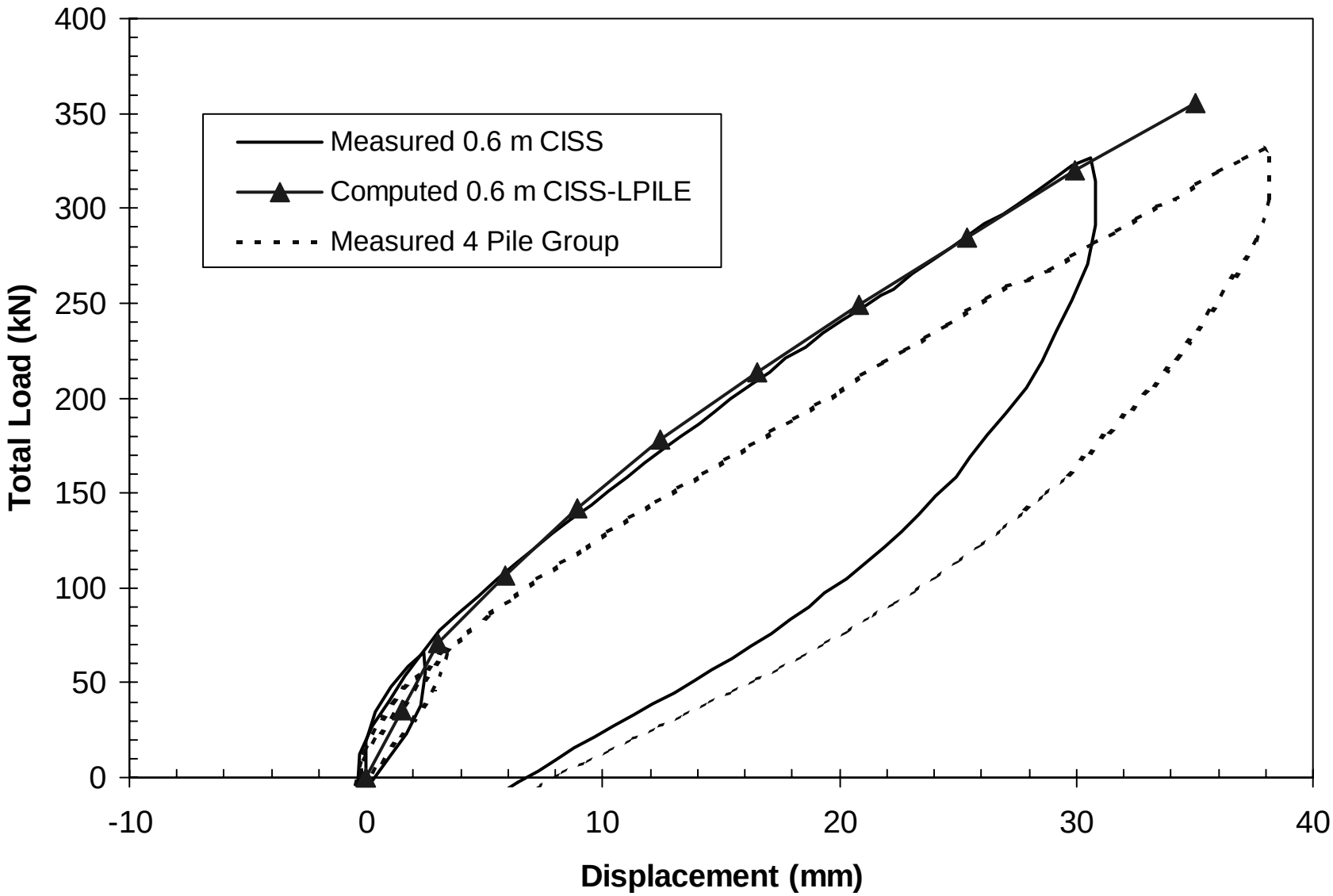

Figure 8.15 Measured total load-displacement curves for 0.6 m CISS pile and four pile group after stone column treatment along with curve computed using LPILE.

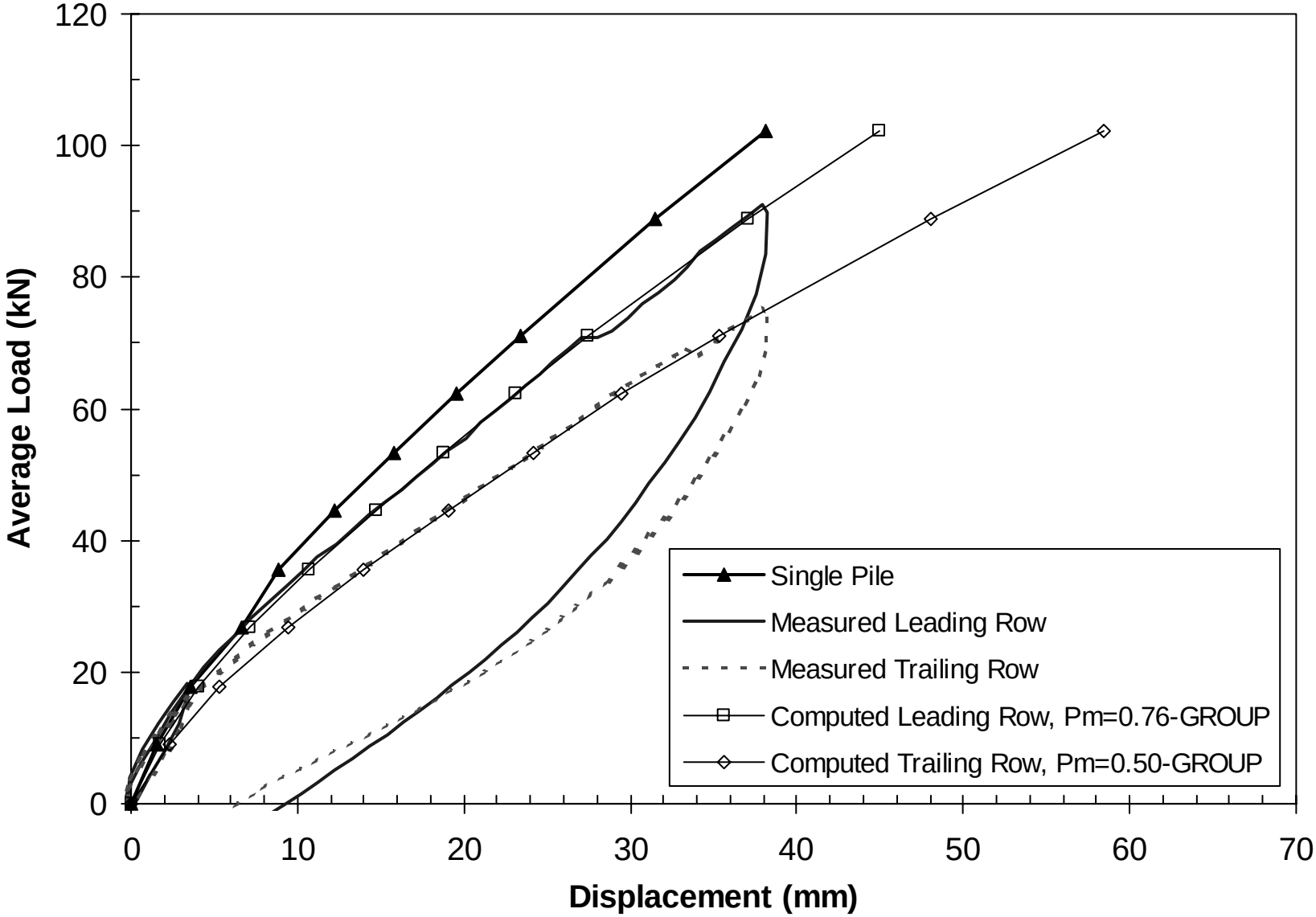

Figure 8.16 Measured average load-displacement curves for two rows in four pile group after stone column treatment along with curves computed using GROUP with indicated p-multipliers.

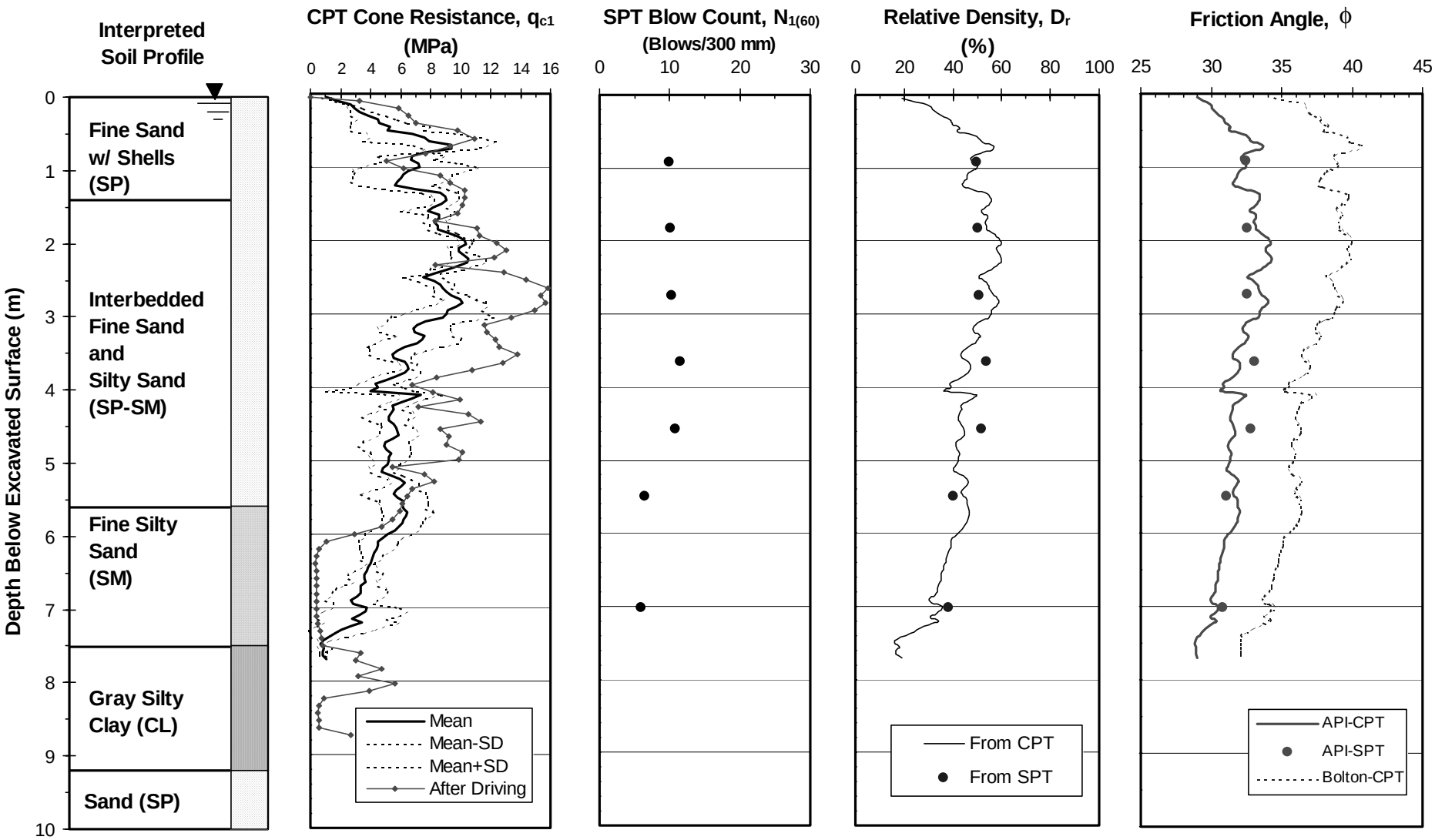

Figure 8.17 Summary of idealized soil profile and in-situ tests along with interpreted relative density and friction angle.

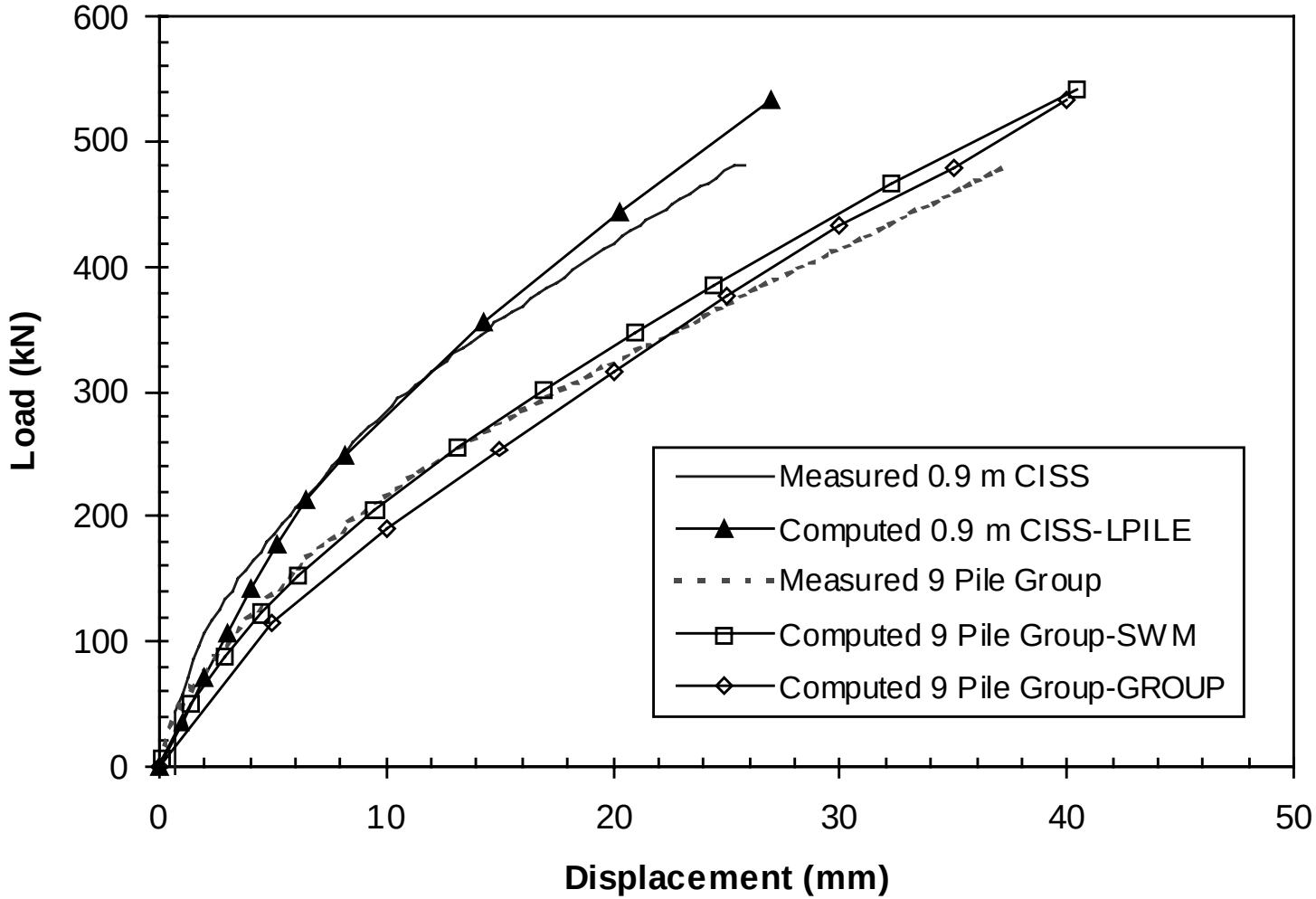

Figure 8.18 Measured total load-displacement curves for 0.9 m CISS pile and nine-pile group along with computed curves using LPILE, GROUP and SWM

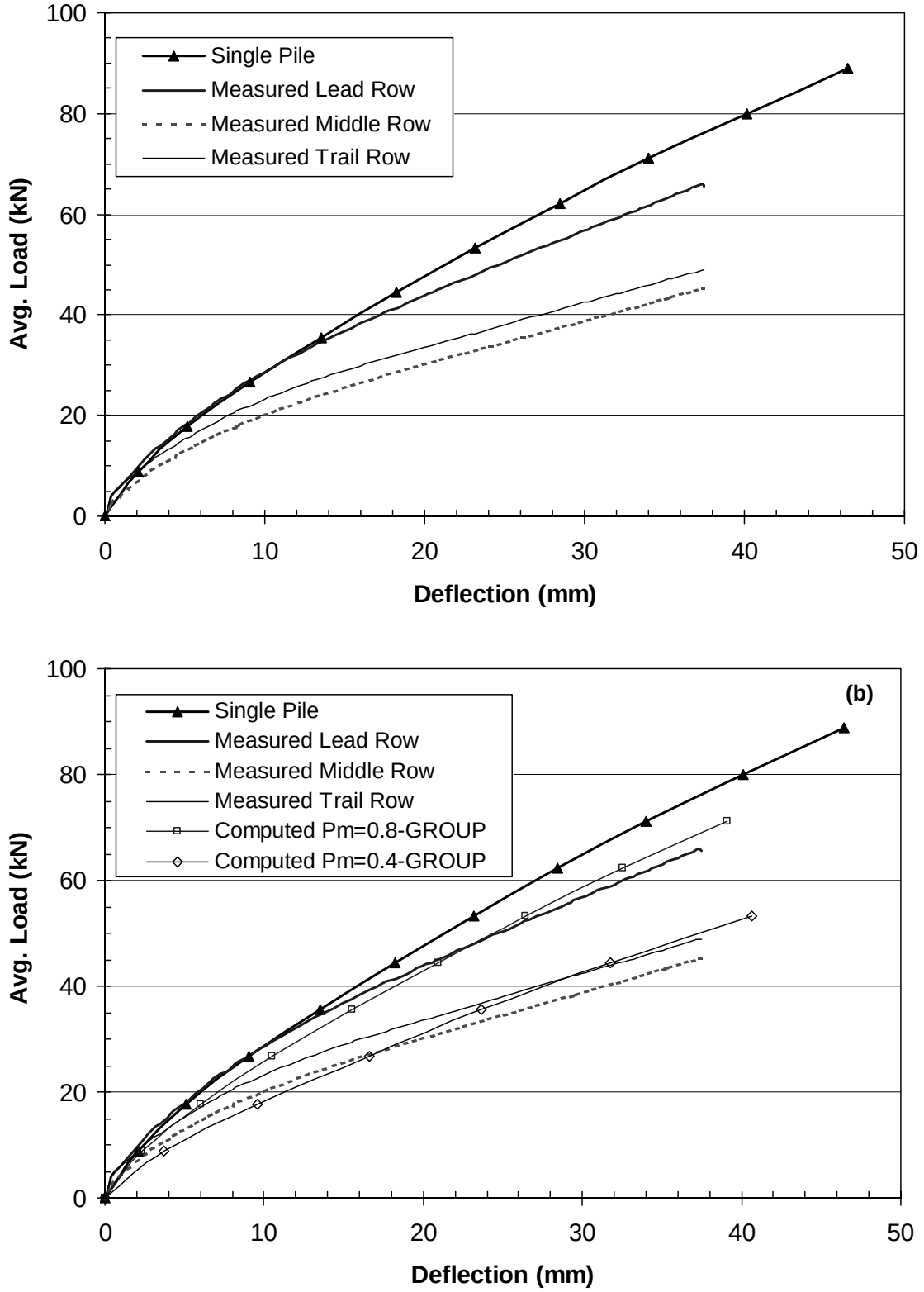

Figure 8.19 (a) Measured average load-displacement curves for each row in the 9 pile group along with (b) computed curves for leading and trailing rows computed using GROUP with p-multipliers of 0.8 and 0.4, respectively.

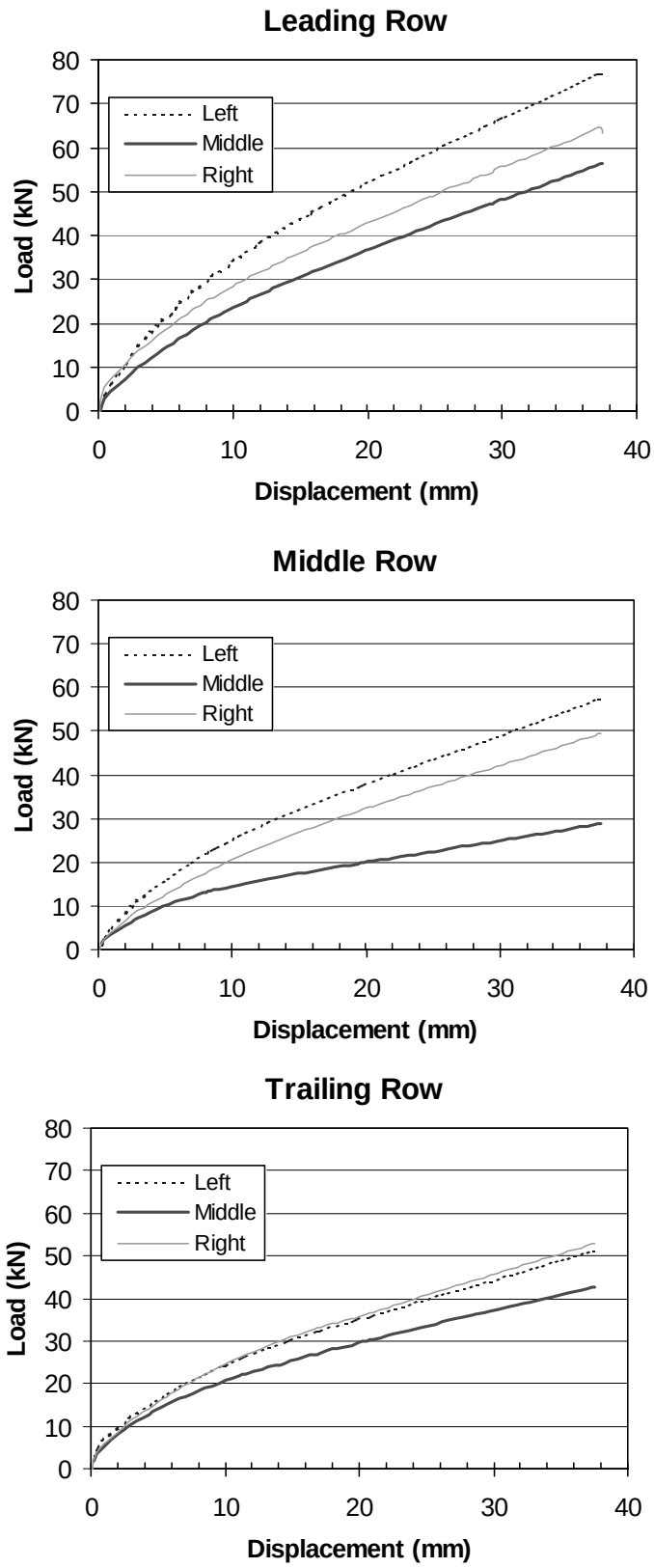

Figure 8.20 Measured load-displacement curves for the left, middle and right piles in each of the three rows in the nine-pile group.

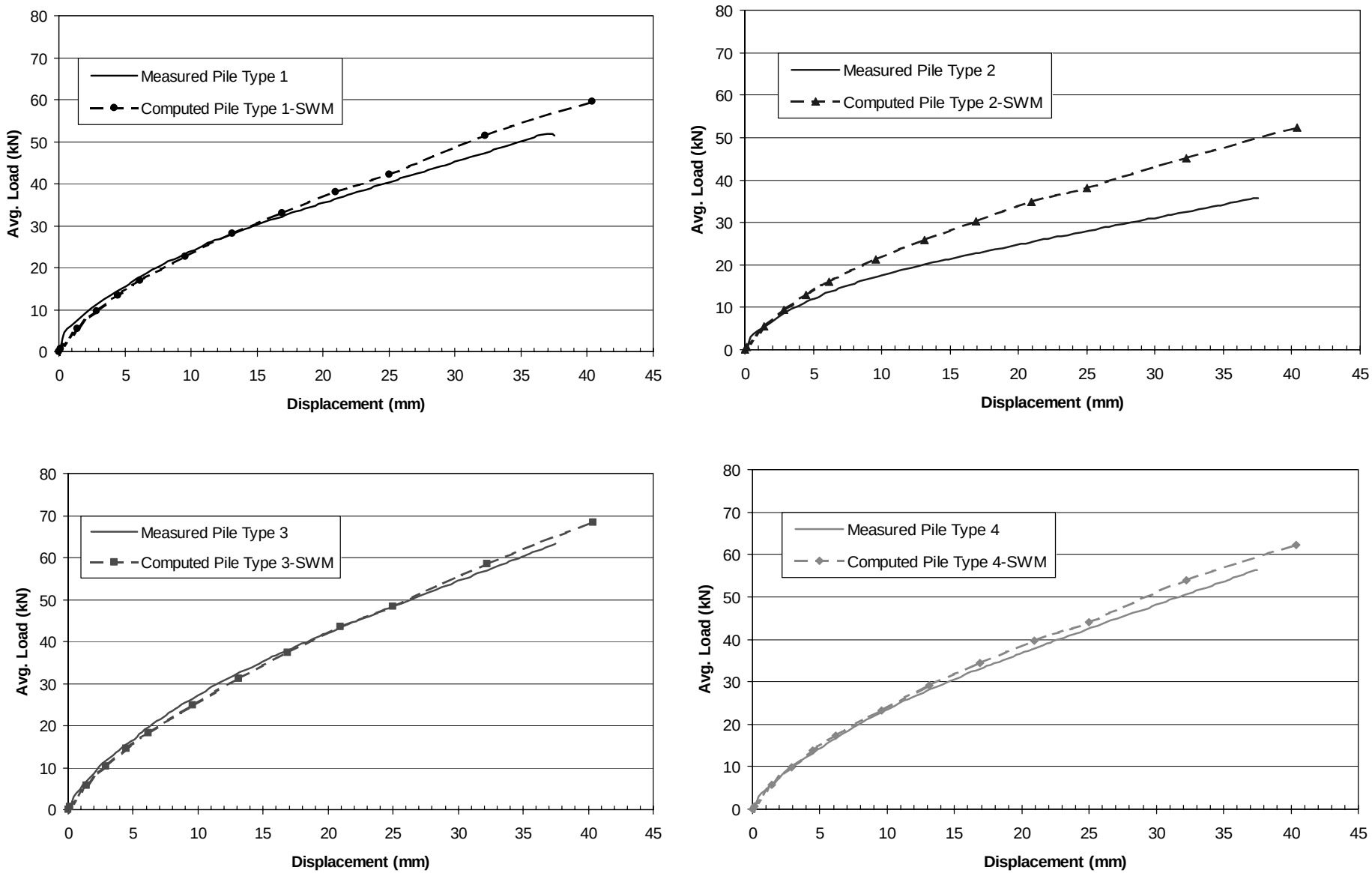

Figure 8.21 Comparison of measured and computed load-displacement curves for four pile types in the nine-pile group using SWM.

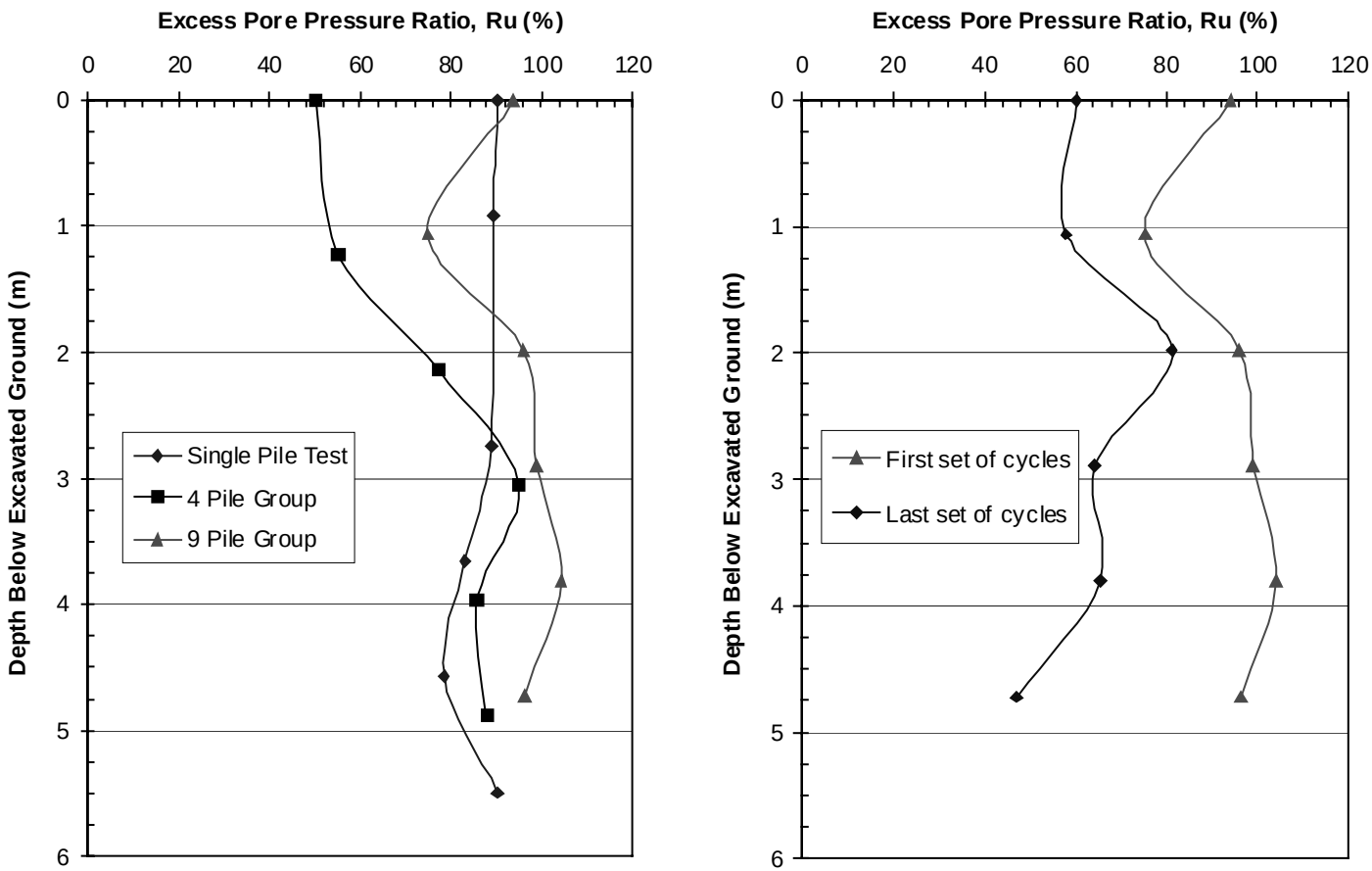

Figure 8.22 Average R_u versus depth curves (a) for the first series of load cycles following blasting at each test site and (b) for the first and last series of load cycles at the nine pile group.

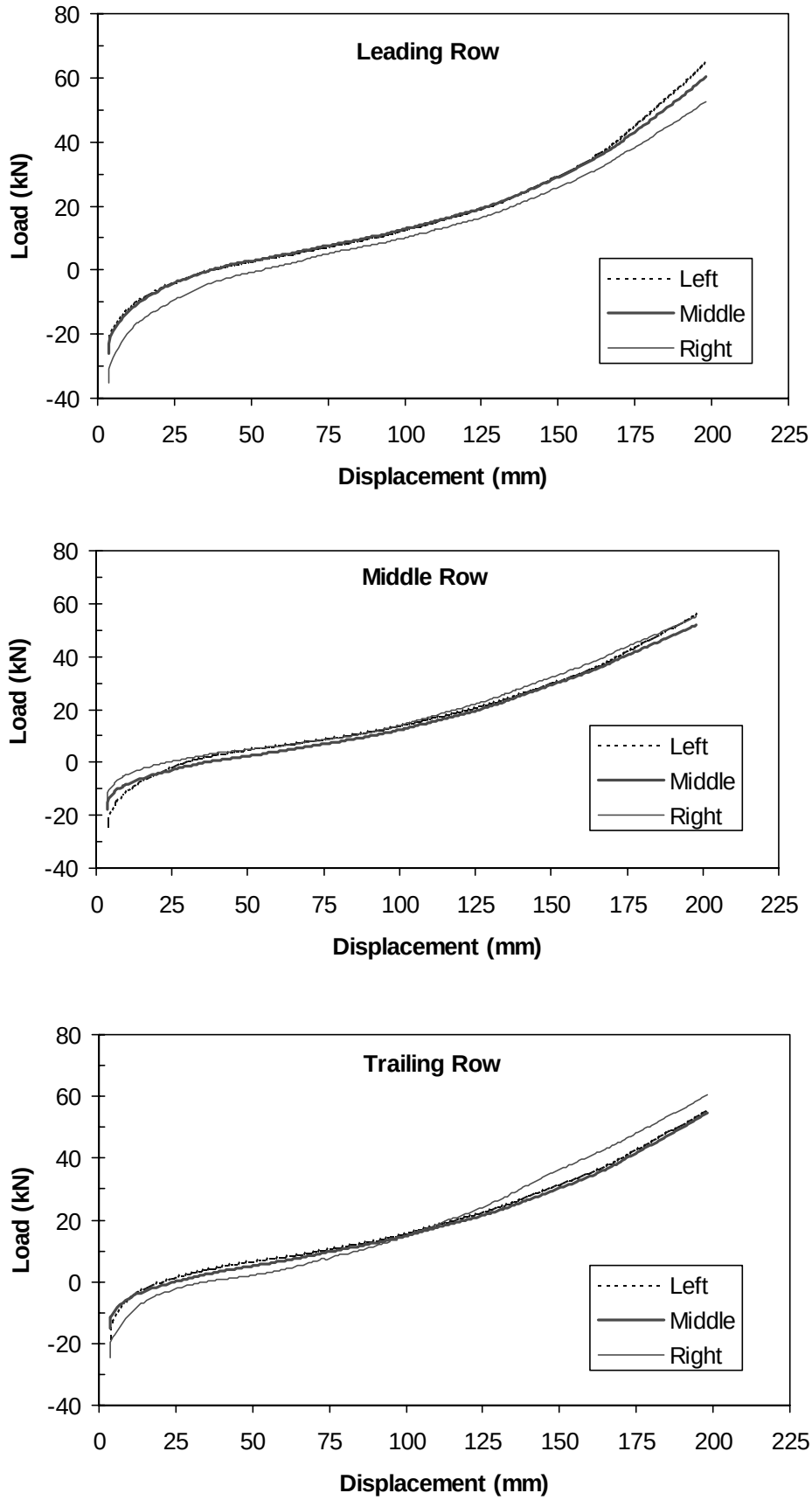

Figure 8.23 Measured load-displacement curves for the left, middle and right piles in each row in the nine-pile group after six cycles of loading following blasting.

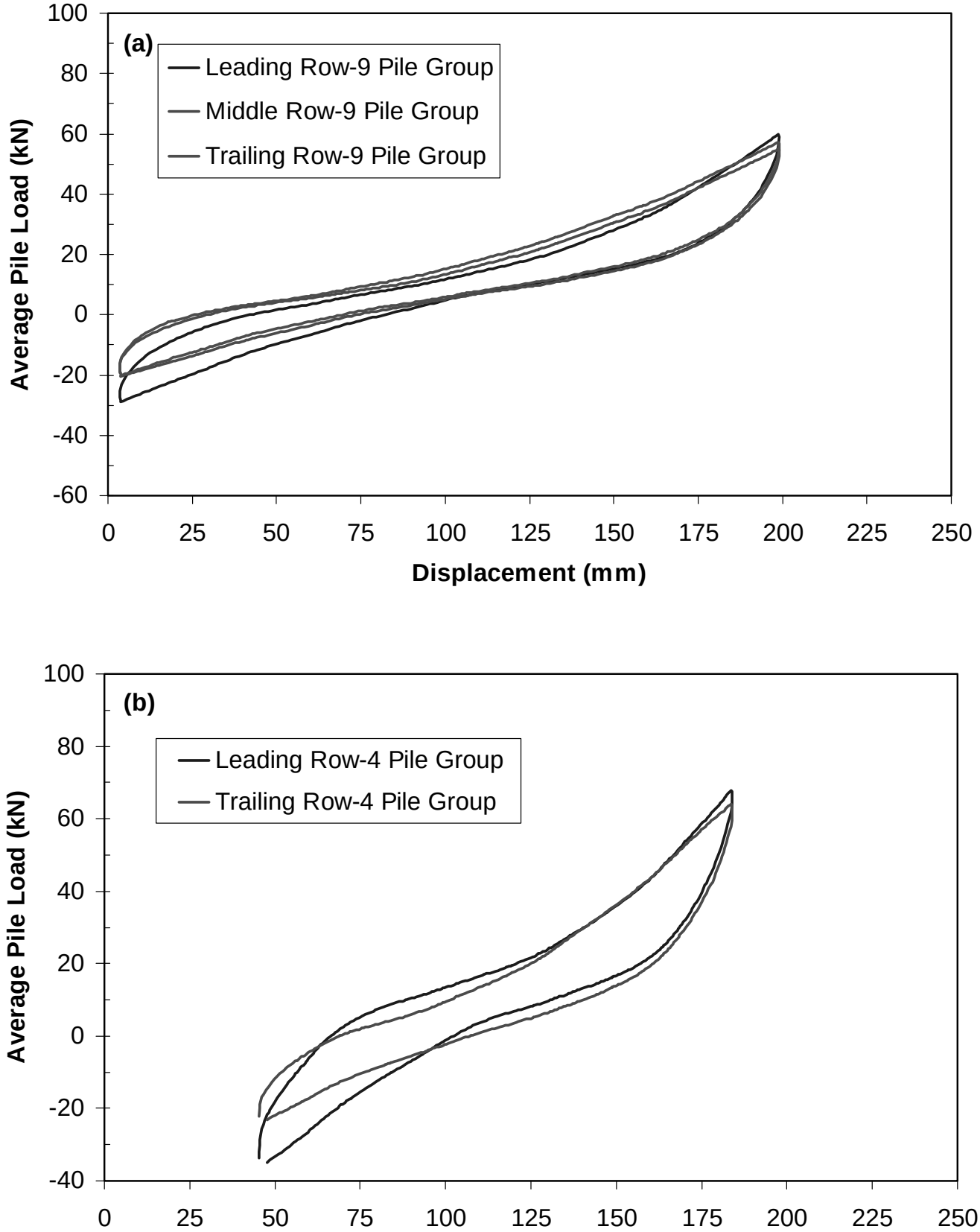

Figure 8.24 Measured average load-displacement curves for (a) the two rows in the four pile group and (b) the three rows in the nine pile group after six cycles of loading following blasting.

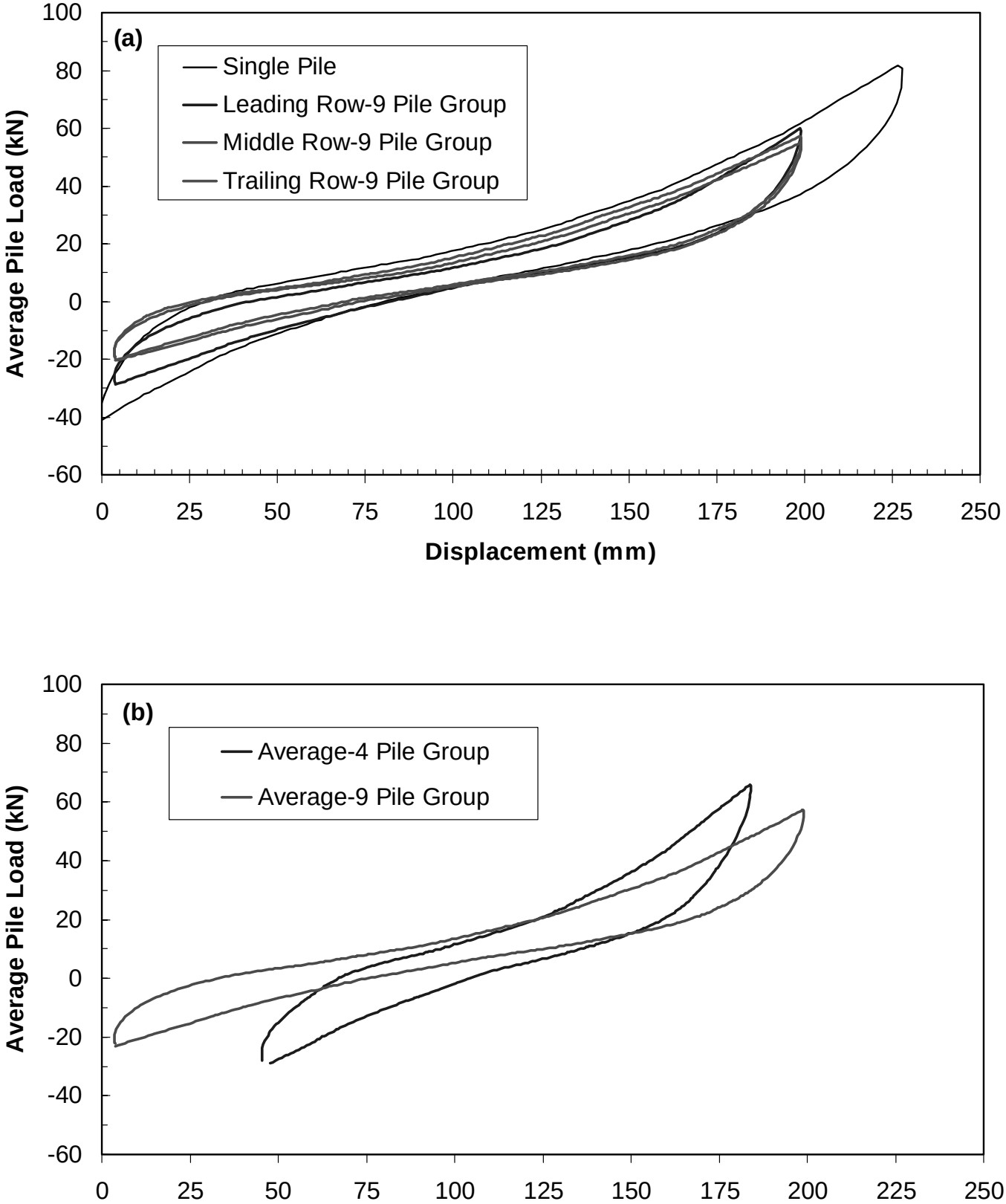

Figure 8.25 Measured average load-displacement curves for (a) the single pile in comparison with those for the three rows in the nine pile group and (b) the 4 pile group and 9-pile group.

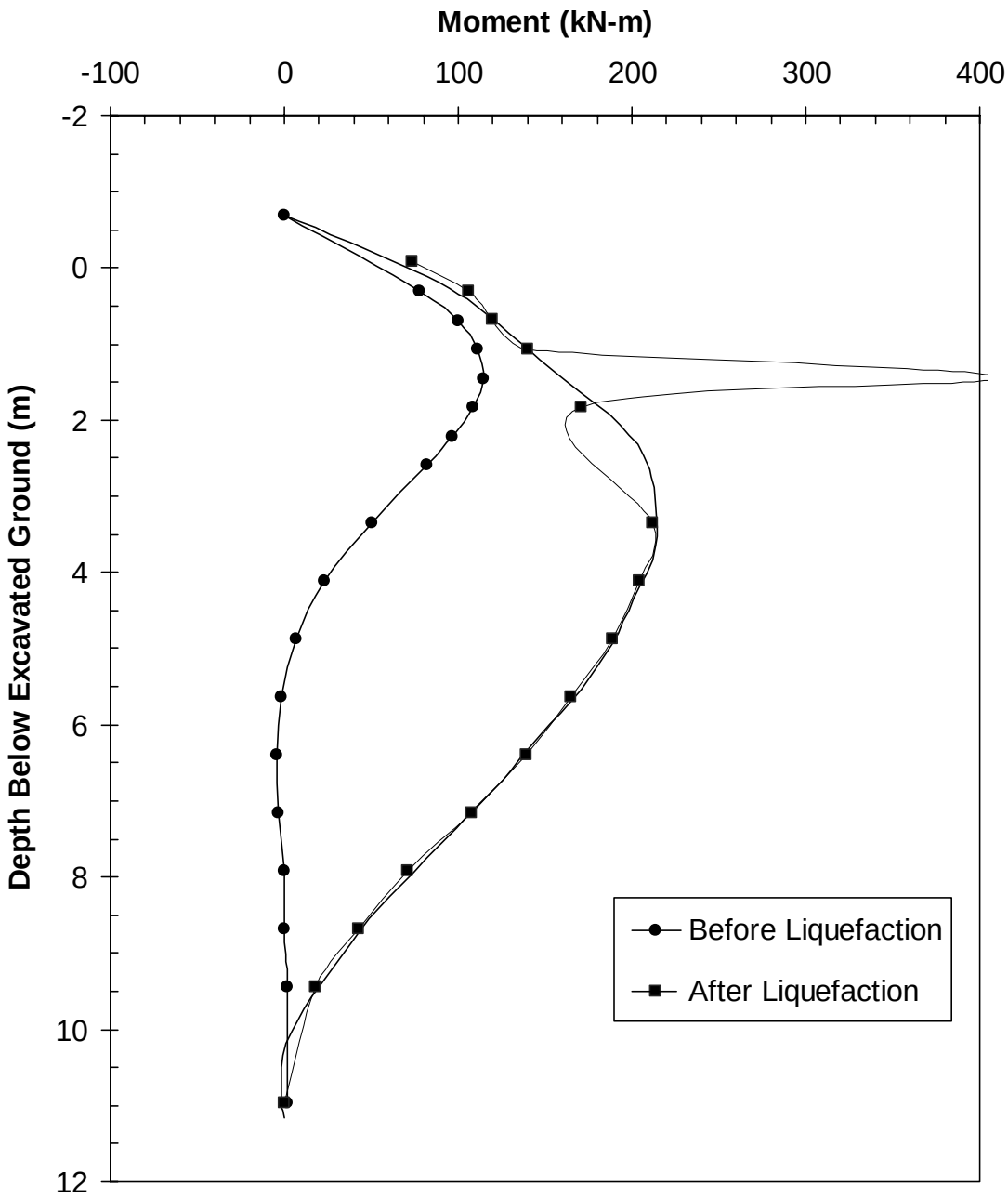

Figure 8.26 Bending moment versus depth curves for the single pile before liquefaction and after liquefaction with an applied load of 69 kN in both cases.

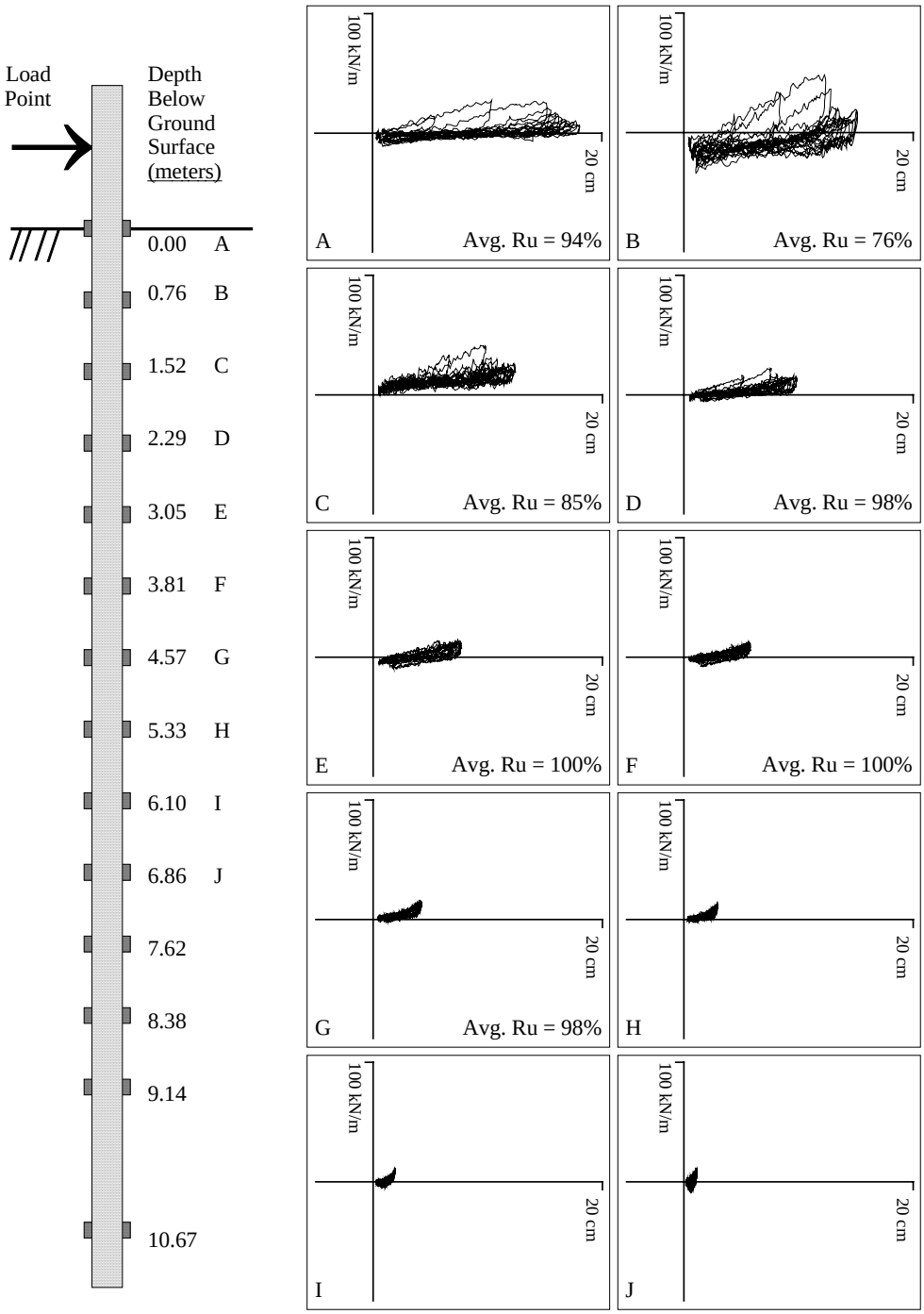

Figure 8.27 Diagrammatic summary of calculated p-y curves for the east center pile in 3x3 group, during the first 23-cm load cycle (from 2.6 to 12.2 min)

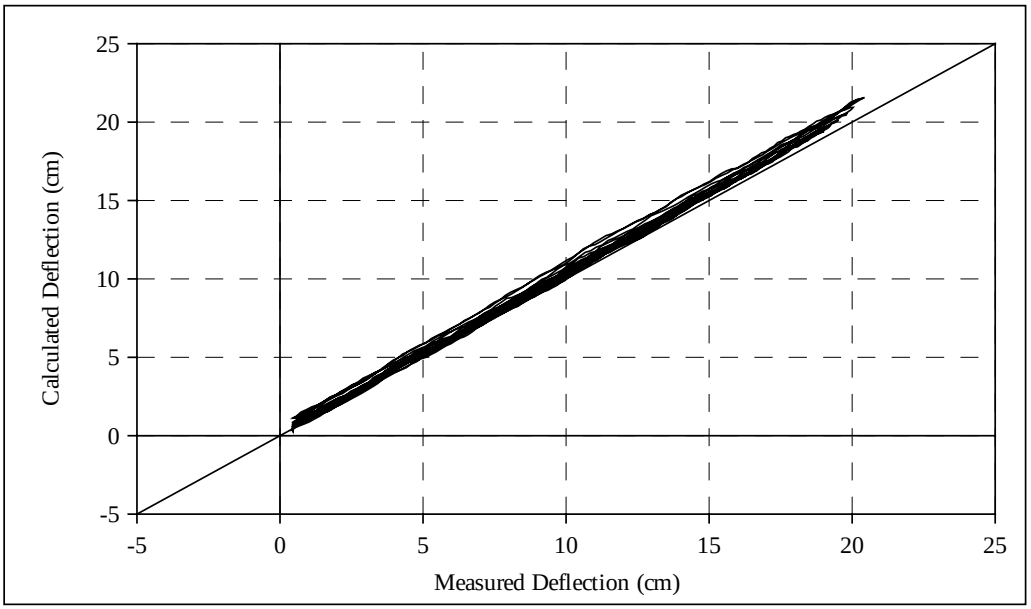

Figure 8.28 Comparison of measured versus calculated pile deflection at load point for the east center pile in 3x3 group during the first 23-cm load cycle (from 2.6 to 12.2 min)

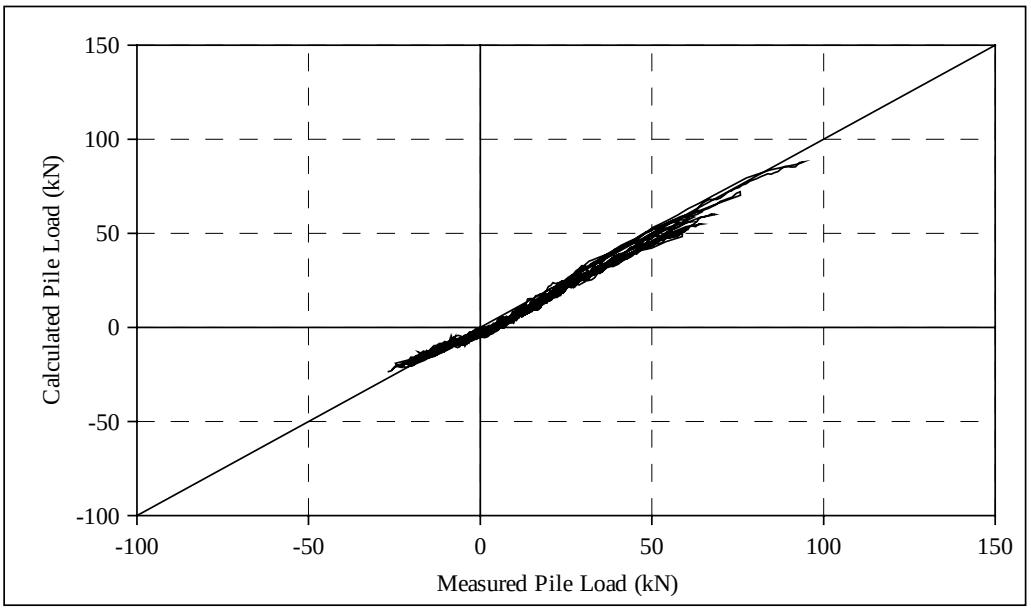

Figure 8.29 Comparison of measured versus calculated pile load (at load point) for the east center pile in 3x3 group during the first 23-cm load cycle (from 2.6 to 12.2 min)

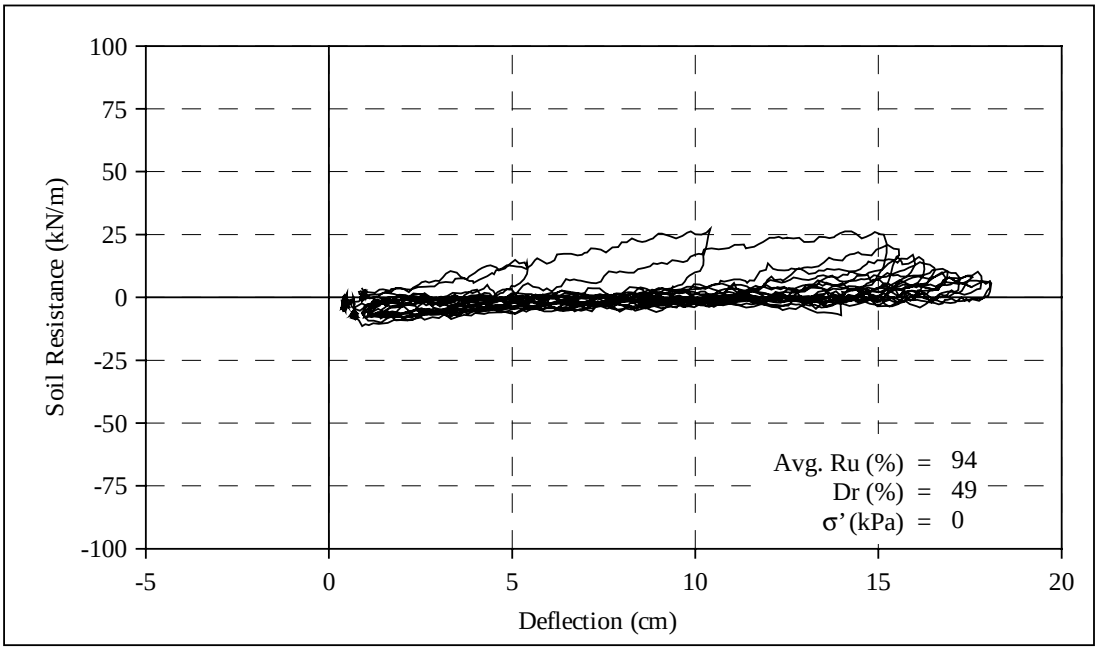

Figure 8.30 Calculated deflection versus soil resistance for the east center pile in 3x3 group, at a depth of 0.00 meters during the first 23-cm load cycle (from 2.6 to 12.2 min)

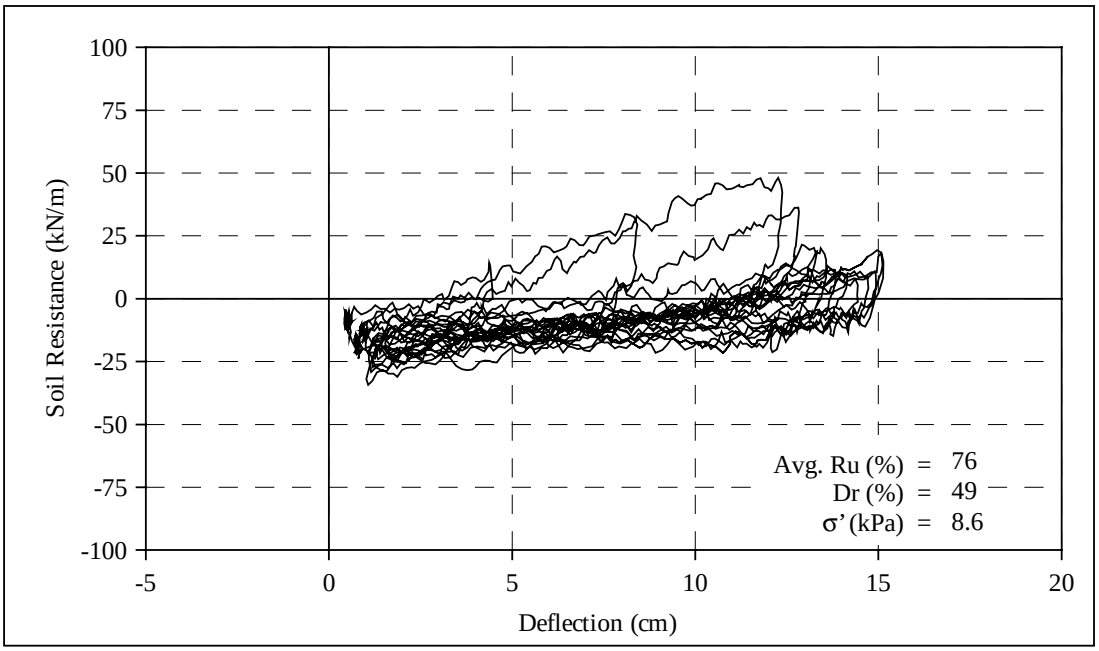

Figure 8.31 Calculated deflection versus soil resistance for the east center pile in 3x3 group, at a depth of 0.76 meters during the first 23-cm load cycle (from 2.6 to 12.2 min)

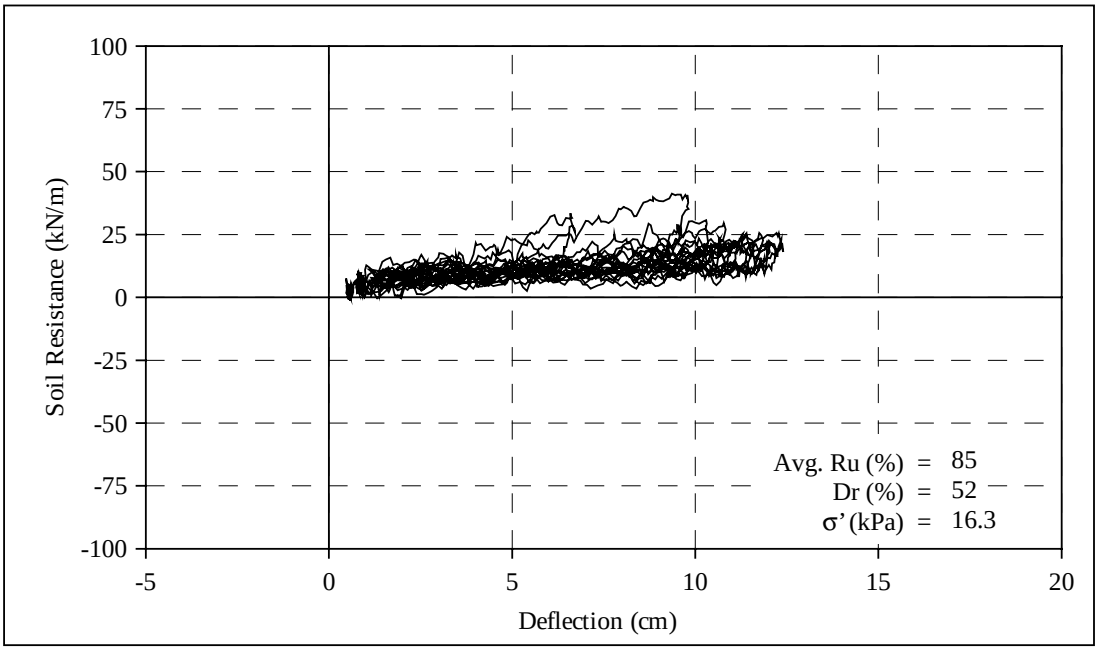

Figure 8.32 Calculated deflection versus soil resistance for the east center pile in 3x3 group, at a depth of 1.52 meters during the first 23-cm load cycle (from 2.6 to 12.2 min)

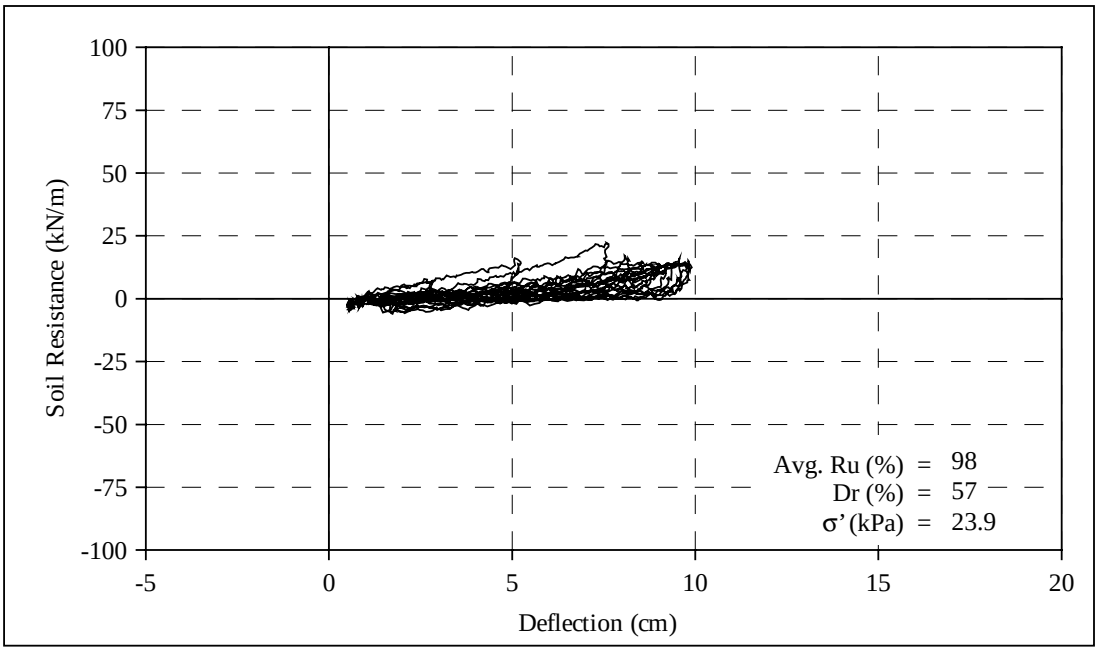

Figure 8.33 Calculated deflection versus soil resistance for the east center pile in 3x3 group, at a depth of 2.29 meters during the first 23-cm load cycle (from 2.6 to 12.2 min)

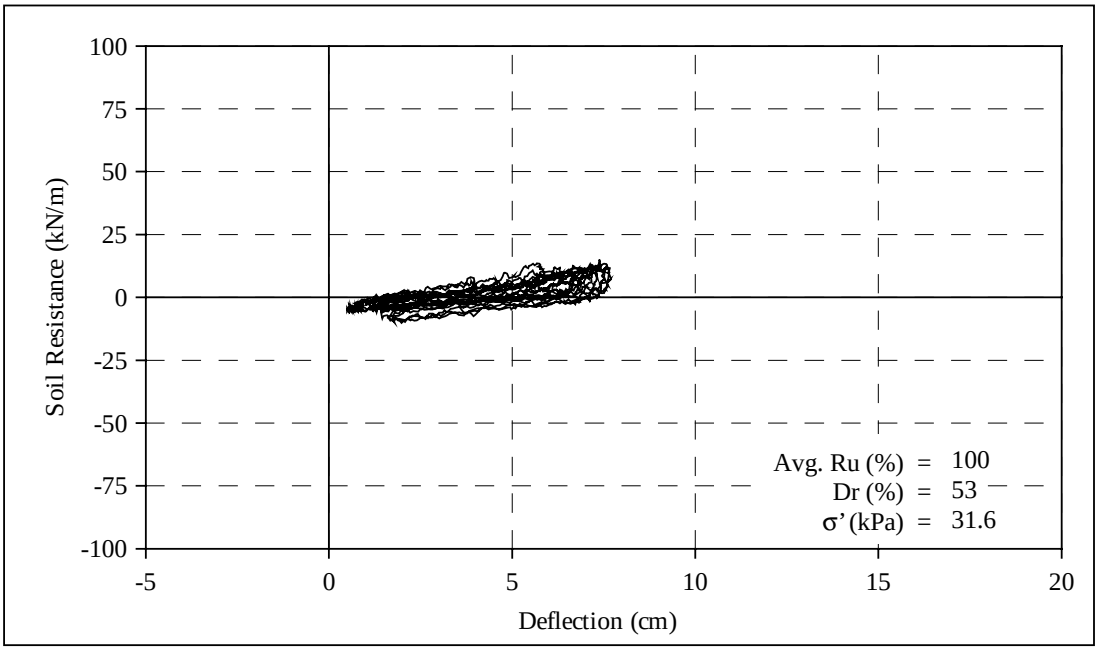

Figure 8.34 Calculated deflection versus soil resistance for the east center pile in 3x3 group, at a depth of 3.05 meters during the first 23-cm load cycle (from 2.6 to 12.2 min)

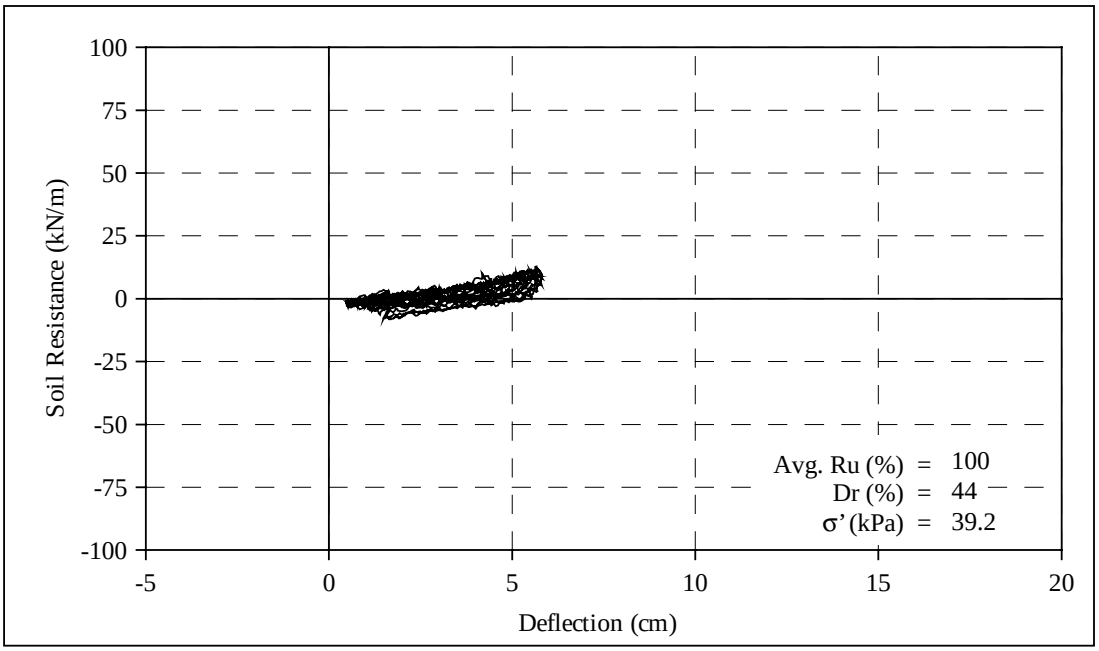

Figure 8.35 Calculated deflection versus soil resistance for the east center pile in 3x3 group, at a depth of 3.81 meters during the first 23-cm load cycle (from 2.6 to 12.2 min)

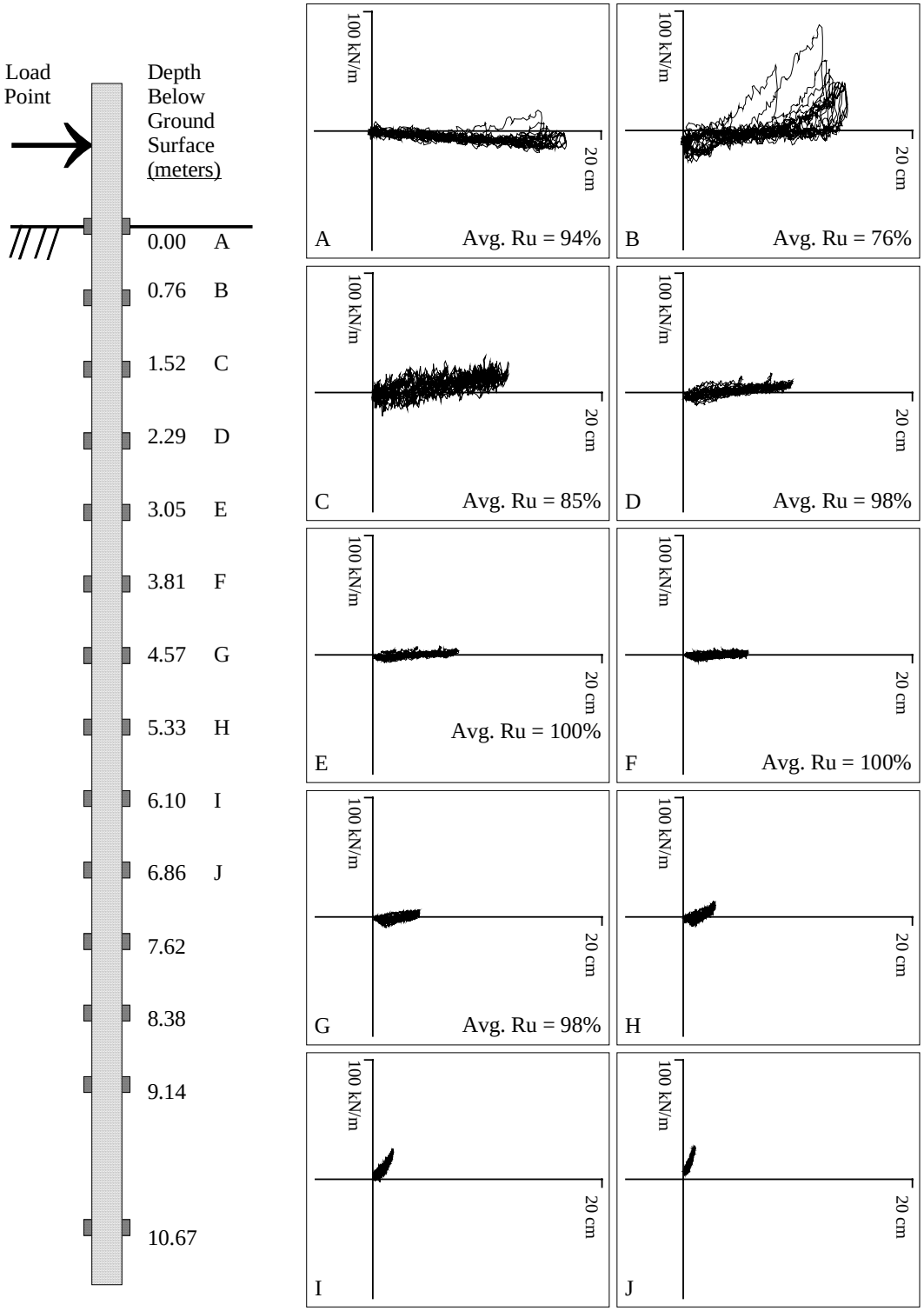

Figure 8.36 Diagrammatic summary of calculated p-y curves for the north center pile in 3x3 group, during the first 23-cm load cycle (from 2.6 to 12.2 min)

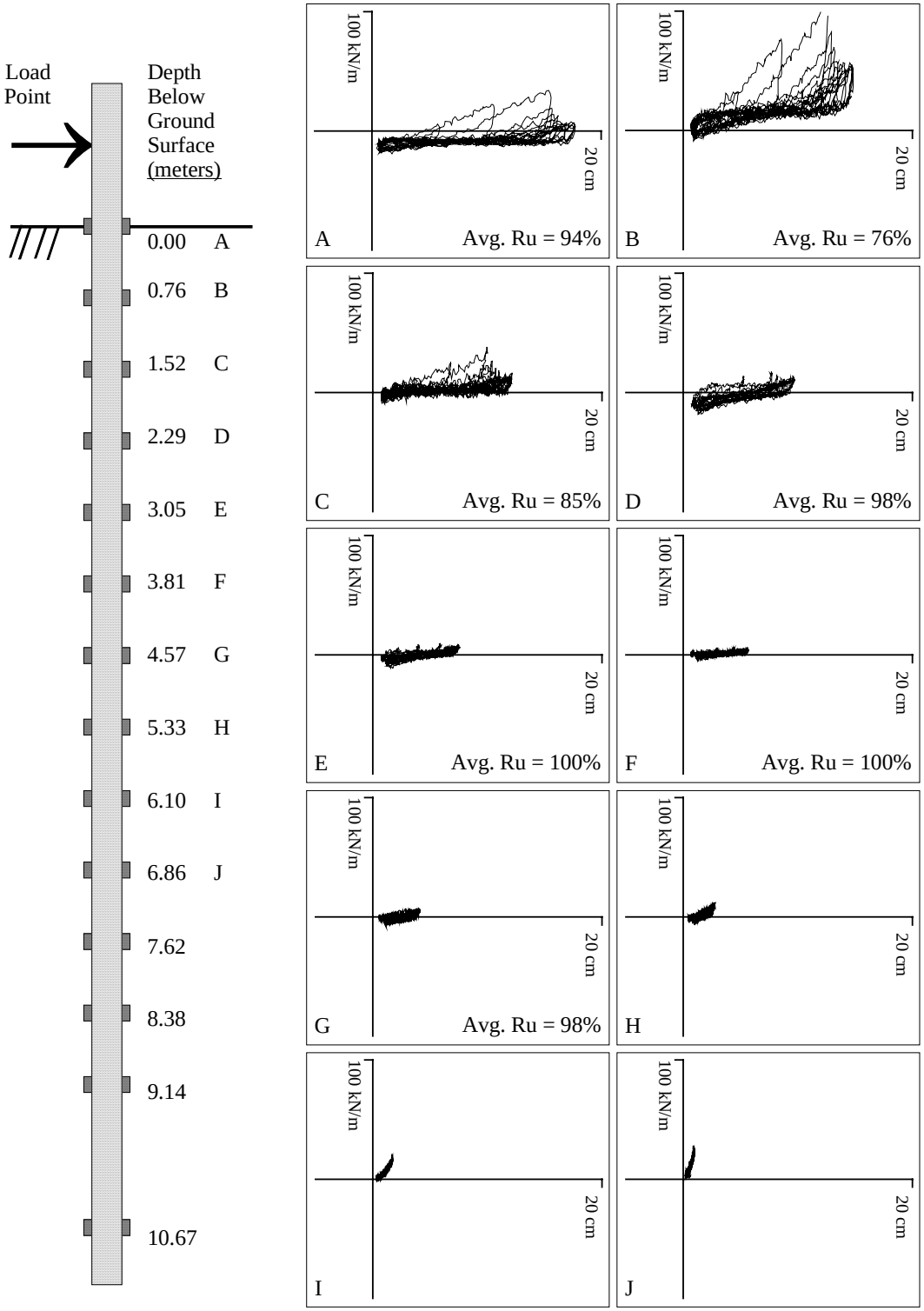

Figure 8.37 Diagrammatic summary of calculated p-y curves for the northeast pile in 3x3 group, during the first 23-cm load cycle (from 2.6 to 12.2 min)

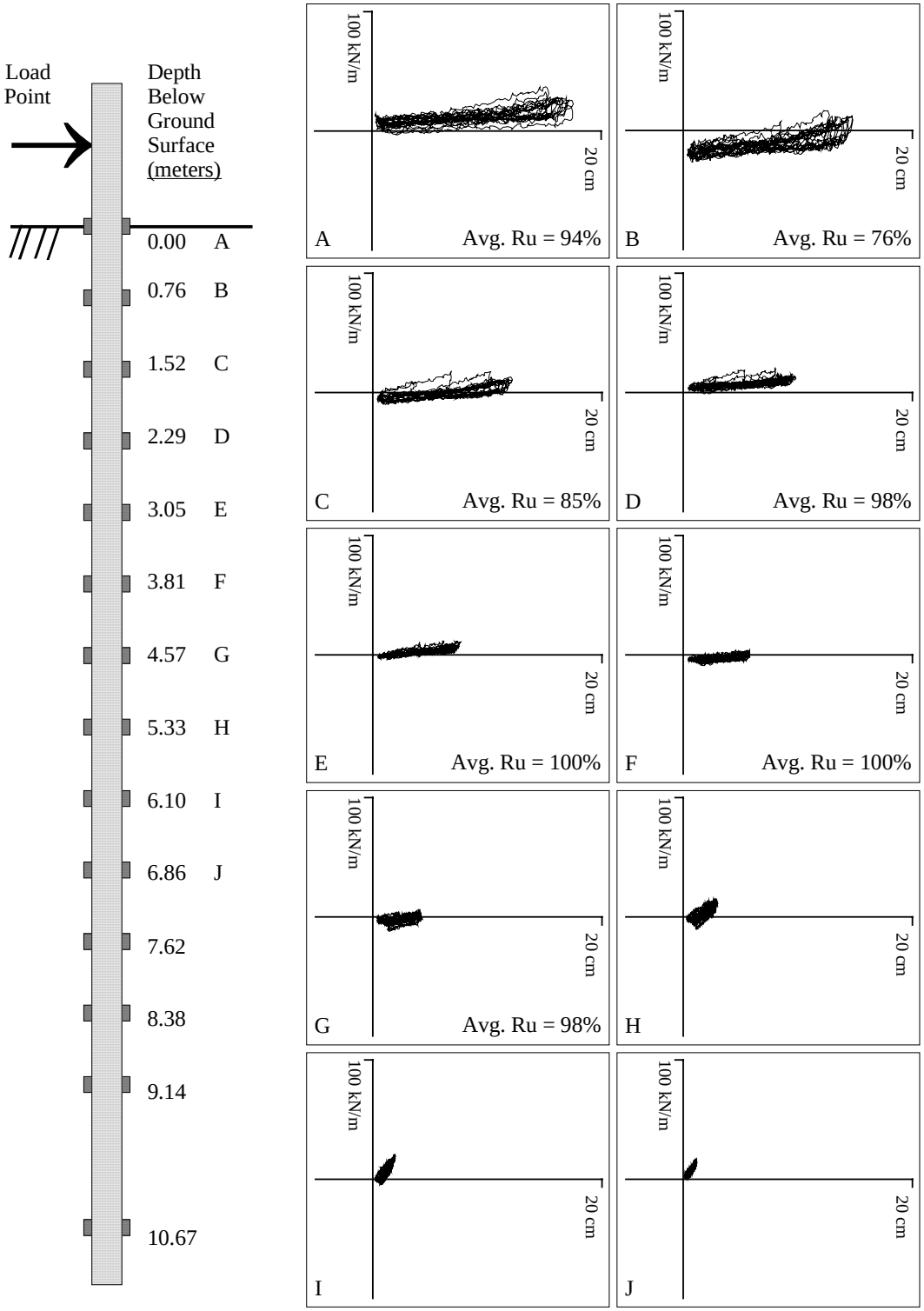

Figure 8.38 Diagrammatic summary of calculated p-y curves for the center pile in 3x3 group, during the first 23-cm load cycle (from 2.6 to 12.2 min)

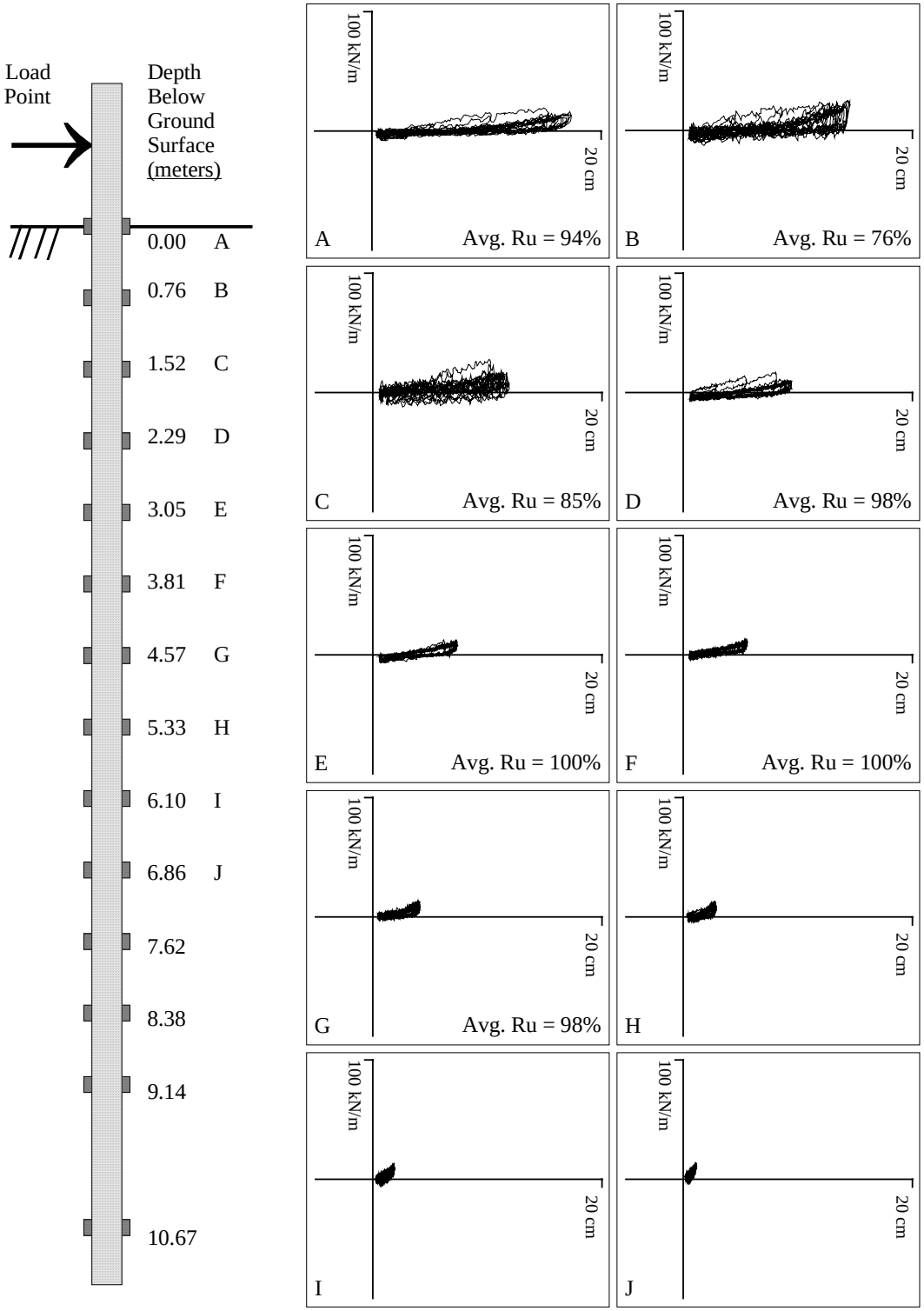

Figure 8.39 Diagrammatic summary of calculated p-y curves for the south center pile in 3x3 group, during the first 23-cm load cycle (from 2.6 to 12.2 min)

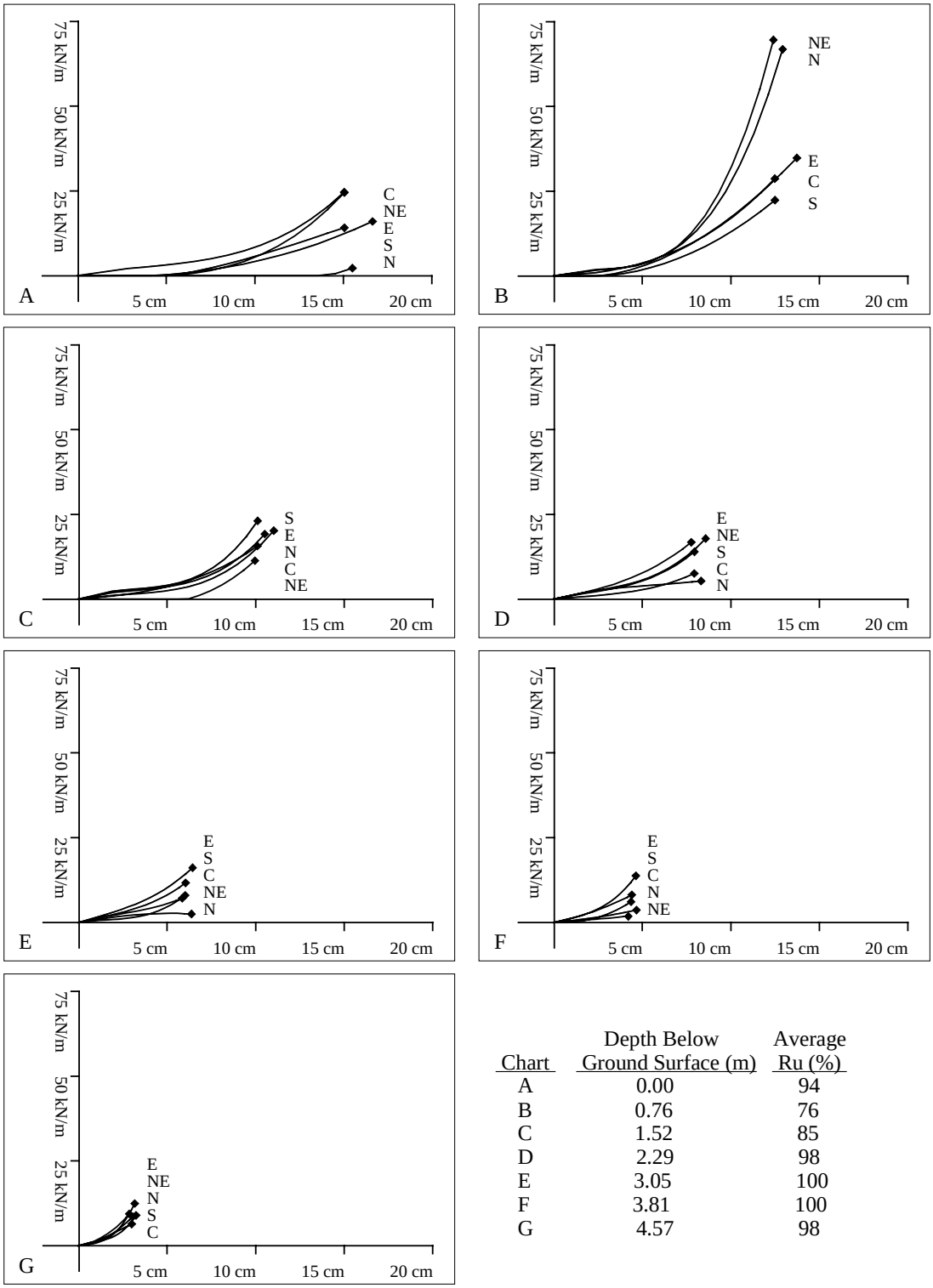

Chart	Depth Below Ground Surface (m)	Average Ru (%)
A	0.00	94
B	0.76	76
C	1.52	85
D	2.29	98
E	3.05	100
F	3.81	100
G	4.57	98

Figure 8.40 Calculated p-y curves for different piles in the 3x3 group at various depths during the first 23-cm load cycle, relative to zero pile head load

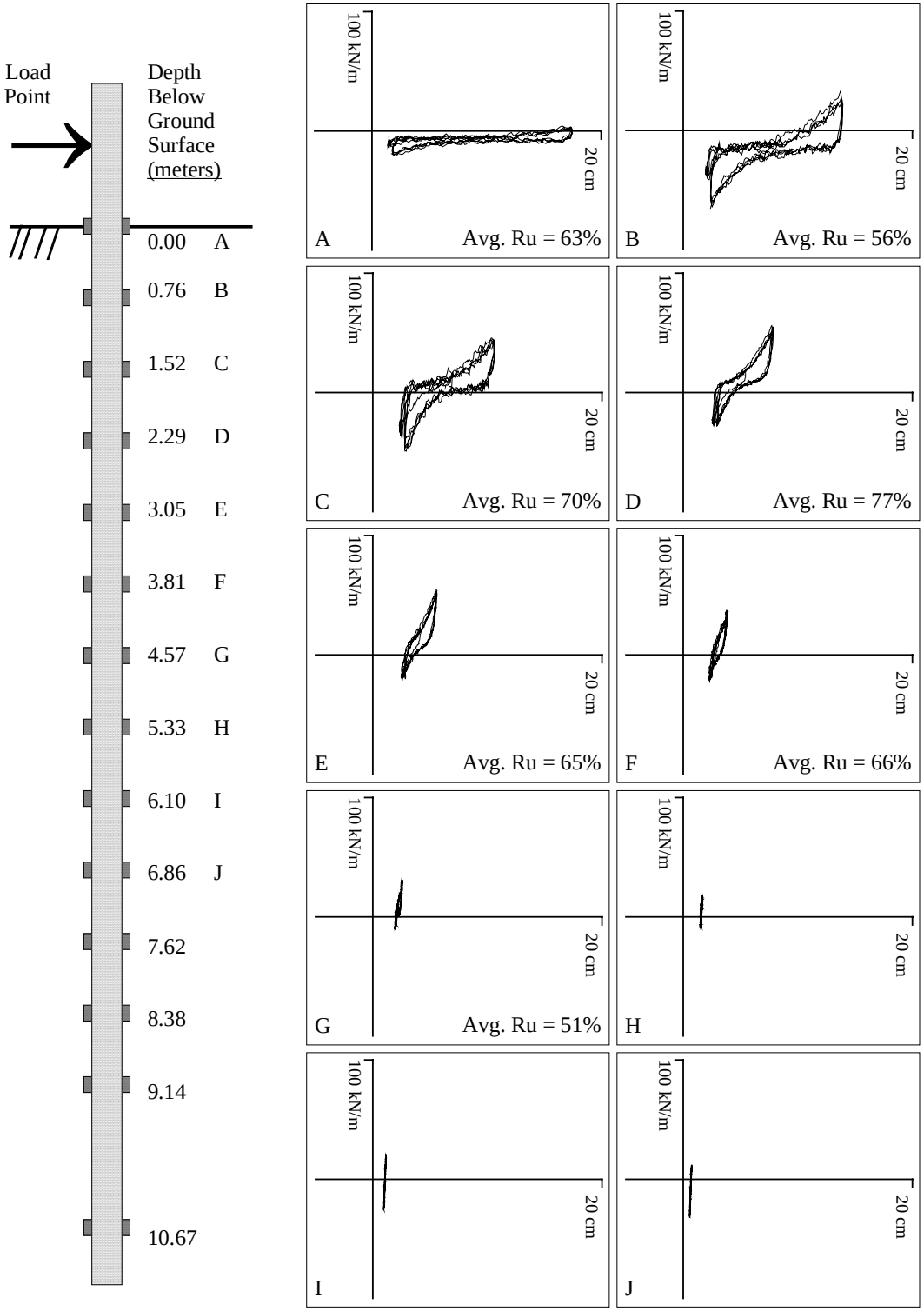

Figure 8.41 Diagrammatic summary of calculated p-y curves for the east center pile in 3x3 group, during the tenth 23-cm load cycle (from 58.4 to 62.2 min)

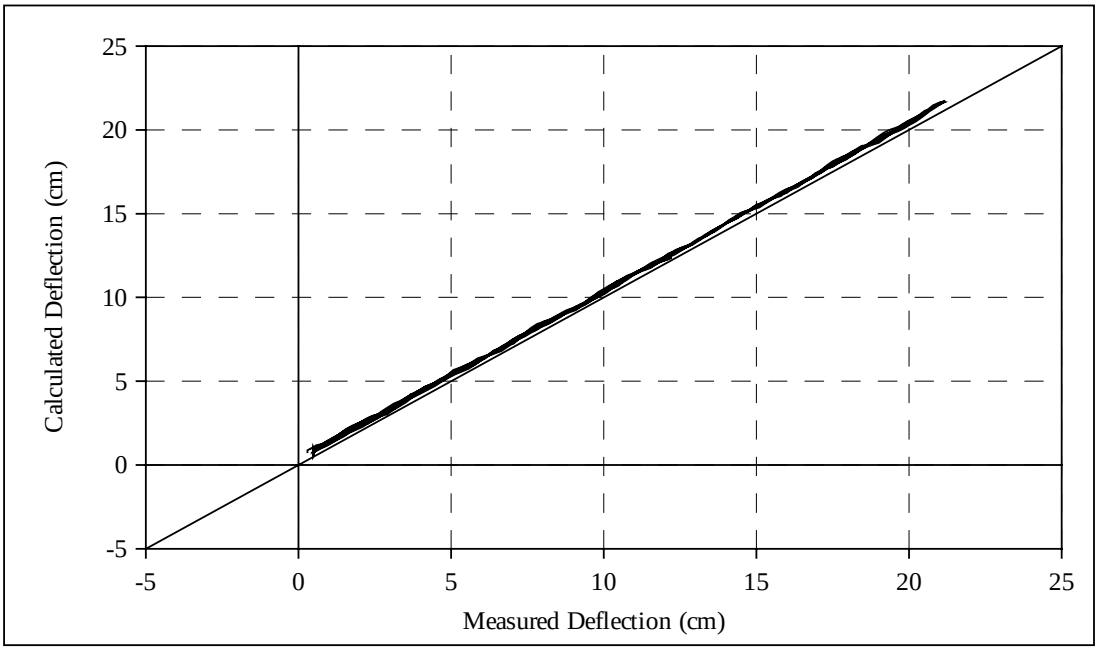

Figure 8.42 Comparison of measured versus calculated pile deflection at load point for the east center pile in 3x3 group during the tenth 23-cm load cycle (from 58.4 to 62.2 min)

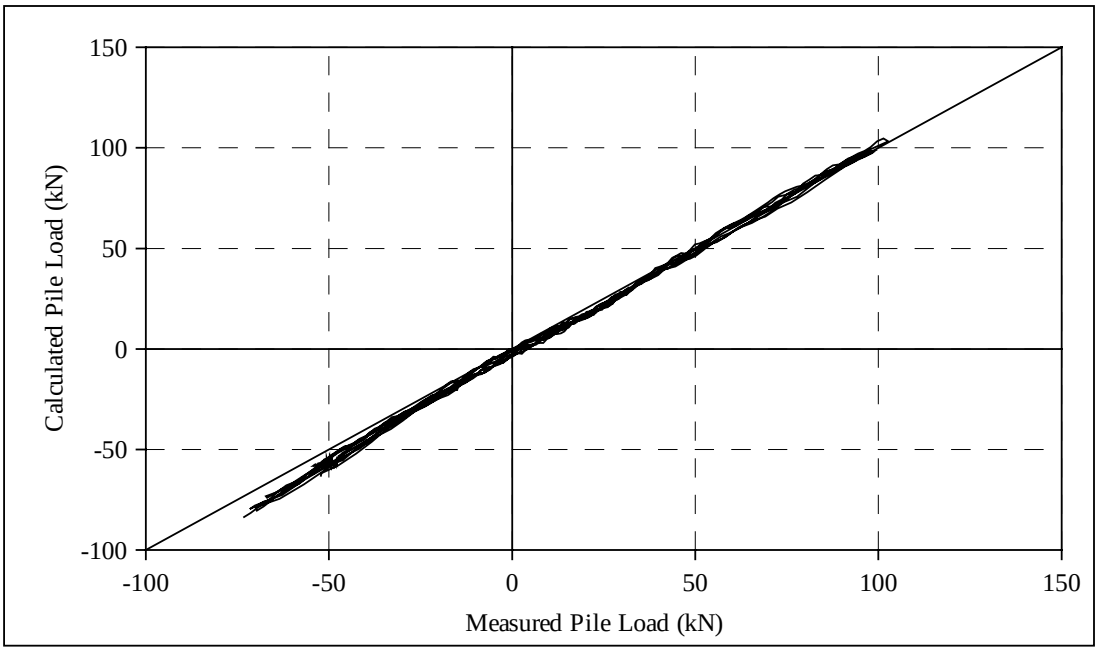

Figure 8.43 Comparison of measured versus calculated pile load (at load point) for the east center pile in 3x3 group during the tenth 23-cm load cycle (from 58.4 to 62.2 min)

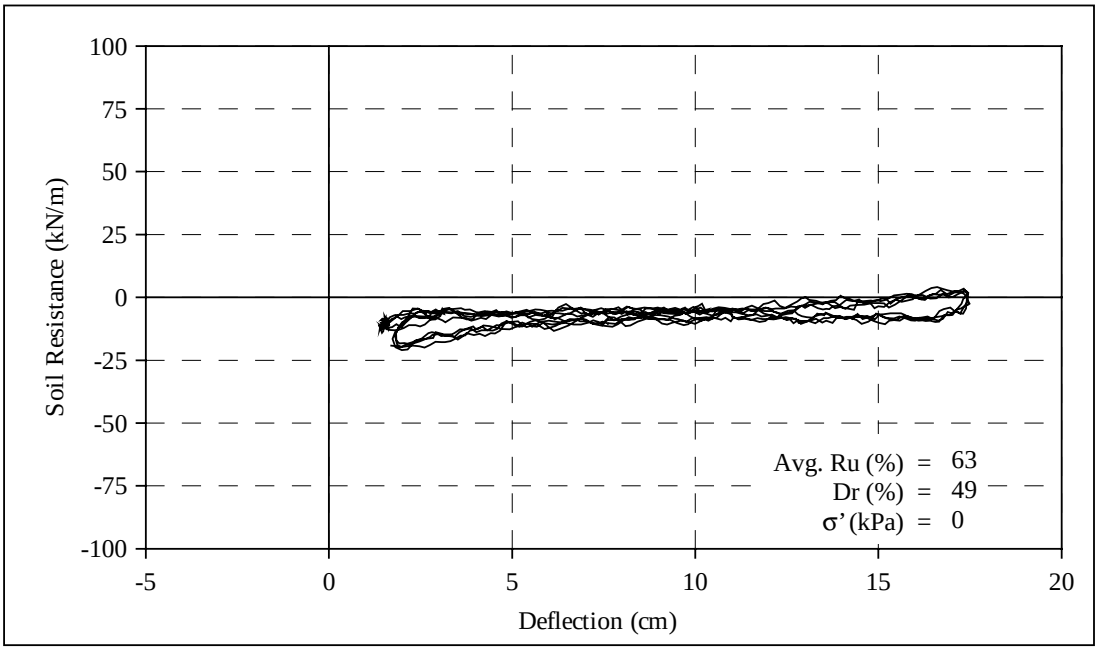

Figure 8.44 Calculated deflection versus soil resistance for the east center pile in 3x3 group, at a depth of 0.00 meters during the tenth 23-cm load cycle (from 58.4 to 62.2 min)

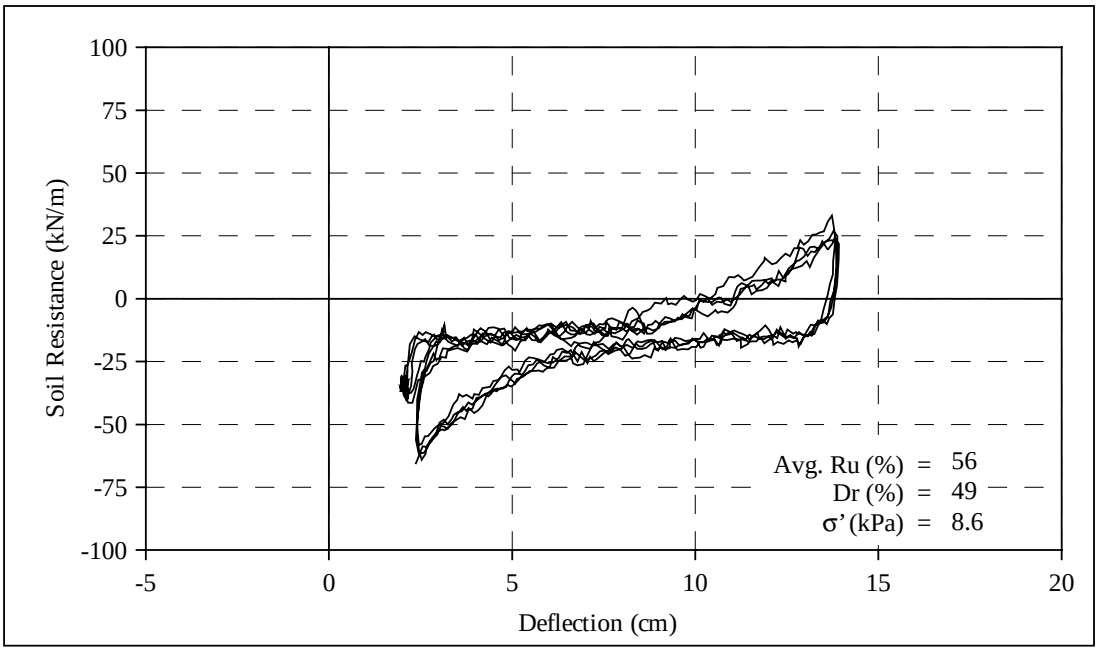

Figure 8.45 Calculated deflection versus soil resistance for the east center pile in 3x3 group, at a depth of 0.76 meters during the tenth 23-cm load cycle (from 58.4 to 62.2 min)

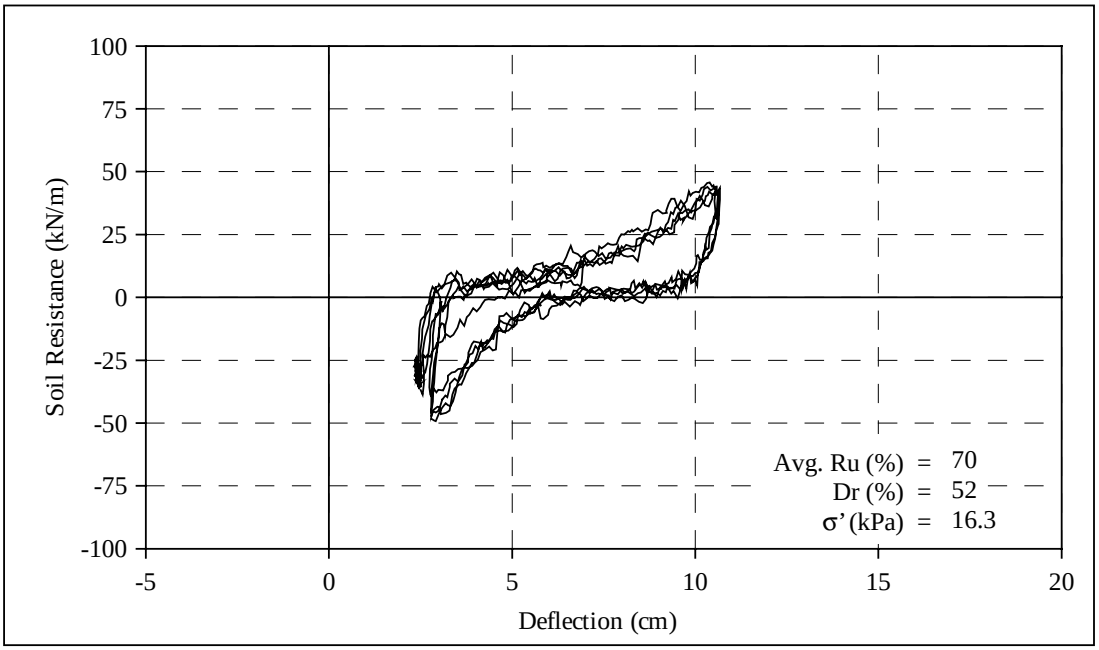

Figure 8.46 Calculated deflection versus soil resistance for the east center pile in 3x3 group, at a depth of 1.52 meters during the tenth 23-cm load cycle (from 58.4 to 62.2 min)

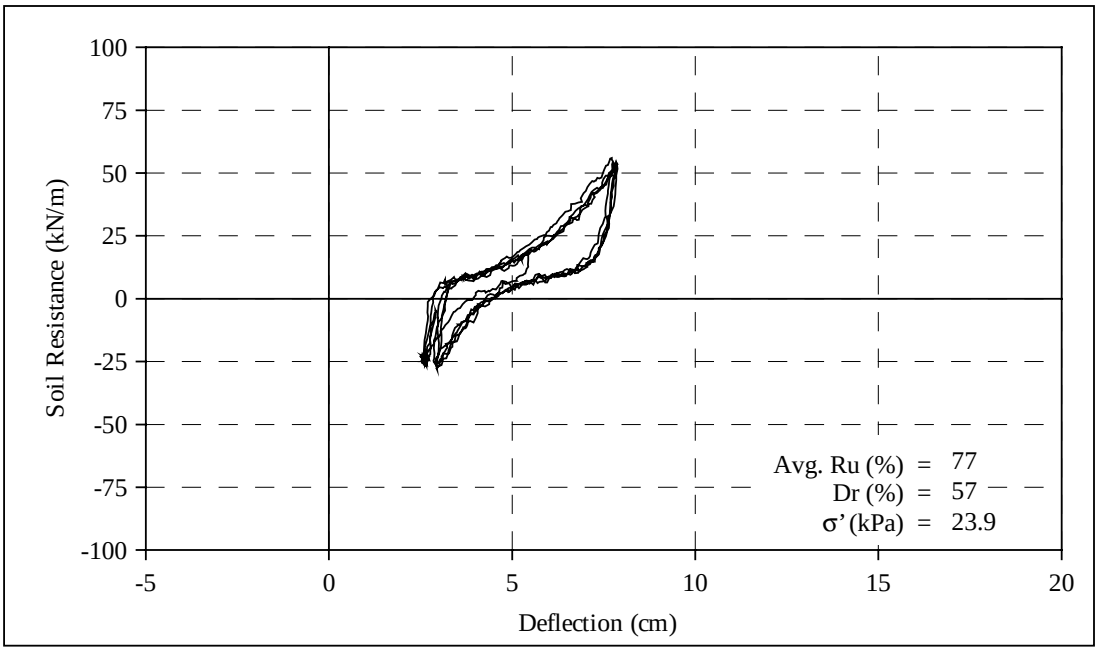

Figure 8.47 Calculated deflection versus soil resistance for the east center pile in 3x3 group, at a depth of 2.29 meters during the tenth 23-cm load cycle (from 58.4 to 62.2 min)

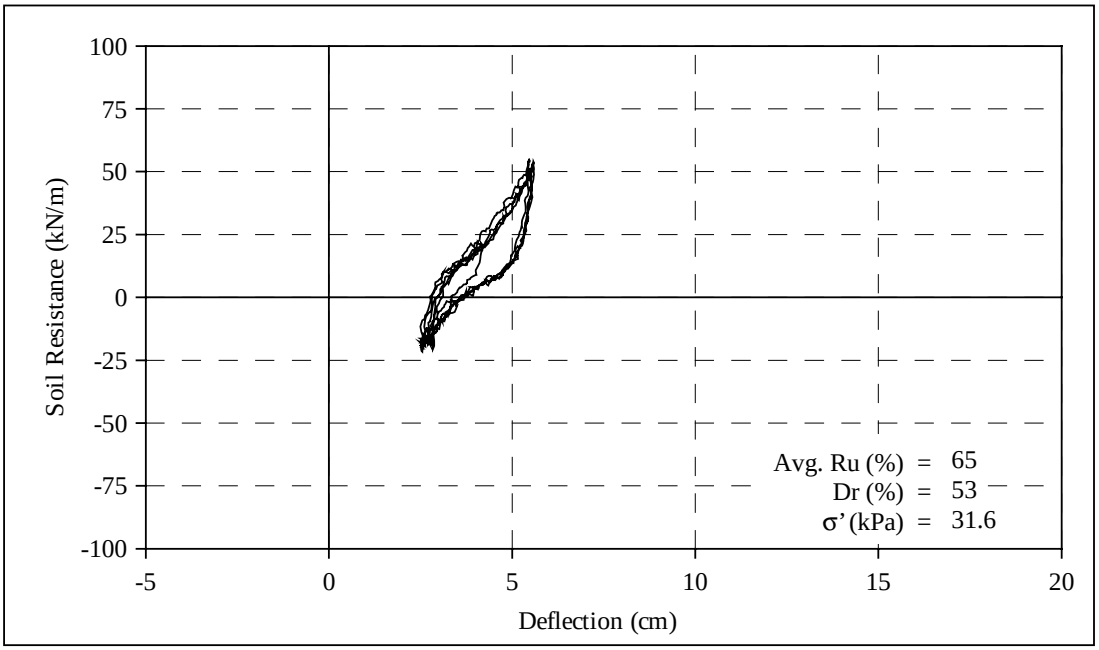

Figure 8.48 Calculated deflection versus soil resistance for the east center pile in 3x3 group, at a depth of 3.05 meters during the tenth 23-cm load cycle (from 58.4 to 62.2 min)

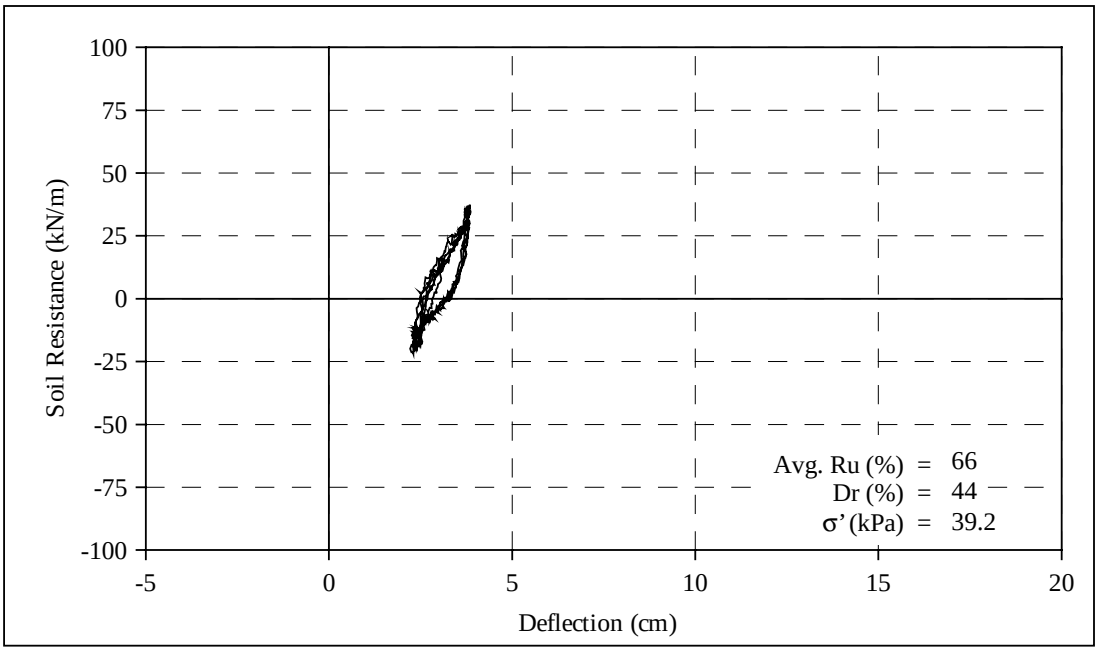

Figure 8.49 Calculated deflection versus soil resistance for the east center pile in 3x3 group, at a depth of 3.81 meters during the tenth 23-cm load cycle (from 58.4 to 62.2 min)

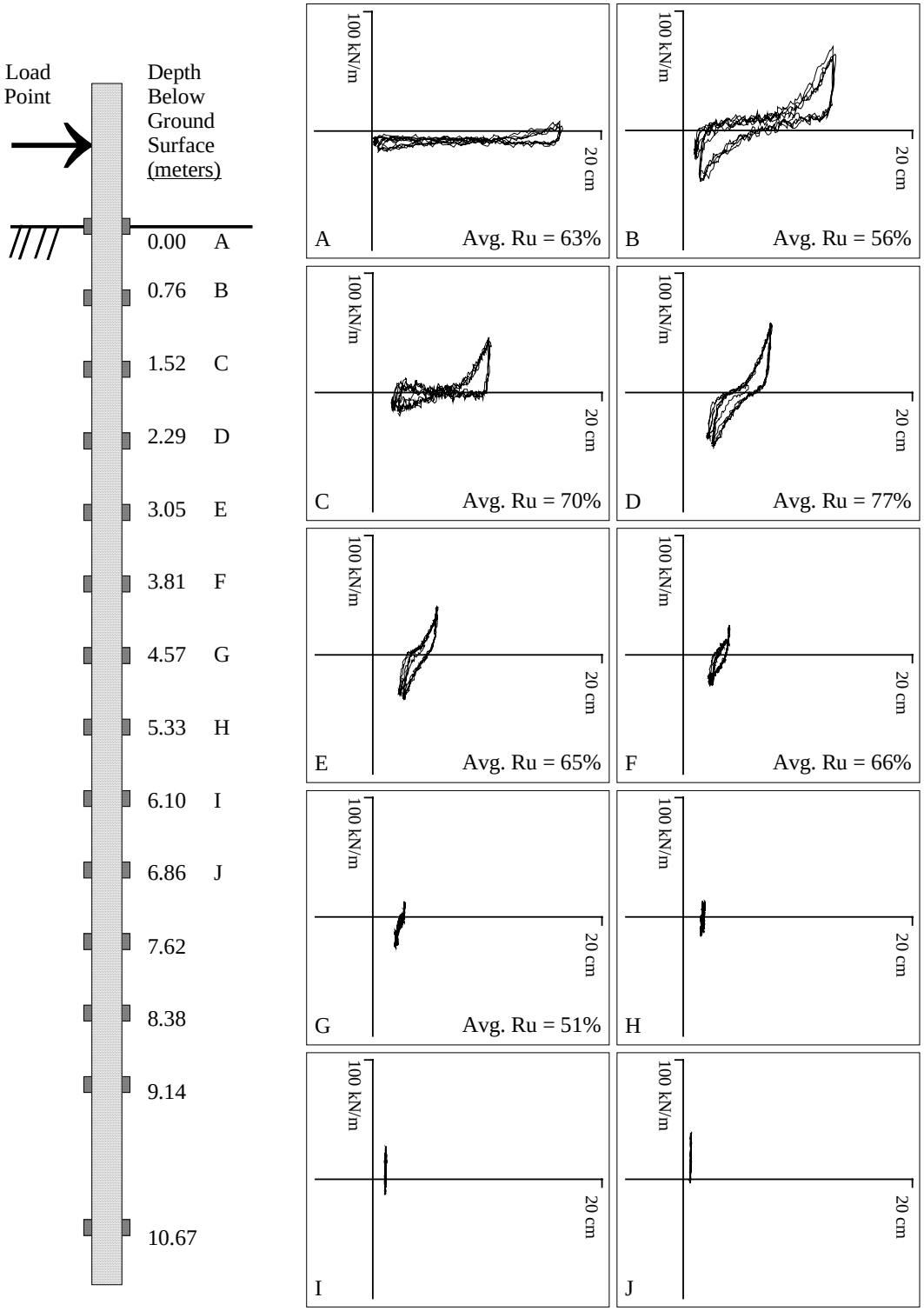

Figure 8.50 Diagrammatic summary of calculated p-y curves for the northeast pile in 3x3 group, during the tenth 23-cm load cycle (from 58.4 to 62.2 min)

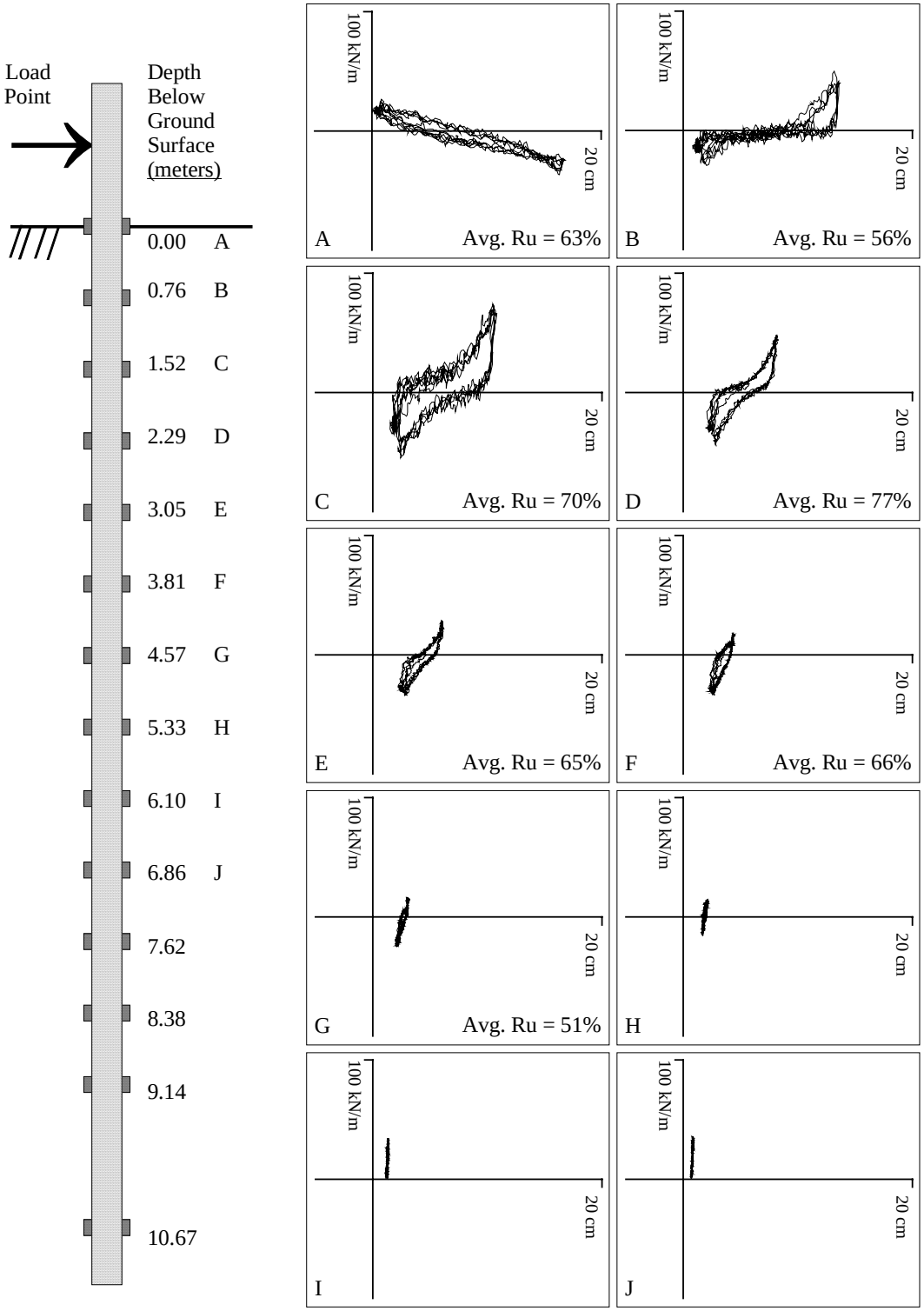

Figure 8.51 Diagrammatic summary of calculated p-y curves for the north center pile in 3x3 group, during the tenth 23-cm load cycle (from 58.4 to 62.2 min)

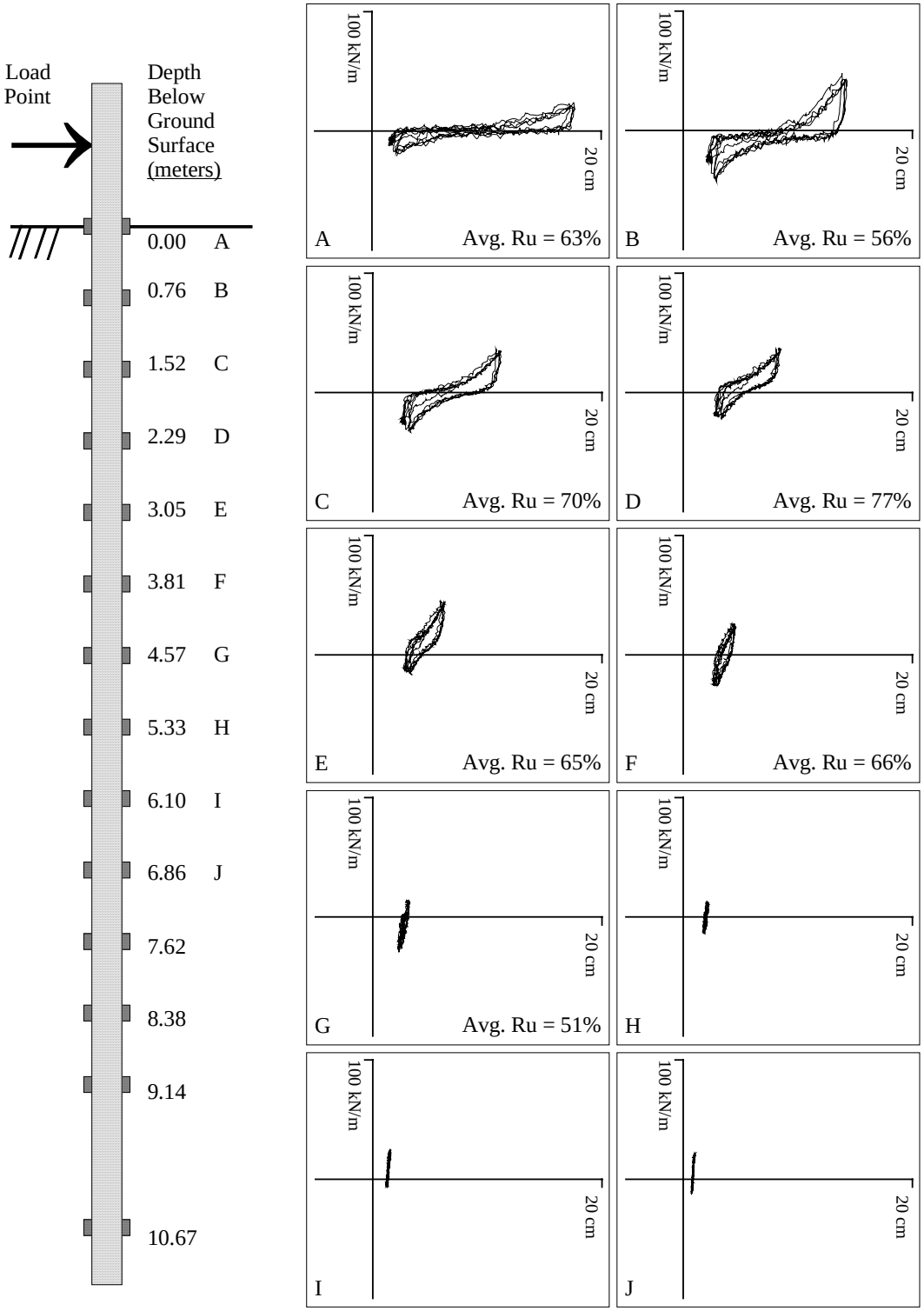

Figure 8.52 Diagrammatic summary of calculated p-y curves for the center pile in 3x3 group, during the tenth 23-cm load cycle (from 58.4 to 62.2 min)

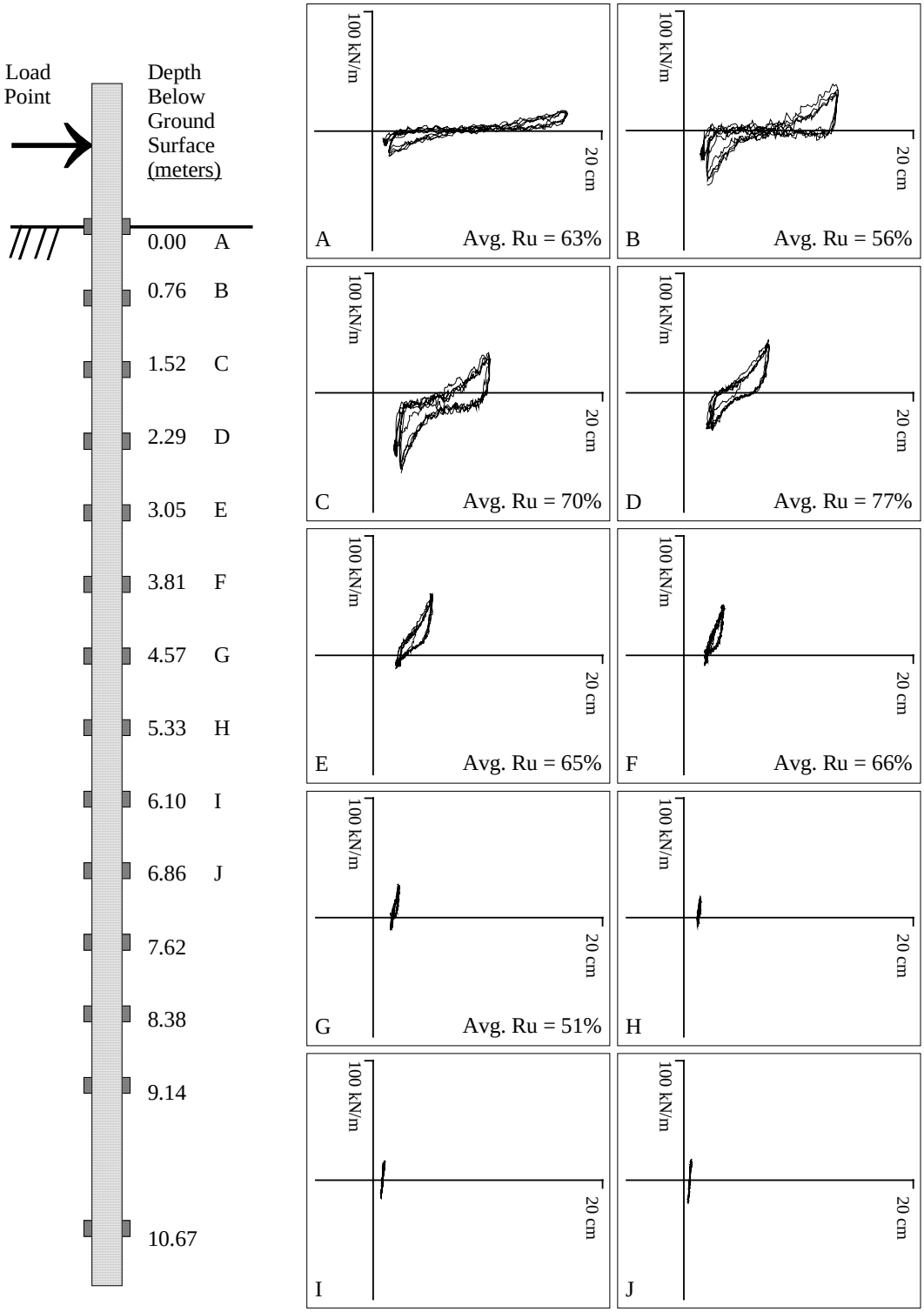

Figure 8.53 Diagrammatic summary of calculated p-y curves for the south center pile in 3x3 group, during the tenth 23-cm load cycle (from 58.4 to 62.2 min)

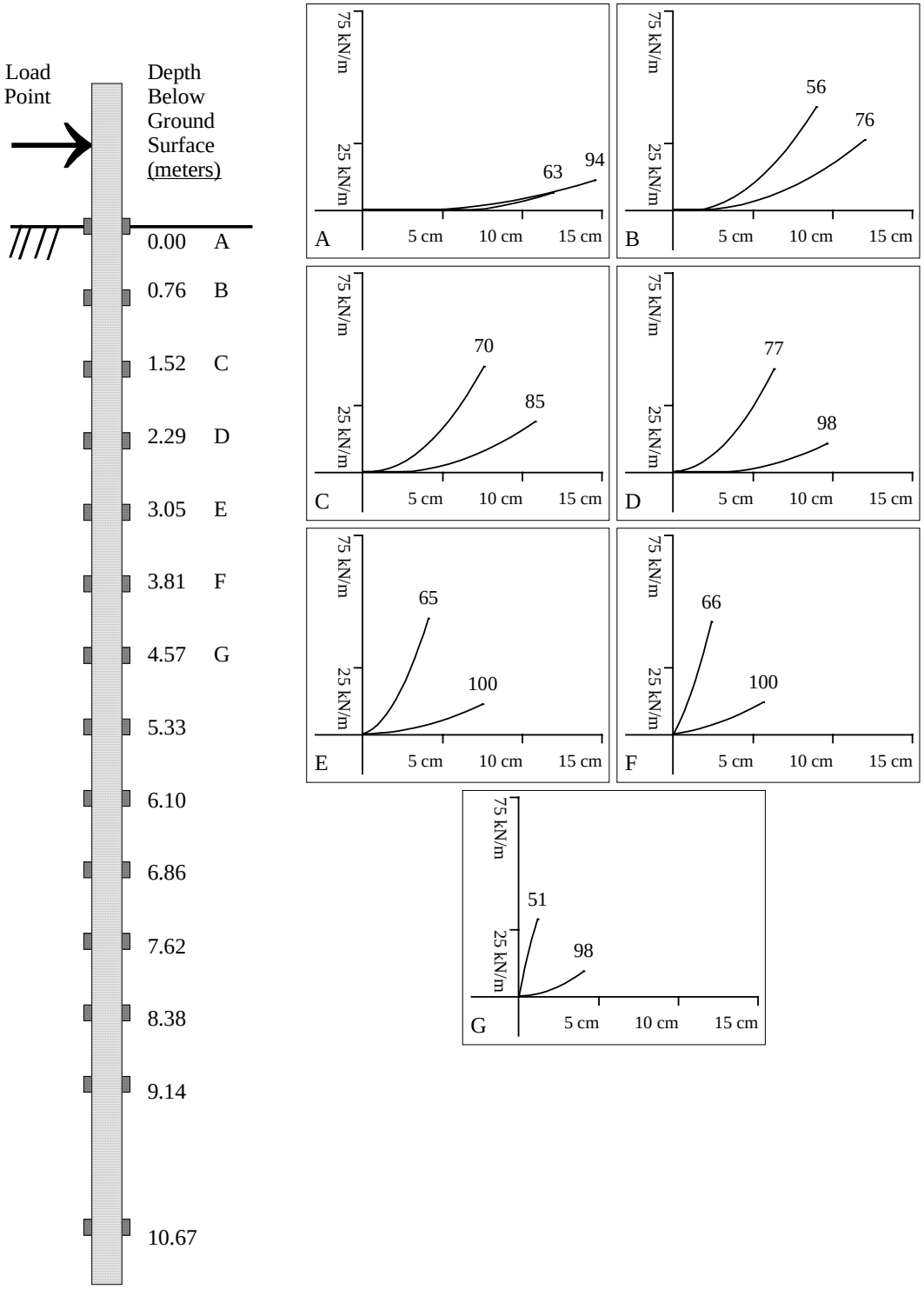

Figure 8.54 Representative p-y curves at various depths for different values of Ru (shown above the respective curves, in percent) for the 3x3 group

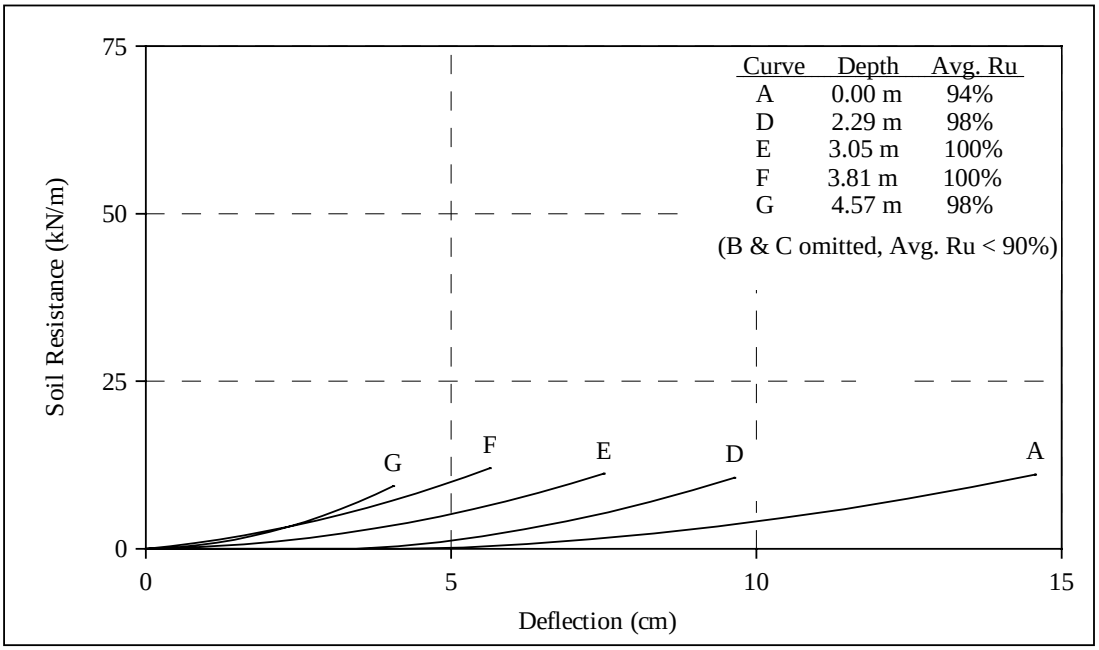

Figure 8.55 Comparison of representative p-y curves at various depths for the 3x3 group during the first 23-cm load cycle (from 2.6 to 12.2 min)

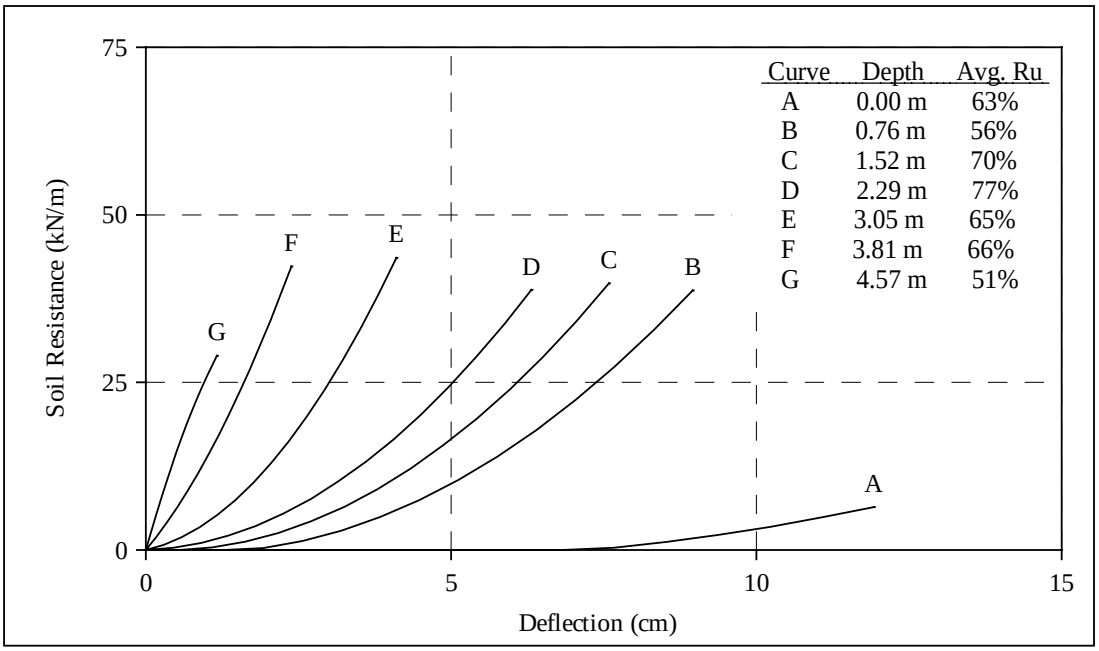

Figure 8.56 Comparison of representative p-y curves at various depths for the 3x3 group during the tenth 23-cm load cycle (from 58.4 to 62.2 min)

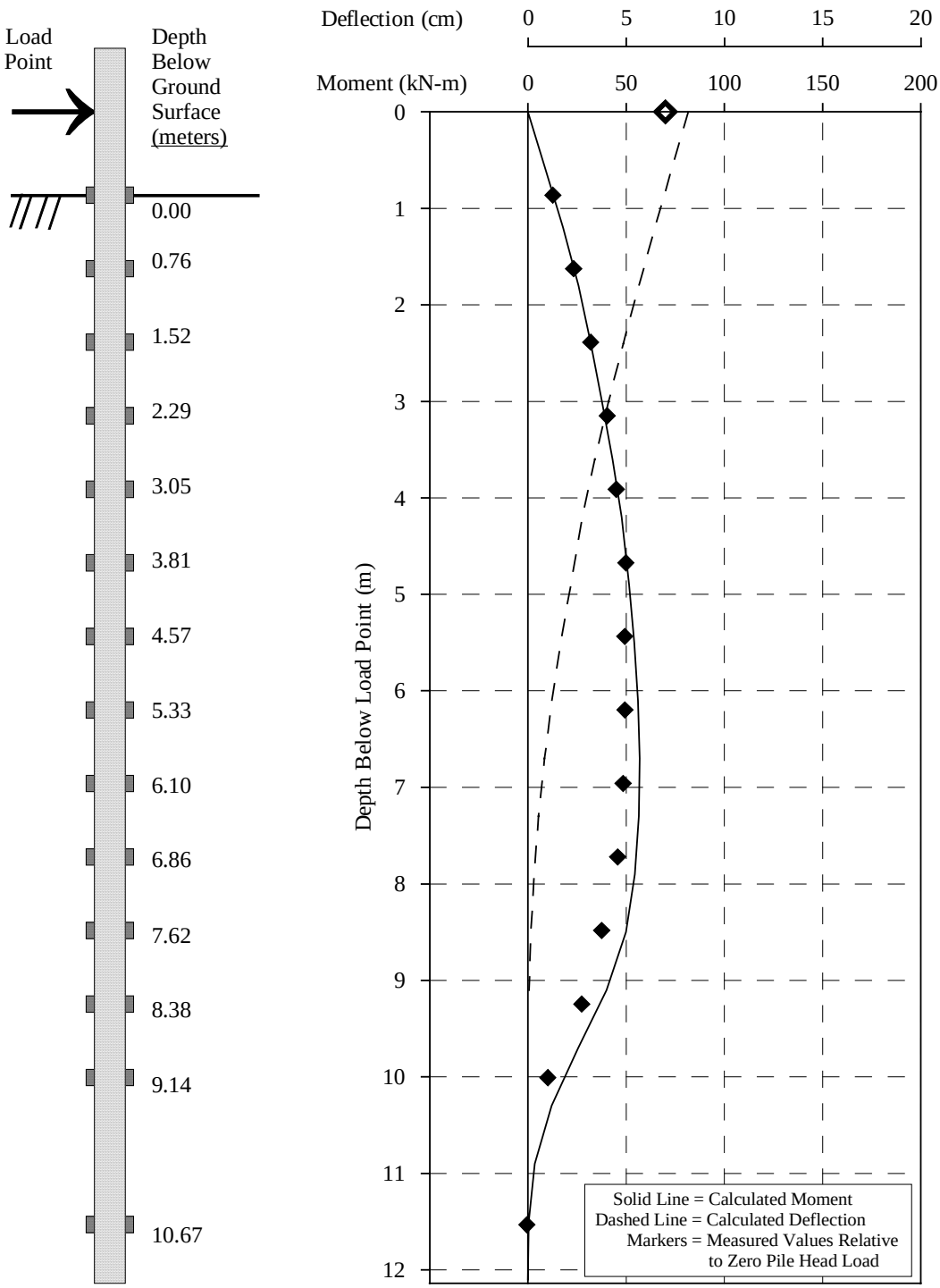

Figure 8.57 Comparison of measured and computed bending moments and pile head deflection using developed p-y curves (east center pile in 3x3 group, measured pile head load = 15.0 kN)

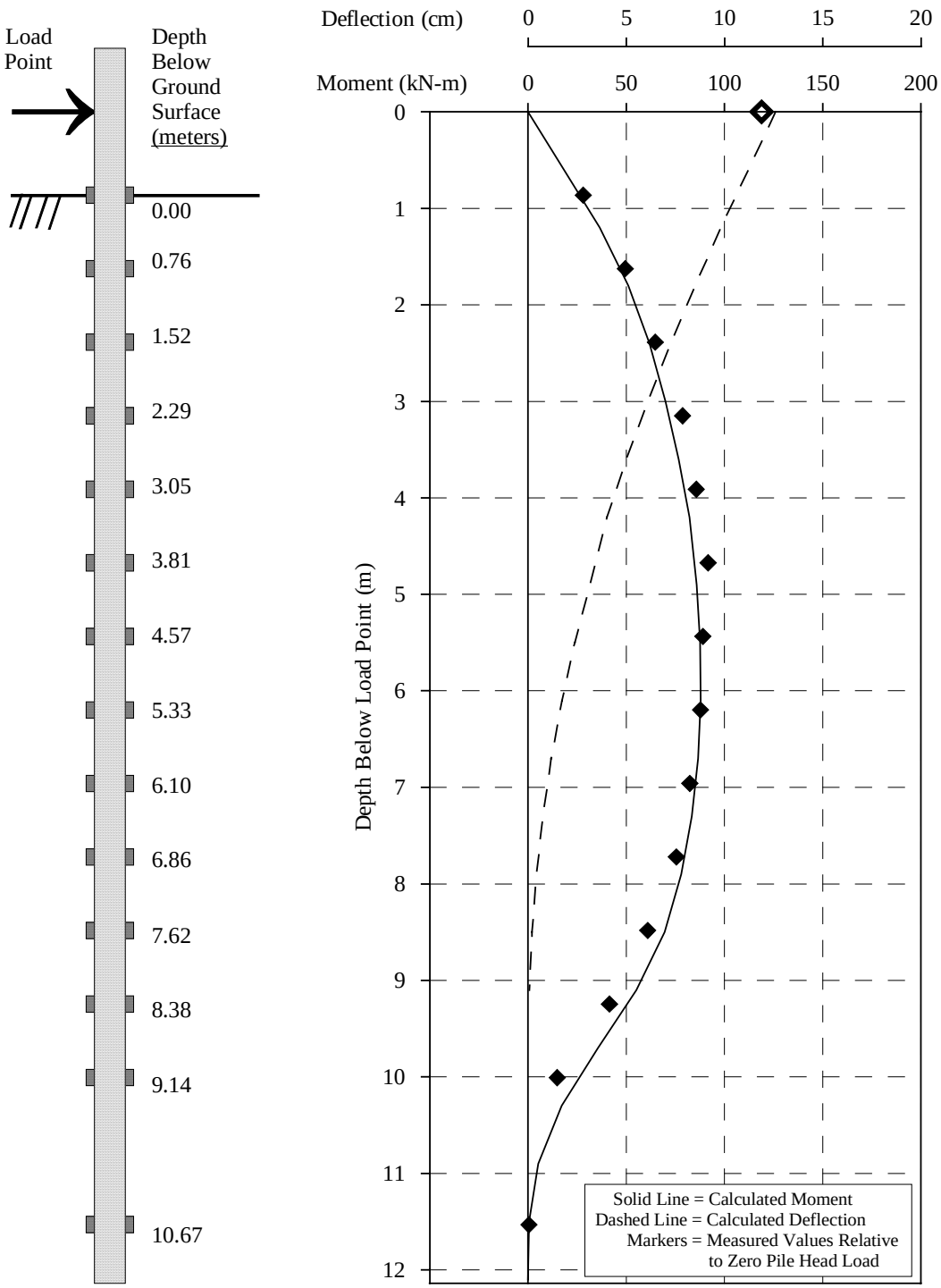

Figure 8.58 Comparison of measured and computed bending moments and pile head deflection using developed p-y curves (east center pile in 3x3 group, measured pile head load = 30.5 kN)

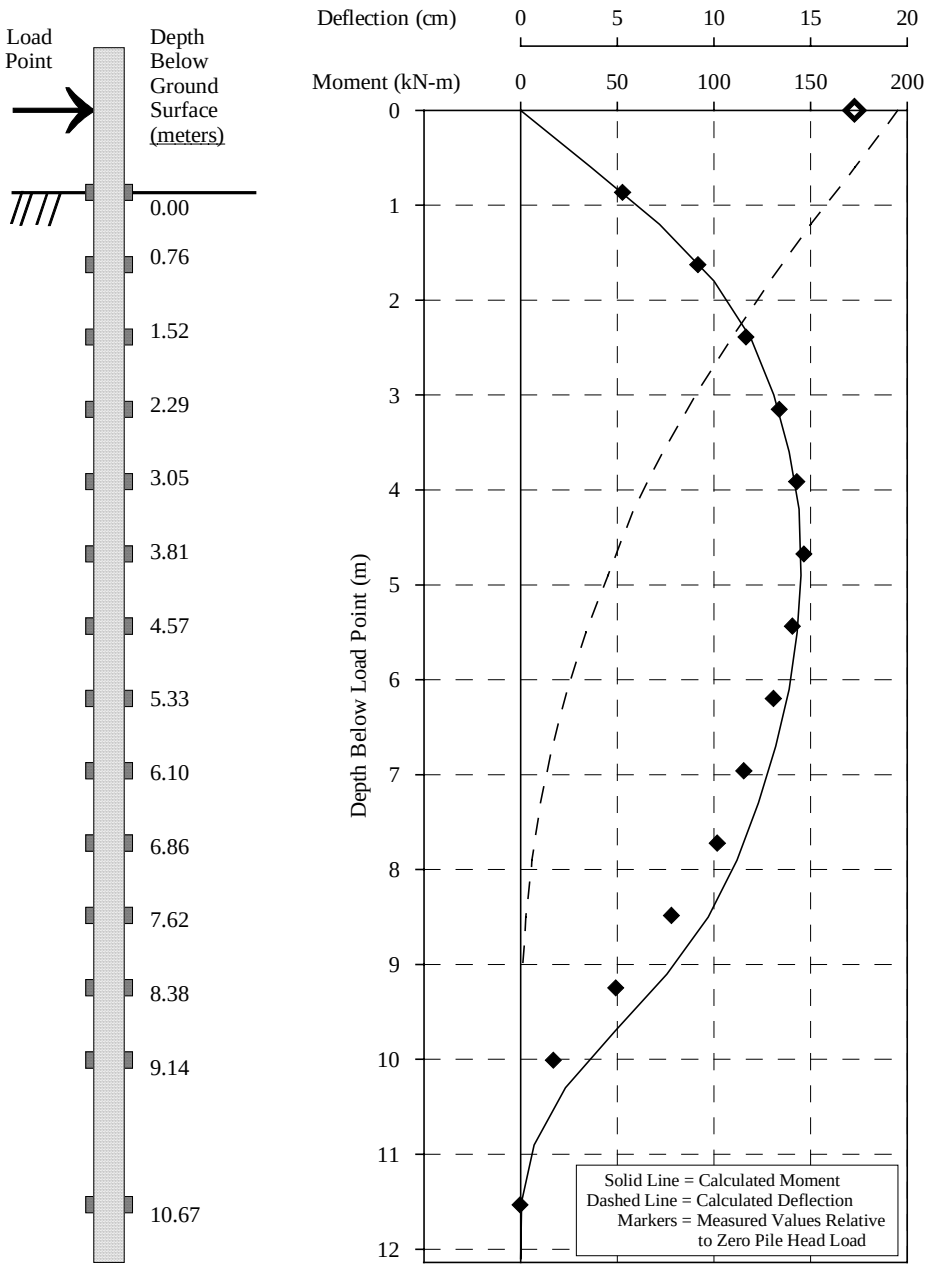

Figure 8.59 Comparison of measured and computed bending moments and pile head deflection using developed p-y curves (east center pile in 3x3 group, measured pile head load = 60.0 kN)

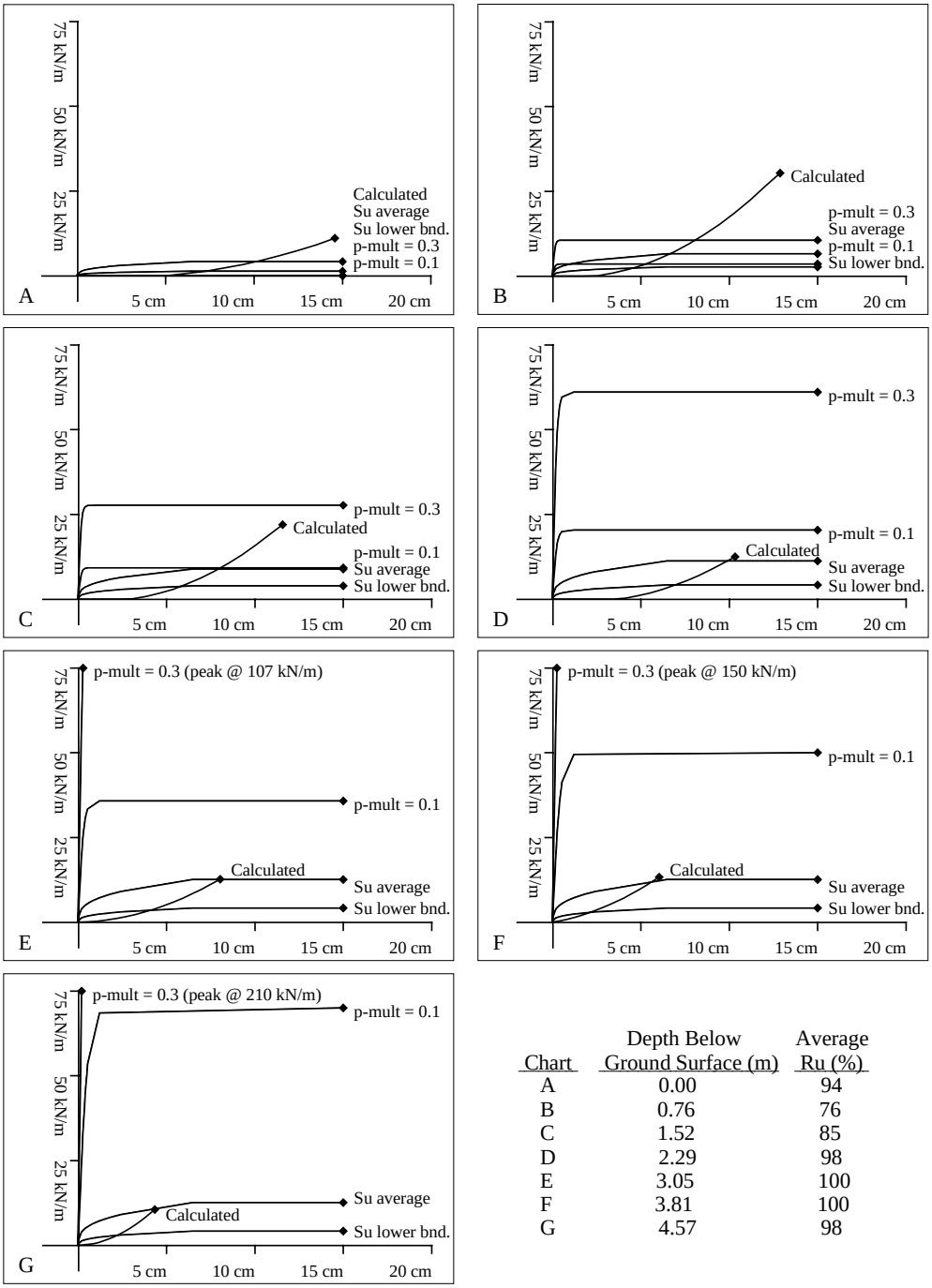

Chart	Depth Below Ground Surface (m)	Average Ru (%)
A	0.00	94
B	0.76	76
C	1.52	85
D	2.29	98
E	3.05	100
F	3.81	100
G	4.57	98

Figure 8.60 Comparison of calculated p-y curves with p-y curve approximations using p-multipliers and residual undrained shear strengths

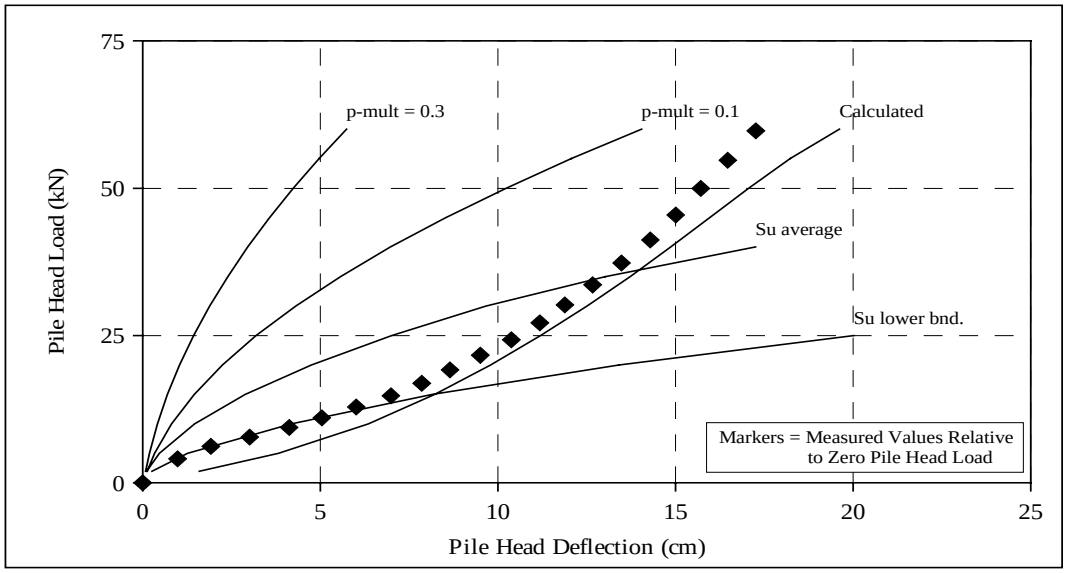

Figure 8.61 Comparison of measured deflection and load with deflection and load using calculated p-y curves and various p-y curve approximations

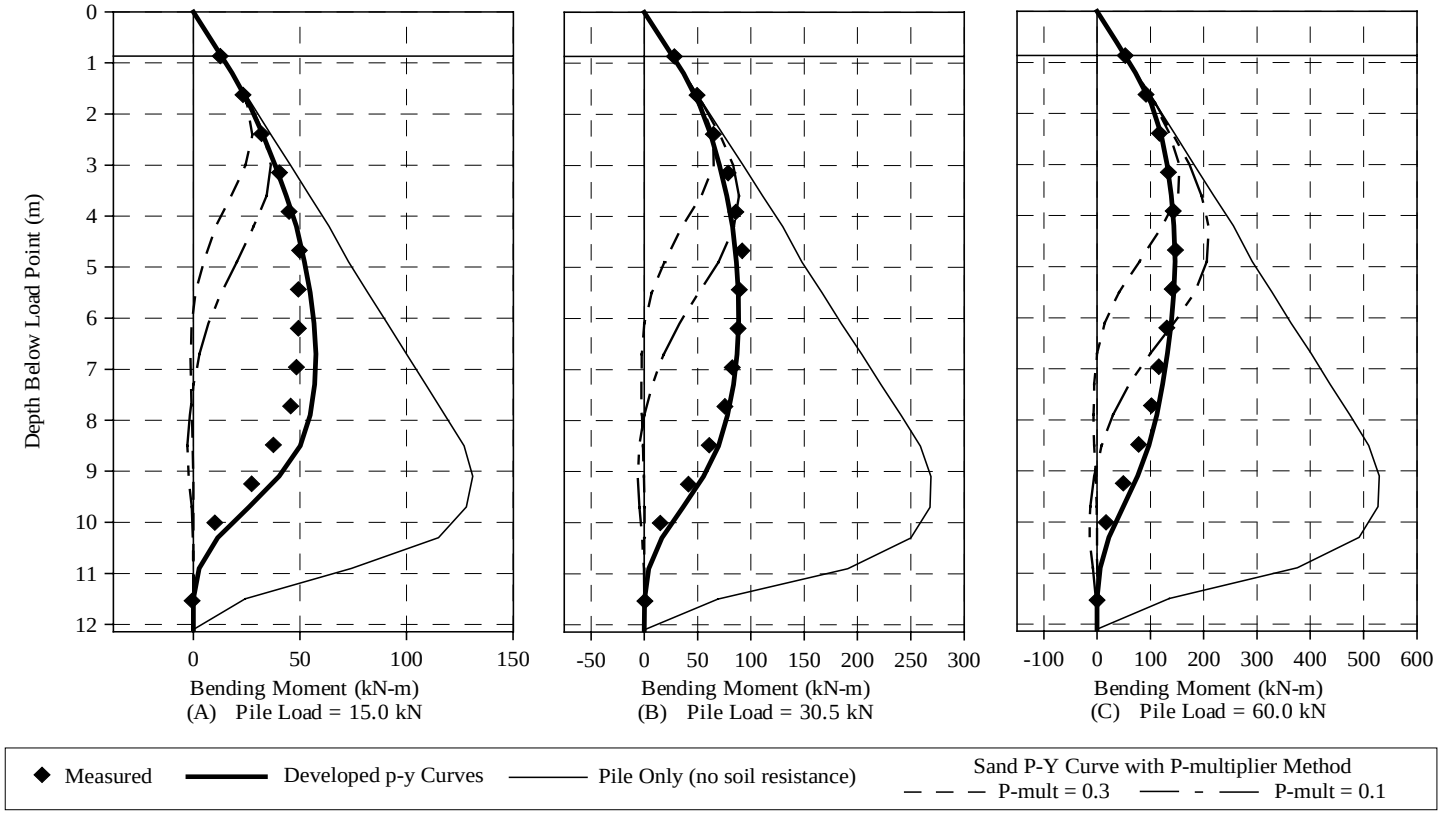

Figure 8.62 Comparison of bending moment versus depth using calculated p-y curves and p-y curve approximation using p-multipliers

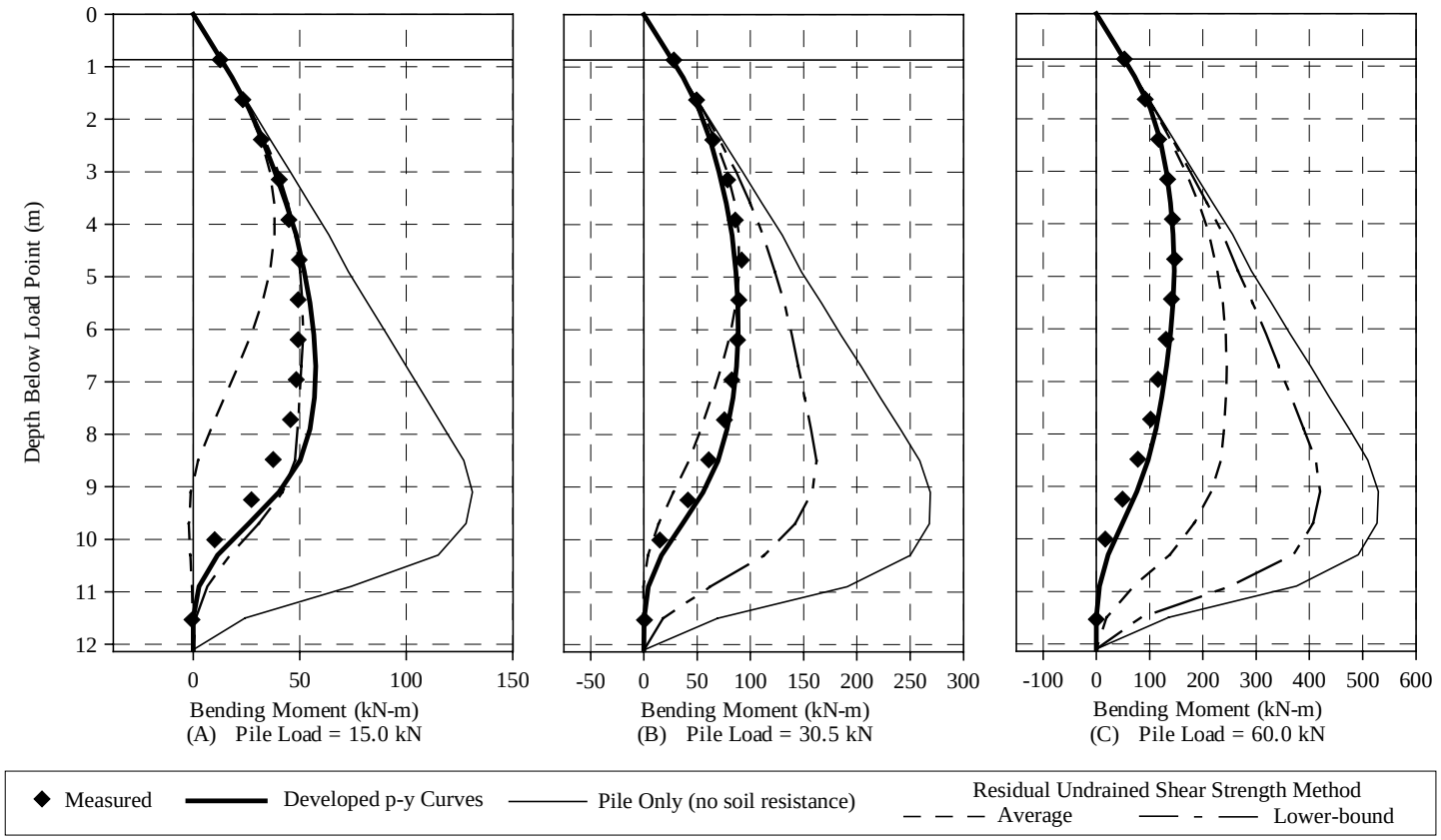

Figure 8.63 Comparison of bending moment versus depth using calculated p-y curves and p-y curve approximation using residual undrained shear strengths

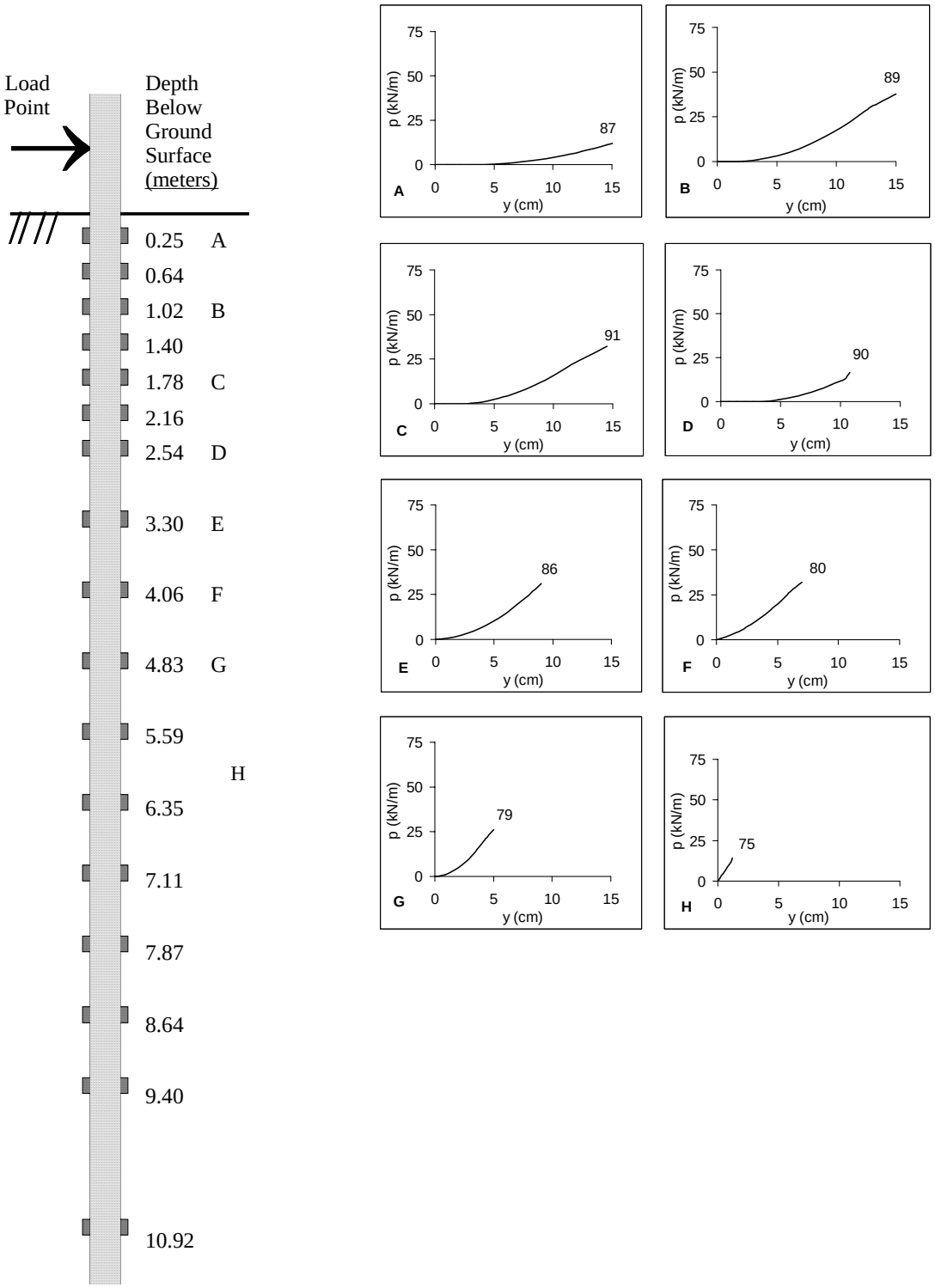

Figure 8.64 Representative p-y curves at various depths for different values of Ru (shown above the respective curves, in percent) for the single pile

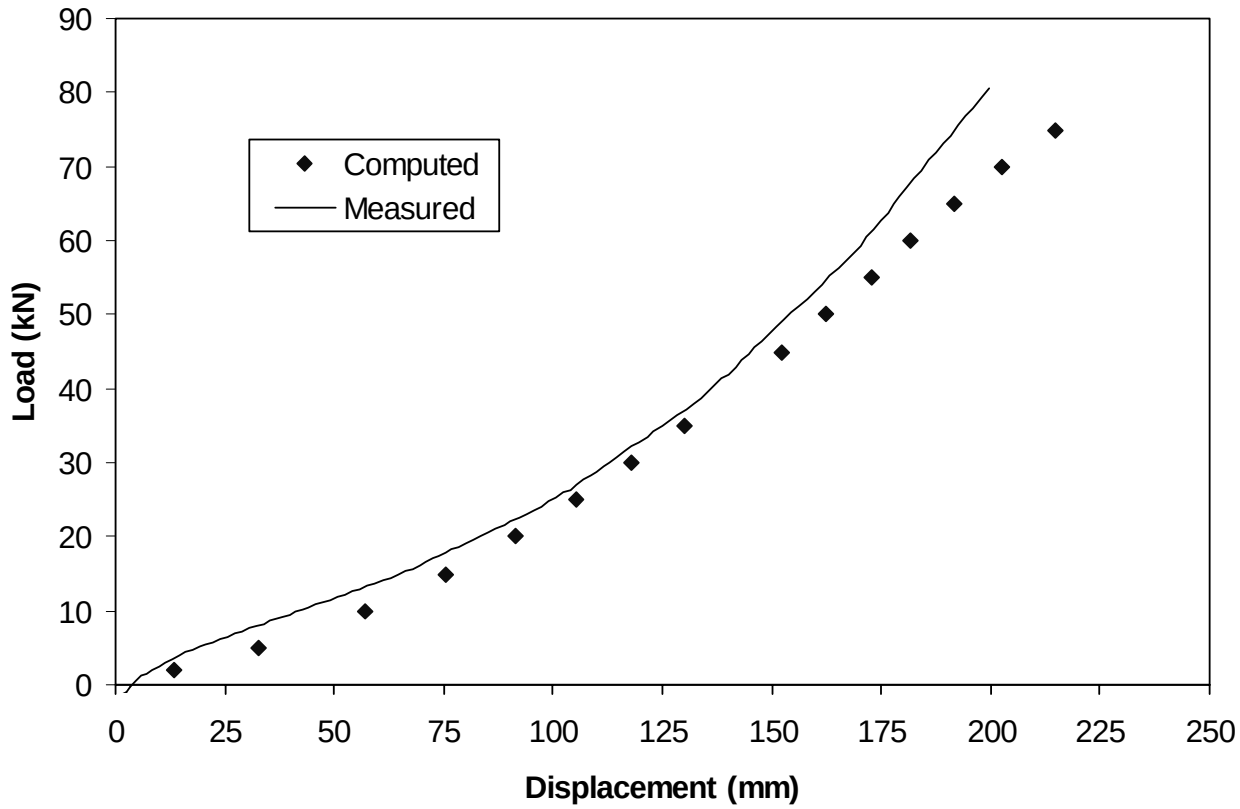

Figure 8.65 Comparison of measured load-displacement curve computed by LPILE using p-y curves for liquefied sand developed during this study.

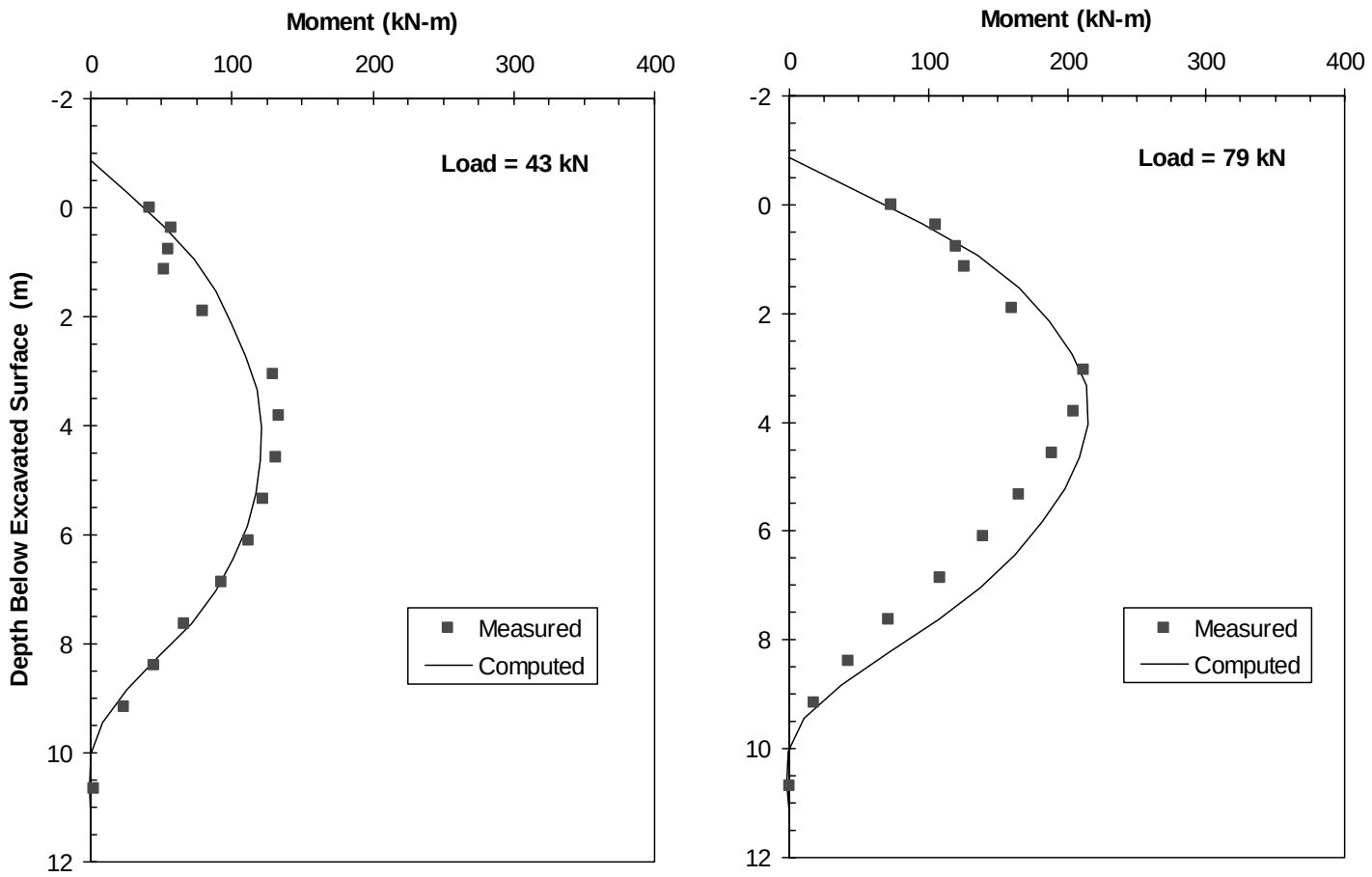

Figure 8.66 Comparison of measured bending moment versus depth curves along with curves computed using LPILE and p-y curves for liquefied sand developed during this study at two load levels.

9 CONCLUSIONS AND RECOMMENDATIONS

This chapter contains the conclusions and recommendations relative to pile behavior in liquefied sand. Other conclusions, such as for behavior in non-liquefied sand or the performance of E-Quake drains, can be found in the body of the report.

1. General agreement was observed between the *p-y* curves back-calculated from the full-scale testing at Treasure Island and those back-calculated from Caltrans sponsored centrifuge testing at UC Davis, with the exception that significantly more displacement was required in the full-scale testing for the soil to provide appreciable resistance.

2. The shape of the back-calculated *p-y* curves is significantly different than those currently recommended for design, using either the p-multiplier approach or the soft clay approach with residual strengths. Specifically, the *p-y* curves for liquefied sand obtained from this study show a concave up shape, rather than a concave down shape typical of clay and non-liquefied sand.

3. The *p-y* curves increase in stiffness as the depth increases, or alternatively, as the initial effective stress increases.

4. The *p-y* curves increase in stiffness as pile diameter increases, though not in a directly proportional manner. In addition, the zone of liquefied soil providing resistance increases with pile diameter.

5. The *p-y* curves increase in stiffness as the average excess pore-pressure ratio (r_u) decreases. Curves are provided in the report for r_u ranging from 35 to 100 percent.

6. Based on full-scale and centrifuge testing, sand with an initial relative density of 50 percent or greater may show significant dilative behavior while liquefied under lateral loading.

7. Group effects appear to be relatively inconsequential for pile groups in liquefied sand. For both the 4-pile group and the 9-pile group, the load-displacement curves for the individual piles within a group were essentially the same. In addition, the load-displacement curve for the single pile was very similar to that for the piles in the 9-pile group.

8. For design purposes, p-multipliers for group effects can be taken as 1.0 for liquefied sand. However, as the average r_u decreases and the frictional resistance increases, group effects will also become important and will need to be accounted for with appropriate p-multipliers.

9. Alternative methods for developing *p-y* curves in liquefied sand (i.e. p-multipliers or soft clay curves using residual strengths) may result in computed displacements and bending moments that adequately capture the measured response over a limited range of depth and load. If these alternative *p-y* curves are used, the effect of their shape on the computed foundation and superstructure response should be considered for the anticipated loading.

10. Pushover analyses should only be used if kinematic loads are not expected to contribute significantly to the foundation and superstructure response.

11. When performing a pushover analysis, pile response should be assessed under lateral loads applied before and after the onset of liquefaction.

12. If a dynamic/time history analysis which implements *p-y* curves to model the soil is required, the effect of dilational soil response should be incorporated into the *p-y* curves. Current procedures only account for pore pressure changes due to free-field soil strains and neglect the effect of pore pressure changes resulting from interaction with the foundation.

10 REFERENCES

Ashour, M., Pilling, P., Norris, G., and Perez, H. (1996). “Development of Strain Wedge Model Program for Pile Group Interference and Pile Cap Contribution Effects.” Report No. CCEER-94-4, Civil Engineering Dept.,University of Nevada, Reno, June 1996, Federal Study No. F94TL16C, Submitted to State of California Department of transportation (CalTrans).

Bennett, M. (1994) “Subsurface Investigation for Liquefaction Analysis and Piezometer Calibration at Treasure Island Naval Station, California,” Open File Report 94-709, U.S. Geological Survey, 41 p.

Bolton, M.D. (1986). “The strength and dilatancy of sands”, *Geotechniq*ue, Vol. 36, No. 1, Mar, p. 65-78.

Brown, D.A., Morrison, C., and Reese, L.C., (1988). "Lateral load behavior of a pile group in sand, *J. Geotech. Engrg.*, ASCE, 114(11), 1261-1276.

Brown, D.A., Reese, L.C., and O'Neill, M.W., (1987). "Behavior of a large scale pile group subjected to cyclic lateral loading", *J. Geotech.l Engrg.*, ASCE, 113(11), 1326-1343.

Carroll, R.G. Jr. (1983). “Geotextile Filter Criteria”, Transportation Research Record 916, Transportation Research Board, Washington, D.C. p. 46-53.

Das, B.M. (1994). Principles of Geotechnical Engineering, PWS Publishing Co., Boston, Massachussetts.

De Alba, P., Benoit, J., Pass, D.G. and Carter, J.J. (1994). “Deep instrumentation array at the Treasure Island Naval Station”, The Loma Prieta, California Earthquake of Oct. 17, 1989-Strong Ground motion, U.S. Geological Survey Professional Paper 1551-A, A155-168, US Gov. Printing Office, Washington, D.C.

Dobry, R. and Abdoun, T. (1998). “Post-Triggering Response of Liquefied Sand in the Free Field and Near Foundations,” Geotechnical Special Publication 75, Vol 1, p. 270-300.

Dobry, R., Abdoun, T., and O’Rourke, T.D. (1996). “Evaluation of Pile Response Due to Liquefaction Induced Lateral Spreading of the Ground,” Proceedings of the Fourth Caltrans Seismic Design Workshop, 10 p.

Faris, R. (1997). Personnel communication.

Giroud, J.P., (1982). “Filter criteria for geotextiles”, Procs. 2nd Intl. Conf. on Geotextiles, Las Vegas, Nevada, Vol. 1, p. 103-109.

Kulhawy, F.H. and Mayne, P.W. (1990). Manual on estimating soil properties for foundation design, Research Project 1493-6, EL-6800, Electric Power Research Institute, Palo Alto, CA.

Kutter, B.L. and Wilson, D.W. (1999). “De-Liquefaction Shock Waves,” Proceedings of the 7th U.S.-Japan Workshop on Earthquake Resistant Design of Lifeline Facilities and Countermeasures Against Soil Liquefaction, Seattle, August, pp. 295-310.

Liu, Lee and Dobry R. (2000). “Effect of liquefaction on lateral response of piles by centrifuge model tests”, Research Report on MCEER-FHWA Project DTFH-621-92-C-00106.

Matlock, H. and Ripperger, E.A. (1958). “Measurement of soil pressure on a laterally loaded pile”, Procs. American Society for Testing Materials, Vol. 58, p. 1245-1260.

McVay, M., Casper, R. and Shang, Te-I (1995). “Lateral response of three-row groups in loose to dense sands at 3D and 5D pile spacing”, *J. Geotech. Engrg.*, 112(5), 436-441.

Narin van Court, W.A. and Mitchell, J.K. (1995). “New Insights into Explosive Compaction of Loose, Saturated, Cohesionless Soils,” Soil Improvement for Earthquake Hazard Mitigation, Geotechnical Special Pub. No. 49, p. 51-65.

Onoue, A. (1988). “Diagrams considering well resistance for design spacing ratio of gravel drains,” Soils and Foundations, Japanese Society of Soil Mechanics and Foundation Engineering, Vol 28, No. 3, 160-168.

Orense, R., Ishihara, K, Yasuda, S., Morimoto, I., and Takagi, M. (2000). “Soil Spring Constants During Lateral Flow of Liquefied Ground,” 12th World Conference on Earthquake Engineering, Auckland, New Zealand, paper 2099.

Pestana, J.M., Hunt, C.E. and Goughnour, R.R., (1997). “FEQDrain: A finite element computer program for the analysis of the earthquake generation and dissipation of pore water pressure in layered sand deposits with vertical drains”, Report No. EERC97-17, Earthquake Engineering Research Center, Univ. of California, Berkeley.

Reese, L.C. and Wang, S.T. (1996) Documentation of computer program LPILE plus version 3.0 for windows, Ensoft, Inc., Austin, Texas, 365 p.

Reese, L.C., Wang, S.T., Arrellaga, J.A. and Hendrix, J. (1996) “Computer

program GROUP for Windows, User's Manual, version 4.0", Ensoft, Inc., Austin, Texas, 370 p.

Rollins, K.M., Peterson, K.T., Weaver, T.J. (1998). "Lateral load behavior of a full-scale pile group in clay", *J. Geotech. & Geoenv. Engrg.*, 124(6), 468-478.

Ruesta, P.F. and Townsend, F.C. (1997). "Evaluation of laterally loaded pile group at Roosevelt Bridge, *J. Geotech. and Geoenv. Engrg.*, ASCE, 123(12), 1153-1161.

Seed, H.B. and Booker, J.R. (1977). "Stabilization of potentially liquefiable sand deposits using gravel drains", *J. of Geotech. Engrg,*, ASCE, 103(7), 757-768.

Seed, H.B., Martin, P.P., and Lysmer, J. (1975). "The generation and dissipation of pore water pressures during soil liquefaction", Report No. EERC 75-26, Earthquake Engineering Research Center, Univ. of California, Berkeley.

Seed, R.B. and Harder, L.F. (1990). "SPT-based analysis of cyclic pore pressure generation and undrained residual strength." Seed Memorial Proceedings, J.M. Duncan, Ed., Vol. 2,p. 351-376.

Studer, J. and Kok, L. (1980). “Blast Induced Excess Porewater Pressure and Liquefaction Experience and Application,” Proceedings of the Intl. Symp. On Soils under Cyclic and Transient Loading, Swansea, Wales, p. 581-593.

Wang, S-T and Reese, L. (1998). “Design of pile foundations in liquefied sand”, Geotech. Special Publication No. 75, Geotechnical earthquake engineering and soil dynamics III, Vol. 2, p. 1331-1343.

Weaver, T.J. (2001). “Behavior of liquefying sand and CISS piles during full-scale lateral load tests,” Ph.D. Dissertation, University of California, San Diego.

Wilson, D.W., Boulanger, R.W., Kutter, B.L., and Abghari, A. (1996). “Soil-Pile-Superstructure Interaction Experiments with Liquefiable Sand in the Centrifuge,” Proceedings of the Fourth Caltrans Seismic Design Workshop, 12 p.

Youd, T.L. and Idriss, I.M. (2001). “Liquefaction resistance of soils: Summary report from the 1996 NCEER and 1998 NCEER/NSF Workshops on evaluation of liquefaction resistance of soils”, J. of Geoech. and Geoenv. Engrg., ASCE, 127(4), 297-313.

APPENDIX A

Liquefaction Mitigation Using Stone Columns Around Deep Foundations: Full Scale Test Results

A.1 ABSTRACT

The results presented in this paper were developed as part of a larger project analyzing the behavior of full-scale laterally loaded piles in liquefied soil, the first full-scale testing of its kind. This paper presents the results of a series of full-scale tests performed on deep foundations in liquefiable sand, both before and after ground improvement, where controlled blasting was used to liquefy the soil surrounding the foundations. Data was collected showing the behavior of laterally loaded piles before and after liquefaction. After the installation of stone columns, the tests were repeated. Based on the results of these tests, it can be concluded that the installation of stone columns can significantly increase the density of the improved ground as indicated by the cone penetration test. Furthermore, it was found that the stone column installation limited the excess pore pressure increase from the controlled blasting and substantially increased the rate of excess pore pressure dissipation. Finally, the stone columns were found to significantly increase the stiffness of the foundation system, by more than 2.5 to 3.5 times that in the liquefied soil. This study provides some of the first full-scale quantitative results on the improvement of foundation performance due to stone columns in a liquefiable deposit.

A.2 INTRODUCTION

Installation of stone columns, also referred to as vibro-replacement and vibro-displacement, is a ground improvement technique often used to mitigate liquefaction hazards in saturated loose granular soils. Stone columns can improve the performance of these deposits in four main ways. First, the installation of the stone columns densifies the deposit by vibration and replacement. Second, this technique increases the lateral stresses in the surrounding soil. Third, stone columns provide reinforcement, as the stone columns are stiffer, stronger and denser than the surrounding soils. Finally, stone columns provide drainage, reducing the potential for build-up of excess porewater pressures. Though the effect of each of these factors will vary between deposits, combined they make stone columns an efficient and popular liquefaction hazard mitigation technique (*1*).

There is considerable qualitative data available showing that stone column installation is an effective means of ground improvement for mitigating liquefaction hazards. A 1995 report by Mitchell *et al.* (*2*) gives case histories for the performance of improved ground during earthquakes for more than 30 sites. Five of these sites, from the 1989 Loma Prieta Earthquake and the 1994 Northridge Earthquake, were treated with stone columns. In each case, good performance was observed following the earthquake. Priebe, in a 1990 report (*3*), describes additional case histories for improved sites that performed well in earthquakes. Other reports have discussed the design of stone column ground improvement and the extent of improvement that can be expected from the use of stone columns (e.g. *4*, *5*, and *6*).

While qualitative information from past earthquakes is valuable in confirming that stone columns can be an effective means of ground improvement, quantitative data is

needed for design purposes. This paper is a result of a series of full-scale tests performed on deep foundations in liquefiable sand, before and after ground improvement, and were part of a larger project analyzing the full-scale behavior of laterally loaded piles in liquefied soil, the first full-scale testing of its kind. Controlled blasting was used to liquefy the soil surrounding the piles, and data was collected showing the behavior of laterally loaded piles before and after liquefaction. After the installation of stone columns, the tests were repeated. This paper provides quantitative results on the behavior of laterally loaded piles during liquefaction, and the amount of improvement that results from the installation of stone columns.

A.3 PROJECT DESCRIPTION

The stone column tests presented in this paper were part of a larger series of tests on the full-scale behavior of laterally loaded piles in liquefied sand. This project, known as the Treasure Island Liquefaction Test (TILT), was a joint venture between the University of California, San Diego and Brigham Young University. As part of the TILT project, a 4-pile group of 324-mm diameter pipe piles was loaded laterally against a 0.6-m Cast-In-Steel-Shell (CISS) pile in a 15- by 21-m excavation, approximately 1.5-m deep. A high-speed hydraulic actuator was used to apply the lateral loads. The first lateral load test was conducted before the installation of stone columns and before blasting. Liquefaction was then induced using controlled blasting, and the piles were tested again. Stone columns were then installed, and the tests were repeated for both pre-blast and post-blast behavior. Load-displacement and pore pressure information was gathered for all tests.

The testing took place on Treasure Island, a man-made island built on a shoal of Yerba Buena Island in the San Francisco Bay. Treasure Island has been a naval base for a number of years, but is currently being transferred from the U.S. Navy to the City of San Francisco as part of a national base closure program. The site at Treasure Island was selected for a number of reasons. Approvals for the use of explosives were relatively easy to obtain for the portion of the island still operated by the U.S. Navy. In addition, the site is only 300 meters away from the Treasure Island Fire Station, the location of a National Geotechnical Experimentation Site (NGES). The NGES status of the site, as well as numerous other geotechnical investigations on the island, provides a wealth of geotechnical data to draw from for the TILT project. Furthermore, there is a known liquefaction hazard at the site due to the high groundwater level and loose nature of the hydraulic fill. In fact, liquefaction was observed across the island during the 1989 Loma Prieta earthquake (*7*).

The generalized soil profile at the project site is shown in Figure 1, along with values for the Standard Penetration Test (SPT) $N_1(60)$ values. The groundwater level was at a depth of approximately 1.5 meters. The soil profile generally consists of uniformly graded sand with silt to a depth of approximately 6 meters. Sieve analyses shows the fines content ranges between 5 and 15 percent. This would classify the soil as SP-SM based on ASTM D-2488. This surfical sand is the layer where all of the controlled blasting took place. It is underlain by soft fat clay (CH) to a depth of approximately 10 meters, loose silty sand (SM) to 13.5 meters in depth, and again soft fat clay to the bottom of the borehole at 19 meters. Though the top 1.5 meters of soil at the site was

excavated for the experiments, all depths given are from the original ground surface unless indicated otherwise.

A.4 METHODS AND TESTING PROCEDURE

The field portion of this project lasted between September 1998 and June 1999. All of the lateral load tests were carried out in February 1999. Below is a description of the test set-up, controlled blasting and testing procedures, as well as a description of the stone column installation.

A.4.1 Test Set-up

Figure 2 presents a plan view of the test set-up. The 4-pile group consisted of four 342-mm O.D. steel pipe piles with a 10-mm wall thickness, connected by a load frame that allowed for the free rotation of the pile heads while maintaining the same lateral displacement for all four piles in the group. The CISS pile was 0.6 m in diameter, with a nominal wall thickness of 13 mm. The hydraulic actuator used had a double swivel connection to both the CISS pile and pile group load frame thus allowing for free rotation at the CISS load stub. All of the piles were driven to depths between 12 and 14 meters below the excavated surface. For the CISS pile, the steel shell was driven into place, drilled out, and then filled with steel reinforcement and concrete. No water was observed in the steel shell prior to placement of the concrete.

The site was excavated to a depth of approximately 1.5 meters. The objective of this was to conduct the lateral load test primarily in the loose saturated sand by removing the medium dense sand and lowering the excavated surface closer to the ground water

table. Prior to excavation, SPTs and CPTs were performed. Following completion of the pre-treatment load tests, the site was backfilled to the original elevation, and the stone columns were installed. A second set of CPTs was then performed. The site was then re-excavated to the same level as before, and the post-treatment series of tests were performed.

A 1500-kN high-speed hydraulic actuator was used to laterally load the piles, with the loading point approximately 0.8 meters above the excavated surface. The speed of the actuator was approximately 10 mm/second. This actuator was connected between the load frame of the pile group and the load stub of the CISS pile, such that load-displacement information for the pile group and the CISS pile was obtained simultaneously. The applied load was measured in the actuator using an array of three 500-kN load cells. Relative displacement between the pile group and CISS pile was measured in the actuator as well, using a linear variable displacement transformer (LVDT). In addition, absolute displacement measurements of the piles were obtained using string activated linear potentiometers fixed to a reference post outside of the excavation. These were attached to the foundations in such a way as to allow for monitoring of displacement, tilt, and rotation. In order to monitor the effectiveness of the controlled blasting, pore pressures were measured using piezoceramic pore pressure transducers arranged at various depths immediately adjacent to the piles.

A.4.2 Controlled Blasting

In order to determine the blasting procedure to be used at the site, a pilot liquefaction study was performed on an adjacent site. This pilot study confirmed that

liquefaction could be induced by controlled blasting techniques. For safety reasons, two-part explosives were used on the project. When mixed, the nitromethane and ammonium nitrate had the equivalent explosive power of 0.5 kg of TNT (trinitrotoluene) per charge. The explosives used to raise pore pressures in the vicinity of the piles consisted of two sets of eight 0.5-kg charges, placed in 5-m diameter circles around each of the piles. All charges were placed at a depth of approximately 3.5 meters below the excavated ground surface. The sixteen charges were set off in one sequence, with a delay of approximately 250 milliseconds between each pair of charges. For the post-treatment blast, the same charge pattern was used. In addition, 14 charges were added around the perimeter of the excavation in an attempt to induce liquefaction in the area surrounding the stone columns. These additional charges had no effect on the soil immediately surrounding the foundations, but this was an attempt to study the behavior of an "improved island" and will be discussed in a future publication.

A.4.3 Stone Column Installation

After the first series of tests, the site was backfilled and stone columns were installed around the piles. Twenty-four 0.9-m diameter stone columns were installed in a 4 by 6 grid around the piles, with a spacing of approximately 2.4 meters on center, as shown in Figure 2. The stone columns extended through the surfical sand layer at the site, to depths of approximately 5.5 to 6.0 meters. After the installation, the site was re-excavated to the same depth as for the pre-treatment tests.

The stone columns used were installed using the dry bottom feed method. "Dry" in this context refers to the fact that the vibratory probe was driven into the ground using

compressed air instead of water. The term “bottom feed” is in reference to the way gravel is fed through the tip of the probe rather than being placed into the soil from the ground surface. Compressed air, vibration, and the weight of the probe itself drove the probe into the ground. Once the probe reached full depth, it was lifted up and the hole was backfilled with gravel from the probe tip. As the probe was approximately 0.5 m in diameter, multiple passes were required to create a column 0.9 m in diameter. The probe was raised in 0.9-m lifts, and gravel was placed into the soil. The probe was then re-lowered into the gravel that had just been placed, forcing it outward and further densifying the surrounding soil. Lifting the probe multiple times inserts more gravel into the column. To determine the number of passes required for complete site treatment, the operator monitored the amperage of the vibrating probe. As the soil was densified, the probe required more power to maintain its vibration. Once a set level of increase in amperage had been reached, the operator proceeded to the next 0.9-m lift.

A.4.4 Loading Sequence

The piles were first loaded before the installation of stone columns and before blasting had taken place. For this first test, the piles were pulled towards each other until one pile was displaced 38 mm. The load was reduced until one of the piles returned to its original position. After this test, the charges were set off. Ten seconds after the blast, the piles were loaded again, cycled under displacement control to 75 mm, 150 mm, and 225 mm of absolute displacement, then cycled at 225 mm of displacement nine times. For these tests, the load level was approximately 0.8 meters above the excavated surface.

The procedure for the post-treatment tests was essentially the same as for the pre-treatment testing. After the first tests were completed, stone columns were installed and the post treatment testing took place. For the post-treatment testing, the same loading sequence as the pre-treatment tests was attempted. However, the capacity of individual load cells within the pile group was exceeded before the piles had reached 150 mm of absolute displacement, so the piles were cycled under load control instead of displacement control.

A.5 RESULTS

The improvement to the upper sand layer is apparent from review of Figure 3, which shows the CPT tip resistance values (q_c) for the upper sand layer, both before (Figure 3a) and after (Figure 3b) treatment with stone columns. Excluding the top 1.5 meters that was excavated prior to testing, a substantial increase in the tip resistance can be seen throughout the sand layer. Prior to installation of the stone columns, the average tip resistance in the upper sand was approximately 4 MPa. After installation of the stone columns, the average tip resistance in the upper sand ranged between 10 and 50 MPa, and below a depth of 2 meters (i.e. 0.5 meters below the excavated surface) the average is well above 20 MPa. This amount of improvement can be expected from the installation of stone columns (e.g. *3* and *6*). Clearly, this substantial increase in tip resistance corresponds to a substantial decrease in the susceptibility of the upper sand to liquefaction.

This increased resistance to liquefaction can be observed in comparison of the pre- and post-treatment excess pore pressures (R_u). Figures 4 and 5 show the pre-

treatment blast-induced excess pore pressure ratios for the 4-pile group and the CISS pile, respectively. Each of the pore pressure transducers that obtained these recordings was located within 0.5 meters of the respective foundations. An immediate increase in R_u at all depths can be seen at the time of the blast, near the beginning of the record. Elevated pore pressures are maintained for at least the 10 minutes of loading, and are generally in excess of R_u equal to 80 percent for depths greater than 2.7 meters. Though R_u was not found to be 100 percent throughout the profile, observations confirmed that the site was essentially liquefied. These observations included numerous sand boils, water flowing freely from the ground (see Figure 6), and considerable surface settlement. With the load also shown on Figures 4 and 5, it is clear that the loading of the soil by the foundation has a significant impact on the pore pressure. A dramatic decrease, and subsequent increase, in pore pressure can be observed with each cycle of loading. This trend decreases with depth, which is likely associated with reduced soil displacement. For the recording at 0.9-m depth adjacent to the 4-pile group, this trend is very strong, for both loading and unloading. This behavior is indicative of soil dilation during loading, as would be expected.

The excess pore pressure ratios for the post-treatment tests, presented in Figures 7 and 8, are in sharp contrast to those recorded before installation of the stone columns. Though a sudden increase in R_u is apparent at the beginning of the record following the blast, the increase is much less than in the pre-treatment case. Furthermore, there is a rapid dissipation of excess pore pressures. At the end of 10 minutes, pore pressures are near hydrostatic, and in fact are slightly negative in some cases. Observations were consistent with these measurements, in that no visible signs of liquefaction were

apparent. No sand boil, surface settlement, or flowing water was observed, and there was actually significant gapping around the piles during the cyclic loading. The pore pressure response to cyclic loading is similar to that observed in the pre-treatment blast, with pore pressure decreasing with each cycle. The unusual response of the 2.7-m deep transducer adjacent to the 4–pile group should be noted. A likely cause is the presence of a clay pocket at the transducer tip. These clay pockets were commonly encountered in the excavated material.

Perhaps the most dramatic indicator of the amount of improvement that the soil has undergone as a result of stone column installation are the load-displacement curves. Reviewing first the pre-treatment plots for both the 4-pile group and the CISS pile, shown respectively in Figures 9 and 10, the pre-blast secant stiffness from the plots is approximately 7.5 kN/mm. These values are immediately reduced by over 60 percent due to the increased pore pressure from the blast. As the number of cycles increase and the soil structure is broken down, the secant stiffness is further reduced a total of nearly 70 percent for the 4-pile group and 80 percent for the CISS pile. The higher excess pore pressures surrounding the CISS pile may explain the lower stiffness values.

In contrast, the post-treatment load-displacement curves are shown in Figures 11 and 12 for the 4-pile group and the CISS pile, respectively. The initial secant stiffness prior to blasting is approximately 9.3 kN/mm for the 4-pile group and 10.8 kN/mm for the CISS pile. This is an increase of 25 to 45 percent over the pre-treatment, pre-blast test results. In both cases, however, the secant stiffness after blasting is approximately 7 kN/mm. This is only a 25 to 35 percent decrease from the pre-blast values and 2.5 to 3.5

times greater than the post-blast values prior to the installation of stone columns. This is a significant improvement over the pre-treatment test results.

As mentioned previously, in the pilot study as well as in a single pile test carried out earlier, it was found the a site could be liquefied at least twice using the same blast pattern with nearly identical results. This indicates that the lack of liquefaction in the post-treatment test, along with the improved performance from the measured data, can be attributed to the installation of the stone columns.

A.6 CONCLUSIONS

This paper presents the results of full-scale lateral load tests in liquefiable sands before and after ground improvement with stone columns. In each case, controlled blasting was used to elevate pore pressures in an attempt to liquefy the soil surrounding the deep foundations. Based on these results, several conclusions can be made regarding the stone column effectiveness in improving the performance of the foundation system under lateral loading in liquefiable soils.

- As has been observed in previous studies, the installation of stone columns significantly increased the density of the ground surrounding the foundations as indicated by the cone penetrometer test.
- The excess pore pressure increase resulting from controlled blasting was limited following ground improvement, as compared to pre-improvement tests.
- The rate of excess pore pressure dissipation after blasting was significantly increased as a result as the installation of stone columns.

- The installation of stone columns significantly increased the stiffness of the foundation system before and after blasting. This increase was 2.5 to 3.5 times that of the system in the liquefied soil.

A.7 REFERENCES

(1)Kramer, Steven L. *Geotechnical Earthquake Engineering*. Prentice-Hall, Inc., New Jersey, 1996.

(2)Mitchell, James K., Christopher D. P. Baxter and Travis C. Munson. Performance of Improved Ground During Earthquakes. *Soil Improvement for Earthquake Hazard Mitigation*, American Society of Civil Engineers, Geotechnical Special Publication No. 49, 1995, pp. 1-36.

(3)Priebe, H. J. The prevention of liquifaction by vibro replacement. *Proceedings of the International Conference on Earthquake Resistant Construction and Design.* S. A. Savidis, editor. A. A. Balkema Publishers, Rotterdam, Netherlands, 1991, pp. 211-219

(4)Somasundaram, Suji, Gamini Weeratunga, and John Best. Ground Improvement at the Long Beach Aquarium of the Pacific – A Case Study. *Ground Improvement, Ground Reinforcement, Ground Treatment, Developments 1987 – 1997*, American

Society of Civil Engineers, Geotechnical Special Publication No. 69, 1997, pp. 457-475.

(5)Saxena, D. S. and J. D. Hussin. Stone Column Improved and Piezocone Tested Site Supports Mid Rise Building Complex – A Case History. *Ground Improvement, Ground Reinforcement, Ground Treatment, Developments 1987 – 1997*, American Society of Civil Engineers, Geotechnical Special Publication No. 69, 1997, pp. 476-491.

(6)Soydemir, Cetin, Frank J. Swekosky, Juan I. Baez and Joel S. Mooney. Ground Improvement at Albany Airport, New York. *Ground Improvement, Ground Reinforcement, Ground Treatment, Developments 1987 – 1997*, American Society of Civil Engineers, Geotechnical Special Publication No. 69, 1997.

(7)Andrus, Ronald D., Kenneth H. Stokoe, II, Riley M. Chung, and James A. Bay. *Liquefaction Evaluation of Densified Sand at Approach to Pier 1 on Treasure Island, California, Using SASW Method.* Report NISTIR 6230. National Institute of Standards and Technology, 1998.

LIST OF FIGURES

Figure 1: Soil profile and Standard Penetration Test results.

Figure 2: Plan view of test set-up.

Figure 3: Pre- and post-treatment cone penetration test results. Maximum and minimum values are shown in grey, average values in black

Figure 4: Pre-treatment blast-induced excess pore-pressure ratio around 4-pile group.

Figure 5: Pre-treatment blast-induced excess pore-pressure ratio around CISS pile.

Figure 6: Water flowing from ground near CISS pile following pre-treatment blast.

Figure 7: Post-treatment blast-induced excess pore-pressure ratio around 4-pile group.

Figure 8: Post-treatment blast-induced excess pore-pressure ratio around CISS pile.

Figure 9: Load-displacement curves for 4-pile group (pre-treatment blast).

Figure 10: Load-displacement curves for 0.6-m diameter CISS pile (pre-treatment blast).

Figure 11: Load-displacement curves for 4-pile group (post-treatment blast).

Figure 12: Load-displacement curves for CISS pile (post-treatment blast).

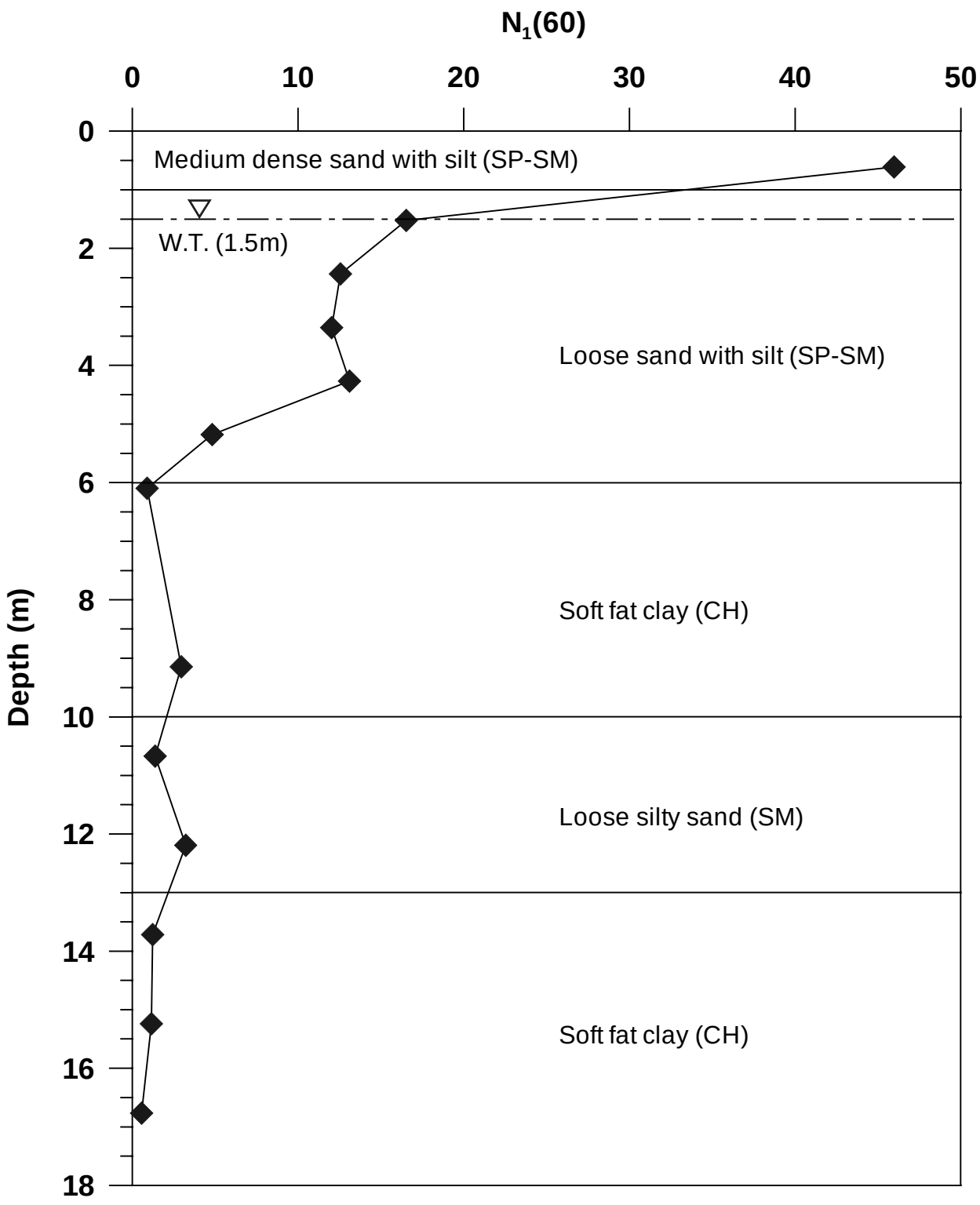

FIGURE 1: Soil profile and standard penetration test results.

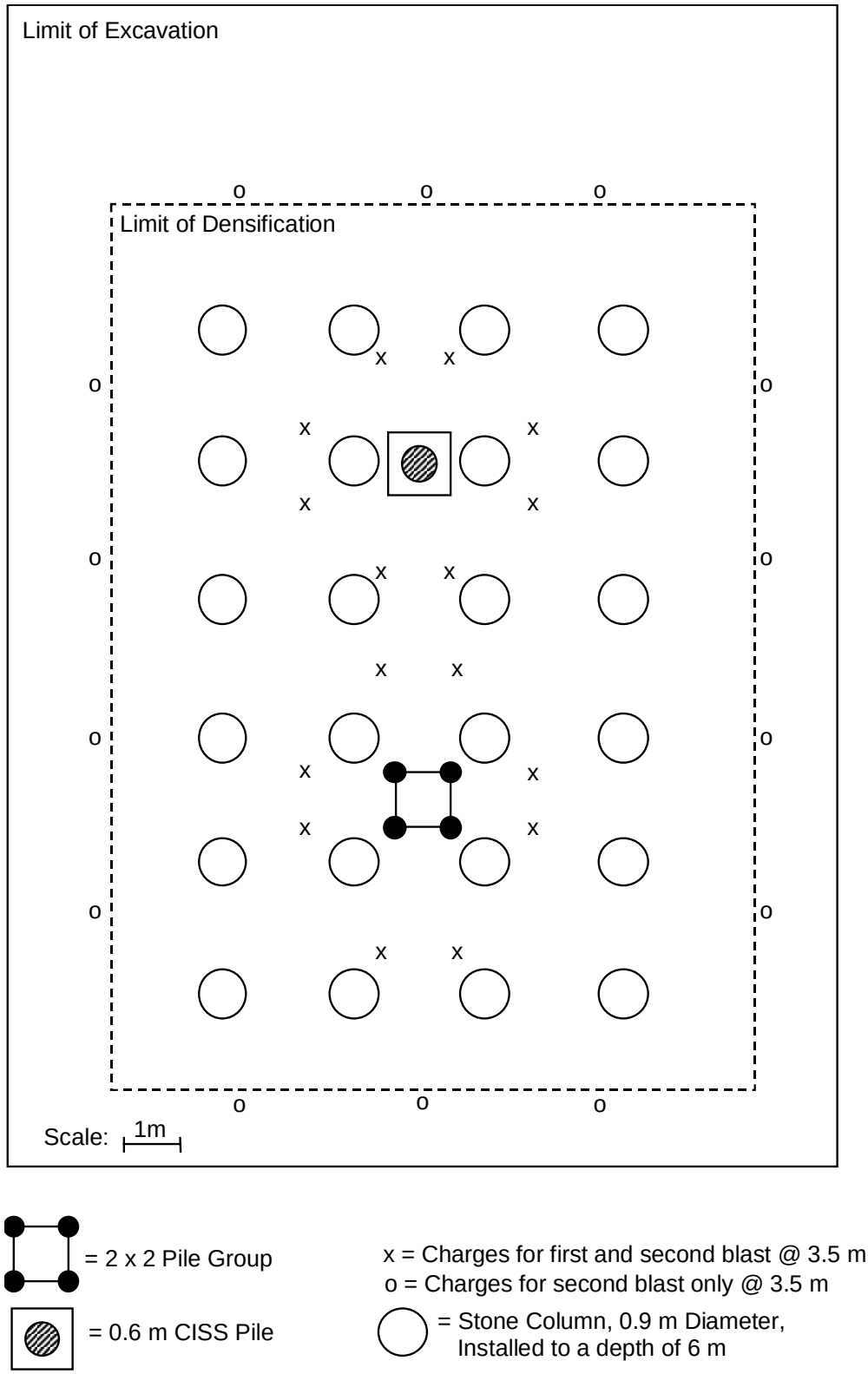

Figure 2: Plan View of test set-up.

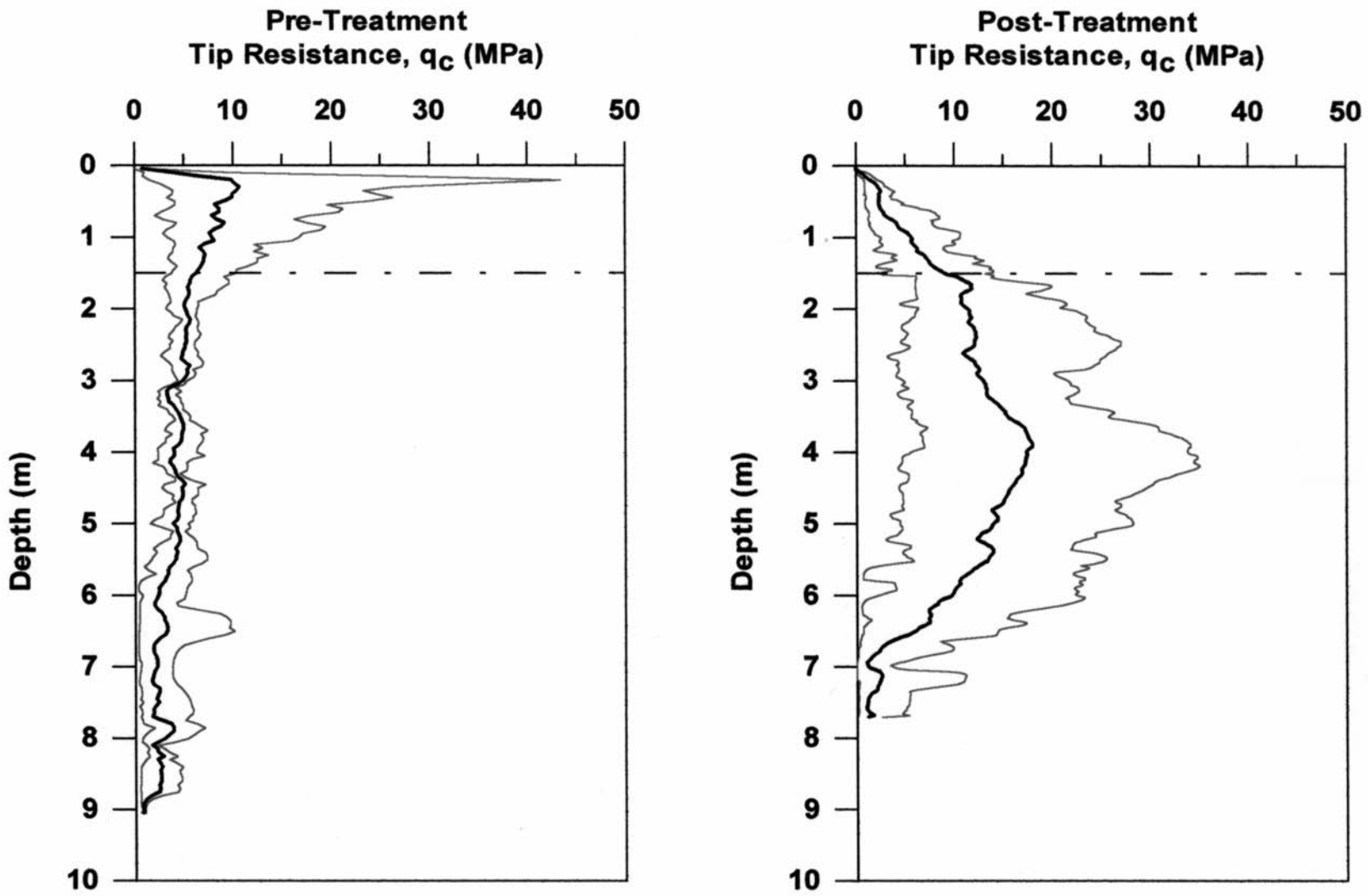

FIGURE 3: Pre- and post-treatment cone penetration test results. Maximum and minumum values are shown in gray, average values in black.

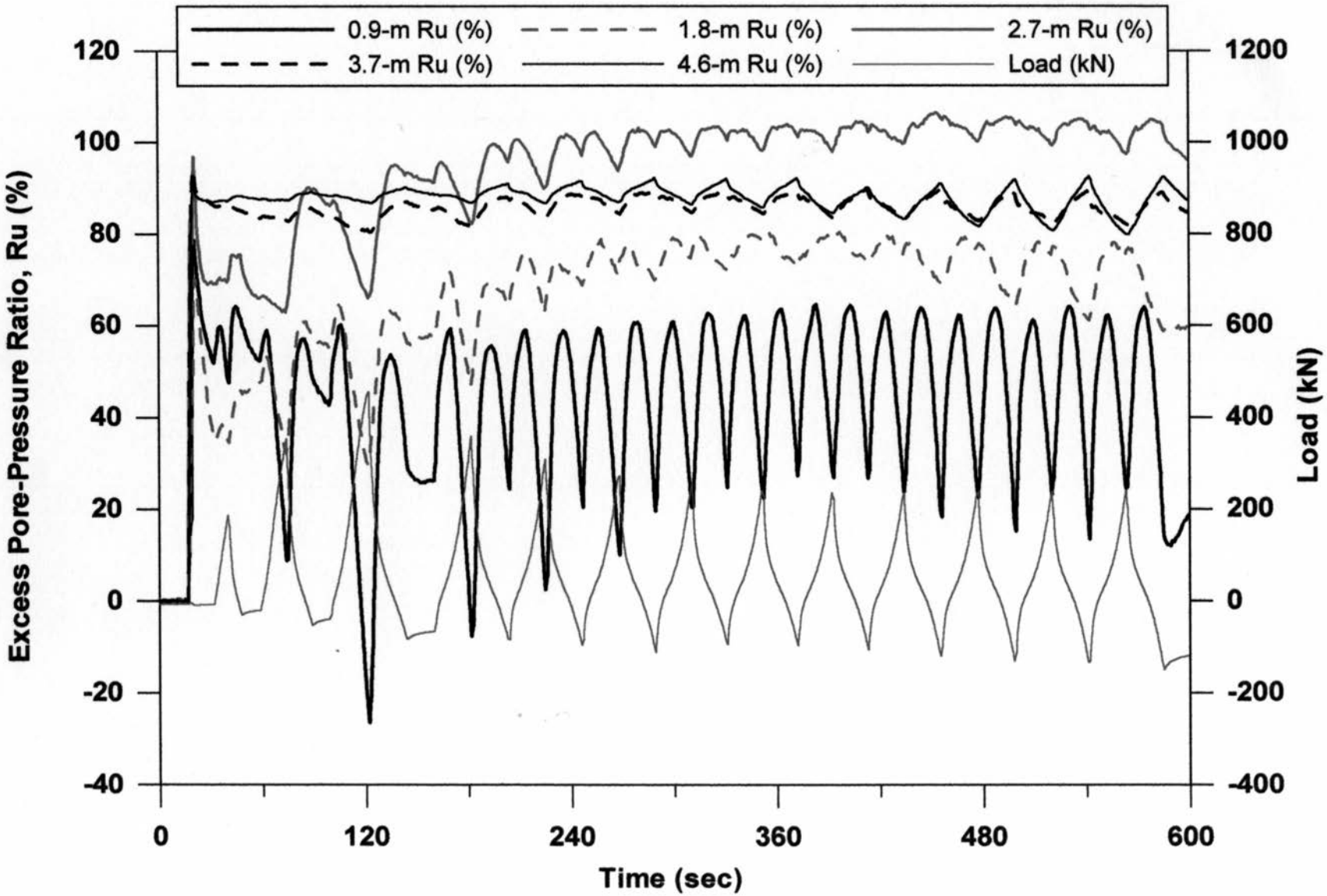

FIGURE 4: Pre-treatment blast-induced excess pore-pressure ratio around 4-pile group.

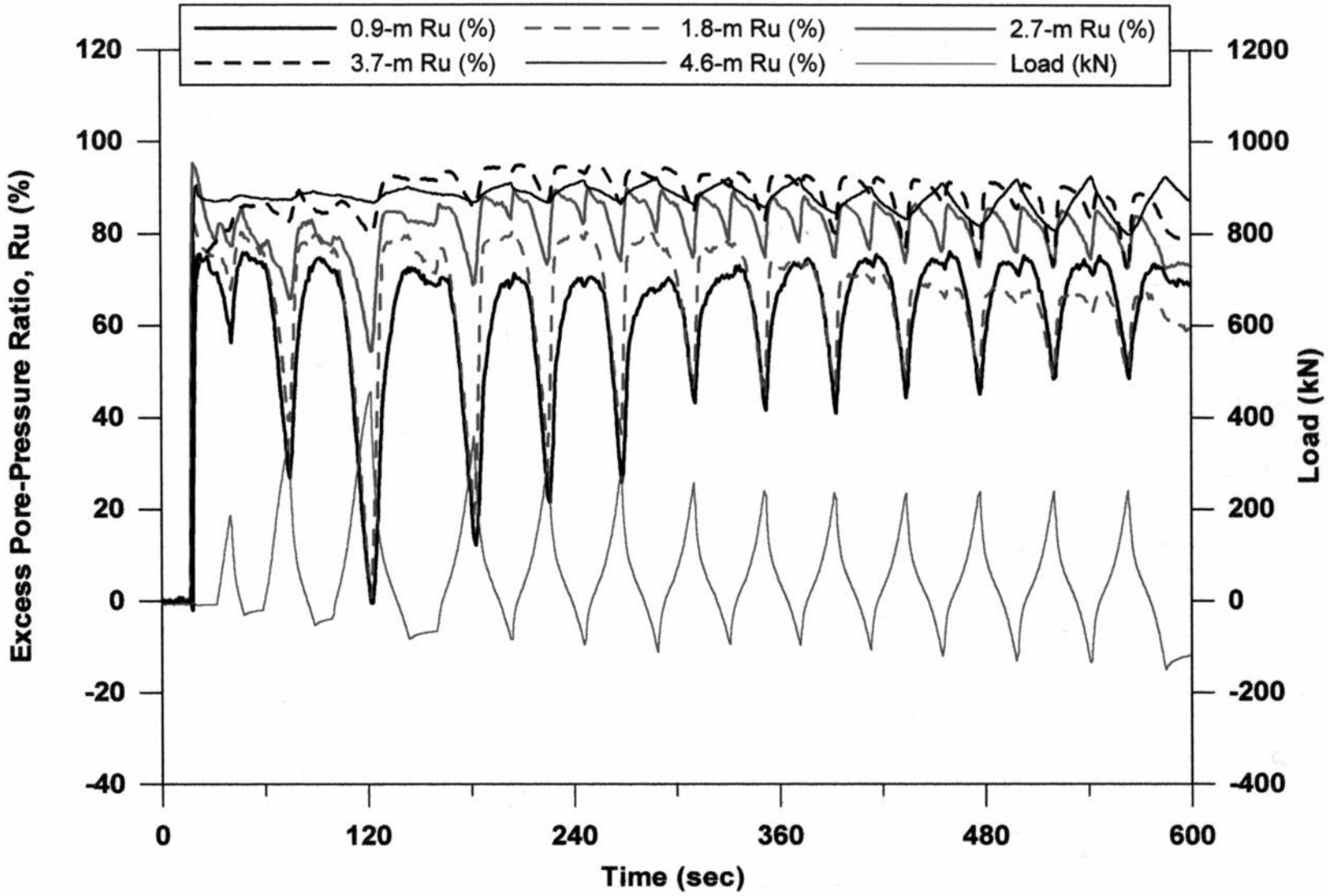

FIGURE 5: Pre-treatment blast-induced excess pore-pressure ratio around CISS pile.

Figure 6: Water flowing from ground near CISS pile following pre-treatment blast.

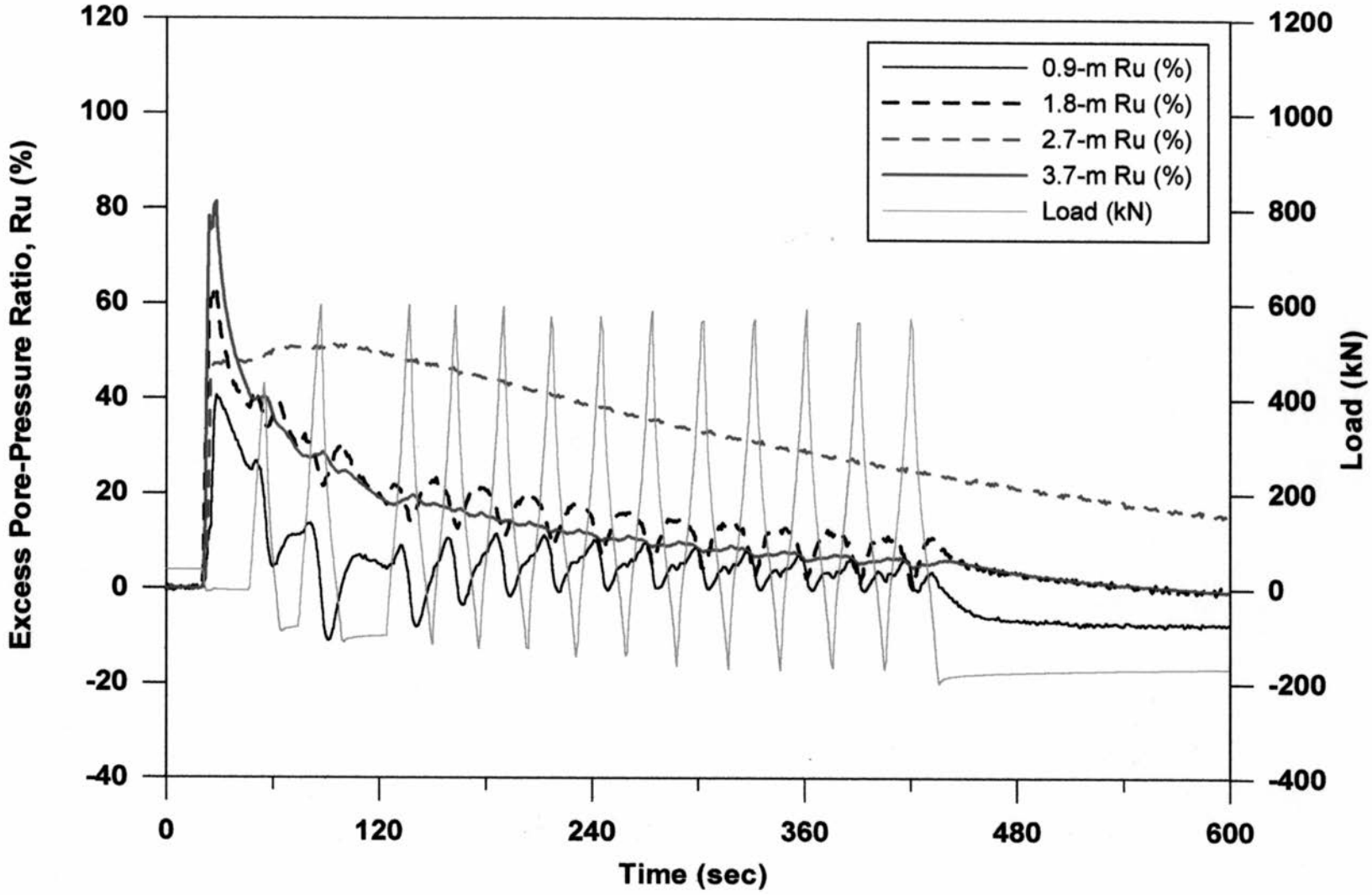

FIGURE 7: Post-treatment blast-induced excess pore-pressure ratio around 4-pile group.

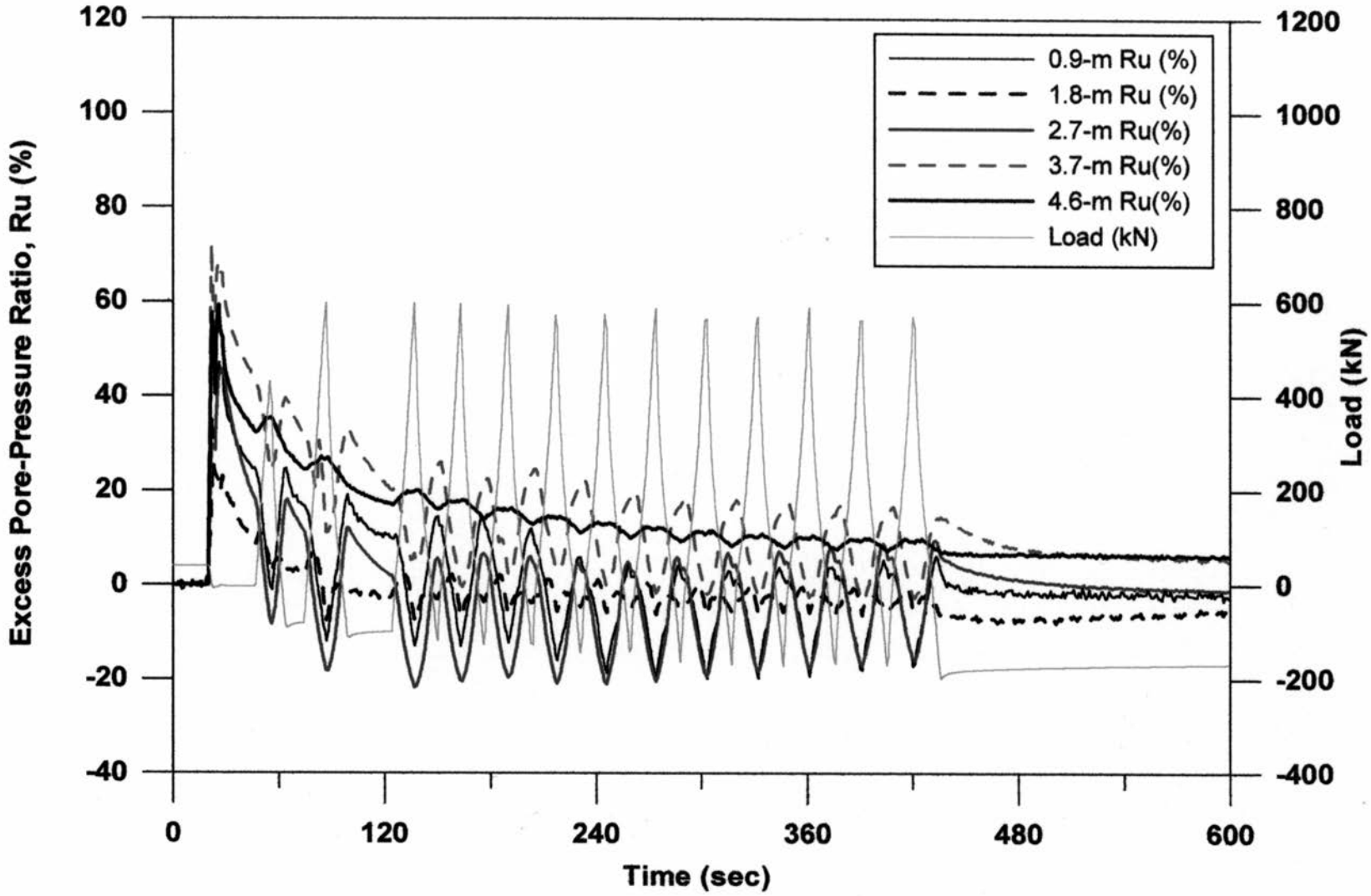

FIGURE 8: Post-treatment blast-induced excess pore-pressure ratio around CISS pile.

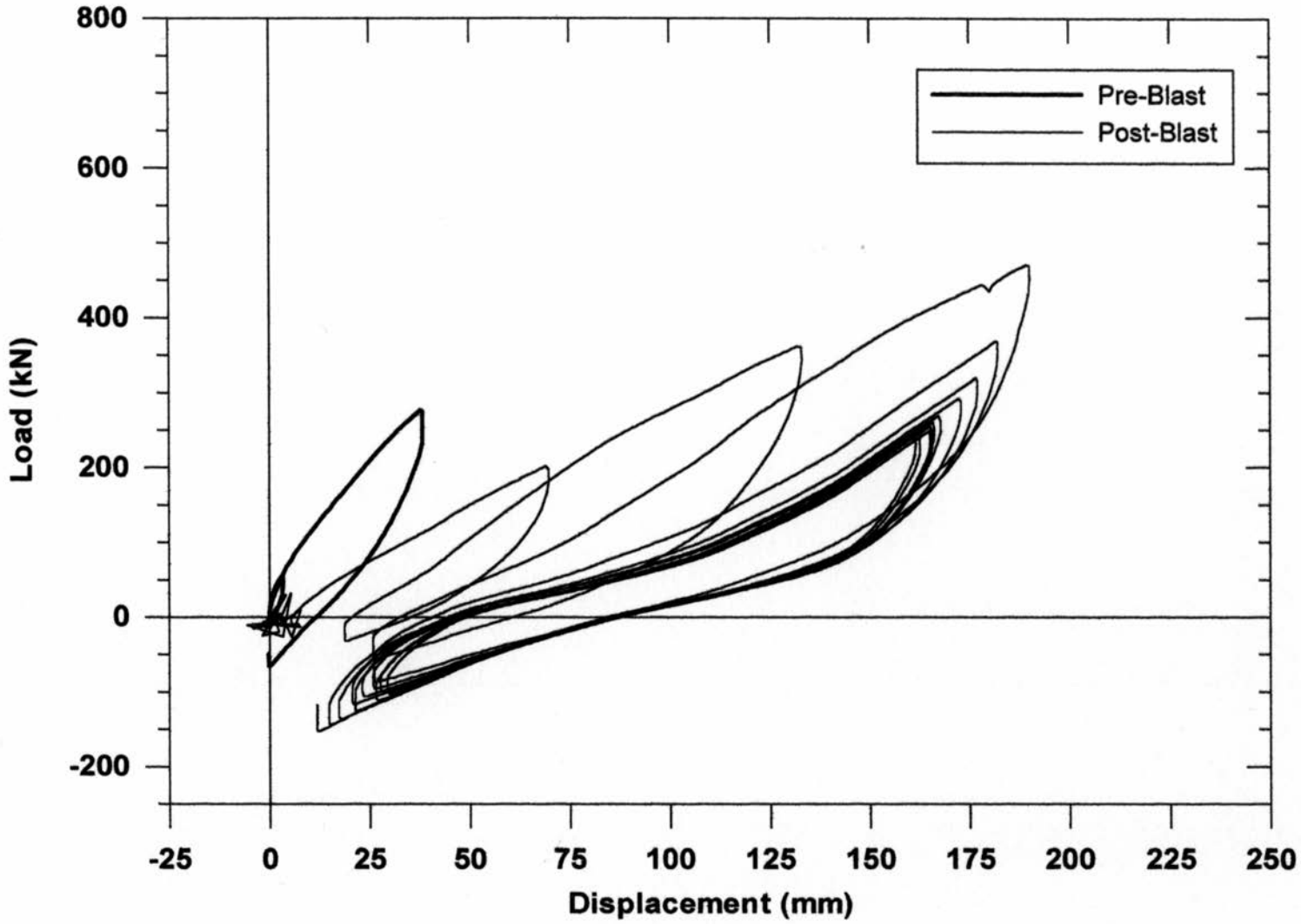

FIGURE 9: Load-displacement curves for 4-pile group (pre-treatment blast).

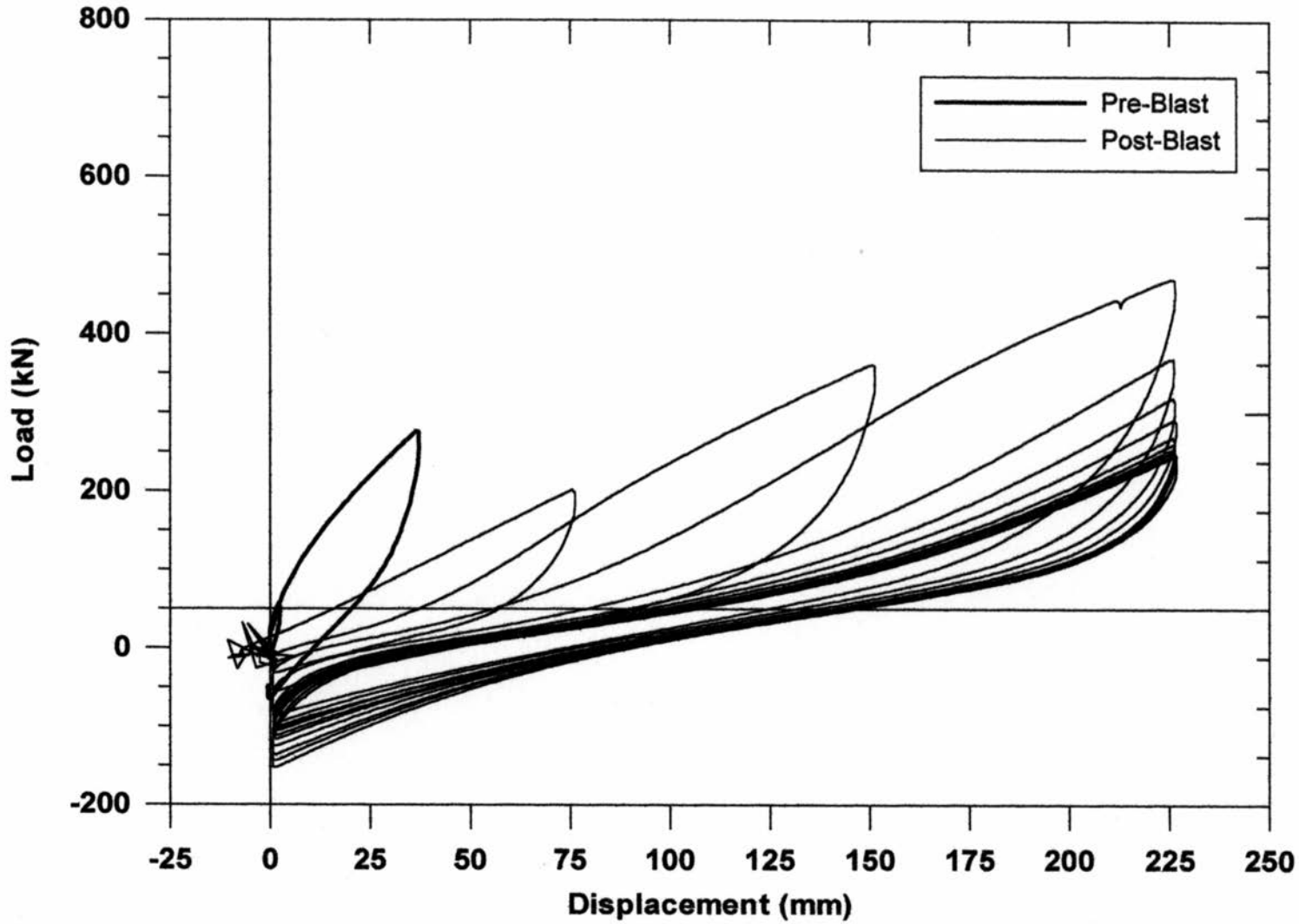

FIGURE 10: Load-displacement curves for 0.6-m diameter CISS pile (pre-treatment blast).

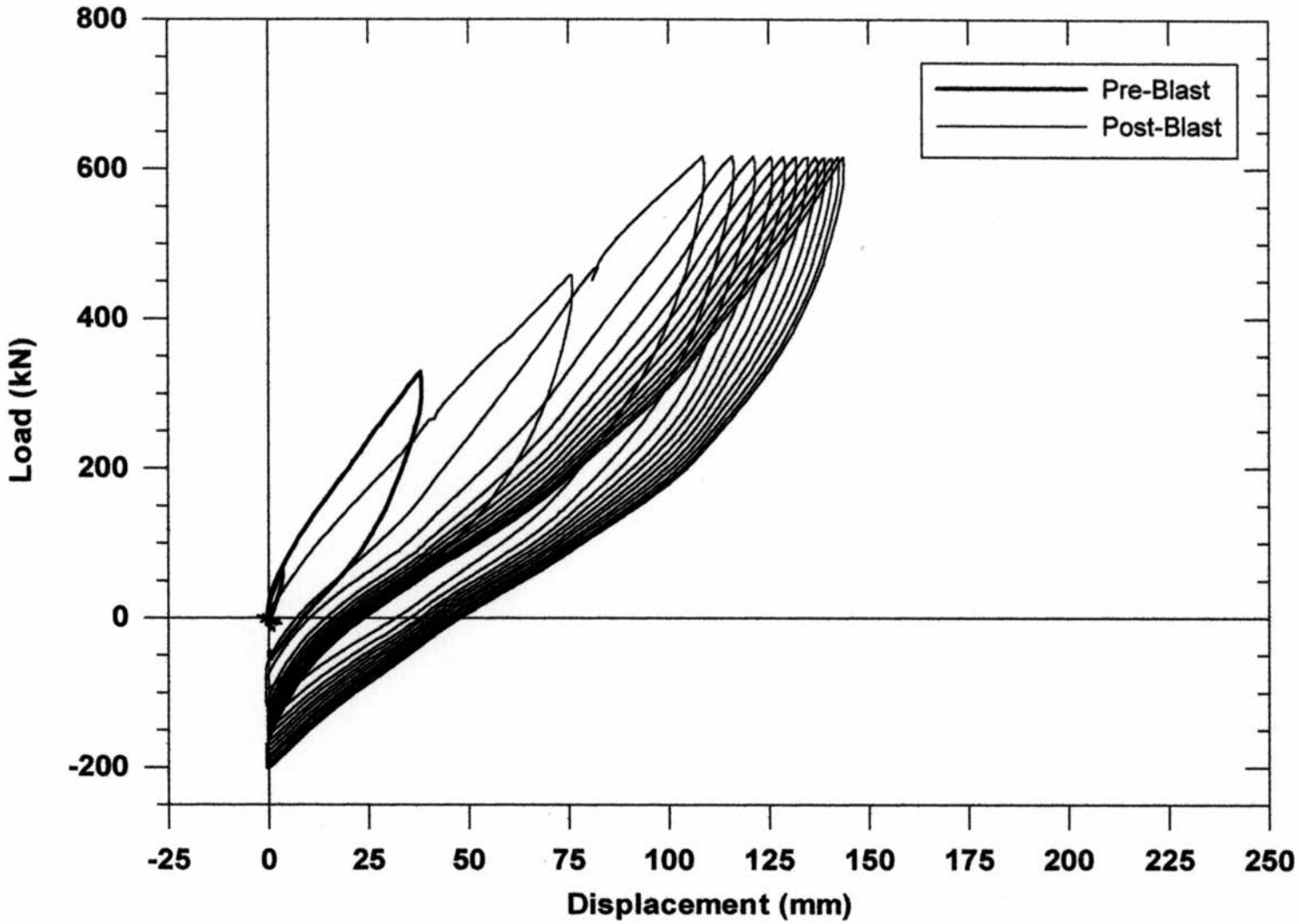

FIGURE 11: Load-displacement curves for 4-pile group (post-treatment blast).

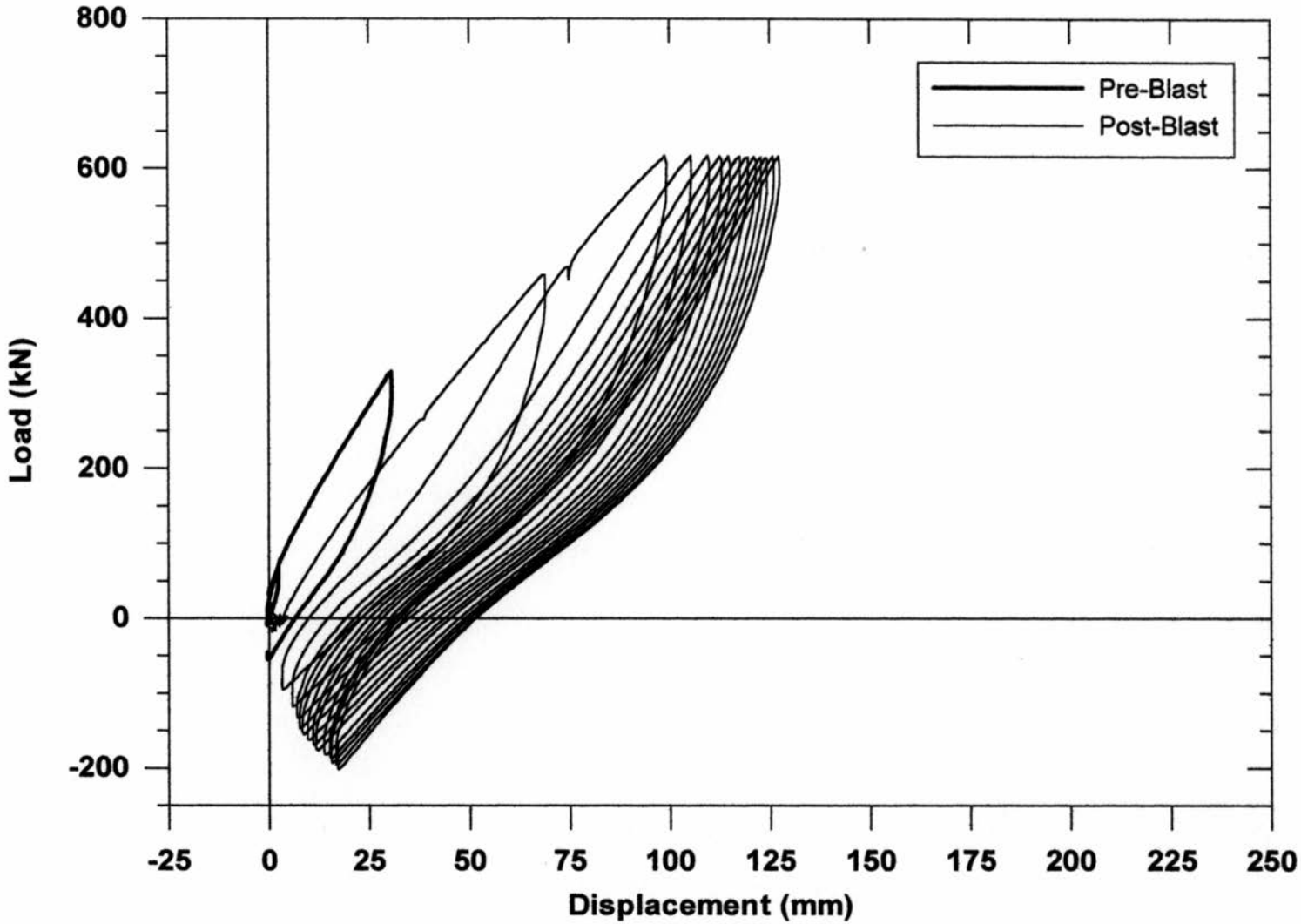

FIGURE 12: Load-displacement curves for 0.6-m diameter CISS pile (post-treatment blast).